Status and Trends of North American Bats

Summer Occupancy Analysis 2010-2019

North American Bat Monitoring Program | May 2022

By Bradley J. Udell[1], Bethany R. Straw[1], Tina L. Cheng[2], Kyle Enns[1], Winifred F. Frick[2, 3], Benjamin Gotthold[1], Kathryn M. Irvine[4], Cori Lausen[5], Susan Loeb[6], Jonathan Reichard[7], Tom Rodhouse[8], Dane Smith[1], Christian Stratton[9], Wayne E. Thogmartin[10], and Brian E. Reichert[1]

[1] U.S. Geological Survey, Fort Collins Science Center, Fort Collins, Colorado, 80526, USA

[2] Bat Conservation International, Austin, Texas, 78746, USA

[3] University of California Santa Cruz, Department of Ecology and Evolutionary Biology, Santa Cruz, California, 95060, USA

[4] U.S. Geological Survey, Northern Rocky Mountain Science Center, Bozeman, Montana, 59717, USA

[5] Wildlife Conservation Society Canada, Toronto, Ontario, M5S 3A7, CA

[6] U.S. Forest Service, Southern Research Station, Clemson, South Carolina, 29634, USA

[7] U.S. Fish and Wildlife Service, Ecological Services, Hadley, Massachusetts, 01035, USA

[8] National Parks Service, Upper Columbia Basin Network, Bend, Oregon, 97701 USA

[9] Montana State University, Department of Mathematical Sciences, Bozeman, Montana, 59717, USA

[10] U.S. Geological Survey, Upper Midwest Environmental Sciences Center, La Crosse, Wisconsin, 54603, USA

NABat NORTH AMERICAN BAT MONITORING PROGRAM

The North American Bat Monitoring Program (NABat) is a multi-national, multi-agency coordinated bat monitoring program across North America. NABat seeks to address the historic lack of information on status and trends of North American Bats through coordinated, standardized, long-term data collection and integrated data analysis. Bat monitoring data contributed to the NABat database are used to estimate bat distributions and abundance and how these metrics are changing over time. This information fills critical knowledge gaps that support the management of bat populations in the face of multiple threats.

NABat is committed to iterative improvement throughout the life of the program. To deliver the best available science, we will continue to pursue opportunities for improvement throughout the greater bat monitoring system—from data collection to information delivery.

To learn more about NABat visit nabatmonitoring.org.

Acknowledgements

Fundamental to the success of the NABat program is the collaborative network upon which it stands. We express our deep thanks to all our collaborators who contribute to the collection and collation of bat monitoring data across North America. Without the committed efforts of these partners, none of this work is possible. We would like to specifically acknowledge all the data contributors from the following organizations whose NABat Partner Portal project data were used in this assessment:

Alaska Department of Fish and Game
Arizona Game & Fish Department
Arizona State Parks and Trails
Army Corps of Engineers
Bat Conservation International
Bat Survey Solutions, LLC
Bureau of Land Management
California Department of Fish & Wildlife
Camp Blanding Joint Training Center
Canadian Wildlife Health Cooperative
Canadian Wildlife Service
Colorado Natural Heritage Program
Colorado Parks and Wildlife
Corduroy Brook Enhancement Association
Delaware Division of Fish & Wildlife
Environmental Solutions & Innovations, Inc.
Florida Fish & Wildlife Conservation Commission
Georgia Department of Natural Resources
Idaho Department of Fish & Game
Illinois Bat Conservation Program
Indiana Department of Natural Resources, Division of Fish & Wildlife
Indiana Department of Natural Resources, Division of Forestry
Iowa Department of Natural Resources
Kansas Department of Wildlife, Parks & Tourism
Keweenaw Bay Indian Community Natural Resources Department
Maine Department of Inland Fisheries & Wildlife
Massachusetts Department of Transportation, Highway Division
Midwest Bat Hub
Minnesota Department of Natural Resources
Missouri Department of Conservation
Montana Natural Heritage Program
Myotistar
National Park Service
Nebraska Game & Parks Commission
Nevada Department of Wildlife
New Jersey Division of Fish and Wildlife - Endangered and Nongame Species Program
Newfoundland & Labrador Department of Fisheries & Land Resources
North Carolina Wildlife Resources Commission
Nova Scotia Department of Lands and Forestry Wildlife Division
Ohio Department of Natural Resources
One Tam

Oregon Military Department
Oregon State University
Parks Canada
Phoenix College
Quebec Chiroptera Group
Rhode Island Division of Fish & Wildlife
San Diego Natural History Museum
South Carolina Department of Natural Resources
Summit Lake Paiute Tribe
Tennessee Wildlife Resources Agency
U.S. Air Force
U.S. Fish and Wildlife Service
U.S. Forest Service
U.S. Geological Survey
U.S. Navy
Unama'ki Institute of Natural Resources
University of North Carolina at Greensboro
Utah Division of Wildlife Resources
Vermont Fish & Wildlife Department
Virginia Department of Game and Inland Fisheries
Virginia Polytechnic Institute and State University
Washington Department of Fish & Wildlife
Western EcoSystems Technology, Inc.
Wildlife Conservation Society Canada
Wisconsin Department of Natural Resources
Wyoming Game & Fish Department

We would like to thank Jeremy Siemers, Dan Neubaum, W. Mark Ford, Jesse De La Cruz, Roger Perry, Andy King, Rich Geboy, Laura Beard, Tina Jackson, Kelli Van Norman, Josh Chapman, Lori Pruitt, and one anonymous reviewer for their thoughtful and helpful feedback on earlier versions of the analyses and report. We thank members of the NABat Core Planning Team for their leadership and input: Jeremy Coleman, Ted Weller, Michelle Verant, Mylea Bayless, Frank Quamen, Charles Francis, and Eric Britzke. We would like to acknowledge James Cox (Contractor - U.S. Geological Survey), Frank Tousley (Contractor - U.S. Geological Survey), Jaclyn Martin (U.S. Geological Survey), Carter Campbell (U.S. Geological Survey) and all others at the North American Bat Monitoring Program that assisted in formatting and collating data for this effort.

Any use of trade, firm, or product names is for descriptive purposes only and does not imply endorsement by the U.S. Government. The findings and conclusions in this article are those of the author(s) and do not necessarily represent the views of the U.S. Fish and Wildlife Service. Information accessed here do not satisfy agency consultation requirements under Section 7(a)(2) of the U.S. Endangered Species Act of 1973 (87 Stat. 884, as amended 16 U.S.C. 1531 et seq.; ESA). For consultation purposes in the U.S., use the U.S. Fish and Wildlife Service's IPaC program, or contact your local field office. Funding support provided by USGS Ecosystems Mission Area (Species Management Research Program, Biological Threats and Invasive Species Research Program), U.S. Fish and Wildlife Service, and Bureau of Land Management.

Executive Summary

- We developed an analytical pipeline supported by web-based infrastructure for integrating continental scale bat monitoring data (stationary acoustic, mobile acoustic, and capture records) to estimate summer (May 1–Aug 31) occupancy probabilities and changes in occupancy over time for 12 North American bat species. This serves as one of multiple lines of evidence that inform the status and trends of bat populations.
- We analyzed data from a total of 12 bat species (Table 1), 11 of which have tested positive for *Pseudogymnoascus destructans (Pd),* a fungal pathogen that causes white-nose syndrome (WNS)—a disease that has led to significant rates of mortality for subterranean hibernating bat species in North America. A twelfth species was also selected because of high rates of mortality at wind energy facilities. Additional species were considered but not selected due to data limitations.
- We estimated occupancy probabilities for 2010 through 2019 for three species (*Myotis lucifugus*, MYLU; *Myotis septentrionalis*, MYSE; and *Perimyotis subflavus*, PESU). For an additional nine species, we estimated occupancy probabilities for 2016 through 2019 (*Myotis evotis*, MYEV; *Myotis grisescens*, MYGR; *Myotis leibii*, MYLE; *Myotis thysanodes*, MYTH; *Myotis volans*, MYVO; *Myotis yumanensis*, MYYU; *Eptesicus fuscus*, EPFU; *Lasionycteris noctivagans*, LANO; and *Lasiurus cinereus*, LACI).
- For each species, we provide range-wide occupancy probability predictions (e.g., predicted summer occupancy distribution maps) each year at a spatial resolution of 100 km^2 and provide regional estimates of mean occupancy probability aggregated at larger spatial scales (state/province/territory, range-wide).
- For each species, we also provide trends over time (average annual change rate and total change rate) in mean occupancy probabilities at multiple spatial scales (state/province/territory, range-wide) and when possible, over multiple timescales (short, medium, long).
- Results suggest that over the short-term (2016-2019), two (*Myotis lucifugus* and *Perimyotis subflavus)* of 12 species have experienced declines in range-wide average occupancy probability with at least 95% certainty. Seven species showed either minor increases or decreases in range-wide average occupancy probability but with less than 95% certainty in both trend indicators. Results over the longer term (eight years and 10 years of sampling) suggest that three hibernating species known to be highly affected by white-nose syndrome (*Myotis lucifugus, Myotis septentrionalis,* and *Perimyotis subflavus*) have experienced marked declines in range-wide average occupancy probabilities, with severity varying by species and region. Finally, the results for three species (*Eptesicus fuscus, Lasiurus cinereus, Lasionycteris noctivagans*) were inconclusive due to 1) borderline convergence issues in the model fitting procedure which suggests potentially unreliable estimates, 2) failure to reliably distinguish between false positives and true positive detections for ambiguous detections, and 3) largely uninformative covariates for occupancy and detection.
- For *Myotis lucifugus, Myotis septentrionalis,* and *Perimyotis subflavus* we found meaningful associations in space and time between declining winter populations (likely a result of WNS) and summer occupancy distributions.

- The representativeness of sampling data for each species' status and trend estimates (e.g., state/province/territory) were also evaluated based on the percent of grid cells sampled each year with a goal of understanding the reliability of regional estimates and improving future monitoring efforts.
- This work represents the most comprehensive effort to date to model North American bat distributions across their continental ranges. Despite current limitations highlighted in the discussion, the analytical methods and resulting status and trends estimates provide the best available science on summer bat populations across North America and will continue to improve over time as monitoring data sets and analytical methods improve.
- Moving forward, our occupancy analyses will continue to improve with submission of more 1) data from currently underrepresented areas (i.e., improved geographic representation), 2) manually-vetted acoustic recordings, 3) capture records, and 4) roost location and count data (summer and winter).

Table 1. Species included in this analysis, with corresponding white-nose syndrome (WNS) status and federal listing status. WNS Status includes Confirmed = species identified with diagnostic symptoms of white-nose syndrome, Pd positive = species on which *Pseudogymnoascus destructans* (Pd) has been detected but WNS has not been confirmed, and Not detected = species which WNS and Pd have not been detected (whitenosesyndrome.org, accessed 2021-12-10). Federal listing status was obtained from Government of Canada Species at Risk Public Registry (https://species-registry.canada.ca/index-en.html#/species?sortBy=commonNameSort&sortDirection=asc&pageSize=10, accessed 2021-12-10), U.S. Fish and Wildlife Service Endangered Species List (https://www.fws.gov/endangered/, accessed 2021-12-10), and Mexico's Enciclo Vida (https://enciclovida.mx/, accessed 2022-01-10). *Indicates species currently undergoing species status assessment by U.S. Fish and Wildlife Service. **Indicates species currently under review by the Committee on the Status of Endangered Wildlife in Canada (https://www.cosewic.ca/index.php/en-ca/reports/status-reports-preparation.html, accessed 2022-01-10).

Species Code	Scientific Name	WNS Status	Federal Listing Status
MYLU	*Myotis lucifugus*	Confirmed	Canada: Endangered USA: None*
MYSE	*Myotis septentrionalis*	Confirmed	Canada: Endangered USA: Threatened*
PESU	*Perimyotis subflavus*	Confirmed	Canada: Endangered USA: None*
MYEV	*Myotis evotis*	Confirmed	Mexico: Subject to special protection
MYGR	*Myotis grisescens*	Confirmed	USA: Endangered
MYLE	*Myotis leibii*	Confirmed	None
MYTH	*Myotis thysanodes*	Confirmed	None
MYVO	*Myotis volans*	Confirmed	None
MYYU	*Myotis yumanensis*	Confirmed	None
EPFU	*Eptesicus fuscus*	Confirmed	None
LANO	*Lasionycteris noctivagans*	*Pd* positive	Canada: None** Mexico: Subject to special protection
LACI	*Lasiurus cinereus*	Not detected	Canada: None**

Table of Contents

Acknowledgements ii
Executive Summary iv
1. Introduction and Purpose 1
2. Methods - Datasets 3
2.1 Response data 3
2.1.1 Stationary acoustic sampling 3
2.1.2 Mobile transect acoustic sampling methods 4
2.1.3 Capture records 5
2.1.4 Summary of response types 5
2.1.5 Data sources and contributors 6
2.2 Covariates 7
2.2.1 Site-level covariates 7
2.2.2 Seasonal connectivity metrics (integrating winter count data) 8
2.2.3 Other derived grid cell-level covariates sourced from spatial data sets 11
2.2.4 Detection-level covariates 12
2.3 Range maps 13
3. Results 15
3.1 Useful definitions for interpreting results 15
3.2 Organization of results 16
3.3 *Myotis lucifugus* 18
3.4 *Myotis septentrionalis* 23
3.5 *Perimyotis subflavus* 28
3.6 *Myotis evotis* 34
3.7 *Myotis grisescens* 40
3.8 *Myotis leibii* 45
3.9 *Myotis thysanodes* 50
3.10 *Myotis volans* 56
3.11 *Myotis yumanensis* 62
3.12 Inconclusive Results 67
3.12.1 *Eptesicus fuscus* 69
3.12.2 *Lasionycteris noctivagans* 74
3.12.3 *Lasiurus cinereus* 79

4. Discussion 84
4.1 Interpreting occupancy estimates and trends 85
4.2 Data limitations 86
4.3 Analytical limitations 87
4.4 Looking forward 89
References 90
Appendix A: Statistical Method Used for the False-positive Occupancy Modeling and Predictions 95
A.1 Statistical methods used for the false-positive occupancy modeling 95
A.2 Observation model 95
A.2.1 Data fusion and aggregation for occupancy modeling 95
A.2.2 Additional model assumptions 96
A.2.3 Statistical model 97
A.2.4 Constraints on p11 and p10 for identifiability 98
A.3 Ecological model for grid cell-level occupancy 98
A.3.1 Hierarchical ecoregion effects in space and time 104
A.3.2 Winter-to-summer connectivity metric 106
A.3.3 Spatial splines 107
A.4 Model fitting 108
A.5 Predicting occupancy maps and deriving status and trend across the species range 108
A.5.1 Temporal scope 108
A.5.2 Spatial scope 108
A.5.3 Measures of status and trend 109
References cited in Appendix A 111
Appendix B: State/Province/Territory Level Results 113
B.1 *Myotis lucifugus* 113
B.2 *Myotis septentrionalis* 122
B.3 *Perimyotis subflavus* 131
B.4 *Myotis evotis* 139
B.5 *Myotis grisescens* 144
B.6 *Myotis leibii* 149
B.7 *Myotis thysanodes* 155
B.8 *Myotis volans* 160
B.9 *Myotis yumanensis* 165

B.10 *Eptesicus fuscus* 170
B.11 *Lasionycteris noctivagans* 178
B.12 *Lasiurus cinereus* 186
Appendix C: Occupancy Modeling Covariate Effects 194
C.1 *Myotis lucifugus* 194
C.2 *Myotis septentrionalis* 196
C.3 *Perimyotis subflavus* 198
C.4 *Myotis evotis* 200
C.5 *Myotis grisescens* 202
C.6 *Myotis leibii* 204
C.7 *Myotis thysanodes* 206
C.8 *Myotis volans* 208
C.9 *Myotis yumanensis* 210
C.10 *Eptesicus fuscus* 212
C.11 *Lasionycteris noctivagans* 214
C.12 Lasiurus cinereus 216
Appendix D: Comparing predicted occupancy probabilities to monitoring data 219
D.1 *Myotis lucifugus* 220
D.2 *Myotis septentrionalis* 221
D.3 *Perimyotis subflavus* 222
D.4 *Myotis evotis* 223
D.5 *Myotis grisescens* 224
D.6 *Myotis leibii* 225
D.7 *Myotis thysanodes* 226
D.8 *Myotis volans* 227
D.9 *Myotis yumanensis* 228
D.10 *Eptesicus fuscus* 229
D.11 *Lasionycteris noctivagans* 230
D.12 *Lasiurus cinereus* 231

List of Tables

Table 1. Species included in this analysis, with corresponding white-nose syndrome (WNS) status and federal listing status.....v
Table 2. Summary of data available for the Summer Occupancy Analysis.. 6
Table 3. Name and source of the site-level covariates in the North American Bat Monitoring Program (NABat) database... 7
Table 4. Name and source of site-level covariates obtained from Google Earth Engine. 7
Table 5. Species mean seasonal migration distance, and sample size of records from the literature and/or the U.S. Historic Bat Banding Database. 9
Table 6. Additional spatial covariates geo-processed and joined to each grid cell in the continental North American Bat Monitoring Program (NABat) sampling grid using either ArcMap or the spatial features (sf) package in R.....11
Table 7. Summary of night-level covariates aggregated across seven-day periods and included in the false-positive occupancy model for each bat species**..** 13
Table 8. Sources of species range maps for bats that occur in North America.....13
Table 9. A summary table depicting the total number of monitoring data points (grid-cell*observation) of each detection history type (0: no-detection, 1: ambiguous detection, 2: unambiguous detection) for each bat species, including the number of points of each type that fell inside and outside of the reference ranges.....14
Table 10. The numerical values represented in Figure 7 for average annual change and total average change of *Myotis lucifugus* (MYLU) over short-term (2016–2019, three year), medium-term (2012–2019, seven year), and long-term (2010–2019, nine year) periods. CRI = 95 credible interval. 22
Table 11. The numerical values represented in Figure 12 for average annual change and total average change over short-term (2016–2019, three year), medium-term (2012–2019, seven year), and long-term (2010–2019, nine year) periods. CRI = 95% credible interval.....27
Table 12. The numerical values represented in Figure 17 for average annual change and total average change *Perimyotis subflavus* (PESU) over short-term (2016–2019, three year), medium-term (2012–2019, seven year), and long-term (2010–2019, nine year) periods. CRI = 95 % credible interval. 33
Table 13. The numerical values represented in Figure 22 for average annual change and total average change over a short-term (2016–2019, three year) period. CRI= 95% credible intervals. 39
Table 14. The numerical values represented in Figure 27 for average annual change and total average change over a short-term (2016–2019, three year) period. CRI = 95% credible intervals. 44
Table 15. The numerical values represented in Figure 32 for average annual change and total average change over a short-term (2016–2019, three year) period. CRI = 95% credible interval. 49
Table 16. The numerical values represented in Figure 37 for average annual change and total average change of Myotis thysanodes (MYTH) over a short-term (2016–2019, three year) period. CRI = 95% credible interval. 55
Table 17. The numerical values represented in Figure 42 for average annual change and total average change over a short-term (2016–2019, three year) period. CRI = 95% credible interval. 61
Table 18. The numerical values represented in Figure 47 for average annual change and total average change over a short-term (2016–2019, three year) period. CRI= 95% credible interval.....67
Table 19. The numerical values represented in Figure 52 for average annual change and total average change over a short-term (2016–2019, three year) period.....73
Table 20. The numerical values represented in Figure 57 for average annual change and total average change over a short-term (2016–2019, three year) period.....78
Table 21. The numerical values represented in Figure 62 for average annual change and total average change over a short-term (2016–2019, three year) period.....83
Table A.1. A description of the ecological model for predicting grid cell-level occupancy for each bat species. Note the parameter estimates from fitted models and the relative strength of effects are provided in Appendix C. AR1 = autoregressive 100

List of Figures

Figure 1. Winter-to-summer population connectivity values have declined for (A) *Myotis lucifufus* (MYLU), (B) *Myotis septentrionalis* (MYSE), and (C) *Perimyotis subflavus* (PESU) (color bar shows connectivity values after transformation [log +1 then centering] for visualization) for years 2010 and 2019 based on the modeled species counts at winter hibernacula each year and the species specific, winter-to-summer, mean migration distance... ...10
Figure 2. Ecological regions of North America at levels 1, 2, and 3 (Environmental Protection Agency 2013)... 12
Figure 3. *Myotis lucifugus* (MYLU) mean occupancy probabilities (color bar) predicted in each North American Bat Monitoring Program (NABat) grid cell in the modeled species range for 2019… 18
Figure 4. *Myotis lucifugus* (MYLU) mean predicted occupancy probabilities in 2010, 2012, 2016, and 2019 predicted for all North American Bat Monitoring Program (NABat) grid cells in the modeled species range based on site-level covariates for each grid cell and year... 19
Figure 5. The total change rate in mean grid cell occupancies (color bar) for *Myotis lucifugus* (MYLU) between 2010 and 2019 for all North American Bat Monitroing Program (NABat) grid cells in the modeled species range based on site-level covariates for each grid cell and year.....20
Figure 6. Estimates of the average occupancy probability (ψt) of *Myotis lucifugus* (MYLU) each year, aggregated across all NABat grid cells in the modeled range each year... 21
Figure 7. Estimates of average annual change (avg_annual_change = lambda_avg – 1) and total change (total_change = lambda_tot - 1) of *Myotis lucifugus* (MYLU) over the short-term (2016–2019, three years of change), medium-term (2012–2019, seven years of change) and long-term (2010–2019, nine years of change).....22
Figure 8. *Myotis septentrionalis* (MYSE) mean occupancy probabilities (color bar) predicted in each North American Bat Monitoring Program (NABat) grid cell in the modeled species range for 2019.....23
Figure 9. Mean predicted occupancy probabilities of *Myotis septentrionalis* (MYSE) in 2010, 2012, 2016, and 2019 predicted for all North American Bat Monitoring Program (NABat) grid cells in the modeled species range based on site-level covariates for each grid cell and year.....24
Figure 10. The total change rate in mean grid cell occupancies (color bar) for *Myotis septentrionalis* (MYSE) between 2010 and 2019 for all North American Bat Monitoring Program (NABat) grid cells in the modeled species range based on site-level covariates for each grid cell and year... 25
Figure 11. Estimates of the average occupancy probability (ψt) for *Myotis septentrionalis* (MYSE) each year, aggregated across all North American Bat Monitoring Program (NABat) grid cells in modeled range each year… 26
Figure 12. Estimates of average annual change (avg_annual_change = lambda_avg – 1) and total change (total_change = lambda_tot - 1) for *Myotis septentrionalis* (MYSE) over the short-term (2016–2019, three years of change), medium-term (2012–2019, seven years of change) and long-term (2010–2019, nine years of change). 27
Figure 13. *Perimyotis subflavus* (PESU) mean occupancy probabilities (color bar) predicted in each North American Bat Monitoring Program (NABat) grid cell in the modeled species range for 2019…. 29
Figure 14. Mean predicted occupancy probabilities of *Perimyotis subflavus* (PESU) in 2010, 2012, 2016, and 2019 predicted for all North American Bat Monitoring Program (NABat) grid cells in the modeled species range based on site-level covariates for each grid cell and year… 30
Figure 15. The total change rate in mean grid cell occupancies (color bar) of *Perimyotis subflavus* (PESU) between 2010 and 2019 for all North American Bat Monitoring Program (NABat) grid cells in the modeled species range based on site-level covariates for each grid cell and year… 31
Figure 16. Estimates of the average occupancy probability (ψt) each year of *Perimyotis subflavus* (PESU), aggregated across all North American Bat Monitoring Program (NABat) grid cells in modeled range each year... 32
Figure 17. Estimates of average annual change (avg_annual_change = lambda_avg – 1) and total change (total_change = lambda_tot - 1) of *Perimyotis subflavus* (PESU), over the short-term (2016–2019, three years of change), medium-term (2012–2019, seven years of change) and long-term (2010–2019, nine years of change)....33
Figure 18. *Myotis evotis* (MYEV) mean occupancy probabilities (color bar) predicted in each North American Bat Monitoring Program (NABat) grid cell in the modeled species range for 2019.....35

FIGURE 19. MEAN PREDICTED OCCUPANCY PROBABILITIES OF *MYOTIS EVOTIS* (MYEV) IN 2016–2019 PREDICTED FOR ALL NORTH AMERICAN BAT MONITORING PROGRAM (NABAT) GRID CELLS IN THE MODELED SPECIES RANGE BASED ON SITE-LEVEL COVARIATES FOR EACH GRID CELL AND YEAR... 36
FIGURE 20. THE TOTAL CHANGE RATE IN MEAN GRID CELL OCCUPANCIES (COLOR BAR) FOR *MYOTIS EVOTIS* (MYEV) BETWEEN 2016 AND 2019 FOR ALL NORTH AMERICAN BAT MONITORING PROGRAM (NABAT) GRID CELLS IN THE MODELED SPECIES RANGE BASED ON SITE-LEVEL COVARIATES FOR EACH GRID CELL AND YEAR... 37
FIGURE 21. ESTIMATES OF THE AVERAGE OCCUPANCY PROBABILITY (ψt) EACH YEAR FOR *MYOTIS EVOTIS* (MYEV), AGGREGATED ACROSS ALL NORTH AMERICAN BAT MONITORING PROGRAM (NABAT) GRID CELLS IN MODELED RANGE EACH YEAR... 38
FIGURE 22. ESTIMATES OF AVERAGE ANNUAL CHANGE (AVG_ANNUAL_CHANGE = LAMBDA_AVG – 1) AND TOTAL CHANGE (TOTAL_CHANGE = LAMBDA_TOT - 1) FOR *MYOTIS EVOTIS* (MYEV) OVER THE SHORT-TERM (2016–2019, THREE YEARS OF CHANGE)... 39
FIGURE 23. A MAP OF *MYOTIS GRISESCENS* (MYGR) MEAN OCCUPANCY PROBABILITIES (COLOR BAR) PREDICTED IN EACH NORTH AMERICAN BAT MONITORING PROGRAM (NABAT) GRID CELL IN THE MODELED SPECIES RANGE FOR 2019... 40
FIGURE 24. MEAN PREDICTED OCCUPANCY PROBABILITIES FOR *MYOTIS GRISESCENS* (MYGR) IN 2016–2019 PREDICTED FOR ALL NORTH AMERICAN BAT MONITORING PROGRAM (NABAT) GRID CELLS IN THE MODELED SPECIES RANGE BASED ON SITE-LEVEL COVARIATES FOR EACH GRID CELL AND YEAR... 41
FIGURE 25. THE TOTAL CHANGE RATE IN MEAN GRID CELL OCCUPANCIES (COLOR BAR) FOR *MYOTIS GRISESCENS* (MYGR) BETWEEN 2016 AND 2019 FOR ALL NORTH AMERICAN BAT MONITORING PROGRAM (NABAT) GRID CELLS IN THE MODELED SPECIES RANGE BASED ON SITE-LEVEL COVARIATES FOR EACH GRID CELL AND YEAR.... 42
FIGURE 26. ESTIMATES OF THE AVERAGE OCCUPANCY PROBABILITY (ψt) FOR *MYOTIS GRISESCENS* (MYGR) EACH YEAR, AGGREGATED ACROSS ALL NORTH AMERICAN BAT MONITORING PROGRAM (NABAT) GRID CELLS IN MODELED RANGE EACH YEAR... 43
FIGURE 27. ESTIMATES OF AVERAGE ANNUAL CHANGE (AVG_ANNUAL_CHANGE = LAMBDA_AVG – 1) AND TOTAL CHANGE (TOTAL_CHANGE = LAMBDA_TOT - 1) FOR *MYOTIS GRISESCENS* (MYGR) OVER THE SHORT-TERM (2016–2019, THREE YEARS OF CHANGE)... 44
FIGURE 28. A MAP OF *MYOTIS LEIBII* (MYLE) MEAN OCCUPANCY PROBABILITIES (COLOR BAR) PREDICTED IN EACH NORTH AMERICAN BAT MONITORING PROGRAM (NABAT) GRID CELL IN THE MODELED SPECIES RANGE FOR 2019.... 45
FIGURE 29. MEAN PREDICTED OCCUPANCY PROBABILITIES FOR *MYOTIS LEIBII* (MYLE) IN 2016–2019 PREDICTED FOR ALL NORTH AMERICAN BAT MONITORING PROGRAM (NABAT) GRID CELLS IN THE MODELED SPECIES RANGE BASED ON SITE-LEVEL COVARIATES FOR EACH GRID CELL AND YEAR... 46
FIGURE 30. THE TOTAL CHANGE RATE IN MEAN GRID CELL OCCUPANCIES (COLOR BAR) FOR *MYOTIS LEIBII* (MYLE) BETWEEN 2016 AND 2019 FOR ALL NORTH AMERICAN BAT MONITORING PROGRAM (NABAT) GRID CELLS IN THE MODELED SPECIES RANGE BASED ON SITE-LEVEL COVARIATES FOR EACH GRID CELL AND YEAR... 47
FIGURE 31. ESTIMATES OF THE AVERAGE OCCUPANCY PROBABILITY (ψt) FOR *MYOTIS LEIBII* (MYLE) EACH YEAR, AGGREGATED ACROSS ALL NORTH AMERICAN BAT MONITORING PROGRAM (NABAT) GRID CELLS IN MODELED RANGE EACH YEAR... 48
FIGURE 32. ESTIMATES OF AVERAGE ANNUAL CHANGE (AVG_ANNUAL_CHANGE = LAMBDA_AVG – 1) AND TOTAL CHANGE (TOTAL_CHANGE = LAMBDA_TOT - 1) FOR *MYOTIS LEIBII* (MYLE) OVER THE SHORT-TERM (2016–2019, THREE YEARS OF CHANGE)... 49
FIGURE 33. *MYOTIS THYSANODES* (MYTH) MEAN OCCUPANCY PROBABILITIES (COLOR BAR) PREDICTED IN EACH NORTH AMERICAN BAT MONITORING PROGRAM (NABAT) GRID CELL IN THE MODELED SPECIES RANGE FOR 2019.... 51
FIGURE 34. MEAN PREDICTED OCCUPANCY PROBABILITIES OF *MYOTIS THYSANODES* (MYTH) IN 2016–2019 PREDICTED FOR ALL NORTH AMERICAN BAT MONITORING PROGRAM (NABAT) GRID CELLS IN THE MODELED SPECIES RANGE BASED ON SITE-LEVEL COVARIATES FOR EACH GRID CELL AND YEAR... 52
FIGURE 35. THE TOTAL CHANGE RATE IN MEAN GRID CELL OCCUPANCIES (COLOR BAR) OF *MYOTIS THYSANODES* (MYTH) BETWEEN 2016 AND 2019 FOR ALL NORTH AMERICAN BAT MONITORING PROGRAM (NABAT) GRID CELLS IN THE MODELED SPECIES RANGE BASED ON SITE-LEVEL COVARIATES FOR EACH GRID CELL AND YEAR.... 53
FIGURE 36. ESTIMATES OF THE AVERAGE OCCUPANCY PROBABILITY (ψt) OF *MYOTIS THYSANODES* (MYTH) EACH YEAR, AGGREGATED ACROSS ALL NORTH AMERICAN BAT MONITORING PROGRAM (NABAT) GRID CELLS IN MODELED RANGE EACH YEAR... 54

FIGURE 37. ESTIMATES OF AVERAGE ANNUAL CHANGE (AVG_ANNUAL_CHANGE = LAMBDA_AVG – 1) AND TOTAL CHANGE (TOTAL_CHANGE = LAMBDA_TOT - 1) FOR *MYOTIS THYSANODES* (MYTH) OVER THE SHORT-TERM (2016–2019, THREE YEARS OF CHANGE).. 55
FIGURE 38. A MAP OF *MYOTIS VOLANS* (MYVO) MEAN OCCUPANCY PROBABILITIES (COLOR BAR) PREDICTED IN EACH NORTH AMERICAN BAT MONITORING PROGRAM (NABAT) GRID CELL IN THE MODELED SPECIES RANGE FOR 2019... 57
FIGURE 39. MEAN PREDICTED OCCUPANCY PROBABILITIES OF *MYOTIS VOLANS* (MYVO) IN 2016–2019 PREDICTED FOR ALL NORTH AMERICAN BAT MONITORING PROGRAM (NABAT) GRID CELLS IN THE MODELED SPECIES RANGE BASED ON SITE-LEVEL COVARIATES FOR EACH GRID CELL AND YEAR.. 58
FIGURE 40. THE TOTAL CHANGE RATE IN MEAN GRID CELL OCCUPANCIES (COLOR BAR) FOR *MYOTIS VOLANS* (MYVO) BETWEEN 2016 AND 2019 FOR ALL NORTH AMERICAN BAT MONITORING PROGRAM (NABAT) GRID CELLS IN THE MODELED SPECIES RANGE BASED ON SITE-LEVEL COVARIATES FOR EACH GRID CELL AND YEAR... 59
FIGURE 41. ESTIMATES OF THE AVERAGE OCCUPANCY PROBABILITY (ψt) OF *MYOTIS VOLANS* (MYVO) EACH YEAR, AGGREGATED ACROSS ALL NORTH AMERICAN BAT MONITORING PROGRAM (NABAT) GRID CELLS IN MODELED RANGE EACH YEAR... 60
FIGURE 42. ESTIMATES OF AVERAGE ANNUAL CHANGE (AVG_ANNUAL_CHANGE = LAMBDA_AVG – 1) AND TOTAL CHANGE (TOTAL_CHANGE = LAMBDA_TOT - 1) FOR *MYOTIS VOLANS* (MYVO) OVER THE SHORT-TERM (2016–2019, THREE YEARS OF CHANGE).. 61
FIGURE 43. *MYOTIS YUMANENSIS* (MYYU) MEAN OCCUPANCY PROBABILITIES (COLOR BAR) PREDICTED IN EACH NORTH AMERICAN BAT MONITORING PROGRAM (NABAT) GRID CELL IN THE MODELED SPECIES RANGE FOR 2019.. 63
FIGURE 44. MEAN PREDICTED OCCUPANCY PROBABILITIES OF *MYOTIS YUMANENSIS* (MYYU) IN 2016–2019 PREDICTED FOR ALL NORTH AMERICAN BAT MONITORING PROGRAM (NABAT) GRID CELLS IN THE MODELED SPECIES RANGE BASED ON SITE-LEVEL COVARIATES FOR EACH GRID CELL AND YEAR... 64
FIGURE 45. THE TOTAL CHANGE RATE IN MEAN GRID CELL OCCUPANCIES (COLOR BAR) OF *MYOTIS YUMANENSIS* (MYYU) BETWEEN 2016 AND 2019 FOR ALL NORTH AMERICAN BAT MONITORING PROGRAM (NABAT) GRID CELLS IN THE MODELED SPECIES RANGE BASED ON SITE-LEVEL COVARIATES FOR EACH GRID CELL AND YEAR.. 65
FIGURE 46. ESTIMATES OF THE AVERAGE OCCUPANCY PROBABILITY (ψt) OF *MYOTIS YUMANENSIS* (MYYU) EACH YEAR, AGGREGATED ACROSS ALL NORTH AMERICAN BAT MONITORING PROGRAM (NABAT) GRID CELLS IN MODELED RANGE EACH YEAR... 66
FIGURE 47. ESTIMATES OF AVERAGE ANNUAL CHANGE (AVG_ANNUAL_CHANGE = LAMBDA_AVG – 1) AND TOTAL CHANGE (TOTAL_CHANGE = LAMBDA_TOT - 1) OF *MYOTIS YUMANENSIS* (MYYU) OVER THE SHORT-TERM (2016–2019, THREE YEARS OF CHANGE). MEANS (POINTS) AND 95% CREDIBLE INTERVALS (BARS) ARE DEPICTED ACCORDING TO THE PERCENT OF GRID CELLS SAMPLED IN THE MODELED SPECIES RANGE EACH YEAR (LEGEND).. 67
FIGURE 48. A MAP OF *EPTESICUS FUSCUS* (EPFU) MEAN OCCUPANCY PROBABILITIES (COLOR BAR) PREDICTED IN EACH NORTH AMERICAN BAT MONITORING PROGRAM (NABAT) GRID CELL IN THE MODELED SPECIES RANGE FOR 2019... 70
FIGURE 49. MEAN PREDICTED OCCUPANCY PROBABILITIES FOR *EPTESICUS FUSCUS* (EPFU) IN 2016–2019 PREDICTED FOR ALL NABAT GRID CELLS IN THE MODELED SPECIES RANGE BASED ON SITE-LEVEL COVARIATES FOR EACH GRID CELL AND YEAR... 70
FIGURE 50. THE TOTAL CHANGE RATE IN MEAN GRID CELL OCCUPANCIES (COLOR BAR) FOR *EPTESICUS FUSCUS* (EPFU) BETWEEN 2016 AND 2019 FOR ALL NABAT GRID CELLS IN THE MODELED SPECIES RANGE BASED ON SITE-LEVEL COVARIATES FOR EACH GRID CELL AND YEAR.. 71
FIGURE 51. ESTIMATES OF THE AVERAGE OCCUPANCY PROBABILITY (ψt) EACH YEAR FOR *EPTESICUS FUSCUS* (EPFU), AGGREGATED ACROSS ALL NABAT GRID CELLS IN MODELED RANGE EACH YEAR... 72
FIGURE 52. ESTIMATES OF AVERAGE ANNUAL CHANGE (AVG_ANNUAL_CHANGE = LAMBDA_AVG – 1) AND TOTAL CHANGE (TOTAL_CHANGE = LAMBDA_TOT - 1) FOR *EPTESICUS FUSCUS* (EPFU) OVER THE SHORT-TERM (2016–2019, THREE YEARS OF CHANGE).. 73
FIGURE 53. A MAP OF *LASIONYCTERIS NOCTIVAGANS* (LANO) MEAN OCCUPANCY PROBABILITIES (COLOR BAR) PREDICTED IN EACH NABAT GRID CELL IN THE MODELED SPECIES RANGE FOR 2019... 75
FIGURE 54. MEAN PREDICTED OCCUPANCY PROBABILITIES FOR *LASIONYCTERIS NOCTIVAGANS* (LANO) IN 2016–2019 PREDICTED FOR ALL NABAT GRID CELLS IN THE MODELED SPECIES RANGE BASED ON SITE-LEVEL COVARIATES FOR EACH GRID CELL AND YEAR... 75
FIGURE 55. THE TOTAL CHANGE RATE IN MEAN GRID CELL OCCUPANCIES (COLOR BAR) FOR *LASIONYCTERIS NOCTIVAGANS* (LANO) BETWEEN 2016 AND 2019 FOR ALL NABAT GRID CELLS IN THE MODELED SPECIES RANGE BASED ON SITE-LEVEL COVARIATES FOR EACH GRID CELL AND YEAR... 76

FIGURE 56. ESTIMATES OF THE AVERAGE OCCUPANCY PROBABILITY (ψt) FOR *LASIONYCTERIS NOCTIVAGANS* (LANO) EACH YEAR, AGGREGATED ACROSS ALL NABAT GRID CELLS IN MODELED RANGE EACH YEAR... 77
FIGURE 57. ESTIMATES OF AVERAGE ANNUAL CHANGE (AVG_ANNUAL_CHANGE = LAMBDA_AVG – 1) AND TOTAL CHANGE (TOTAL_CHANGE = LAMBDA_TOT - 1) FOR *LASIONYCTERIS NOCTIVAGANS* (LANO) OVER THE SHORT-TERM (2016–2019, THREE YEARS OF CHANGE)... 78
FIGURE 58. A MAP OF *LASIURUS CINEREUS* (LACI) MEAN OCCUPANCY PROBABILITIES (COLOR BAR) PREDICTED IN EACH NABAT GRID CELL IN THE MODELED SPECIES RANGE FOR 2019... 80
FIGURE 59. MEAN PREDICTED OCCUPANCY PROBABILITIES DOE *LASIURUS CINEREUS* (LACI) IN 2016–2019 PREDICTED FOR ALL NABAT GRID CELLS IN THE MODELED SPECIES RANGE BASED ON SITE-LEVEL COVARIATES FOR EACH GRID CELL AND YEAR... 80
FIGURE 60. THE TOTAL CHANGE RATE IN MEAN GRID CELL OCCUPANCIES (COLOR BAR) *LASIURUS CINEREUS* (LACI) BETWEEN 2016 AND 2019 FOR ALL NABAT GRID CELLS IN THE MODELED SPECIES RANGE BASED ON SITE-LEVEL COVARIATES FOR EACH GRID CELL AND YEAR.....81
FIGURE 61. ESTIMATES OF THE AVERAGE OCCUPANCY PROBABILITY (ψt) FOR *LASIURUS CINEREUS* (LACI) EACH YEAR, AGGREGATED ACROSS ALL NABAT GRID CELLS IN MODELED RANGE EACH YEAR... 82
FIGURE 62. ESTIMATES OF AVERAGE ANNUAL CHANGE (AVG_ANNUAL_CHANGE = LAMBDA_AVG – 1) AND TOTAL CHANGE (TOTAL_CHANGE = LAMBDA_TOT - 1) FOR *LASIURUS CINEREUS* (LACI) OVER THE SHORT-TERM (2016–2019, THREE YEARS OF CHANGE)... 83
FIGURE B.1. ESTIMATES OF THE AVERAGE OCCUPANCY PROBABILITY (ψt) FOR *MYOTIS LUCIFUGUS* (MYLU) AGGREGATED OVER ALL GRID CELLS FOR EACH STATE, TERRITORY OR PROVINCE IN THE MODELED SPECIES RANGE EACH YEAR... 115
FIGURE B.2. AVERAGE ANNUAL RATES OF CHANGE IN MEAN OCCUPANCY PROBABILITIES (AVG_ANNUAL_CHANGE = LAMBDA_AVG - 1) FOR *MYOTIS LUCIFUGUS* (MYLU) BETWEEN YEARS OVER THE DESIGNATED TIME PERIOD (THREE YEARS: 2016-2019, SEVEN YEARS: 2012-2019, OR NINE YEARS: 2010-2019) AGGREGATED ACROSS A STATE, PROVINCE, OR TERRITORY WITHIN THE MODELED SPECIES RANGE... 118
FIGURE B.3. THE TOTAL CHANGE RATE IN MEAN OCCUPANCY (TOTAL_CHANGE = LAMBDA_TOT - 1) FOR *MYOTIS LUCIFUGUS* (MYLU) GIVEN THE MEAN OCCUPANCY ESTIMATE IN LAST YEAR OF SAMPLING (2019) AND THE MEAN OCCUPANCY ESTIMATES THREE YEARS (2016), SEVEN YEARS (2012), AND NINE YEARS (2010) PRIOR AGGREGATED ACROSS A STATE, PROVINCE, OR TERRITORY WITHIN THE MODELED SPECIES RANGE.....121
FIGURE B.4. ESTIMATES OF THE AVERAGE OCCUPANCY PROBABILITY (ΨT) FOR *MYOTIS SEPTENTRIONALIS* (MYSE) AGGREGATED OVER ALL GRID CELLS FOR EACH STATE, TERRITORY OR PROVINCE IN THE MODELED SPECIES RANGE EACH YEAR... 124
FIGURE B.5. AVERAGE ANNUAL RATES OF CHANGE IN MEAN OCCUPANCY PROBABILITIES (AVG_ANNUAL_CHANGE = LAMBDA_AVG - 1) FOR *MYOTIS SEPTENTRIONALIS* (MYSE) BETWEEN YEARS OVER THE DESIGNATED TIME PERIOD (THREE YEARS: 2016-2019, SEVEN YEARS: 2012-2019, OR NINE YEARS: 2010-2019) AGGREGATED ACROSS A STATE, PROVINCE, OR TERRITORY WITHIN THE MODELED SPECIES RANGE... 127
FIGURE B.6. THE TOTAL CHANGE RATE IN MEAN OCCUPANCY (TOTAL_CHANGE = LAMBDA_TOT - 1) FOR *MYOTIS SEPTENTRIONALIS* (MYSE) GIVEN THE MEAN OCCUPANCY ESTIMATE IN LAST YEAR OF SAMPLING (2019) AND THE MEAN OCCUPANCY ESTIMATES THREE YEARS (2016), SEVEN YEARS (2012), AND NINE YEARS (2010) PRIOR AGGREGATED ACROSS A STATE, PROVINCE, OR TERRITORY WITHIN THE MODELED SPECIES RANGE... 130
FIGURE B.7. ESTIMATES OF THE AVERAGE OCCUPANCY PROBABILITY (ψt) FOR *PERIMYOTIS SUBFLAVUS* (PESU) AGGREGATED OVER ALL GRID CELLS IN THE MODELED SPECIES RANGE FOR EACH STATE, TERRITORY OR PROVINCE AND YEAR. MEANS (POINTS) AND 95% CREDIBLE INTERVALS (BARS) ARE DEPICTED ACCORDING TO THE PERCENT OF GRID CELLS SAMPLED (LEGEND) IN THE ENTIRE STATE, PROVINCE OR TERRITORY EACH YEAR (A-D)... 132
FIGURE B.8. AVERAGE ANNUAL RATES OF CHANGE IN MEAN OCCUPANCY PROBABILITIES (AVG_ANNUAL_CHANGE = LAMBDA_AVG - 1) FOR *PERIMYOTIS SUBFLAVUS* (PESU) BETWEEN YEARS OVER THE DESIGNATED TIME PERIOD (THREE YEARS: 2016-2019, SEVEN YEARS: 2012-2019, OR NINE YEARS: 2010-2019) AGGREGATED ACROSS A STATE, PROVINCE, OR TERRITORY WITHIN THE MODELED SPECIES RANGE... 135
FIGURE B.9. THE TOTAL CHANGE RATE IN MEAN OCCUPANCY (TOTAL_CHANGE = LAMBDA_TOT - 1) FOR *PERIMYOTIS SUBFLAVUS* (PESU) GIVEN THE MEAN OCCUPANCY ESTIMATE IN LAST YEAR OF SAMPLING (2019) AND THE MEAN OCCUPANCY ESTIMATES THREE YEARS (2016), SEVEN YEARS (2012), AND NINE (2010) PRIOR AGGREGATED ACROSS A STATE, PROVINCE, OR TERRITORY WITHIN THE

modeled species range. For example, if total_change_9yr = -0.25, the mean occupancy rate has declined by 25% over the nine years since 2010, while a value of 0.25 would indicate an increase of 25%... 138
Figure B.10. Estimates of the average occupancy probability (Ψ) for *Myotis evotis* (MYEV) aggregated over all grid cells for each state, territory or province in the modeled species range each year....139
Figure B.11. Average annual rates of change in mean occupancy probabilities (avg_annual_change = lambda_avg - 1) for *Myotis evotis* (MYEV) between years over the three-year (2016-2019) time period aggregated across a state, province, or territory within the modeled species range. For example, if avg_change_3yr = -0.05, the mean occupancy rate has declined on average by 5% each year over the three years since 2016....141
Figure B.12. The total change rate in mean occupancy (*total_change* = lambda_tot - 1) for *Myotis evotis* (MYEV) given the mean occupancy estimate in last year of sampling (2019) and the mean occupancy estimates three years (2016) prior aggregated across a state, province, or territory within the modeled species range....143
Figure B.13. Estimates of the average occupancy probability (ψt) for *Myotis grisescens* (MYGR) aggregated over all grid cells for each state in the modeled species range each year... 144
Figure B.14. Average annual rates of change in mean occupancy probabilities (avg_annual_change = lambda_avg - 1) for *Myotis grisescens* (MYGR) between years over the three-year (2016-2019) time period aggregated across a state within the modeled species range... 145
Figure B.15. The total change rate in mean occupancy (total_change = lambda_tot - 1) for *Myotis grisescens* (MYGR) given the mean occupancy estimate in last year of sampling (2019) and the mean occupancy estimates three years (2016) prior aggregated across a state within the modeled species range... 148
Figure B.16. Estimates of the average occupancy probability (ψt) for *Myotis leibii* (MYLE) aggregated over all grid cells for each state in the modeled species range each year.. 150
Figure B.17. Average annual rates of change in mean occupancy probabilities (avg_annual_change = lambda_avg - 1) for *Myotis leibii* (MYLE) between years over the three-year (2016-2019) time period aggregated across a state within the modeled species range... 152
Figure B.18. The total change rate in mean occupancy (total_change = lambda_tot - 1) for *Myotis leibii* (MYLE) given the mean occupancy estimate in last year of sampling (2019) and the mean occupancy estimates three years (2016) prior aggregated across a state within the modeled species range... 154
Figure B.19. Estimates of the average occupancy probability (psi_bar) for *Myotis thysanodes* (MYTH) aggregated over all grid cells for each state, territory or province in the modeled species range each year... 155
Figure B.20. Average annual rates of change in mean occupancy probabilities (avg_annual_change = lambda_avg - 1) for *Myotis thysanodes* (MYTH) between years over the three-year time (2016-2019) period aggregated across a state, province, or territory within the modeled species range....157
Figure B.21. The total change rate in mean occupancy (total_change = lambda_tot - 1) for *Myotis thysanodes* (MYTH) given the mean occupancy estimate in last year of sampling (2019) and the mean occupancy estimates three years (2016) prior aggregated across a state, province, or territory within the modeled species range... 159
Figure B.22. Estimates of the average occupancy probability (Ψ) for *Myotis volans* (MYVO) aggregated over all grid cells for each state, territory or province in the modeled species range each year. Means (points) and 95% credible intervals (bars) are depicted according to the percent of grid cells sampled (legend) in the entire state, province or territory each year (A and B)... 160
Figure B.23. Average annual rates of change in mean occupancy probabilities (avg_annual_change = lambda_avg - 1) for *Myotis volans* (MYVO) between years over the three-year (2016-2019) time period aggregated across a state, province, or territory within the modeled species range... 162
Figure B.24. The total change rate in mean occupancy (total_change = lambda_tot - 1) for *Myotis volans* (MYVO) given the mean occupancy estimate in last year of sampling (2019) and the mean occupancy estimates three years (2016) prior aggregated across a state, province, or territory within the modeled species range....164
Figure B.25. Estimates of the average occupancy probability (Ψ) for *Myotis yumanensis* (MYYU) aggregated over all grid cells for each state, territory or province in the modeled species range each year. Means (points) and 95% credible intervals (bars) are depicted according to the percent of grid cells sampled (legend) in the entire state, province or territory each year (A and B)... 165

FIGURE B.26. AVERAGE ANNUAL RATES OF CHANGE IN MEAN OCCUPANCY PROBABILITIES (AVG_ANNUAL_CHANGE = LAMBDA_AVG - 1) FOR *MYOTIS YUMANENSIS* (MYYU) BETWEEN YEARS OVER THE THREE-YEAR (2016-2019) TIME PERIOD AGGREGATED ACROSS A STATE, PROVINCE, OR TERRITORY WITHIN THE MODELED SPECIES RANGE.....167
FIGURE B.27. THE TOTAL CHANGE RATE IN MEAN OCCUPANCY (TOTAL_CHANGE = LAMBDA_TOT - 1) FOR *MYOTIS YUMANENSIS* (MYYU) GIVEN THE MEAN OCCUPANCY ESTIMATE IN LAST YEAR OF SAMPLING (2019) AND THE MEAN OCCUPANCY ESTIMATES THREE YEARS (2016) PRIOR AGGREGATED ACROSS A STATE, PROVINCE, OR TERRITORY WITHIN THE MODELED SPECIES RANGE... 169
FIGURE B.28. ESTIMATES OF THE AVERAGE OCCUPANCY PROBABILITY (ΨT) FOR *EPTESICUS FUSCUS* (EPFU) AVERAGE OCCUPANCY PROBABILITY AGGREGATED OVER ALL GRID CELLS FOR EACH STATE IN THE MODELED SPECIES RANGE EACH YEAR.....171
FIGURE B.29. AVERAGE ANNUAL RATES OF CHANGE IN MEAN OCCUPANCY PROBABILITIES (AVG_ANNUAL_CHANGE = LAMBDA_AVG - 1) FOR *EPTESICUS FUSCUS* (EPFU) BETWEEN YEARS OVER THE THREE-YEAR (2016-2019) TIME PERIOD AGGREGATED ACROSS A STATE, PROVINCE, OR TERRITORY WITHIN THE MODELED SPECIES RANGE... 174
FIGURE B.30. THE TOTAL CHANGE RATE IN MEAN OCCUPANCY (TOTAL_CHANGE = LAMBDA_TOT - 1) FOR *EPTESICUS FUSCUS* (EPFU) GIVEN THE MEAN OCCUPANCY ESTIMATE IN LAST YEAR OF SAMPLING (2019) AND THE MEAN OCCUPANCY ESTIMATES THREE YEARS (2016) PRIOR AGGREGATED ACROSS EACH STATE WITHIN THE MODELED SPECIES RANGE.....177
FIGURE B.31. ESTIMATES OF THE AVERAGE OCCUPANCY PROBABILITY (ΨT) FOR *LASIONYCTERIS NOCTIVAGANS* (LANO) AGGREGATED OVER ALL GRID CELLS FOR EACH STATE IN THE MODELED SPECIES RANGE EACH YEAR.....179
FIGURE B.32. AVERAGE ANNUAL RATES OF CHANGE IN MEAN OCCUPANCY PROBABILITIES (AVG_ANNUAL_CHANGE = LAMBDA_AVG - 1) FOR *LASIONYCTERIS NOCTIVAGANS* (LANO) BETWEEN YEARS OVER THE THREE-YEAR (2016-2019) TIME PERIOD AGGREGATED ACROSS A STATE WITHIN THE MODELED SPECIES RANGE.....182
FIGURE B.33. THE TOTAL CHANGE RATE IN MEAN OCCUPANCY (TOTAL_CHANGE = LAMBDA_TOT - 1) FOR *LASIONYCTERIS NOCTIVAGANS* (LANO) GIVEN THE MEAN OCCUPANCY ESTIMATE IN LAST YEAR OF SAMPLING (2019) AND THE MEAN OCCUPANCY ESTIMATES THREE YEARS (2016) PRIOR AGGREGATED ACROSS A STATE WITHIN THE MODELED SPECIES RANGE... 185
FIGURE B.34. ESTIMATES OF THE AVERAGE OCCUPANCY PROBABILITY (ΨT) FOR *LASIURUS CINEREUS* (LACI) AGGREGATED OVER ALL GRID CELLS FOR EACH STATE IN THE MODELED SPECIES RANGE EACH YEAR... 187
FIGURE B.35. AVERAGE ANNUAL RATES OF CHANGE IN MEAN OCCUPANCY PROBABILITIES (AVG_ANNUAL_CHANGE = LAMBDA_AVG - 1) FOR *LASIURUS CINEREUS* (LACI) BETWEEN YEARS OVER THE THREE-YEAR (2016-2019) TIME PERIOD AGGREGATED ACROSS A STATE WITHIN THE MODELED SPECIES RANGE.....190
FIGURE B.36. THE TOTAL CHANGE RATE IN MEAN OCCUPANCY (*TOTAL_CHANGE* = LAMBDA_TOT - 1) FOR *LASIURUS CINEREUS* (LACI) GIVEN THE MEAN OCCUPANCY ESTIMATE IN LAST YEAR OF SAMPLING (2019) AND THE MEAN OCCUPANCY ESTIMATES THREE YEARS (2016) PRIOR AGGREGATED ACROSS A STATE WITHIN THE MODELED SPECIES RANGE... 193
FIGURE C.1. ESTIMATES OF COVARIATE EFFECTS ON GRID CELL OCCUPANCY FOR *MYOTIS LUCIFUGUS* (MYLU), EXCLUDING INTERCEPT ESTIMATES WHICH VARIED BY ECOREGIONS AND YEAR.....195
FIGURE C.2. ESTIMATES OF OBSERVATION COVARIATES ON THE DETECTION RATE FOR *MYOTIS LUCIFUGUS* (MYLU). 196
FIGURE C.3. ESTIMATES OF OCCUPANCY AND DETECTION COVARIATES FOR *MYOTIS SEPTENTRIONALIS* (MYSE). 197
FIGURE C.4. ESTIMATES OF OCCUPANCY AND DETECTION COVARIATES *MYOTIS SEPTENTRIONALIS* (MYSE). 198
FIGURE C.5. ESTIMATES OF OCCUPANCY AND DETECTION COVARIATES FOR *PERIMYOTIS SUBFLAVUS* (PESU).....199
FIGURE C.6. ESTIMATES OF OCCUPANCY AND DETECTION COVARIATES FOR *PERIMYOTIS SUBFLAVUS* (PESU).....200
FIGURE C.7. ESTIMATES OF OCCUPANCY AND DETECTION COVARIATES FOR *MYOTIS EVOTIS* (MYEV).....201
FIGURE C.8. ESTIMATES OF OCCUPANCY AND DETECTION COVARIATES FOR *MYOTIS EVOTIS* (MYEV).....202
FIGURE C.9. ESTIMATES OF OCCUPANCY AND DETECTION COVARIATES FOR *MYOTIS GRISESCENS* (MYGR).....203
FIGURE C.10. ESTIMATES OF OCCUPANCY AND DETECTION COVARIATES FOR *MYOTIS GRISESCENS* (MYGR).....204
FIGURE C.11. ESTIMATES OF OCCUPANCY AND DETECTION COVARIATES FOR *MYOTIS LEIBII* (MYLE).....205
FIGURE C.12. ESTIMATES OF OCCUPANCY AND DETECTION COVARIATES FOR *MYOTIS LEIBII* (MYLE).....206
FIGURE C.13. ESTIMATES OF OCCUPANCY AND DETECTION COVARIATES FOR *MYOTIS THYSANODES* (MYTH). 207
FIGURE C.14. ESTIMATES OF OCCUPANCY AND DETECTION COVARIATES FOR *MYOTIS THYSANODES* (MYTH). 208
FIGURE C.15. ESTIMATES OF OCCUPANCY AND DETECTION COVARIATES FOR *MYOTIS VOLANS* (MYVO).....209
FIGURE C.16. ESTIMATES OF OCCUPANCY AND DETECTION COVARIATES *MYOTIS VOLANS* (MYVO).....210
FIGURE C.17. ESTIMATES OF OCCUPANCY AND DETECTION COVARIATES FOR *MYOTIS YUMANENSIS* (MYYU). 211
FIGURE C.18. ESTIMATES OF OCCUPANCY AND DETECTION COVARIATES *MYOTIS YUMANENSIS* (MYYU). 212

FIGURE C.19. ESTIMATES OF OCCUPANCY AND DETECTION COVARIATES FOR *EPTESICUS FUSCUS* (EPFU). 213
FIGURE C.20. ESTIMATES OF OCCUPANCY AND DETECTION COVARIATES FOR *EPTESICUS FUSCUS* (EPFU). 214
FIGURE C.21. ESTIMATES OF OCCUPANCY AND DETECTION COVARIATES FOR *LASIONYCTERIS NOCTIVAGANS* (LANO). 215
FIGURE C.22. ESTIMATES OF OCCUPANCY AND DETECTION COVARIATES *LASIONYCTERIS NOCTIVAGANS* (LANO). 216
FIGURE C.23. ESTIMATES OF OCCUPANCY AND DETECTION COVARIATES FOR *LASIURUS CINEREUS* (LACI). 217
FIGURE C.24. ESTIMATES OF OCCUPANCY AND DETECTION COVARIATES FOR *LASIURUS CINEREUS* (LACI). 218
FIGURE D.1. VIOLIN PLOTS DEPICT PREDICTED OCCUPANCY PROBABILITIES FOR *MYOTIS LUCIFUGUS* (MYLU) COMPARED TO THE HIGHEST LEVEL OF SPECIES DETECTION OBSERVED FOR EACH GRID CELL AND YEAR... 220
FIGURE D.2. VIOLIN PLOTS DEPICT PREDICTED OCCUPANCY PROBABILITIES FOR *MYOTIS SEPTENTRIONALIS* (MYSE) COMPARED TO THE HIGHEST LEVEL OF SPECIES DETECTION OBSERVED FOR EACH GRID CELL AND YEAR... 221
FIGURE D.3. VIOLIN PLOTS DEPICT PREDICTED OCCUPANCY PROBABILITIES FOR *PERIMYOTIS SUBFLAVUS* (PESU) COMPARED TO THE HIGHEST LEVEL OF SPECIES DETECTION OBSERVED FOR EACH GRID CELL AND YEAR... 222
FIGURE D.4. VIOLIN PLOTS DEPICT PREDICTED OCCUPANCY PROBABILITIES FOR *MYOTIS EVOTIS* (MYEV) COMPARED TO THE HIGHEST LEVEL OF SPECIES DETECTION OBSERVED FOR EACH GRID CELL AND YEAR... 223
FIGURE D.5. VIOLIN PLOTS DEPICT PREDICTED OCCUPANCY PROBABILITIES FOR *MYOTIS GRISESCENS* (MYGR) COMPARED TO THE HIGHEST LEVEL OF SPECIES DETECTION OBSERVED FOR EACH GRID CELL AND YEAR... 224
FIGURE D.6. VIOLIN PLOTS DEPICT PREDICTED OCCUPANCY PROBABILITIES FOR *MYOTIS LEIBII* (MYLE) COMPARED TO THE HIGHEST LEVEL OF SPECIES DETECTION OBSERVED FOR EACH GRID CELL AND YEAR... 225
FIGURE D.7. VIOLIN PLOTS DEPICT PREDICTED OCCUPANCY PROBABILITIES FOR *MYOTIS THYSANODES* (MYTH) COMPARED TO THE HIGHEST LEVEL OF SPECIES DETECTION OBSERVED FOR EACH GRID CELL AND YEAR... 226
FIGURE D.8. VIOLIN PLOTS DEPICT PREDICTED OCCUPANCY PROBABILITIES FOR *MYOTIS VOLANS* (MYVO) COMPARED TO THE HIGHEST LEVEL OF SPECIES DETECTION OBSERVED FOR EACH GRID CELL AND YEAR... 227
FIGURE D.9. VIOLIN PLOTS DEPICT PREDICTED OCCUPANCY PROBABILITIES FOR *MYOTIS YUMANENSIS* (MYYU) COMPARED TO THE HIGHEST LEVEL OF SPECIES DETECTION OBSERVED FOR EACH GRID CELL AND YEAR... 228
FIGURE D.10. VIOLIN PLOTS DEPICT PREDICTED OCCUPANCY PROBABILITIES FOR *EPTESICUS FUSCUS* (EPFU) COMPARED TO THE HIGHEST LEVEL OF SPECIES DETECTION OBSERVED FOR EACH GRID CELL AND YEAR... 229
FIGURE D.11. VIOLIN PLOTS DEPICT PREDICTED OCCUPANCY PROBABILITIES FOR *LASIONYCTERIS NOCTIVAGANS* (LANO) COMPARED TO THE HIGHEST LEVEL OF SPECIES DETECTION OBSERVED FOR EACH GRID CELL AND YEAR... 230
FIGURE D.12. VIOLIN PLOTS DEPICT PREDICTED OCCUPANCY PROBABILITIES FOR *LASIURUS CINEREUS* (LACI) COMPARED TO THE HIGHEST LEVEL OF SPECIES DETECTION OBSERVED FOR EACH GRID CELL AND YEAR... 231

1. Introduction and Purpose

The primary objective of the North American Bat Monitoring Program (NABat) is to provide reliable status and trend information for the 46 species of bats occurring in the United States, including species shared by Mexico and Canada. NABat status and trend information is intended to inform conservation decision making, leading to the long-term viability of bat populations across the continent (Loeb et al. 2015). Multiple lines of evidence are often necessary to provide insight into population status and trends because North American bats have varied and complex life histories (Loeb et al. 2015) and face multiple stressors. Several species of North American bats have experienced significant declines due to white-nose syndrome (WNS) (Cheng et al. 2021a), and others may be at future risk to WNS impacts and/or other population stressors, such as land use change, climate change, and collisions with wind energy turbines (Sherwin et al. 2013; O'Shea et al. 2016; Frick et al. 2020; Friedenberg and Frick 2021). The objectives of the status and trends analyses presented here were to evaluate and synthesize multiple streams of NABat monitoring data to estimate annual summer population distributions (occupancy probabilities) of bats across their North American ranges and infer how their distributions have changed over time (trends). This report documents the scope, methods, and results of the NABat Summer Occupancy Analyses, including objectives, data types, data sources, data contributors, species-specific results, current limitations, and future directions.

Species occupancy (i.e., presence or space-use by at least one individual versus absence) in space and time is a key ecological state variable used to understand the distribution of a species. Sampling methods for bats are imperfect, and biases from both false-negatives (i.e., species was present but not detected) and false-positives (e.g., an acoustic recording was misclassified) are important considerations (Loeb et al. 2018). Using an occupancy modeling framework permits estimation of and accounting for observation errors of both types (e.g., MacKenzie et al. 2002, MacKenzie et al. 2006, Royle and Link 2006, Chambert et al. 2015) while estimating occupancy probabilities and relationships with ecological predictors. Occupancy probability is the probability that a species occurs (i.e., is present or uses space) within a location (e.g., NABat 10 km x 10 km grid cell, Loeb et al. 2015) over a specified timeframe. Occupancy models can be used to predict species occupancy probabilities beyond locations where data were collected, by leveraging the modeled relationships between spatiotemporal predictors and species occupancy probabilities. This in turn allows for producing species-specific maps of predicted species occupancy probabilities across a variety of spatial extents (e.g., all parts of the species' range with adequate monitoring data). The use of a spatially balanced sampling design (e.g., NABat master sample, Talbert and Reichert 2018) helps to ensure a representative sample and minimize potential biases of out of sample predictions. Quantifying changes between occupancy probabilities at different periods of time can be used to infer temporal trends (i.e., rates of change) in occupancy probabilities along with estimates of uncertainty.

Species occupancy of a NABat grid cell is directly related to its population abundance within a grid cell (and in grid cells within bat dispersal distances), the spatial unit of interest (100 km^2) (He and Gaston 2000, Steenweg et al. 2018), the spatial clustering of bat activity centers (i.e., summer roosts), bat movement behavior, and habitat use (Efford and Dawson 2012). Trends in occupancy probabilities over time are generally expected to correlate with changes in species abundance (i.e., higher expected abundances correspond with higher expected occupancy probabilities given constant movement behavior, Holt et al. 2002). We expect trends in bat occupancy probability over time to be less sensitive than changes in abundance since they are 1) dependent on processes besides abundance, 2) based on binary detection/non-detection data, and 3) in some cases difficult to disentangle from the changes in detection probabilities linked to changes in abundance (Royle and Nichols 2003). However, measures of occupancy such as occupancy probability can provide an important quantifiable indicator for understanding the range-wide status and trend of a wildlife population and their use of space over time (Joseph et al. 2006, Noon et al. 2012).

We analyzed summer (May 1 – August 31) occupancy distributions of bats using multiple streams of monitoring data (response data including stationary acoustic, mobile acoustic, and capture records) in false positive occupancy models (Appendix A). Specifically, we estimated occupancy probabilities for 2010 through 2019 and changes in this metric over time for three species (*Myotis lucifugus,* MYLU; *Myotis septentrionalis,* MYSE; and *Perimyotis subflavus,* PESU). For an additional nine species, we estimated occupancy probabilities for 2016 through 2019 (*Myotis evotis,* MYEV; *Myotis grisescens,* MYGR; *Myotis leibii,* MYLE; *Myotis thysanodes,* MYTH; *Myotis volans,* MYVO; *Myotis yumanensis,* MYYU; *Eptesicus fuscus*, EPFU; *Lasionycteris noctivagans,* LANO; and *Lasiurus cinereus,* LACI). Of these 12 bat species, 11 have tested positive for *Pseudogymnoascus destructans* (Pd) (Table 1), the fungal pathogen that causes white-nose syndrome (WNS)—a disease that has led to significant rates of mortality for subterranean hibernating bat species in North America (Cheng et al. 2021a, Hoyt et al. 2021). A twelfth species was also selected because of high rates of mortality at wind energy facilities. Additional species were considered but not selected due to data limitations.

For each species, we 1) fit false-positive occupancy models to monitoring data and estimated ecological covariate effects in space and time on the occupancy probability of 100 km^2 areas (i.e., NABat grid cells), 2) predicted species' occupancy probabilities across all NABat grid cells in the 'modeled ranges' (i.e., the spatial extent for each species' range for which there were adequate monitoring data) for every year of interest, 3) derived regional predictions of the mean occupancy probability each year across all grid cells in each region of interest and at multiple scales (state/province/territory, range-wide), 4) derived annual trends (rates of change) and cumulative trends in average occupancy probabilities over time for each species and region of interest, and 5) calculated the percent of grid cells sampled in each region and year of interest to assess the degree of representation of each regional trend. These results are included in this report and the associated USGS data release (Udell et al., 2022).

2. Methods - Datasets

We used data in the NABat database for summer occupancy analyses. Here we describe the types of data used, and statistical considerations. For detailed statistical methods, refer to Appendix A.

2.1 Response data

Our statistical analyses used two main types of summer monitoring response data: acoustic call-sequences (i.e., bat echolocation sequences, sometimes referred to as a bat pass, captured as ultrasonic recordings) and capture records. Acoustic sampling was conducted using two different survey methods, stationary surveys and mobile transect surveys. The call-sequences from each acoustic sampling method were classified via two different approaches: automated identification software (i.e., auto ID), and manually vetted by a human observer (manual IDs). Altogether, this resulted in 5 different response types (stationary acoustic-auto IDs, stationary acoustic-manual IDs, mobile transect acoustic-auto IDs, mobile transect acoustic-manual IDs, and capture records). We compiled response data from records submitted to the NABat Partner Portal[1] by a variety of data contributors and partners including state, federal, and tribal agencies, non-governmental organizations, academic researchers, and private individuals.

2.1.1 Stationary acoustic sampling

When data were collected following NABat protocols, 2–4 stationary acoustic detectors were deployed within an NABat grid cell (10 km x 10 km) (Chapter 4, Loeb et al. 2015), with grid cells selected for sampling according to the priority sampling order of the NABat master sample (Talbert and Reichert 2018). In such cases, detectors were deployed for 1–4 nights, with detectors recording from dusk through dawn. However, all data collected between 2010–2015 pre-dates NABat survey protocols as documented in Loeb et al. (2015), and some data submitted to NABat after 2015 did not follow NABat survey protocols or the master sample. For example, many projects contributed data spanning several weeks throughout the summer monitoring period and did not follow NABat probabilistic sampling order. While the variable effort between NABat protocol data and non-NABat protocol data are monitored and accounted for in statistical models, non-NABat protocol data present possible issues due to unknown data collection protocols. Examples include violations of independence between detectors (see Appendix A: A.2.1 and A.2.2), unrepresentative sampling, and unbalanced spatiotemporal sampling (i.e., the set of grid cells sampled each year changes in space and time), which can bias inferences about status and trends.

2.1.1.1 Automatically identified call-sequences from stationary sampling (stationary auto IDs)

Data contributors assigned automated species identifications to recorded call-sequences using various commercially available software types, software versions, and filters. We accepted data from all types and refer to such automatically classified call-sequences as auto IDs. The response for auto IDs in the occupancy analyses is the number of call-sequences classified to the species of interest via automated classification software, which is further summarized as species presence/absence (0/1). At the recording-night level, a '0' could indicate the bat was

[1] https://sciencebase.usgs.gov/nabat/#/results

not present or the bat was present but not detected. A bat being present but not detectable or identifiable is a false negative, and these are known considerations for bat surveys (Loeb et al. 2015). These can occur when 1) a bat was present but not echolocating, or 2) was echolocating but was too far from the microphone to be recorded by the detector, or 3) the echolocation call-sequence could not be identified to species or is misclassified. Issues with identification can occur when the recording quality is poor, when echolocation pulse parameters overlap among species, when call sequences are non-diagnostic, or when there are multiple species in a recording such that the auto identification software cannot reach consensus for one species assignment. False-positives due to misclassification error are also common, thus a positive identification can occur either from correctly detecting and identifying a call-sequence to species (true positive) or from an incorrect species classification (false-positive).

2.1.1.2 Manually vetted acoustic call-sequences from stationary sampling

Manual vetting refers to the process of a human reviewing a call-sequence recording and assigning or confirming a species identification after an automatic classification has been assigned. Data contributors conduct manual vetting or hand review in a variety of ways. Typically, only a subset of the highest quality automatically identified call-sequences are manually vetted, however, some NABat data contributors vet all auto IDs. Vetted acoustic data in the NABat database comes in two types: one that is unconditional on a positive species auto ID and one that is conditional on a positive species auto ID. Unconditional vetting includes all records for which there is a manual ID (e.g., auto IDs that were originally classified as noise files or as a different species); it is the more inclusive data type, and it is the only data type that existed in the NABat database when the false positive occupancy modeling methods were originally developed (Stratton and Irvine 2022). For these reasons, we only included unconditional vetting data in these occupancy analyses. Since the vetting procedures of individual data contributors may vary and are mostly unknown, properly inferring ‘0’ data is problematic for unconditional vetting data. Thus, we conservatively assume unconditional manual vetting represents presence-only data. This is because a value of ‘0’ could be: 1) the result of confirming no call-sequences were from the species of interest, 2) a result of overturning an auto ID recorded as the species of interest (false positive for the auto ID, zero for manual ID), or 3) because no effort was put towards vetting a given recording (i.e., what should be a n/a value). Consequently, these data also represent detection-only information. These data can be considered an unambiguous detection method, and we make this assumption in our analyses.

Conditionally vetted data provide information about numbers of auto IDs reviewed and confirmed for each sampling night. Conditionally vetted data are now available in the NABat database and our future analyses will capitalize on these. However, they require statistical extensions (e.g., Chambert et al. 2015, Doser et al. 2021) to the current ‘site-confirmation’ analytical methods used in these analyses.

2.1.2 Mobile transect acoustic sampling methods

When data were collected following NABat protocols, a mobile transect (25–48 km in length) was driven within an NABat cell (10 x 10 km) at a minimum speed of 32 km/hr (Chapter 5, Loeb et al. 2015). Transects were designed such that routes refrain from doubling back, and, when a

constant speed is maintained throughout, the assumption can be made that each recorded call-sequence corresponds to a single individual. Transects were driven for multiple nights, commencing 45 minutes after sunset. Ultrasonic acoustic detectors were mounted on top of vehicles to record bat calls. All data collected between 2010–2014 pre-date NABat survey protocols as documented in Loeb et al. (2015), and some data submitted to NABat after 2014 did not follow NABat survey protocols or the master sample.

2.1.2.1 Automatically identified call-sequences from mobile sampling (mobile auto IDs)

Auto IDs for the mobile transect data stream were classified similarly to auto IDs from the stationary data stream. The response for mobile auto IDs in summertime analyses is the number of call-sequences automatically classified each night to the species of interest, which is further aggregated into species presence/absence (0/1) for the occupancy analysis. This data stream is similarly subject to false negatives and false positives.

2.1.2.2 Manually vetted acoustic call-sequences from mobile sampling

Manually vetted acoustic records for mobile sampling were classified the same as for stationary (i.e., unconditional vetting), and the same statistical considerations (presence-only data, unambiguous detections) are relevant. Thus, the only difference from the stationary vetted records is the physical mode (stationary or mobile transect) of acoustic sampling used to record call-sequences. Conditional vetting data for mobile transects are now available in the NABat database but were not included in these analyses.

2.1.3 Capture records

Capture records came from field biologists who captured bats in mist nets, harp traps or other devices. The observation unit for capture data was the individual bat. We aggregated capture records by species by night and grid cell for compatibility. Note that these data represent presence-only data because no information is available for capture attempts where no bats were captured. Furthermore, we assume that capture records are an unambiguous detection method with no incorrect species classification, which can aid in the estimation of false positive occupancy models. In reality, there are some species misidentifications in capture data, but for the purposes of these analyses, we assume these error rates are negligible when bats are ’in-hand.’

2.1.4 Summary of response types

We have taken an integrated approach to our occupancy analyses by incorporating multiple data types. Here we summarize those data types (Table 2).

Table 2. Summary of data available for the Summer Occupancy Analysis. Source refers to the five data types described, 'Temporal resolution' refers to the finest time period resolution used for each data type, 'Spatial resolution' is the finest spatial resolution used for each data type, 'Type' denotes whether the data type was considered detection/non-detection information or presence-only information, and 'False-positive status' refers to whether the data are considered ambiguous (subject to false positives) or unambiguous (no false positives) for use in the occupancy analyses. NABat = North American Bat Monitoring Program.

Source	Temporal resolution	Spatial resolution	Type	False-positive status
Auto ID stationary	Night	NABat grid cell	Detection/ non-detection	ambiguous
Manual ID stationary (unconditional)	Night	NABat grid cell	Presence only	unambiguous
Auto ID Mobile	Night	NABat grid cell	Detection/ non-detection	ambiguous
Manual ID mobile	Night	NABat grid cell	Presence only	unambiguous
Capture	Night	NABat grid cell	Presence only	unambiguous

2.1.5 Data sources and contributors

The stationary and mobile acoustic data sets were contributed by NABat partners (see Acknowledgements) and sourced from the NABat Monitoring Database via a data request process (https://www.nabatmonitoring.org/get-data). Data were pulled from the NABat Database on October 18, 2021:

North American Bat Monitoring Program (NABat) Database v7.0.2 (Provisional Release): U.S. Geological Survey. Accessed 2021-10-18. NABat Request Number 35. https://doi.org/10.5066/P9UXA6CF

North American Bat Monitoring Program (NABat) Database v7.0.2 (Provisional Release): U.S. Geological Survey. Accessed 2021-10-18. NABat Request Number 34. https://doi.org/10.5066/P9UXA6CF

North American Bat Monitoring Program (NABat) Database v7.0.14 (Provisional Release): U.S. Geological Survey. Accessed 2021-10-18. NABat Request Number 73. https://doi.org/10.5066/P9UXA6CF

2.2 Covariates

We incorporated into our statistical analyses a suite of ecological predictor variables (covariates) including those that influence where bats occur in space and time and those that influence bat detectability in space and time. We used grid cell-level (occupancy) and observation-level (detection) covariates. In order to be incorporated into these analyses, spatial predictors for a species occupancy probability needed to be available at the NABat grid cell level across all grid cells in a species range, while spatiotemporal covariates also needed to be available at an annual temporal resolution. Detection-level covariates needed to be available at the nightly resolution for sampled NABat grid cells. We also incorporated a winter-to-summer population connectivity metric which allowed for linking the potential influence of known winter populations (and regional declines due to WNS impacts) with a species' summer occupancy distribution space and time.

2.2.1 Site-level covariates

2.2.1.1. In the NABat database

We used site-level (i.e., a 100 km^2 NABat grid cell) covariates available in the NABat database to inform site-level occupancy when analyzing acoustic data sets (Table 3).

Table 3. Name and source of the site-level covariates in the North American Bat Monitoring Program (NABat) database.

Name	Source
Annual mean precipitation Annual mean temperature	Fick, S.E. and R.J. Hijmans, 2017. Worldclim 2: New 1-km spatial resolution climate surfaces for global land areas. International Journal of Climatology. http://www.worldclim.com/version2
Percent forest cover Percent water Percent wetland	2010 North American Land Cover at 250 m spatial resolution. Produced by Natural Resources Canada/Canada Centre for Remote Sensing (NRCan/CCRS), United States Geological Survey (USGS); Insituto Nacional de Estadística y Geografía (INEGI), Comisión Nacional para el Conocimiento y Uso de la Biodiversidad (CONABIO) and Comisión Nacional Forestal (CONAFOR). http://www.cec.org/north-american-environmental-atlas/land-cover-2010-modis-250m/

2.2.1.2 Sourced from Google Earth Engine

Additional covariates were extracted from Google Earth Engine and summarized at the NABat grid cell level (Table 4).

Table 4. Name and source of site-level covariates obtained from Google Earth Engine.

Name	Source
Max elevation	U.S. Geological Survey. 1999. GTOPO30. https://doi.org/10.5066/F7DF6PQS
Physiographic diversity	Theobald, D.M., Harrison-Atlas, D., Monahan, W.B. and Albano, C.M., 2015. Ecologically-relevant maps of landforms and physiographic diversity for climate adaptation planning. PloS one, 10(12), p.e0143619.

We aggregated mean elevation across each NABat grid cell (10 km x 10 km) by taking the maximum across all pixels (at a 30 arc second resolution) within each grid cell. Next, we aggregated physiographic diversity across each NABat grid cell by taking the mean across pixels at a 30 m resolution (Theobald 2015). Physiographic diversity (Theobald et al. 2015) is a variable the combines information on elevation (mean and standard deviation at multiple spatial scales), slope, aspect, multi-scale topographical position index, latitude, continuous heat load index, and parent material to classify landforms (e.g., valleys, ridges, cliffs) and physiographic classes, then summarizes the diversity of physiographic classes at a 30 m resolution. This variable is a measure of landscape complexity (i.e., ruggedness), including geographic and physiographic characteristics. Meaningful correlations between physiographic diversity and vertebrate diversity across the USA suggest that this metric captures key ecosystem features that structure biodiversity (Theobald et al. 2015), and previous work has also suggested that landscape complexity and areas of topographic relief are important predictors of bats distributions (Armstrong et al. 1994, Patten 2004).

2.2.2 Seasonal connectivity metrics (integrating winter count data)

We calculated a winter-to-summer seasonal population connectivity metric for *Myotis lucifugus* (MYLU), *Myotis septentrionalis* (MYSE), and *Perimyotis subflavus* (PESU) to link the potential spatiotemporal influence of abundance in the known winter range to occupancy in the summer range. Winter counts for these species have declined drastically since the arrival of white-nose syndrome (WNS), with regional differences depending on the timing of WNS arrival (Cheng et al. 2021a). We used a seasonal connectivity approach to examine whether there is a measurable spatiotemporal influence of known winter populations (and observed declines due to WNS) on the summer distribution of bats. We also included seasonal connectivity metrics in species' occupancy models to leverage the spatiotemporal information in the winter population monitoring data to help predict species' occupancy probabilities in space and time across summer distributions. For example, suitable habitat that was historically occupied at high rates may no longer be occupied due to severe regional WNS impacts.

The winter-to-summer seasonal population connectivity metric quantifies the hypothesis that spatial proximity of known winter hibernacula to summer grid cells (scaled by seasonal migration distance of the species) and the abundances of each known winter hibernacula (i.e., counts of hibernating bats at winter roost sites) over time are related to occupancy probability of a grid cell during each summer. We hypothesized that bat abundances declining over time in winter hibernacula due to mortality from WNS would reduce occupancy probabilities of summer habitat, with the largest declines in occupancy occurring in grid cells in close proximity to the largest declines in winter population counts. We define a 'potential connectivity' metric based on metapopulation theory (Hanski and Ovaskainen 2000, Moilanen and Hanski 2001), where the seasonal connectivity of a grid cell in the summer range is dependent on three factors: 1) the spatial distribution of all known winter hibernacula in the species range and the species abundance at each, 2) the distances between each hibernaculum and the summer grid cell of interest, and 3) the seasonal migration movement behavior of the bats (See Appendix A, Section A.3.2 for more details)

Because this is a spatiotemporal covariate, it provides an additional source of information to estimate occupancy probabilities and trends over space and time, which could be especially useful in years and/or regions of interest with sparse summer monitoring data. In regions of interest without winter monitoring data and known hibernacula locations, this metric may not appropriately reflect the true winter-to-summer connectivity because extremely low values represent no data rather that lack of winter populations. In these cases, the effects of this variable were set to zero so that occupancy probabilities and trends over time were not influenced by lack of data.

Seasonal connectivity metrics are species-specific and use hibernacula locations (at the resolution of the NABat grid cell centroid), annual abundances, and mean migration distances for each species. Locations were joined to the NABat grid cell, and these centroid coordinates were used as the locations for each hibernaculum when calculating distances. We used the modeled hibernacula counts and locations for MYLU, MYSE, and PESU from the Cheng et al. (2021b) analysis of colony counts, which utilized colony count data contained in the NABat database. The seasonal connectivity metric was calculated for MYLU, MYSE, and PESU for years 2010–2019, and maps from 2010 can be viewed for each species range (Fig. 2). To estimate the average migration distance of each species, we relied mostly on documented migration records in the literature. Some historic records from the U.S. Bat Banding Database were also used when calculating migration distance for MYLU (Table 5).

Table 5. Species mean seasonal migration distance, and sample size of records from the literature and/or the U.S. Historic Bat Banding Database.

Species	Mean	Number of studies or individual movements
MYLU	119.69 km	219 individuals
MYSE	62 km	2 studies
PESU	227 km	3 studies

Some populations have experienced large declines in estimated winter colony counts due to WNS (Cheng et al. 2021a, Cheng et al 2021b). As such, seasonal connectivity also declines steeply over the same time, which represents a decline in the expected number of winter-to-summer migrants in summer grid cells (Figure 1).

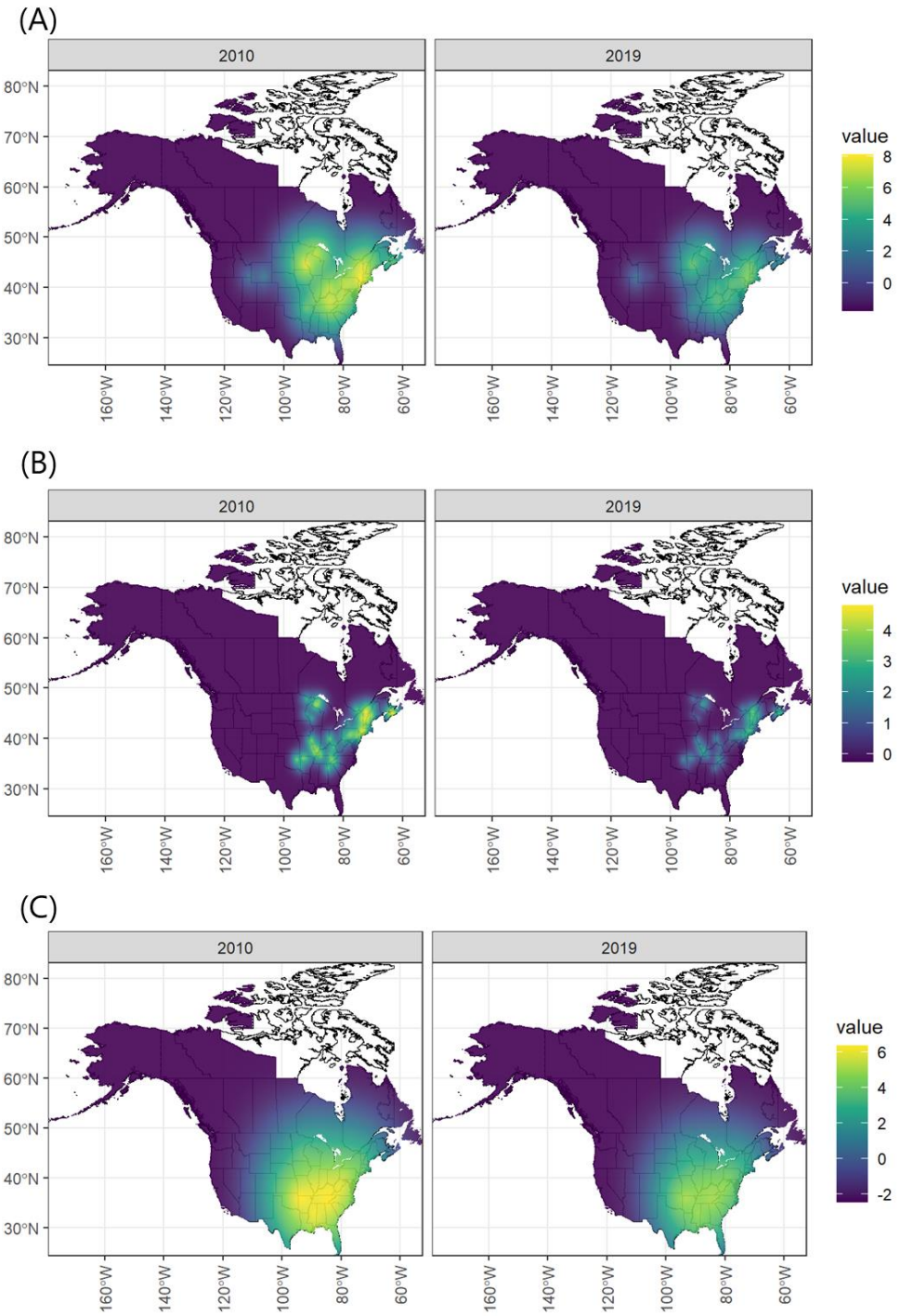

Figure 1. Winter-to-summer population connectivity values have declined for (A) *Myotis lucifufus* (MYLU), (B) *Myotis septentrionalis* (MYSE), and (C) *Perimyotis subflavus* (PESU) (color bar shows connectivity values after transformation [log +1 then centering] for visualization) for years 2010 and 2019 based on the modeled species counts at winter hibernacula each year and the species specific, winter-to-summer, mean migration distance. The decline in this metric seen between 2010-2019 reflects a decline in winter counts due to WNS, and a corresponding decline in potential seasonal connectivity (i.e., relative number of predicted seasonal migrants).

2.2.3 Other derived grid cell-level covariates sourced from spatial data sets

Several habitat features may affect bat occurrence; however, however only a few were available in the NABat database. We thus geo-processed and incorporated several additional ecological predictors of bat occupancy probability for each grid cell for use in the occupancy analysis (Table 6).

Table 6. Additional spatial covariates geo-processed and joined to each grid cell in the continental North American Bat Monitoring Program (NABat) sampling grid using either ArcMap or the spatial features (sf) package in R.

Name	Description	Source
Ecoregions of North America (Levels 1, 2 and 3)	Hierarchal ecoregion names and numbers. For example, where numbers are encoded as level1.level2.level3. Grid cells classified as "water" were reassigned to the nearest ecoregion.	U.S. Environmental Protection Agency, 2013, Level III ecoregions of the continental United States: Corvallis, Oregon, U.S. EPA–National Health and Environmental Effects Research Laboratory, map scale 1:7,500,000, https://www.epa.gov/eco-research/level-iii-and-iv-ecoregions-continental-united-states. Omernik, J.M. and G.E. Griffith. 2014. Ecoregions of the conterminous United States: evolution of a hierarchical spatial framework. Environmental Management 54(6):1249–1266.
Karst indicator	All grid cells that intersected the karst polygons were assigned a value of 1, else 0.	Chen, Z., Auler, A.S., Bakalowicz, M. et al. The World Karst Aquifer Mapping project: concept, mapping procedure and map of Europe. Hydrogeol J 25, 771–785 (2017). https://doi.org/10.1007/s10040-016-1519-3
Mines	The distance from the centroid of each grid cell to the nearest mine polygon.	Maus, Victor; Giljum, Stefan; Gutschlhofer, Jakob; da Silva, Dieison M; Probst, Michael; Gass, Sidnei L B; Luckeneder, Sebastian; Lieber, Mirko; McCallum, Ian (2020): Global-scale mining polygons (Version 1). PANGAEA, https://doi.org/10.1594/PANGAEA.910894
Rivers and Shorelines indicator	All grid cells that intersected rivers or shorelines were assigned a value of 1, else 0.	Commission for Environmental Cooperation. 2006. North American Rivers and Lakes. https://www.sciencebase.gov/catalog/item/4fb55df0e4b04cb937751e02

Ecological regions (i.e., Ecoregions) of North America provide natural and hierarchical classifications of spatial regions based on meaningful ecological characteristics, the underlying ecological communities, and geographic space. Thus, in comparison to arbitrary geopolitical boundaries such as states, provinces, or territories, they provide an ecologically grounded approach to including regional spatiotemporal structure into the occupancy model. Ecoregions may capture regional variation in bat occupancy distributions above and beyond the range-wide influences of other ecological predictors (e.g., elevation, temperature). The hierarchical nature of these ecoregions (level-3 within level-2 within level-1) helps describe regional influences on occupancy at several spatial scales given the underlying ecological communities in each (which may be important for explaining bat occupancy, bat detection, and misclassification rates). Thus, ecoregions provide useful hierarchical structure to account for spatial autocorrelation at several spatial scales (i.e., all other unmeasured influences in bat occupancy that vary spatially). Finally, ecoregions provide useful spatial units to structure changes in occupancy probabilities over time, especially compared to the null model of modeling temporal change as constant across a species range.

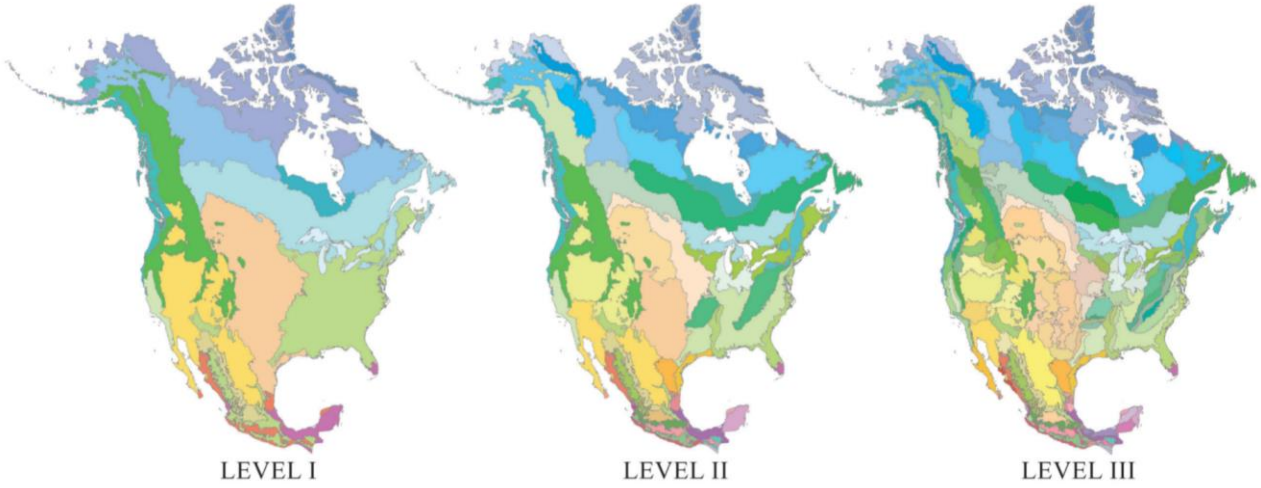

Figure 2. Ecological regions of North America at levels 1, 2, and 3 (Environmental Protection Agency 2013). Names of ecoregions and shapefiles are available at https://www.epa.gov/eco-research/ecoregions.

2.2.4 Detection-level covariates

The detectability of a bat species in a grid cell on a given night is dependent on many factors, most notably factors that affect bat activity and the amount of time over which monitoring occurs (Table 7). For example, monitoring on longer and/or warmer nights is generally more likely to result in more recorded call-sequences than on shorter and/or cooler nights.

Table 7. Summary of night-level covariates aggregated across seven-day periods and included in the false-positive occupancy model for each bat species**.** Effort index = length of detection history aggregated over for each seven-day observation period (e.g., aggregating over 4 nights in 7-day period at a single stationary detector would result in an effort of 4). Effort index was derived from monitoring data while all other night-level covariates came from Daymet.

Name	Source
Day length	Thornton, M.M., R. Shrestha, Y. Wei, P.E. Thornton, S. Kao, and B.E. Wilson. 2020. Daymet: Annual Climate Summaries on a 1-km Grid for North America, Version 4. ORNL DAAC, Oak Ridge, Tennessee, USA. https://doi.org/10.3334/ORNLDAAC/1852
Day of year	
Maximum air temperature	
Minimum air temperature	
Water vapor pressure	
Effort index	Derived from monitoring data

2.3 Range maps

Numerous sources for species range maps exist and maps vary in range extent and boundaries (Table 8). Many species range maps have not been updated in the last 10 years despite evidence that some species' ranges are expanding due to climate change (McCracken et al. 2018). In this analysis, we bound the total geographic extent of occupancy predictions (hereafter 'modeled species range') for each species by the geographic scope of monitoring data rather than the published species range (hereafter 'reference range'). This approach ensured that predictions were not extrapolated beyond the bounds of the data. In some cases, model predictions may extend beyond the reference range, or may only cover a portion of the reference range based on the extent of monitoring data. Discrepancies between the modeled species' range and reference range are shown in the figures in Section 3. Note, the polygon depicting the reference range is for illustrative purposes only and does not indicate a modeling parameter.

In most cases, the reference ranges reflected are from the National Atlas of the United States (2011); however, in two instances (MYGR and PESU) we instead have used recently updated and refined range maps provided by the U.S. Fish and Wildlife Service's species leads. These maps were developed using a combination of known roosts, historical capture records, and expert elicitation. In the case of MYGR only, the modeled species range was clipped to the reference range provided by the U.S. Fish and Wildlife Service to bound predictions within the recently established boundaries.

Table 8. Sources of species range maps for bats that occur in North America.

Source	URL
National Atlas of the United States	https://purl.stanford.edu/pz329xp4277
U.S. Fish and Wildlife Service Environmental Conservation Online System	https://ecos.fws.gov/ecp/report/current-range-all
International Union for Conservation on Nature	https://www.iucnredlist.org/resources/spatial-data-download
NatureServe	https://www.natureserve.org/conservation-tools/digital-distribution-maps-mammals-western-hemisphere

Table 9. A summary table depicting the total number of monitoring data points (grid-cell*observation) of each detection history type (0: no-detection, 1: ambiguous detection, 2: unambiguous detection) for each bat species, including the number of points of each type that fell inside and outside of the reference ranges.

Species	Total 0's	Inside 0's	Outside 0's	Total 1's	Inside 1's	Outside 1's	Total 2's	Inside 2's	Outside 2's
MYLU	4731	4468	263	4255	3891	364	2985	2700	285
PESU	4067	3959	108	4717	4659	58	1474	1417	57
MYSE	7440	5992	1448	1323	935	388	928	845	83
MYYU	973	597	376	461	299	162	647	595	52
MYTH	1444	793	651	410	197	213	387	272	115
MYVO	902	642	260	994	846	148	654	619	35
MYEV	967	608	359	460	301	159	1059	942	117
MYLE	2818	1567	1251	333	256	77	175	139	36
MYGR	3546	352	3194	1047	478	569	154	134	20
EPFU	3691	3497	194	5743	5558	185	4267	4062	205
LANO	4707	4276	431	3617	3373	244	2555	2331	224
LACI	3417	3227	190	5788	5521	267	2812	2588	224

3. Results

3.1 Useful definitions for interpreting results

- **Occupancy state**: The presence/absence status of a species in a NABat 100 km^2 grid cell during a summer season. Bats are mobile animals, therefore occupancy is interpreted as space-use (i.e., whether or not a grid cell is used by a species, where use is any type of space use in a grid cell including flying through or accessing water sources).
- **Species distribution**: The geographical distribution of species' occurrence across its' range. For the purpose of these analyses, it is the true but unknown spatial configuration of species occupancy (i.e., space use) across grid cells each year.
- **Occupancy probability**: The probability (ranging between zero and one) that a species occupies/uses a grid cell in a summer season. We make predictions for the occupancy probability for each species and year across all grid cells in each modeled species range.
- **Range:** The geographic limits of a particular species' distribution.
- **Modeled species range**: The geographic extent of occupancy probability predictions that were modeled for each species, based on the geographic scope of the species detections in the monitoring data.
- **Posterior distribution (Posterior probability distribution)**: A probability distribution for a parameter estimate given information in the data, and the resulting inference from a Bayesian analysis. Point estimates (the posterior mean) and 95% credible intervals are used to summarize the posterior distribution of each parameter for inference.
- **Posterior mean**: The mean of the posterior distribution, which we use as the point estimate (best single point guess) for each parameter.
- **95% credible interval (95% CRI)**: The interval of credible values for a parameter for which there is a 95% probability that the true (unknown) value is contained within the interval. Also, a measure of uncertainty for each parameter estimate (larger the interval = more uncertain). We calculate an equal tailed 95% credible interval and define the lower and upper limits based on the 2.5% and 97.5% quantiles. Thus, all values for a parameter outside of this interval together have 5% probability of being true, with a 2.5% probability of being less than the lower limit, and a 2.5% probability of being greater than upper limit. These intervals also provide information on the 'significance' (or certainty) of direction of association (positive or negative) of an estimate. If the 95% credible intervals are entirely negative (i.e., intervals do not overlap zero or contain positive values), we can infer that parameter value is negative with at least 0.95 probability (95% certainty). The same logic holds for 95% credible intervals that are entirely positive, that is, there is at least a 95% certainty that the parameter is positive. When the 95% credible interval overlaps zero and spans both negative and positive values, there is less than a 95% certainty that the parameter is 'significantly' negative or positive.
- **Region**: The term 'region', or 'regional' in the results refers to various geographic or geopolitical areas of interest for which aggregate measures of status occupancy and trends were calculated including states, provinces, and territories, and the modeled species ranges.

- **Average occupancy probability (regional or range-wide):** The average occupancy probability across all grid cells in a region of interest (e.g., state/province/territory or species range). Also, the expected value for the proportion of occupied grid cells in the region.
- **Annual change:** The proportional rate of change in average occupancy probability between two subsequent years.
- **Average annual change:** The average annual proportional rate of change in the average occupancy probability over a time period of interest.
- **Total change:** The total proportional rate of change in the average occupancy probability between the first and last year of sampling.
- **Proportion of grid cells sampled**: The proportion of grid cells sampled for each region, species, and year. Higher values indicate a higher degree of representativeness of the sampling data for each regional estimate.

3.2 Organization of results

In this section, we depict several occupancy status and trend results for each species at the grid cell and range-wide spatial extents. Sections are organized by species.

- For each species, we first present range-wide occupancy probability maps across all grid cells in each species' modeled range including the most recent occupancy probability map in 2019, the same map with sampled locations and detection histories are shown, and a time series of maps of four years of occupancy probabilities and visit histories.
- For the time series maps, years 2010, 2012, 2016, and 2019 are displayed for MYLU, PESU, and MYSE, while years 2016–2019 are displayed for all other species
- We provide a map of change in grid cell-level occupancy probabilities for each species, with the total change between 2010–2019 for MYLU, PESU, and MYSE and from 2016–2019 for all other species.
- Next, we depict the time series of average occupancy probability each year aggregated across all grid cells in the modeled species' range, while also depicting the percent of grid cells in the modeled species' range that were surveyed each year. Means and 95% credible intervals are provided for each parameter.
- We also provide two trend metrics based on average occupancy probability per year, average annual change and total change between the starting and ending year.
    - We provide these trend estimates at three different temporal windows for MYLU, PESU, and MYSE (three years of change: 2016–2019; seven years of change: 2012–2019; and nine years of change: 2010–2019) and only for short time scales for all other species.
    - For example, if avg_change_9yr = -0.05, the average occupancy rate for a region of interest declined on average by 5% each year over the nine years since 2010. Likewise, if total_change_9yr = -0.25, the average occupancy rate for a region of interest declined by a total of 25% over the nine years since 2010, while a value of 0.25 would indicate an increase of 25%.
    - We infer the 'significance' of a trend estimate based on the 95% credible intervals. When 95% credible intervals are entirely positive (i.e., not overlapping

zero or containing any negative values), or entirely negative, then there is at least a 0.95 probability (95% certainty) that the predicted occupancy probabilities are truly increasing (for positive intervals) or decreasing (for negative intervals). Otherwise, we have less than 95% certainty that the estimate is truly different than zero.

- Similar regional estimates of the average occupancy probability aggregated across all grid cells in a region of interest are provided for each state/province/territory for each species and year (Appendix B).
- The proportion of grid cells sampled in each region of interest and year for each species is also depicted in the same figures to delineate the representativeness of each estimate.
- Both trend indicators (average annual change and total change) were also calculated for these time series, the same as for the range-wide trends (Appendix B).
- Results of parameter estimates from each species occupancy model, including grid cell-level occupancy predictor effects and detection effects, are presented in Appendix C.
- Finally, Appendix D contains plots that depict an informal model assessment for each species, comparing the predicted occupancy probabilities to the monitoring data.

3.3 *Myotis lucifugus*

(A)

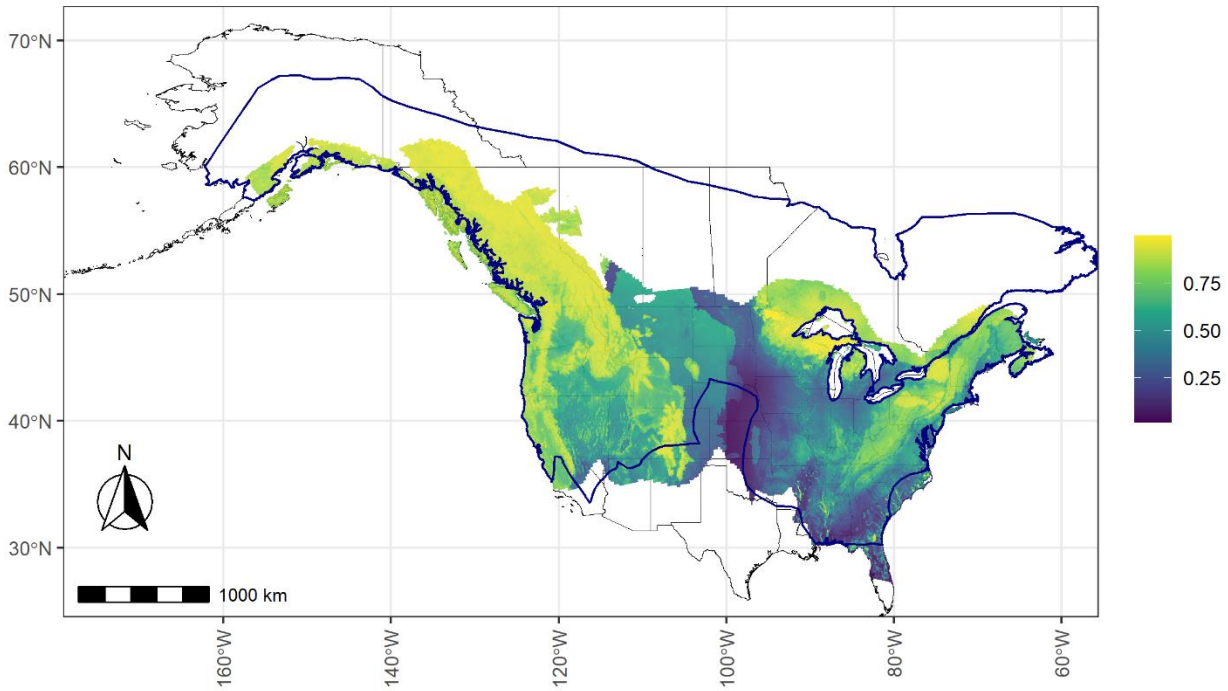

(B)

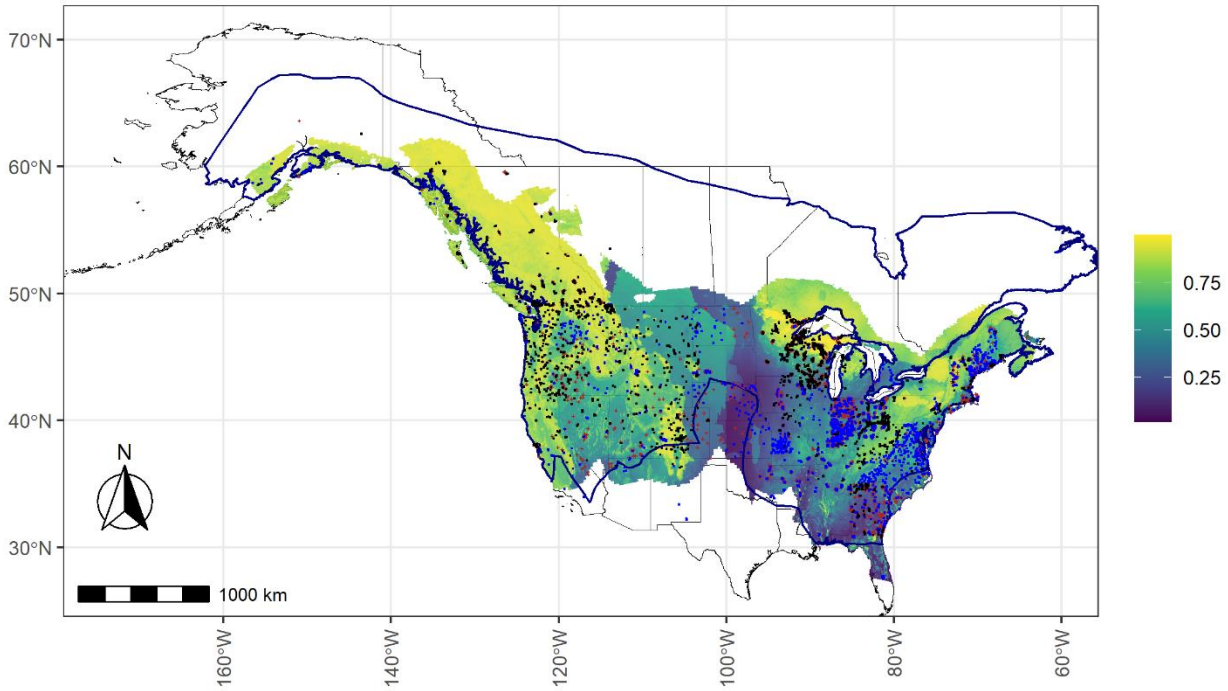

Figure 3. *Myotis lucifugus* (MYLU) mean occupancy probabilities (color bar) predicted in each North American Bat Monitoring Program (NABat) grid cell in the modeled species range for 2019. Probabilities are depicted against the reference range map (blue polygon; National Atlas of the United States, 2011)

and borders of U.S. states and Canadian provinces/territories (A and B). Note, the polygon depicting the reference range is for illustrative purposes only and was not used to bound occupancy probability predictions – instead, the analyses are bound by the geographic scope of monitoring data. All sampled locations (2010–2019) and detection summaries are also overlaid (B), including sampled locations where the species was never detected (brown '+' signs), locations where the species was detected at least once by acoustic auto IDs (blue dots), and locations where the species was detected either by manually verified acoustic records or capture data (black dots).

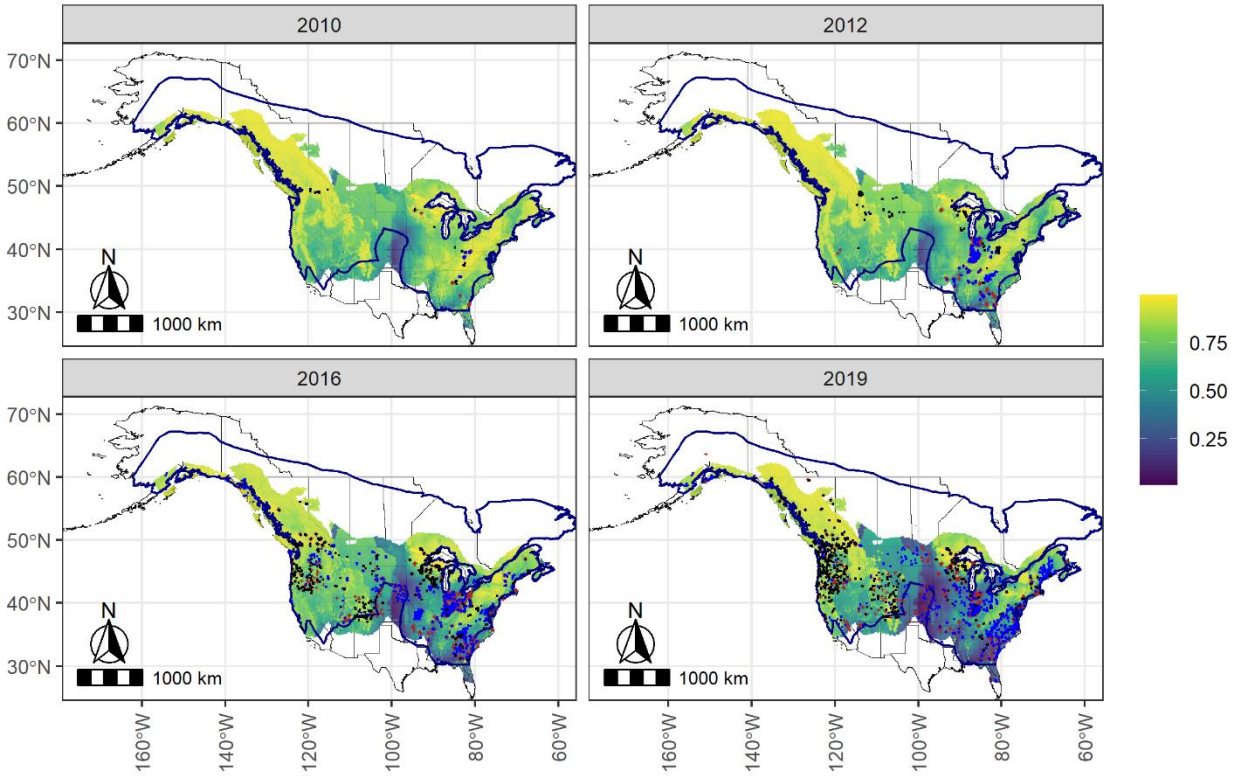

Figure 4. *Myotis lucifugus* (MYLU) mean predicted occupancy probabilities in 2010, 2012, 2016, and 2019 predicted for all North American Bat Monitoring Program (NABat) grid cells in the modeled species range based on site-level covariates for each grid cell and year. This is depicted against the reference range map (blue polygon; National Atlas of the United States, 2011) and borders of U.S. states and Canadian provinces/territories. Note, the polygon depicting the reference range is for illustrative purposes only and was not used to bound occupancy probability predictions – instead, the analyses are bound by the geographic scope of monitoring data. The grid cells sampled each year are also displayed based on detection histories as: brown '+' signs= never detected, blue dots = detected with an auto ID, black dots = detected with manual vetting and/or capture.

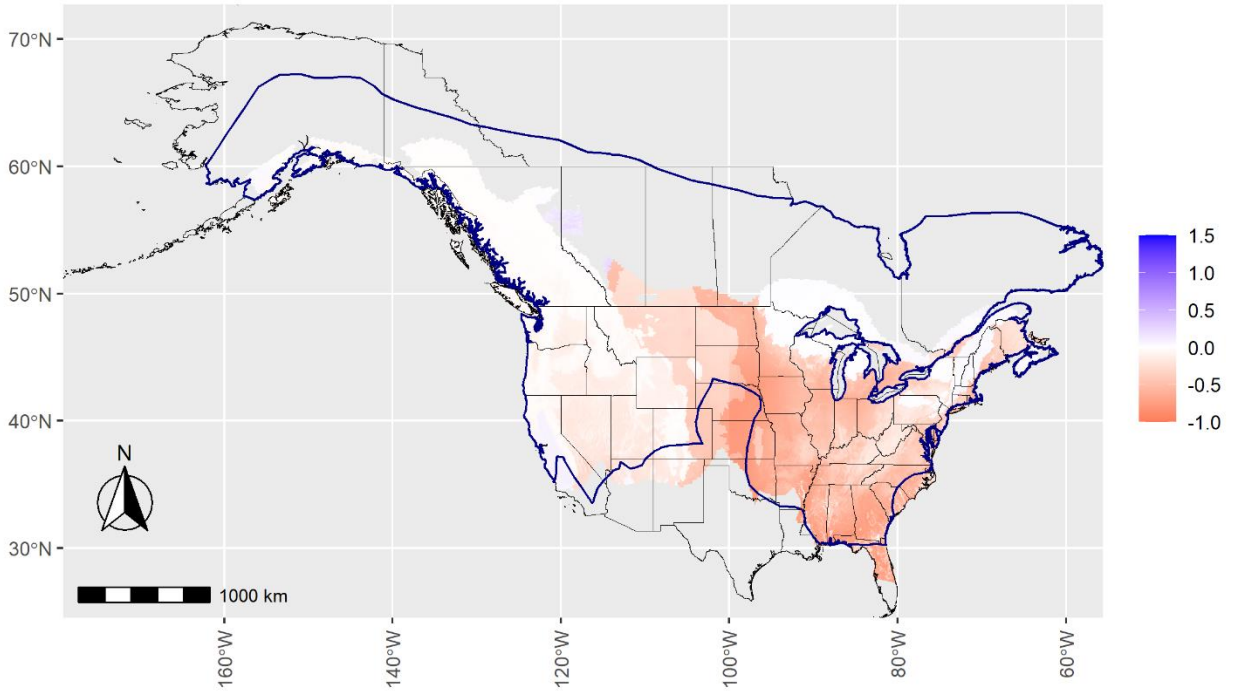

Figure 5. The total change rate in mean grid cell occupancies (color bar) for *Myotis lucifugus* (MYLU) between 2010 and 2019 for all North American Bat Monitoring Program (NABat) grid cells in the modeled species range based on site-level covariates for each grid cell and year. This is depicted against the reference range map (blue polygon; National Atlas of the United States, 2011) and borders of U.S. states and Canadian provinces/territories. Note, the polygon depicting the reference range is for illustrative purposes only and was not used to bound occupancy probability predictions – instead, the analyses are bound by the geographic scope of monitoring data. For visualization purposes, the upper bound of the scalebar is truncated at 1.5 (150%) and corresponds to values of 1.5 and above, while the lower bound is naturally bounded at -1 (-100%).

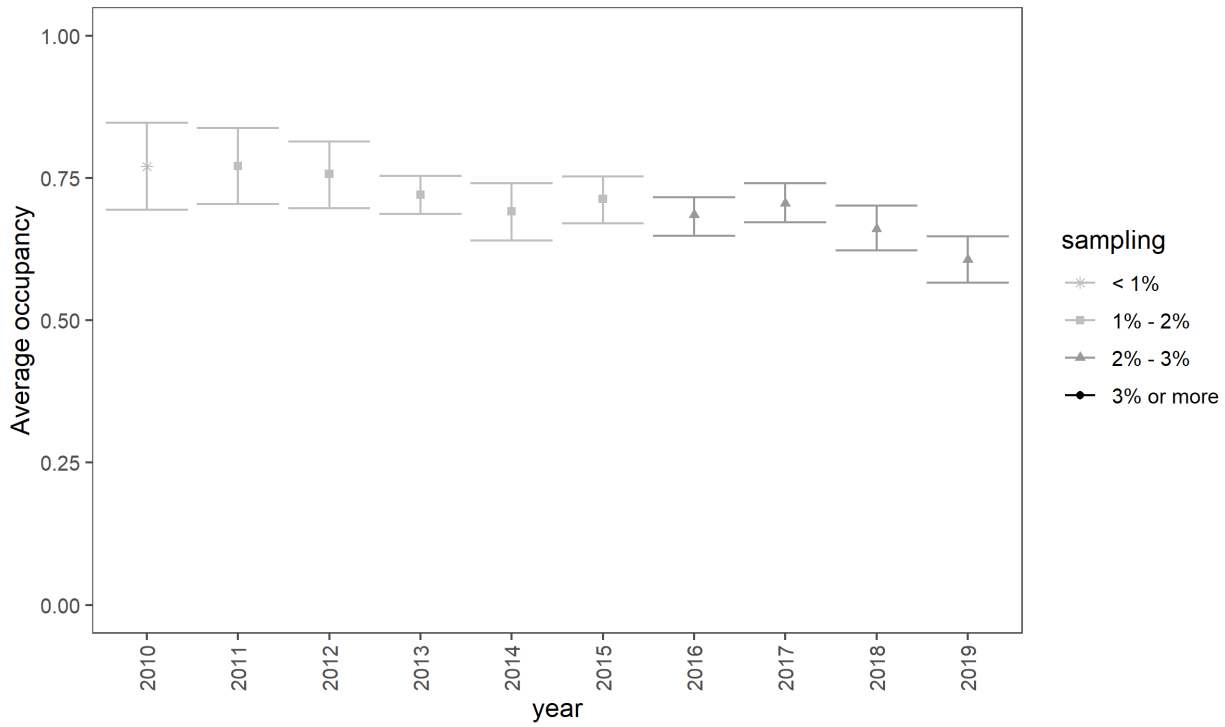

Figure 6. Estimates of the average occupancy probability ($\hat{\psi}_t$) of *Myotis lucifugus* (MYLU) each year, aggregated across all NABat grid cells in the modeled range each year. Means (points) and 95% credible intervals (bars) are depicted according to the percent of grid cells sampled in the modeled species range that each year (legend).

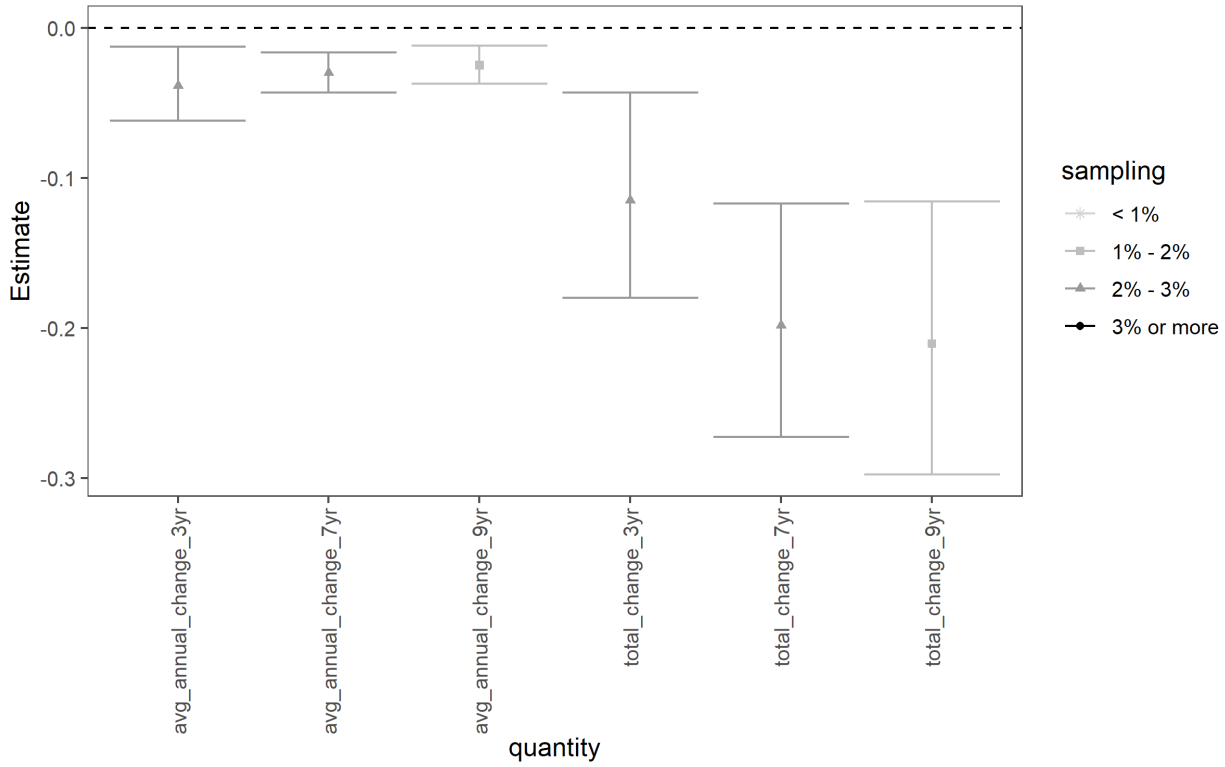

Figure 7. Estimates of average annual change (avg_annual_change = lambda_avg – 1) and total change (total_change = lambda_tot - 1) of *Myotis lucifugus* (MYLU) over the short-term (2016–2019, three years of change), medium-term (2012–2019, seven years of change) and long-term (2010–2019, nine years of change). Means (points) and 95% credible intervals (bars) are depicted according to the percent of grid cells sampled in the modeled species range each year (legend). Note the 95% credible intervals do not overlap zero, meaning there is at least 95% certainty that trends in MYLU occupancy are negative.

Table 10. The numerical values represented in Figure 7 for average annual change and total average change of *Myotis lucifugus* (MYLU) over short-term (2016–2019, three year), medium-term (2012–2019, seven year), and long-term (2010–2019, nine year) periods. CRI = 95 credible interval.

Trend Type	Quantity	Mean	Lower CRI	Upper CRI
Annual	avg_annual_change_3yr	-0.0383	-0.0618	-0.0125
Annual	avg_annual_change_7yr	-0.0298	-0.0429	-0.0162
Annual	avg_annual_change_9yr	-0.0248	-0.0370	-0.0118
Total	total_change_3yr	-0.1147	-0.1799	-0.0430
Total	total_change_7yr	-0.1981	-0.2724	-0.1168
Total	total_change_9yr	-0.2103	-0.2974	-0.1157

3.4 *Myotis septentrionalis*

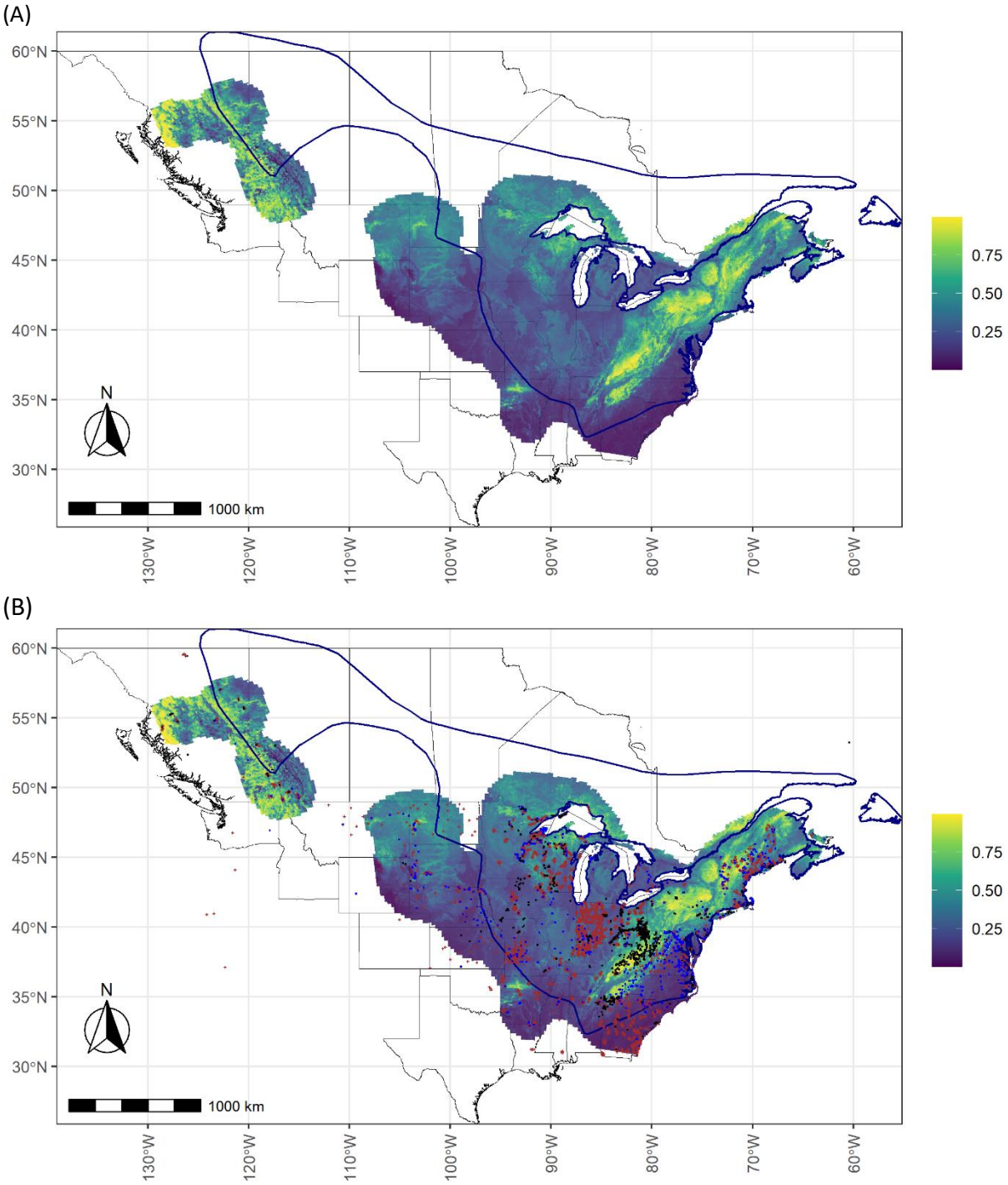

Figure 8. *Myotis septentrionalis* (MYSE) mean occupancy probabilities (color bar) predicted in each North American Bat Monitoring Program (NABat) grid cell in the modeled species range for 2019. Probabilities are depicted against the reference range map (blue polygon; National Atlas of the United States, 2011) and borders of U.S. states and Canadian provinces/territories (A and B). Note, the polygon depicting the reference range is for illustrative purposes only and was not used to bound occupancy probability predictions – instead, the analyses are bound by the geographic scope of monitoring data. All

sampled locations (2010–2019) and detection summaries are also overlaid (B), including sampled locations where the species was never detected (brown '+' sign), locations where the species was detected at least once by acoustic auto IDs (blue dots), and locations where the species was detected either by manually verified acoustic records or capture data (black dots).

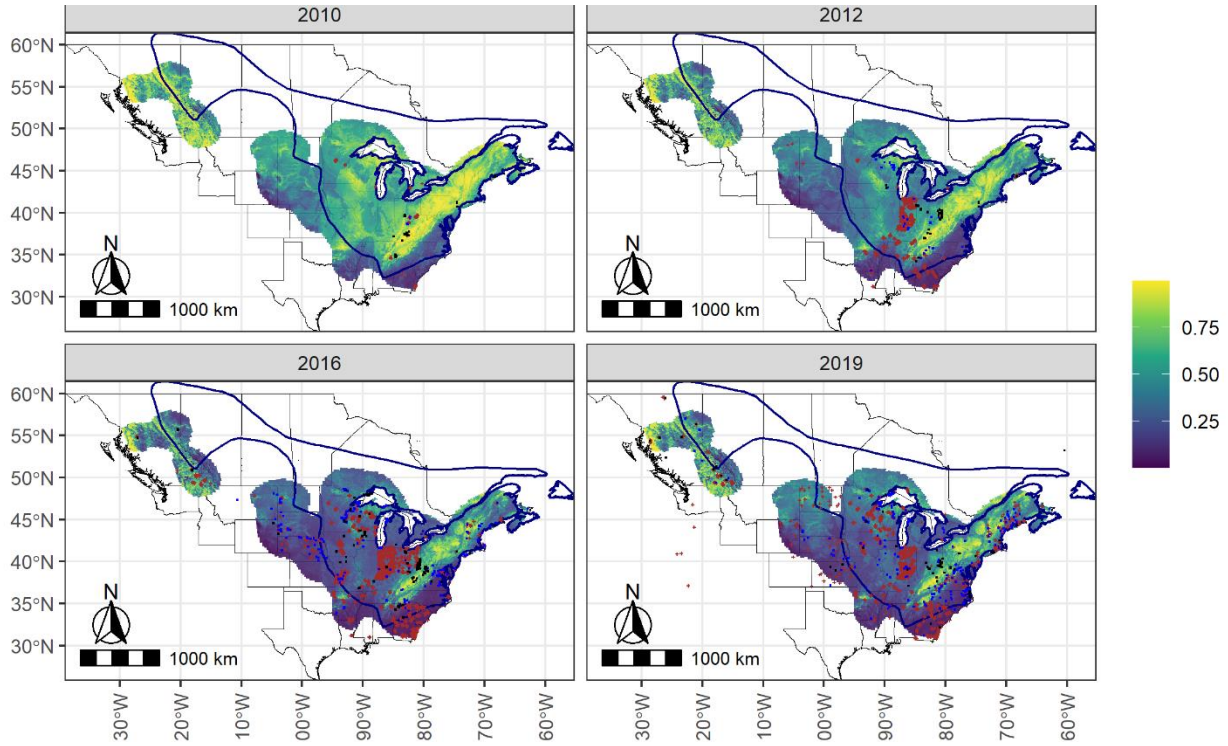

Figure 9. Mean predicted occupancy probabilities of *Myotis septentrionalis* (MYSE) in 2010, 2012, 2016, and 2019 predicted for all North American Bat Monitoring Program (NABat) grid cells in the modeled species range based on site-level covariates for each grid cell and year. This is depicted against the reference range map (blue polygon; National Atlas of the United States, 2011) and borders of U.S. states and Canadian provinces/territories. Note, the polygon depicting the reference range is for illustrative purposes only and was not used to bound occupancy probability predictions – instead, the analyses are bound by the geographic scope of monitoring data. The grid cells sampled each year are also displayed based on detection histories as: brown '+' sign = never detected, blue dots = detected with an auto ID, black dots= detected with manual vetting and/or capture.

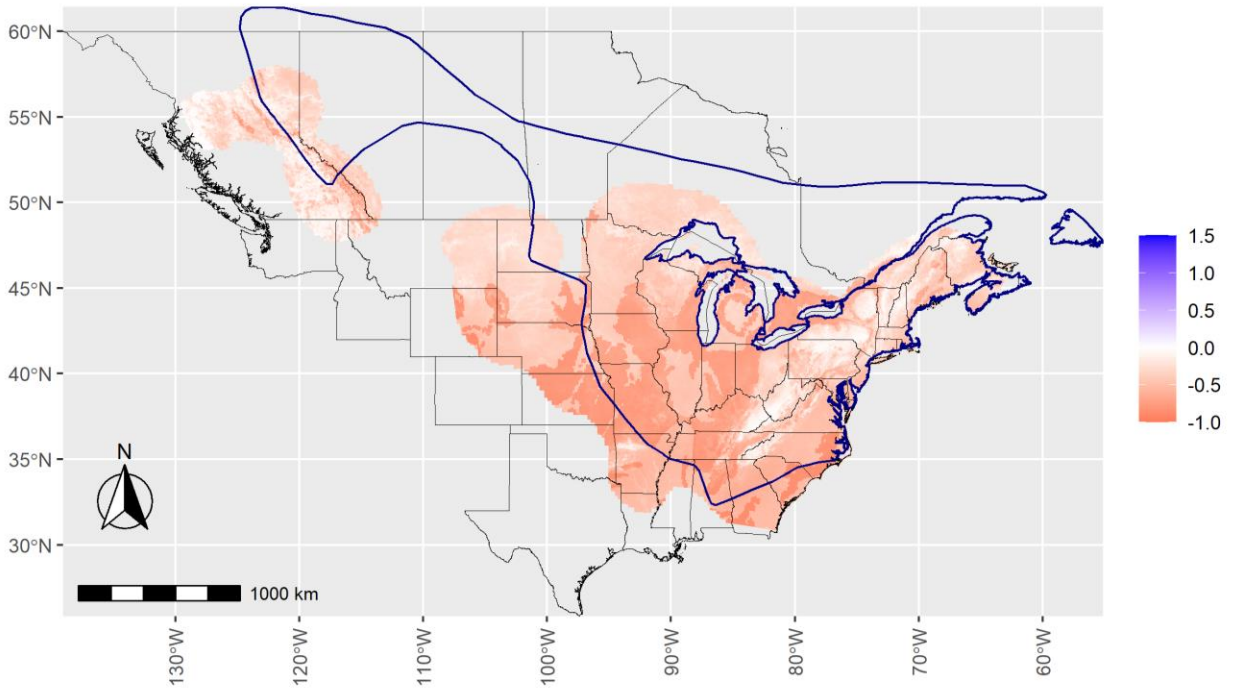

Figure 10. The total change rate in mean grid cell occupancies (color bar) for *Myotis septentrionalis* (MYSE) between 2010 and 2019 for all North American Bat Monitoring Program (NABat) grid cells in the modeled species range based on site-level covariates for each grid cell and year. This is depicted against the reference range map (blue polygon; National Atlas of the United States, 2011) and borders of U.S. states and Canadian provinces/territories. Note, the polygon depicting the reference range is for illustrative purposes only and was not used to bound occupancy probability predictions – instead, the analyses are bound by the geographic scope of monitoring data. For visualization purposes, the upper bound of the scalebar is truncated at 1.5 (150%) and corresponds to values of 1.5 and above, while the lower bound is naturally bounded at -1 (-100%).

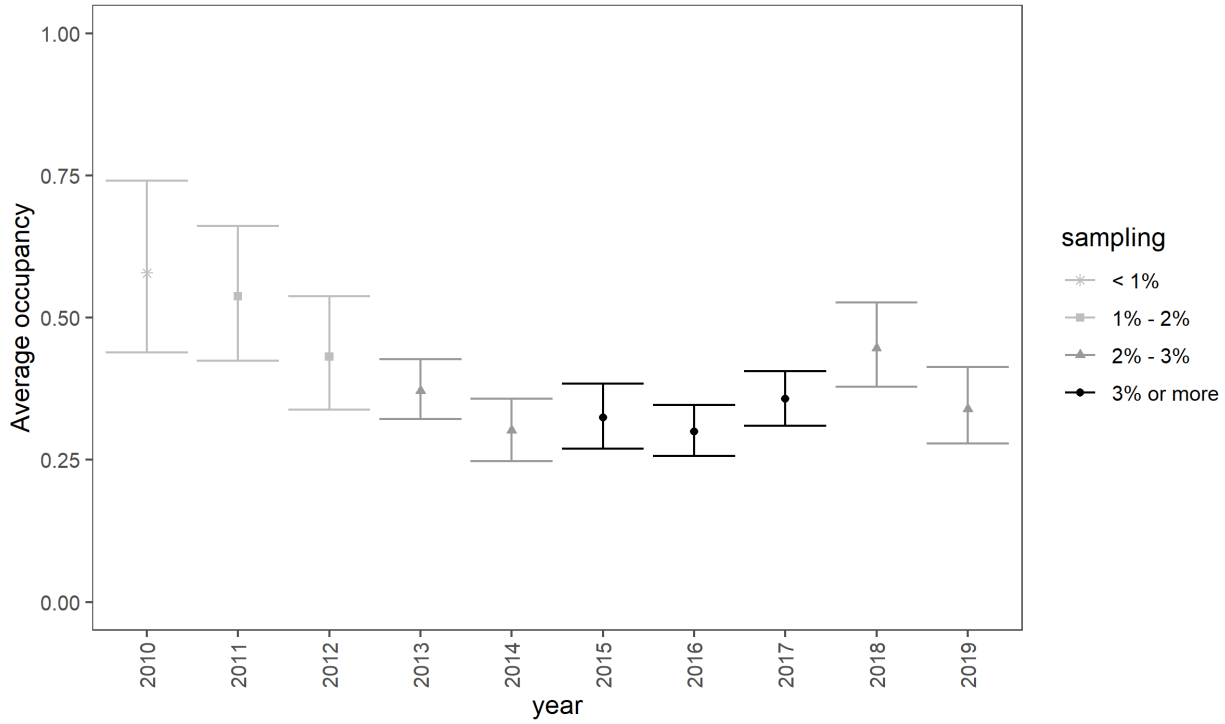

Figure 11. Estimates of the average occupancy probability ($\hat{\psi}_t$) for *Myotis septentrionalis* (MYSE) each year, aggregated across all North American Bat Monitoring Program (NABat) grid cells in modeled range each year. Means (points) and 95% credible intervals (bars) are depicted according to the percent of grid cells sampled in the modeled species range each year (legend).

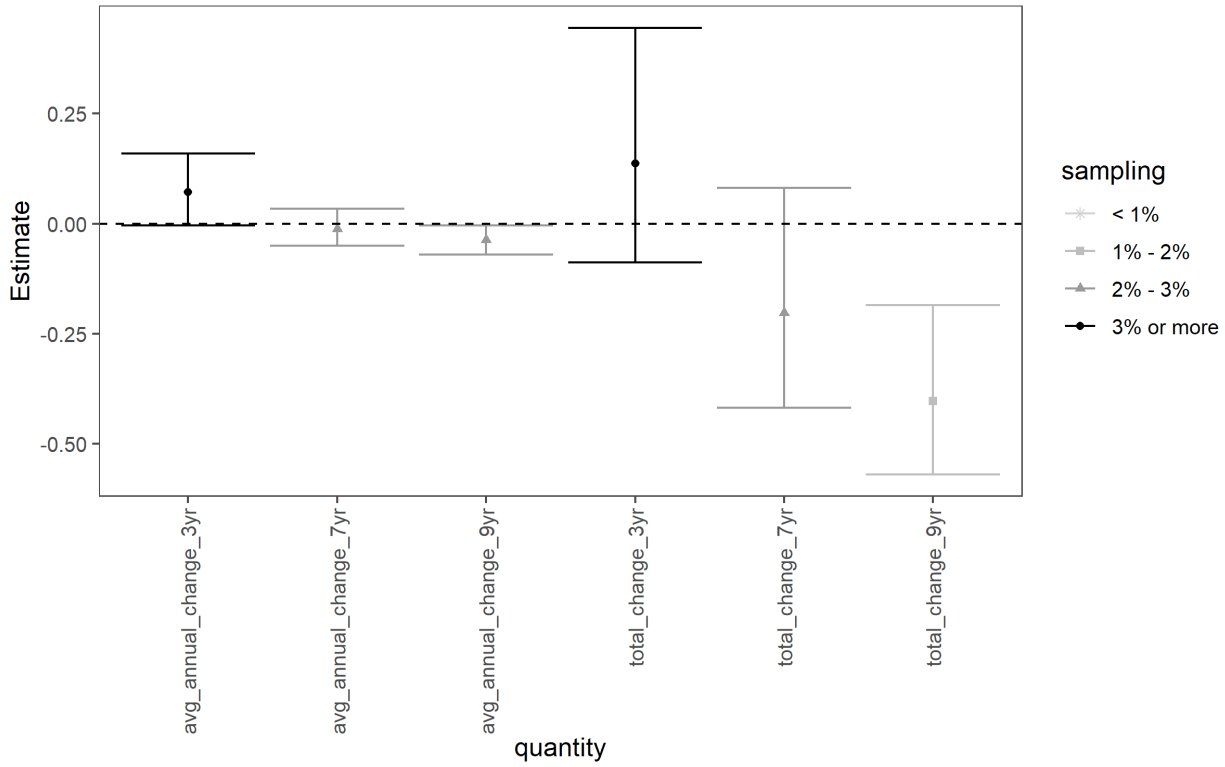

Figure 12. Estimates of average annual change (avg_annual_change = lambda_avg – 1) and total change (total_change = lambda_tot - 1) for *Myotis septentrionalis* (MYSE) over the short-term (2016–2019, three years of change), medium-term (2012–2019, seven years of change) and long-term (2010–2019, nine years of change). Means (points) and 95% credible intervals (bars) are depicted according to the percent of grid cells sampled in the modeled species range each year (legend). Note that when the 95% credible intervals do not overlap zero, there is at least 95% certainty that trends in species occupancy are either negative or positive. When credible intervals overlap zero, there is less than 95% certainty that these trends are different than zero.

Table 11. The numerical values represented in Figure 12 for average annual change and total average change over short-term (2016–2019, three year), medium-term (2012–2019, seven year), and long-term (2010–2019, nine year) periods. CRI = 95% credible interval.

Trend Type	Quantity	Mean	Lower CRI	Upper CRI
Annual	avg_annual_change_3yr	0.0717	-0.0042	0.1597
Annual	avg_annual_change_7yr	-0.0120	-0.0497	0.0340
Annual	avg_annual_change_9yr	-0.0371	-0.0699	-0.0035
Total	total_change_3yr	0.1366	-0.0881	0.4443
Total	total_change_7yr	-0.2026	-0.4185	0.0808
Total	total_change_9yr	-0.4028	-0.5693	-0.1853

3.5 *Perimyotis subflavus*

(A)

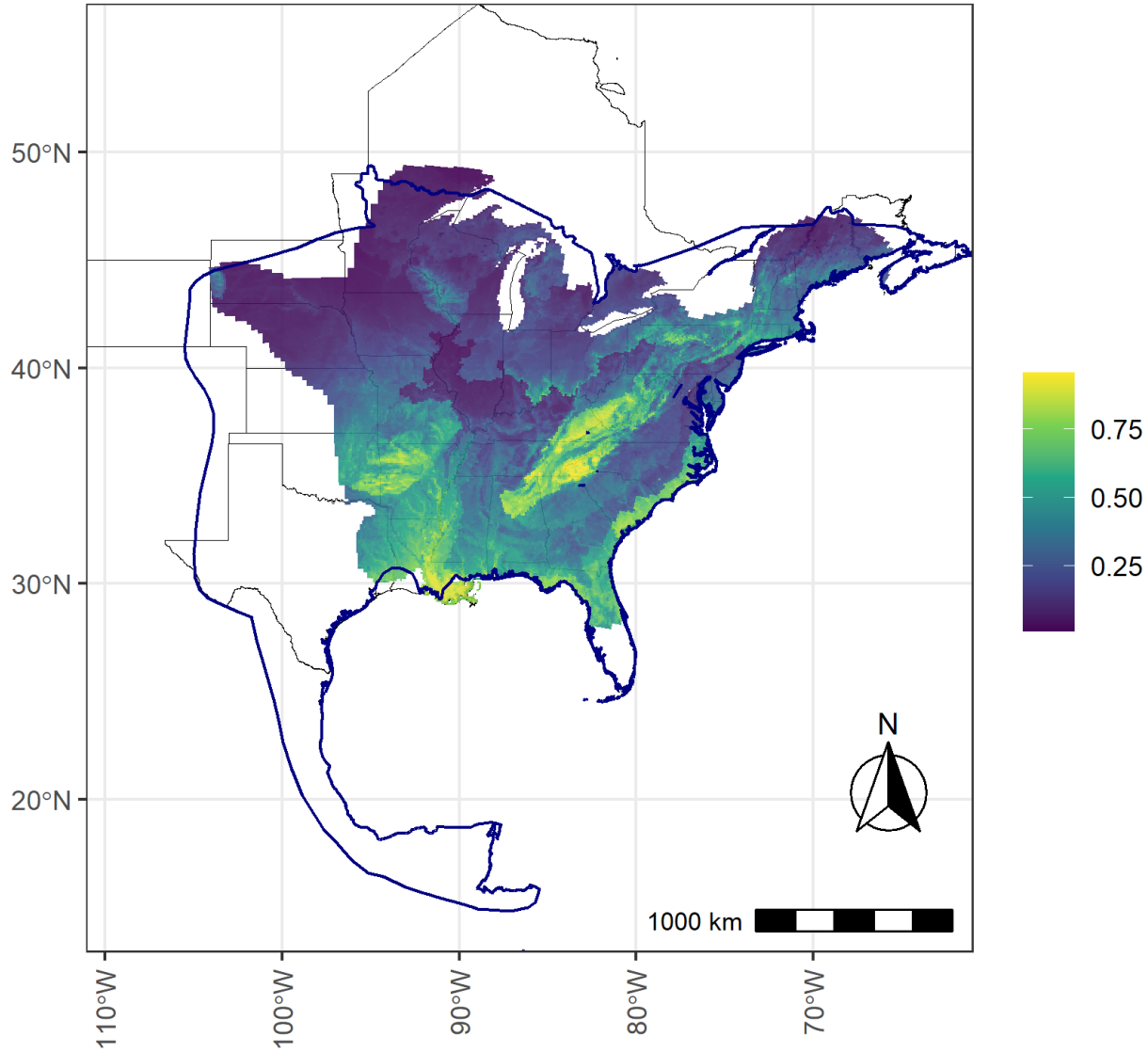

(B)

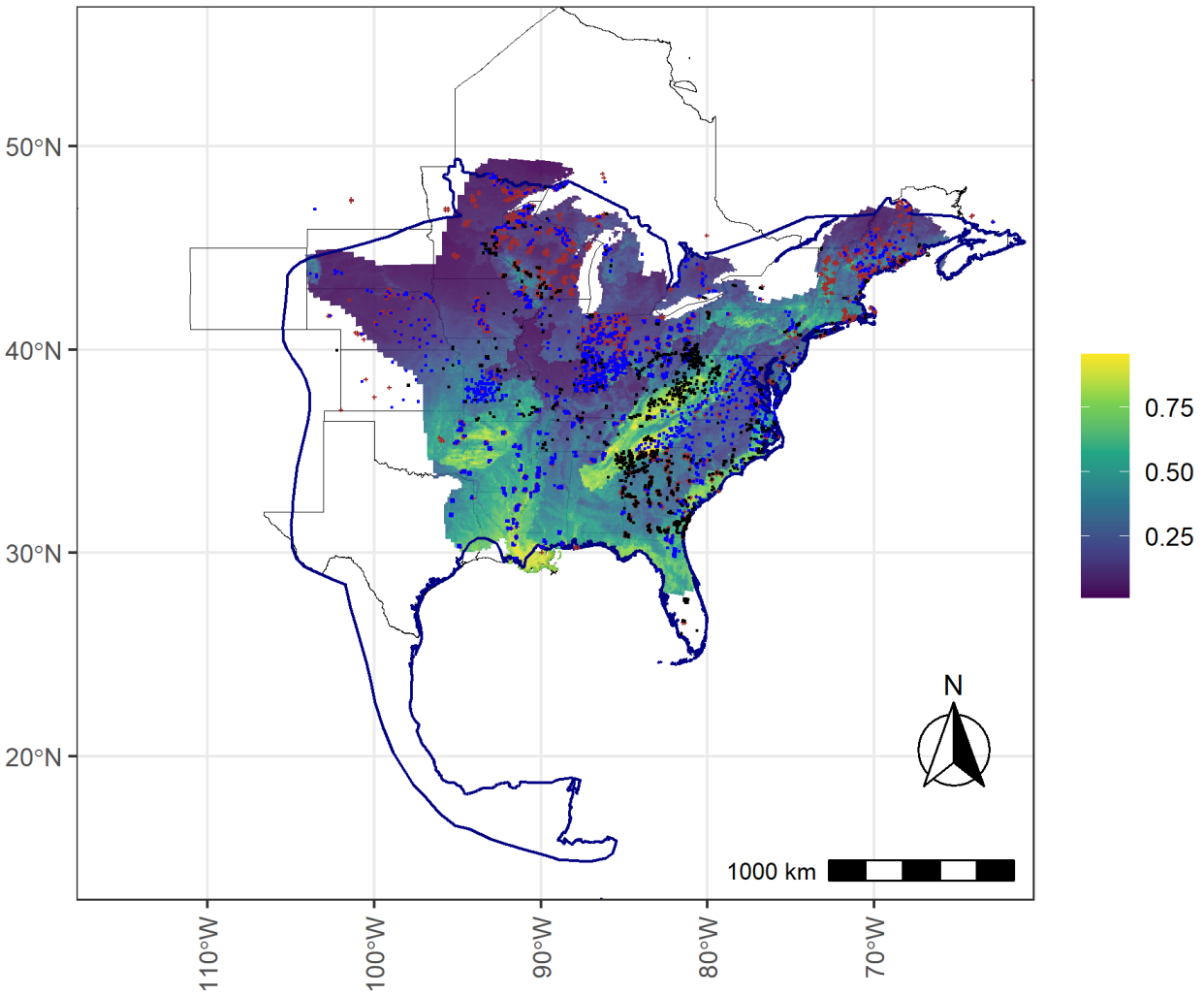

Figure 13. *Perimyotis subflavus* (PESU) mean occupancy probabilities (color bar) predicted in each North American Bat Monitoring Program (NABat) grid cell in the modeled species range for 2019. Probabilities are depicted against the reference range map (blue polygon range map provided by M. Turner, U.S. Fish and Wildlife Service, written communication, August 20, 2021) and borders of U.S. states and Canadian provinces/territories (A and B). Note, the polygon depicting the reference range is for illustrative purposes only and was not used to bound occupancy probability predictions – instead, the analyses are bound by the geographic scope of monitoring data. All sampled locations (2010–2019) and detection summaries are also overlaid (B), including sampled locations where the species was never detected (brown '+' sign), locations where the species was detected at least once by acoustic auto IDs (blue dots), and locations where the species was detected either by manually verified acoustic records or capture data (black dots).

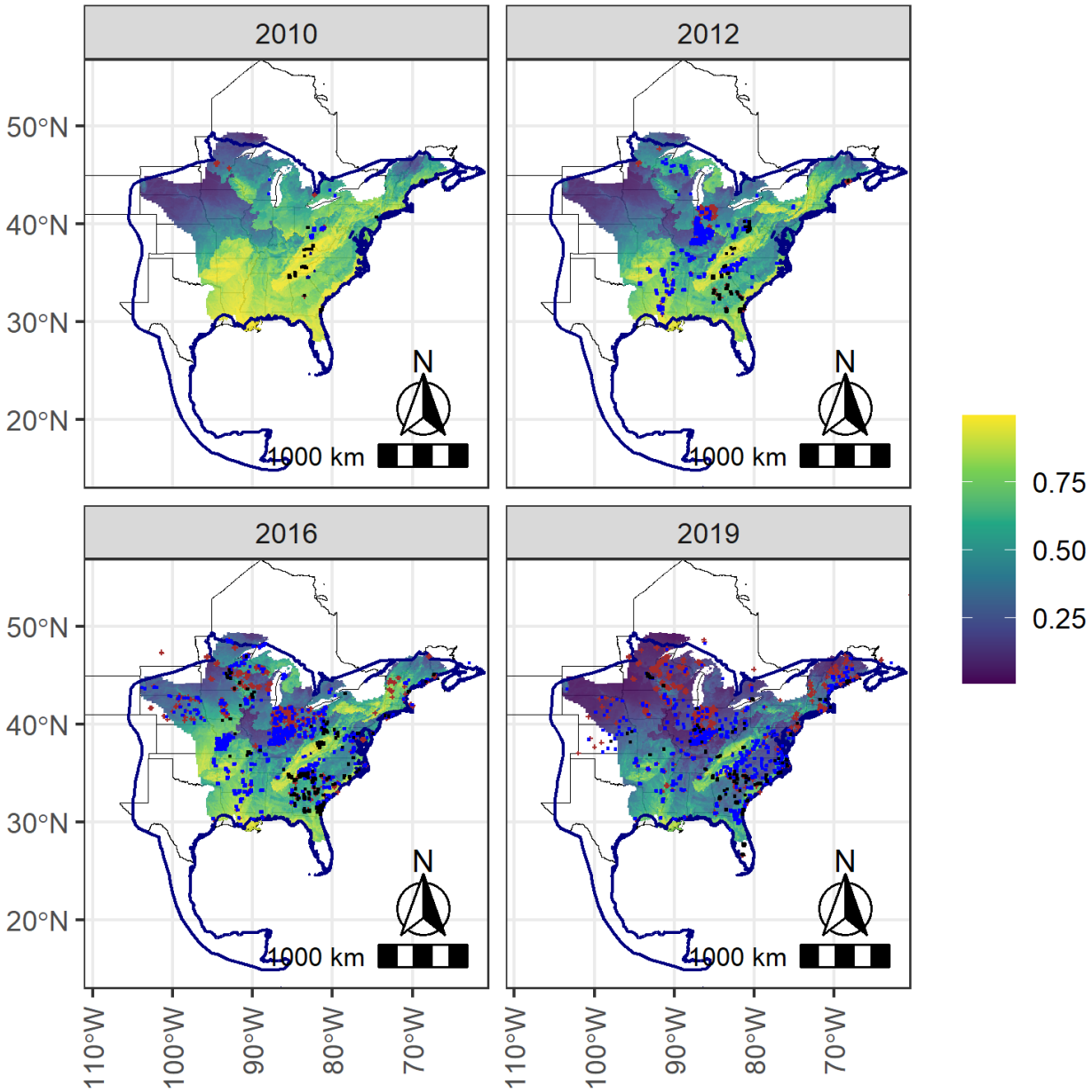

Figure 14. Mean predicted occupancy probabilities of *Perimyotis subflavus* (PESU) in 2010, 2012, 2016, and 2019 predicted for all North American Bat Monitoring Program (NABat) grid cells in the modeled species range based on site-level covariates for each grid cell and year. This is depicted against the reference range map (blue polygon range map provided by M. Turner, U.S. Fish and Wildlife Service, written communication, August 20, 2021) and borders of U.S. states and Canadian provinces/territories. Note, the polygon depicting the reference range is for illustrative purposes only and was not used to bound occupancy probability predictions – instead, the analyses are bound by the geographic scope of monitoring data. The grid cells sampled each year are also displayed based on detection histories as: brown '+' sign = never detected, blue dots = detected with an auto ID, black dots= detected with manual vetting and/or capture.

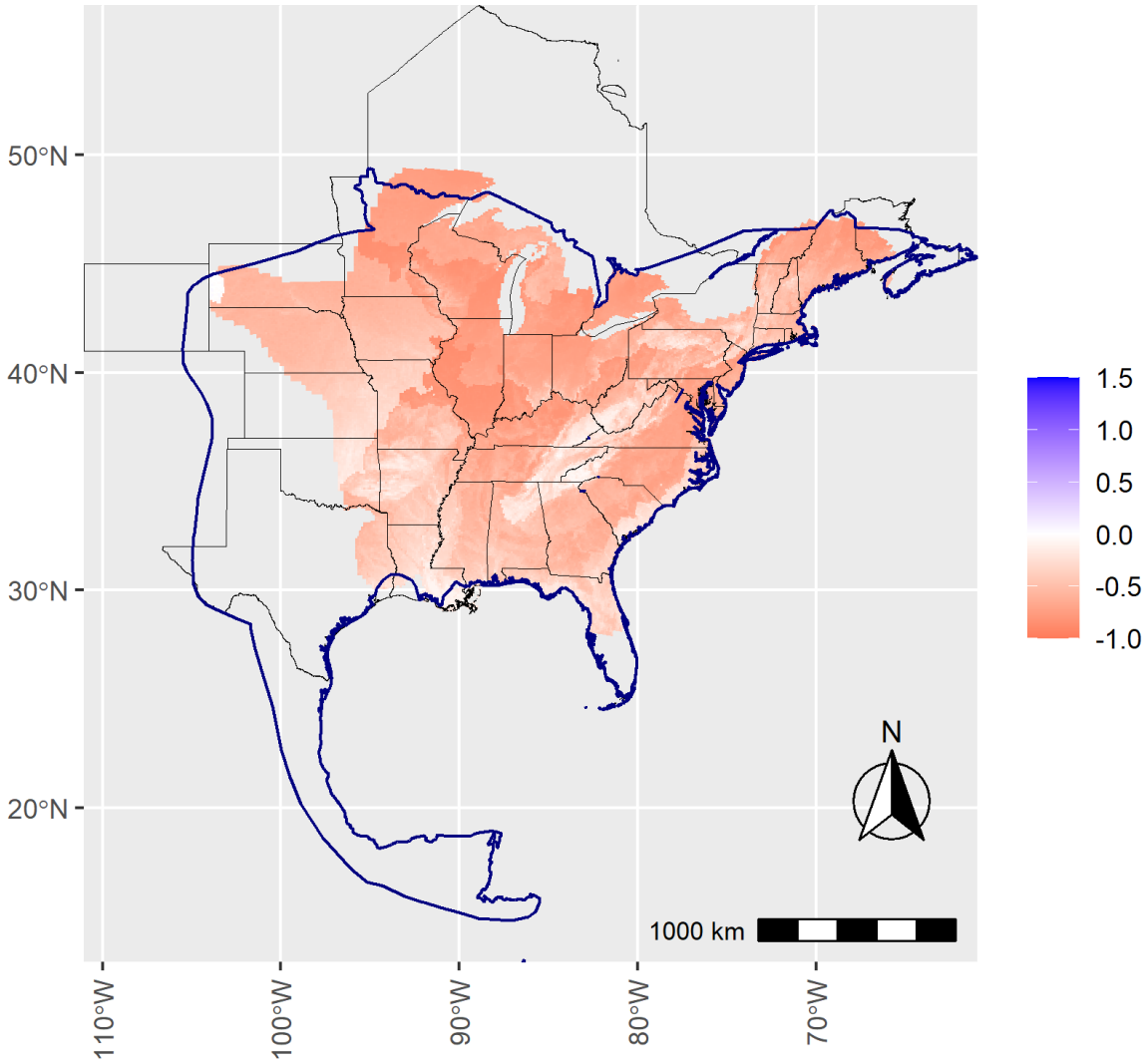

Figure 15. The total change rate in mean grid cell occupancies (color bar) of *Perimyotis subflavus* (PESU) between 2010 and 2019 for all North American Bat Monitoring Program **(**NABat) grid cells in the modeled species range based on site-level covariates for each grid cell and year. This is depicted against the reference range map (blue polygon range map provided by M. Turner, U.S. Fish and Wildlife Service**,** written communication, August 20, 2021) and borders of U.S. states and Canadian provinces/territories. Note, the polygon depicting the reference range is for illustrative purposes only and was not used to bound occupancy probability predictions – instead, the analyses are bound by the geographic scope of monitoring data. For visualization purposes, the upper bound of the scalebar is truncated at 1.5 (150%) and corresponds to values of 1.5 and above, while the lower bound is naturally bounded at -1 (-100%).

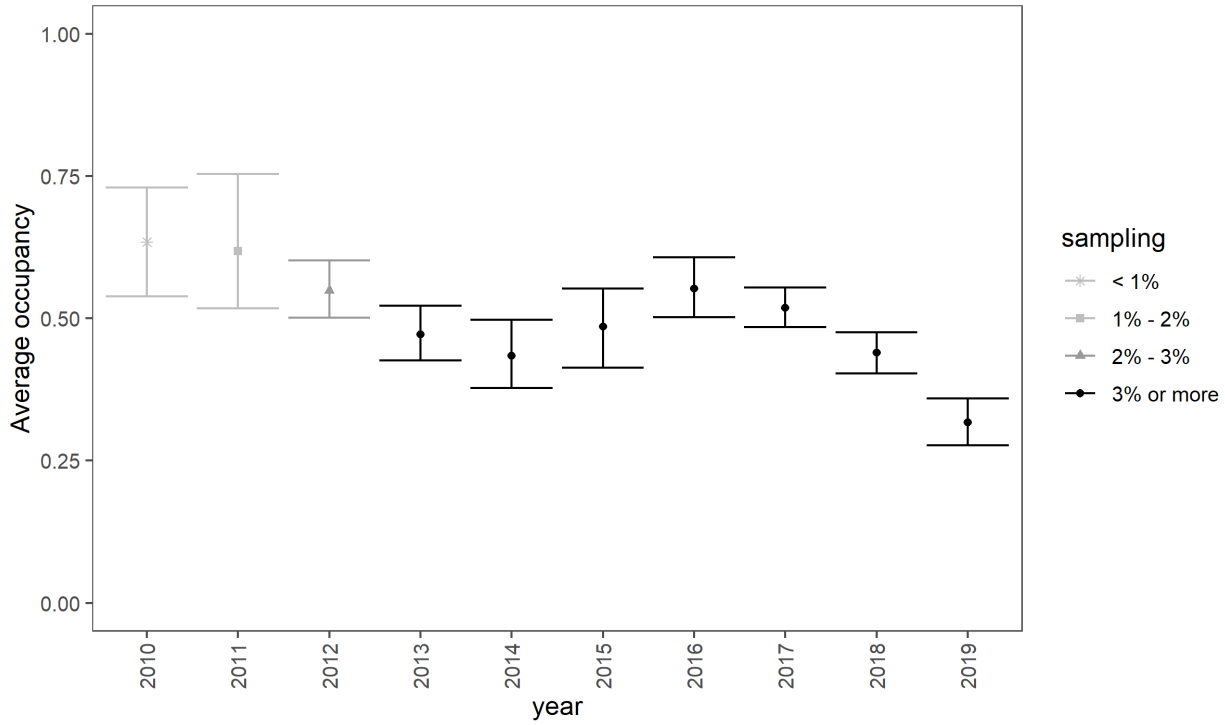

Figure 16. Estimates of the average occupancy probability ($\hat{\psi}_t$) each year of *Perimyotis subflavus* (PESU), aggregated across all North American Bat Monitoring Program (NABat) grid cells in modeled range each year. Means (points) and 95% credible intervals (bars) are depicted according to the percent of grid cells sampled in the modeled species range each year (legend).

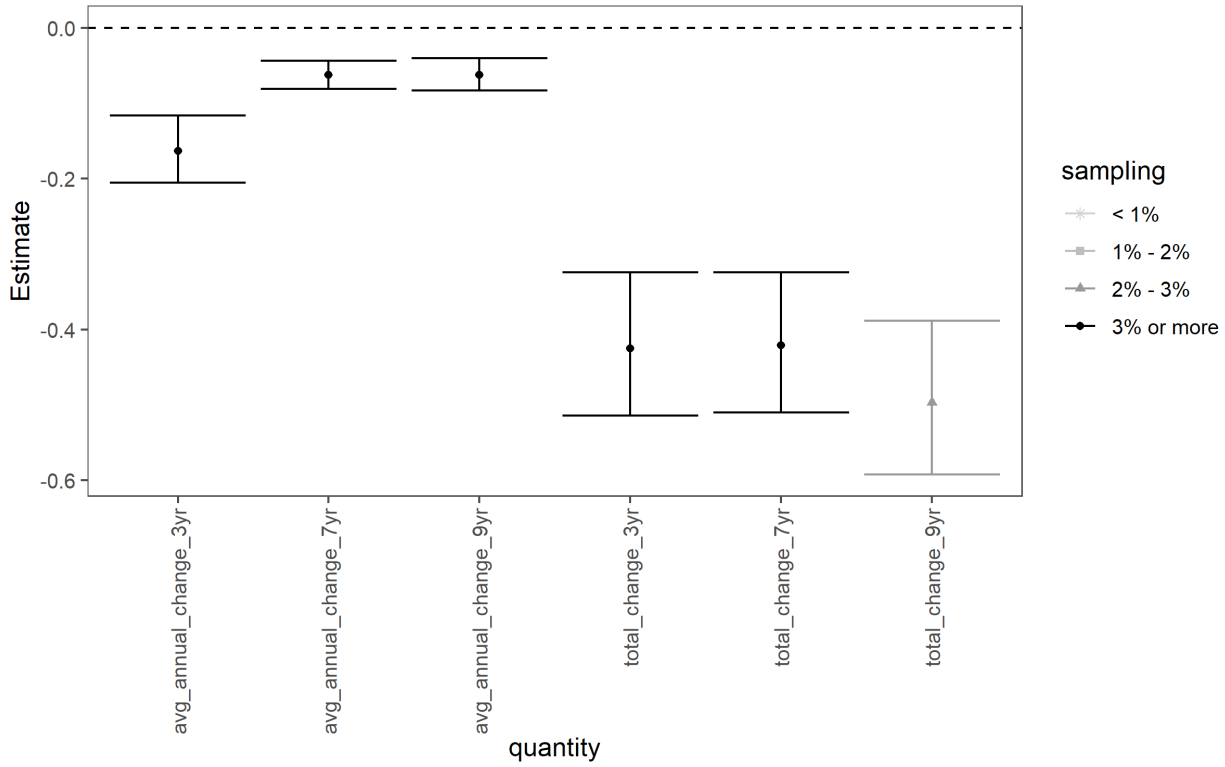

Figure 17. Estimates of average annual change (avg_annual_change = lambda_avg – 1) and total change (total_change = lambda_tot - 1) of *Perimyotis subflavus* (PESU), over the short-term (2016–2019, three years of change), medium-term (2012–2019, seven years of change) and long-term (2010–2019, nine years of change). Means (points) and 95% credible intervals (bars) are depicted according to the percent of grid cells sampled in the modeled species range each year (legend). Note that the 95% credible intervals do not overlap zero, meaning there is at least 95% certainty that trends in PESU occupancy are negative.

Table 12. The numerical values represented in Figure 17 for average annual change and total average change *Perimyotis subflavus* (PESU) over short-term (2016–2019, three year), medium-term (2012–2019, seven year), and long-term (2010–2019, nine year) periods. CRI = 95 % credible interval.

Trend Type	Quantity	Mean	Lower CRI	Upper CRI
Annual	avg_annual_change_3yr	-0.1628	-0.2050	-0.1159
Annual	avg_annual_change_7yr	-0.0624	-0.0806	-0.0432
Annual	avg_annual_change_9yr	-0.0623	-0.0831	-0.0400
Total	total_change_3yr	-0.4249	-0.5147	-0.3243
Total	total_change_7yr	-0.4210	-0.5101	-0.3240
Total	total_change_9yr	-0.4968	-0.5922	-0.2883

3.6 *Myotis evotis*

(A)

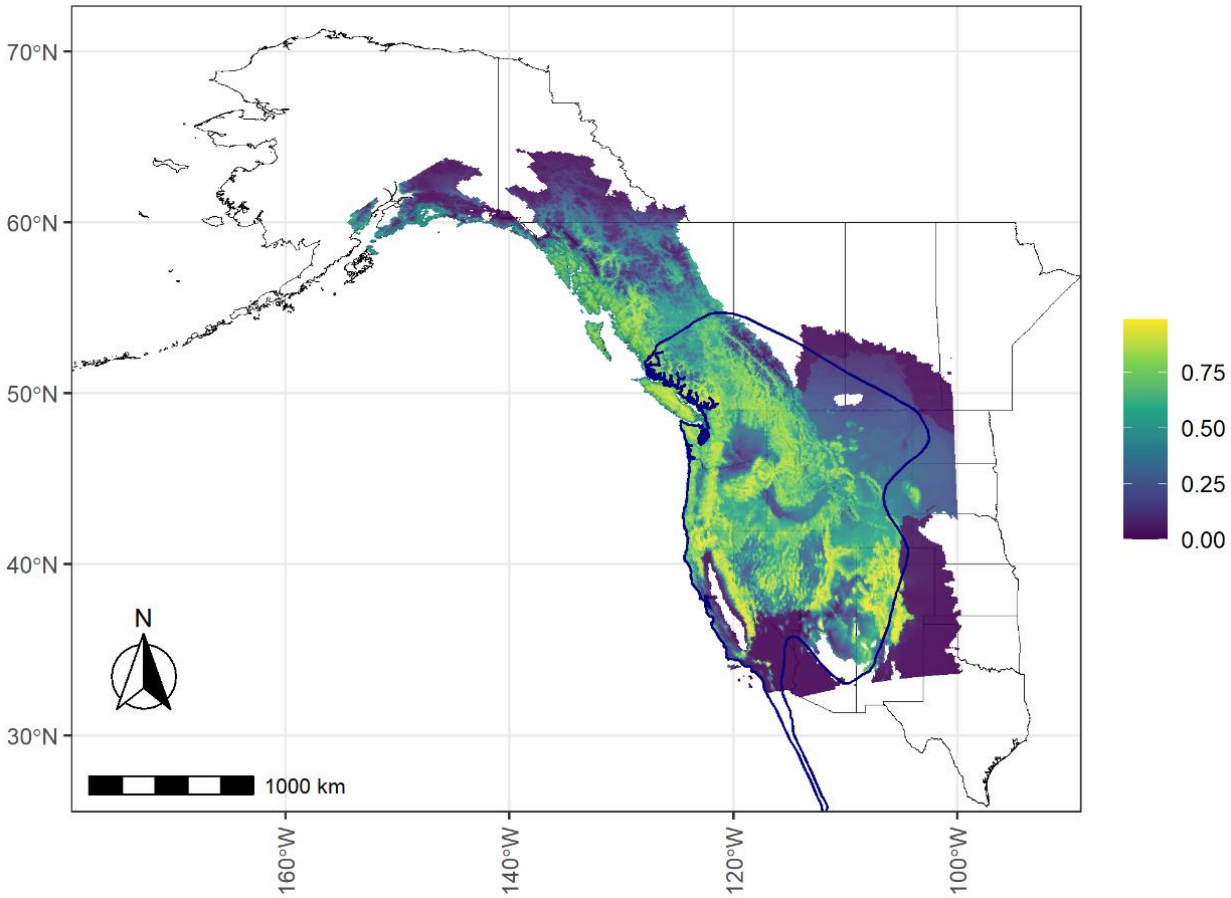

(B)

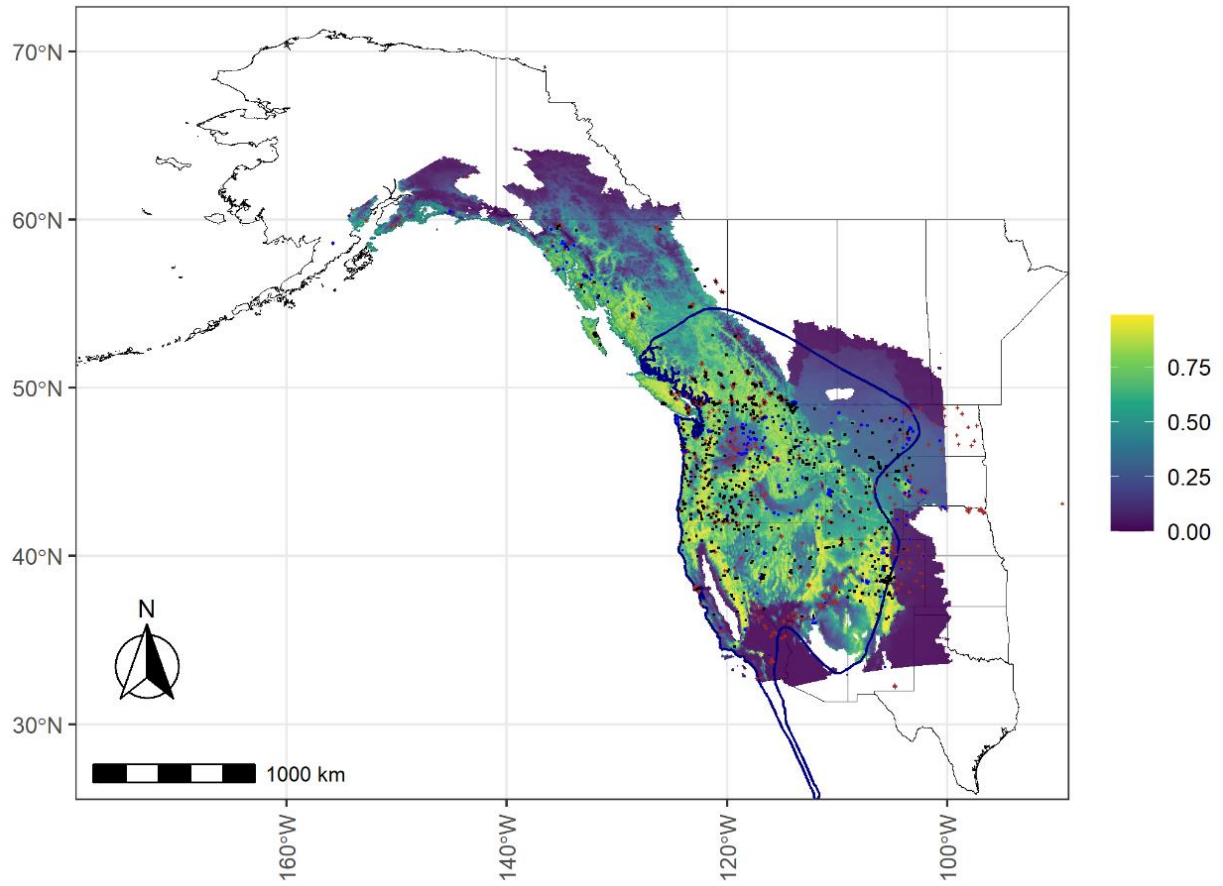

Figure 18. *Myotis evotis* (MYEV) mean occupancy probabilities (color bar) predicted in each North American Bat Monitoring Program (NABat) grid cell in the modeled species range for 2019. Probabilities are depicted against the reference range map (blue polygon; National Atlas of the United States, 2011) and borders of U.S. states and Canadian provinces/territories (A and B). Note, the polygon depicting the reference range is for illustrative purposes only and was not used to bound occupancy probability predictions – instead, the analyses are bound by the geographic scope of monitoring data. All sampled locations (2016–2019) and detection summaries are also overlaid (B), including sampled locations where the species was never detected (brown '+' sign), locations where the species was detected at least once by acoustic auto IDs (blue dots), and locations where the species was detected either by manually verified acoustic records or capture data (black dots).

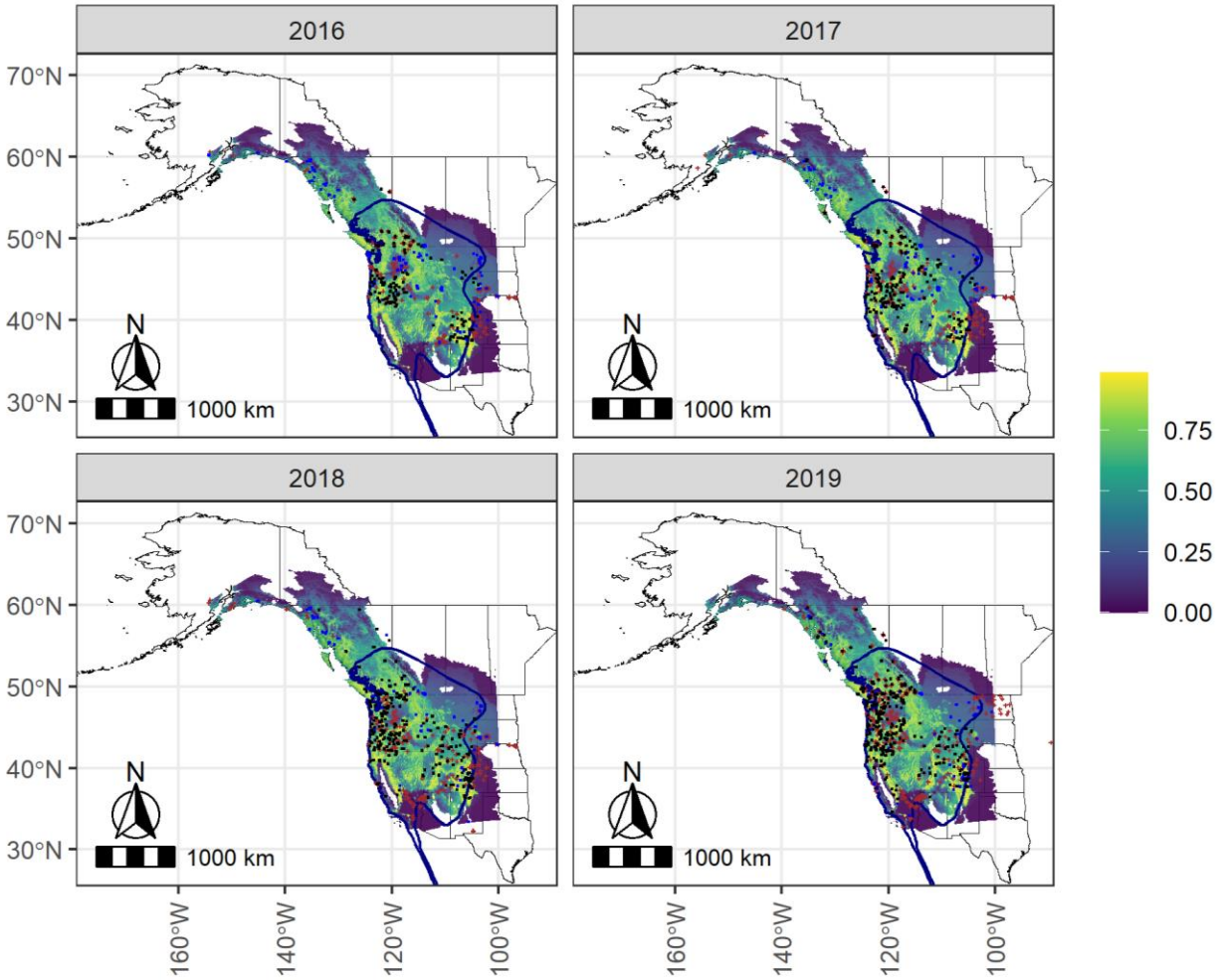

Figure 19. Mean predicted occupancy probabilities of *Myotis evotis* (MYEV) in 2016–2019 predicted for all North American Bat Monitoring Program (NABat) grid cells in the modeled species range based on site-level covariates for each grid cell and year. This is depicted against the reference range map (blue polygon; National Atlas of the United States, 2011) and borders of U.S. states and Canadian provinces/territories. Note, the polygon depicting the reference range is for illustrative purposes only and was not used to bound occupancy probability predictions – instead, the analyses are bound by the geographic scope of monitoring data. The grid cells sampled each year are also displayed based on detection histories as: brown '+' sign = never detected, blue dots= detected with an auto ID, black dots= detected with manual vetting and/or capture.

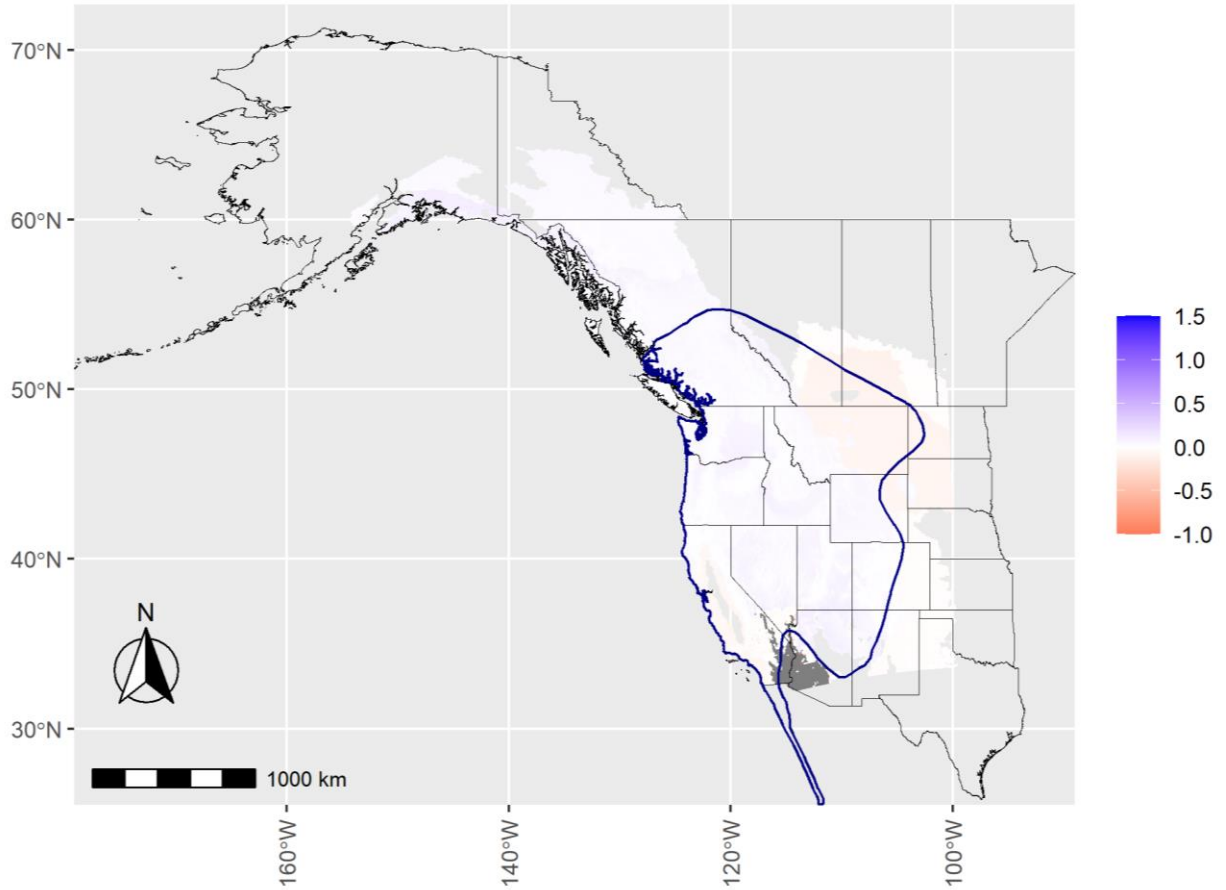

Figure 20. The total change rate in mean grid cell occupancies (color bar) for *Myotis evotis* (MYEV) between 2016 and 2019 for all North American Bat Monitoring Program (NABat) grid cells in the modeled species range based on site-level covariates for each grid cell and year. This is depicted against the reference range map (blue polygon; National Atlas of the United States, 2011) and borders of U.S. states and Canadian provinces/territories. Note, the polygon depicting the reference range is for illustrative purposes only and was not used to bound occupancy probability predictions – instead, the analyses are bound by the geographic scope of monitoring data. For visualization purposes, the upper bound of the scalebar is truncated at 1.5 (150%) and corresponds to values of 1.5 and above, while the lower bound is naturally bounded at -1 (-100%).

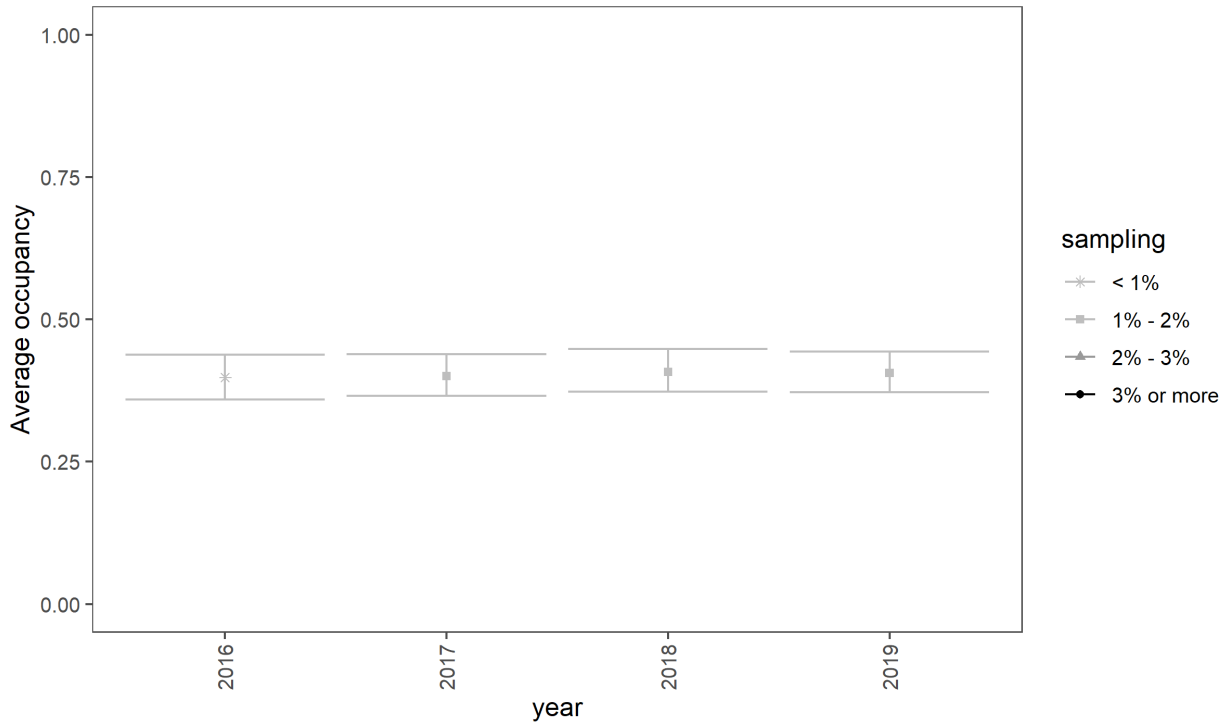

Figure 21. Estimates of the average occupancy probability ($\hat{\psi}_t$) each year for *Myotis evotis* (MYEV), aggregated across all North American Bat Monitoring Program (NABat) grid cells in modeled range each year. Means (points) and 95% credible intervals (bars) are depicted according to the percent of grid cells sampled in the modeled species range each year (legend).

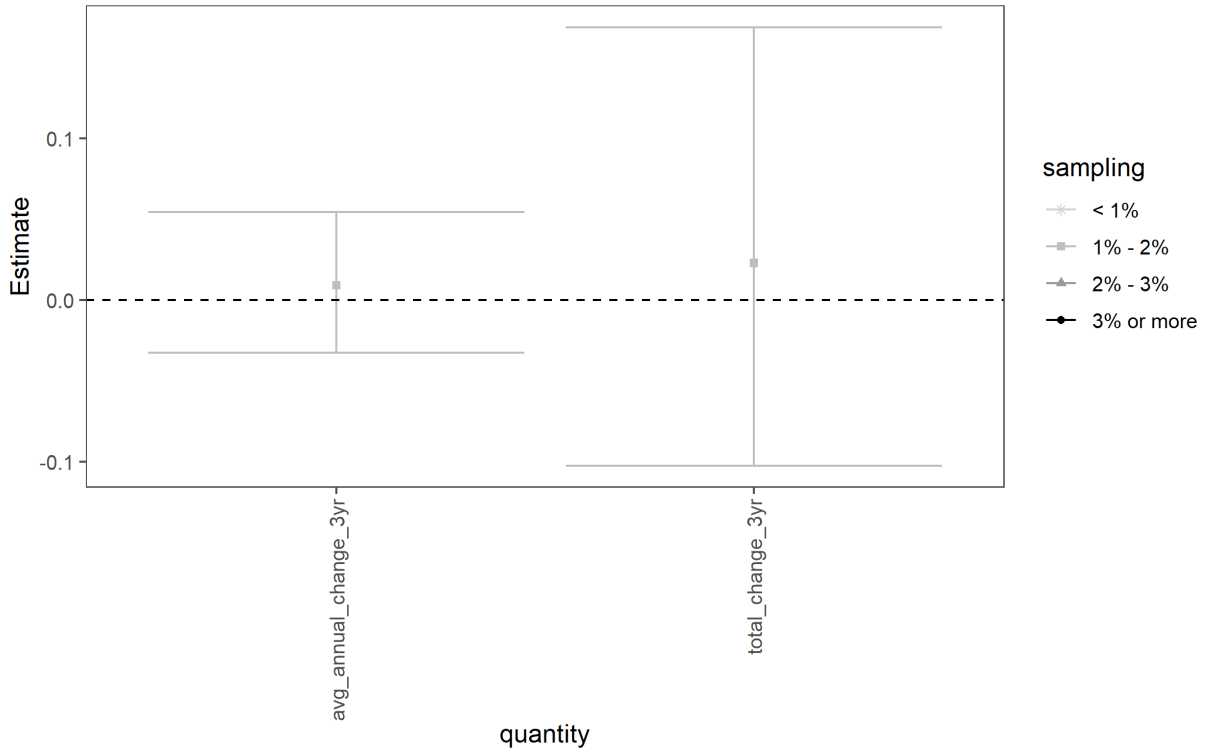

Figure 22. Estimates of average annual change (avg_annual_change = lambda_avg – 1) and total change (total_change = lambda_tot - 1) for *Myotis evotis* (MYEV) over the short-term (2016–2019, three years of change). Means (points) and 95% credible intervals (bars) are depicted according to the percent of grid cells sampled in the modeled species range each year (legend). Note that the 95% credible intervals overlap zero, meaning there is less than 95% certainty that trends in MYEV occupancy different than zero.

Table 13. The numerical values represented in Figure 22 for average annual change and total average change over a short-term (2016–2019, three year) period. CRI= 95% credible intervals.

Trend Type	Quantity	Mean	Lower CRI	Upper CRI
Annual	avg_annual_change_3yr	0.0091	-0.0327	0.0543
Total	total_change_3yr	0.0229	-0.1025	0.1687

3.7 *Myotis grisescens*

(A)

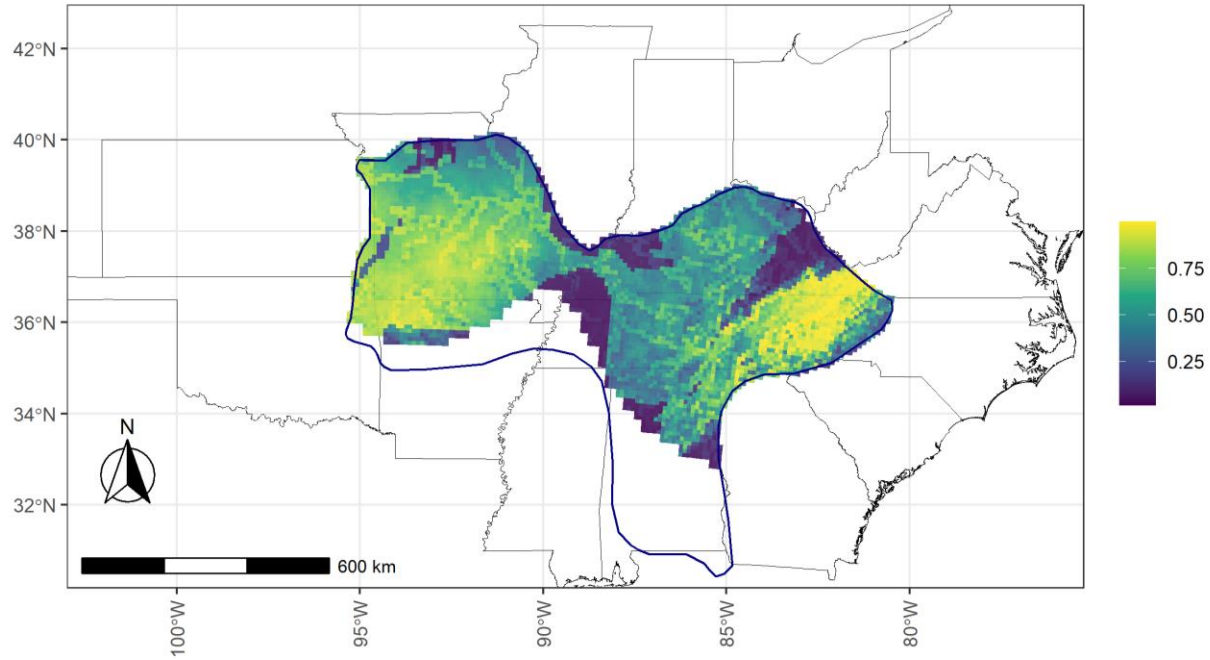

(B)

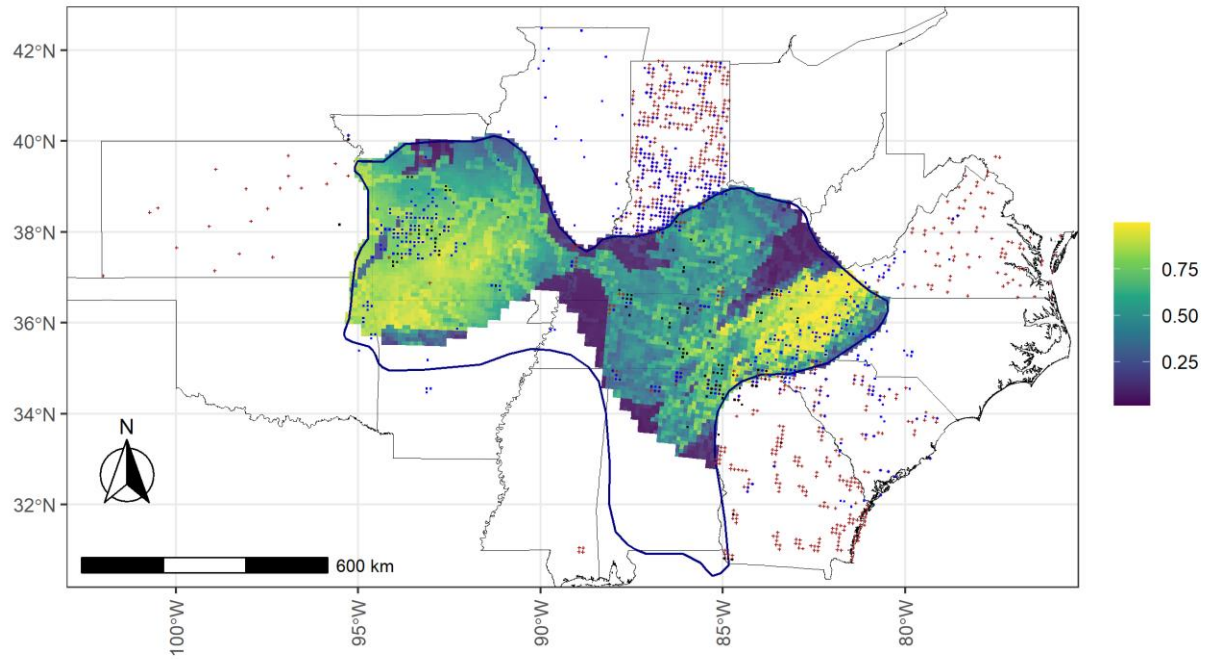

Figure 23. A map of *Myotis grisescens* (MYGR) mean occupancy probabilities (color bar) predicted in each North American Bat Monitoring Program (NABat) grid cell in the modeled species range for 2019. Probabilities are depicted against the reference range map (blue polygon range map provided by I. Kuczynska, U.S. Fish and Wildlife Service, written communication, September 30, 2021) and borders of U.S. states (A and B). All sampled locations (2016–2019) and detection summaries are also overlaid (B),

including sampled locations where the species was never detected (brown '+' sign), locations where the species was detected at least once by acoustic auto IDs (blue dots), and locations where the species was detected either by manually verified acoustic records or capture data (black dots).

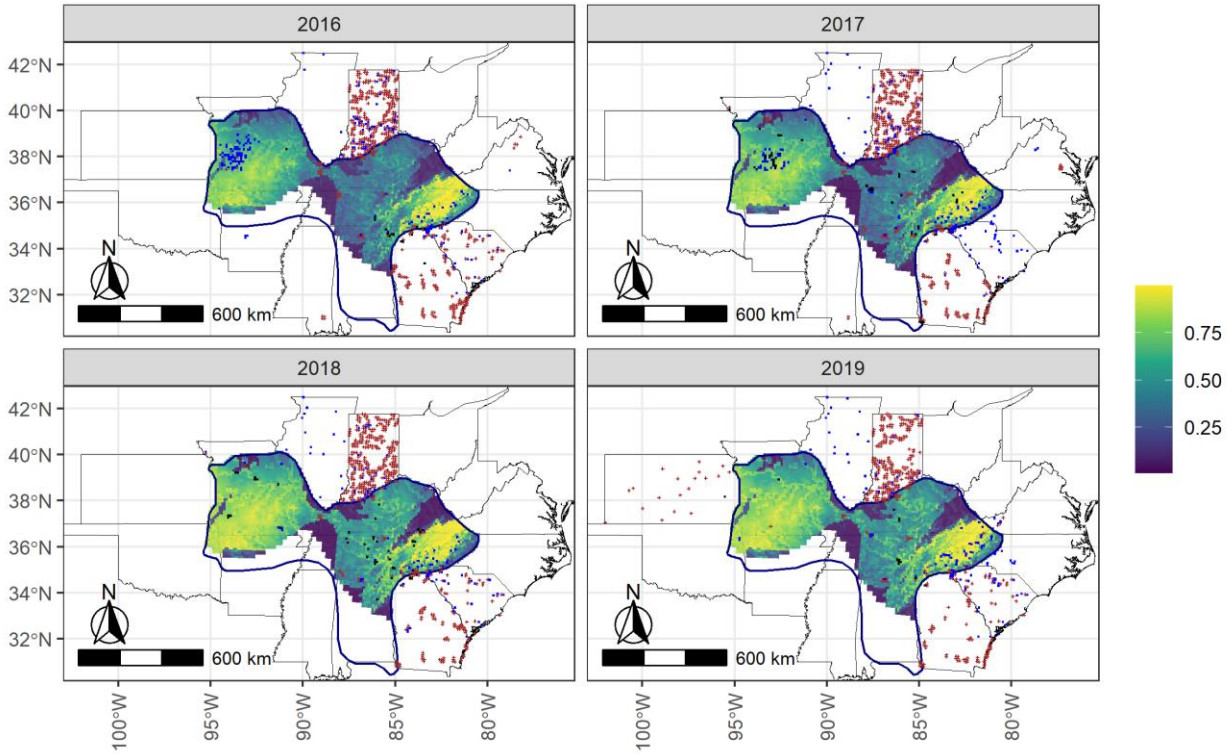

Figure 24. Mean predicted occupancy probabilities for *Myotis grisescens* (MYGR) in 2016–2019 predicted for all North American Bat Monitoring Program (NABat) grid cells in the modeled species range based on site-level covariates for each grid cell and year. This is depicted against the reference range map (blue polygon range map provided by I. Kuczynska, U.S. Fish and Wildlife Service, written communication, September 30, 2021) and borders of U.S. states. The grid cells sampled each year are also displayed based on detection histories as: brown '+' sign = never detected, blue dots = detected with an auto ID, black dots = detected with manual vetting and/or capture.

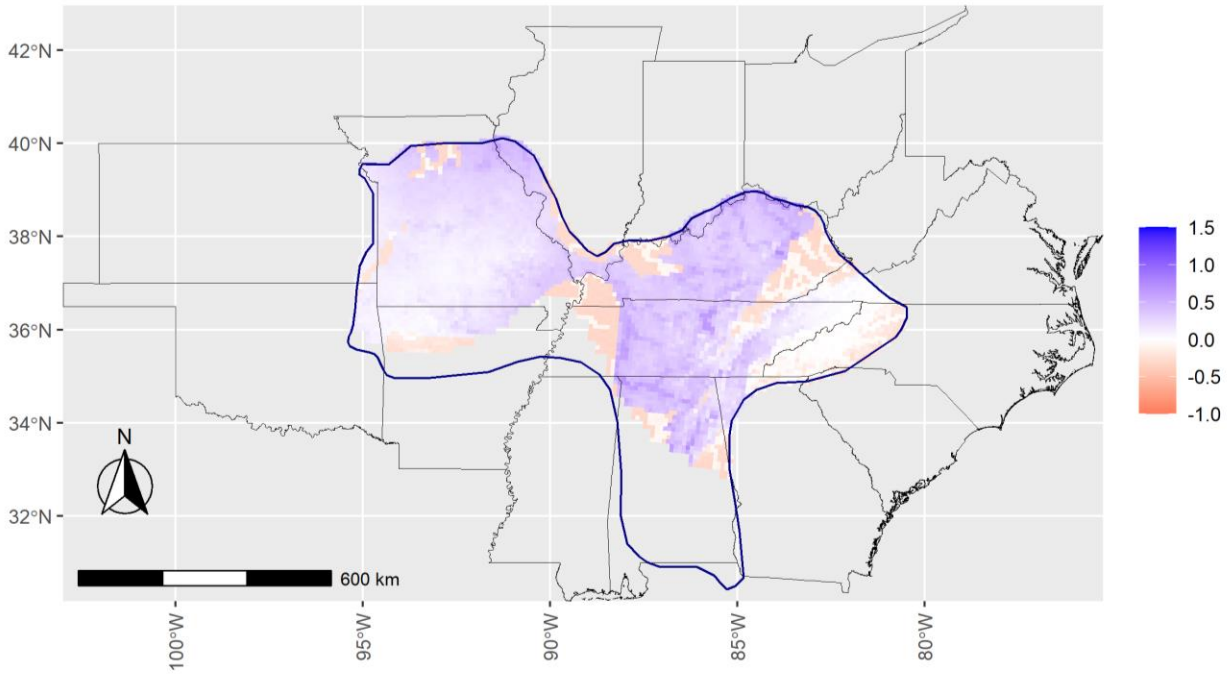

Figure 25. The total change rate in mean grid cell occupancies (color bar) for *Myotis grisescens* (MYGR) between 2016 and 2019 for all North American Bat Monitoring Program (NABat) grid cells in the modeled species range based on site-level covariates for each grid cell and year. This is depicted against the reference range map (blue polygon range map provided by I. Kuczynska, U.S. Fish and Wildlife Service, written communication, September 30, 2021) and borders of U.S. states. For visualization purposes, the upper bound of the scalebar is truncated at 1.5 (150%) and corresponds to values of 1.5 and above, while the lower bound is naturally bounded at -1 (-100%).

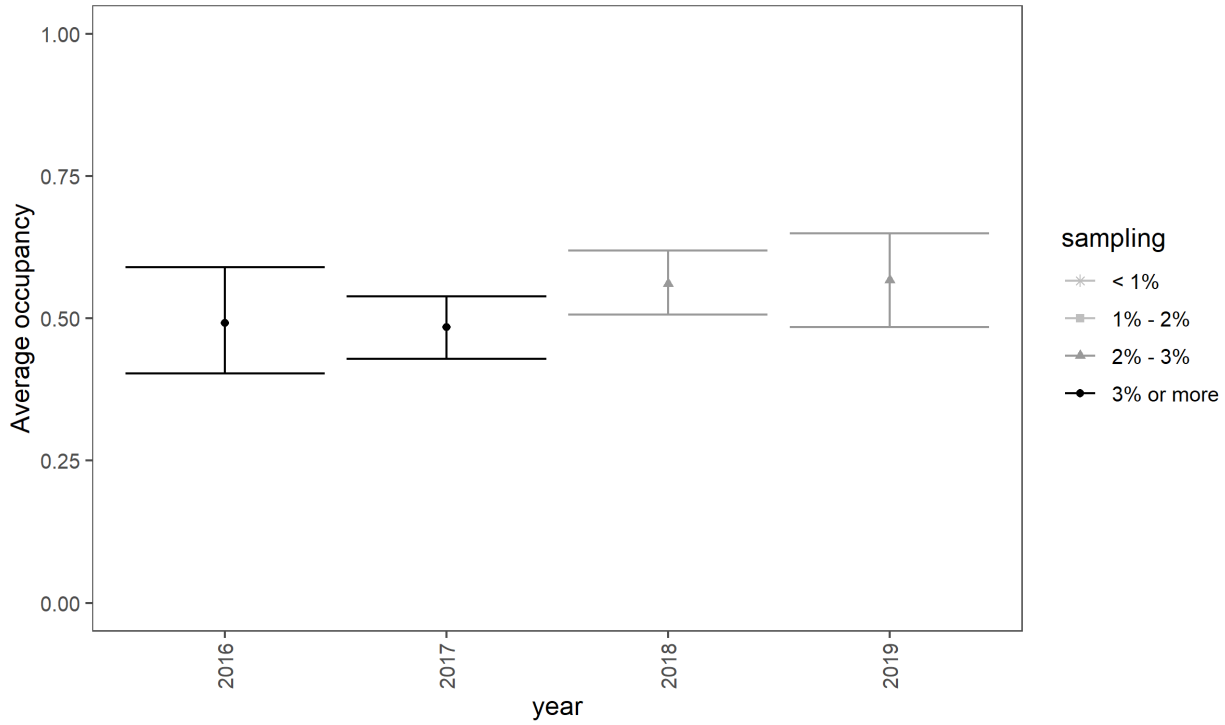

Figure 26. Estimates of the average occupancy probability ($\hat{\psi}_t$) for *Myotis grisescens* (MYGR) each year, aggregated across all North American Bat Monitoring Program (NABat) grid cells in modeled range each year. Means (points) and 95% credible intervals (bars) are depicted according to the percent of grid cells sampled in the modeled species range each year (legend).

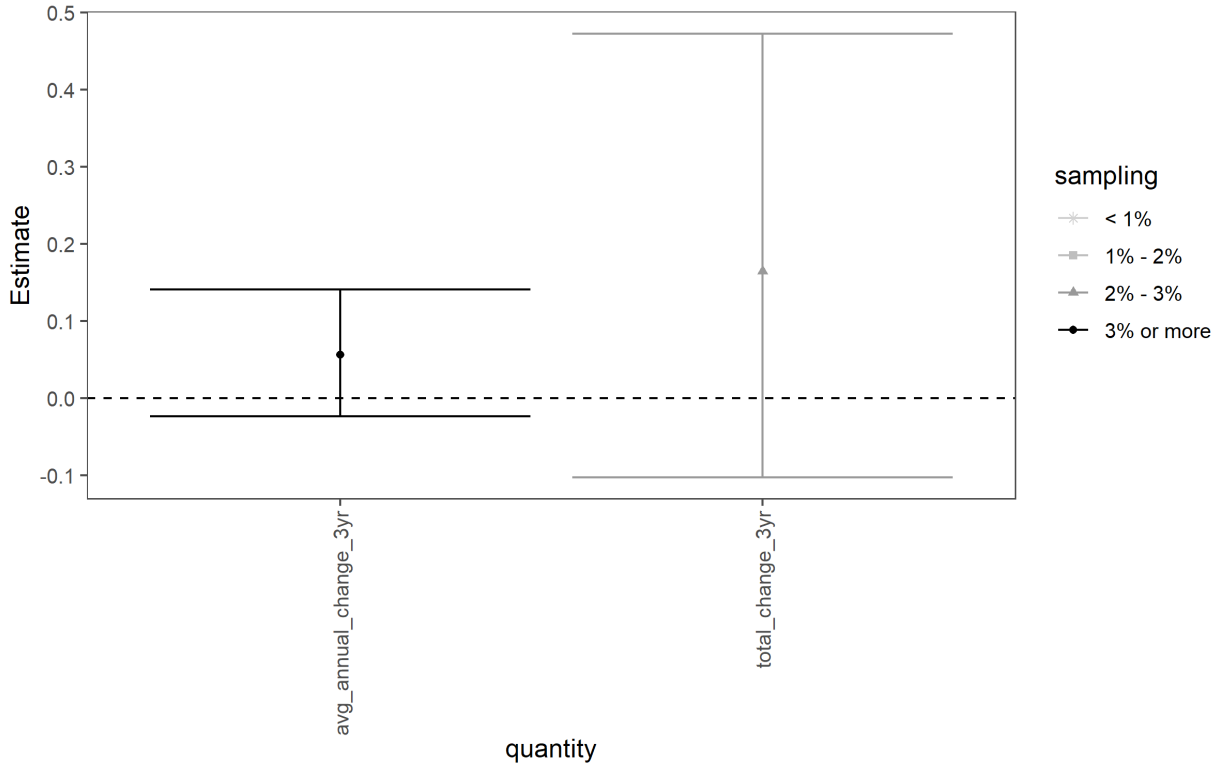

Figure 27. Estimates of average annual change (avg_annual_change = lambda_avg – 1) and total change (total_change = lambda_tot - 1) for *Myotis grisescens* (MYGR) over the short-term (2016–2019, three years of change). Means (points) and 95% credible intervals (bars) are depicted according to the percent of grid cells sampled in the modeled species range each year (legend). Note that the 95% credible intervals overlap zero, meaning there is less than 95% certainty that trends in MYGR occupancy are different than zero.

Table 14. The numerical values represented in Figure 27 for average annual change and total average change over a short-term (2016–2019, three year) period. CRI = 95% credible intervals.

Trend Type	Quantity	Mean	Lower CRI	Upper CRI
Annual	avg_annual_change_3yr	0.0568	-0.0234	0.1410
Total	total_change_3yr	0.1645	-0.1023	0.4725

3.8 *Myotis leibii*

(A)

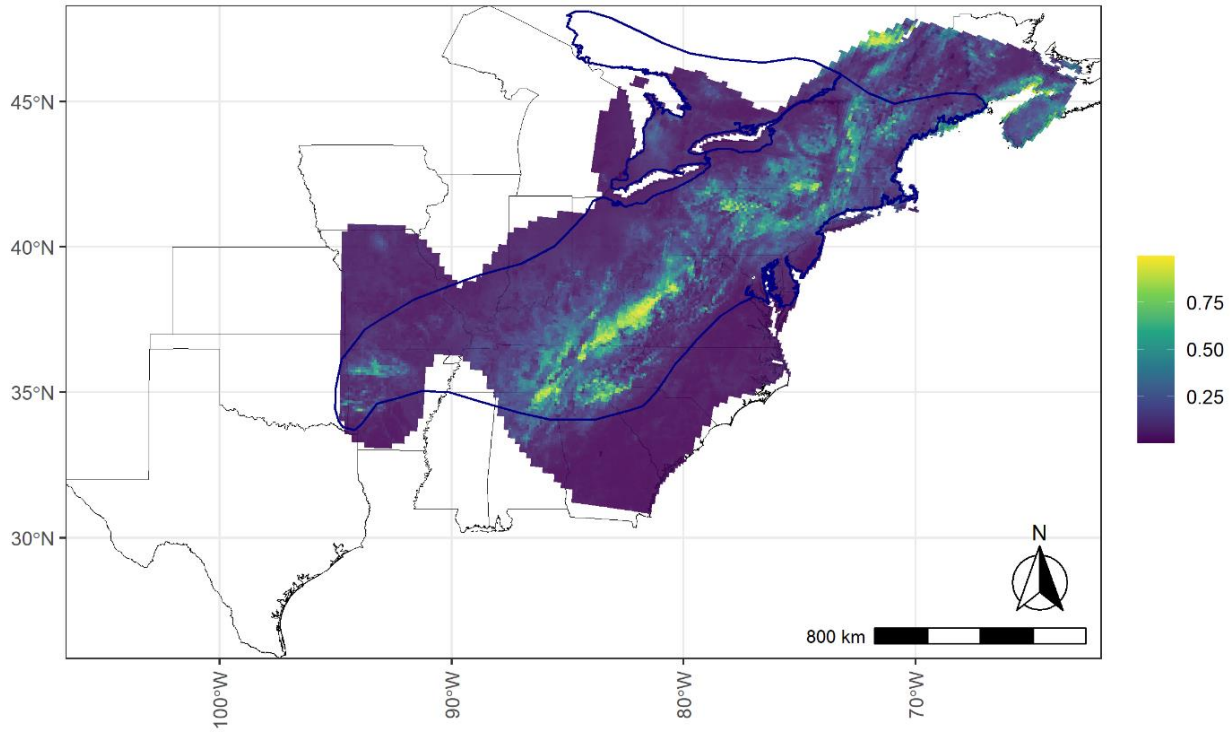

(B)

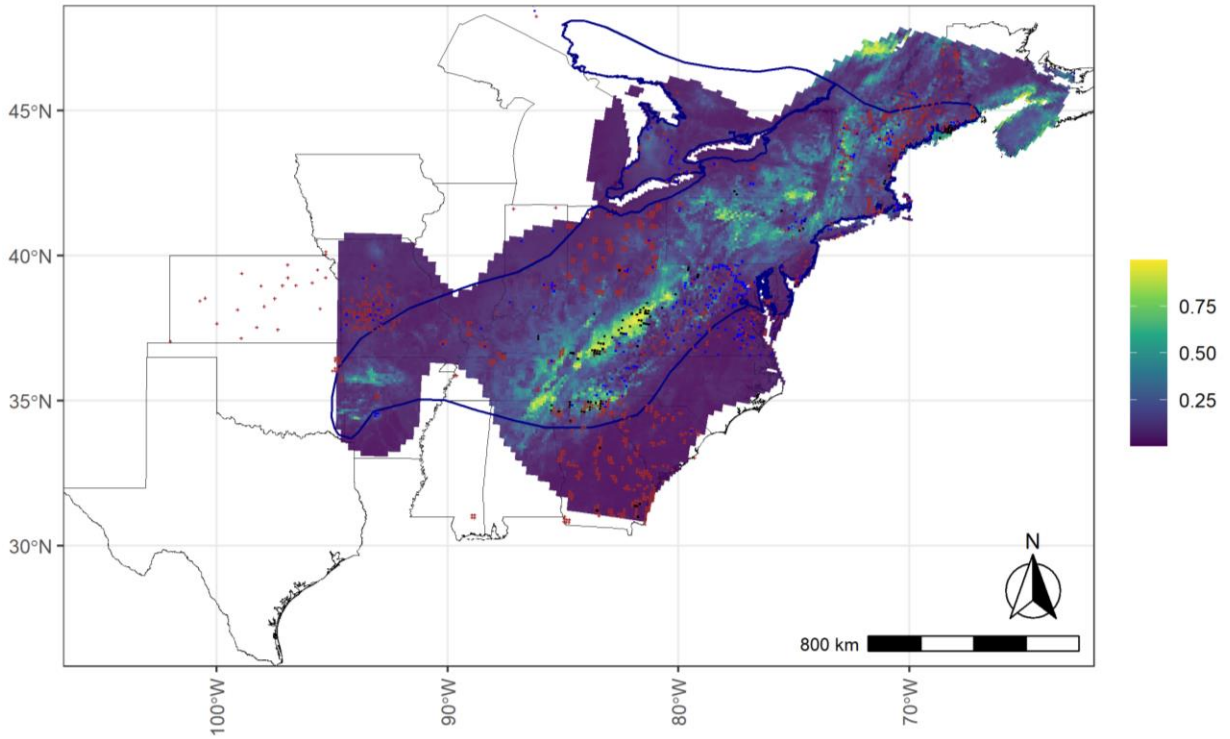

Figure 28. A map of *Myotis leibii* (MYLE) mean occupancy probabilities (color bar) predicted in each North American Bat Monitoring Program (NABat) grid cell in the modeled species range for 2019. Probabilities are depicted against the reference range map (blue polygon; National Atlas of the United

States, 2011) and borders of U.S. states and Canadian provinces/territories (A and B). Note, the polygon depicting the reference range is for illustrative purposes only and was not used to bound occupancy probability predictions – instead, the analyses are bound by the geographic scope of monitoring data. All sampled locations (2016–2019) and detection summaries are also overlaid (B), including sampled locations where the species was never detected (brown '+' sign), locations where the species was detected at least once by acoustic auto IDs (blue dots), and locations where the species was detected either by manually verified acoustic records or capture data (black dots).

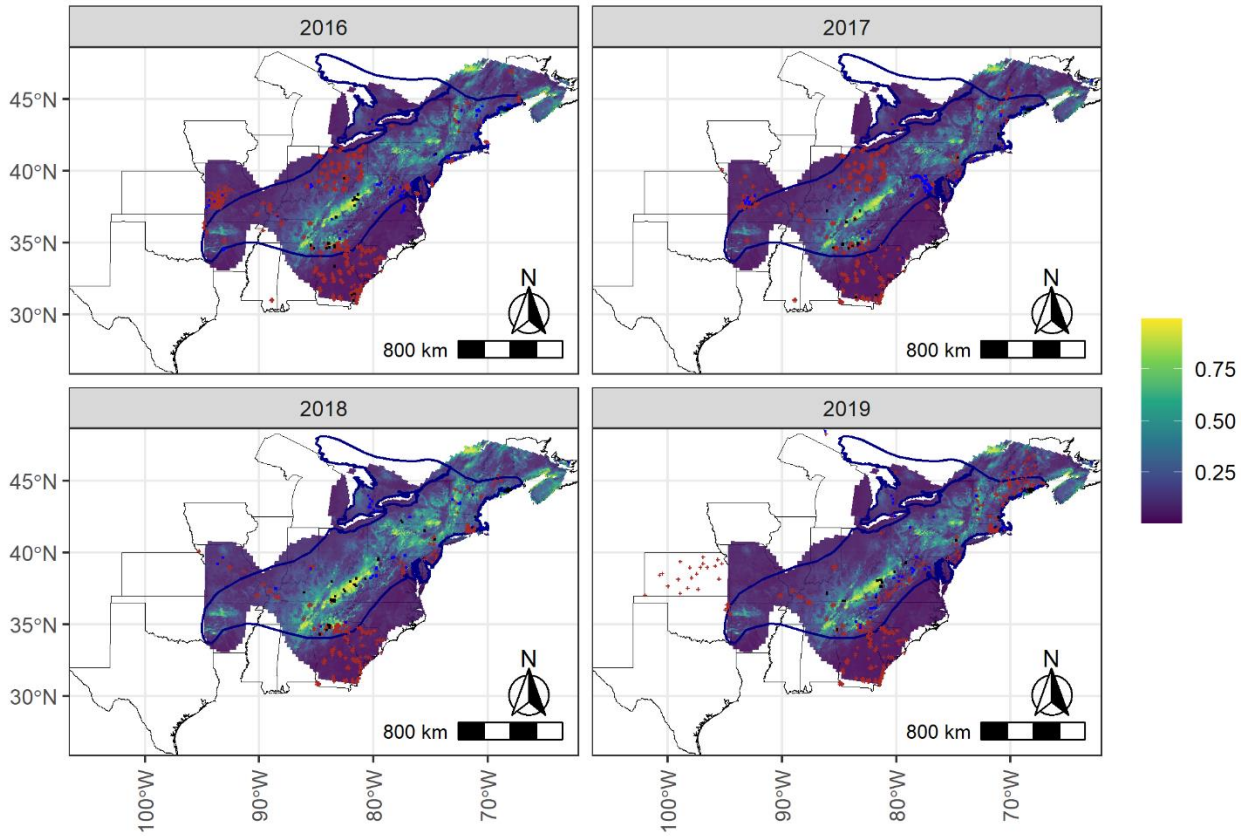

Figure 29. Mean predicted occupancy probabilities for *Myotis leibii* (MYLE) in 2016–2019 predicted for all North American Bat Monitoring Program (NABat) grid cells in the modeled species range based on site-level covariates for each grid cell and year. This is depicted against the reference range map (blue polygon; National Atlas of the United States, 2011) and borders of U.S. states and Canadian provinces/territories. Note, the polygon depicting the reference range is for illustrative purposes only and was not used to bound occupancy probability predictions – instead, the analyses are bound by the geographic scope of monitoring data. The grid cells sampled each year are also displayed based on detection histories as: brown '+' sign = never detected, blue dots = detected with an auto ID, black dots = detected with manual vetting and/or capture.

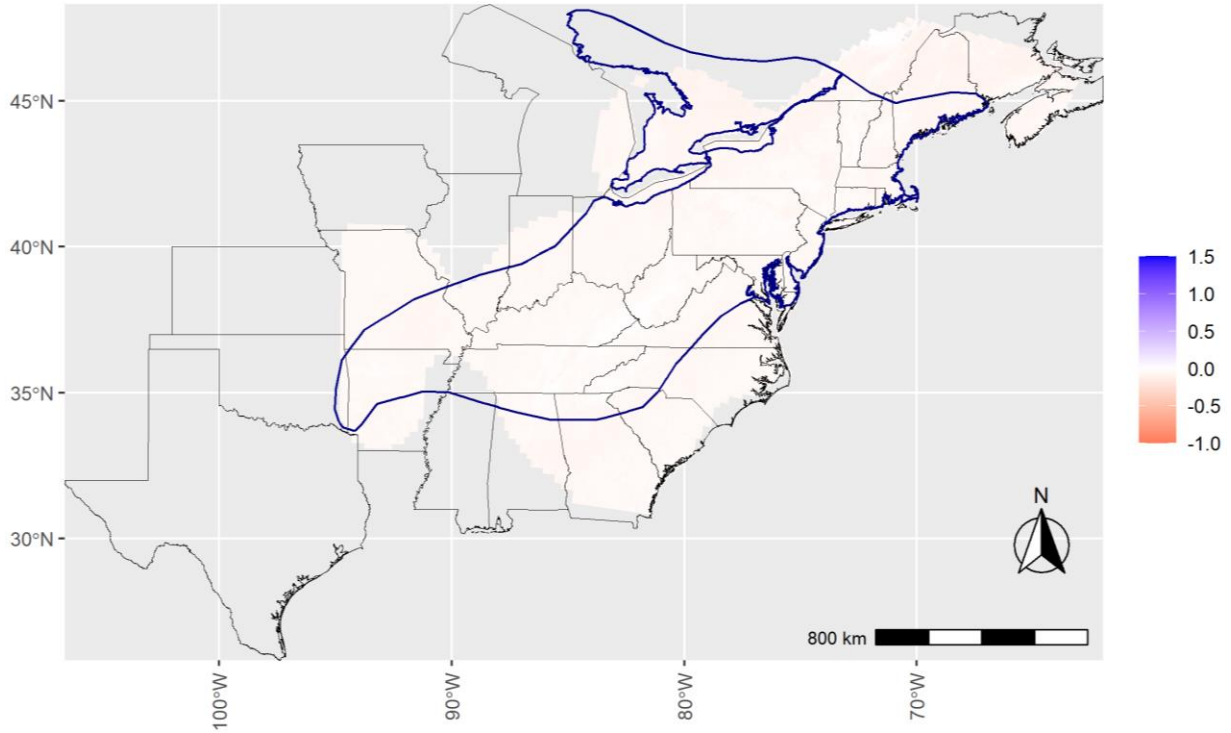

Figure 30. The total change rate in mean grid cell occupancies (color bar) for *Myotis leibii* (MYLE) between 2016 and 2019 for all North American Bat Monitoring Program (NABat) grid cells in the modeled species range based on site-level covariates for each grid cell and year. This is depicted against the reference range map (blue polygon; National Atlas of the United States, 2011) and borders of U.S. states and Canadian provinces/territories. Note, the polygon depicting the reference range is for illustrative purposes only and was not used to bound occupancy probability predictions – instead, the analyses are bound by the geographic scope of monitoring data. For visualization purposes, the upper bound of the scalebar is truncated at 1.5 (150%) and corresponds to values of 1.5 and above, while the lower bound is naturally bounded at -1 (-100%).

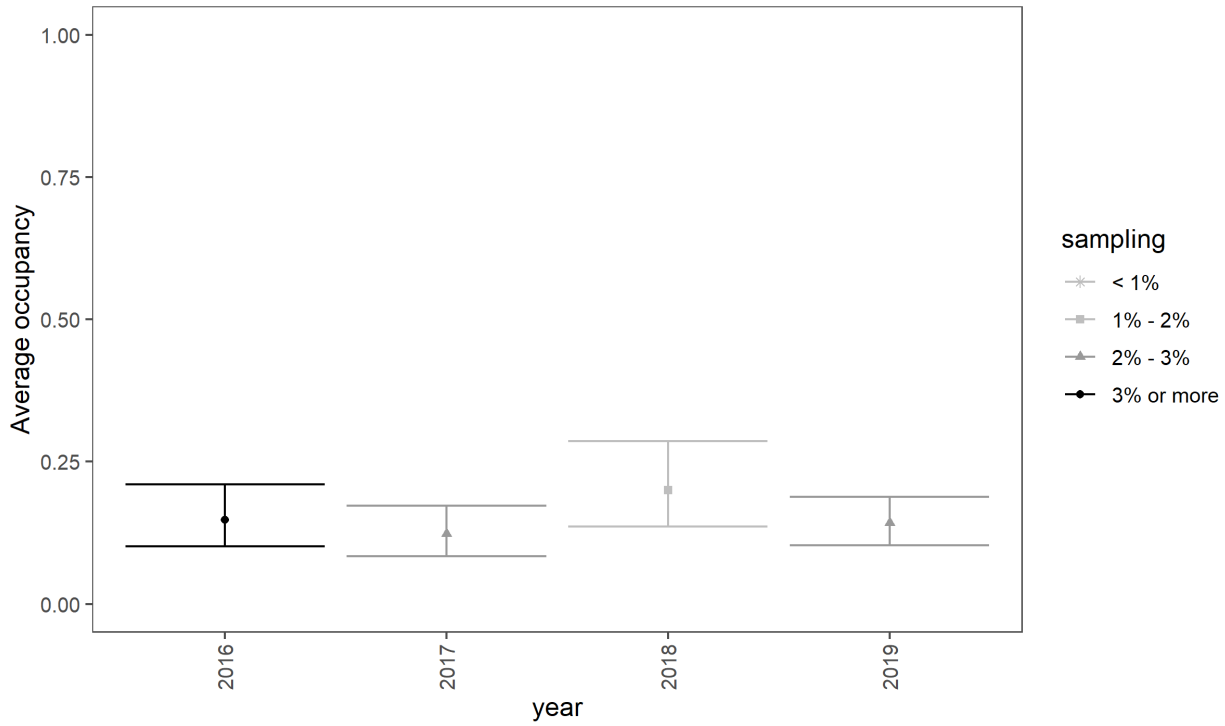

Figure 31. Estimates of the average occupancy probability ($\hat{\psi}_t$) for *Myotis leibii* (MYLE) each year, aggregated across all North American Bat Monitoring Program (NABat) grid cells in modeled range each year. Means (points) and 95% credible intervals (bars) are depicted according to the percent of grid cells sampled in the modeled species range that each year (legend).

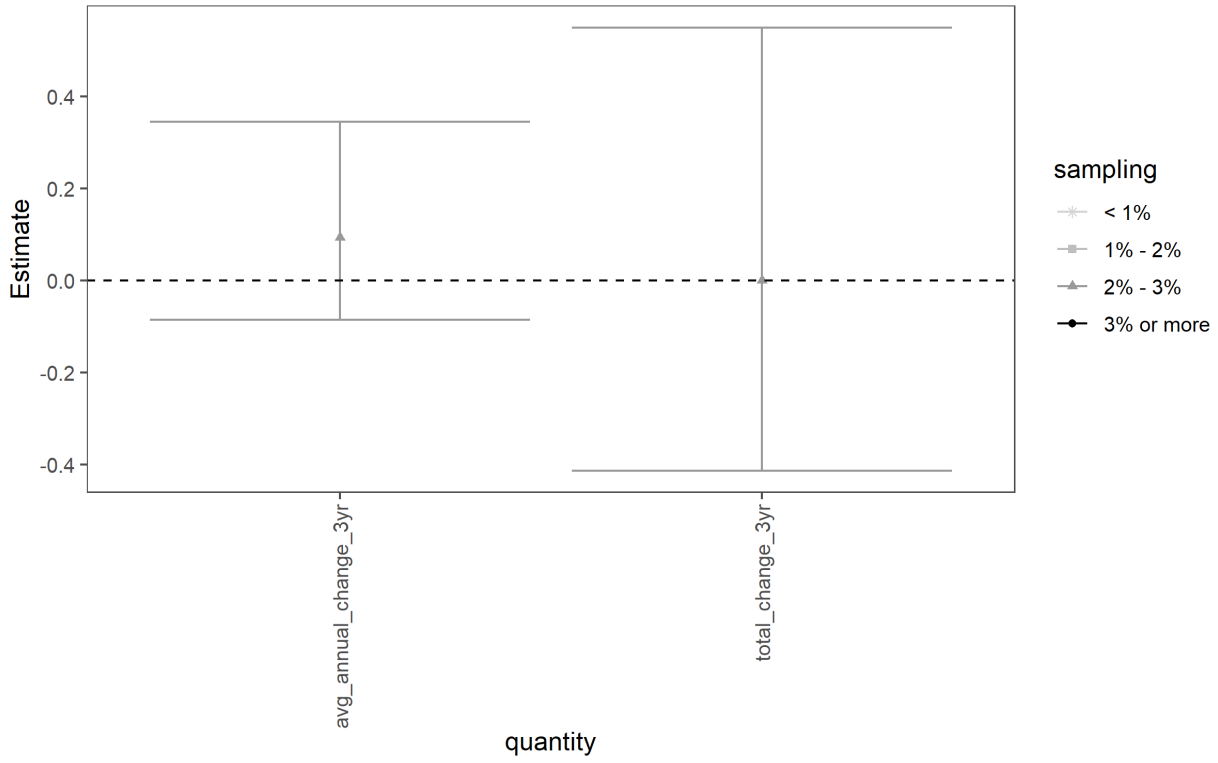

Figure 32. Estimates of average annual change (avg_annual_change = lambda_avg – 1) and total change (total_change = lambda_tot - 1) for *Myotis leibii* (MYLE) over the short-term (2016–2019, three years of change). Means (points) and 95% credible intervals (bars) are depicted according to the percent of grid cells sampled in the modeled species range each year (legend). Note that the 95% credible intervals overlap zero, meaning there is less than 95% certainty that trends in MYLE occupancy different than zero.

Table 15. The numerical values represented in Figure 32 for average annual change and total average change over a short-term (2016–2019, three year) period. CRI = 95% credible interval.

Trend Type	Quantity	Mean	Lower CRI	Upper CRI
Annual	avg_annual_change_3yr	0.0934	-0.0856	0.3456
Total	total_change_3yr	0.0002	-0.4131	0.5495

3.9 *Myotis thysanodes*

(A)

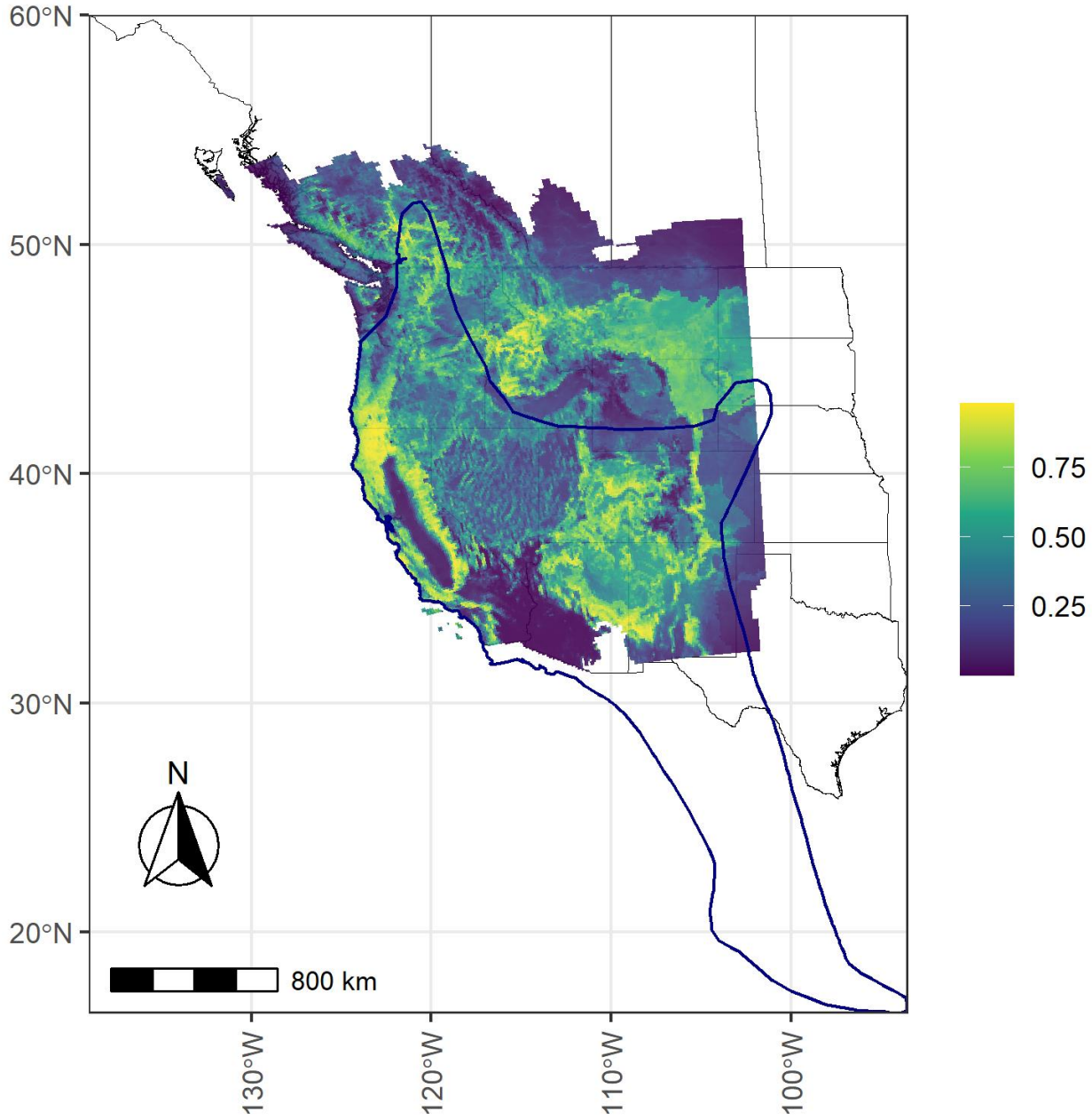

(B)

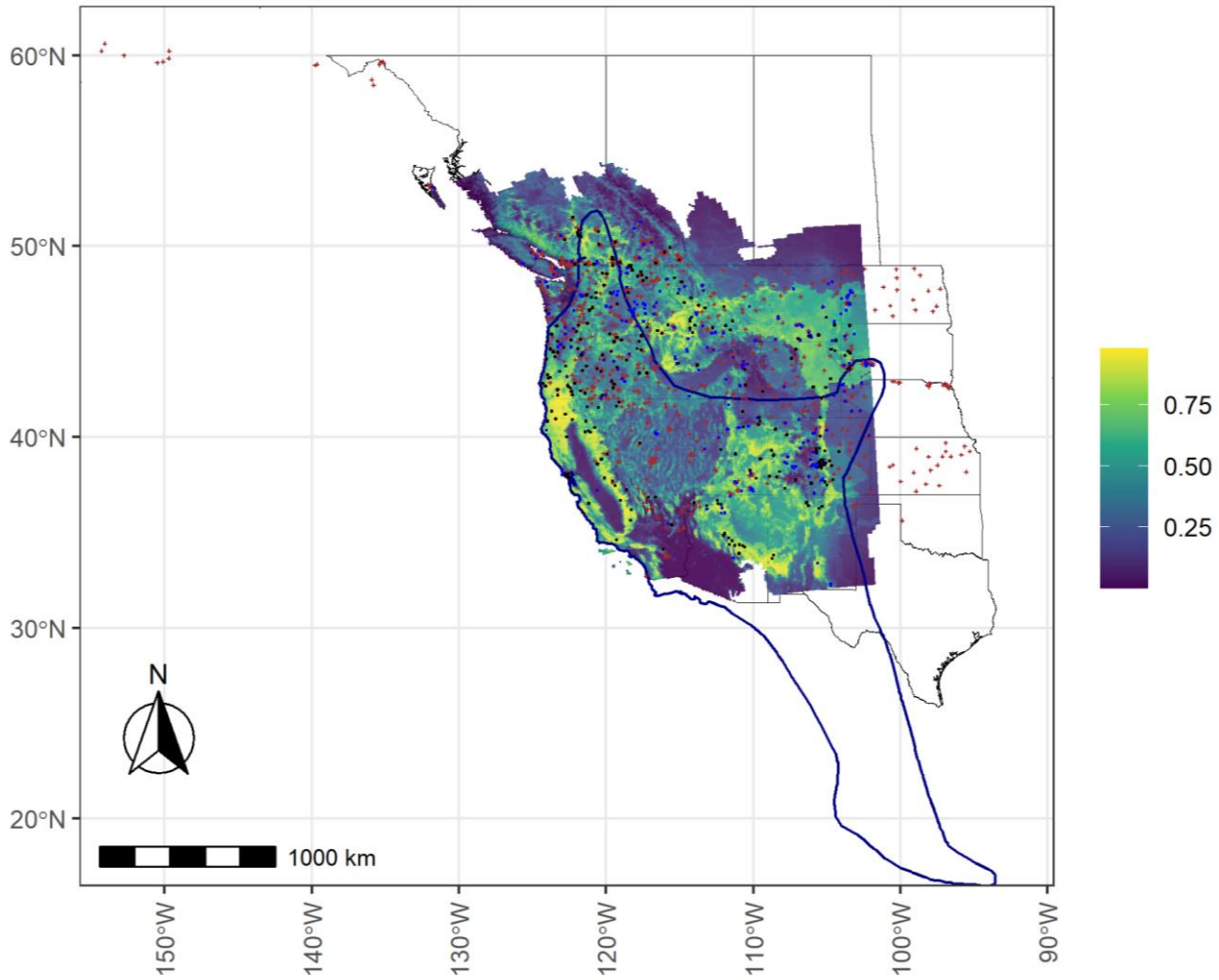

Figure 33. *Myotis thysanodes* (MYTH) mean occupancy probabilities (color bar) predicted in each North American Bat Monitoring Program (NABat) grid cell in the modeled species range for 2019. Probabilities are depicted against the reference range map (blue polygon; National Atlas of the United States, 2011) and borders of U.S. states and Canadian provinces/territories (A and B). Note, the polygon depicting the reference range is for illustrative purposes only and was not used to bound occupancy probability predictions – instead, the analyses are bound by the geographic scope of monitoring data. All sampled locations (2016–2019) and detection summaries are also overlaid (B), including sampled locations where the species was never detected (brown '+' sign), locations where the species was detected at least once by acoustic auto IDs (blue dots), and locations where the species was detected either by manually verified acoustic records or capture data (black dots).

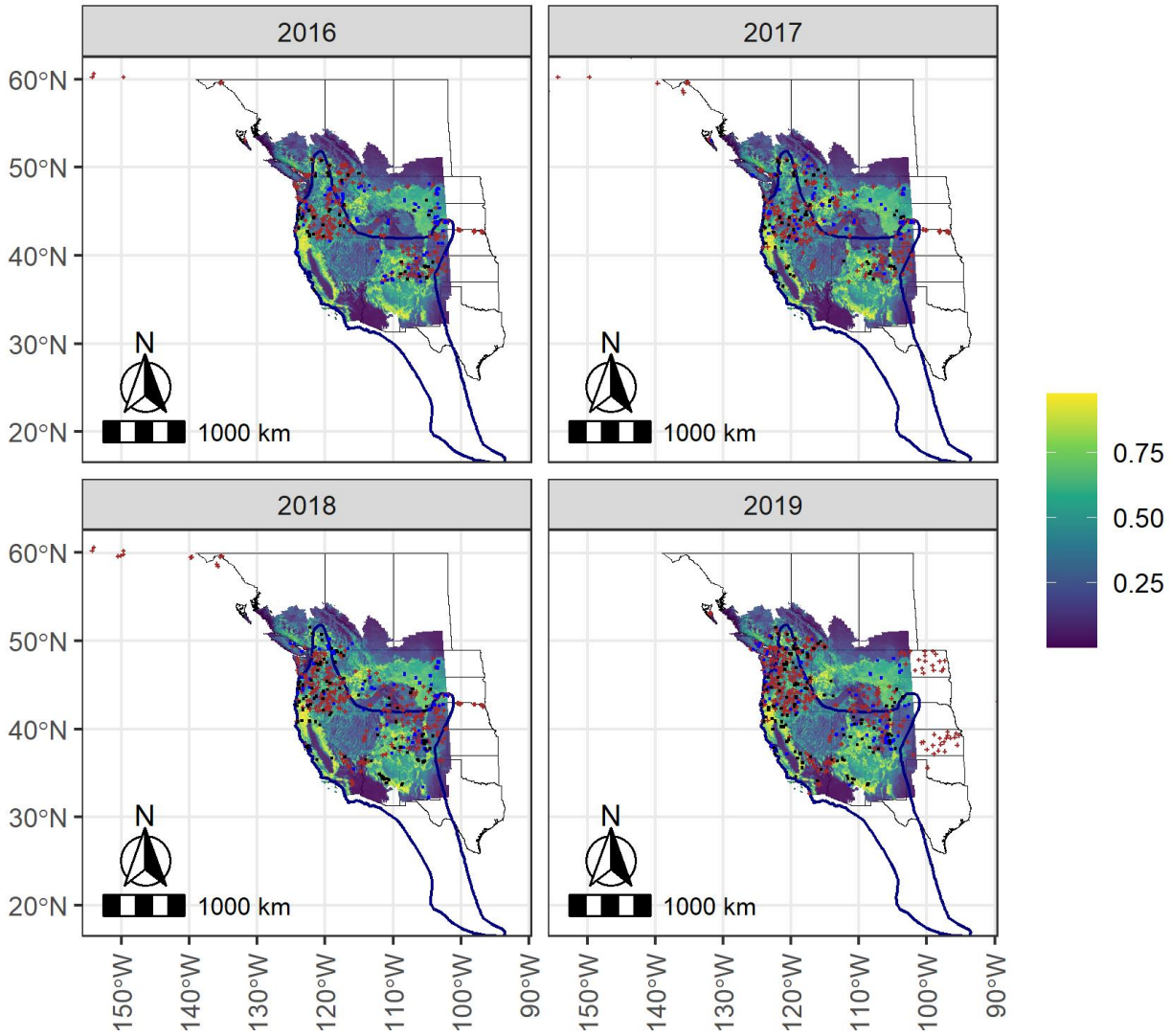

Figure 34. Mean predicted occupancy probabilities of *Myotis thysanodes* (MYTH) in 2016–2019 predicted for all North American Bat Monitoring Program (NABat) grid cells in the modeled species range based on site-level covariates for each grid cell and year. This is depicted against the reference range map (blue polygon; National Atlas of the United States, 2011) and borders of U.S. states and Canadian provinces/territories. Note, the polygon depicting the reference range is for illustrative purposes only and was not used to bound occupancy probability predictions – instead, the analyses are bound by the geographic scope of monitoring data. The grid cells sampled each year are also displayed based on detection histories as: red = never detected, blue = detected with an auto ID, black= detected with manual vetting and/or capture.

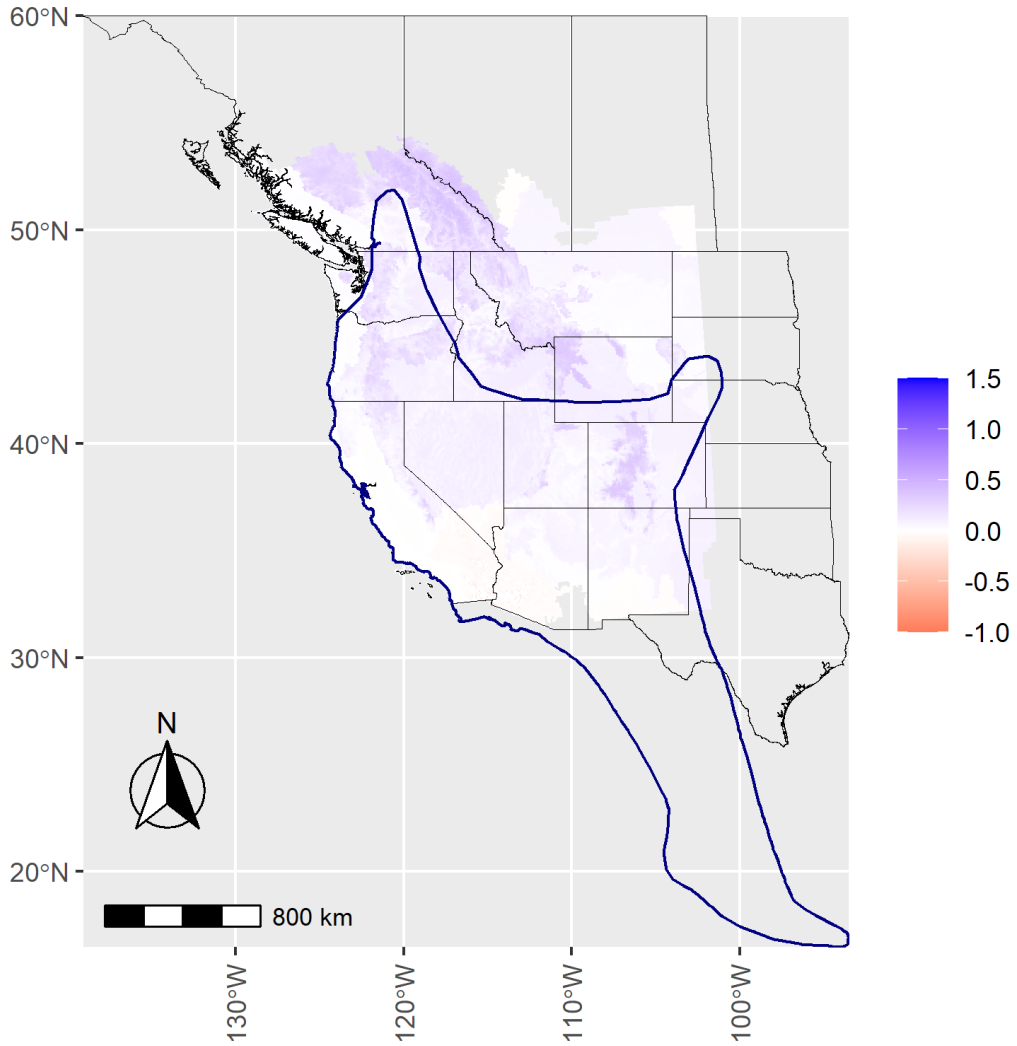

Figure 35. The total change rate in mean grid cell occupancies (color bar) of *Myotis thysanodes* (MYTH) between 2016 and 2019 for all North American Bat Monitoring Program (NABat) grid cells in the modeled species range based on site-level covariates for each grid cell and year. This is depicted against the reference range map (blue polygon; National Atlas of the United States, 2011) and borders of U.S. states and Canadian provinces/territories. Note, the polygon depicting the reference range is for illustrative purposes only and was not used to bound occupancy probability predictions – instead, the analyses are bound by the geographic scope of monitoring data. For visualization purposes, the upper bound of the scalebar is truncated at 1.5 (150%) and corresponds to values of 1.5 and above, while the lower bound is naturally bounded at -1 (-100%).

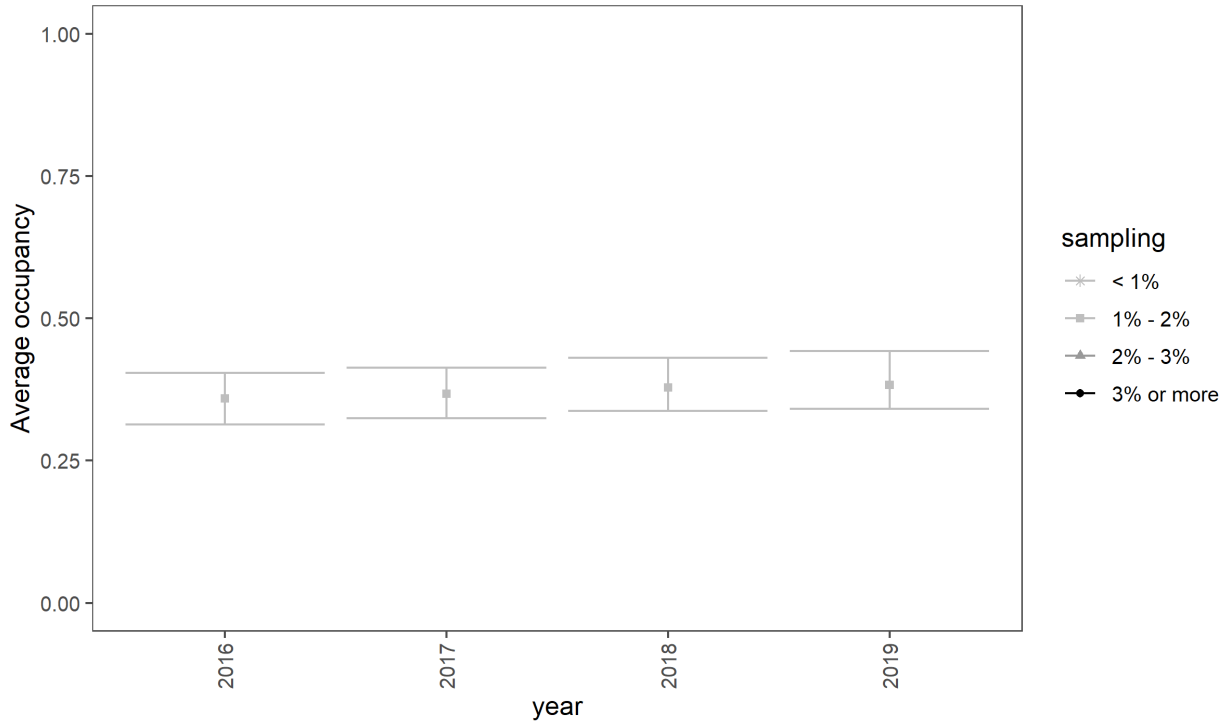

Figure 36. Estimates of the average occupancy probability ($\hat{\psi}_t$) of *Myotis thysanodes* (MYTH) each year, aggregated across all North American Bat Monitoring Program (NABat) grid cells in modeled range each year. Means (points) and 95% credible intervals (bars) are depicted according to the percent of grid cells sampled in the modeled species range each year (legend).

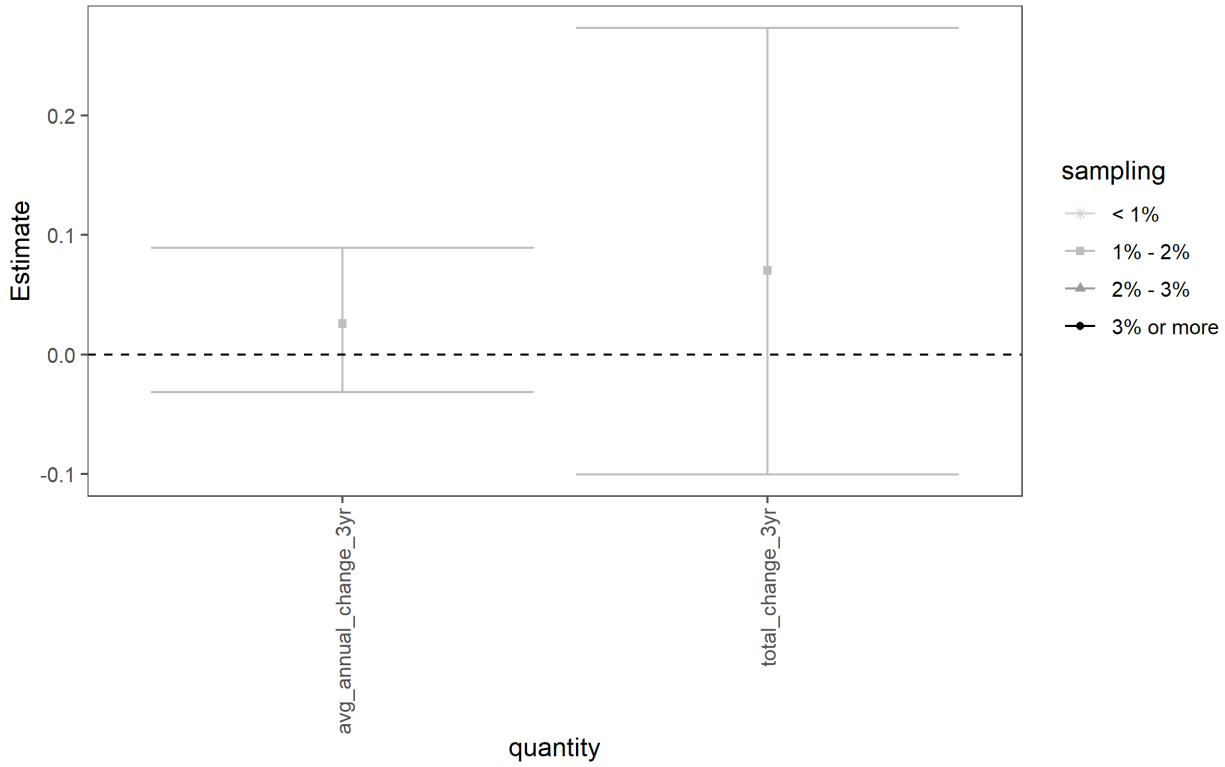

Figure 37. Estimates of average annual change (avg_annual_change = lambda_avg – 1) and total change (total_change = lambda_tot - 1) for *Myotis thysanodes* (MYTH) over the short-term (2016–2019, three years of change). Means (points) and 95% credible intervals (bars) are depicted according to the percent of grid cells sampled in the modeled species range each year (legend). Note that the 95% credible intervals overlap zero, meaning there is less than a 95% certainty that trends in MYTH occupancy are different than zero.

Table 16. The numerical values represented in Figure 37 for average annual change and total average change of *Myotis thysanodes* (MYTH) over a short-term (2016–2019, three year) period. CRI = 95% credible interval.

Trend Type	Quantity	Mean	Lower CRI	Upper CRI
Annual	avg_annual_change_3yr	0.0257	-0.317	0.0892
Total	total_change_3yr	0.0702	-0.1003	0.2731

3.10 *Myotis volans*

(A)

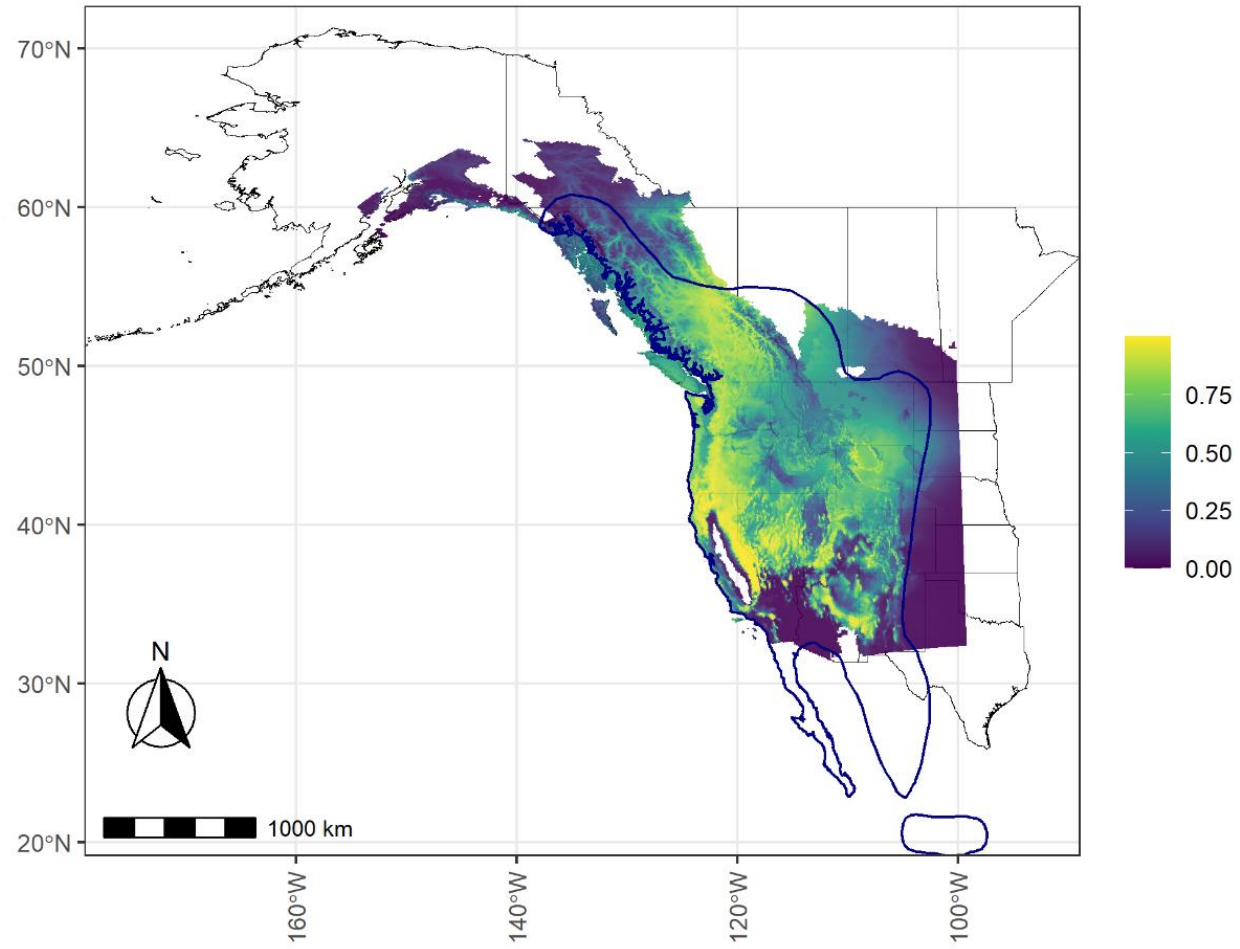

(B)

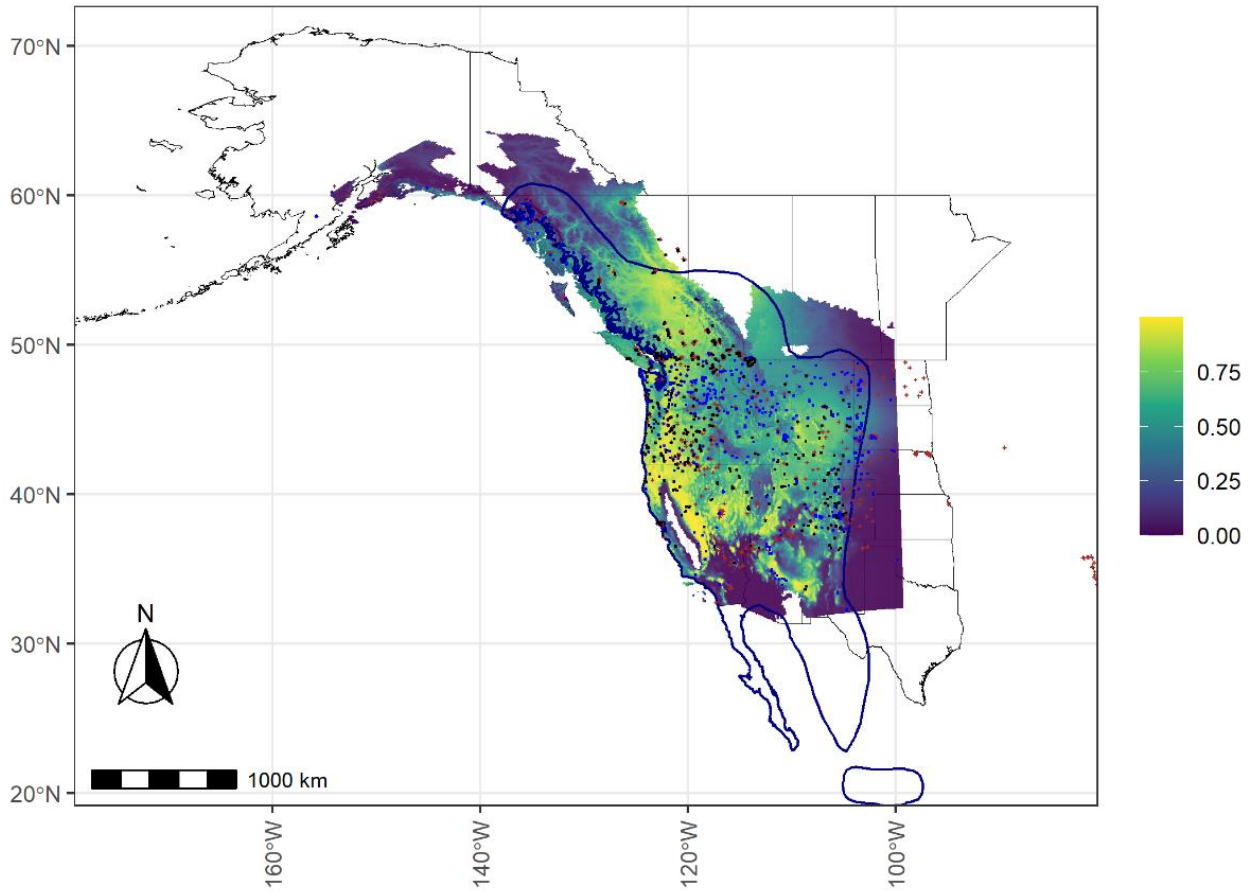

Figure 38. A map of *Myotis volans* (MYVO) mean occupancy probabilities (color bar) predicted in each North American Bat Monitoring Program (NABat) grid cell in the modeled species range for 2019. Probabilities are depicted against the reference range map (blue polygon; National Atlas of the United States, 2011) and borders of U.S. states and Canadian provinces/territories (A and B). Note, the polygon depicting the reference range is for illustrative purposes only and was not used to bound occupancy probability predictions – instead, the analyses are bound by the geographic scope of monitoring data. All sampled locations (2016–2019) and detection summaries are also overlaid (B), including sampled locations where the species was never detected (brown '+' sign), locations where the species was detected at least once by acoustic auto IDs (blue dots), and locations where the species was detected either by manually verified acoustic records or capture data (black dots).

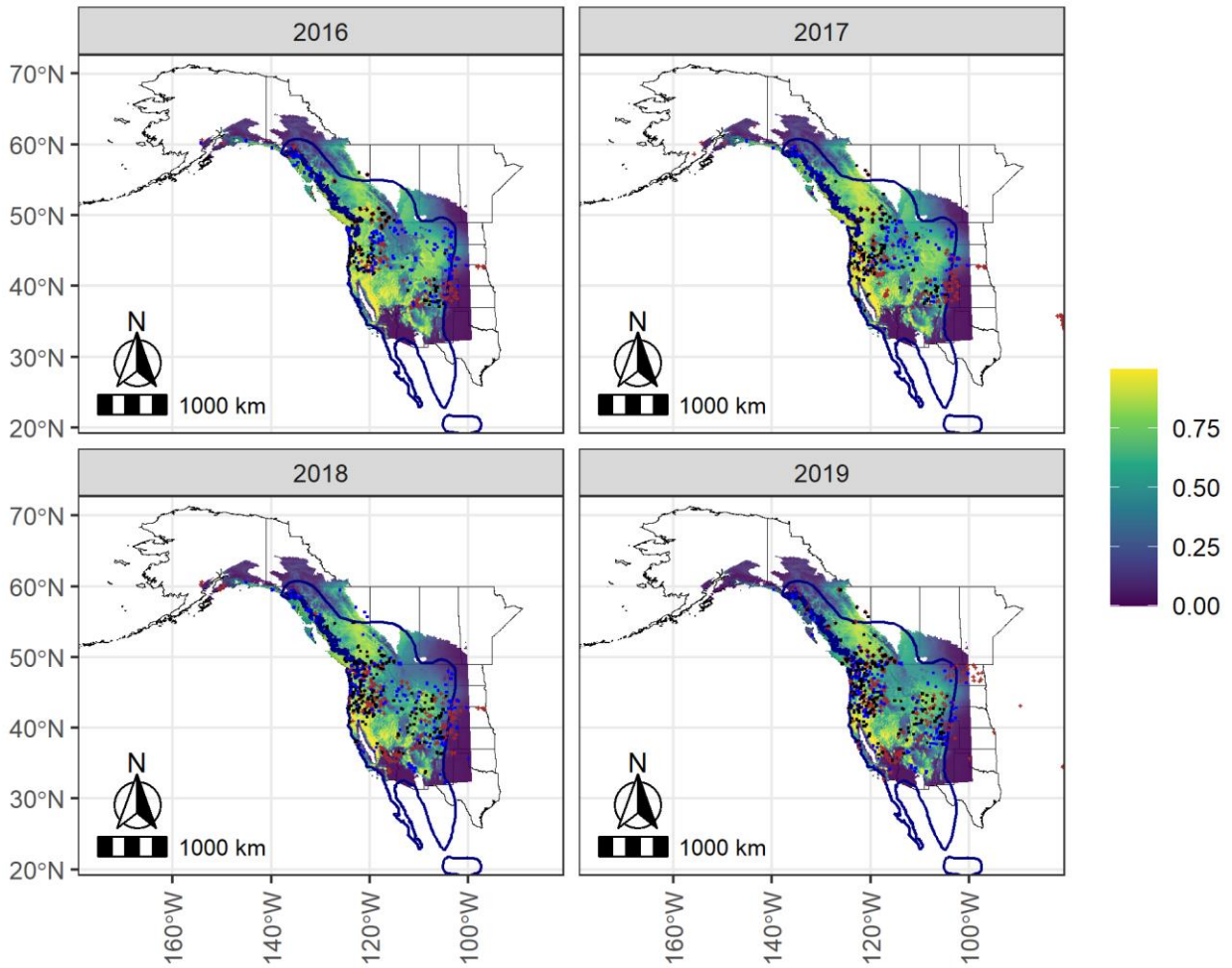

Figure 39. Mean predicted occupancy probabilities of *Myotis volans* (MYVO) in 2016–2019 predicted for all North American Bat Monitoring Program (NABat) grid cells in the modeled species range based on site-level covariates for each grid cell and year. This is depicted against the reference range map (blue polygon; National Atlas of the United States, 2011) and borders of U.S. states and Canadian provinces/territories. Note, the polygon depicting the reference range is for illustrative purposes only and was not used to bound occupancy probability predictions – instead, the analyses are bound by the geographic scope of monitoring data. The grid cells sampled each year are also displayed based on detection histories as: brown '+' sign = never detected, blue dots = detected with an auto ID, black dots = detected with manual vetting and/or capture.

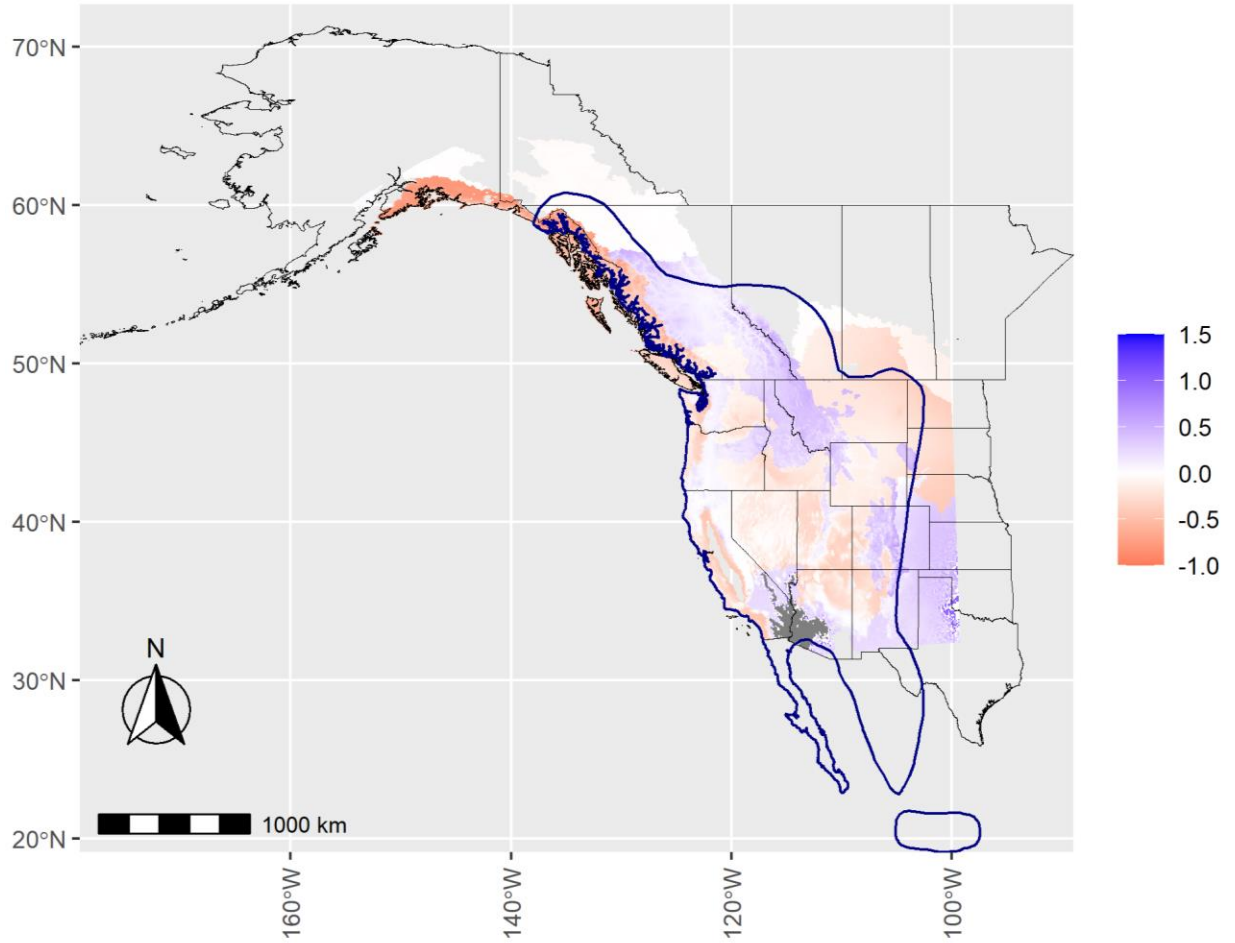

Figure 40. The total change rate in mean grid cell occupancies (color bar) for *Myotis volans* (MYVO) between 2016 and 2019 for all North American Bat Monitoring Program (NABat) grid cells in the modeled species range based on site-level covariates for each grid cell and year. This is depicted against the reference range map (blue polygon; National Atlas of the United States, 2011) and borders of U.S. states and Canadian provinces/territories. Note, the polygon depicting the reference range is for illustrative purposes only and was not used to bound occupancy probability predictions – instead, the analyses are bound by the geographic scope of monitoring data. For visualization purposes, the upper bound of the scalebar is truncated at 1.5 (150%) and corresponds to values of 1.5 and above, while the lower bound is naturally bounded at -1 (-100%).

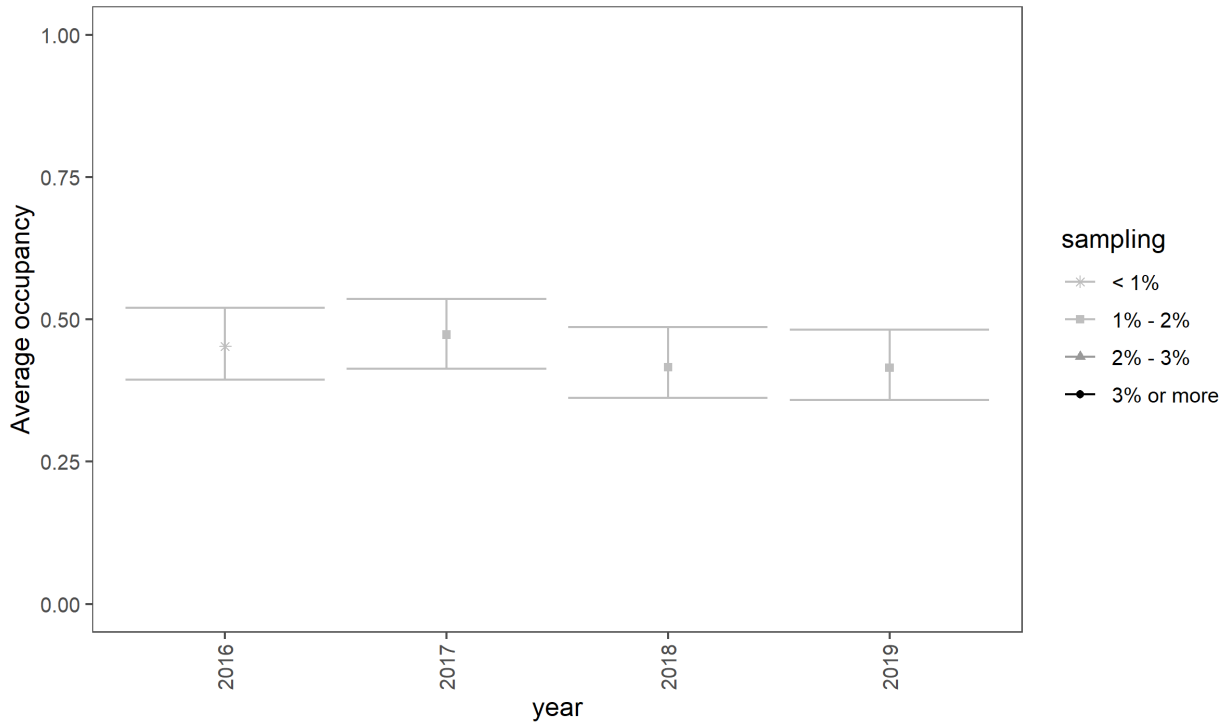

Figure 41. Estimates of the average occupancy probability ($\hat{\psi}_t$) of *Myotis volans* (MYVO) each year, aggregated across all North American Bat Monitoring Program (NABat) grid cells in modeled range each year. Means (points) and 95% credible intervals (bars) are depicted according to the percent of grid cells sampled in the modeled species range each year (legend).

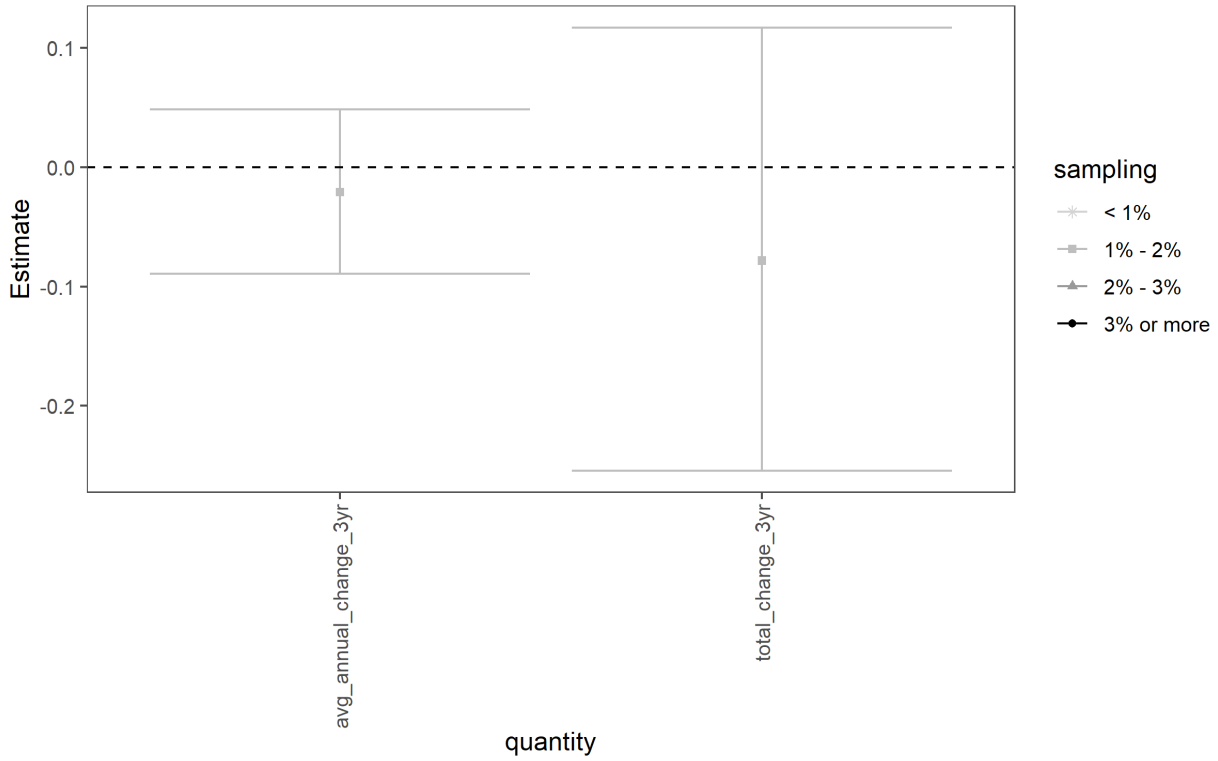

Figure 42. Estimates of average annual change (avg_annual_change = lambda_avg – 1) and total change (total_change = lambda_tot - 1) for *Myotis volans* (MYVO) over the short-term (2016–2019, three years of change). Means (points) and 95% credible intervals (bars) are depicted according to the percent of grid cells sampled in the modeled species range each year (legend). Note that the 95% credible intervals overlap zero, meaning there is less than 95% certainty that trends in MYVO occupancy are different than zero.

Table 17. The numerical values represented in Figure 42 for average annual change and total average change over a short-term (2016–2019, three year) period. CRI = 95% credible interval.

Trend Type	Quantity	Mean	Lower CRI	Upper CRI
Annual	avg_annual_change_3yr	-0.0209	-0.0894	0.0486
Total	total_change_3yr	-0.0783	-0.2544	0.1170

3.11 *Myotis yumanensis*

(A)

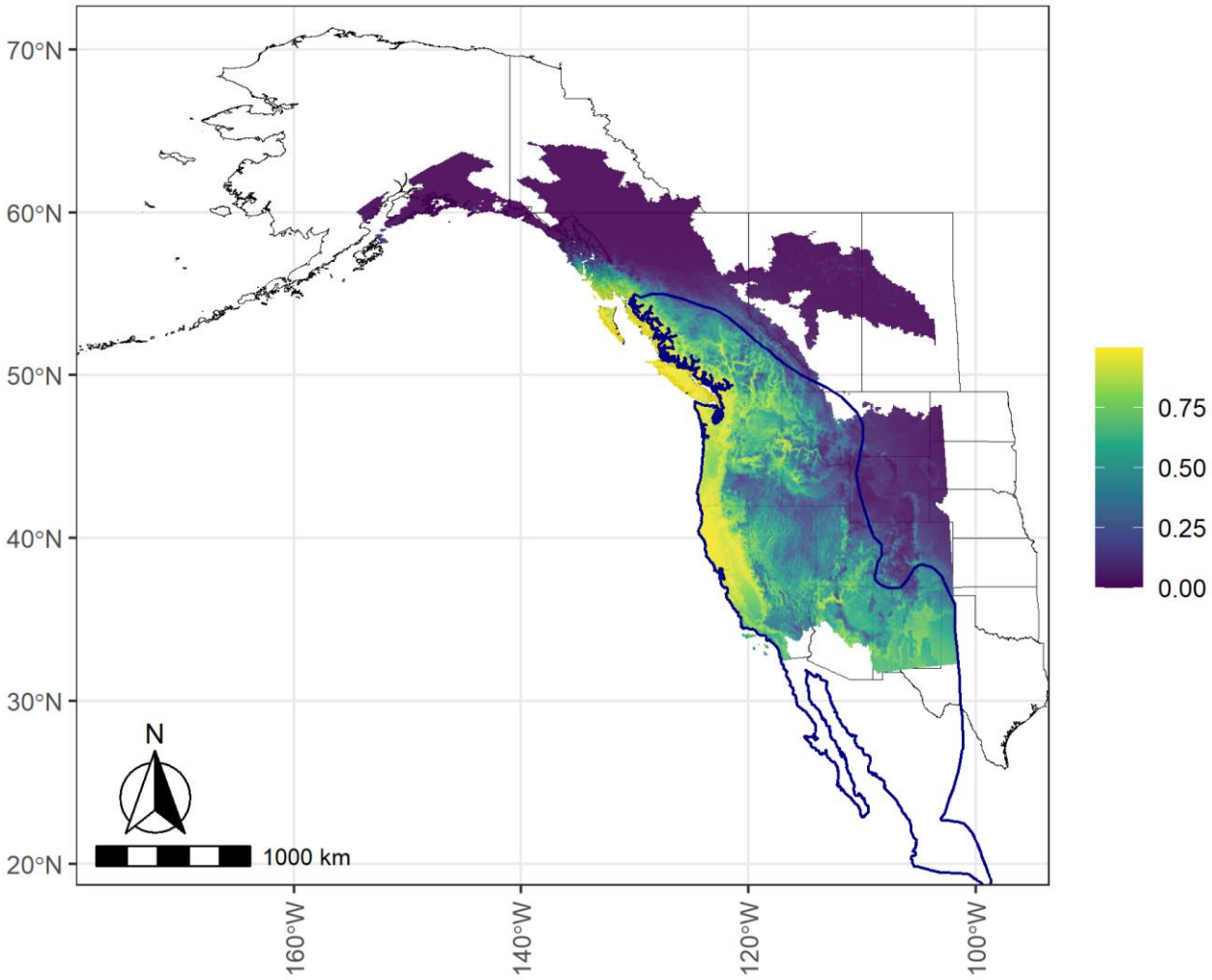

(B)

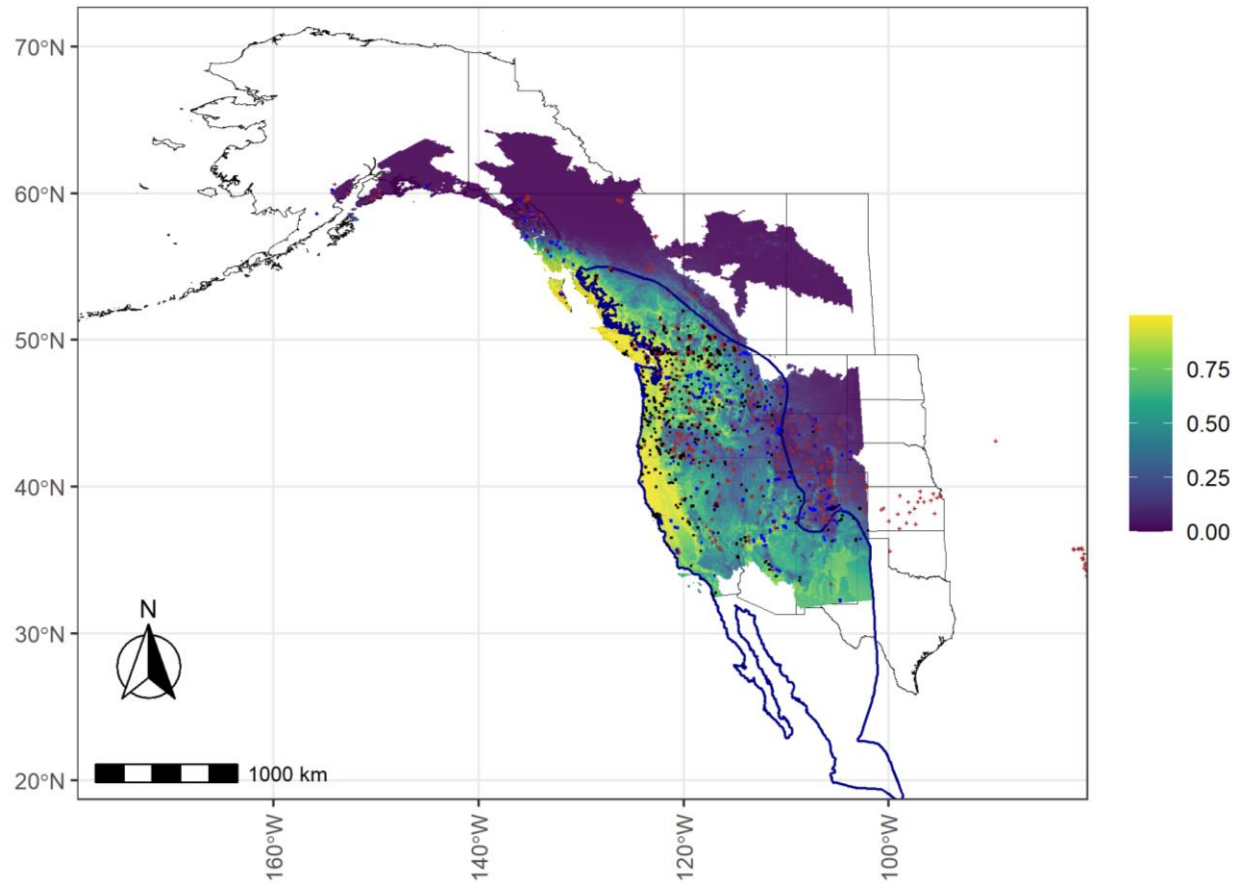

Figure 43. *Myotis yumanensis* (MYYU) mean occupancy probabilities (color bar) predicted in each North American Bat Monitoring Program (NABat) grid cell in the modeled species range for 2019. Probabilities are depicted against the reference range map (blue polygon; National Atlas of the United States 2011) and borders of U.S. states and Canadian provinces/territories (A and B). Note, the polygon depicting the reference range is for illustrative purposes only and was not used to bound occupancy probability predictions – instead, the analyses are bound by the geographic scope of monitoring data. All sampled locations (2016–2019) and detection summaries are also overlaid (B), including sampled locations where the species was never detected (brown '+' sign), locations where the species was detected at least once by acoustic auto IDs (blue dots), and locations where the species was detected either by manually verified acoustic records or capture data (black dots).

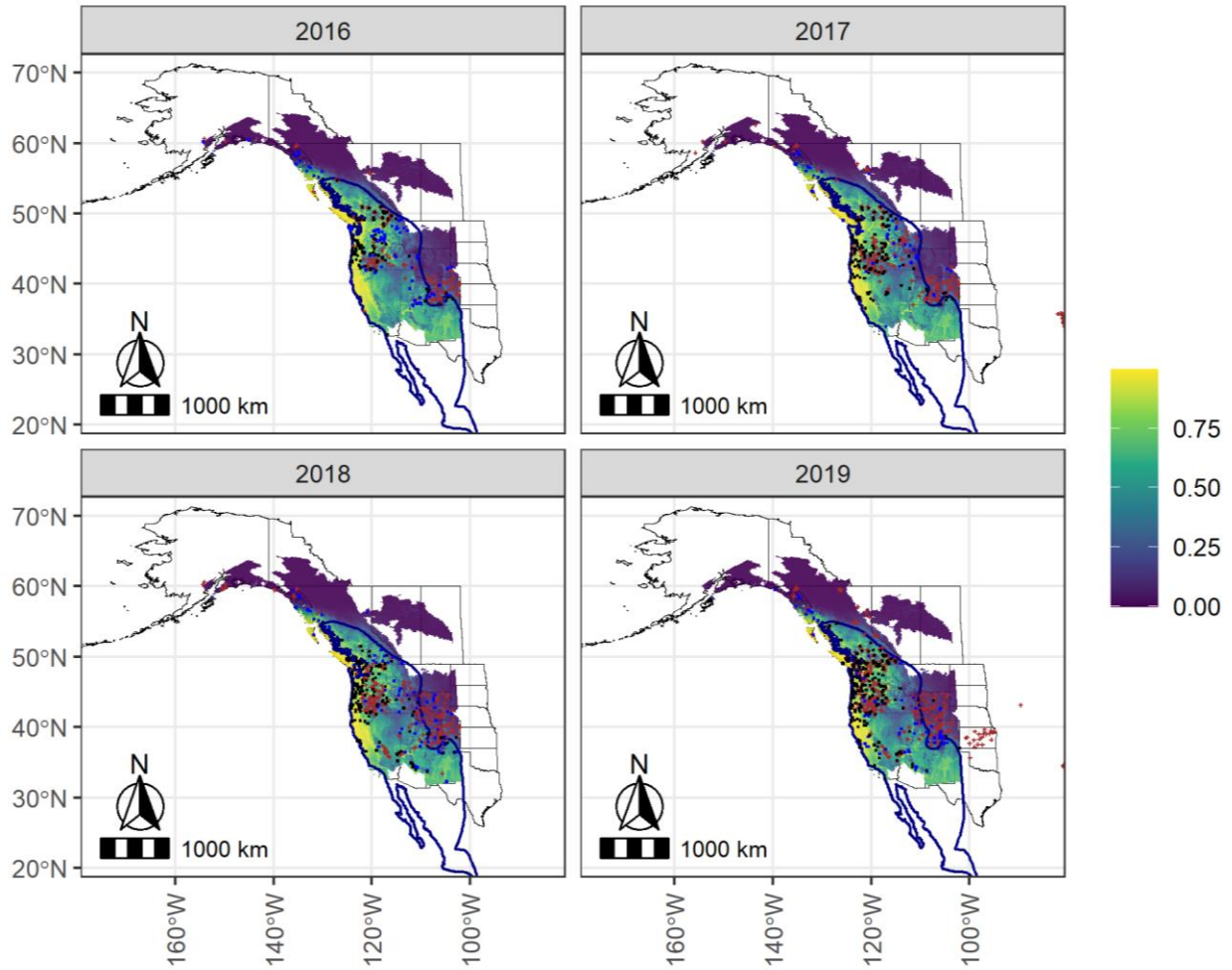

Figure 44. Mean predicted occupancy probabilities of *Myotis yumanensis* (MYYU) in 2016–2019 predicted for all North American Bat Monitoring Program (NABat) grid cells in the modeled species range based on site-level covariates for each grid cell and year. This is depicted against the reference range map (blue polygon; National Atlas of the United States, 2011) and borders of U.S. states and Canadian provinces/territories. Note, the polygon depicting the reference range is for illustrative purposes only and was not used to bound occupancy probability predictions – instead, the analyses are bound by the geographic scope of monitoring data. The grid cells sampled each year are also displayed based on detection histories as: brown '+' sign = never detected, blue dots = detected with an auto ID, black dots= detected with manual vetting and/or capture.

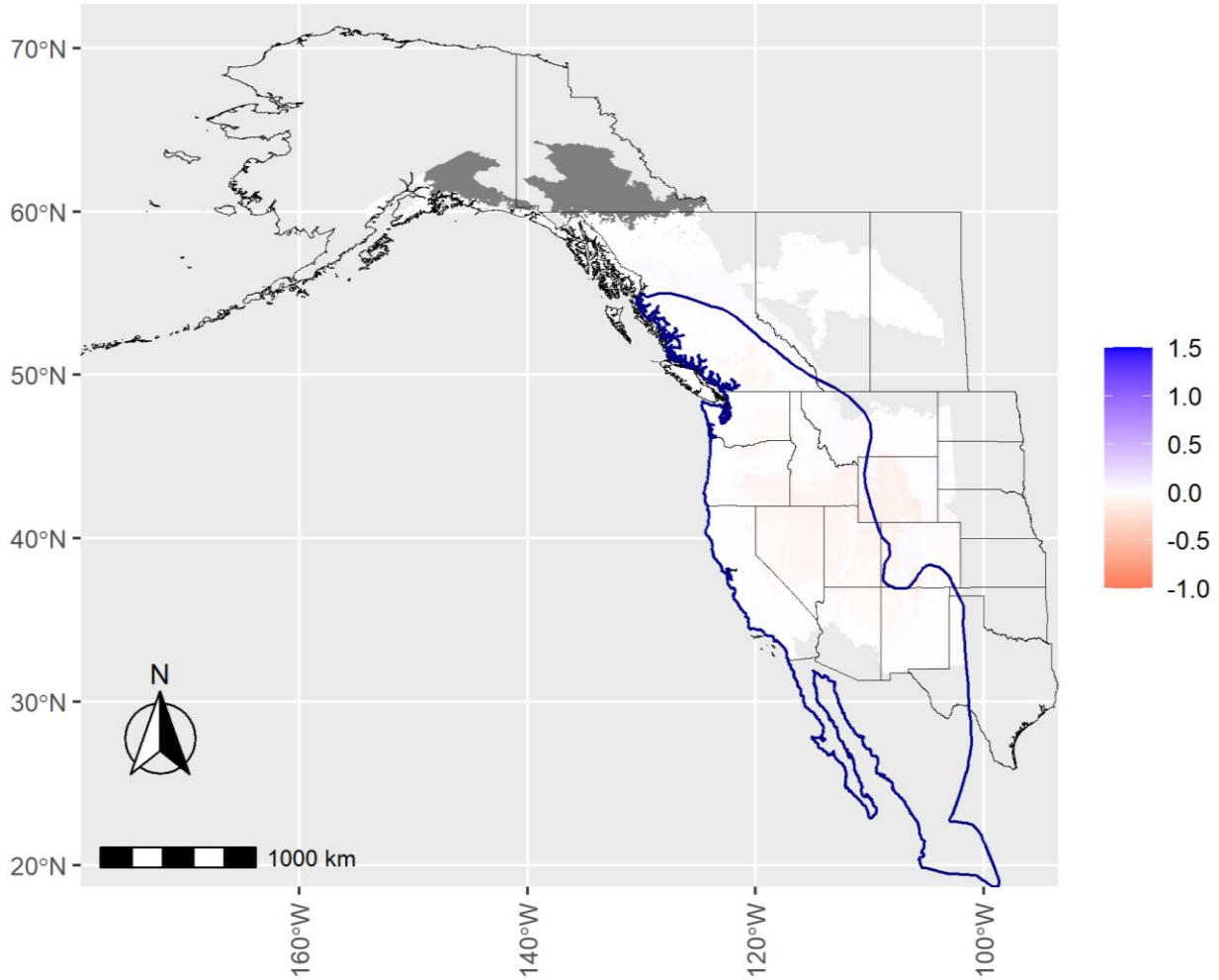

Figure 45. The total change rate in mean grid cell occupancies (color bar) of *Myotis yumanensis* (MYYU) between 2016 and 2019 for all North American Bat Monitoring Program (NABat) grid cells in the modeled species range based on site-level covariates for each grid cell and year. This is depicted against the reference range map (blue polygon; National Atlas of the United States, 2011) and borders of U.S. states and Canadian provinces/territories. Note, the polygon depicting the reference range is for illustrative purposes only and was not used to bound occupancy probability predictions – instead, the analyses are bound by the geographic scope of monitoring data. For visualization purposes, the upper bound of the scalebar is truncated at 1.5 (150%) and corresponds to values of 1.5 and above, while the lower bound is naturally bounded at -1 (-100%).

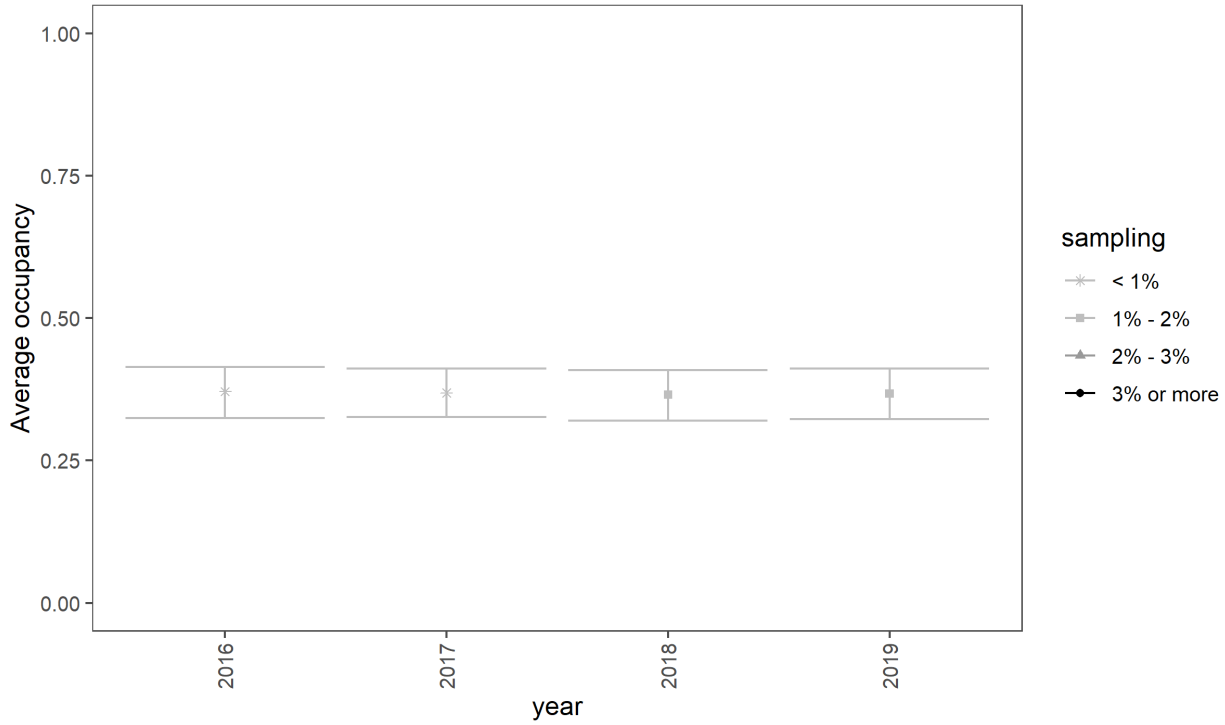

Figure 46. Estimates of the average occupancy probability ($\hat{\psi}_t$) of *Myotis yumanensis* (MYYU) each year, aggregated across all North American Bat Monitoring Program (NABat) grid cells in modeled range each year. Means (points) and 95% credible intervals (bars) are depicted according to the percent of grid cells sampled in the modeled species range each year (legend).

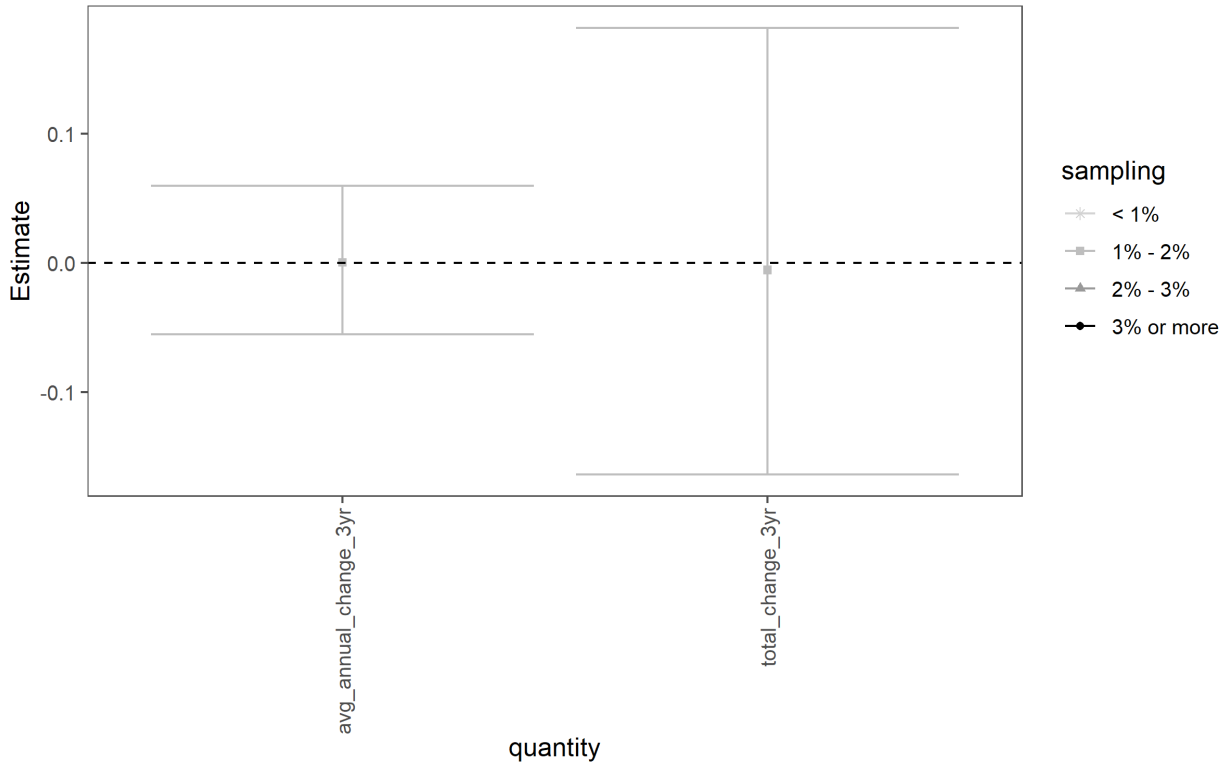

Figure 47. Estimates of average annual change (avg_annual_change = lambda_avg – 1) and total change (total_change = lambda_tot - 1) of *Myotis yumanensis* (MYYU) over the short-term (2016–2019, three years of change). Means (points) and 95% credible intervals (bars) are depicted according to the percent of grid cells sampled in the modeled species range each year (legend). Note that the 95% credible intervals overlap zero, meaning there is less than 95% certainty that trends in MYYU occupancy are different than zero.

Table 18. The numerical values represented in Figure 47 for average annual change and total average change over a short-term (2016–2019, three year) period. CRI= 95% credible interval.

Trend Type	Quantity	Mean	Lower CRI	Upper CRI
Annual	avg_annual_change_3yr	0.0006	-0.0551	0.0598
Total	total_change_3yr	-0.0054	-0.1635	0.1819

3.12 Inconclusive Results

The results for three species (*Eptesicus fuscus, Lasionycteris noctivagans, Lasiurus cinereus*), were inconclusive due to 1) borderline convergence issues in the model fitting procedure leading to potentially unreliable estimates, 2) largely uninformative covariates for occupancy and detectability, which led to both estimation and prediction issues, and 3) failure to reliably distinguish between false positives and true positives for ambiguous species detections. All three species required very long model runs (in comparison to species with similar amounts for data) to achieve convergence. A high degree of autocorrelation in the MCMC chains led to very slow mixing and low effective sample sizes, which can indicate issues with model identifiability (Ogle and Barber 2020) or multi-modality in posterior distributions.

Monitoring effort (the length of the detection history aggregated over each 7-day observation period) was estimated to have large effect sizes, while most other detection covariates had effect sizes near zero (Appendix C.10 – C.12). Whether the lack of informative detection covariates reflects species behavior or analytical limitations is unclear, but this resulted in a poor ability of the model to distinguish between true positive and false positive detections in the ambiguous detection data of two species (*Eptesicus fuscus* and *Lasiurus cinereus*; Appendix D.10 -D.11). Thus, relatively little information was gleaned about species occupancy from these detections. Furthermore, there were large geographic biases in the unambiguous data compared to ambiguous detections for all 3 species, with mostly unambiguous detections in the west, and ambiguous detections in the east.

An additional consideration for these species was that effects of ecoregions largely overpowered all other grid cell level covariates (e.g., physiographic diversity, elevation) for predicting species' occupancy. This was despite the use of regularization priors to minimize the strength of these effects (Appendix A.2). Predictions for occupancy probabilities in space and time were largely driven by ecoregion effects, resulting in mostly homogenous occupancy probabilities within each ecoregion and year, and unrealistic hard boundaries between ecoregions. There were also large swings in ecoregion effects over time, which led to trends of especially large magnitude compared to trends for the other nine species evaluated. While these swings could be driven by species' movement behavior and differences in space use from year to year, they could also be driven by sampling artifacts compounded with otherwise weak predictors to explain spatiotemporal variation.

Finally, there are common estimation issues with false-positive occupancy models that must be overcome by either including site-level confirmation data, observation-level confirmation data, or parameter constraints (e.g., constraining detectability to be greater than the false-positive rate, Royle and Link 2006, Chambert et al. 2015). Furthermore, simply collecting more data to obtain larger sample sizes does not help overcome limitations of false-positives; in fact, according to the third law of mark-recapture (Kéry and Royle 2020) and its corollary: "the problem of false positives does not vanish as sample sizes grow, quite on the contrary, more false positive errors accumulate when more surveys are conducted." These three species are relatively widespread throughout North America and are often included in species lists when processing acoustic monitoring files. They also had the most data collected from 2016-2019 (Table 9), comparable in total sample size to MYLU, MYSE, and PESU, but with only 4 years of monitoring data. We used a combination of site-level confirmation data and parameter constraints when fitting species occupancy models, and the addition of the parameter constraints improved model estimation for the other 9 species. However, it could be that these parameter constraints are too restrictive for EPFU, LACI, and LANO, especially when aggregating detections at 7-day periods.

3.12.1 *Eptesicus fuscus*

(A)

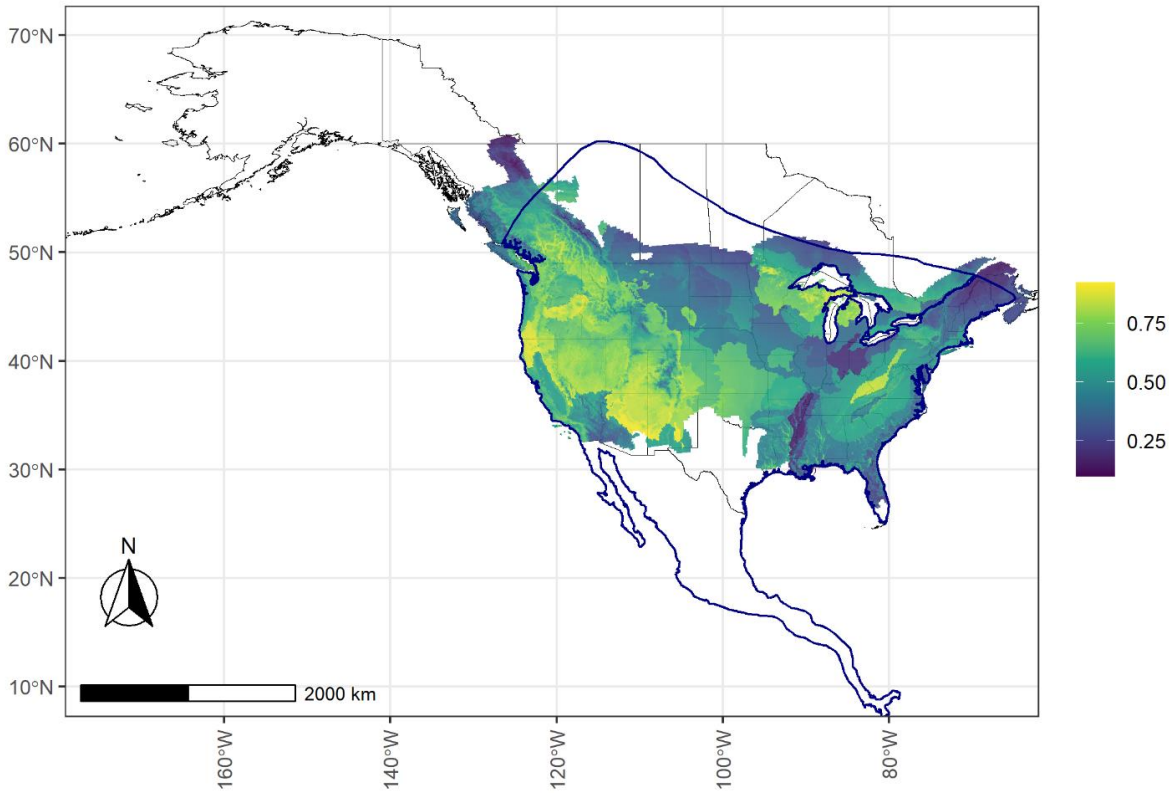

(B)

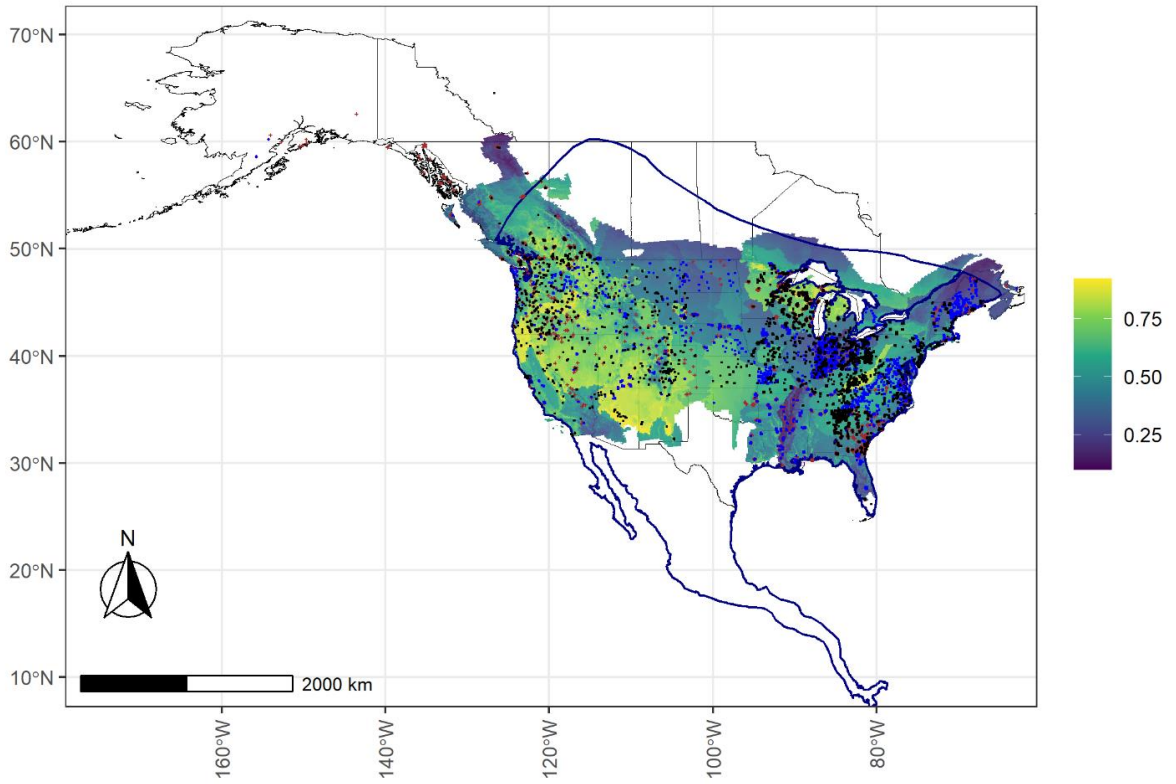

Figure 48. A map of *Eptesicus fuscus* (EPFU) mean occupancy probabilities (color bar) predicted in each North American Bat Monitoring Program (NABat) grid cell in the modeled species range for 2019. Probabilities are depicted against the reference range map (blue polygon; National Atlas of the United States, 2011) and borders of U.S. states and Canadian provinces/territories (A and B). Note, the polygon depicting the reference range is for illustrative purposes only and was not used to bound occupancy probability predictions – instead, the analyses are bound by the geographic scope of monitoring data. All sampled locations (2016–2019) and detection summaries are also overlaid (B), including sampled locations where the species was never detected (brown '+' sign), locations where the species was detected at least once by acoustic auto IDs (blue dots), and locations where the species was detected either by manually verified acoustic records or capture data (black dots). Note the results for EPFU were inconclusive due to issues reported in section 3.12.

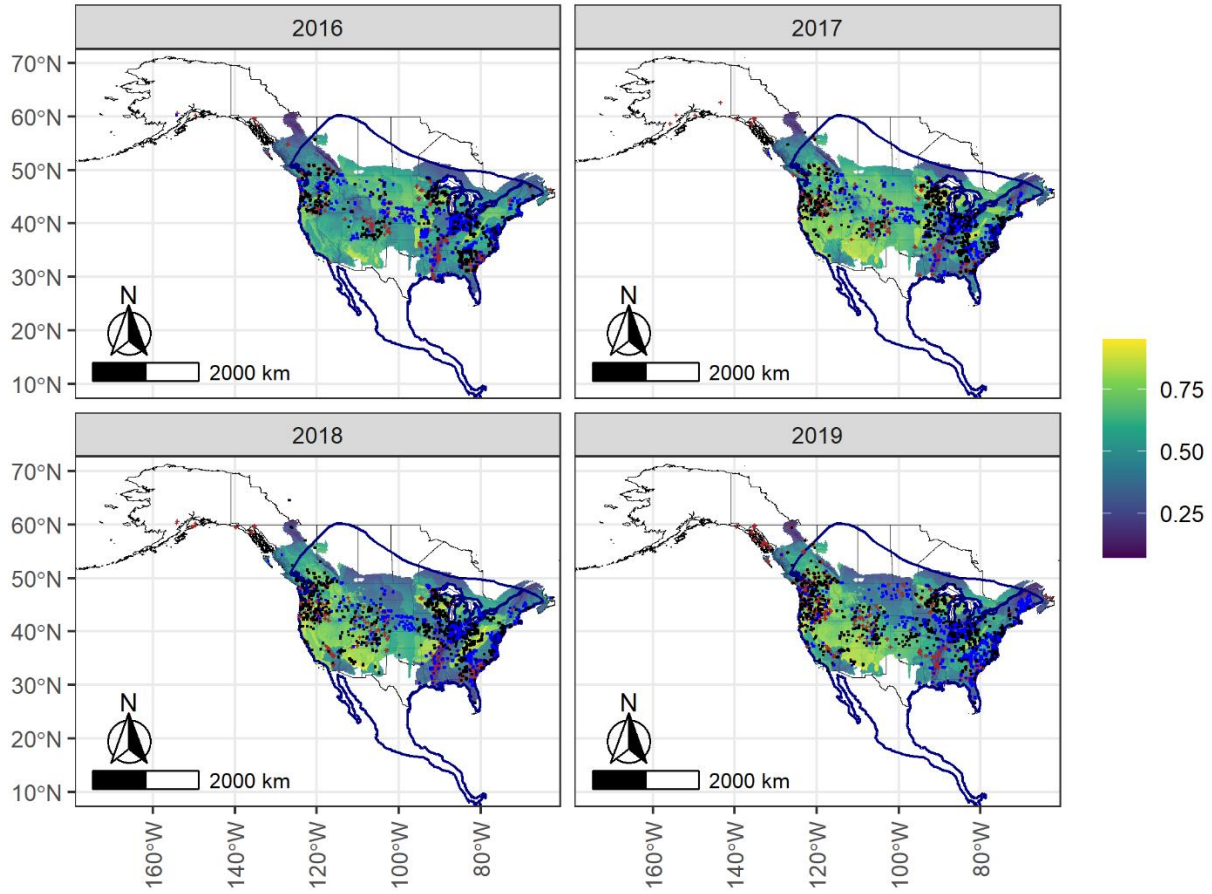

Figure 49. Mean predicted occupancy probabilities for *Eptesicus fuscus* (EPFU) in 2016–2019 predicted for all NABat grid cells in the modeled species range based on site-level covariates for each grid cell and year. This is depicted against the reference range map (blue polygon; National Atlas of the United States, 2011) and borders of U.S. states and Canadian provinces/territories. Note, the polygon depicting the reference range is for illustrative purposes only and was not used to bound occupancy probability predictions – instead, the analyses are bound by the geographic scope of monitoring data. The grid cells sampled each year are also displayed based on detection histories as: brown '+' sign = never detected, blue dots = detected with an auto ID, black dots = detected with manual vetting and/or capture. Note the results for EPFU were inconclusive due to issues reported in section 3.12.

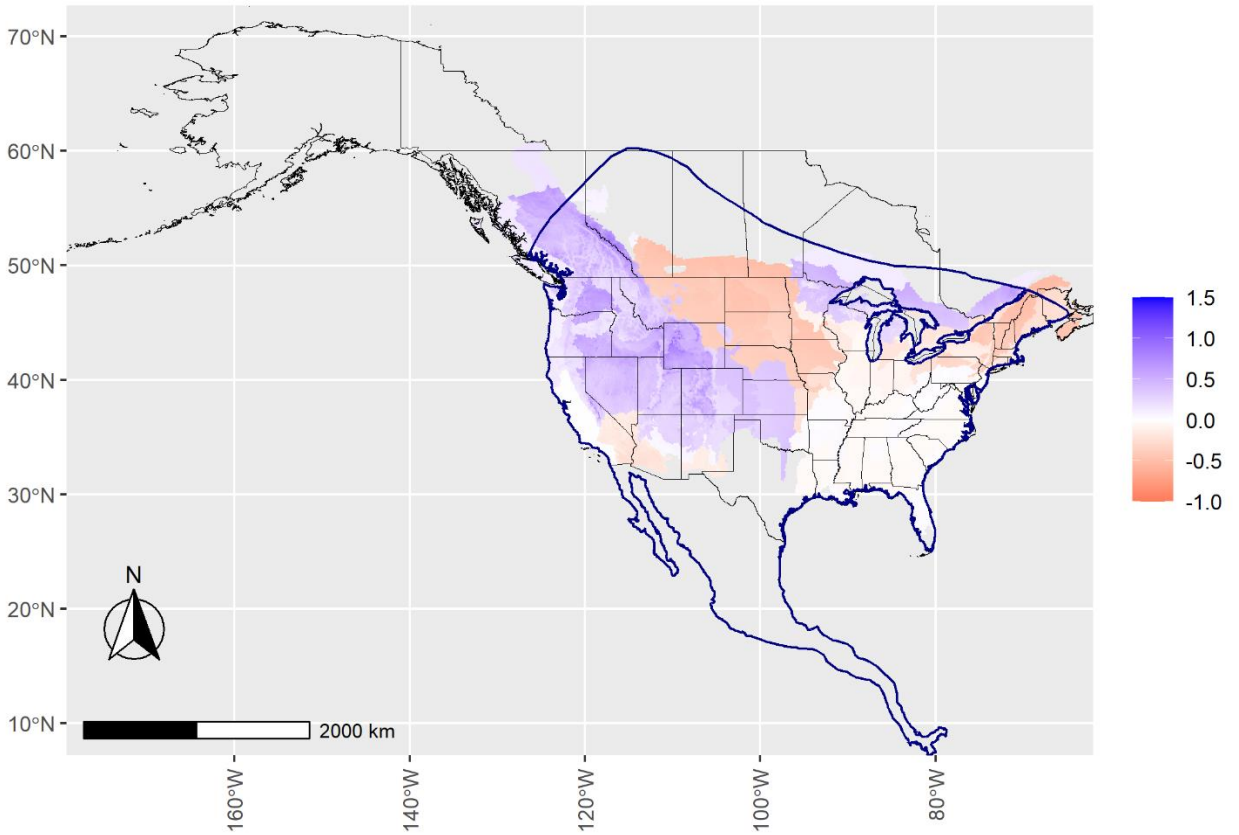

Figure 50. The total change rate in mean grid cell occupancies (color bar) for *Eptesicus fuscus* (EPFU) between 2016 and 2019 for all NABat grid cells in the modeled species range based on site-level covariates for each grid cell and year. This is depicted against the reference range map (blue polygon; National Atlas of the United States, 2011) and borders of U.S. states and Canadian provinces/territories. Note, the polygon depicting the reference range is for illustrative purposes only and was not used to bound occupancy probability predictions – instead, the analyses are bound by the geographic scope of monitoring data. For visualization purposes, the upper bound of the scalebar is truncated at 1.5 (150%) and corresponds to values of 1.5 and above, while the lower bound is naturally bounded at -1 (-100%). Note the results for EPFU were inconclusive due to issues reported in section 3.12.

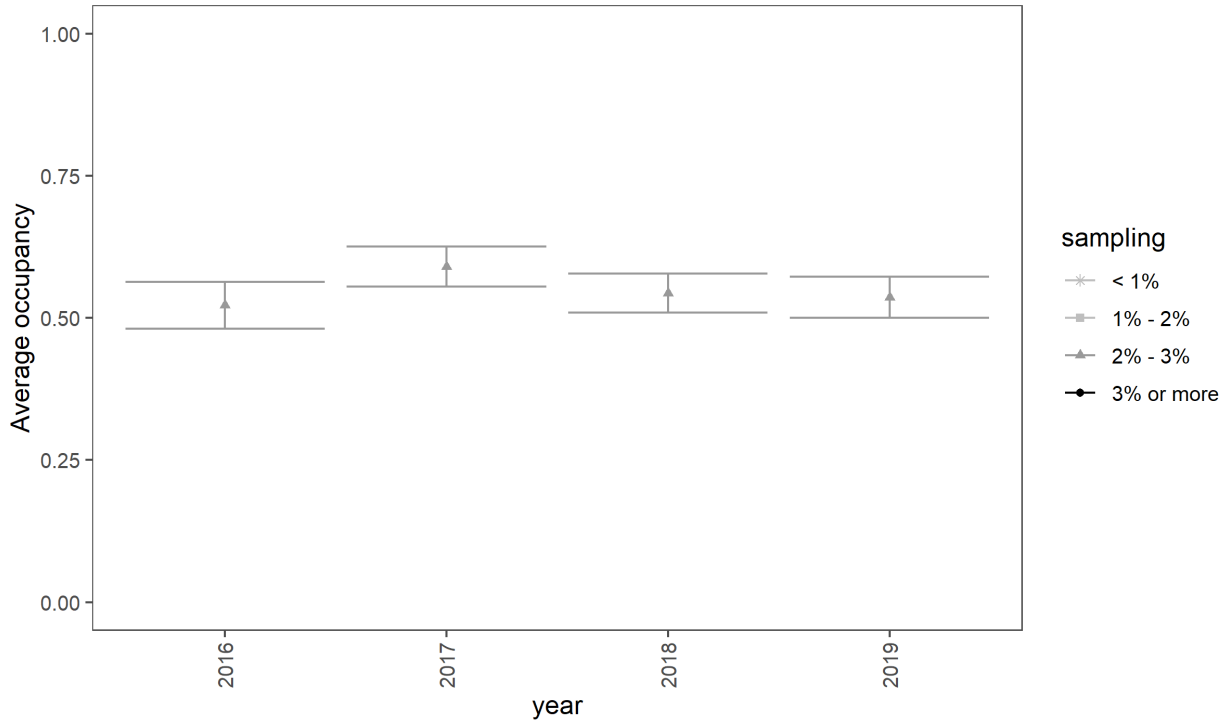

Figure 51. Estimates of the average occupancy probability ($\hat{\psi}_t$) each year for *Eptesicus fuscus* (EPFU), aggregated across all NABat grid cells in modeled range each year. Means (points) and 95% credible intervals (bars) are depicted according to the percent of grid cells sampled in the modeled species range each year (legend). Note the results for EPFU were inconclusive due to issues reported in section 3.12.

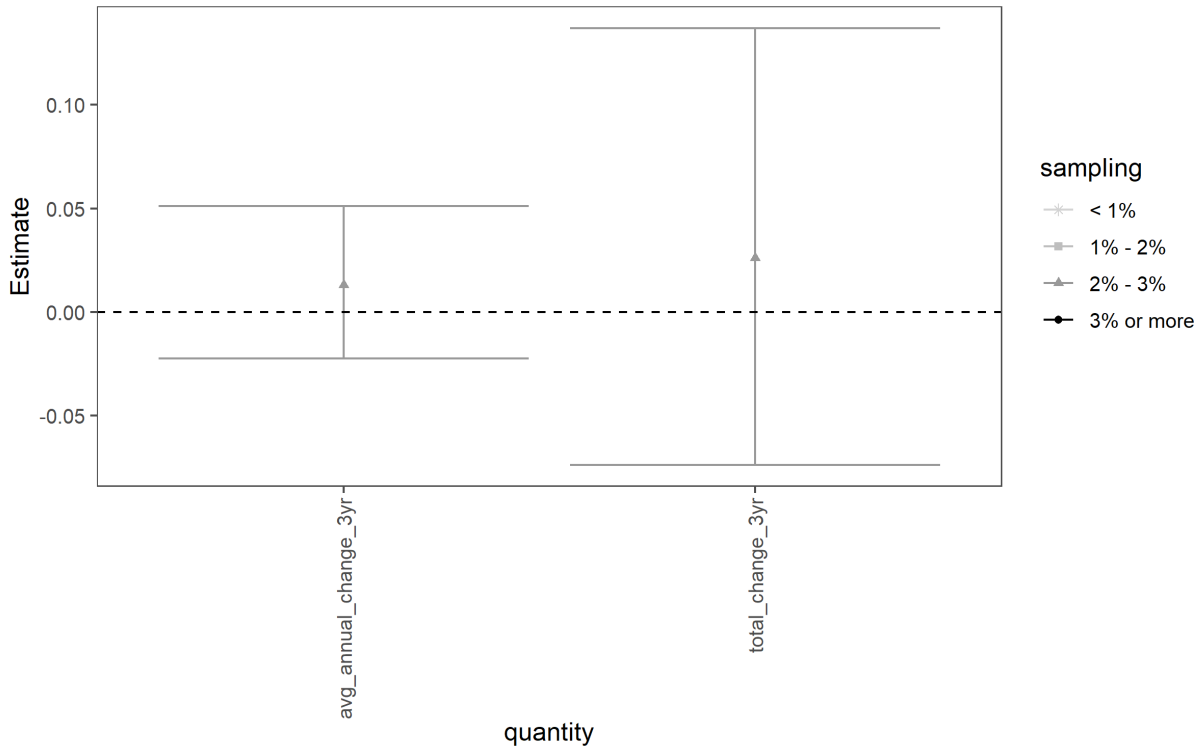

Figure 52. Estimates of average annual change (avg_annual_change = lambda_avg – 1) and total change (total_change = lambda_tot - 1) for *Eptesicus fuscus* (EPFU) over the short-term (2016–2019, three years of change). Means (points) and 95% credible intervals (bars) are depicted according to the percent of grid cells sampled in the modeled species range each year (legend). Note that the credible intervals overlap zero, meaning there is less than 95% certainty that trends in EPFU occupancy are different than zero. Note the results for EPFU were inconclusive due to issues reported in section 3.12.

Table 19. The numerical values represented in Figure 52 for average annual change and total average change over a short-term (2016–2019, three year) period.

Trend Type	Quantity	Mean	Lower CRI	Upper CRI
Annual	avg_annual_change_3yr	0.0131	-0.0223	0.0512
Total	total_change_3yr	0.0262	-0.0737	0.1369

3.12.2 *Lasionycteris noctivagans*

(A)

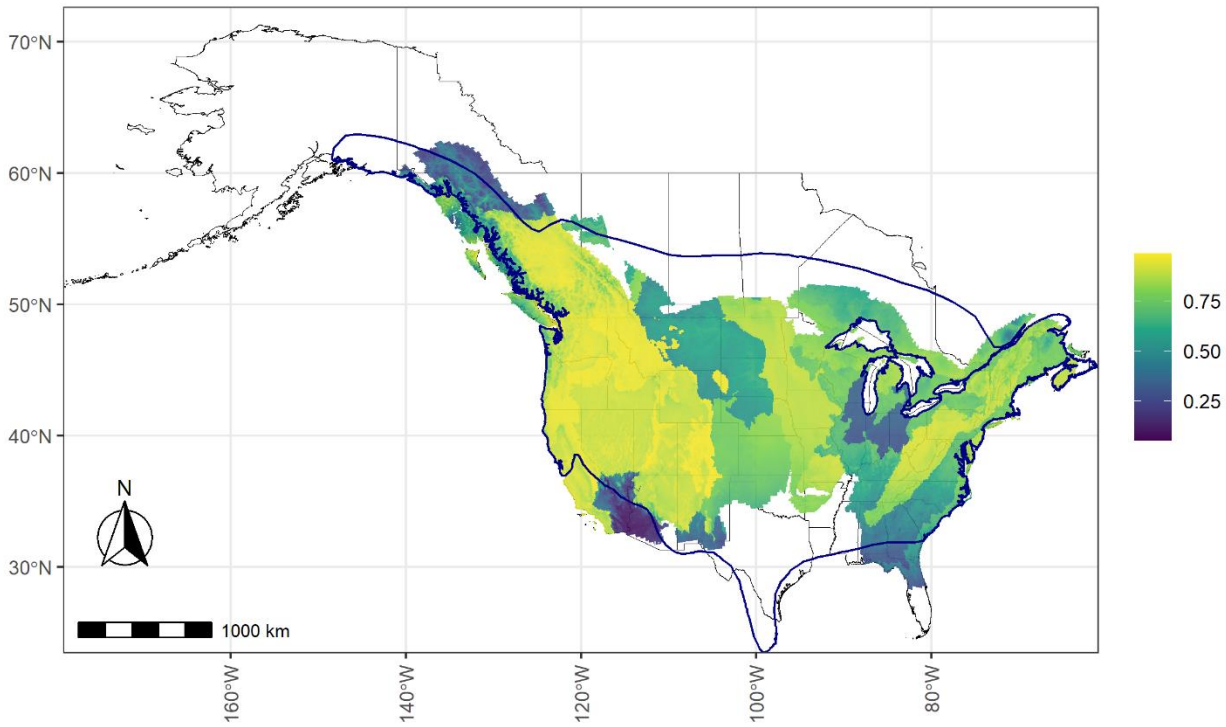

(B)

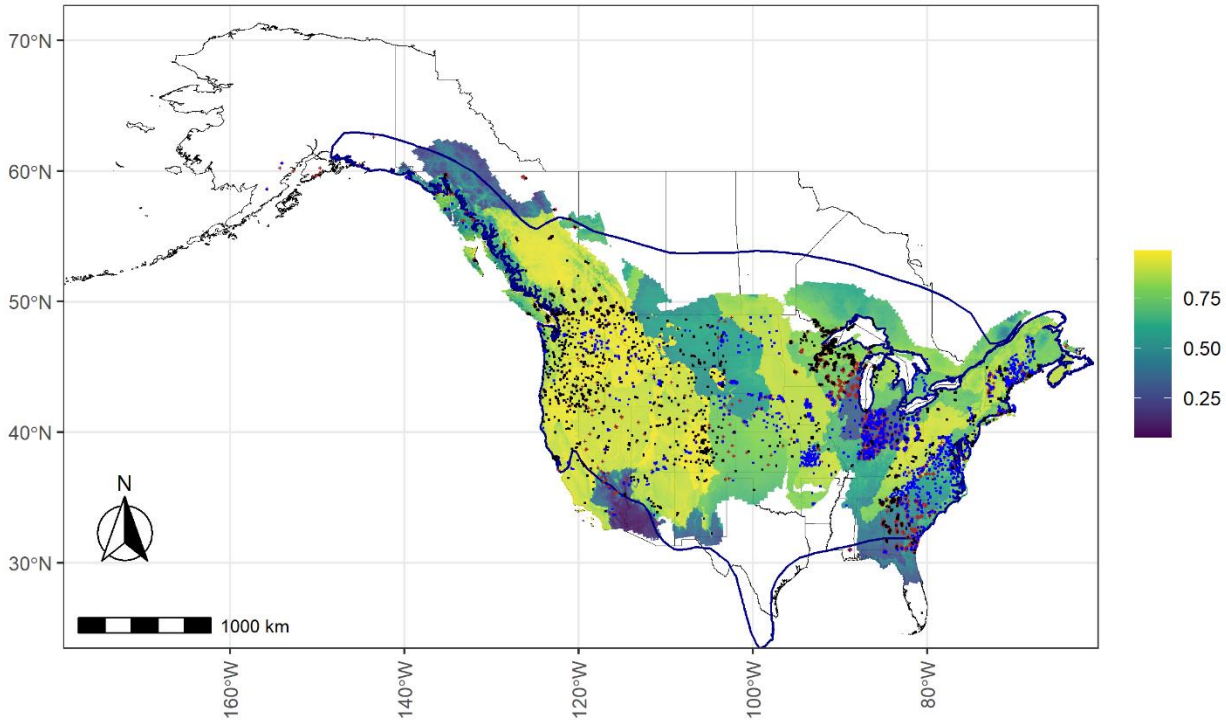

Figure 53. A map of *Lasionycteris noctivagans* (LANO) mean occupancy probabilities (color bar) predicted in each NABat grid cell in the modeled species range for 2019. Probabilities are depicted against the reference range map (blue polygon; National Atlas of the United States, 2011) and borders of U.S. states and Canadian provinces/territories (A and B). Note, the polygon depicting the reference range is for illustrative purposes only and was not used to bound occupancy probability predictions – instead, the analyses are bound by the geographic scope of monitoring data. All sampled locations (2016–2019) and detection summaries are also overlaid (B), including sampled locations where the species was never detected (brown '+' sign), locations where the species was detected at least once by acoustic auto IDs (blue dots), and locations where the species was detected either by manually verified acoustic records or capture data (black dots). Note the results for LANO were inconclusive due to issues reported in section 3.12.

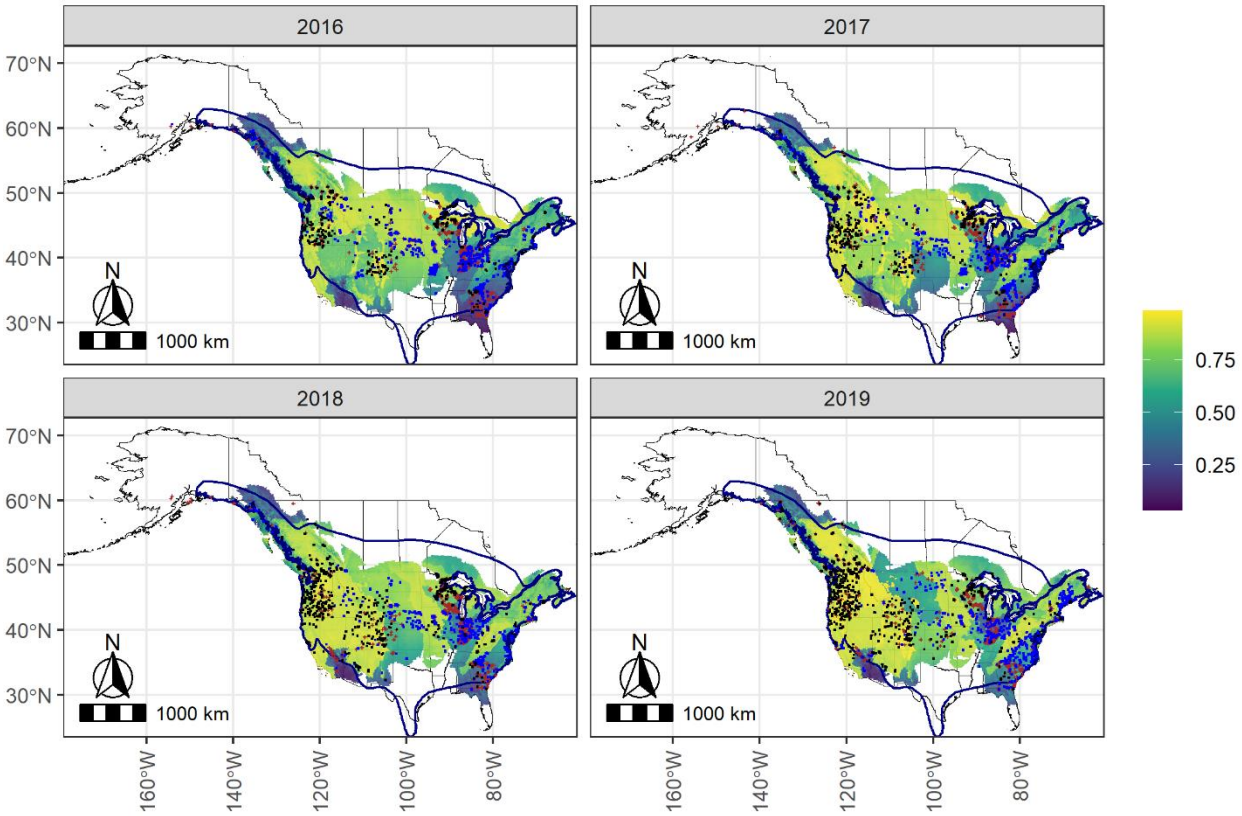

Figure 54. Mean predicted occupancy probabilities for *Lasionycteris noctivagans* (LANO) in 2016–2019 predicted for all NABat grid cells in the modeled species range based on site-level covariates for each grid cell and year. This is depicted against the reference range map (blue polygon; National Atlas of the United States, 2011) and borders of U.S. states and Canadian provinces/territories. Note, the polygon depicting the reference range is for illustrative purposes only and was not used to bound occupancy probability predictions – instead, the analyses are bound by the geographic scope of monitoring data. The grid cells sampled each year are also displayed based on detection histories as: brown '+' sign = never detected, blue dots = detected with an auto ID, black dots = detected with manual vetting and/or capture. Note the results for LANO were inconclusive due to issues reported in section 3.12.

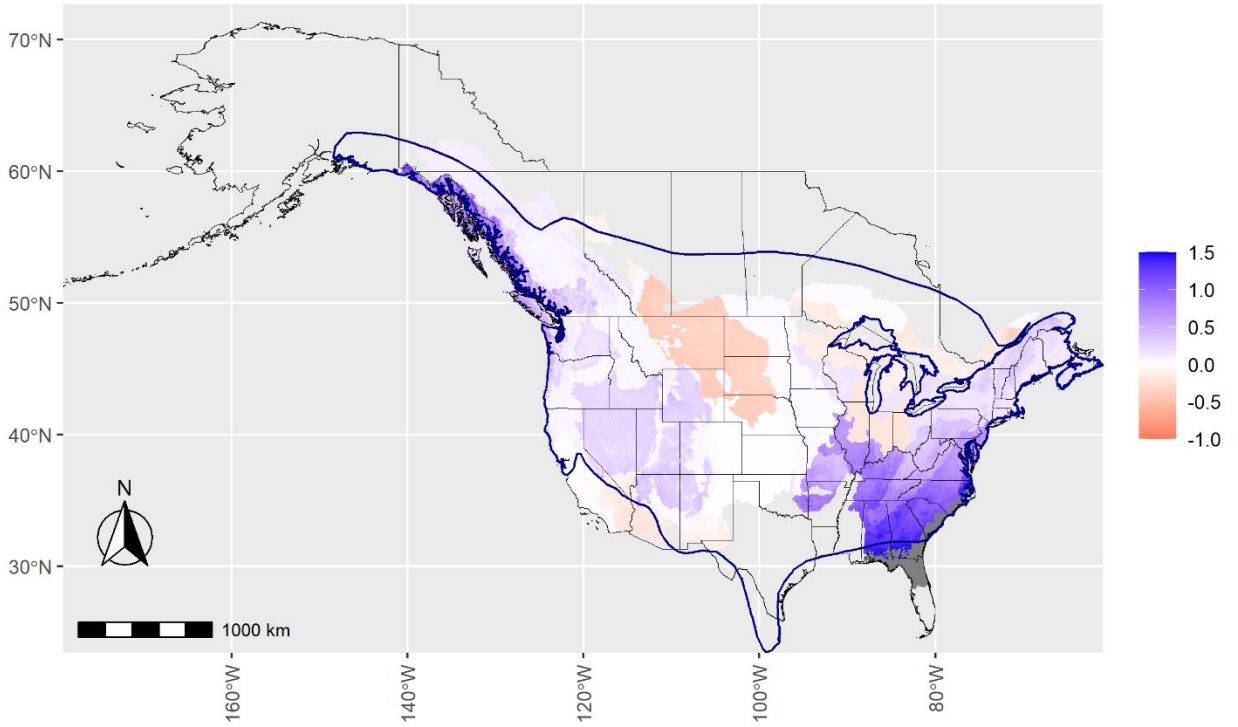

Figure 55. The total change rate in mean grid cell occupancies (color bar) for *Lasionycteris noctivagans* (LANO) between 2016 and 2019 for all NABat grid cells in the modeled species range based on site-level covariates for each grid cell and year. This is depicted against the reference range map (blue polygon; National Atlas of the United States, 2011) and borders of U.S. states and Canadian provinces/territories. Note, the polygon depicting the reference range is for illustrative purposes only and was not used to bound occupancy probability predictions – instead, the analyses are bound by the geographic scope of monitoring data. For visualization purposes, the upper bound of the scalebar is truncated at 1.5 (150%) and corresponds to values of 1.5 and above, while the lower bound is naturally bounded at -1 (-100%). Note the results for LANO were inconclusive due to issues reported in section 3.12.

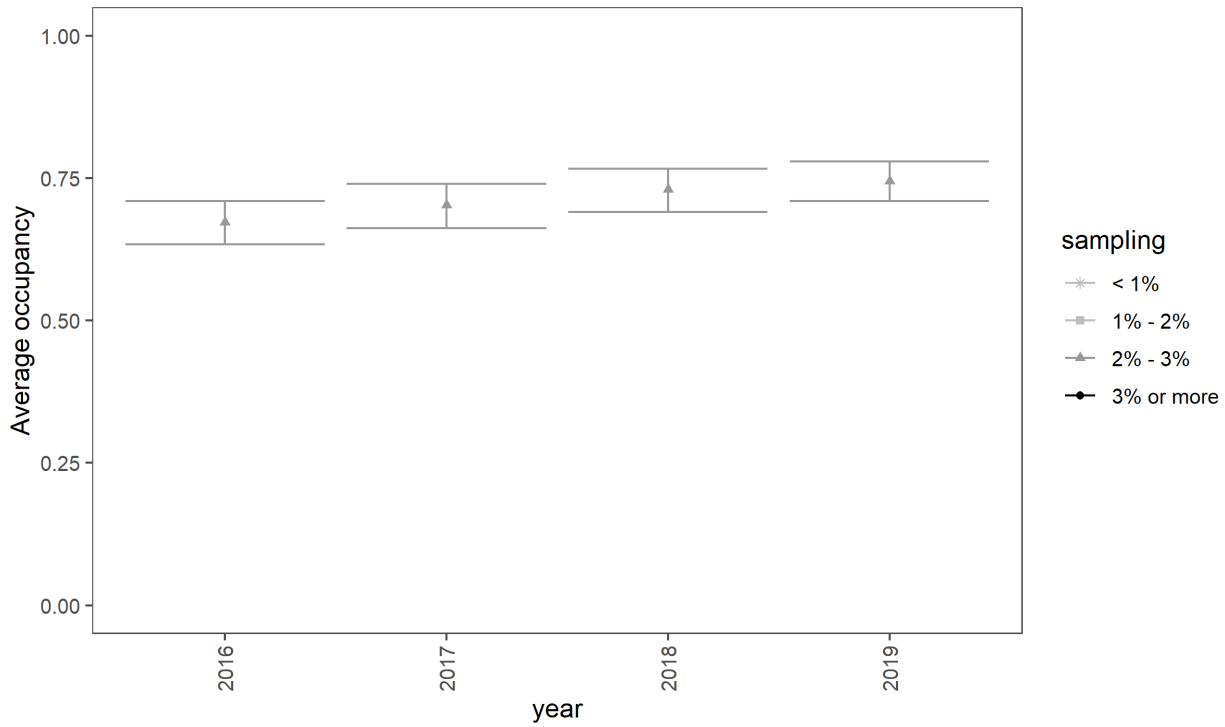

Figure 56. Estimates of the average occupancy probability ($\hat{\psi}_t$) for *Lasionycteris noctivagans* (LANO) each year, aggregated across all NABat grid cells in modeled range each year. Means (points) and 95% credible intervals (bars) are depicted according to the percent of grid cells sampled in the modeled species range each year (legend). Note the results for LANO were inconclusive due to issues reported in section 3.12.

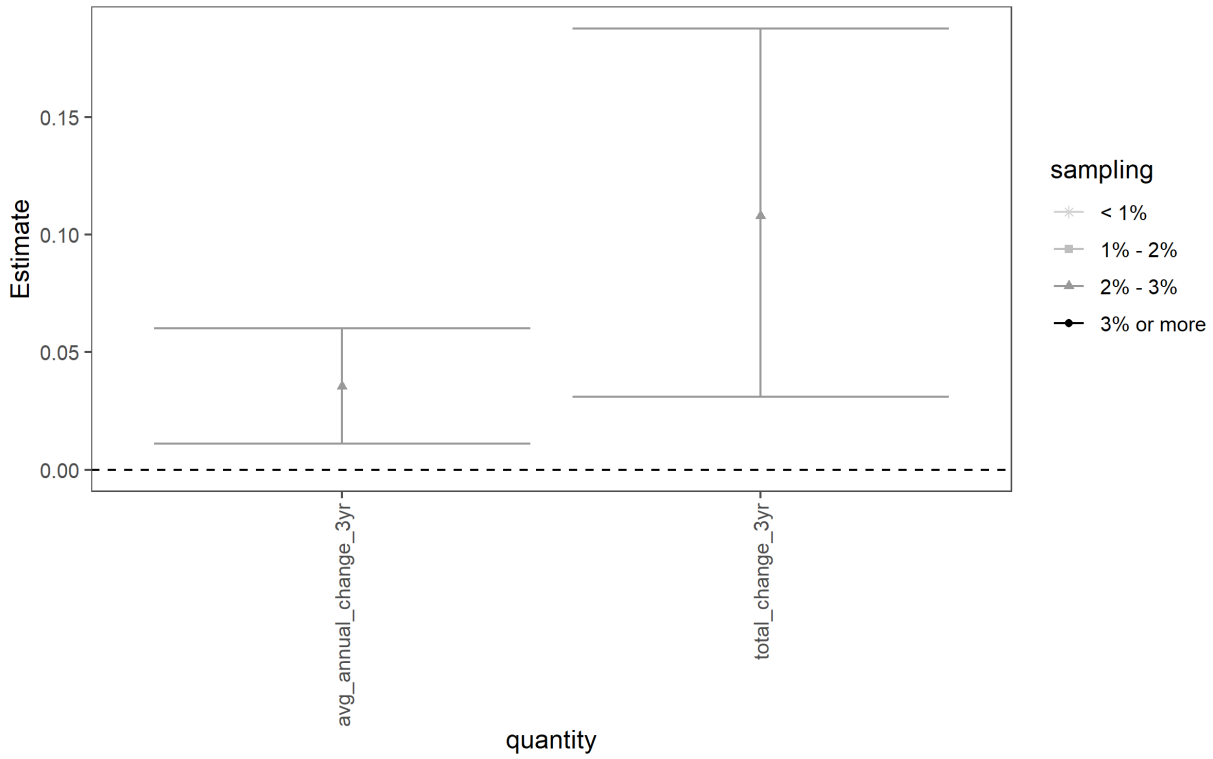

Figure 57. Estimates of average annual change (avg_annual_change = lambda_avg – 1) and total change (total_change = lambda_tot - 1) for *Lasionycteris noctivagans* (LANO) over the short-term (2016–2019, three years of change). Means (points) and 95% credible intervals (bars) are depicted according to the percent of grid cells sampled in the modeled species range each year (legend). Note that the 95% credible intervals do not overlap zero, indicating there is at least 95% certainty that trends in LANO occupancy are positive. Note the results for LANO were inconclusive due to issues reported in section 3.12.

Table 20. The numerical values represented in Figure 57 for average annual change and total average change over a short-term (2016–2019, three year) period.

Trend Type	Quantity	Mean	Lower CRI	Upper CRI
Annual	avg_annual_change_3yr	0.0354	0.0110	0.0601
Total	total_change_3yr	0.1080	0.0310	0.1876

3.12.3 *Lasiurus cinereus*

(A)

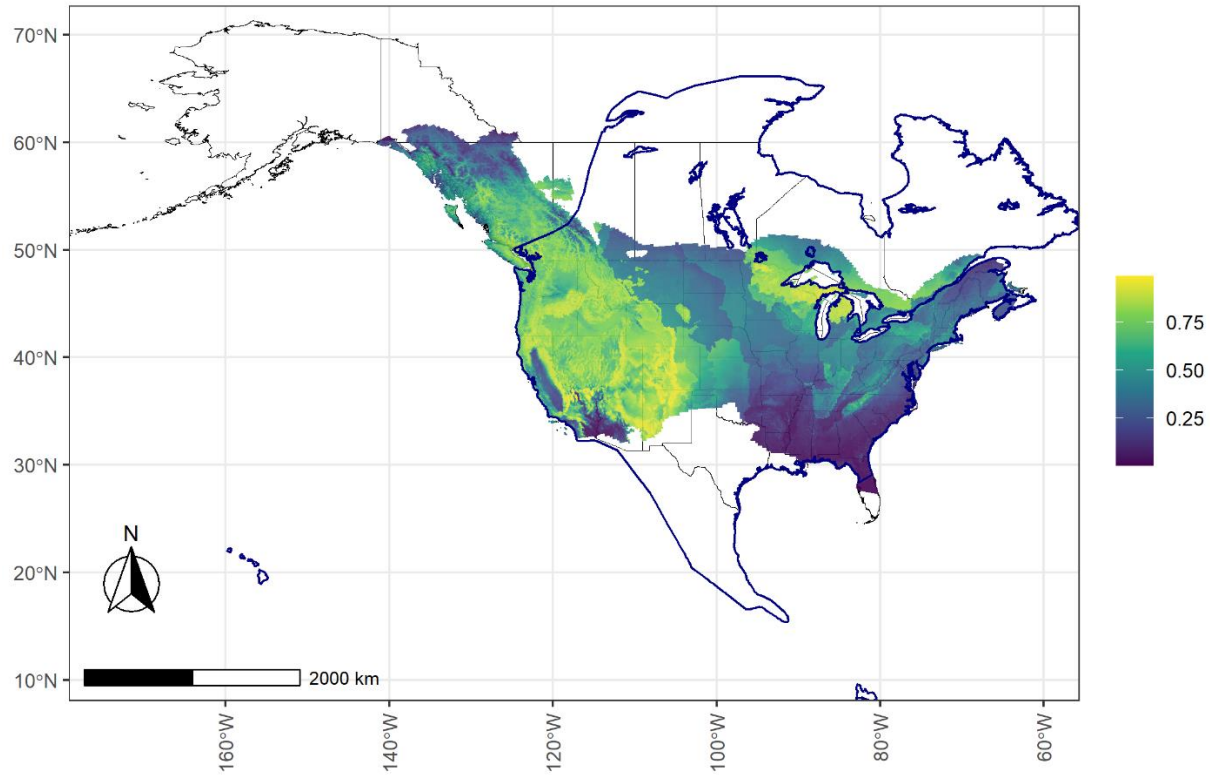

(B)

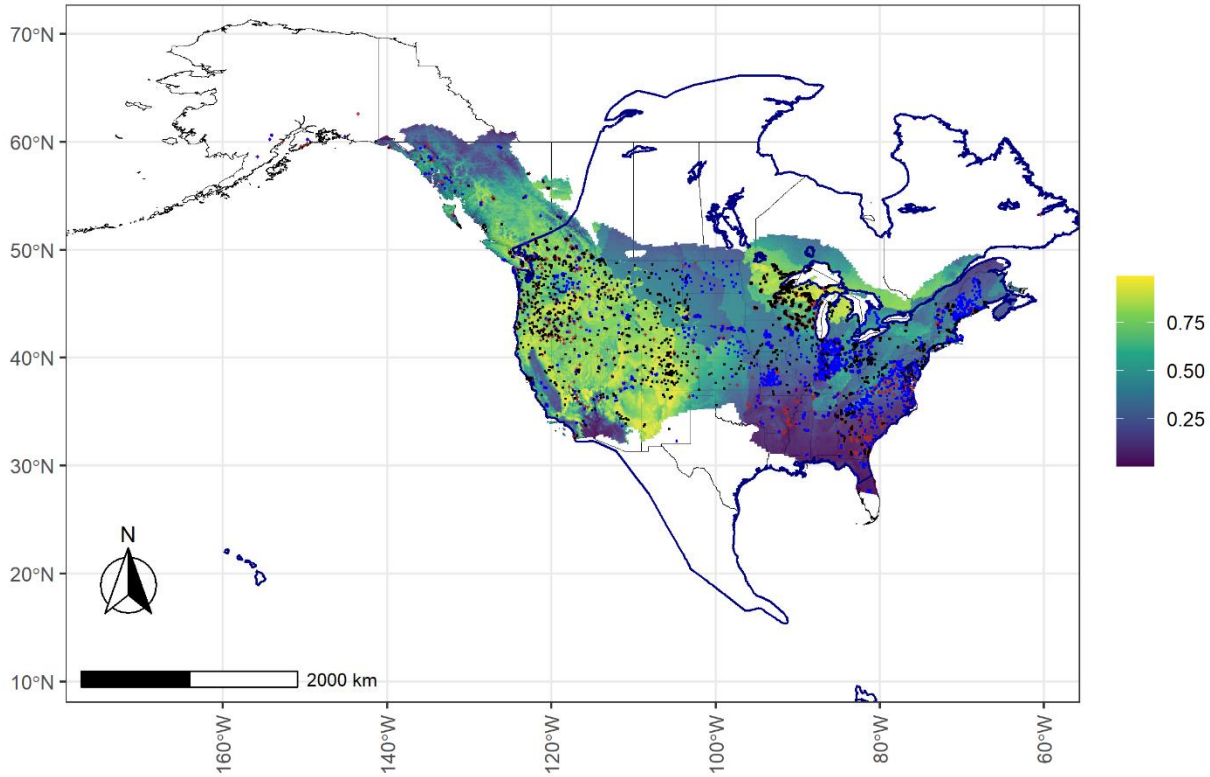

Figure 58. A map of *Lasiurus cinereus* (LACI) mean occupancy probabilities (color bar) predicted in each NABat grid cell in the modeled species range for 2019. Probabilities are depicted against the reference range map (blue polygon; National Atlas of the United States, 2011) and borders of U.S. states and Canadian provinces/territories (A and B). Note, the polygon depicting the reference range is for illustrative purposes only and was not used to bound occupancy probability predictions – instead, the analyses are bound by the geographic scope of monitoring data. All sampled locations (2016–2019) and detection summaries are also overlaid (B), including sampled locations where the species was never detected (brown '+' sign), locations where the species was detected at least once by acoustic auto IDs (blue dots), and locations where the species was detected either by manually verified acoustic records or capture data (black dots). Note the results for LACI were inconclusive due to issues reported in section 3.12.

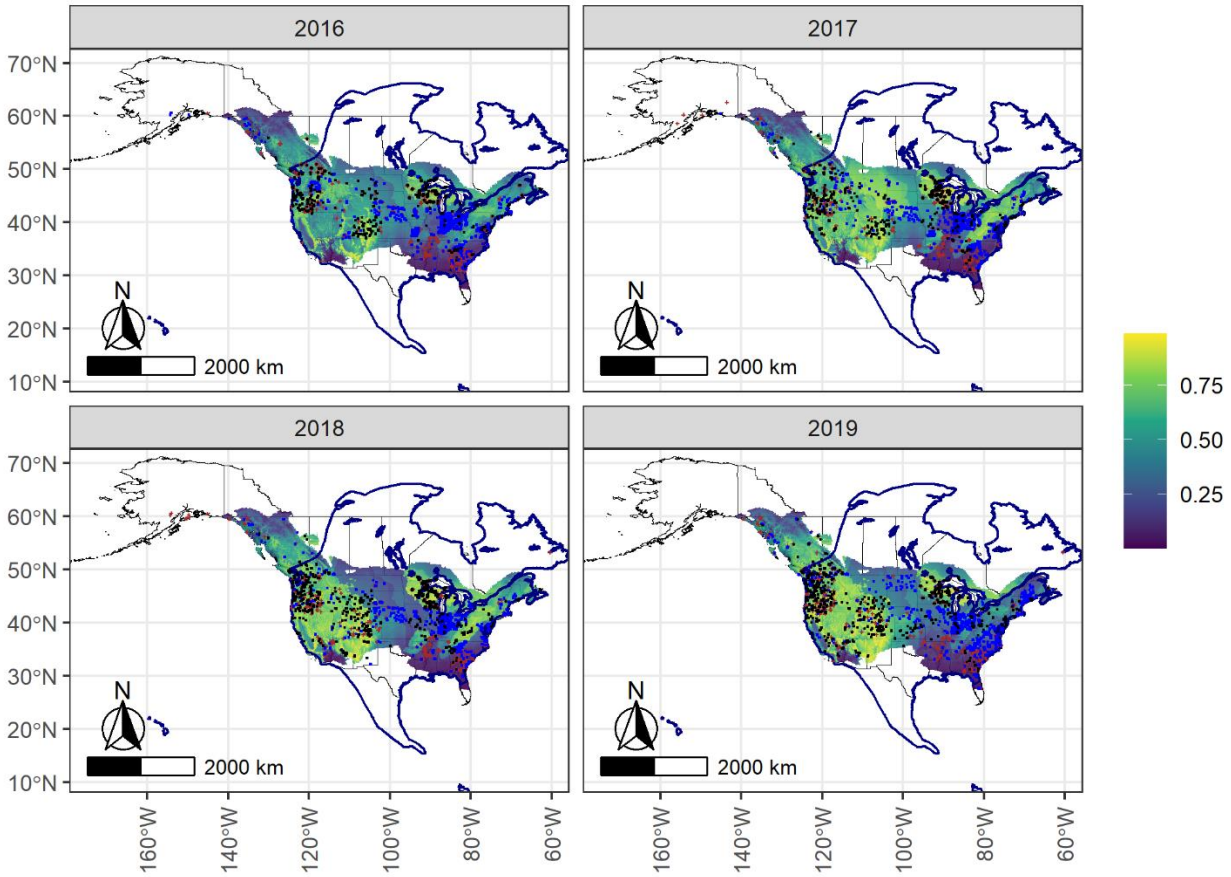

Figure 59. Mean predicted occupancy probabilities doe *Lasiurus cinereus* (LACI) in 2016–2019 predicted for all NABat grid cells in the modeled species range based on site-level covariates for each grid cell and year. This is depicted against the reference range map (blue polygon; National Atlas of the United States, 2011) and borders of U.S. states and Canadian provinces/territories. Note, the polygon depicting the reference range is for illustrative purposes only and was not used to bound occupancy probability predictions – instead, the analyses are bound by the geographic scope of monitoring data. The grid cells sampled each year are also displayed based on detection histories as: brown '+' sign = never detected, blue dots = detected with an auto ID, black dots = detected with manual vetting and/or capture. Note the results for LANO were inconclusive due to issues reported in section 3.12.

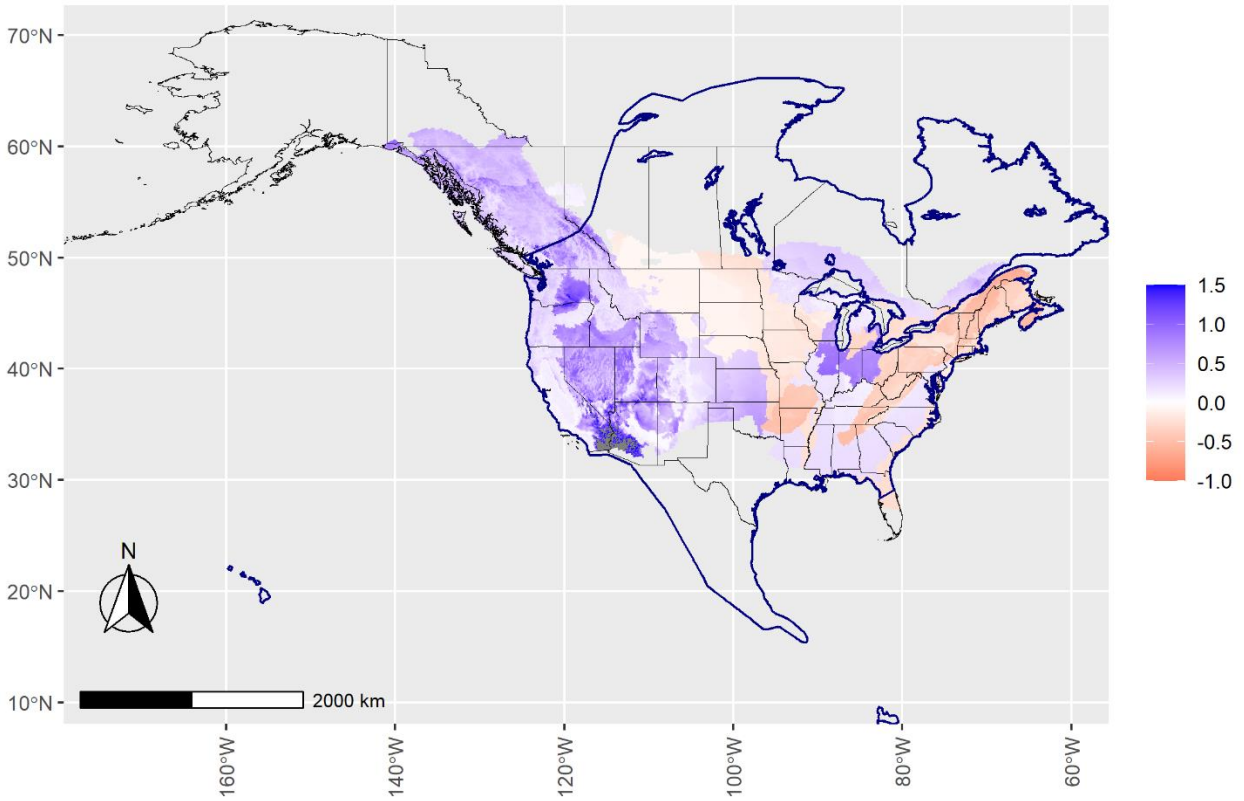

Figure 60. The total change rate in mean grid cell occupancies (color bar) *Lasiurus cinereus* (LACI) between 2016 and 2019 for all NABat grid cells in the modeled species range based on site-level covariates for each grid cell and year. This is depicted against the reference range map (blue polygon; National Atlas of the United States, 2011) and borders of U.S. states and Canadian provinces/territories. Note, the polygon depicting the reference range is for illustrative purposes only and was not used to bound occupancy probability predictions – instead, the analyses are bound by the geographic scope of monitoring data. For visualization purposes, the upper bound of the scalebar is truncated at 1.5 (150%) and corresponds to values of 1.5 and above, while the lower bound is naturally bounded at -1 (-100%). Note the results for LANO were inconclusive due to issues reported in section 3.12.

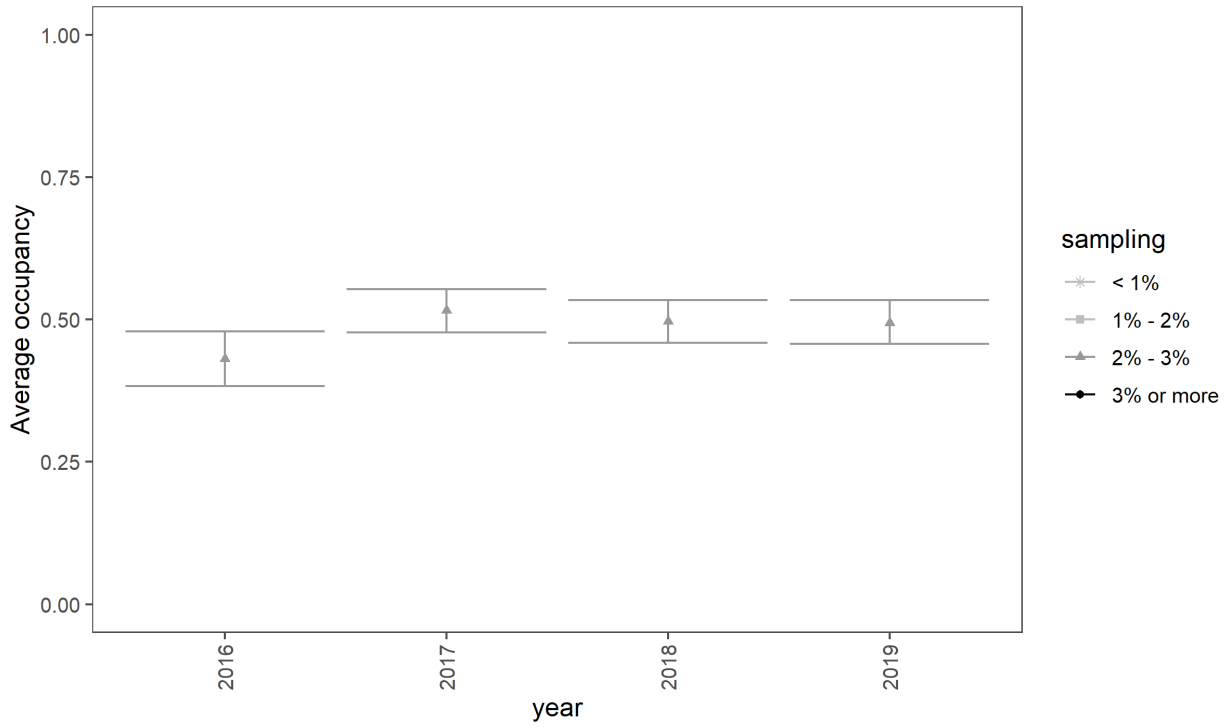

Figure 61. Estimates of the average occupancy probability ($\hat{\psi}_t$) for *Lasiurus cinereus* (LACI) each year, aggregated across all NABat grid cells in modeled range each year. Means (points) and 95% credible intervals (bars) are depicted according to the percent of grid cells sampled in the modeled species range each year (legend). Note the results for LACI were inconclusive due to issues reported in section 3.12.

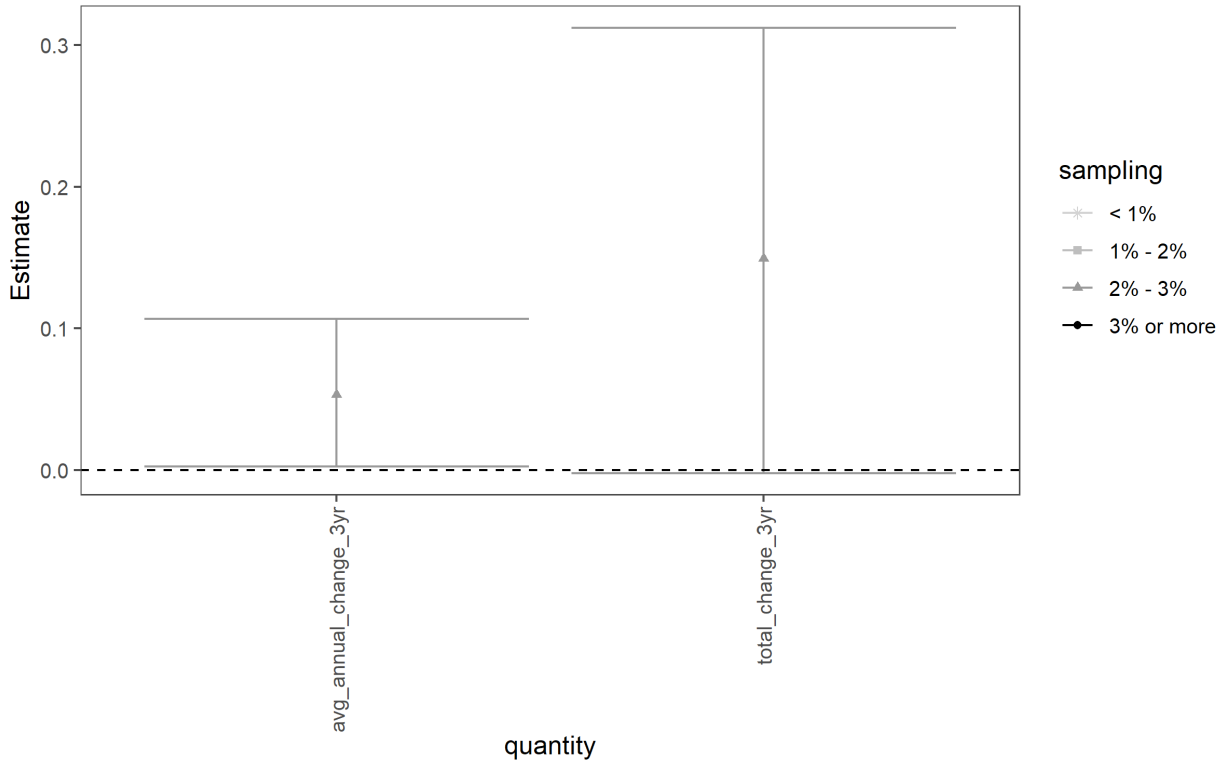

Figure 62. Estimates of average annual change (avg_annual_change = lambda_avg – 1) and total change (total_change = lambda_tot - 1) for *Lasiurus cinereus* (LACI) over the short-term (2016–2019, three years of change). Means (points) and 95% credible intervals (bars) are depicted according to the percent of grid cells sampled in the modeled species range each year (legend). Note that when the 95% credible intervals do not overlap zero, there is at least 95% certainty that trends in species occupancy are either negative or positive. When credible intervals overlap zero, there is less than a 95% certainty that these trends are different than zero. Note the results for LACI were inconclusive due to issues reported in section 3.12.

Table 21. The numerical values represented in Figure 62 for average annual change and total average change over a short-term (2016–2019, three year) period.

Trend Type	Quantity	Mean	Lower CRI	Upper CRI
Annual	avg_annual_change_3yr	0.0535	0.0026	0.1069
Total	total_change_3yr	0.1494	-0.0020	0.3120

4. Discussion

Bats in North America follow a complex seasonal life cycle with a maternity season in summer (Loeb et al. 2015). In this report, we used summer population monitoring data (acoustic and capture records) from the NABat database as a line of evidence to better understand the status and trends of 12 bat species across their North American ranges. Specifically, we used occupancy analysis (e.g., MacKenzie et al. 2002, MacKenzie et al. 2008, Chambert et al. 2015) to produce occupancy probability distribution maps and related metrics based on modeled habitat relationships. While summer occupancy is often positively correlated with changes in local abundance, occupancy provides additional insight into species' distributions, which are driven by a variety of factors including animal movement, space use, and habitat selection (Gaston 2003). These analyses represent one of multiple lines of evidence necessary to provide a full picture of the status and trends of bat populations (Loeb et al. 2015). The results provided here should be taken in context with additional NABat status and trends analyses on summer abundance analyses (e.g., from analyzing just the mobile acoustic data) and winter abundance (from analyzing internal roost counts), both of which are currently underway for species which sufficient data are available.

We calculated several status and trend-related metrics based on species occupancy probabilities across multiple spatial and temporal scales. Maps of species occupancy probabilities are useful for informing management decisions that are influenced by where and in what likelihood a bat species may be present (e.g., forest management practices) during a specific period of time. Estimates of grid cell-level occupancy can be useful for comparisons across space (regions of high and low occurrence) or comparing trends over time. Aggregate measures of occupancy at larger spatial scales (i.e., the average over all grid cells in a region of interest) can be similarly compared across space and time to gain insights into the status and trends of species distributions. Time series in the average occupancy probabilities at the range-wide scale and at state/province/territories (Appendix B) can be useful for these comparisons. We calculated two different trend indicators (average annual change and total change) over short-, medium-, and long-term trends for all 12 species at multiple spatial scales, which can help to inform species' conservation efforts (e.g., status assessments, prioritization efforts).

We found marked long-term declines in the range-wide average occupancy probabilities of three species of North American bats (MYLU, PESU, and MYSE). For MYLU, we found average annual declines in range-wide occupancy probability between 2010 and 2019 of -2.48% (95%CRI = -3.7% – -1.18%) per year and a total change between 2010 and 2019 of -21.03% (95%CRI = -29.74% – -11.57%). For PESU, we found average annual declines in range-wide occupancy probability between 2010 and 2019 of -6.23% (95%CRI = -8.31% – -4.00%) per year and a total change between 2010 and 2019 of -49.68% (95%CRI = -59.22% – -38.83%). For MYSE between 2010 and 2019, we found average annual declines in range-wide occupancy probability of -3.71% (95%CRI = -6.99% – -3.50%) per year and total change between 2010 and 2019 of -40.28% (95%CRI = -56.93% – -18.53%). These large declines in average occupancy probability corresponded with the continued progression of white-nose syndrome since its discovery in 2006, and the coincident declines in winter colony counts (Cheng et al. 2021a). This

was also evidenced by the meaningful spatiotemporal associations we found between winter-to-summer connectivity metrics and summer occupancy probabilities (Appendix C, C.1 – C.3).

4.1 Interpreting occupancy estimates and trends

Estimates of species occupancy are associated with a specific geographic region of interest and year. As different trends can arise at different spatial scales (e.g., range-wide declines despite some regional increases), it is important to keep the geographic extent of a trend estimate in mind when interpreting results. We provide estimates of 'range-wide' occupancy, yet they do not correspond with the entire reference range of each species because 1) a lack of data and 2) uncertainty regarding the true range limit of each species (e.g., confirmation data exist outside of the published species' ranges). Furthermore, reference range maps often vary between sources and there is a lack of consensus on the most accurate source for each species. We make the distinction between the 'modeled species range (summer),' which we used throughout these analyses when referring to 'range-wide' estimates, and the true but unknown species range across all North America. We infer range-wide status and trends based on the extent of the occupancy map predictions. As a result, range-wide species occupancy estimates may evolve as better approximations of the true extent of species ranges emerge. In the future, as more data become available and modeling approaches are refined, occupancy analyses may themselves be used to update species range maps.

The degree to which monitoring data and inferences drawn from monitoring data (e.g., species-habitat relationships, trends in average occupancy probability) are representative of a given region of interest (state/province/territory or modeled range) and/or year are dependent on the percent of grid cells sampled and the representativeness of the underlying environmental covariates at sampled locations. In some cases, average occupancy probability estimates for an ecoregion can be quite precise, despite very little sampling in an overlapping state, province, or territory. This occurs when there are sufficient data within the ecoregions used to fit the models and make the predictions, but relatively few data from the state, province, or territory of interest. To acknowledge this source of uncertainty in occupancy estimates, we depicted the percent of grid cells sampled in each region of interest and year for each species using a grey scale and shapes. Several regional estimates had less than 3% sampling each year and these results may motivate future monitoring efforts with an eye towards improving representation for all states, provinces, and territories.

We found that short-term trend indicators may provide early insight into the most recent changes in occupancy, but were generally prone to issues of small sample sizes and the potential for a single year to drive averages. Furthermore, we found that short-term trends might be positive despite long-term declines, especially if most severe declines pre-dated the sampling period. For MYSE, the estimated low point of the time series for range-wide average occupancy probability occurred in 2016 (the first year of the short-term time period), which is followed by a small increase in 2017, a very large increase in 2018, and a decline in 2019 to near 2017 levels. The point estimates for both short-term trend indicators (average annual change and total change) were positive, while the 95% credible intervals suggest there was less than (but quite close to) a 0.95 probability that the trend was positive. However, the point estimates for both medium-term indicators were negative with less than 95% certainty (i.e., credible

intervals overlapping zero), and the point estimates for both long-term indicators were negative with greater than 95% certainty (i.e., 95% credible intervals not overlapping zero). So, in this case, the positive short-term trend is driven by an all-time low point in MYSE's occupancy estimates in 2016 and a single high point average occupancy probability in 2018.

Medium-term and long-term trends are more robust to issues of small sample sizes but require longer-term data sets to estimate. Given the spread of WNS over time and declines in winter colony counts (Cheng et al. 2021a), longer-term trends are also more likely to capture historical impacts of WNS (if pre-WNS monitoring data are available). However, it is worth noting that severe impacts due to WNS had already been realized in parts of the Northeastern United States before 2010 (Cheng et al. 2021a). For most species, monitoring data are only available starting in 2016. For other species, data are relatively sparse prior to 2015 and don't follow NABat monitoring guidelines (Loeb et al. 2015). Uncertainty in estimates for these earlier years are appropriately higher than later years due to small sample sizes. So, despite the strengths of long-term trend indicators, they also have limitations in the current analyses. To help mitigate these sampling limitations in early years, we included winter-to-summer connectivity metrics as predictors of summer occupancy probabilities for MYLU, MYSE, and PESU. Winter-to-summer connectivity metrics can change in space and time based on winter hibernacula counts each year (Section 2.2.3). We also included an autoregressive (AR1) process to account for biologically plausible temporal autocorrelation on occupancy intercepts over time (Appendix A). However, estimates in early years in regions of interest without known hibernacula (e.g., the western U.S. for MYLU) were more uncertain. With an additional five years of NABat monitoring data, these limitations in medium- and long-term trend indicators may become less problematic. Similarly, additional years of data will allow for medium- and long-term trend estimates to be calculated for the additional nine species in these analyses for which we currently only provide short-term trend estimates.

4.2 Data limitations

There were several limitations of the available monitoring data. First, acoustic monitoring methods for bat populations are subject to both false positive and false negatives, which required statistical consideration (Banner et al. 2018). Second, manually vetted data and capture data were conservatively treated as presence only, and this limited the types of false positive occupancy models that could be implemented (Stratton and Irvine 2022). Next, while the NABat protocol (Loeb et al. 2015) was specifically designed to follow a probabilistic sampling order to ensure spatial randomness and representation, these data were combined with historical data that did not follow a probabilistic sampling framework for selecting grid cells to sample, which could result in analytical biases (Irvine et al. 2018). Next, there are clear geographic biases in regions of interest with no sampling data or limited sampling data, and these regions of interest are underrepresented in the analyses. While predictions in occupancy and trends can be made for these regions of interest (and sometimes with high precision based on underlying ecoregion sampling), estimates in geographic regions of interest with little to no data are less representative than those with higher sampling effort.

Another limitation of the available monitoring data was that sampled locations were often different between years (i.e., a non-spatiotemporally balanced sample). As a result, estimates

of occupancy relationships and trends over time may be biased due to sampling artifacts (Irvine et al. 2018). This limited the types and the spatial scale of spatiotemporal dynamics that could be built into these occupancy models (Appendix A, Section A.2). There may also be potential geographic biases in mobile transect surveys from a non-random distribution of roads with respect to bat habitat. Finally, the summer space use distribution of many bat species is strongly tied to summer roost locations. Inclusion of summer roost locations and abundances over time may help to improve occupancy estimates of some species. For example, based on the distribution of summer roost locations and counts, the occupancy probabilities for MYGR may be overpredicted for parts of eastern Tennessee and western North Carolina (where bat counts at individual summer roosts are often less than a few hundred individuals), and underpredicted in central Kentucky and central Tennessee (where populations in individual summer roosts can be greater than 50,000 bats; I. Kuczynska, U.S. Fish and Wildlife Service, written communication, February 15, 2022). However, while occupancy and abundance are related (especially at the grid cell level), a region with lower abundances at summer roost could feasibly have a higher proportion of grid cells occupied than a region with higher abundances if summer roosts are more widely dispersed across the landscape. Inclusion of known roost location data (and counts when available) in future analyses may help to reconcile these differences and contributing these data to the NABat database is encouraged.

4.3 Analytical limitations

The observation component of our false positive occupancy model allowed us to account for both false positives and false negatives by combining information on auto IDs with manually vetted data and capture data. However, due to data limitations (i.e., presence-only representations of manual vetting and capture data), we were limited to using site-level confirmation methods (Chambert et al. 2015, Stratton and Irvine 2022). These methods are generally less estimable than observation-level confirmation methods and are more prone to biases (Chambert et al. 2015, Section A.2.4). Following suggestions in the literature for site-confirmation false-positive methods (Royle and Link 2006), we included an additional constraint that true positive rates (aggregated over a seven-day observation period) must be higher than false positive rates to improve estimation and reduce potential biases (Section A.2.4). This assumption is likely to hold better for some species than others. In fact, fitting models for EPFU, LANO, and LACI was considerably more difficult than for other species, which is likely related to higher false positive rates for these species paired with mostly small and unimportant estimated effects of detection covariates (Section 3.12, Appendix C). A recent development of ‘conditional vetting’ in the NABat database, for which the number of auto IDs reviewed and the number of auto IDs confirmed can be inferred, allows for observation confirmation methods (at the individual call-sequence level) to be implemented in future modeling efforts. A final limitation of the observation model was aggregating detector-level responses at the sampling night across seven-day observation periods. This was done to mitigate concerns of non-independence in time (Appendix A.1.1); however, this precluded the inclusion of nightly level resolution of predictors on the observation process. We will investigate options in the future for how to account for these finer scale sources of variation.

The ecological component of each species occupancy model estimated species-specific environmental relationships, and, in conjunction with additional spatiotemporal effects,

allowed for making predictions in species occupancy probabilities across modeled species ranges. The degree to which the predicted occupancy map and trends over time reflect the 'true' distribution and trends of a species is thus dependent on how well the important factors that determine species distributions and their changes over time are captured in these models. Despite the inclusion of abiotic and biotic covariates, predictions of occupancy probability can diverge from the true species distribution for all the same reasons that the realized niche of a species diverges from the fundamental niche (e.g., unaccounted for influences of biotic interactions, dispersal limitation, disturbance, source-sink dynamics, anthropogenic impacts). Furthermore, these statistical models are rough approximations of biological processes. Ideally, we would fit fully spatiotemporally dynamic occupancy models at the grid cell spatial scale (e.g., Rodhouse et al. 2015, Wright et al. 2021). However, we cannot currently meet the data and computational requirements of these models given issues of non-spatiotemporally balanced sampling and further complications of spatiotemporal models, and of false positive occupancy models. Instead, we used a combination of hierarchical ecoregion random effects in space and time, a temporal autoregressive (AR1) process, spatial grid cell-level predictors (e.g., elevation, temperature, physiographic diversity, percent forest cover) and, in some cases (MYYU, MYVO), a grid cell-level multivariate spatial spline to account for unmeasured, spatial continuous influences at large spatial scales (Appendix 3.2). Also, in the case of MYLU, MYSE, and PESU, a winter-to-summer connectivity metric (Section 2.2.3) provided additional spatiotemporal information for predicting summer occupancy probabilities in space and time.

A general set of ecological predictors was included for each species (Section 2.2, Section A.3), and additional covariates were included based on discussions with species experts and the availability of data-sets across the entirety of North America. Strong correlations in potential predictor variables sometimes precluded the inclusion of some pairs of predictor variables (e.g., both percent forest cover and Normalized Difference Vegetation Index, NDVI). Moderate correlations between some important predictor variables were mostly unavoidable given the correlated physical and biological processes that influence these factors (e.g., temperature and elevation, physiographic diversity and percent forest). Correlations in predictor variables make interpreting covariate effects in isolation problematic. For example, MYSE is dependent on deciduous or mixed hardwood-coniferous forests for summer habitat (e.g., Henderson et al. 2008); however, the estimated effect for percent forest cover (of any forest type) was negative for MYSE after accounting for all other correlated covariate effects (e.g., elevation, physiographic diversity, winter to summer connectivity). Furthermore, the inclusion of additional ecoregion effects or spatial splines can sometimes absorb the influence of spatially correlated predictors. Given the correlations in predictor variables, these current models are currently better suited for making predictions of occupancy probabilities as opposed to testing specific hypotheses of influences on species occupancy in isolation of other covariate effects. Three final complications include: 1) we are missing regional covariates that may only be relevant in portions of the range, 2) we do not capture interaction differences in covariate effects across geographic regions (e.g., the effects of elevation on species occupancy may in fact be different at 5,000 ft in the interior Rocky Mountains versus the mountains on the Pacific coast), and 3) some predictor variables (e.g., percent forest of any kind) may not fully capture

important heterogeneity in the ecological relationships of specialist species (e.g., selection for deciduous versus coniferous forest).

4.4 Looking forward

Together with the NABat community, we have developed a pipeline for assessing status and trends of North American bat populations from multiple sources of monitoring data. This pipeline allows us to make data-driven, repeatable, and transparent inferences by constructing the best possible approximation of reality given limitations in the data and available analytical methods. All forms of ecological inference (formal or informal) depend on assumptions (either explicit or implicit) and are subject to observation biases (e.g., detectability). This report reflects the current state of the science and can serve to identify specific areas for improvement. Our ability to assess bat populations will improve as additional years of data are collected, geographic gaps in sampling are rectified, and the representativeness of sampling is increased. Additionally, uploading the actual recording files will facilitate our ability to reprocess call-sequences as new software become available with improved classification accuracy. Also, increasing the proportion of unambiguous data sets (e.g. manually-vetted acoustic observations and capture data) would help to improve inference by overcoming limitations for false-positives introduced by ambiguous acoustic detections. Obtaining and including data on summer and winter roost locations and abundances could also help to improve summer occupancy predictions by anchoring on known population centers. We will continue to incorporate feedback from NABat Technical Working Groups and Community of Practice to improve data quality and efficiencies in data collection and upload procedures, while developing novel statistical methods to maximize the utility of available data. Thus, NABat reports on status and trends of North American bat species will evolve as the state of the science and NABat monitoring data advance over time.

References

2010 North American Land Cover at 250 m spatial resolution. Produced by Natural Resources Canada/Canada Centre for Remote Sensing (NRCan/CCRS), United States Geological Survey (USGS); Insituto Nacional de Estadística y Geografía (INEGI), Comisión Nacional para el Conocimiento y Uso de la Biodiversidad (CONABIO) and Comisión Nacional Forestal (CONAFOR). http://www.cec.org/north-american-environmental-atlas/land-cover-2010-modis-250m/

Armstrong, D. M., Adams, R. A., & Freeman, J. 1994. Distribution and ecology of bats of Colorado. *Natural history inventory of Colorado (USA). no. 15.*

Balantic, C., and T. Donovan. 2019. "Dynamic Wildlife Occupancy Models Using Automated Acoustic Monitoring Data." *Ecological Applications* 0 (0): 1–14.

Banner, K. M., K. M. Irvine, T. J. Rodhouse, W. J. Wright, R. M. Rodriguez, and A. R. Litt. 2018. Improving Geographically Extensive Acoustic Survey Designs for Modeling Species Occurrence with Imperfect Detection and Misidentification. *Ecology and Evolution* 8 (12): 6144–56. https://doi.org/10.1002/ece3.4162.

Barr, E. L., Silvis, A., Armstrong, M. P., & Ford, W. M. 2021. White-nose Syndrome and Environmental Correlates to Landscape-Scale Bat Presence. *Wildlife Society Bulletin*, *45*(3), 410-421.

Chambert, T., D. A. W. Miller, and J. D. Nichols. 2015. Modeling False Positive Detections in Species Occurrence Data Under Different Study Designs. *Ecology* 96 (2): 332–39. https://doi.org/10.1890/14- 1507.1.

Chambert, T., Waddle, J.H., Miller, D.A., Walls, S.C. and Nichols, J.D., 2018. A new framework for analysing automated acoustic species detection data: Occupancy estimation and optimization of recordings post-processing. *Methods in Ecology and Evolution*, *9*(3), pp.560-570.

Chen, Z., Auler, A.S., Bakalowicz, M. *et al.* The World Karst Aquifer Mapping project: concept, mapping procedure and map of Europe. *Hydrogeol J* **25,** 771–785 (2017). https://doi.org/10.1007/s10040-016-1519-3

Cheng, T.L., Reichard, J.D., Coleman, J.T., Weller, T.J., Thogmartin, W.E., Reichert, B.E., Bennett, A.B., Broders, H.G., Campbell, J., Etchison, K. and Feller, D.J. 2021 A. The scope and severity of white-nose syndrome on hibernating bats in North America. *Conservation Biology*.

Cheng, T., Frick, W., Reichert, B.E., Thogmartin, W.E., Udell, B.J., Wiens, A., Whitby, M., Reichard, J., Szymanski, J. 2021 B. In Support of the U.S. Fish and Wildlife Service 3-Bat Species Status Assessment: Winter Colony Count Analysis: U.S. Geological Survey data release, https://doi.org/10.5066/P9YG45TG.

Commission for Environmental Cooperation. 2006. North American Rivers and Lakes. https://www.sciencebase.gov/catalog/item/4fb55df0e4b04cb937751e02

Doser, J.W., Finley, A.O., Weed, A.S. and Zipkin, E.F. 2021. Integrating automated acoustic vocalization data and point count surveys for estimation of bird abundance. *Methods in Ecology and Evolution*, *12*(6), pp.1040-1049.

Efford, M.G. and Dawson, D.K., 2012. Occupancy in continuous habitat. *Ecosphere*, 3(4), pp.1-15.

Fick, S.E. and R.J. Hijmans, 2017. Worldclim 2: New 1-km spatial resolution climate surfaces for global land areas. International Journal of Climatology. http://www.worldclim.com/version2

Frick, W.F., Kingston, T. and Flanders, J. 2020. A review of the major threats and challenges to global bat conservation. *Ann. N.Y. Acad. Sci.*, 1469: 5-25. https://doi.org/10.1111/nyas.14045

Friedenberg, N.A., Frick, W.F. (2021), Assessing fatality minimization for hoary bats amid continued wind energy development. *Biological Conservation*, Volume 262. 2021. 109309, ISSN 0006-3207, https://doi.org/10.1016/j.biocon.2021.109309

Gaston, K. J. 2003. The structure and dynamics of geographic ranges. Oxford University Press on Demand.

Gelman, A., and D. B. Rubin. 1992. "Inference from Iterative Simulation Using Multiple Sequences." *Statistical Science* 7 (4): 457–511.

Hanski, I., & Ovaskainen, O. 2000. The metapopulation capacity of a fragmented landscape. *Nature*, *404*(6779), 755-758.

He, F. and Gaston, K.J. 2000. Occupancy-abundance relationships and sampling scales. *Ecography*, 23(4), pp.503-511.

Henderson, L.E., Farrow, L.J. and Broders, H.G. 2008. Intra-specific effects of forest loss on the distribution of the forest-dependent northern long-eared bat (Myotis septentrionalis*). Biological Conservation*, 141(7), pp.1819-1828.

Holt, A.R., Gaston, K.J. and He, F. 2002. Occupancy-abundance relationships and spatial distribution: a review. *Basic and Applied Ecology*, *3*(1), pp.1-13.

Hooten, M. B., & Hobbs, N. T. 2015. A guide to Bayesian model selection for ecologists. *Ecological monographs*, *85*(1), pp.3-28.

Hoyt, J.R., Kilpatrick, A.M. and Langwig, K.E., 2021. Ecology and impacts of white-nose syndrome on bats. *Nature Reviews Microbiology*, *19*(3), pp.196-210.

Irvine, K. M., T. J. Rodhouse, W. J. Wright, and T. R. Olsen. 2018. "Occupancy Modeling Species-Environment Relationships with Non-Ignorable Survey Designs." *Ecological Applications* 8 (12): 6144–56. https://doi.org/10.1002/eap.1754.

Joseph, L. N., Field, S. A., Wilcox, C., & Possingham, H. P. 2006. Presence–absence versus abundance data for monitoring threatened species. *Conservation biology*, 20(6), 1679-1687.

Kéry, M., and J. A. Royle. 2020. Applied Hierarchical Modeling in Ecology: Analysis of distribution, abundance and species richness in R and BUGS: Volume 2: Dynamic and Advanced Models. Academic Press.

Loeb, S. C., T. J. Rodhouse, L. E. Ellison, C. L. Lausen, J. D. Reichard, K. M. Irvine, T. E. Ingersoll, et al. 2015. "A plan for the North American Bat Monitoring Program (NABat)." U.S. Department of Agriculture Forest Service, Southern Research Station, Asheville, NC.

Gary F McCracken, Riley F Bernard, Melquisidec Gamba-Rios, Randy Wolfe, Jennifer J Krauel, Devin N Jones, Amy L Russell, Veronica A Brown, Rapid range expansion of the Brazilian free-tailed bat in the southeastern United States, 2008–2016, *Journal of Mammalogy*, Volume 99, Issue 2, 3 April 2018, Pages 312–320, https://doi.org/10.1093/jmammal/gyx188

MacKenzie, D.I., Nichols, J.D., Lachman, G.B., Droege, S., Andrew Royle, J. and Langtimm, C.A. 2002. Estimating site occupancy rates when detection probabilities are less than one. *Ecology*, *83*(8), pp.2248-2255.

MacKenzie, D. I., J. D. Nichols, J. A. Royle, K. H. Pollock, L. L. Bailey, and J. E. Hines. 2006. Occupancy Estimation and Modeling: Inferring Patterns and Dynamics of Species Occurrence. Burlington, MA: Elsevier: Academic Press.

Maus, V., Giljum, S., Gutschlhofer, J., da Silva, D.M., Probst, M., Gass, S.L.B., Luckeneder, S., Lieber, M., McCallum, I. 2020. Global-scale mining polygons (Version 1). PANGAEA, https://doi.org/10.1594/PANGAEA.910894

McDonald, T. L. 2003. "Review of Environmental Monitoring Methods: Survey Designs." *Environmental Monitoring and Assessment* 85: 277–92.

Miller, D. A., J. D. Nichols, B. T. McClintock, E. H. Campbell Grant, L. L. Bailey, and L. A. Weir. 2011. "Improving Occupancy Estimation When Two Types of Observational Error Occur: Non-Detection and Species Misidentification." Ecology 92 (7): 1422–8.

Moilanen, A., Hanski, I., On the Use of Connectivity Measures in Spatial Ecology. 2001. *Oikos* Vol. 95, No. 1, pp. 147-151

National Atlas of the United States. (2011). North American Bat Ranges, 1830-2008. National Atlas of the United States. Available at: http://purl.stanford.edu/pz329xp4277.

Noon, B.R., Bailey, L.L., Sisk, T.D. and McKelvey, K.S., 2012. Efficient species-level monitoring at the landscape scale. *Conservation Biology*, 26(3), pp.432-441.

North American Bat Monitoring Program (NABat) Database v7.0.2 (Provisional Release): U.S. Geological Survey. Accessed 2021-10-18. NABat Request Number 35. https://doi.org/10.5066/P9UXA6CF

North American Bat Monitoring Program (NABat) Database v7.0.2 (Provisional Release): U.S. Geological Survey. Accessed 2021-10-18. NABat Request Number 34. https://doi.org/10.5066/P9UXA6CF

North American Bat Monitoring Program (NABat) Database v7.0.14 (Provisional Release): U.S. Geological Survey. Accessed 2021-10-18. NABat Request Number 73. https://doi.org/10.5066/P9UXA6CF

Ogle, K., & Barber, J. J. (2020). Ensuring identifiability in hierarchical mixed effects Bayesian models. *Ecological Applications*, 30(7), e02159.

Omernik, J.M. and G.E. Griffith. 2014. Ecoregions of the conterminous United States: evolution of a hierarchical spatial framework. Environmental Management 54(6):1249–1266.

O'Shea, T.J., Cryan, P.M., Hayman, D.T., Plowright, R.K. and Streicker, D.G. (2016), Multiple mortality events in bats. *Mammal Review*, 46: 175-190. https://doi.org/10.1111/mam.12064

Patten, M. A. 2004. Correlates of species richness in North American bat families. *Journal of Biogeography*, *31*(6), 975-985.

Plummer, M., 2003, March. JAGS: A program for analysis of Bayesian graphical models using Gibbs sampling. In Proceedings of the 3rd international workshop on distributed statistical computing (Vol. 124, No. 125.10, pp. 1-10).

Reichert, B., and Lausen, C., Loeb, S., Weller, T., Allen, R., Britzke, E., Hohoff, T., Siemers, J., Burkholder, B., Herzog, C., and Verant, M., 2018, A guide to processing bat acoustic data for the North American Bat Monitoring Program (NABat): U.S. Geological Survey Open-File Report 2018–1068, 33 p., https://doi.org/10.3133/ofr20181068.

R Core Team. 2020. R: A language and environment for statistical computing. R Foundation

Rodhouse, T. J., Rodriguez, R. M., Banner, K. M., Ormsbee, P. C., Barnett, J., & Irvine, K. M. (2019). Evidence of region-wide bat population decline from long-term monitoring and Bayesian occupancy models with empirically informed priors. *Ecology and evolution*, *9*(19), 11078-11088.

Royle, J. A., & Nichols, J. D. (2003). Estimating abundance from repeated presence–absence data or point counts. *Ecology*, 84(3), 777-790.

Royle, J. A., and R. M. Dorazio. 2006. Hierarchical models of animal abundance and occurrence. *Journal of Agricultural, Biological, and Environmental Statistics*, 11(3), 249-263.

Royle, J.A. and Link, W.A., 2006. Generalized site occupancy models allowing for false positive and false negative errors. *Ecology*, 87(4), pp.835-841.

Sherwin, H.A., Montgomery, W.I. and Lundy, M.G. (2013), Bats and climate change. *Mammal Review*, 43: 171-182. https://doi.org/10.1111/j.1365-2907.2012.00214.x

Steenweg, R., Hebblewhite, M., Whittington, J., Lukacs, P. and McKelvey, K., 2018. Sampling scales define occupancy and underlying occupancy–abundance relationships in animals. *Ecology*, *99*(1), pp.172-183.

Stratton, C., and K.M. Irvine. 2022. Summertime Analysis Statistical Report for Little Brown, Northern Long-eared, and Tricolored Bat Species Status Assessment. Chapter B *in* Straw, B.R, J. A. Martin, J.D Reichard, and B.E Reichert, editors. Analytical Assessments in Support of the U.S. Fish and Wildlife Service 3-Bat Species Status Assessment. Cooperator Report prepared in cooperation with the U.S. Geological Survey, United States Fish and Wildlife Service and Bat Conservation International. https://doi.org/10.7944/P9B4RWEUTalbert, C., and Reichert, B., 2018, Attributed North American Bat Monitoring Program (NABat) Master Sample and Grid-Based Sampling Frame: U.S. Geological Survey data release, https://doi.org/10.5066/P9RRWXL6.

Theobald, D.M., Harrison-Atlas, D., Monahan, W.B. and Albano, C.M., 2015. Ecologically-relevant maps of landforms and physiographic diversity for climate adaptation planning. *PloS one*, *10*(12), p.e0143619.

Thornton, M.M., R. Shrestha, Y. Wei, P.E. Thornton, S. Kao, and B.E. Wilson. 2020. Daymet: Annual Climate Summaries on a 1-km Grid for North America, Version 4. ORNL DAAC, Oak Ridge, Tennessee, USA. https://doi.org/10.3334/ORNLDAAC/1852

Udell, B.J., Straw, B.R, Cheng, T., Enns, K.D., Winfred, F., Gotthold, B.S, Irvine, K.M., Lausen, C., Loeb, S., Reichard, J., Rodhouse, T., Smith, D.A., Stratton, C., Thogmartin, W.E., Wiens, A.M., and Reichert, B.E., 2022, Status and Trends of North American Bats Summer Occupancy Analysis 2010-2019 Data Release: U.S. Geological Survey data release, https://doi.org/10.5066/P92JGACB.

U.S. Environmental Protection Agency, 2013, Level III ecoregions of the continental United States: Corvallis, Oregon, U.S. EPA–National Health and Environmental Effects Research Laboratory,

map scale 1:7,500,000, https://www.epa.gov/eco-research/level-iii-and-iv-ecoregions-continental-united-states.

U.S. Geological Survey. 1999. GTOPO30. https://doi.org/10.5066/F7DF6PQS

Wood, S., 2012. mgcv: Mixed GAM Computation Vehicle with GCV/AIC/REML smoothness estimation.

Wood, S.N., 2016. Just another gibbs additive modeller: interfacing JAGS and mgcv. *arXiv preprint arXiv:1602.02539*.

Wright, W.J., Irvine, K.M. and Rodhouse, T.J., 2016. A goodness-of-fit test for occupancy models with correlated within-season revisits. *Ecology and Evolution*, *6*(15), pp.5404-5415.

Wright, W.J., Irvine, K.M. and Higgs, M.D., 2019. Identifying occupancy model inadequacies: can residuals separately assess detection and presence?. *Ecology*, *100*(6), p.e02703.

Wright, W. J., Irvine, K. M., Rodhouse, T. J., & Litt, A. R. (2021). Spatial Gaussian processes improve multi-species occupancy models when range boundaries are uncertain and nonoverlapping. *Ecology and Evolution*.

Appendix A: Statistical Method Used for the False-positive Occupancy Modeling and Predictions

A.1 Statistical methods used for the false-positive occupancy modeling

Data collected under the NABat probabilistic sampling protocol are well suited to analysis via occupancy modeling. In fact, they have been specifically designed for analyzing bat distributions using occupancy modeling at continental scales (Loeb et al. 2015). The purpose of occupancy modeling (e.g., MacKenzie et al. 2002, MacKenzie et al. 2006) is to estimate the probability of species presence (i.e., the occupancy probability) each summer in each sampled grid cell (10 km x 10 km) using data from replicated surveys of grid cells within each summer. Then, using the estimated spatial and temporal covariate effects on grid cell-level occupancy for each species, predictions can be made for each grid cell in the species range for each year of interest. Thus, occupancy analysis can provide distributional maps of species occupancy probabilities across their ranges, along with estimates of the mean occupancy probability aggregated across larger spatial regions of interest (e.g., Colorado, range-wide) and how these have changed over time (trends). By conducting these analyses in a hierarchical Bayesian analytical framework, we can also provide estimates of uncertainty for each of these quantities at different spatial scales (grid cell, state/province, range).

A.2 Observation model

A key feature of occupancy models is the ability to separate biases due to observation processes (e.g., detectability and false positives) from the ecological process of interest (e.g., occupancy). False positive occupancy models (Royle and Link 2006, Miller et al. 2011, Chambert et al. 2015) incorporate both false positives (misclassification) and false negatives (species was present but not detected) into the detection process and require confirmation data at the site, site/night, or call-sequence level or explanatory covariates on the detection parameters. Following previous work using false-positive occupancy models in the U.S. Fish and Wildlife Service 3 Bat Species Status Assessment (SSA) by Stratton and Irvine (2022) and work by Miller et al. (2011) on site-level confirmation models, we employed a multiple detection state site confirmation model (MDSM) for the summertime false-positive occupancy modeling. While site confirmation methods are more limited than observation-level models (Chambert et al. 2015), the data requirements are more easily met (i.e., more suitable for presence-only confirmation data such as the unconditional manual vetting data or capture data).

A.2.1 Data fusion and aggregation for occupancy modeling

To incorporate all five data sources into a coherent false-positive occupancy modeling framework, we classify each response as: (0) non-detection, (1) ambiguous detection, or (2) unambiguous detection. This classification system is consistent with the false-positive occupancy models developed by Miller et al. (2011). For our analysis, a manual identification or capture record was considered an unambiguous detection and an automatically identified call-sequence was considered an ambiguous detection. Classifying each response in this manner is consistent with the recent literature applying false-positive models from Miller et al. (2011) to acoustic data (Balantic and Donovan 2019).

One assumption of the occupancy modeling framework is that repeated visits to a site (or 10 x 10 km cell in the context of our analysis) are temporally and spatially independent. Continuous periods of monitoring potentially violate the assumption of temporal independence, as we would expect sequential nights of monitoring to be similar due to runs in bat activity (Wright, Irvine, and Rodhouse 2016; Wright, Irvine, and Higgs 2019). To avoid the violation of temporal independence among revisits to a site, continuous periods of monitoring were aggregated to seven-day periods. Also, reducing the size of otherwise very large monitoring data sets reduced the computational demands and improved the feasibility of Bayesian model fitting. The seven-day period started from the first visit to a grid cell. For example, if the first visit occurred on a Tuesday, the next 6 nights would be included in the seven-day period if there were additional visits to that same grid cell. Detection status for each period was summarized as the highest level of species detection (0: no species detections, 1: at least one ambiguous detection, 2: at least on unambiguous detection) over the entire seven-days. If a site had multiple visits separated by more than seven days, each was treated as an independent revisit.

Multiple assumptions were made regarding the spatial independence of revisits to a site (see below). These assumptions could not be assessed as event-specific coordinates because contributed data were not consistently available. These assumptions included the following conditions:

1) If multiple detectors were deployed simultaneously, they were assumed far enough apart from one another to maintain independence. Because data collected before 2016 predates NABat protocols, this may not strictly hold for all observations. However, because the spatial coordinates of many detectors were missing, this was not possible to evaluate.

2) If multiple detection methods occurred concurrently (i.e., mobile transects and stationary acoustic surveys occurred during the same span of time), they were assumed to be spatially independent.

Based on these assumptions, detection matrices were created for each species.

A.2.2 Additional model assumptions

The occupancy modeling framework includes two key assumptions: 1) the occupancy state at each site is closed for the duration of each summer and 2) detection both within and between sites must be independent. We assume that within each site (10 x 10 km cell) the occupancy state does not change over the course of a summer (May 1–Aug 31). However, the closure assumption for the occupancy modeling framework is made at a species level, which means that individuals may move in and out of the grid cell throughout the summer. Also, the closure assumption does not require that a species roosts within a particular grid cell, only that the species occurs/uses the grid cell (MacKenzie et al. 2006).

We assume both that detection of the target species at one site does not affect detection of that species at another site and that detection of the target species during one visit to a site does not affect detection of that species during subsequent visits to the site. We assume there is no unexplained spatial or temporal correlation among observations both within and among sites after accounting for observation level covariates and other spatial or temporal random

effects. The master sample design outlined in A Plan for the North American Monitoring Program was constructed to ensure that sampled grid cells are far enough apart to be considered spatially independent (Loeb et al. 2015). However, as mentioned previously, the fusion of data types (stationary surveys, mobile surveys, and capture data) and of data that did and did not follow NABat monitoring protocols as documented in Loeb et al. 2015 means the spatial independence assumptions are not necessarily satisfied.

To ensure that the data are consistent with the assumption of independent detections within a site, there must again be no unexplained sources of temporal or spatial correlation. Temporal correlation in detection within a site may arise from continuous periods of monitoring. To account for this potential source of temporal correlation, responses were aggregated up to a weekly level. Spatial correlation in detection within a site may arise from detection methods being deployed too close in proximity to each other. Loeb et al. (2015) provides suggested protocols for how to deploy multiple detection methods simultaneously within the same site while still maintaining spatial independence in detections. However, point specific coordinates for detections were unavailable. Therefore, a direct assessment of the spatial independence assumption within a grid cell is not possible. As a result, we conduct these analyses under the assumption that if multiple detection methods were deployed within a cell concurrently (multiple stationary detection devices deployed simultaneously, stationary and mobile acoustic detectors deployed concurrently, etc.) they were deployed far enough apart to be spatially independent. Data collected following the NABat plan adhere to this assumption, but data collected prior to the existence of the NABat plan or under different conditions may not.

A.2.3 Statistical model

Each grid cell (i) had one or more 'visits' (j) within a given year. Multiple detector locations in each grid cell, multiple sampling events per location, and observations by different survey types (stationary, mobile, capture) are treated as repeated and independent visits to a grid cell. For example, four locations with a stationary detector in a grid cell result in four independent visits for each observation event (7-day period). . We model the partially observed latent occupancy state (z_i) and the observed response for grid cell i during visit $\left(y_{ij}|\, z_i\right)$ as follows:

$$z_i \sim \text{Bernoulli}(\psi_i)$$

$$y_{ij}|\, z_i \sim \text{Categorical}\left(M_{ij}\right)$$

where $\left[M_{ij}|\, z_{ij} = 0\,\right] = \left[\left\{1 - p_{10_j}\right\}\left\{p_{10_j}\right\}\{0\}\right]$ for observation states $y_{ij} = \{0,1,2\}$ when $z_i = 0$ and $\left[M_{ij}|\, z_{ij} = 1\right] = \left[\left\{1 - p_{11_j}\right\}\left\{\left(1 - b_j\right) * p_{11}\right\}\left\{b_j * p_{11_j}\right\}\right]$ for observation states $y_{ij} = \{0,1,2\}$ when $z_i = 1$.

For this analysis, the probability of the species occurring at site i (ψ_i) was modeled as a function of grid-cell specific covariates (see ecological state model Section A.3) using a logit link. Each of the detection-level parameters (p_{11}, p_{10}, b) was modeled with a random intercept by year and ecoregion level-3 (Section 2.2.4) to account for unmeasured temporal and spatial influences (e.g., ecological communities, bat abundances, environmental conditions, likelihood of capture effort, potential project level differences in monitoring equipment/analysis in each

geographic region) on the observation processes. Furthermore, observation-level covariates collected from Daymet were aggregated temporally (to match the response data) and were included as covariates on the detectability p_{11}. These variables included day length, day of year, precipitation (a 0/1 indicator), minimum air temperature, and water vapor pressure. A rough measure of total effort (the total number of rows in the response data aggregated across for each observation) was also included to account for variable effort.

A.2.4 Constraints on p11 and p10 for identifiability

Lack of identifiability in false-positive occupancy model parameters is a known issue, and sufficient information about classification probabilities is required to resolve the problem (Royle and Link 2006, Chambert et al. 2012, Chambert et al. 2015) This is because in the implicit mixture of true positives and false positives, $p_{11} * z_i + (1 - z_i) * p10$, different values of p11 and p10 can lead to the same likelihood values. Several methods are available to overcome this issue: 1) incorporate observation level confirmation methods instead of site level, 2) include informative, distinct, and non-correlated covariates for each parameter, or 3) constrain the model so that p11 (the true positive rate) must be greater than p10 (the false negative) (Royle and Link 2006). The false positive framework used here is a site-level confirmation method, which precludes option 1. Option 2 requires good covariates for all three observation parameters; however, while we have a priori biologically meaningful covariates for true positive rates, we do not have informative covariates for false positive rates which may be largely driven by the noise in the underlying ecological community (e.g., other bat species) and classification software types. Nor do we have predictive covariates for the confirmation rate, which is the product of the probability of confirmation effort and the probability that at least one observation over each seven-day period was a true positive. The confirmation rate is also a mix of acoustic confirmation, and capture confirmation, which further complicates the interpretation of this parameter.

Thus, we are left with option 3, constraining the model so that p11 is greater than p10. We found that this constraint greatly improved both our model fitting procedures and predicted occupancy maps (based on discussions with species experts). These assumptions also agree with NABat guidance for vetting auto IDs (i.e., when reviewing auto IDs and lacking diagnostic evidence of a misclassification, accept the auto ID; Reichert et al. 2018). This assumption is further justified when considering that p11 and p10 do not correspond to call-sequence level false positives and true positives, but rather to detection rates aggregated over seven-night periods and potentially multiple detectors. Thus, p11 corresponds to the probability of getting at least one true call-sequence over the entire aggregation period, while p10 is the probability that every auto ID detection over the aggregation period is a false negative (Royle and Link 2006). Moving beyond site-level confirmation methods to observation level confirmation methods should allow for this assumption to be relaxed.

A.3 Ecological model for grid cell-level occupancy

An ecological model for predicting grid cell-level occupancy probabilities in space and time for each species was developed following several steps. First, a general set of grid cell level predictors based on the previous literature and conversations with bat species experts were considered, including maximum elevation, average annual temperature, physiographic

diversity, annual precipitation, percent forest, and percent wetlands (Sections 2.2.1 and 2.2.2). Quadratic effects of maximum elevation and average annual temperature were also included to allow for hump shaped relationships rather than strictly logit-linear, which is especially important when modeling ecological relationships range-wide. These covariates provided the base model for each species, which were modeled on species occupancy using a logit link given the intercept (with spatiotemporal structure) and the ecological predictors. Second, the spatiotemporal dynamics were modeled on the intercept by including hierarchical ecoregion spatial effects (at levels 1, 2, and/or 3) and autoregressive (AR1) temporal effects each year at ecoregion level-1 or level-2 depending on the species (See A.3, Table A.1). The inclusion of a temporal AR1 process was to account for correlation in species occupancy over time (i.e., that random year effects are not completely independent of one another, and years closer together in time should be more similar than years that are further apart in time). Third, additional spatiotemporal covariates (i.e., predictors that varied in space and time) were included where available, for example, the winter to summer connectivity metrics for MYLU, PESU, and MYSE (Section 2.2.3).

Next, after preliminary models were fit and predictions for occupancy maps across species' ranges were made, species experts were consulted about the occupancy map predictions and estimated ecological relationships for each species. Additional covariates were sometimes included on a species-by-species basis based on these discussions. For example, for MYLU, MYSE, PESU, and MYGR, a karst indictor was included to capture the effects of caves, and for MYSE, the effects of karst varied by year to capture the expected impacts of White Nose Syndrome (i.e., the a priori prediction was the effect of karst/caves would become increasingly negative over time due to WNS impacts). Distance to mines was also included for MYSE, MYLU, and PESU. For MYSE, the inclusion of time varying effects of karst, and effects of regional WNS impacts (via the winter-to-summer connectivity effects) was also consistent with a recent empirical study (Barr et al. 2021). Finally, a river and shoreline indicator was included for MYGR since summer roost locations and space-use are strongly tied to distance to large bodies of water. For MYYU and MYVO, a multivariate Gaussian spatial spline was also included (using a tensor product interaction via the mgcv R package, Wood 2012, 2016) after finding the model predictions better matched the a priori predictions of species experts with regards to elevational effects and predicted species distributions. See Table A.1 below for a description of each species model.

Table A.1. A description of the ecological model for predicting grid cell-level occupancy for each bat species. Note the parameter estimates from fitted models and the relative strength of effects are provided in Appendix C. AR1 = autoregressive

Species	Intercept	Winter-to-summer connectivity	Spatial covariates	Spatial covariates with AR1 time varying effects	Spatial spline
MYLU	Space: Ecoregions levels 1, 2, and 3 Time (AR1): Ecoregion level-1	Yes Effect set to zero in level-3 ecoregions with a mean connectivity less than -2.5	Elevation Elevation^2 Temp Temp^2 Physiographic diversity Precipitation Percent Forest Percent Wetlands Karst (East Only) Distance to mines (East only)	No	No
PESU	Space: Ecoregions levels 1, 2, and 3 Time (AR1): Ecoregion level-1	Yes	Elevation Elevation^2 Temp Temp^2 Physiographic diversity Precipitation Percent Forest Percent Wetlands Karst Distance to mines	No	No
MYSE	Time (AR1): homogenous across space	Yes	Elevation Elevation^2 Temp Temp^2 Physiographic diversity Precipitation Percent Forest Percent Wetlands Distance to mines	Karst	No

Species	Intercept	Winter-to-summer connectivity	Spatial covariates	Spatial covariates with AR1 time varying effects	Spatial spline
MYYU	Space: Ecoregions levels 2 and 3 Time (AR1): Ecoregion level-2	No	Elevation Elevation^2 Temp Temp^2 Physiographic diversity Precipitation Percent Forest Percent Wetlands	No	Tensor product interaction with 5 knots in each direction (25 total)
MYTH	Space: Ecoregions levels 2 and 3 Time (AR1): Ecoregion level-2	No	Elevation Elevation^2 Temp Temp^2 Physiographic diversity Precipitation Percent Forest Percent Wetlands	No	No
MYEV	Space: Ecoregions levels 2 and 3 Time (AR1): Ecoregion level-2	No	Elevation Elevation^2 Temp Temp^2 Physiographic diversity Precipitation Percent Forest Percent Wetlands	No	No
MYVO	Space: Ecoregions levels 2 and 3 Time (AR1): Ecoregion level-2	No	Elevation Elevation^2 Temp Temp^2 Physiographic diversity Precipitation Percent Forest Percent Wetlands	No	Tensor product interaction with 5 knots in each direction (25 total)

Species	Intercept	Winter-to-summer connectivity	Spatial covariates	Spatial covariates with AR1 time varying effects	Spatial spline
MYEV	Space: Ecoregions levels 2 and 3 Time (AR1): Ecoregion level-2	No	Elevation Elevation^2 Temp Temp^2 Physiographic diversity Precipitation Percent Forest Percent Wetlands	No	No
EPFU	Space: Ecoregions levels 2 and 3 Time (AR1): Ecoregion level-2	No	Elevation Elevation^2 Temp Temp^2 Physiographic diversity Precipitation Percent Forest Percent Wetlands	No	No
LACI	Space: Ecoregions levels 2 and 3 Time (AR1): Ecoregion level-2	No	Elevation Elevation^2 Temp Temp^2 Physiographic diversity Precipitation Percent Forest Percent Wetlands	No	No
LANO	Space: Ecoregions levels 2 and 3 Time (AR1): Ecoregion level-2	No	Elevation Elevation^2 Temp Temp^2 Physiographic diversity Precipitation Percent Forest Percent Wetlands	No	No

Species	Intercept	Winter-to-summer connectivity	Spatial covariates	Spatial covariates with AR1 time varying effects	Spatial spline
MYLE	Time (AR1): homogenous across space	No	Elevation Elevation^2 Temp Temp^2 Physiographic diversity Precipitation Percent Forest Percent Wetlands	No	No
MYGR	Time (AR1): homogenous across space	No	Elevation Elevation^2 Temp Temp^2 Physiographic diversity Precipitation Percent Forest Percent Wetlands	Karst River/Shoreline	No

In general, the finer the spatial scale used for modeling temporal change, the more accurately the model can capture temporal change across a landscape; however, due to the non-spatially balanced nature of sampling data over time (i.e., the sampling effort is shifting in space over time) care was taken to ensure the spatiotemporal component did not stratify the data too finely in space and time. This was to minimize potential biases in occupancy over time due to sampling issues and to minimize the number of regions and years with no sampling data. While Bayesian variants of information criterion can be calculated to help inform the model selection process, metrics such as Deviance Information Criterion (DIC) are not strictly valid for discrete mixture models, and Widely Applicable Information Criterion (WAIC) is not strictly valid when there is spatial or temporal autocorrelation (Hooten and Hobbs 2015). Furthermore, finer scale spatial models (e.g., spatial splines) were often favored by these metrics as opposed to those with less spatial structure, however, we found these effects often overpowered all other predictor effects and lead to overprediction for out of sample data. So, while information criterion metrics (DIC and WIAC) were calculated and were loosely used to guide initial model development, feedback received from species experts on the output of sample predictions (i.e., predicted occupancy maps) was given priority in guiding the final model structure for each species.

Thus, the exact specification of spatiotemporal dynamics was different between species depending on 1) the scope/geographic size of the species range, 2) the amount of sampling in ecoregions over time, and 3) whether additional spatiotemporal covariates were available (Table A.1). For example, for MYLU, MYSE and PESU which all had winter-to-summer connectivity metrics to help explain spatiotemporal dynamics, temporal effects were included at larger spatial scales (Ecoregion level-1 for MYLU and PESU, range-wide for MYSE). Note that we bounded the effect of connectivity to be strictly positive to better disentangle these spatiotemporal effects from other spatially correlated predictors and to reflect the a priori hypothesis for this variable should have a minimum value of zero (i.e., no effect). For other species with large geographic ranges but without connectivity metrics to help explain fine scale temporal change, temporal dynamics were modeled at Ecoregion level-2. We did not include ecoregion effects for some species with limited geographic ranges (e.g., MYGR). In the next section, an example specification of hierarchical spatiotemporal ecoregion effects (the model used for both MYLU and PESU) is described. The same general structure was used for other species, but ecoregion level-1 was dropped, and temporal effects were modeled at ecoregion level-2.

A.3.1 Hierarchical ecoregion effects in space and time

The purpose of including hierarchical ecoregions effects was to, 1) to better account for unmeasured regional spatial influences that are not captured in the other grid cell-level predictors (e.g., spatiotemporal autocorrelation), 2) to provide useful spatiotemporal structure (i.e., allow occupancy to vary across time at different rates in different ecologically meaningful regions), and 3) allow for sharing of information at several hierarchical spatial scales. While fully spatiotemporal dynamic models at the grid cell scale (e.g., Wright et al. 2021) are desirable, we cannot currently meet the data requirements of such models. However, the addition of hierarchical ecoregions effects allowed us to incorporate a more useful spatiotemporal structure beyond a single range-wide intercept.

Let m represent level-1 ecoregions, n represent level-2 ecoregions, t represent level-3 ecoregions, and j represent years. The overall intercept μ_{all}, is the hyperparameter mean of the ecoregion level-1 random intercepts in space μ_{E1_m}, which come from a normal distribution with standard deviation sd_{e1}.

$$\mu_{E1_m} \sim Normal(\mu_{all}, sd_{e1})$$

A vague normal prior is used for μ_{all}.The random intercept each year varied by ecoregion level-1 based on a multivariate normal autoregressive process, where the level-1 ecoregion spatial effects serve as the mean across years for each ecoregion level-1, and the covariance matrix is defined based on the overall temporal variance σ_y^2, and the correlation parameter ρ (which determines the degree of autocorrelation over time) scaled by the distance between years.

$$\mu_{E1Year_{m,j}} \sim MVN\left(\mu_{E1_m}, \Sigma\right)$$

The temporal correlation matrix across years j was constructed as follows. First, a square matrix with the number of rows and columns equal to the total number of years was specified with rows as i and columns as k. Σ was constructed by looping over each entry i and k in the matrix, and when $i = k$, then $\Sigma_{i,k} = \sigma_y^2$, and when $i \neq k$, then $\Sigma_{i,k} = \sigma_y^2 * \rho^{|i-k|}$, where σ_y^2 is the shared variance across level-1 ecoregions for year effects, while ρ is the temporal correlation parameter and determines the degree of covariance between years given the distance between them ($|i - k|$). Level-2 and level-3 Ecoregion spatial effects were drawn from normal distributions with means of zero and standard deviations of sd_{e2} and sd_{e3} respectively, and these effects were added to the Ecoregion level-1 by year random intercepts $\left(\mu_{E1Year_{m,j}}\right)$.

$$\mu_{E2_n} \sim Normal(0, sd_{e2})$$

$$\mu_{E2Year_{n,j}} = \mu_{E1Year_{m[n],j}} + \mu_{E2_n}$$

$$\mu_{E3_t} \sim Normal(0, sd_{e3})$$

$$\mu_{E3Year_{t,j}} = \mu_{E1Year_{n[t],j}} + \mu_{E3_t}$$

The levels of ecoregions used, especially for the temporal component, varied from species to species. An attempt was made to strike a balance between the finest level possible of spatial resolution in temporal change while also not dividing up the data too finely in space and time given limitations in the dataset (e.g., a non-spatiotemporally balanced sample). For MYLU, MYSE, and PESU, a winter to summer connectivity covariate was also incorporated, which accounts for expected grid cell-level spatiotemporal dynamics in the summer distribution given changes in the winter hibernacula counts, so temporal effects in the intercept were able to be modeled at a larger spatial scale than for species without this covariate. For MYSE, MYGR, and MYLE, ecoregions were dropped all together in favor of a range-wide intercept and covariate effects that changed over time (e.g., the effects of karst) and because in the case of MYGR, the range covers a small geographic extent. For MYSE, this was due to expert feedback that models with ecoregions tended to overpredict in some regions and lead to undesirable hard boundaries

between ecoregions, while the model without ecoregions matched more closely with expert expectations.

For MYLU and PESU, temporal effects were modeled at the ecoregion level-1, because when paired with a winter to summer connectivity metric, this allowed for an adequate spatial resolution to temporal change without dividing the data too finely from region and year. For the remaining species (MYYU, MYEV, MYVO, MYTH, EPFU, LACI, and LANO), ecoregion level-1 effects were removed, and year effects included at ecoregion level-2 to provide a finer scale of spatiotemporal change. We also received feedback from some species experts that ecoregion level-1 spatial and temporal effects spanned too large a spatial scale for some species and regions, that ecoregions levels 2 and 3 were a better representation.

Spatial effects of ecoregions often overpowered other grid cell-level covariates and resulted in undesirable and unrealistic 'hard edges' between ecoregions in the predicted occupancy maps. To ameliorate this issue, we included moderately informative regularization priors on the standard deviations of the space and time random effects (i.e., by including a prior with high support at relatively small values and low support at larger values). This is a common way of providing regularization in Bayesian models by pulling the coefficient effects towards zero (or towards the mean depending on parameterization) unless strongly supported in the data (Hooten and Hobbs 2015). Half-t distribution priors were used for these standard deviations, and the hyperparameters for degrees of freedom and scale varied by species depending on the amount of sampling data, where the target for the posterior distribution means on the standard deviations was less than 0.5 for ecoregions at level-1 and 2, and less than 0.25 for ecoregions level-3. Furthermore, the temporal autocorrelation parameter also provides a means of regularization of the change in occupancy over time and controls the degree of smoothness in the resulting time series of annual intercepts. To represent the a priori belief that the time series in bat occupancy should resemble Markovian dynamics (i.e., similar to the previous year) rather than entirely independent estimates from year to year, we put a weakly informative prior on the autocorrelation parameter of Beta (3,1), to ensure moderate amount of smoothness in the resulting time series.

A.3.2 Winter-to-summer connectivity metric

We calculated a winter-to-summer seasonal population connectivity metric for *Myotis lucifugus* (MYLU), *Myotis septentrionalis* (MYSE), and *Perimyotis subflavus* (PESU) to link the potential spatiotemporal influence of abundance in the known winter range to occupancy in the summer range. Winter counts for these species have declined drastically since the arrival of white-nose syndrome (WNS), with regional differences depending on the timing of WNS arrival (Cheng et al. 2021). We used a seasonal connectivity approach to examine whether there is a measurable spatiotemporal influence of known winter populations (and observed declines due to WNS) on the summer distribution of bats. We also included seasonal connectivity metrics in species' occupancy models to leverage the spatiotemporal information in the winter population monitoring data to help predict species' occupancy probabilities in space and time across summer distributions. For example, suitable habitat that was historically occupied at high rates may no longer be occupied due to severe regional WNS impacts.

We define a 'potential connectivity' metric based on metapopulation theory (Hanski and Ovaskainen 2000, Moilanen and Hanski 2001) to quantify winter-to-summer population connectivity, where the seasonal connectivity of a grid cell in the summer range is dependent on three factors: 1) the spatial distribution of all known winter hibernacula in the species range and the species abundance at each, 2) the distances between each hibernaculum and the grid cell of interest for summer occupancy, and 3) the seasonal migration movement behavior of the bats. One critical component of this metric is the seasonal migration/dispersal kernel, which describes the probability (p_{ij}) that summer site *i* (i.e., a grid cell) and winter hibernaculum *j* are connected based on the distance between them (d_{ij}). We chose the commonly used exponential kernel, which has a single parameter (α: the inverse of the mean migration distance), for simplicity and ease of parameterization. Species-specific values for the mean migration distances are given in Table 5 (Section 2.2.3).

$$p_{ij} = \exp(-\alpha * d_{ij})$$

The pairwise connectivity each year *y*, between each grid cell *i* and known winter hibernaculum j, is then calculated by multiplying p_{ij} by hibernaculum abundances each year (A_{jy}).

$$S_{ijy} = p_{ij} * A_{jy}$$

Thus, S_{ijy} is a proxy for the relative number of seasonal migrants between locations. Finally, the total seasonal connectivity in each grid cell and year is calculated by summing the contributions from each hibernaculum to each summer grid cell and year.

$$S_{iy} = \sum_{j} S_{ijy}$$

The winter-to-summer connectivity values for each grid cell and year (S_{iy}) were then included in the occupancy analyses as additional spatiotemporal covariates to estimate and predict trends in occupancy probabilities in space and time. When used as a predictor variable in occupancy analysis which utilizes a logistic regression, non-normal distributions, especially those that span values greater than three or less than negative three, can cause issues with the estimation procedure. This is especially true when all other predictor variables are centered (mean of zero) and scaled to have a standard deviation of one (implying that more than 95% of values should fall between negative two and two). Values were scaled for use in the occupancy models by taking a 'log plus one' transformation and then centering by the mean across sampled locations and years to improve estimation. The log transformation was used to normalize the raw data, which spanned many orders of magnitude, and the 'plus one' was included to limit the precision of values less than one, especially values very close to zero (e.g., 1e-17) which functionally represent zero expected seasonal migrants.

A.3.3 Spatial splines

For two species (MYYU and MYVO), we also included large-scale and continuous spatial effects at a grid cell-level using a multivariate Gaussian spatial spline (Wood 2016). We included this effect as a tensor product interaction (i.e., a different degree of smoothness in either

dimension) on the x and y coordinates. This improved distribution maps and estimated ecological covariate effects for both species based on expert feedback (and based on DIC and WIAC) by resolving problematic areas in the occupancy predictions. All components of the spatial spline (the JAGS code, the matrix spatial knots, and variance matrix) were created by mgcv R package (Wood 2012, 2016) by specifying a null model of the same dimensions as the occupancy model and were incorporated into the JAGS models. Predictions to out of sample grid cells required a matrix of knot values based on the spatial coordinates of each. These were calculated for each grid cell by feeding the spatial coordinates to the mgcv model object used to create the initial components for the JAGS model by making predictions for the 'lpmatrix', or the linear predictor matrix of the spatial knots. This matrix was incorporate in the same fashion as other spatial covariates when making occupancy predictions.

A.4 Model fitting

Due to the computational demands of Bayesian hierarchical models with large data sets, we modeled each species independently. We fit the MDSM false positive occupancy model for each species via MCMC using JAGS 4.3.0 (Plummer 2003) in R (R Core Team 2020). Each model was fit using three independent chains. The base settings were to run 10,000 iterations for each chain, with 5,000 being discarded as burn-in. We monitored convergence via visuals diagnostic criteria and by evaluating the Gelman-Rubin statistic, which suggest convergence with values near one (Gelman and Rubin 1992). If models had not converged after the initial run, we increased the number of iterations and burn-in until convergence was reached or until model runtimes became impractical. For some species with fewer years of data and additional spatial random effects (e.g., MYYU), much longer runs were possible and were sometime needed for convergence (for example, a burn-in of 30,000 with 80,000 total iterations).

A.5 Predicting occupancy maps and deriving status and trend across the species range

A.5.1 Temporal scope

For occupancy models, the period of interest within each year was May 1–Aug 31. Occupancy maps were predicted and status and trends were assessed from 2010–2019 for MYLU, PESU, and MYSE and from 2016–2019 for all other species. For EPFU and LACI, data from 2010–2015 was also included in model fitting to aid convergence, but predictions were only made for 2016–2019.

A.5.2 Spatial scope

Ideally, we would infer the status and trends of species across their entire North American ranges. However, despite several potential sources of species range maps (see section 2.3), there are often species detections assumed to be unambiguous for purposes of these analyses (i.e., manually vetted acoustic files or capture data) in the NABat database which fall outside of these published ranges. Also, when using ecological models to make predictions (e.g., occupancy probability) across a species range, it is best practice to limit the spatial scope of inference within the geographic extent of the sampling data to avoid issues of extrapolation. For these reasons, our general approach for inferring species status and trends at the species level was to make inferences across the 'Modeled Species Range,' which is the region of space where the species may feasibly occur, but within the geographic extent of the sampling data. For each species, we produced a spatial 2-dimensional kernel around all positive species

detections (ambiguous and unambiguous) for each species over all years of sampling. A polygon for the 'modeled species range' was produced by imposing a threshold on the underlying continuous kernel after tuning the threshold for each species to avoid 'islands' in the distribution. Furthermore, we only made predictions to ecoregions (level-3) for which we have sampling data for each species, thus we did not make predictions to level-3 ecoregions in the modeled species range without sampling data.

A.5.3 Measures of status and trend

For this analysis, we defined status as a measure of the ecological population variable of interest (occupancy probability). Site-level occupancy probabilities ψ_{it} in each grid cell i and year t were predicted for each cell in the species range based on the grid cell-level predictor values and the posterior mcmc samples k of each occupancy covariate coefficient from the occupancy model. Summary statistics for ψ_{it} were calculated based on the posterior predictive samples ψ_{it}^{k} for each grid cell and year.

The average occupancy aggregated across all grid cells in a region of interest each year $\hat{\psi}_t$ (or psi_bar) was derived by first taking the mean over all grid cells i for each year t and mcmc sample k, and then taking the mean over all mcmc samples k for each year t.

$$\widehat{\boldsymbol{\psi}}^{\boldsymbol{k}}{}_{\boldsymbol{t}} = \frac{1}{n}\sum_{i=1}^{n} \boldsymbol{\psi}_{\boldsymbol{i,t}}^{\boldsymbol{k}}$$

$$\hat{\psi}_t = \frac{1}{K}\sum_{k=1}^{K} \widehat{\boldsymbol{\psi}}^{\boldsymbol{k}}{}_{\boldsymbol{t}}$$

Where $\widehat{\boldsymbol{\psi}}^{\boldsymbol{k}}{}_{\boldsymbol{t}}$ is a matrix of mcmc samples k for every year t for the average occupancy probability across all grid cells in a region of interest. The ratio of annual change ($\hat{\lambda}_t$) in the average aggregate occupancy $\hat{\psi}_t$ between subsequent years is derived using samples $\widehat{\boldsymbol{\psi}}^{\boldsymbol{k}}{}_{\boldsymbol{t}}$ as

$$\hat{\boldsymbol{\lambda}}^{\boldsymbol{k}}{}_{\boldsymbol{t}} = \frac{\widehat{\boldsymbol{\psi}}^{\boldsymbol{k}}{}_{\boldsymbol{t}}}{\widehat{\boldsymbol{\psi}}^{\boldsymbol{k}}{}_{\boldsymbol{t-1}}}$$

$$\hat{\lambda}_t = \frac{1}{K}\sum_{k=1}^{K} \hat{\boldsymbol{\lambda}}^{\boldsymbol{k}}{}_{\boldsymbol{t}}$$

The trend parameter λ_{tot} estimates cumulative change over the timeframe of interest "[which] can be thought of as change in the mean of total response (McDonald 2003, pg. 279)". The trend parameter λ_{avg} is the average annual change over all years in a timeframe of interest. When this value is less than one, these values indicate a declining population. Following Banner et al. (2018) and Stratton and Irvine (2022), λ_{tot} is an estimate of the total occupancy rate change from 2010 (or the first year of sampling for some species) to 2019 for each species

$$\lambda_{tot} = \frac{1}{K}\sum_{k=1}^{K}\frac{\widehat{\boldsymbol{\psi}}^{k}_{\text{t=2019}}}{\widehat{\boldsymbol{\psi}}^{k}_{\text{t=2010}}}$$

$$\lambda_{avg} = \frac{1}{K}\sum_{k=1}^{K}\frac{1}{T-1}\sum_{t=1}^{T-1}\hat{\boldsymbol{\lambda}}^{\boldsymbol{k}}_{\boldsymbol{t}}$$

For a more natural interpretation, we convert these trend indicators from ratio of change to proportional rates of change (total_change and avg_annual_change) by subtracting one from each, so that values of 0.05 corresponds to a 5% increase, and values of -0.05 correspond to at 5% decrease. In the data release, these variables are called “deltas” instead of ‘lambdas”. For MYLU, MYSE, and PESU, we provide trend estimates over short-term (2016–2019, three years of change), medium-term (2012–2019, seven years of change) and long-term (2010–2019, nine years of change). For all other species, we only calculated short-term trends since occupancy models were fit to years 2016–2019. In rare cases, extremely uncertain (i.e., low confidence) regional trend estimates were dropped due to biologically unrealistic values in the 95% credible intervals (e.g., intervals that contained both positive and negative values, but with upper limits greater than +300%), which reflect either data limitation, model limitations, or extremely small values of starting occupancy (i.e., issues dividing by numbers close to zero). Otherwise, all regional estimates are provided in the results along with summaries of the sampling effort (total number of grid cells and proportion of each region sampled each year).

Any use of trade, firm, or product names is for descriptive purposes only and does not imply endorsement by the U.S. Government.

References cited in Appendix A

Balantic, C., and T. Donovan. 2019. "Dynamic Wildlife Occupancy Models Using Automated Acoustic Monitoring Data." *Ecological Applications* 0 (0): 1–14.

Banner, K. M., K. M. Irvine, T. J. Rodhouse, W. J. Wright, R. M. Rodriguez, and A. R. Litt. 2018. Improving Geographically Extensive Acoustic Survey Designs for Modeling Species Occurrence with Imperfect Detection and Misidentification. *Ecology and Evolution* 8 (12): 6144–56. https://doi.org/10.1002/ece3.4162.

Barr, E. L., Silvis, A., Armstrong, M. P., & Ford, W. M. 2021. White-nose Syndrome and Environmental Correlates to Landscape-Scale Bat Presence. *Wildlife Society Bulletin*, *45*(3), 410-421.

Chambert, T., D. A. W. Miller, and J. D. Nichols. 2015. Modeling False Positive Detections in Species Occurrence Data Under Different Study Designs. *Ecology* 96 (2): 332–39. https://doi.org/10.1890/14- 1507.1.

Chambert, T., Waddle, J.H., Miller, D.A., Walls, S.C. and Nichols, J.D., 2018. A new framework for analysing automated acoustic species detection data: Occupancy estimation and optimization of recordings post-processing. *Methods in Ecology and Evolution*, *9*(3), pp.560-570.

Cheng, T., Frick, W., Reichert, B.E., Thogmartin, W.E., Udell, B.J., Wiens, A., Whitby, M., Reichard, J., Szymanski, J. 2021 B. In Support of the U.S. Fish and Wildlife Service 3-Bat Species Status Assessment: Winter Colony Count Analysis: U.S. Geological Survey data release, https://doi.org/10.5066/P9YG45TG.

Gelman, A., and D. B. Rubin. 1992. "Inference from Iterative Simulation Using Multiple Sequences." *Statistical Science* 7 (4): 457–511.

Hanski, I., & Ovaskainen, O. 2000. The metapopulation capacity of a fragmented landscape. *Nature*, *404*(6779), 755-758.

Hooten, M. B., & Hobbs, N. T. 2015. A guide to Bayesian model selection for ecologists. *Ecological monographs*, *85*(1), pp.3-28.

Irvine, K. M., T. J. Rodhouse, W. J. Wright, and T. R. Olsen. 2018. "Occupancy Modeling Species-Environment Relationships with Non-Ignorable Survey Designs." *Ecological Applications* 8 (12): 6144–56. https://doi.org/10.1002/eap.1754.

Kéry, M., and J. A. Royle. 2020. Applied Hierarchical Modeling in Ecology: Analysis of distribution, abundance and species richness in R and BUGS: Volume 2: Dynamic and Advanced Models. Academic Press.

Loeb, S. C., T. J. Rodhouse, L. E. Ellison, C. L. Lausen, J. D. Reichard, K. M. Irvine, T. E. Ingersoll, et al. 2015. "A plan for the North American Bat Monitoring Program (NABat)." U.S. Department of Agriculture Forest Service, Southern Research Station, Asheville, NC.

MacKenzie, D.I., Nichols, J.D., Lachman, G.B., Droege, S., Andrew Royle, J. and Langtimm, C.A. 2002. Estimating site occupancy rates when detection probabilities are less than one. *Ecology*, *83*(8), pp.2248-2255.

MacKenzie, D. I., J. D. Nichols, J. A. Royle, K. H. Pollock, L. L. Bailey, and J. E. Hines. 2006. Occupancy Estimation and Modeling: Inferring Patterns and Dynamics of Species Occurrence. Burlington, MA: Elsevier: Academic Press.

McDonald, T. L. 2003. “Review of Environmental Monitoring Methods: Survey Designs.” *Environmental Monitoring and Assessment* 85: 277–92.

Miller, D. A., J. D. Nichols, B. T. McClintock, E. H. Campbell Grant, L. L. Bailey, and L. A. Weir. 2011. “Improving Occupancy Estimation When Two Types of Observational Error Occur: Non-Detection and Species Misidentification.” Ecology 92 (7): 1422–8.

Moilanen, A., Hanski, I., On the Use of Connectivity Measures in Spatial Ecology. 2001. *Oikos* Vol. 95, No. 1, pp. 147-151

Plummer, M., 2003, March. JAGS: A program for analysis of Bayesian graphical models using Gibbs sampling. In Proceedings of the 3rd international workshop on distributed statistical computing (Vol. 124, No. 125.10, pp. 1-10).

R Core Team. 2020. R: A language and environment for statistical computing. R Foundation for Statistical Computing, Vienna, Austria. URL https://www.R-project.org/.

Rodhouse, T. J., Rodriguez, R. M., Banner, K. M., Ormsbee, P. C., Barnett, J., & Irvine, K. M. (2019). Evidence of region-wide bat population decline from long-term monitoring and Bayesian occupancy models with empirically informed priors. *Ecology and evolution*, *9*(19), 11078-11088.

Royle, J.A. and Link, W.A., 2006. Generalized site occupancy models allowing for false positive and false negative errors. *Ecology*, 87(4), pp.835-841.

Stratton, C., and K.M. Irvine. 2022. Summertime Analysis Statistical Report for Little Brown, Northern Long-eared, and Tricolored Bat Species Status Assessment. Chapter B *in* Straw, B.R, J. A. Martin, J.D Reichard, and B.E Reichert, editors. Analytical Assessments in Support of the U.S. Fish and Wildlife Service 3-Bat Species Status Assessment. Cooperator Report prepared in cooperation with the U.S. Geological Survey, United States Fish and Wildlife Service and Bat Conservation International. https://doi.org/10.7944/P9B4RWEU

Wood, S., 2012. mgcv: Mixed GAM Computation Vehicle with GCV/AIC/REML smoothness estimation.

Wood, S.N., 2016. Just another gibbs additive modeller: interfacing JAGS and mgcv. *arXiv preprint arXiv:1602.02539*.

Wright, W.J., Irvine, K.M. and Rodhouse, T.J., 2016. A goodness-of-fit test for occupancy models with correlated within-season revisits. *Ecology and Evolution*, *6*(15), pp.5404-5415.

Wright, W.J., Irvine, K.M. and Higgs, M.D., 2019. Identifying occupancy model inadequacies: can residuals separately assess detection and presence?. *Ecology*, *100*(6), p.e02703.

Wright, W. J., Irvine, K. M., Rodhouse, T. J., & Litt, A. R. (2021). Spatial Gaussian processes improve multi-species occupancy models when range boundaries are uncertain and nonoverlapping. *Ecology and Evolution*.

Appendix B: State/Province/Territory Level Results

B.1 *Myotis lucifugus*

(A)

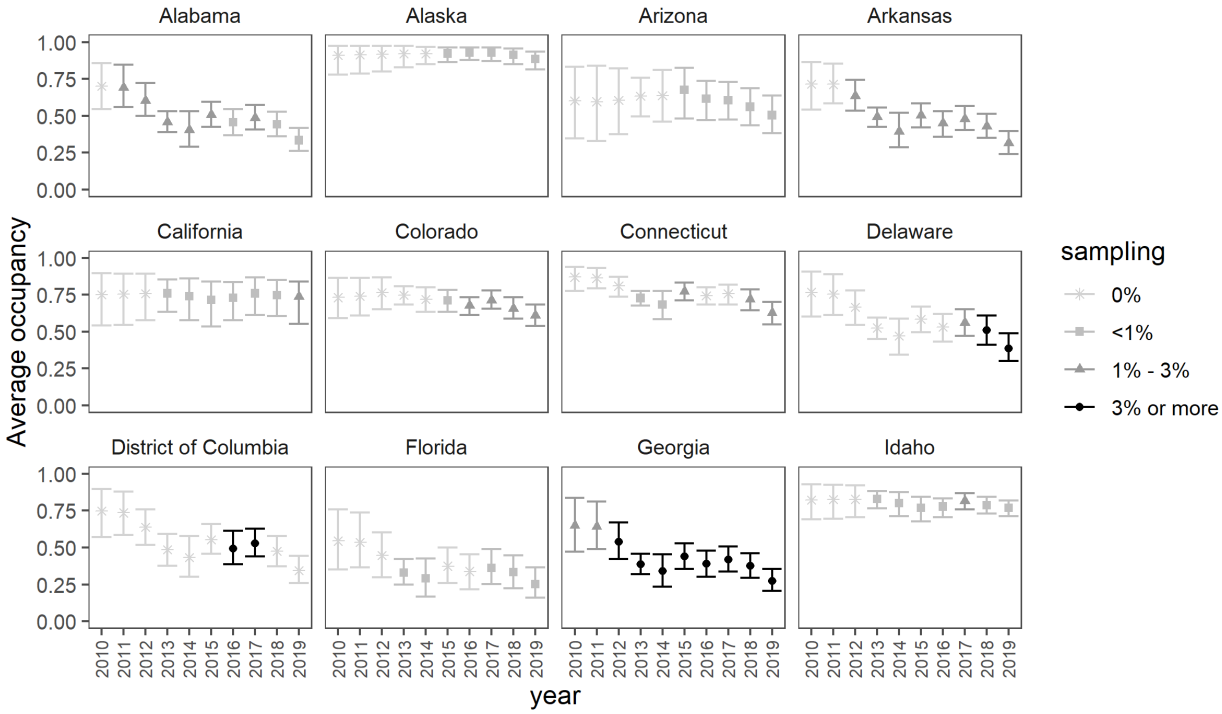

(B)

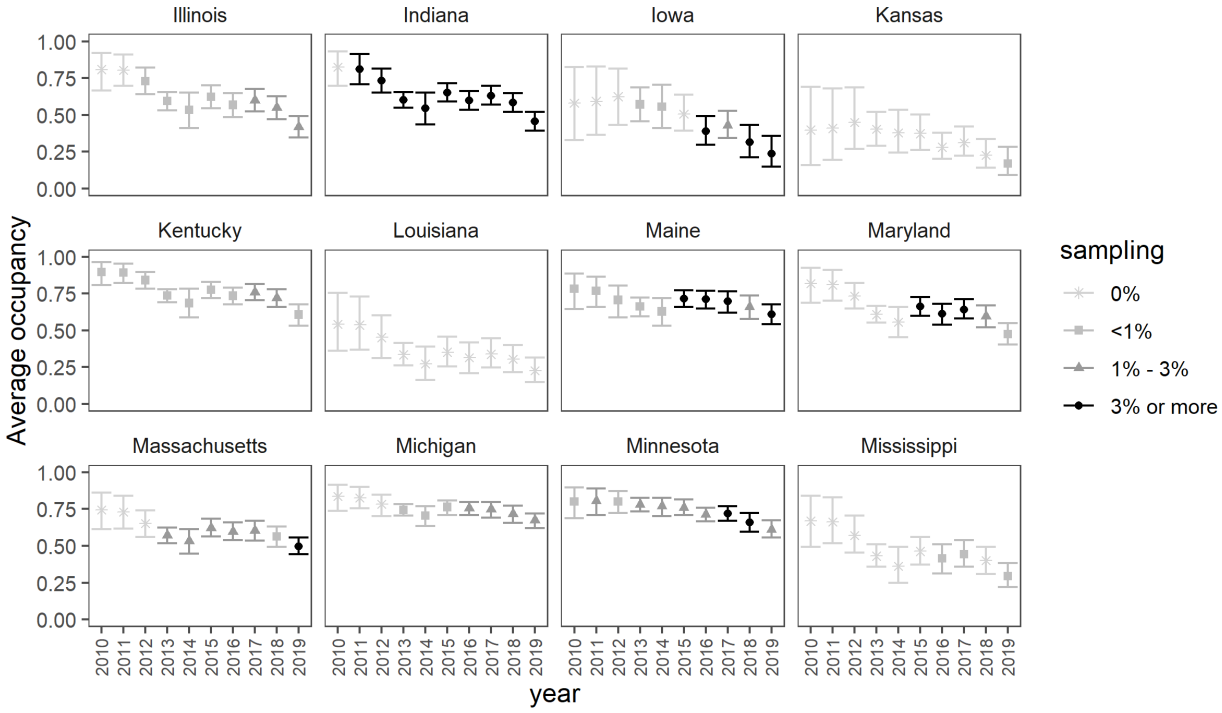

(C)

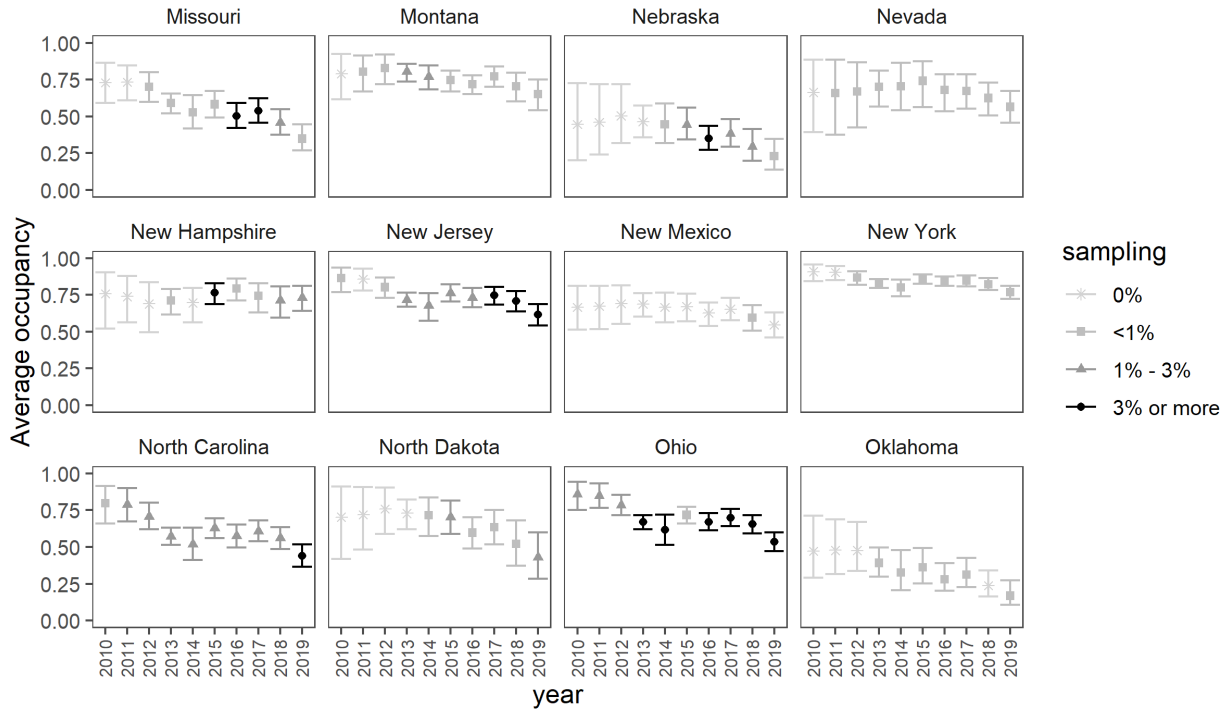
Missouri
Montana
Nebraska
Nevada
New Hampshire
New Jersey
New Mexico
New York
North Carolina
North Dakota
Ohio
Oklahoma
Average occupancy
1.00
0.75
0.50
0.25
0.00
2010
2011
2012
2013
2014
2015
2016
2017
2018
2019
year
sampling
0%
<1%
1% - 3%
3% or more

(D)

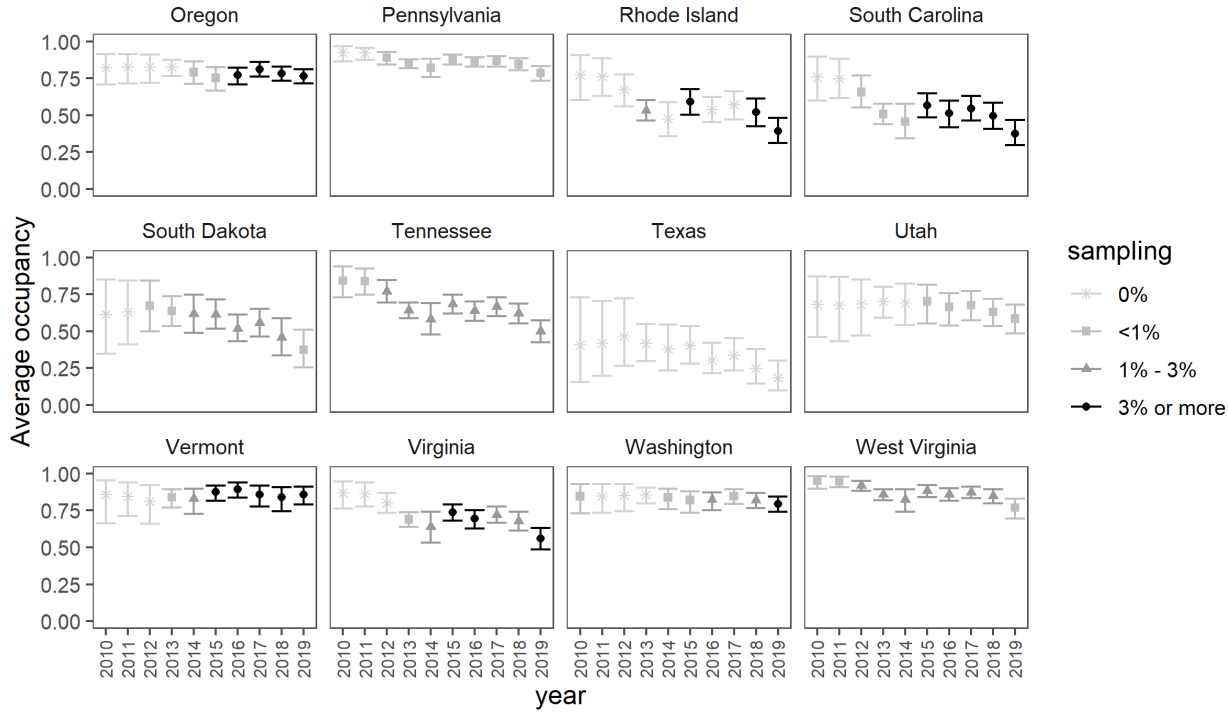
Oregon
Pennsylvania
Rhode Island
South Carolina
South Dakota
Tennessee
Texas
Utah
Vermont
Virginia
Washington
West Virginia
Average occupancy
1.00
0.75
0.50
0.25
0.00
2010
2011
2012
2013
2014
2015
2016
2017
2018
2019
year
sampling
0%
<1%
1% - 3%
3% or more

(E)

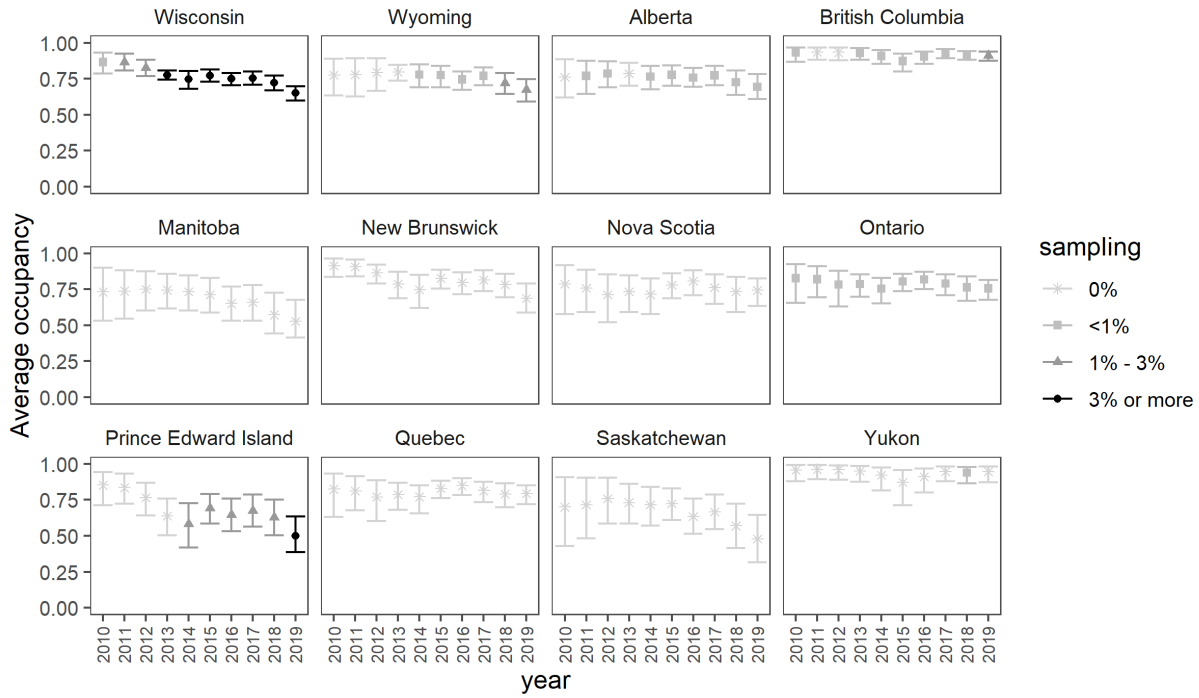

Figure B.1. Estimates of the average occupancy probability ($\hat{\psi}_t$) for *Myotis lucifugus* (MYLU) aggregated over all grid cells for each state, territory or province in the modeled species range each year. Means (points) and 95% credible intervals (bars) are depicted according to the percent of grid cells sampled (legend) are depicted according to the percent of grid cells sampled (legend) in the entire state, province or territory each year (A-E). U.S. states appear first in alphabetic order (A-E), followed by Canadian territories and provinces in alphabetic order (E).

(A)

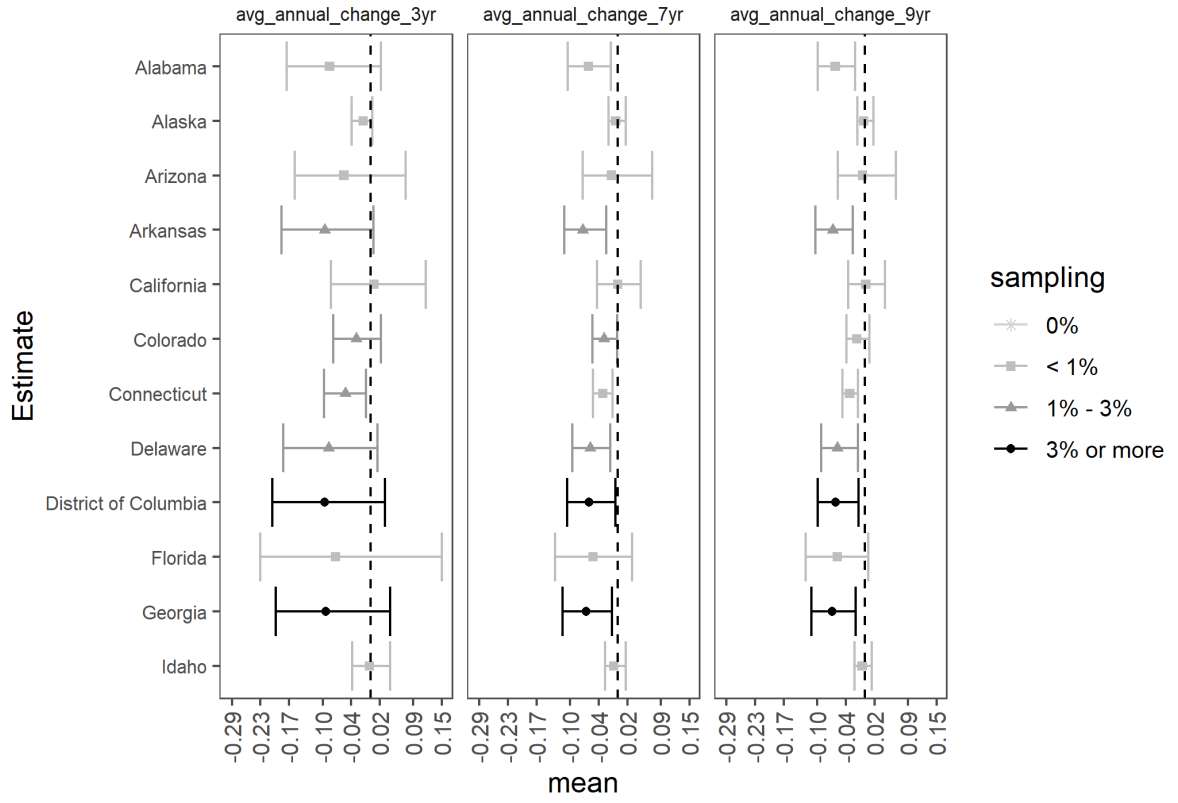
avg_annual_change_3yr
avg_annual_change_7yr
avg_annual_change_9yr
Alabama
Alaska
Arizona
Arkansas
California
Colorado
Connecticut
Delaware
District of Columbia
Florida
Georgia
Idaho
Estimate
-0.29
-0.23
-0.17
-0.10
-0.04
0.02
0.09
0.15
mean
sampling
0%
< 1%
1% - 3%
3% or more

(B)

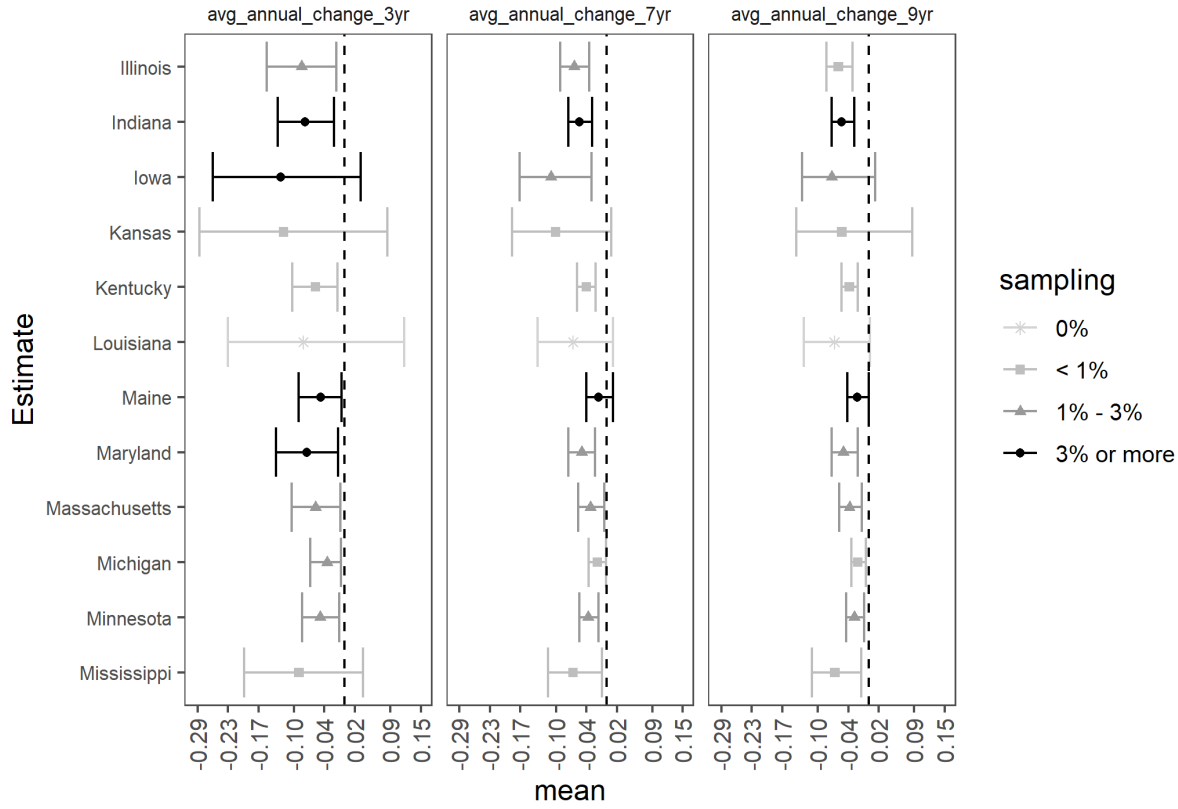
avg_annual_change_3yr
avg_annual_change_7yr
avg_annual_change_9yr
Illinois
Indiana
Iowa
Kansas
Kentucky
Louisiana
Maine
Maryland
Massachusetts
Michigan
Minnesota
Mississippi
Estimate
-0.29
-0.23
-0.17
-0.10
-0.04
0.02
0.09
0.15
mean
sampling
0%
< 1%
1% - 3%
3% or more

(C)

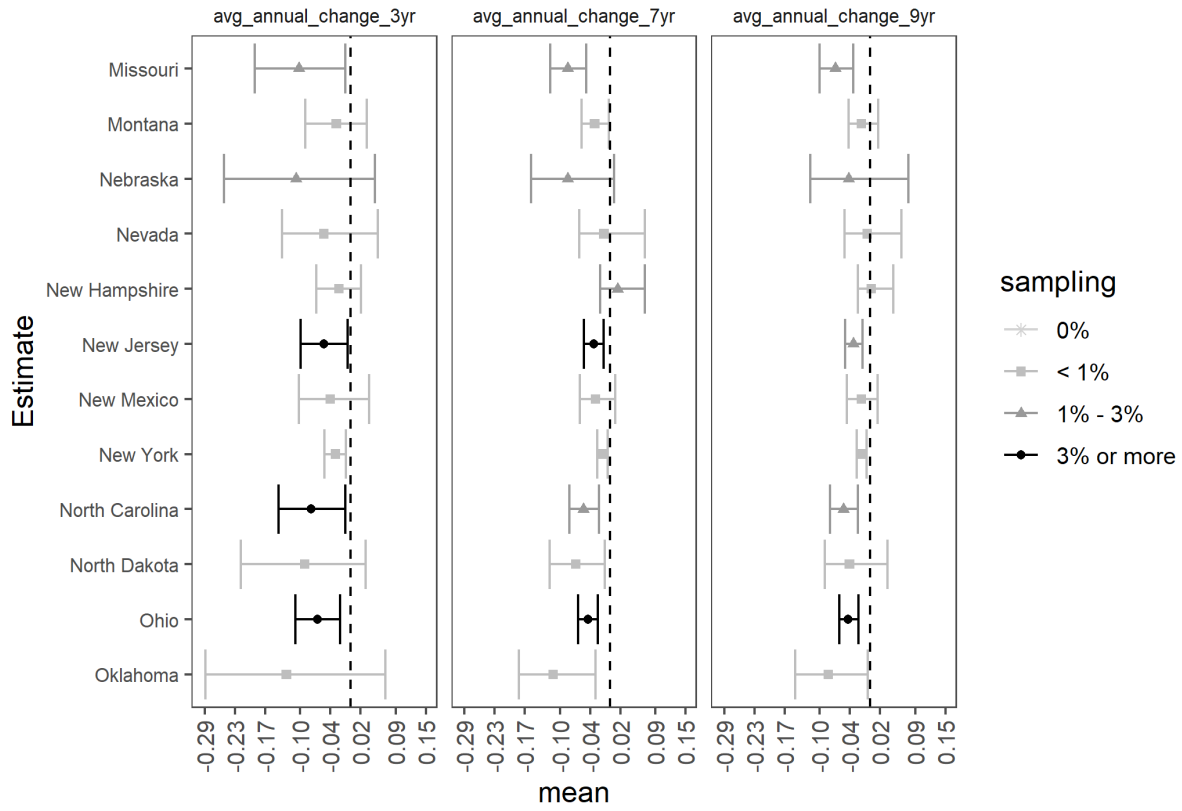
avg_annual_change_3yr
avg_annual_change_7yr
avg_annual_change_9yr
Missouri
Montana
Nebraska
Nevada
New Hampshire
New Jersey
New Mexico
New York
North Carolina
North Dakota
Ohio
Oklahoma
Estimate
-0.29
-0.23
-0.17
-0.10
-0.04
0.02
0.09
0.15
mean
sampling
0%
< 1%
1% - 3%
3% or more

(D)

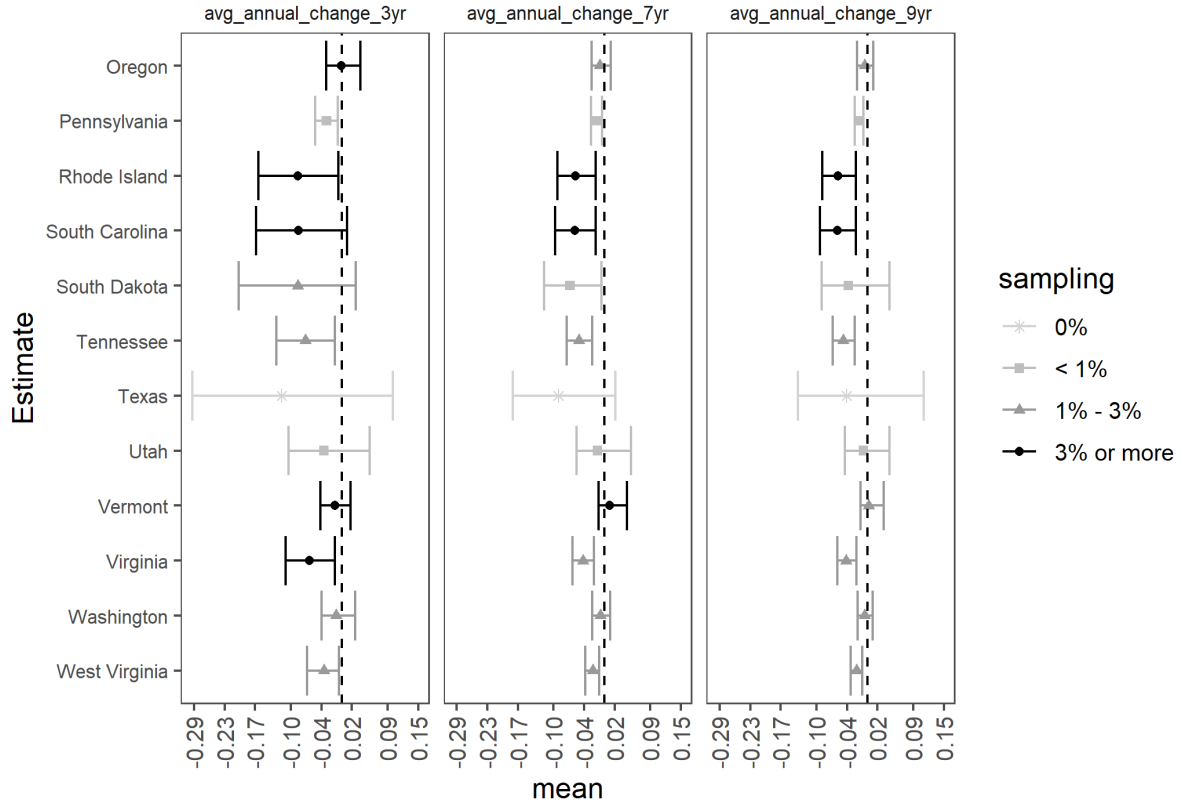
avg_annual_change_3yr
avg_annual_change_7yr
avg_annual_change_9yr
Oregon
Pennsylvania
Rhode Island
South Carolina
South Dakota
Tennessee
Texas
Utah
Vermont
Virginia
Washington
West Virginia
Estimate
-0.29
-0.23
-0.17
-0.10
-0.04
0.02
0.09
0.15
mean
sampling
0%
< 1%
1% - 3%
3% or more

(E)

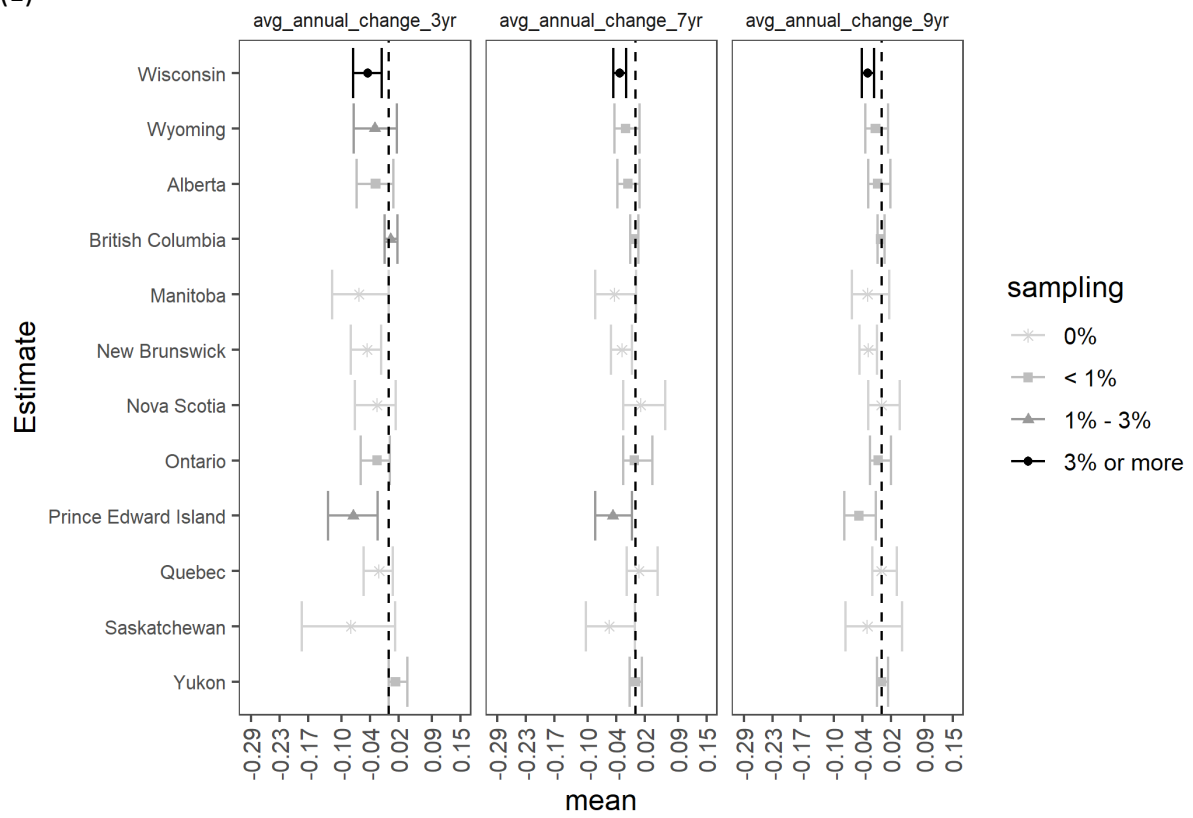

Figure B.2. Average annual rates of change in mean occupancy probabilities (avg_annual_change = lambda_avg - 1) for *Myotis lucifugus* (MYLU) between years over the designated time period (three years: 2016-2019, seven years: 2012-2019, or nine years: 2010-2019) aggregated across a state, province, or territory within the modeled species range. For example, if avg_change_9yr = -0.05, the mean occupancy rate has declined on average by 5% each year over the nine years since 2010. Means (points) and 95% credible intervals (bars) are depicted based on the average percent of grid cells sampled (legend) across all years in the timeframe of interest for each state, province or territory (A-E). Note that when credible intervals do not overlap zero, we have at least 95% certainty that these trends in species occupancy are either negative or positive. When credible intervals overlap zero, we have less than 95% certainty that these trends are different than zero. U.S. states appear first in alphabetic order (A-E), followed by Canadian territories and provinces in alphabetic order (E).

(A)

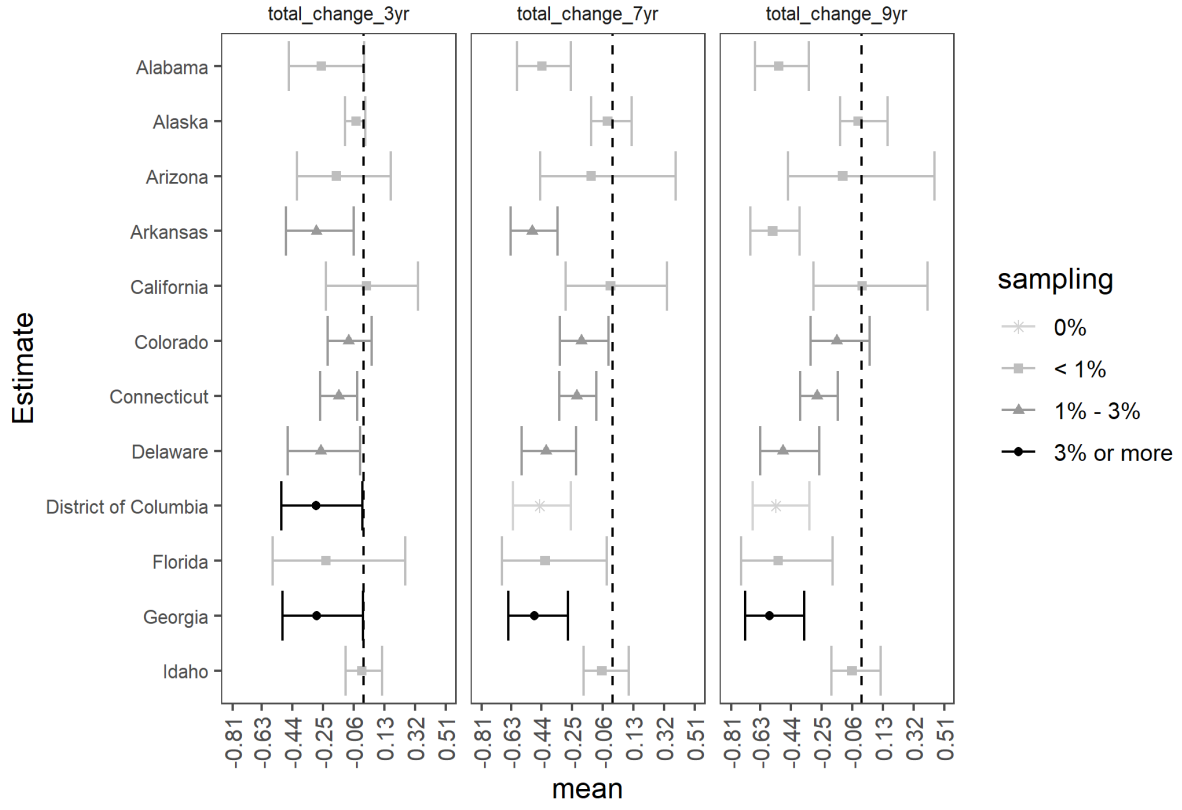
total_change_3yr
total_change_7yr
total_change_9yr
Alabama
Alaska
Arizona
Arkansas
California
Colorado
Connecticut
Delaware
District of Columbia
Florida
Georgia
Idaho
Estimate
-0.81
-0.63
-0.44
-0.25
-0.06
0.13
0.32
0.51
mean
sampling
0%
< 1%
1% - 3%
3% or more

(B)

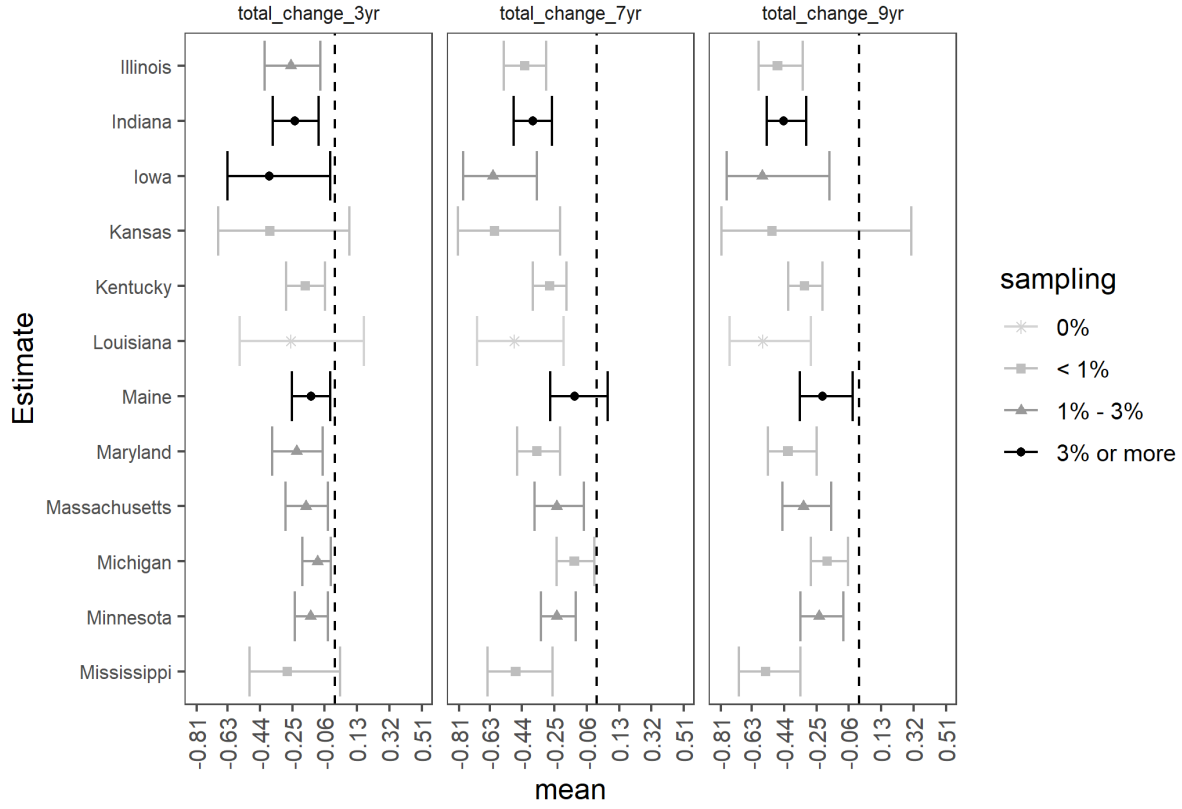
total_change_3yr
total_change_7yr
total_change_9yr
Illinois
Indiana
Iowa
Kansas
Kentucky
Louisiana
Maine
Maryland
Massachusetts
Michigan
Minnesota
Mississippi
Estimate
-0.81
-0.63
-0.44
-0.25
-0.06
0.13
0.32
0.51
mean
sampling
0%
< 1%
1% - 3%
3% or more

(C)

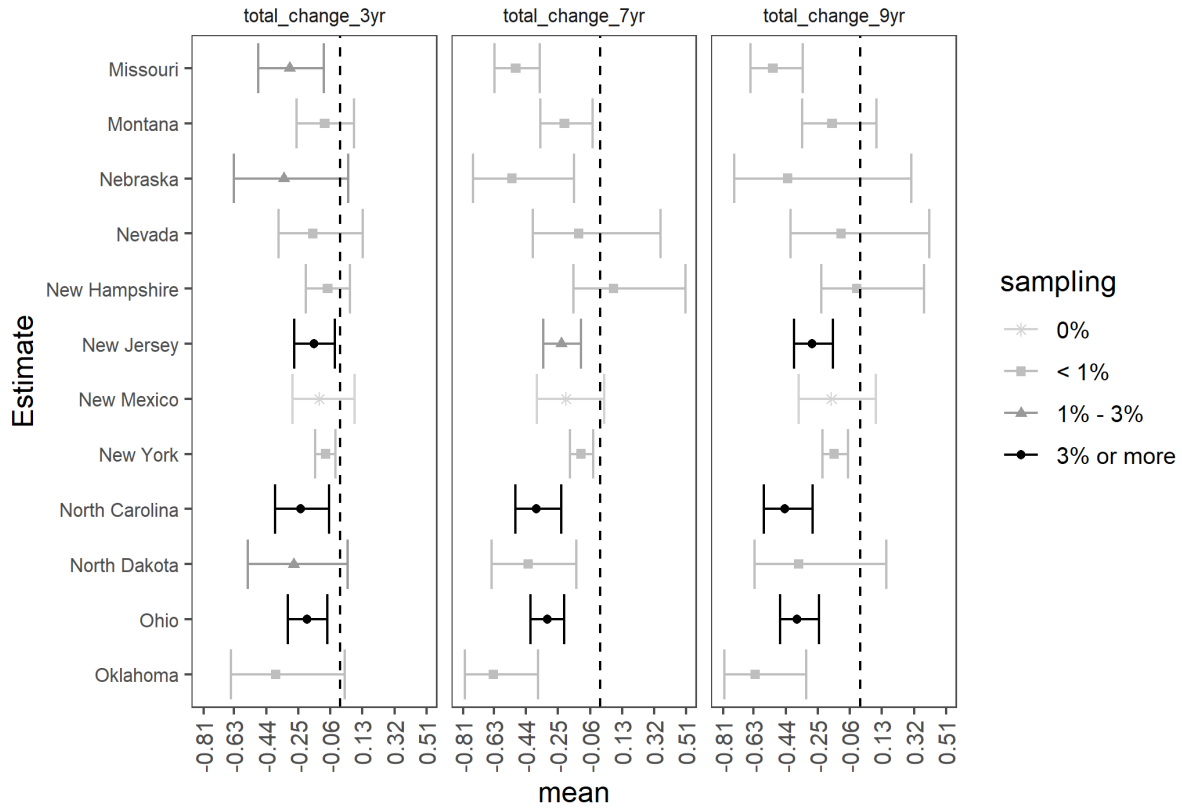
total_change_3yr
total_change_7yr
total_change_9yr
Missouri
Montana
Nebraska
Nevada
New Hampshire
New Jersey
New Mexico
New York
North Carolina
North Dakota
Ohio
Oklahoma
Estimate
-0.81
-0.63
-0.44
-0.25
-0.06
0.13
0.32
0.51
mean
sampling
0%
< 1%
1% - 3%
3% or more

(D)

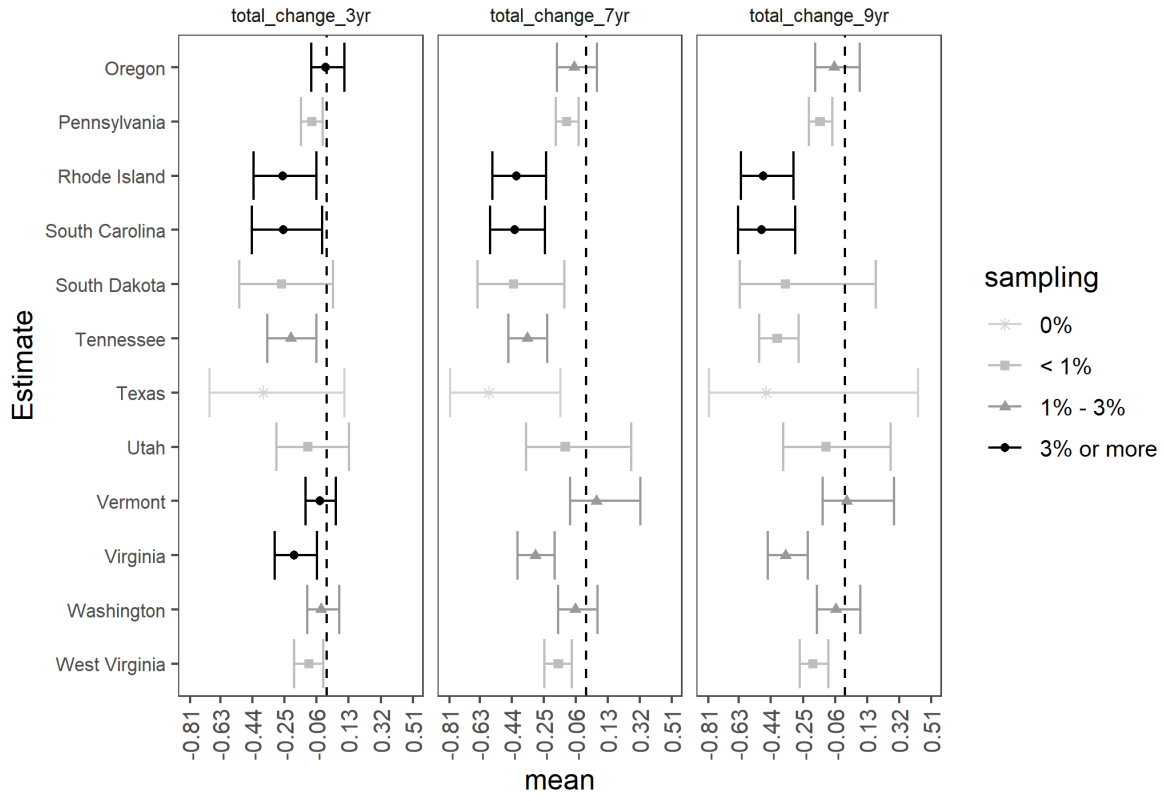
total_change_3yr
total_change_7yr
total_change_9yr
Oregon
Pennsylvania
Rhode Island
South Carolina
South Dakota
Tennessee
Texas
Utah
Vermont
Virginia
Washington
West Virginia
Estimate
-0.81
-0.63
-0.44
-0.25
-0.06
0.13
0.32
0.51
mean
sampling
0%
< 1%
1% - 3%
3% or more

(E)

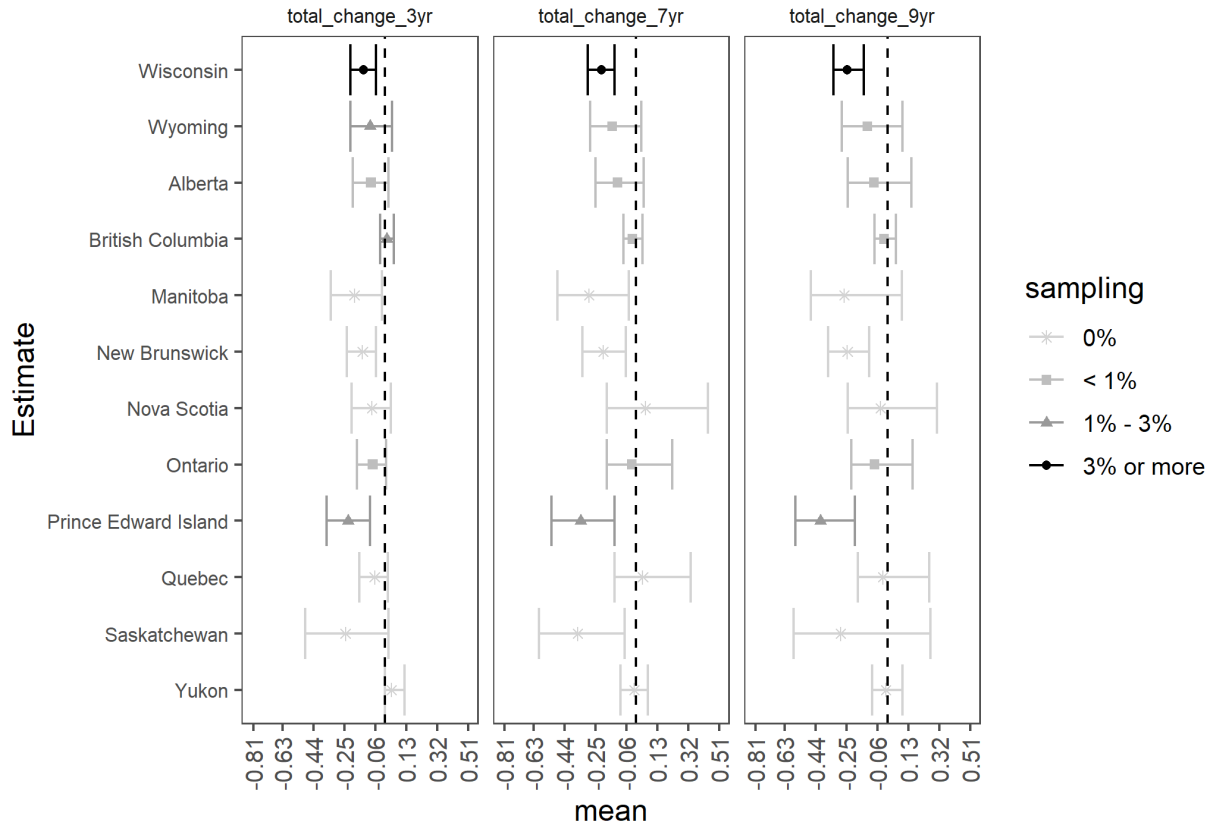

Figure B.3. The total change rate in mean occupancy (total_change = lambda_tot - 1) for *Myotis lucifugus* (MYLU) given the mean occupancy estimate in last year of sampling (2019) and the mean occupancy estimates three years (2016), seven years (2012), and nine years (2010) prior aggregated across a state, province, or territory within the modeled species range. For example, if total_change_9yr = -0.25, the mean occupancy rate has declined by 25% over the nine years since 2010, while a value of 0.25 would indicate an increase of 25%. Means (points) and 95% credible intervals (bars) are depicted based on the average percent of grid cells sampled (legend) in the first and last years of the timeframe of interest for each state, province or territory (A-E). Note that when credible intervals do not overlap zero, we have at least 95% certainty that these trends in species occupancy are either negative or positive. When credible intervals overlap zero, we have less than 95% certainty that these trends are different than zero. U.S. states appear first in alphabetic order (A-E), followed by Canadian territories and provinces in alphabetic order (E).

B.2 *Myotis septentrionalis*

(A)

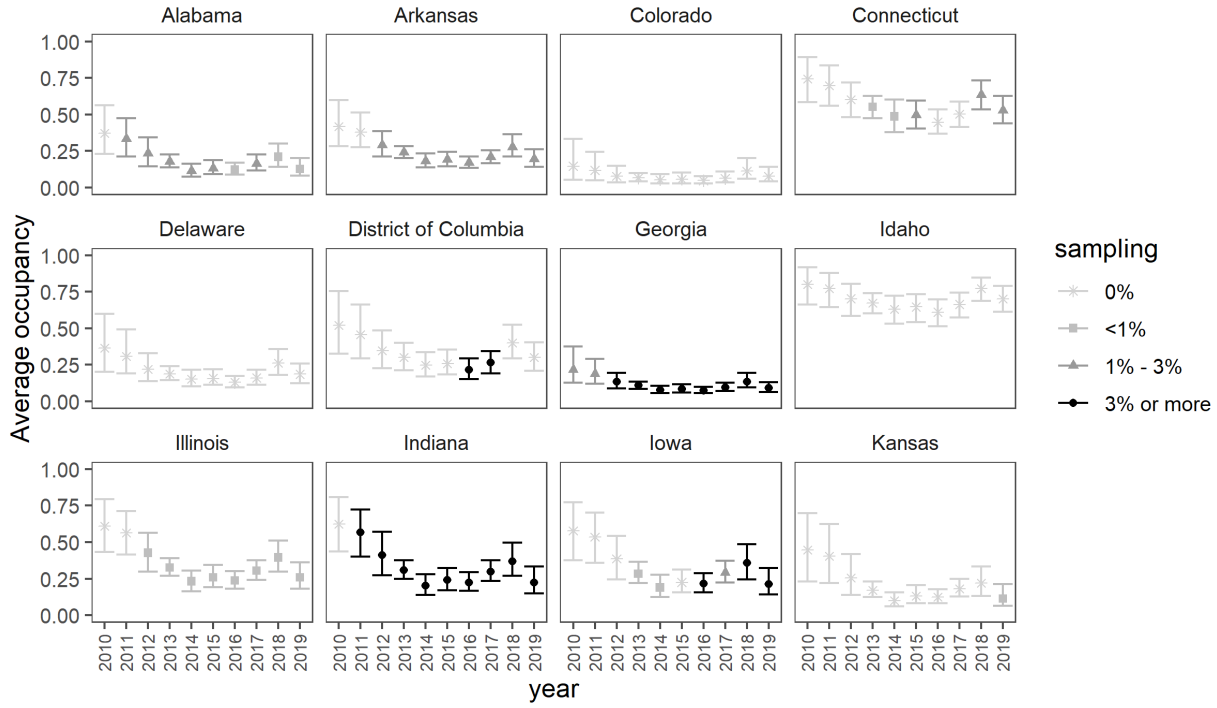

(B)

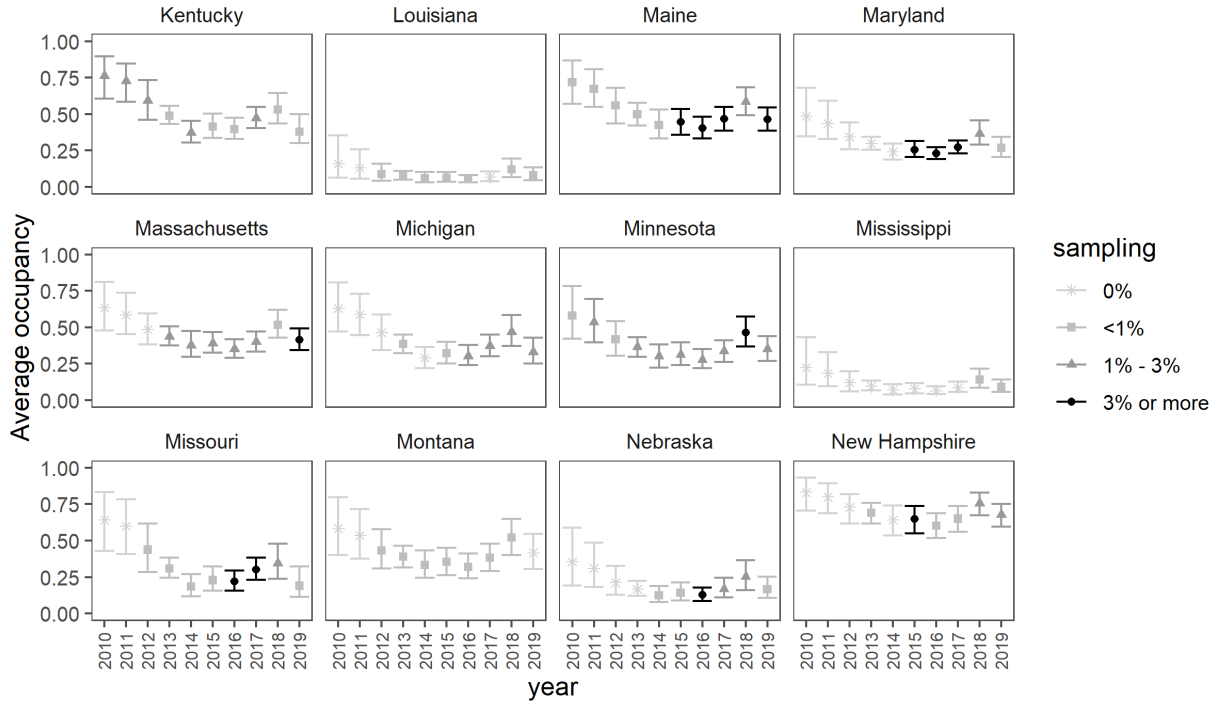

(C)

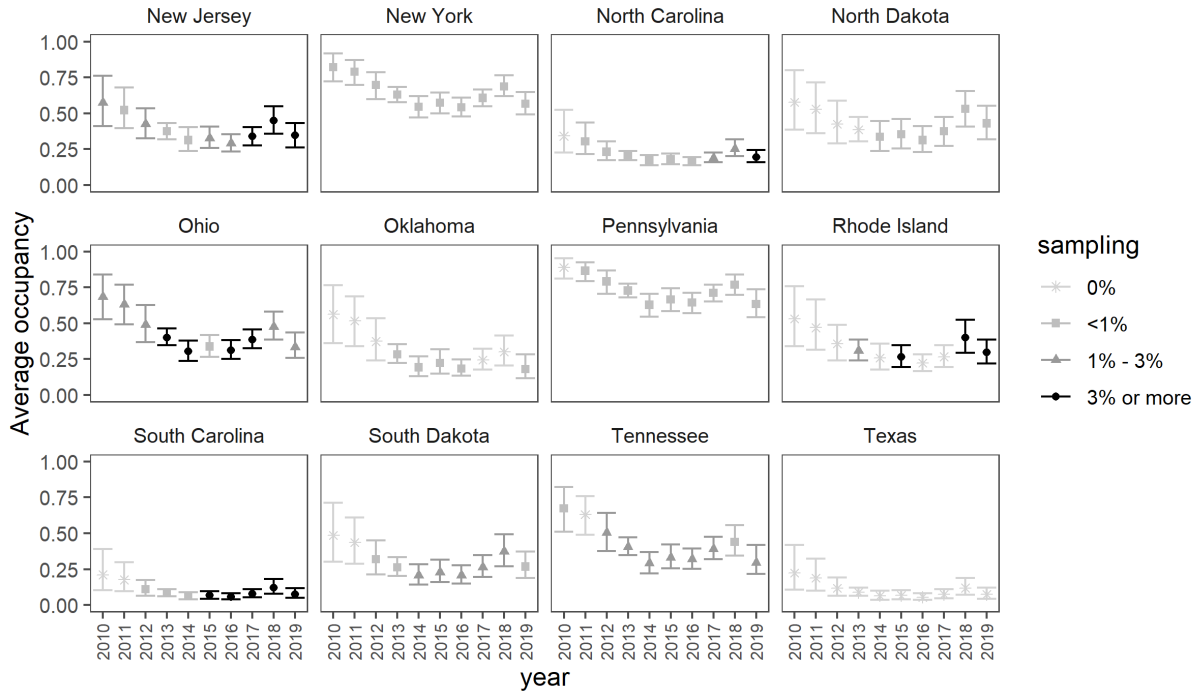
New Jersey
New York
North Carolina
North Dakota
Ohio
Oklahoma
Pennsylvania
Rhode Island
South Carolina
South Dakota
Tennessee
Texas
Average occupancy
1.00
0.75
0.50
0.25
0.00
2010
2011
2012
2013
2014
2015
2016
2017
2018
2019
year
sampling
0%
<1%
1% - 3%
3% or more

(D)

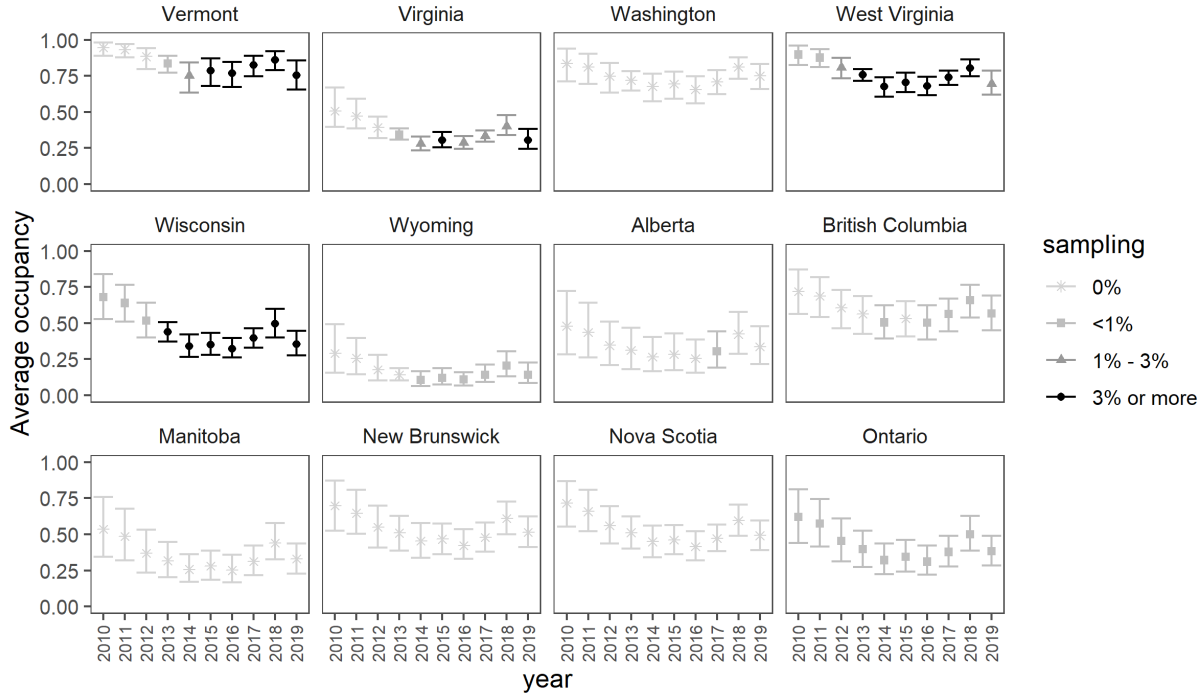
Vermont
Virginia
Washington
West Virginia
Wisconsin
Wyoming
Alberta
British Columbia
Manitoba
New Brunswick
Nova Scotia
Ontario
Average occupancy
1.00
0.75
0.50
0.25
0.00
2010
2011
2012
2013
2014
2015
2016
2017
2018
2019
year
sampling
0%
<1%
1% - 3%
3% or more

(E)

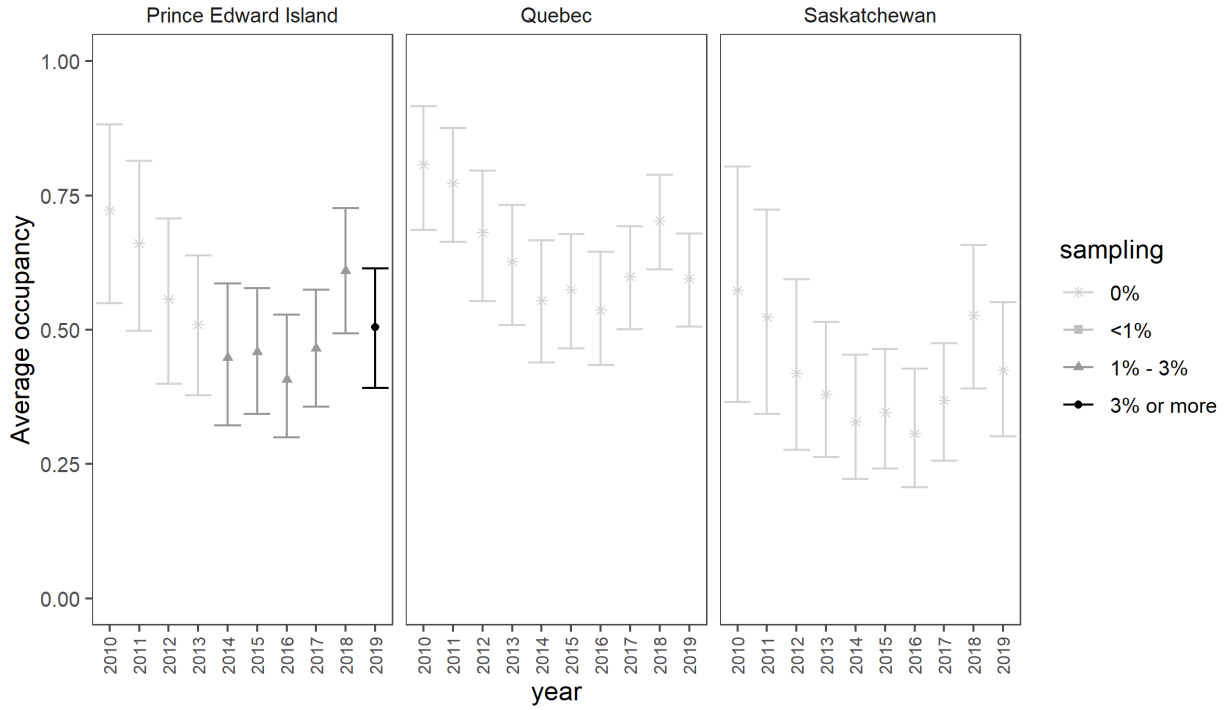

Figure B.4. Estimates of the average occupancy probability ($\widehat{\psi}_t$) for *Myotis septentrionalis* (MYSE) aggregated over all grid cells for each state, territory or province in the modeled species range each year. Means (points) and 95% credible intervals (bars) are depicted according to the percent of grid cells sampled (legend) in the entire state, province or territory each year (A-E). U.S. states appear first in alphabetic order (A-D), followed by Canadian territories and provinces in alphabetic order (D-E).

(A)

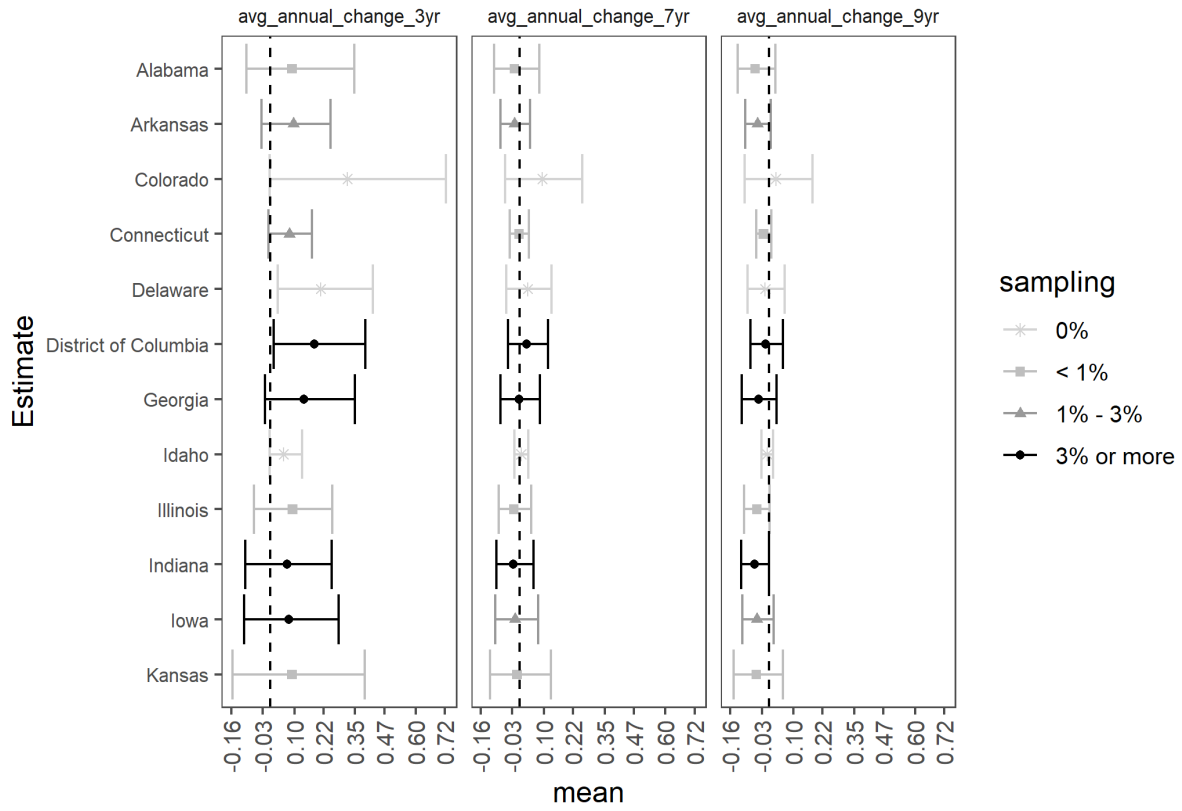
avg_annual_change_3yr
avg_annual_change_7yr
avg_annual_change_9yr
Alabama
Arkansas
Colorado
Connecticut
Delaware
District of Columbia
Georgia
Idaho
Illinois
Indiana
Iowa
Kansas
Estimate
-0.16
-0.03
0.10
0.22
0.35
0.47
0.60
0.72
mean
sampling
0%
< 1%
1% - 3%
3% or more

(B)

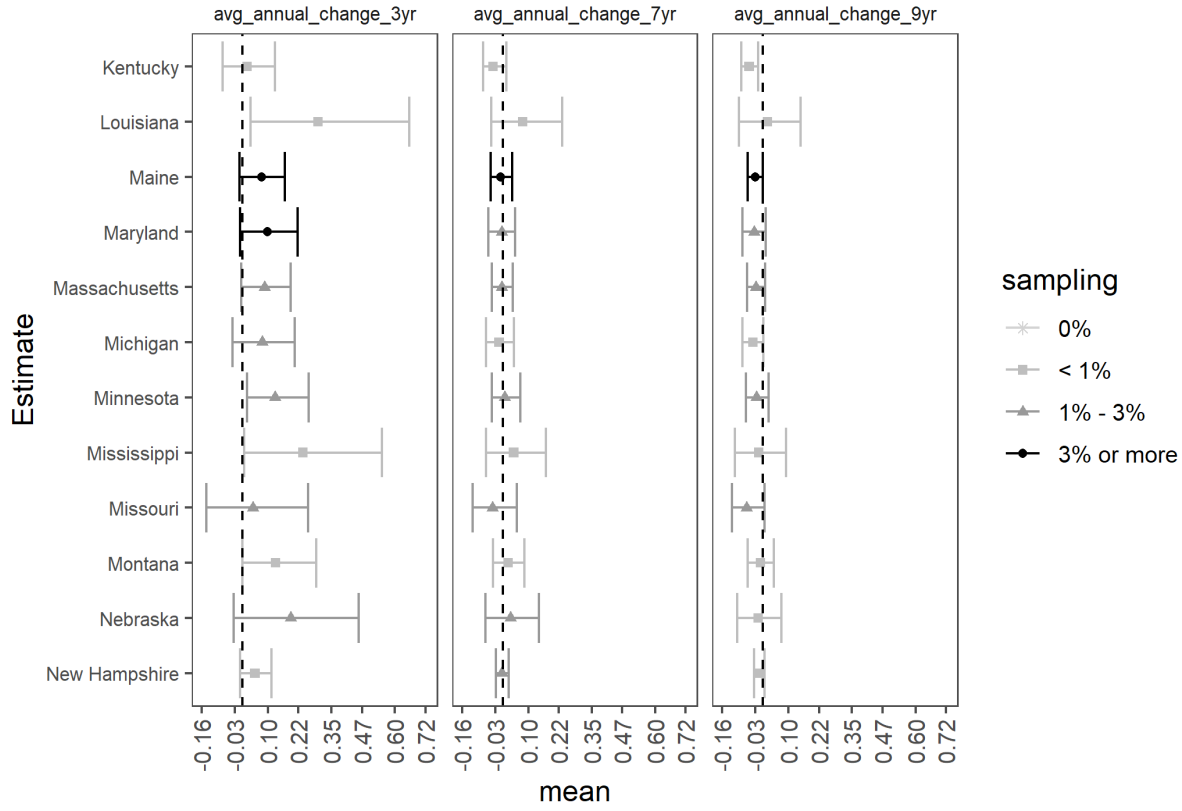
avg_annual_change_3yr
avg_annual_change_7yr
avg_annual_change_9yr
Kentucky
Louisiana
Maine
Maryland
Massachusetts
Michigan
Minnesota
Mississippi
Missouri
Montana
Nebraska
New Hampshire
Estimate
-0.16
-0.03
0.10
0.22
0.35
0.47
0.60
0.72
mean
sampling
0%
< 1%
1% - 3%
3% or more

(C)

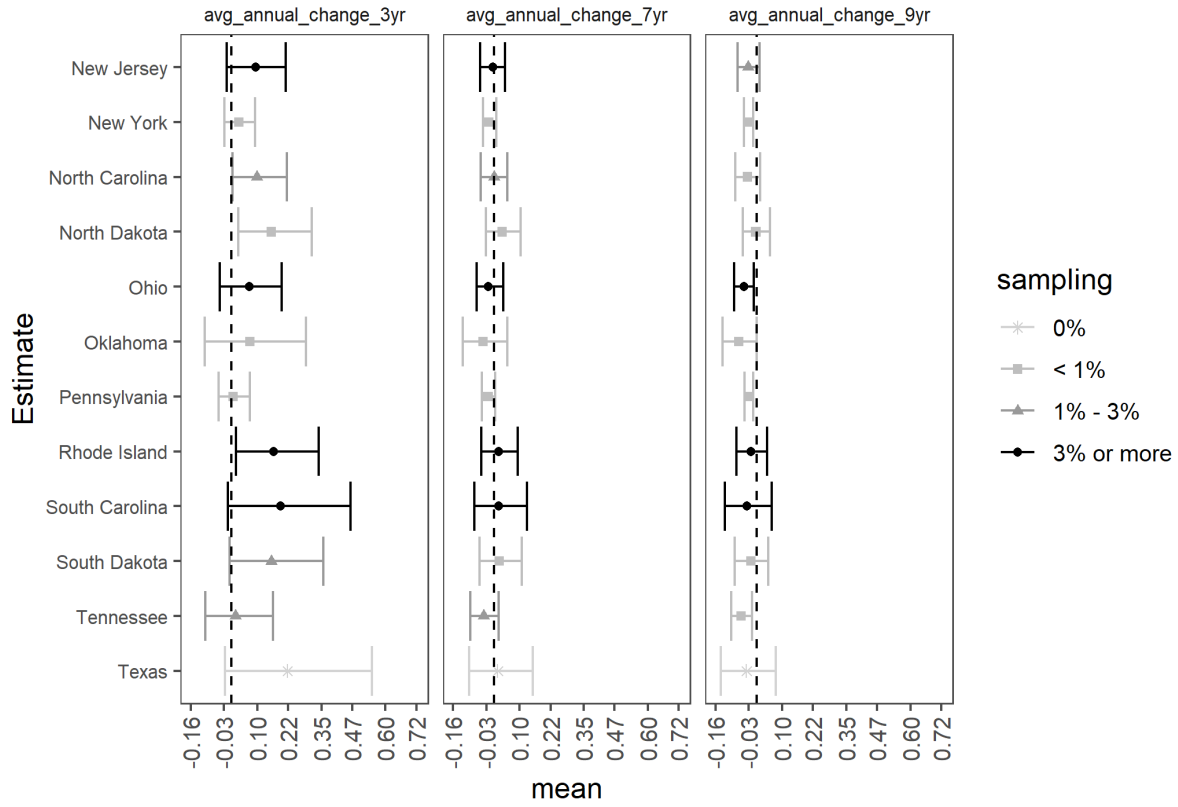
avg_annual_change_3yr
avg_annual_change_7yr
avg_annual_change_9yr
New Jersey
New York
North Carolina
North Dakota
Ohio
Oklahoma
Pennsylvania
Rhode Island
South Carolina
South Dakota
Tennessee
Texas
Estimate
-0.16
-0.03
0.10
0.22
0.35
0.47
0.60
0.72
mean
sampling
0%
< 1%
1% - 3%
3% or more

(D)

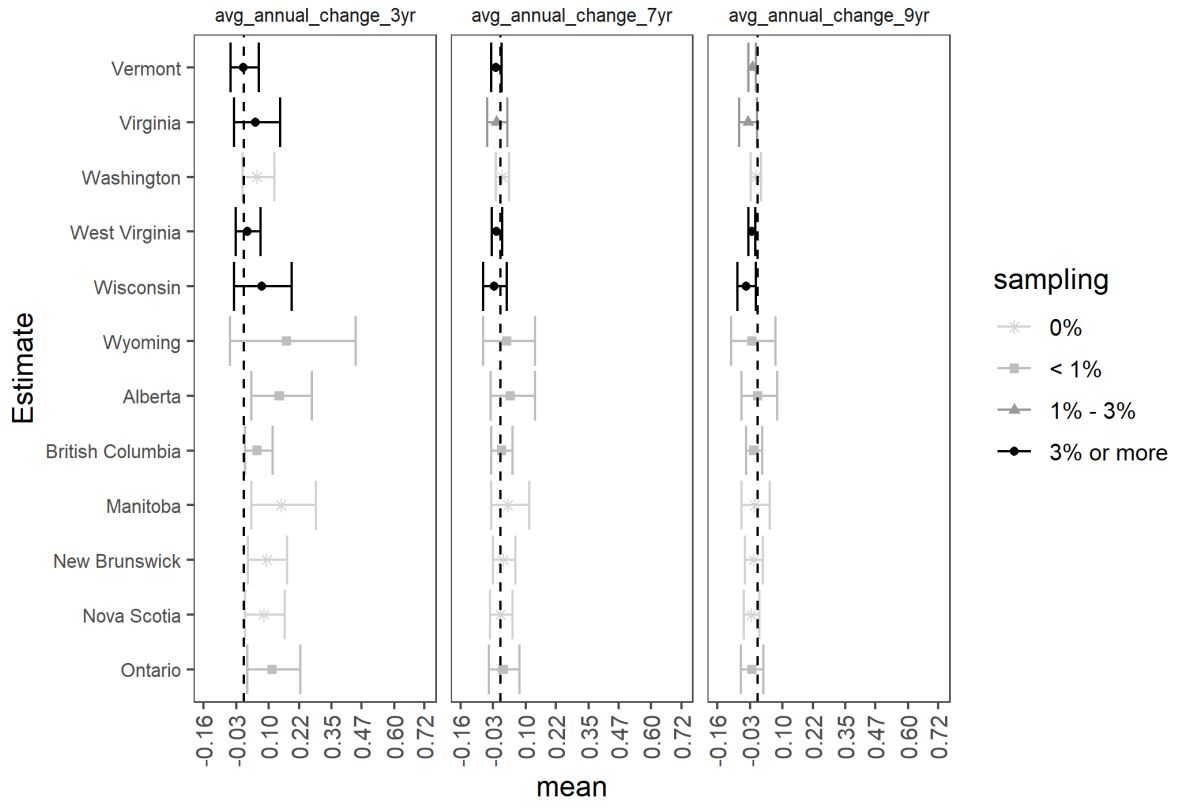
avg_annual_change_3yr
avg_annual_change_7yr
avg_annual_change_9yr
Vermont
Virginia
Washington
West Virginia
Wisconsin
Wyoming
Alberta
British Columbia
Manitoba
New Brunswick
Nova Scotia
Ontario
Estimate
-0.16
-0.03
0.10
0.22
0.35
0.47
0.60
0.72
mean
sampling
0%
< 1%
1% - 3%
3% or more

(E)

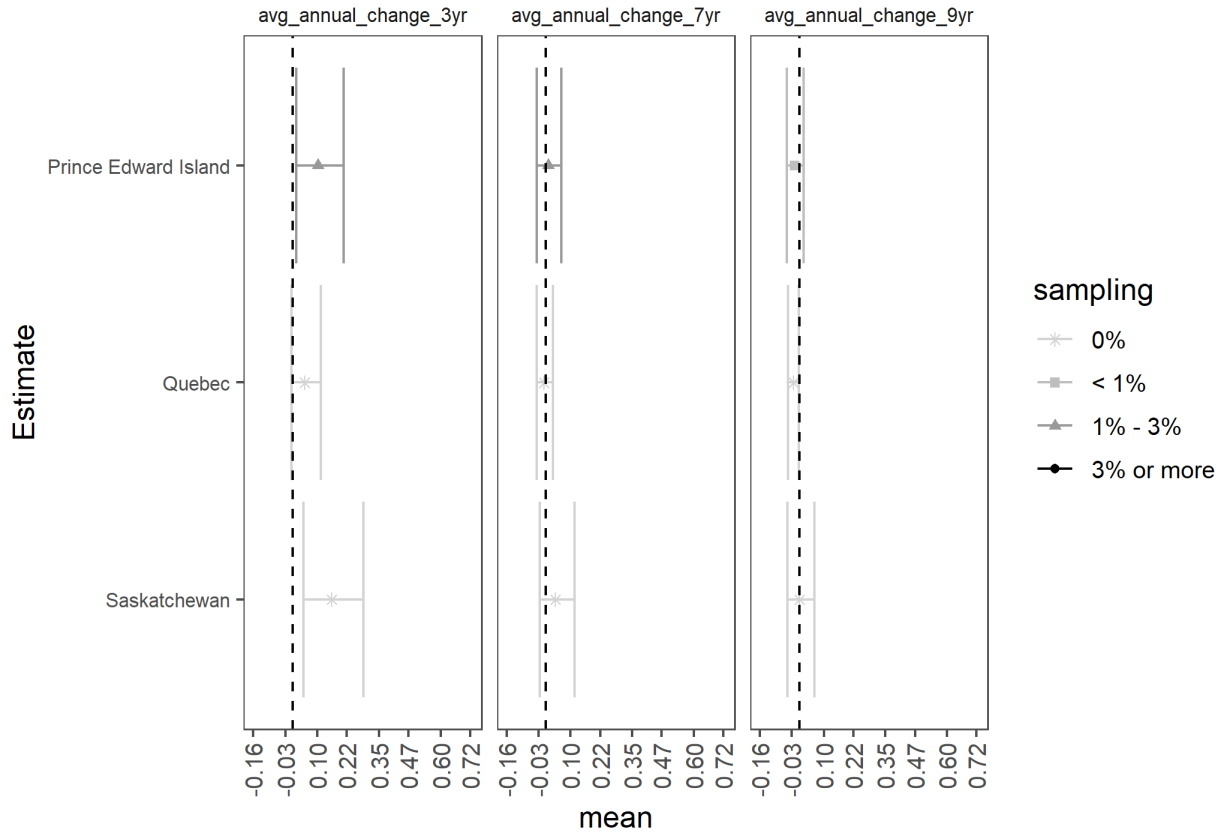

Figure B.5. Average annual rates of change in mean occupancy probabilities (avg_annual_change = lambda_avg - 1) for *Myotis septentrionalis* (MYSE) between years over the designated time period (three years: 2016-2019, seven years: 2012-2019, or nine years: 2010-2019) aggregated across a state, province, or territory within the modeled species range. For example, if avg_change_9yr = -0.05, the mean occupancy rate has declined on average by 5% each year over the nine years since 2010. Means (points) and 95% credible intervals (bars) are depicted based on the average percent of grid cells sampled (legend) across all years in the timeframe of interest for each state, province or territory (A-E). Note that when credible intervals do not overlap zero, we have at least 95% certainty that these trends in species occupancy are either negative or positive. When credible intervals overlap zero, we have less than 95% certainty that these trends are different than zero. U.S. states appear first in alphabetic order (A-D), followed by Canadian territories and provinces in alphabetic order (D-E).

(A)

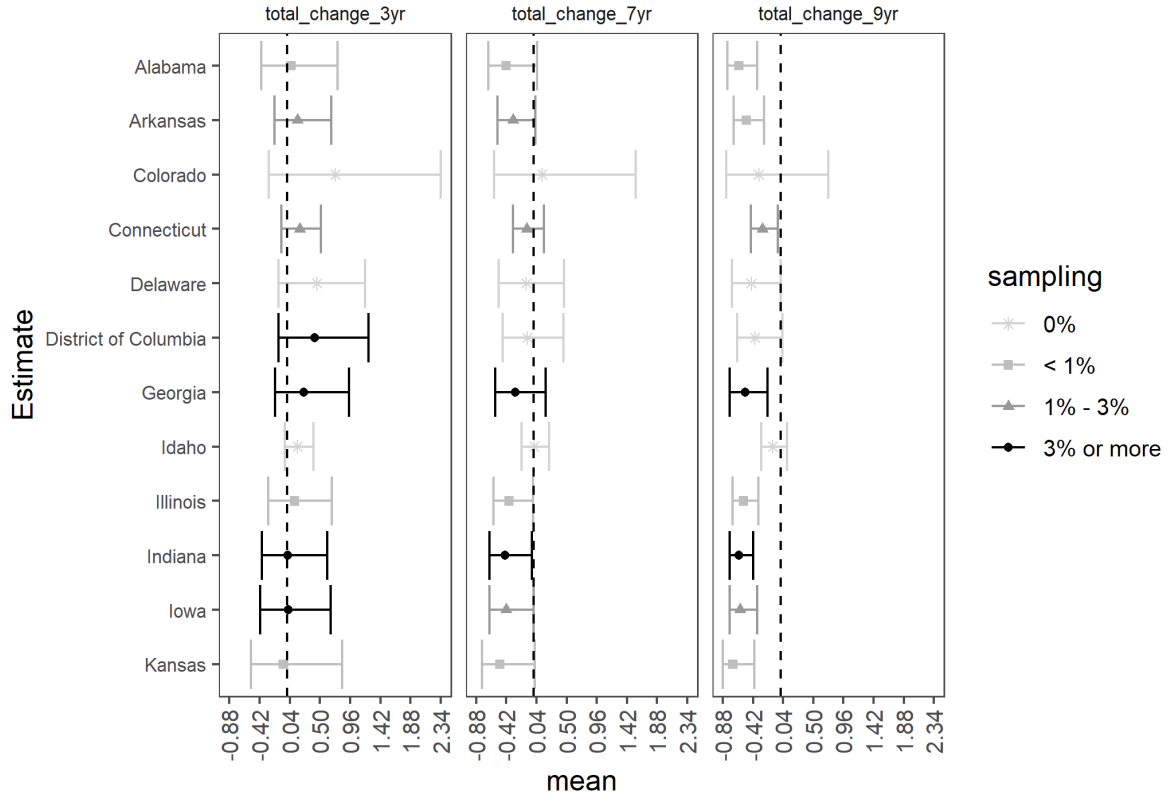
total_change_3yr
total_change_7yr
total_change_9yr
Alabama
Arkansas
Colorado
Connecticut
Delaware
District of Columbia
Georgia
Idaho
Illinois
Indiana
Iowa
Kansas
Estimate
-0.88
-0.42
0.04
0.50
0.96
1.42
1.88
2.34
mean
sampling
0%
< 1%
1% - 3%
3% or more

(B)

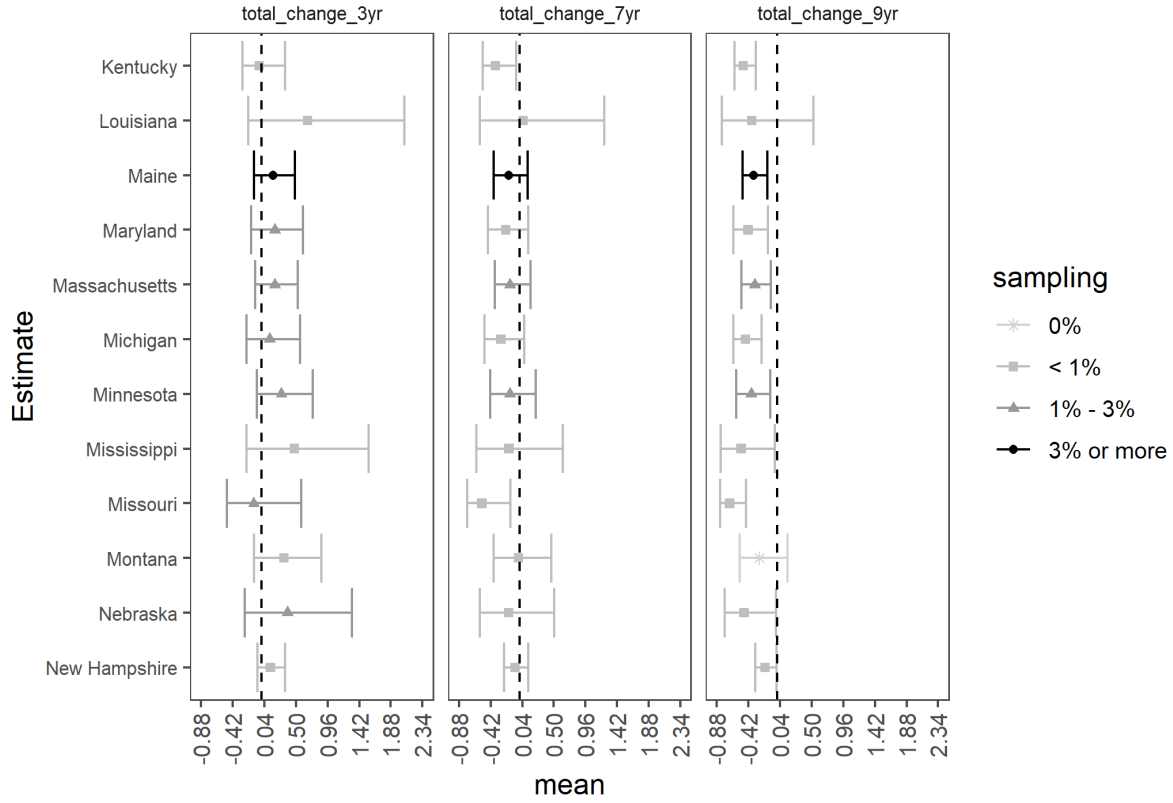
total_change_3yr
total_change_7yr
total_change_9yr
Kentucky
Louisiana
Maine
Maryland
Massachusetts
Michigan
Minnesota
Mississippi
Missouri
Montana
Nebraska
New Hampshire
Estimate
-0.88
-0.42
0.04
0.50
0.96
1.42
1.88
2.34
mean
sampling
0%
< 1%
1% - 3%
3% or more

(C)

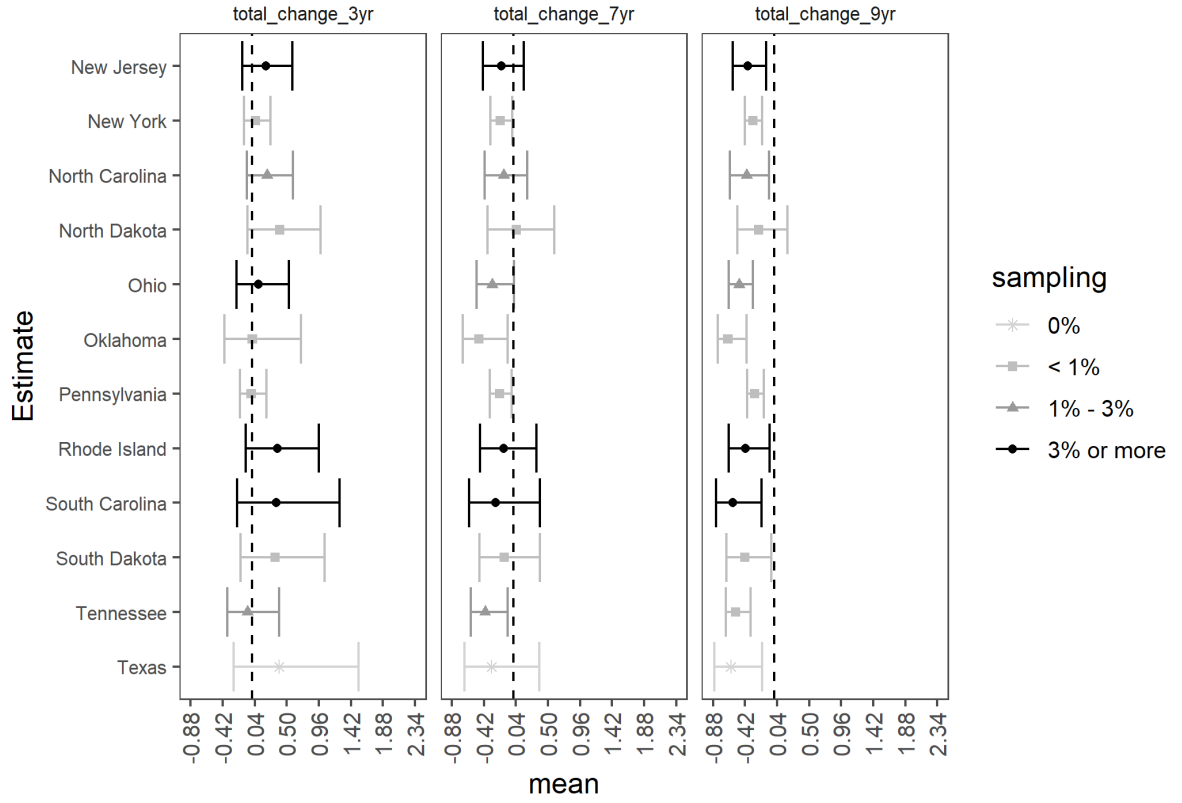
total_change_3yr
total_change_7yr
total_change_9yr
New Jersey
New York
North Carolina
North Dakota
Ohio
Oklahoma
Pennsylvania
Rhode Island
South Carolina
South Dakota
Tennessee
Texas
Estimate
-0.88
-0.42
0.04
0.50
0.96
1.42
1.88
2.34
mean
sampling
0%
< 1%
1% - 3%
3% or more

(D)

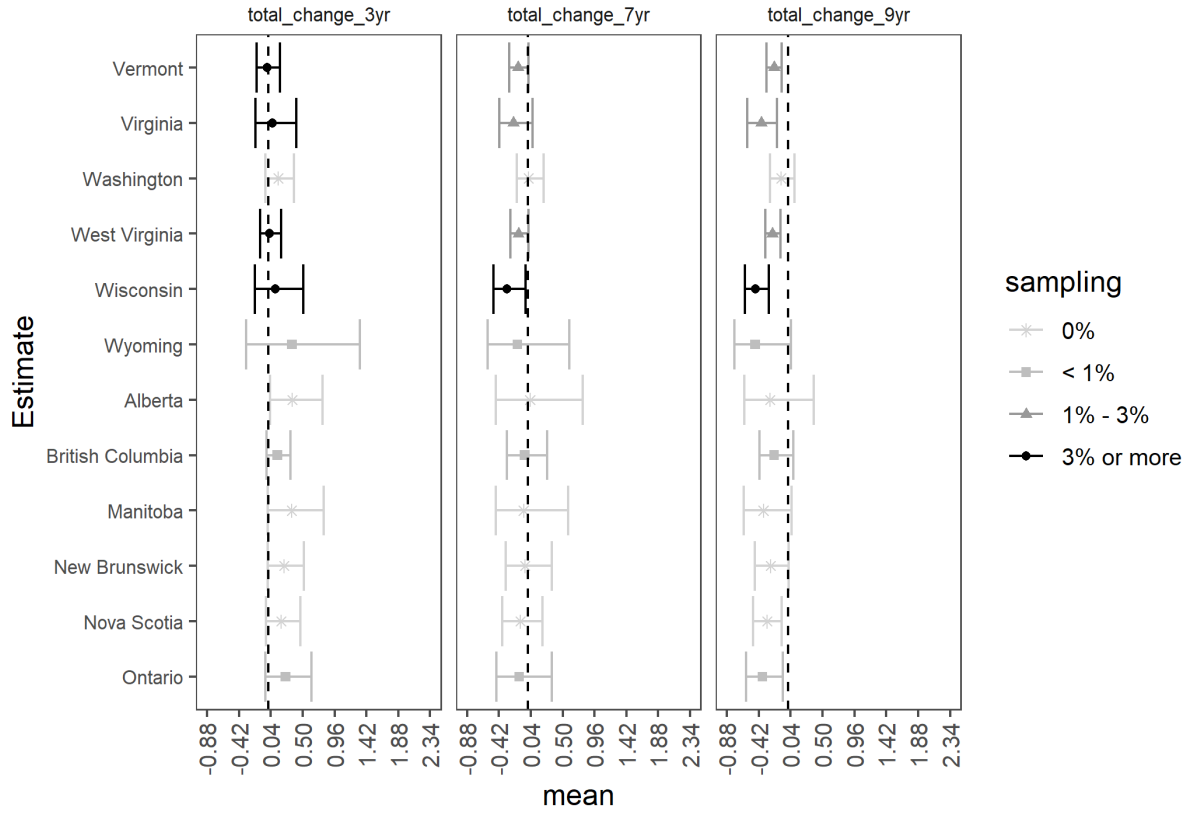
total_change_3yr
total_change_7yr
total_change_9yr
Vermont
Virginia
Washington
West Virginia
Wisconsin
Wyoming
Alberta
British Columbia
Manitoba
New Brunswick
Nova Scotia
Ontario
Estimate
-0.88
-0.42
0.04
0.50
0.96
1.42
1.88
2.34
mean
sampling
0%
< 1%
1% - 3%
3% or more

(E)

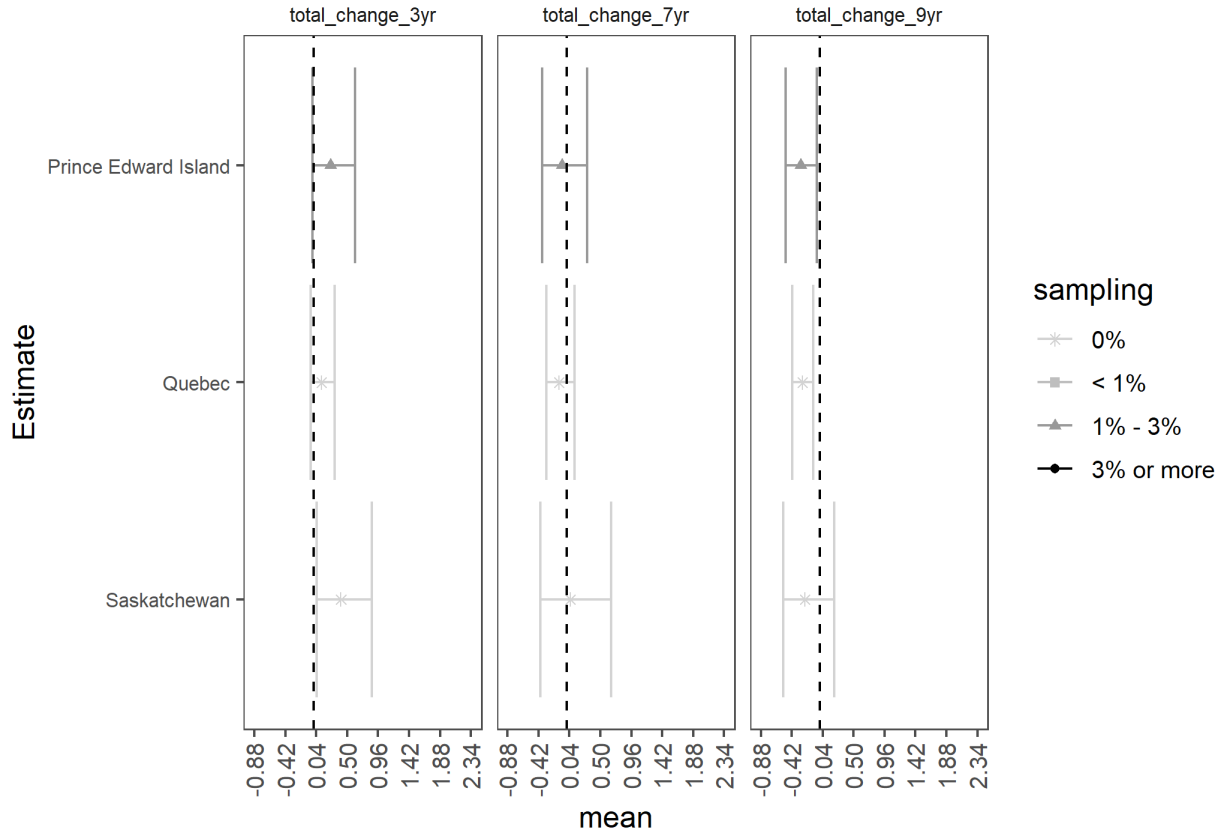

Figure B.6. The total change rate in mean occupancy (total_change = lambda_tot - 1) for *Myotis septentrionalis* (MYSE) given the mean occupancy estimate in last year of sampling (2019) and the mean occupancy estimates three years (2016), seven years (2012), and nine years (2010) prior aggregated across a state, province, or territory within the modeled species range. For example, if total_change_9yr = -0.25, the mean occupancy rate has declined by 25% over the nine years since 2010, while a value of 0.25 would indicate an increase of 25%. Means (points) and 95% credible intervals (bars) are depicted based on the average percent of grid cells sampled (legend) in the first and last years of the timeframe of interest for each state, province or territory (A-E). Note that when credible intervals do not overlap zero, we have at least 95% certainty that these trends in species occupancy are either negative or positive. When credible intervals overlap zero, we have less than 95% certainty that these trends are different than zero. U.S. states appear first in alphabetic order (A-D), followed by Canadian territories and provinces in alphabetic order (D-E).

B.3 *Perimyotis subflavus*

(A)

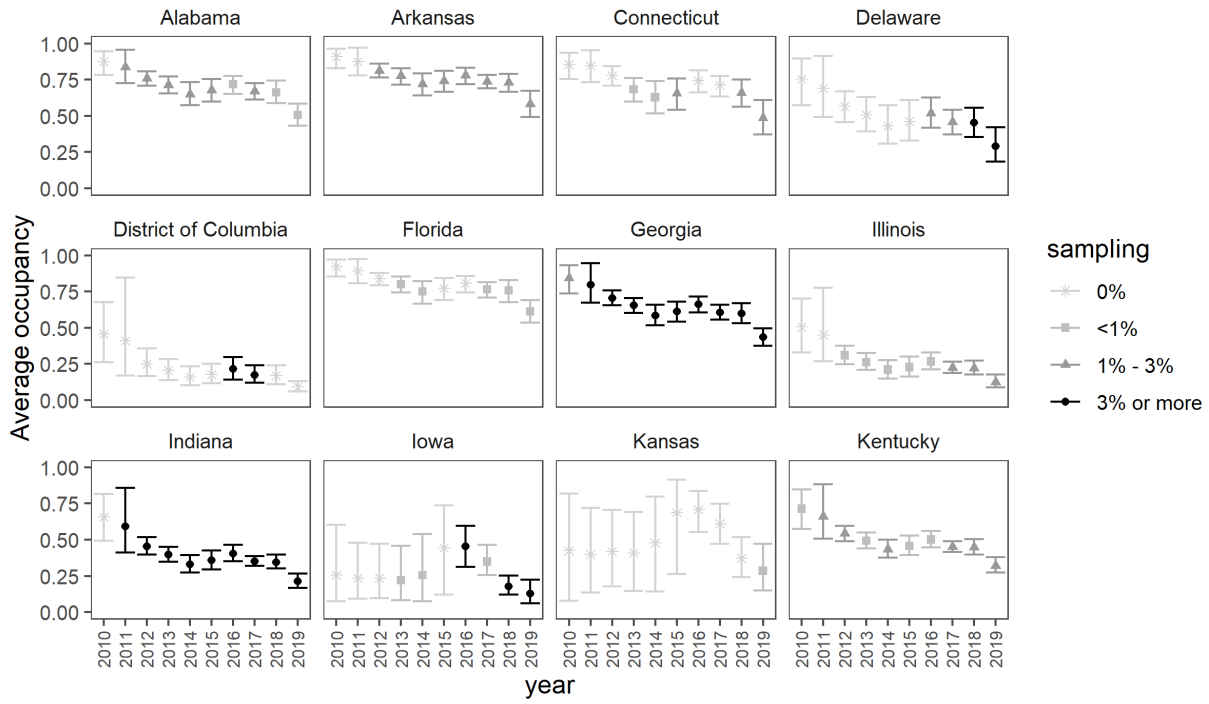

(B)

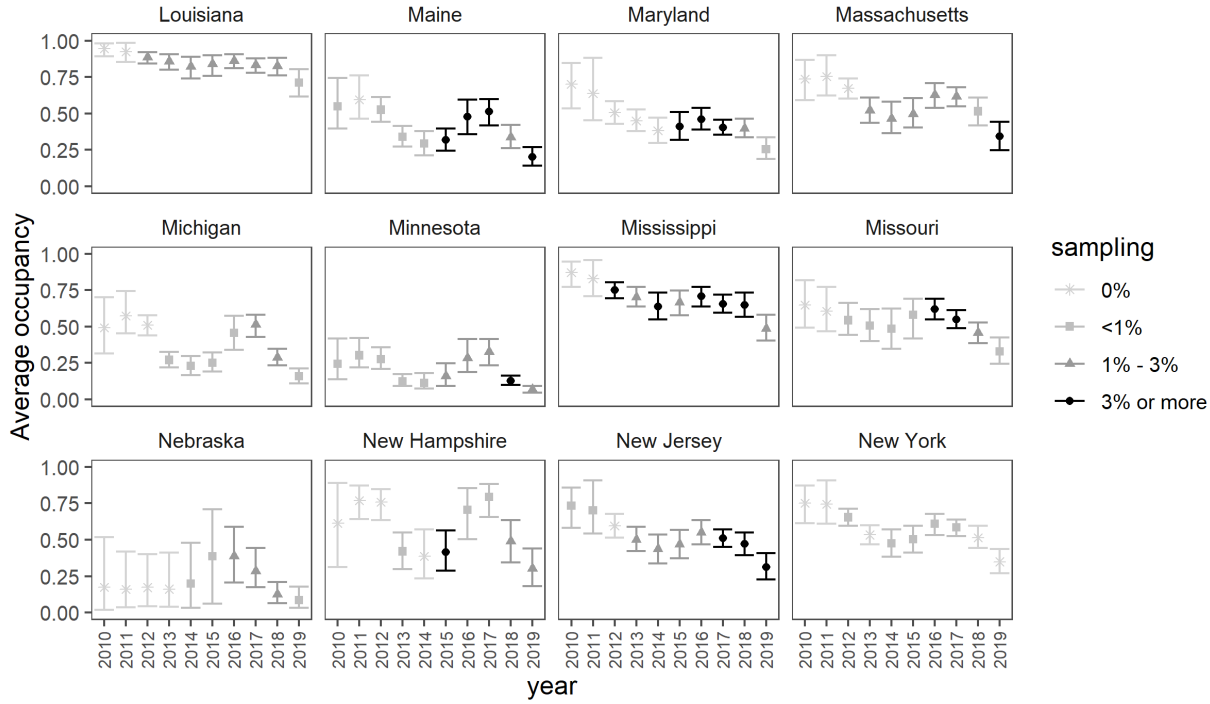

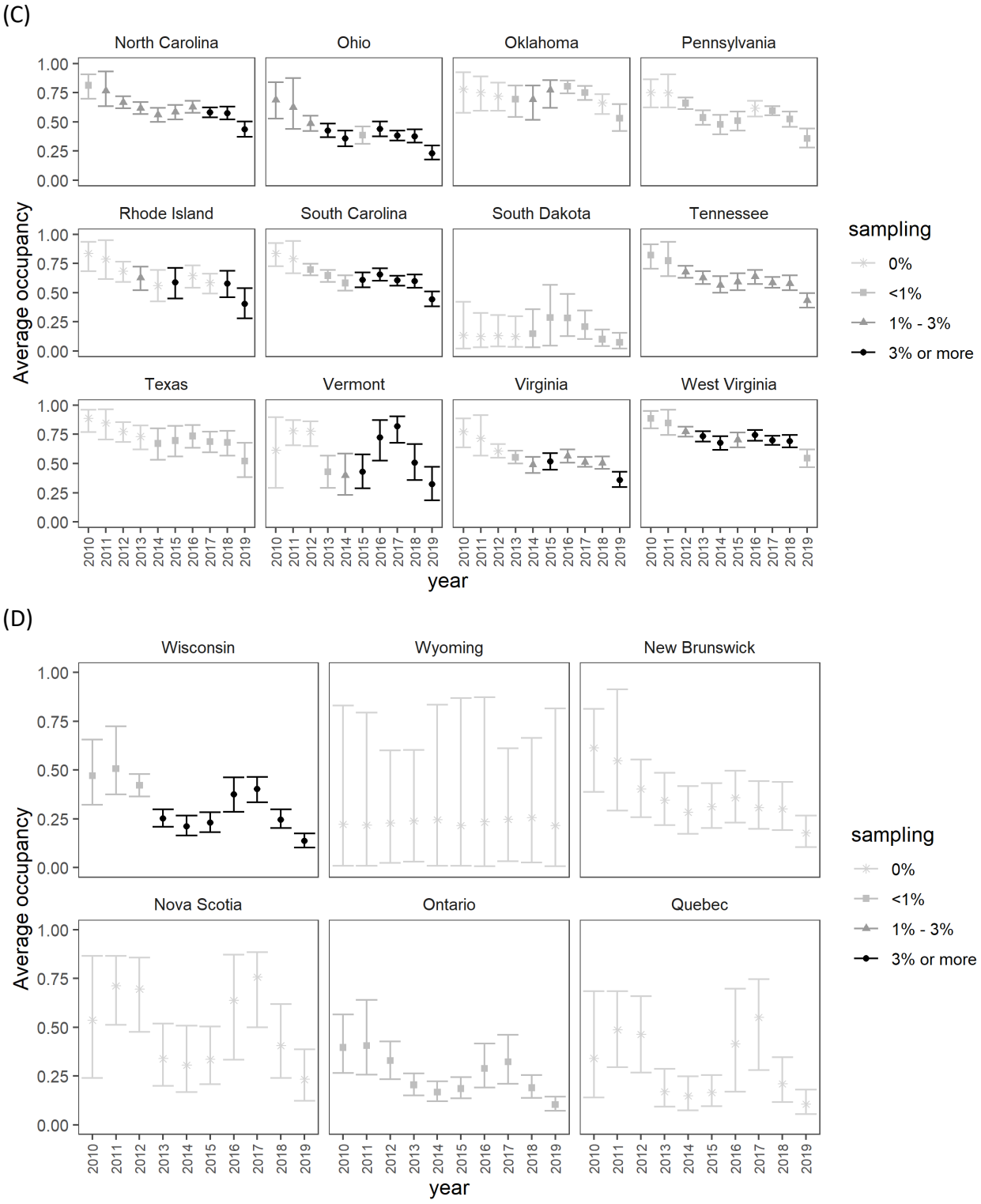

Figure B.7. Estimates of the average occupancy probability ($\hat{\psi}_t$) for *Perimyotis subflavus* (PESU) aggregated over all grid cells in the modeled species range for each state, territory or province and year. Means (points) and 95% credible intervals (bars) are depicted according to the percent of grid cells sampled (legend) in the entire state, province or territory each year (A-D). U.S. states appear first in alphabetic order (A-D), followed by Canadian territories and provinces in alphabetic order (D).

(A)

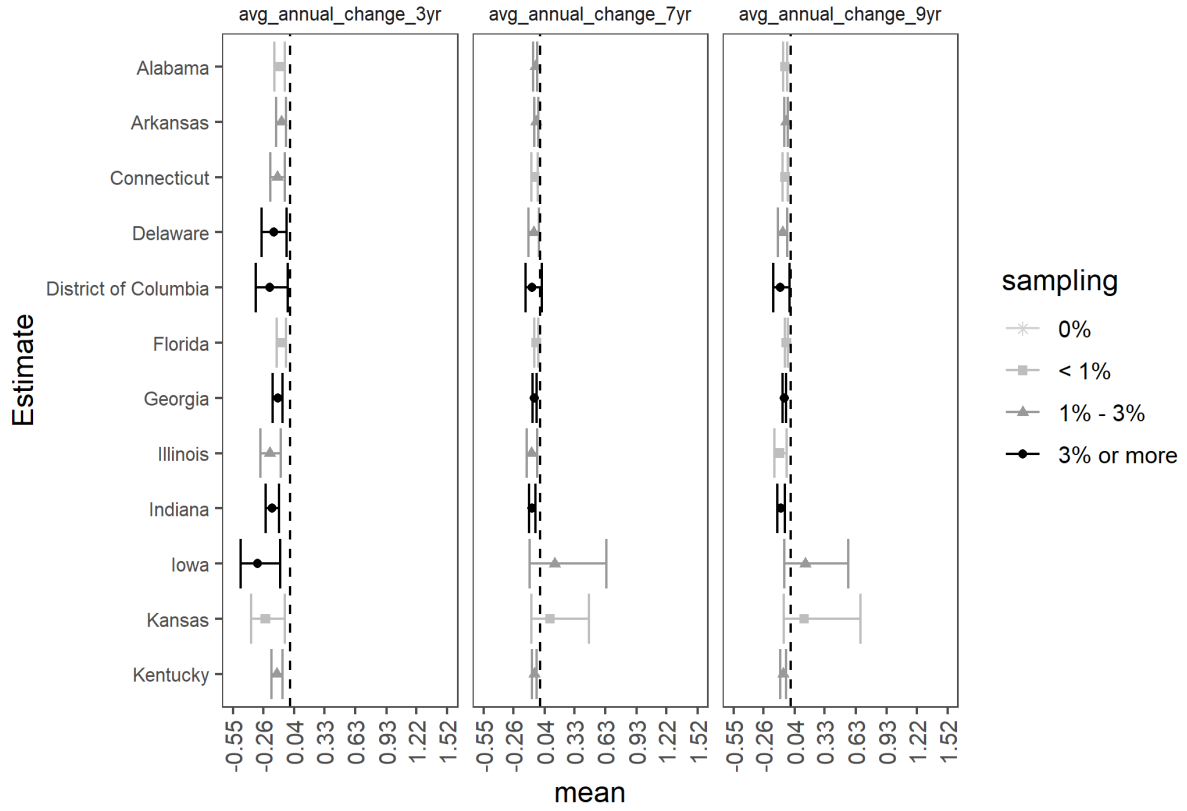
avg_annual_change_3yr
avg_annual_change_7yr
avg_annual_change_9yr
Alabama
Arkansas
Connecticut
Delaware
District of Columbia
Florida
Georgia
Illinois
Indiana
Iowa
Kansas
Kentucky
Estimate
-0.55
-0.26
0.04
0.33
0.63
0.93
1.22
1.52
mean
sampling
0%
< 1%
1% - 3%
3% or more

(B)

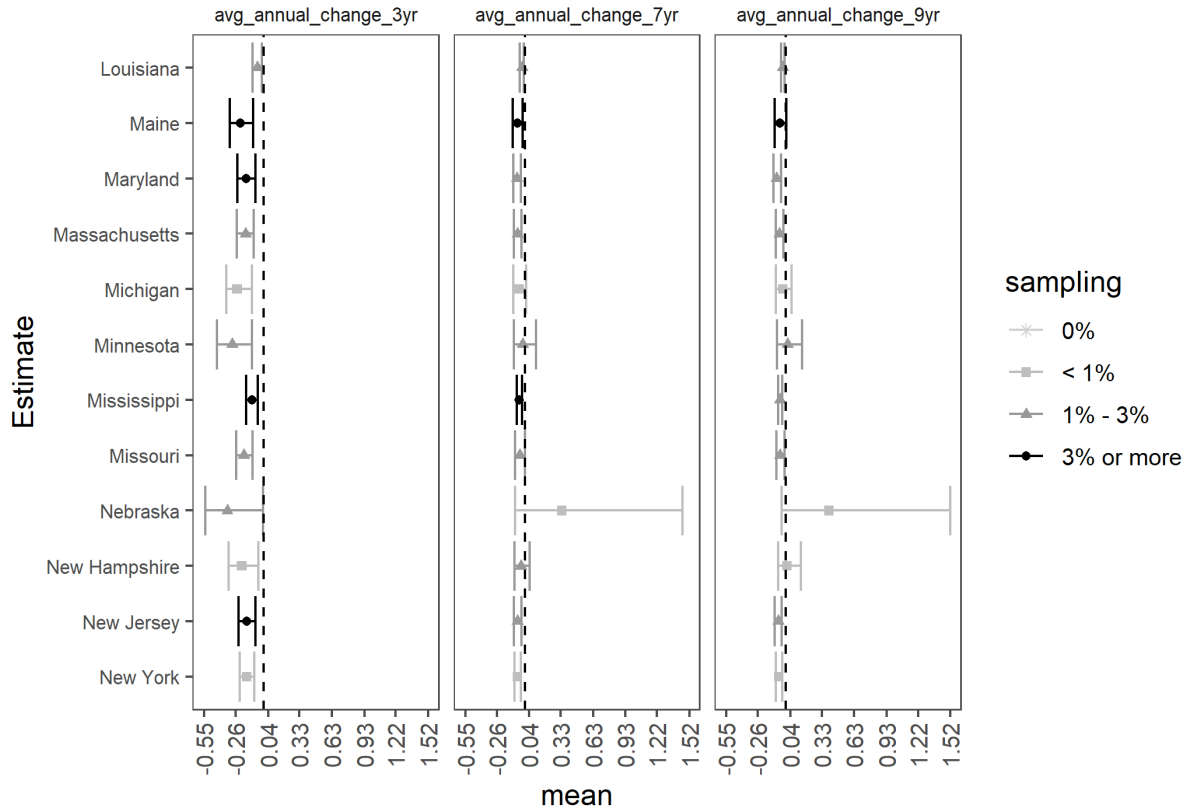
avg_annual_change_3yr
avg_annual_change_7yr
avg_annual_change_9yr
Louisiana
Maine
Maryland
Massachusetts
Michigan
Minnesota
Mississippi
Missouri
Nebraska
New Hampshire
New Jersey
New York
Estimate
-0.55
-0.26
0.04
0.33
0.63
0.93
1.22
1.52
mean
sampling
0%
< 1%
1% - 3%
3% or more

(C)

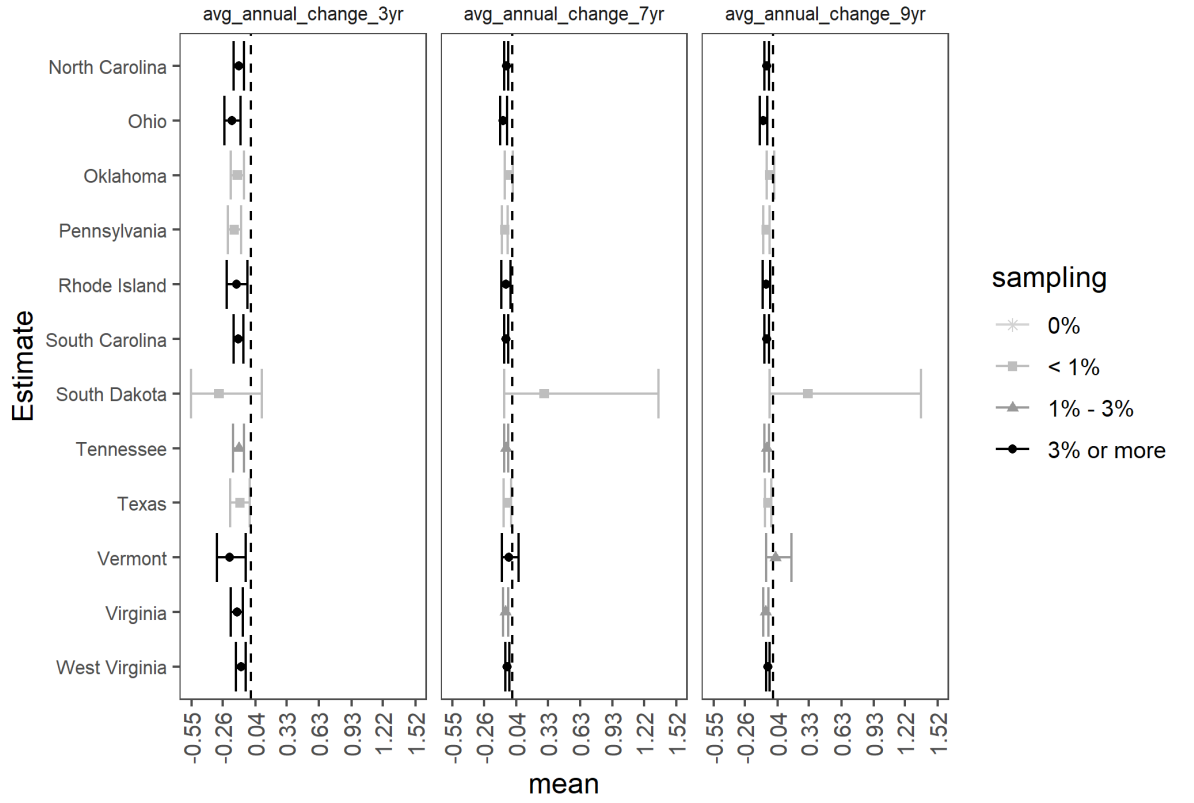
avg_annual_change_3yr
avg_annual_change_7yr
avg_annual_change_9yr
North Carolina
Ohio
Oklahoma
Pennsylvania
Rhode Island
South Carolina
South Dakota
Tennessee
Texas
Vermont
Virginia
West Virginia
Estimate
-0.55
-0.26
0.04
0.33
0.63
0.93
1.22
1.52
mean
sampling
0%
< 1%
1% - 3%
3% or more

(D)

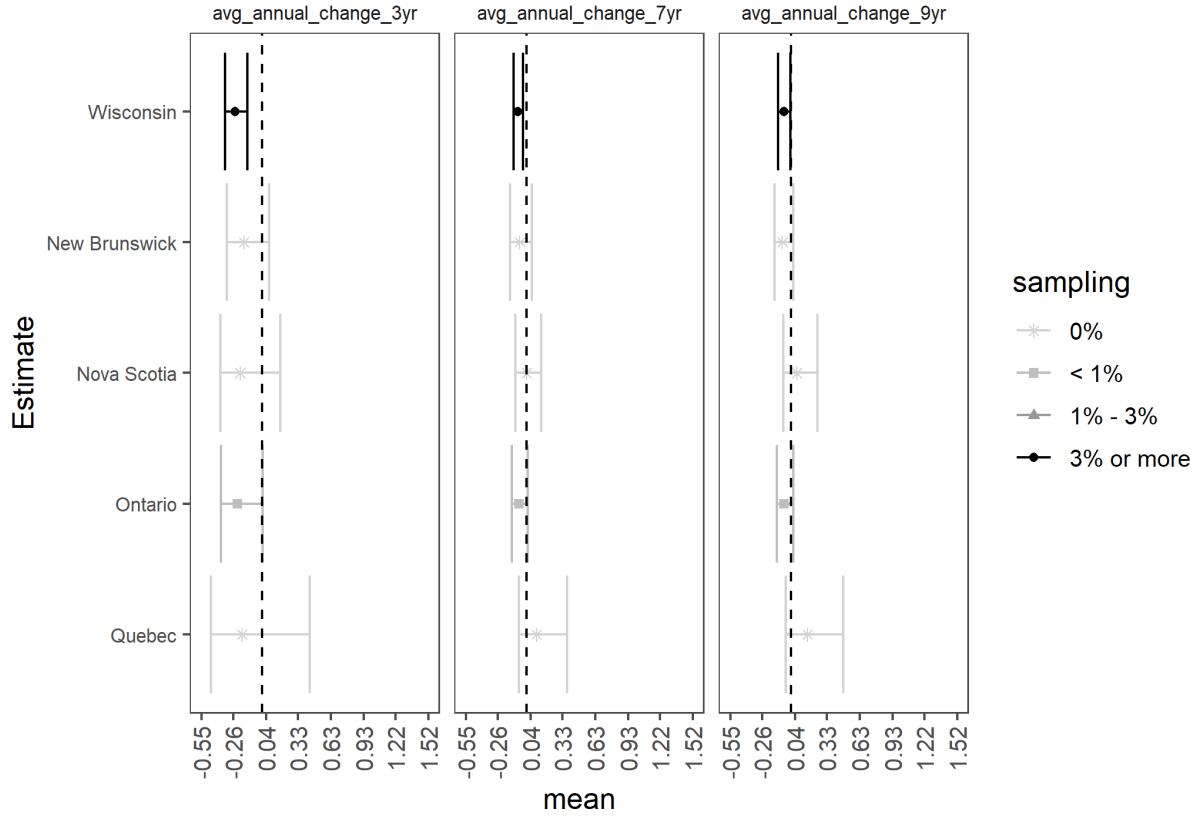
avg_annual_change_3yr
avg_annual_change_7yr
avg_annual_change_9yr
Wisconsin
New Brunswick
Nova Scotia
Ontario
Quebec
Estimate
-0.55
-0.26
0.04
0.33
0.63
0.93
1.22
1.52
mean
sampling
0%
< 1%
1% - 3%
3% or more

Figure B.8. Average annual rates of change in mean occupancy probabilities (avg_annual_change = lambda_avg - 1) for *Perimyotis subflavus* (PESU) between years over the designated time period (three years: 2016-2019, seven years: 2012-2019, or nine years: 2010-2019) aggregated across a state, province, or territory within the modeled species range. For example, if avg_change_9yr = -0.05, the mean occupancy rate has declined on average by 5% each year over the nine years since 2010. Means (points) and 95% credible intervals (bars) are depicted based on the average percent of grid cells sampled (legend) across all years in the timeframe of interest for each state, province or territory (A-D). Note that when credible intervals do not overlap zero, we have at least 95% certainty that these trends in species occupancy are either negative or positive. When credible intervals overlap zero, we have less than 95% certainty that these trends are different than zero. U.S. states appear first in alphabetic order (A-D), followed by Canadian territories and provinces in alphabetic order (D).

(A)

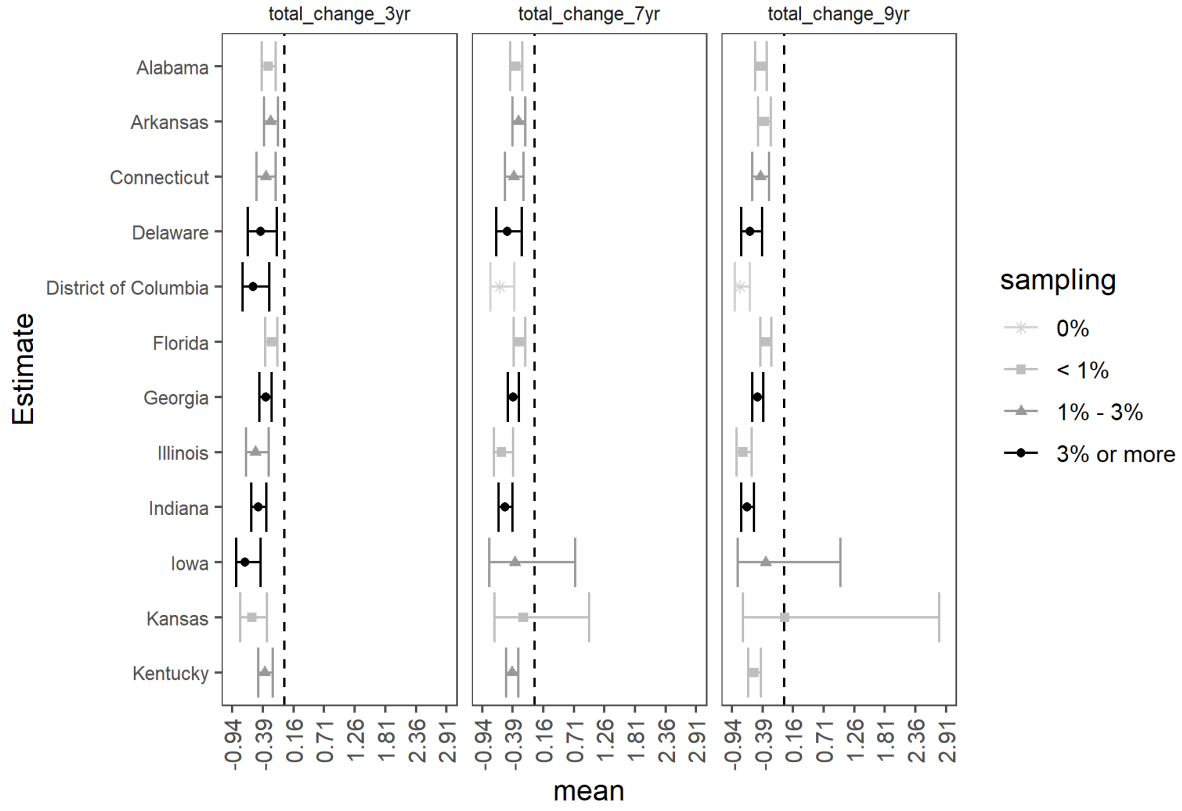
total_change_3yr
total_change_7yr
total_change_9yr
Alabama
Arkansas
Connecticut
Delaware
District of Columbia
Florida
Georgia
Illinois
Indiana
Iowa
Kansas
Kentucky
Estimate
-0.94
-0.39
0.16
0.71
1.26
1.81
2.36
2.91
mean
sampling
0%
< 1%
1% - 3%
3% or more

(B)

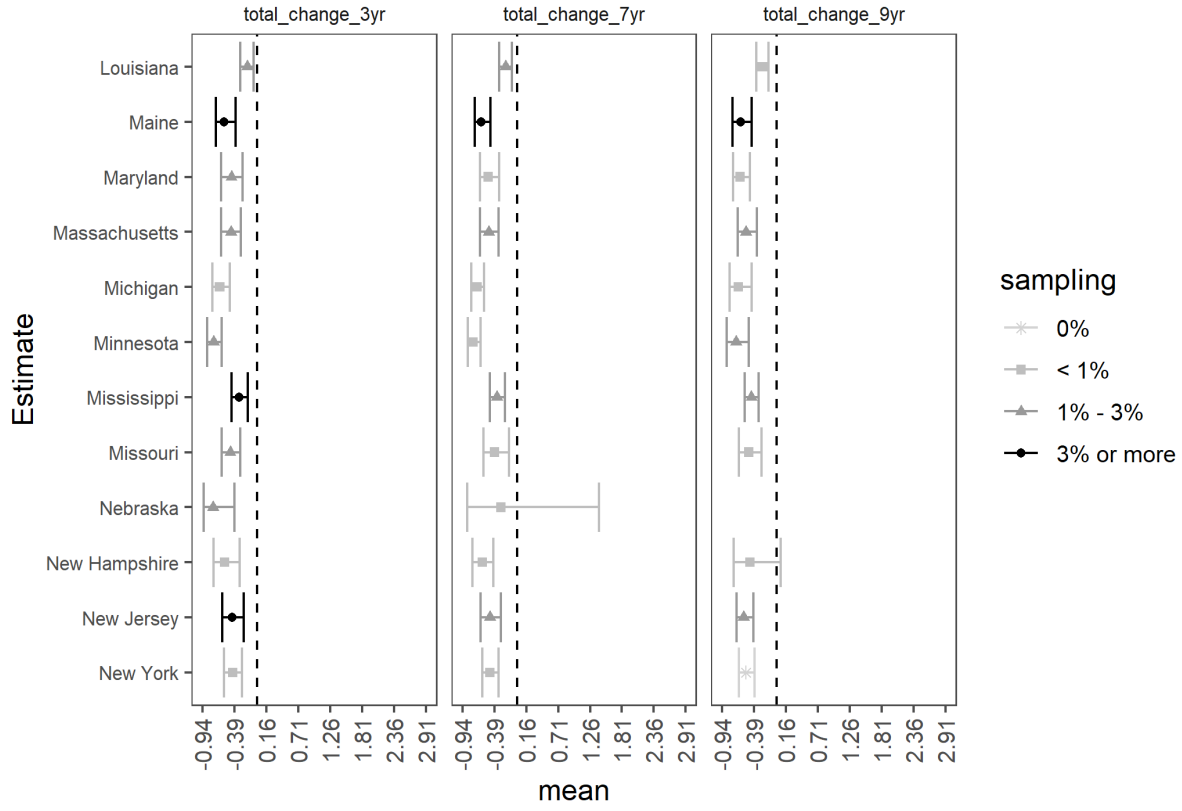
total_change_3yr
total_change_7yr
total_change_9yr
Louisiana
Maine
Maryland
Massachusetts
Michigan
Minnesota
Mississippi
Missouri
Nebraska
New Hampshire
New Jersey
New York
Estimate
-0.94
-0.39
0.16
0.71
1.26
1.81
2.36
2.91
mean
sampling
0%
< 1%
1% - 3%
3% or more

(C)

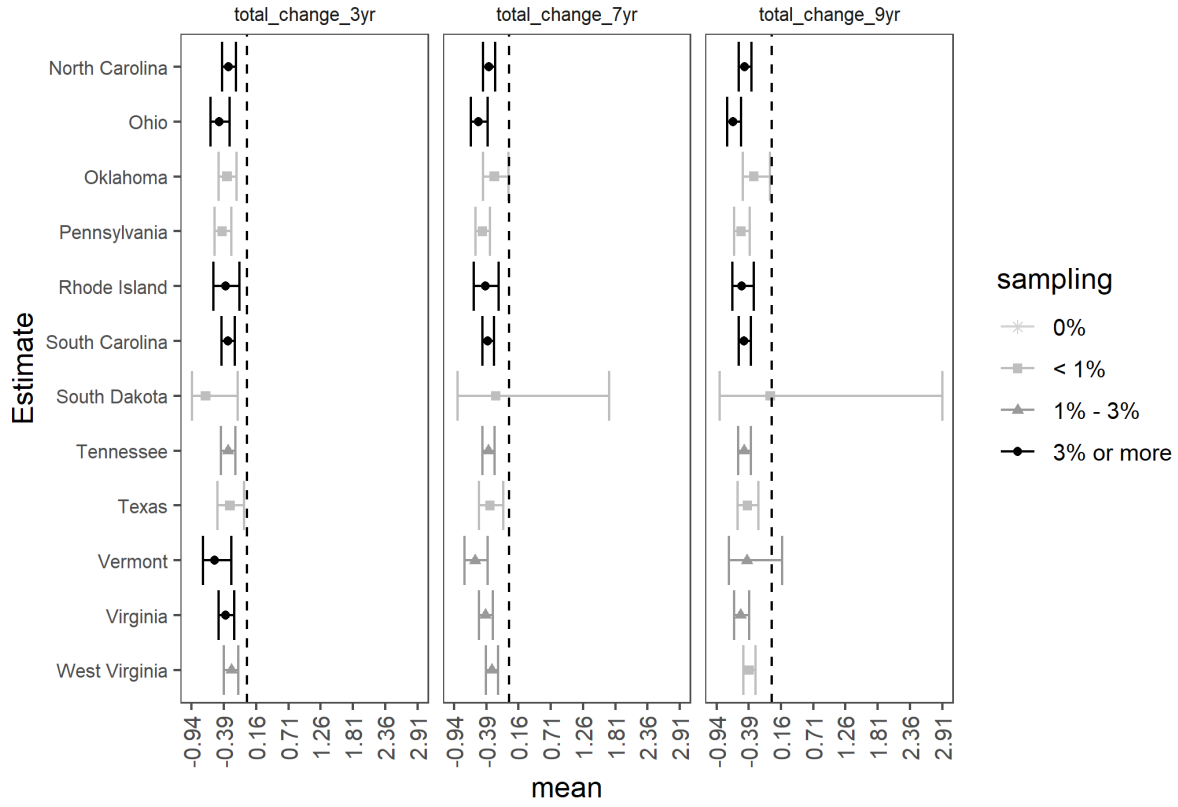
total_change_3yr
total_change_7yr
total_change_9yr
North Carolina
Ohio
Oklahoma
Pennsylvania
Rhode Island
South Carolina
South Dakota
Tennessee
Texas
Vermont
Virginia
West Virginia
Estimate
-0.94
-0.39
0.16
0.71
1.26
1.81
2.36
2.91
mean
sampling
0%
< 1%
1% - 3%
3% or more

(D)

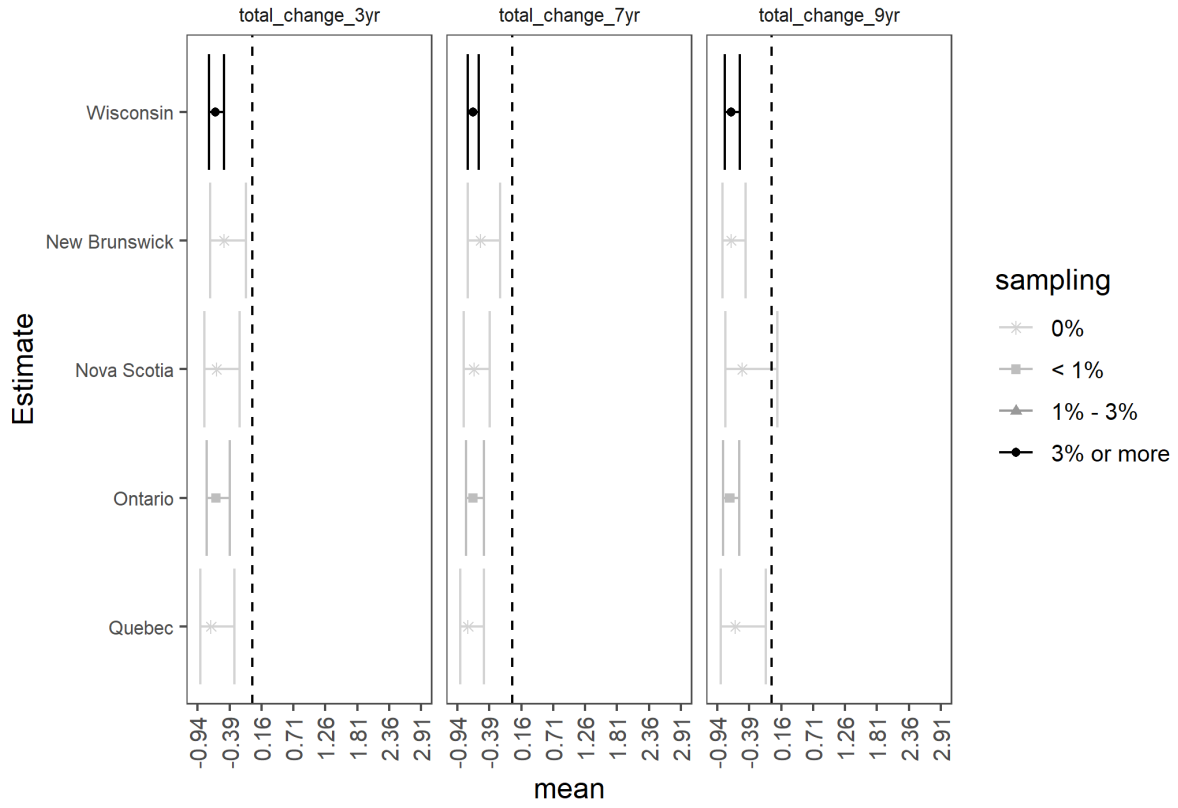
total_change_3yr
total_change_7yr
total_change_9yr
Wisconsin
New Brunswick
Nova Scotia
Ontario
Quebec
Estimate
-0.94
-0.39
0.16
0.71
1.26
1.81
2.36
2.91
mean
sampling
0%
< 1%
1% - 3%
3% or more

Figure B.9. The total change rate in mean occupancy (total_change = lambda_tot - 1) for *Perimyotis subflavus* (PESU) given the mean occupancy estimate in last year of sampling (2019) and the mean occupancy estimates three years (2016), seven years (2012), and nine (2010) prior aggregated across a state, province, or territory within the modeled species range. For example, if total_change_9yr = -0.25, the mean occupancy rate has declined by 25% over the nine years since 2010, while a value of 0.25 would indicate an increase of 25%. Means (points) and 95% credible intervals (bars) are depicted based on the average percent of grid cells sampled (legend) in the first and last years of the timeframe of interest for each state, province or territory (A-D). Note that when credible intervals do not overlap zero, we have at least 95% certainty that these trends in species occupancy are either negative or positive. When credible intervals overlap zero, we have less than 95% certainty that these trends are different than zero. U.S. states appear first in alphabetic order (A-D), followed by Canadian territories and provinces in alphabetic order (D).

B.4 *Myotis evotis*

(A)

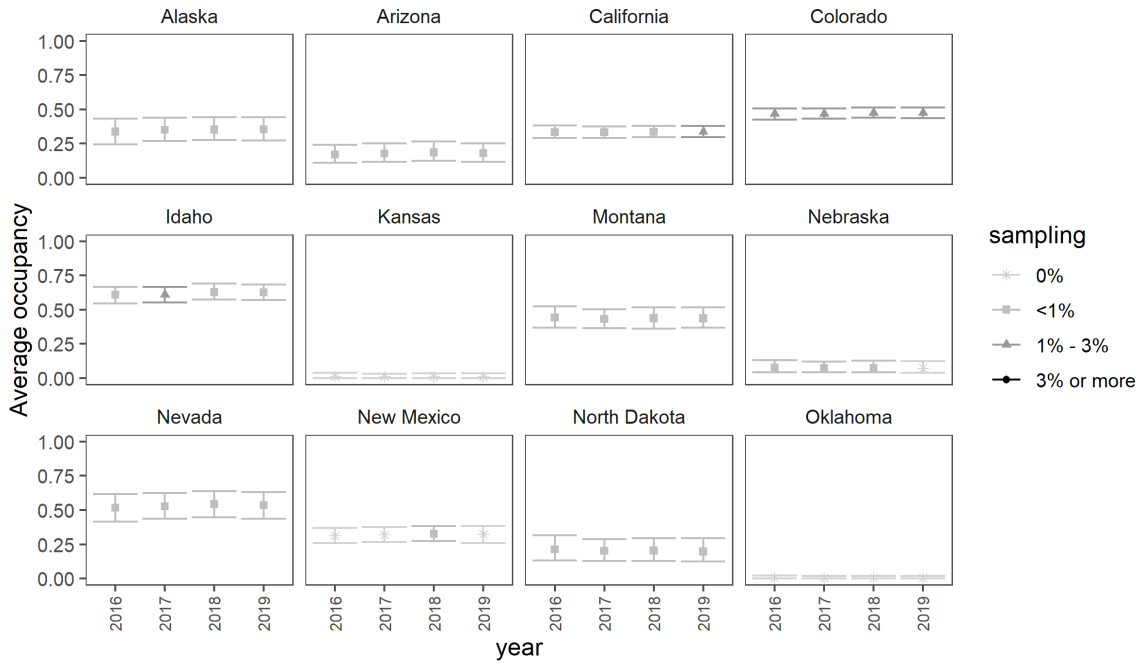

(B)

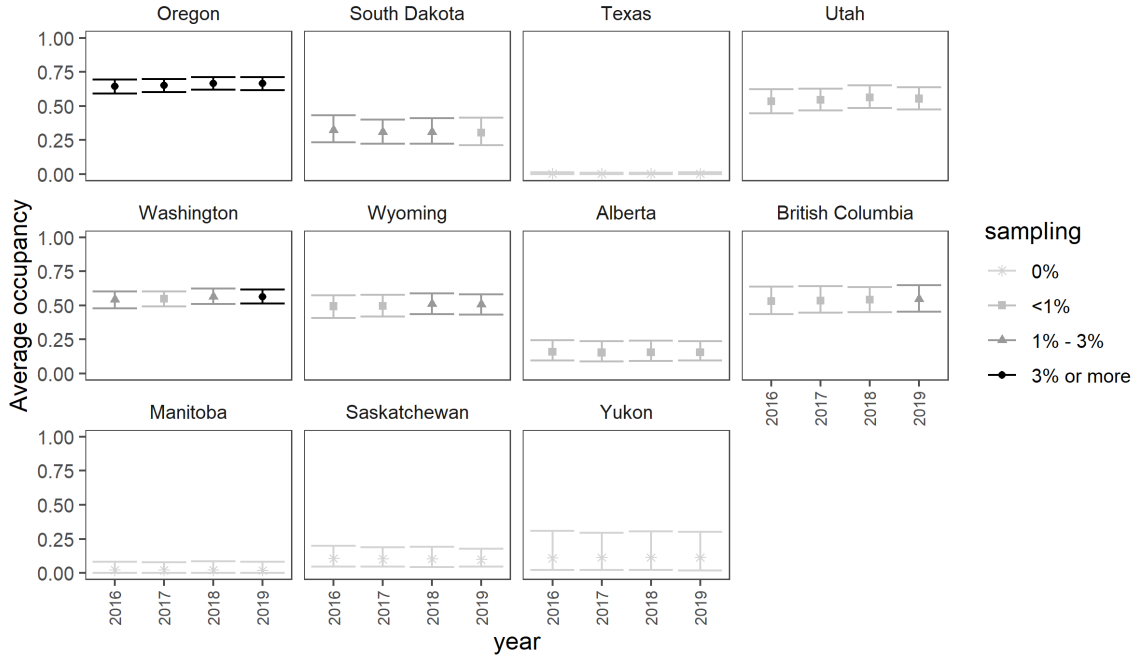

Figure B.10. Estimates of the average occupancy probability ($\widehat{\psi}_t$) for *Myotis evotis* (MYEV) aggregated over all grid cells for each state, territory or province in the modeled species range each year. Means (points) and 95% credible intervals (bars) are depicted according to the percent of grid cells sampled (legend) in the entire state, province or territory each year (A and B). U.S. states appear first in alphabetic order (A and B), followed by Canadian territories and provinces in alphabetic order (B).

(A)

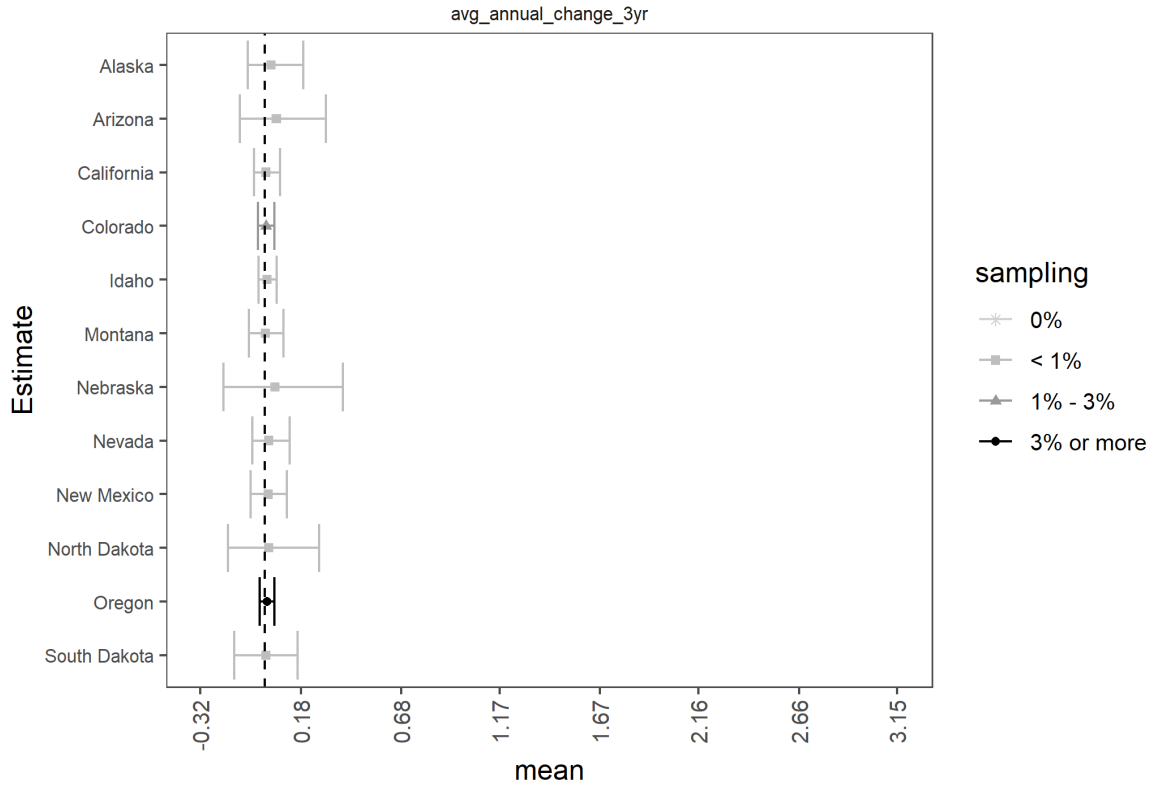
avg_annual_change_3yr
Alaska
Arizona
California
Colorado
Idaho
Montana
Nebraska
Nevada
New Mexico
North Dakota
Oregon
South Dakota
Estimate
-0.32
0.18
0.68
1.17
1.67
2.16
2.66
3.15
mean
sampling
0%
< 1%
1% - 3%
3% or more

(B)

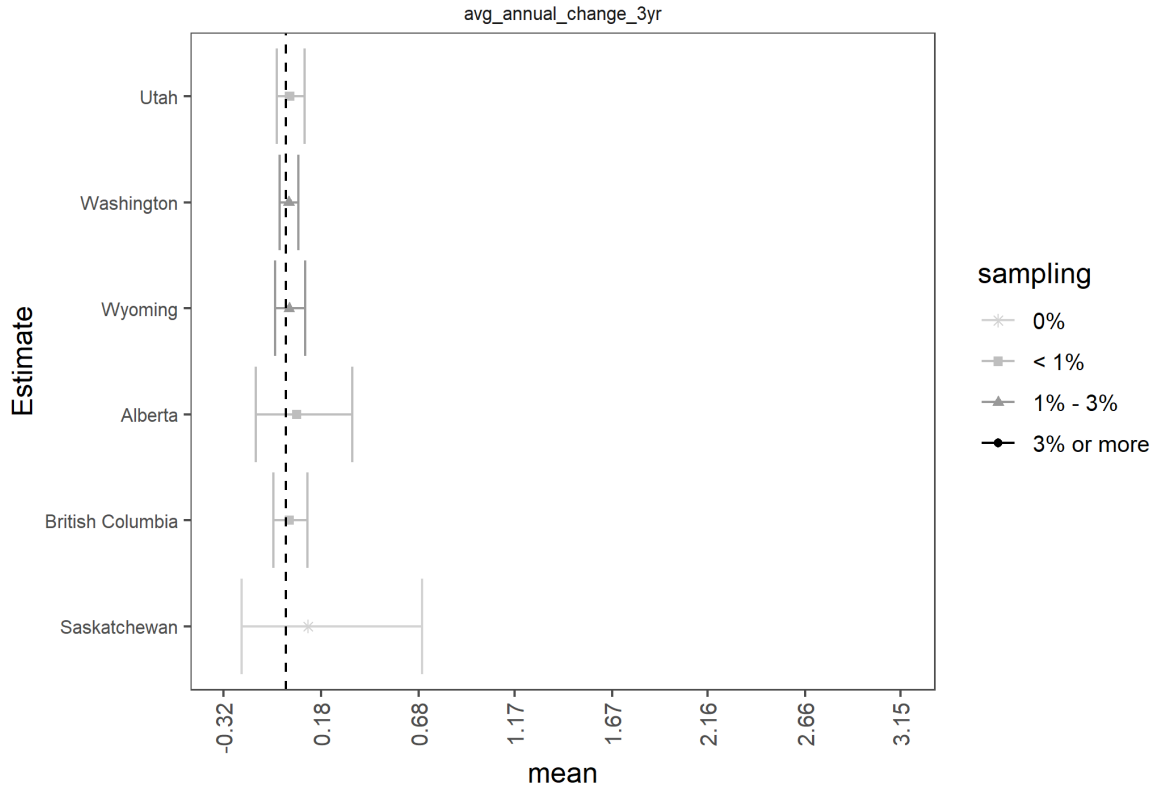
avg_annual_change_3yr
Utah
Washington
Wyoming
Alberta
British Columbia
Saskatchewan
Estimate
-0.32
0.18
0.68
1.17
1.67
2.16
2.66
3.15
mean
sampling
0%
< 1%
1% - 3%
3% or more

Figure B.11. Average annual rates of change in mean occupancy probabilities (avg_annual_change = lambda_avg - 1) for *Myotis evotis* (MYEV) between years over the three-year (2016-2019) time period aggregated across a state, province, or territory within the modeled species range. For example, if avg_change_3yr = -0.05, the mean occupancy rate has declined on average by 5% each year over the three years since 2016. Means (points) and 95% credible intervals (bars) are depicted based on the average percent of grid cells sampled (legend) across all years in the timeframe of interest for each state, province or territory (A and B). Note that when credible intervals do not overlap zero, we have at least 95% certainty that these trends in species occupancy are either negative or positive. When credible intervals overlap zero, we have less than 95% certainty that these trends are different than zero. U.S. states appear first in alphabetic order (A and B), followed by Canadian territories and provinces in alphabetic order (B).

(A)

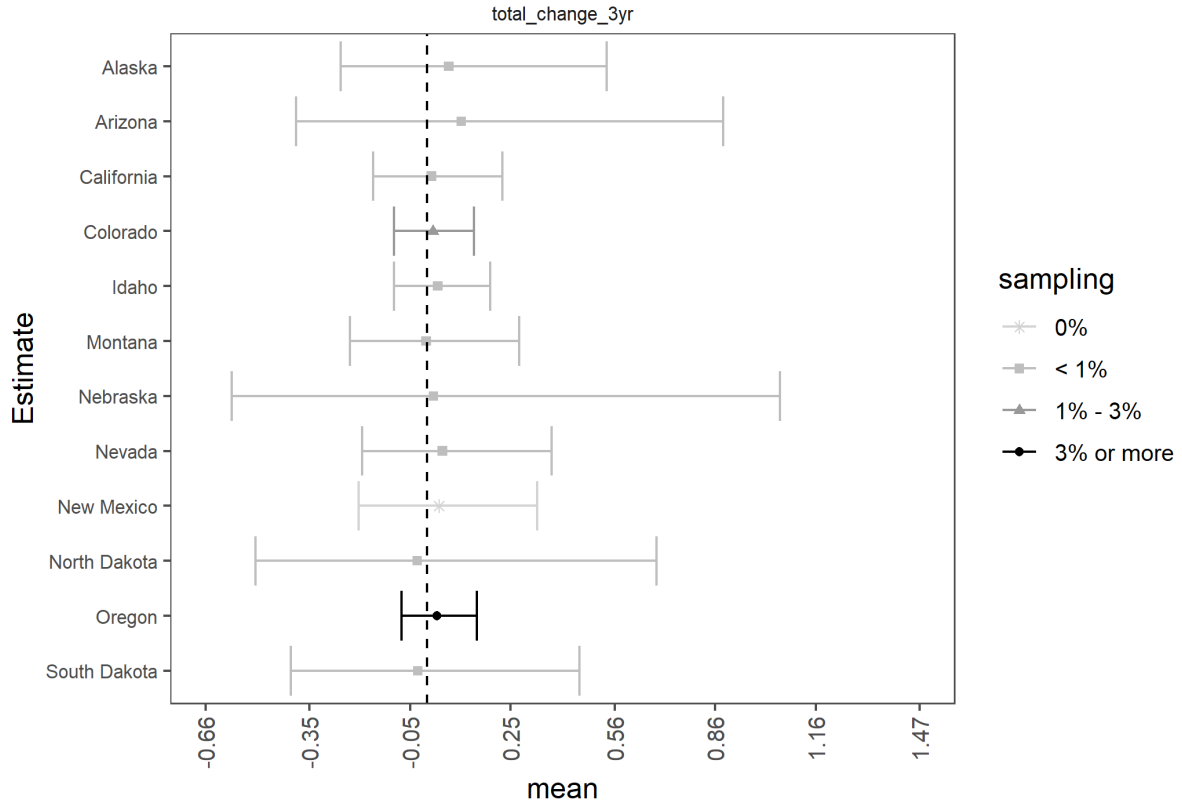
total_change_3yr
Alaska
Arizona
California
Colorado
Idaho
Montana
Nebraska
Nevada
New Mexico
North Dakota
Oregon
South Dakota
Estimate
-0.66
-0.35
-0.05
0.25
0.56
0.86
1.16
1.47
mean
sampling
0%
< 1%
1% - 3%
3% or more

(B)

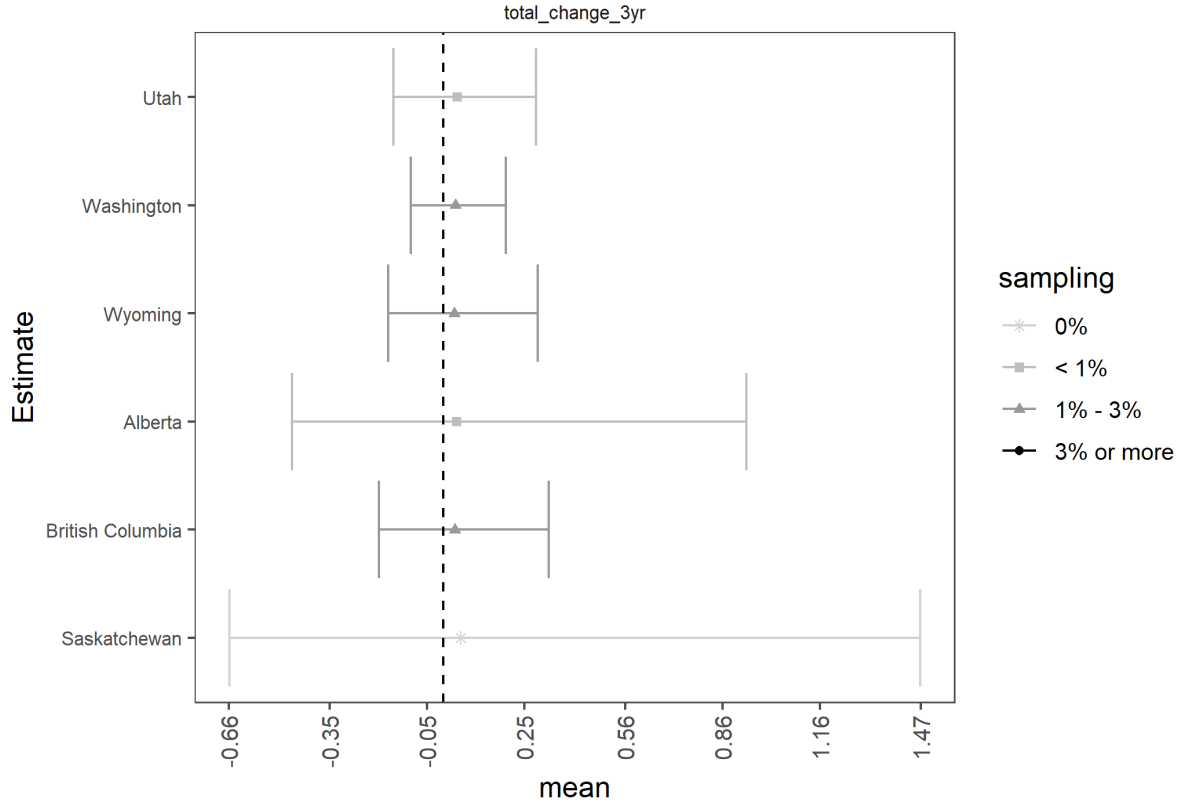
total_change_3yr
Utah
Washington
Wyoming
Alberta
British Columbia
Saskatchewan
Estimate
-0.66
-0.35
-0.05
0.25
0.56
0.86
1.16
1.47
mean
sampling
0%
< 1%
1% - 3%
3% or more

Figure B.12. The total change rate in mean occupancy (total_change = lambda_tot - 1) for *Myotis evotis* (MYEV) given the mean occupancy estimate in last year of sampling (2019) and the mean occupancy estimates three years (2016) prior aggregated across a state, province, or territory within the modeled species range. For example, if total_change_3yr = -0.25, the mean occupancy rate has declined by 25% over the nine years since 2016, while a value of 0.25 would indicate an increase of 25%. Means (points) and 95% credible intervals (bars) are depicted based on the average percent of grid cells sampled (legend) in the first and last years of the timeframe of interest for each state, province or territory (A and B). Note that when credible intervals do not overlap zero, we have at least 95% certainty that these trends in species occupancy are either negative or positive. When credible intervals overlap zero, we have less than 95% certainty that these trends are different than zero. U.S. states appear first in alphabetic order (A and B), followed by Canadian territories and provinces in alphabetic order (B).

B.5 *Myotis grisescens*

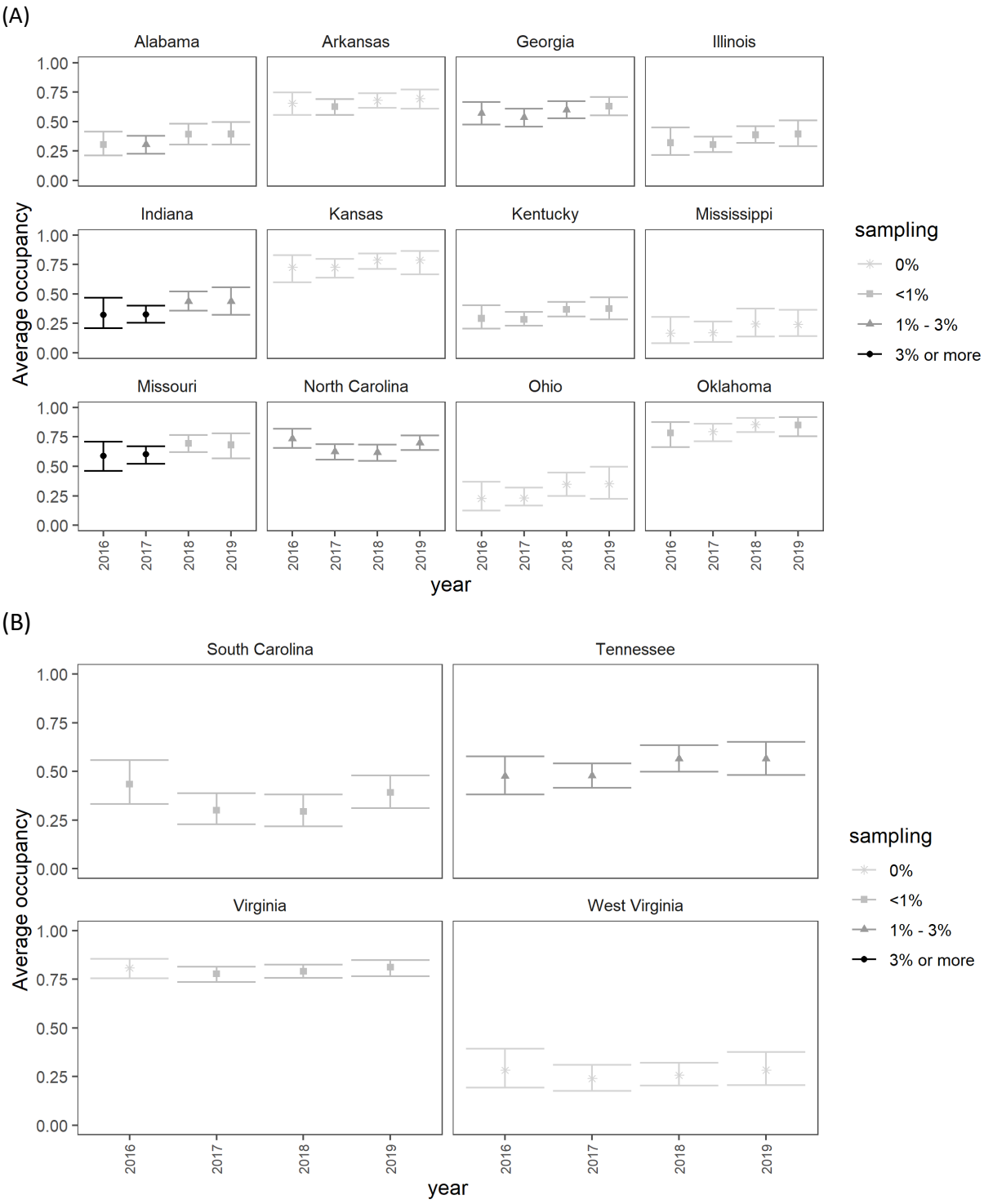

Figure B.13. Estimates of the average occupancy probability ($\hat{\psi}_t$) for *Myotis grisescens* (MYGR) aggregated over all grid cells for each state in the modeled species range each year. Means (points) and 95% credible intervals (bars) are depicted according to the percent of grid cells sampled (legend) in the entire state each year (A and B). U.S. states appear in alphabetic order (A-B).

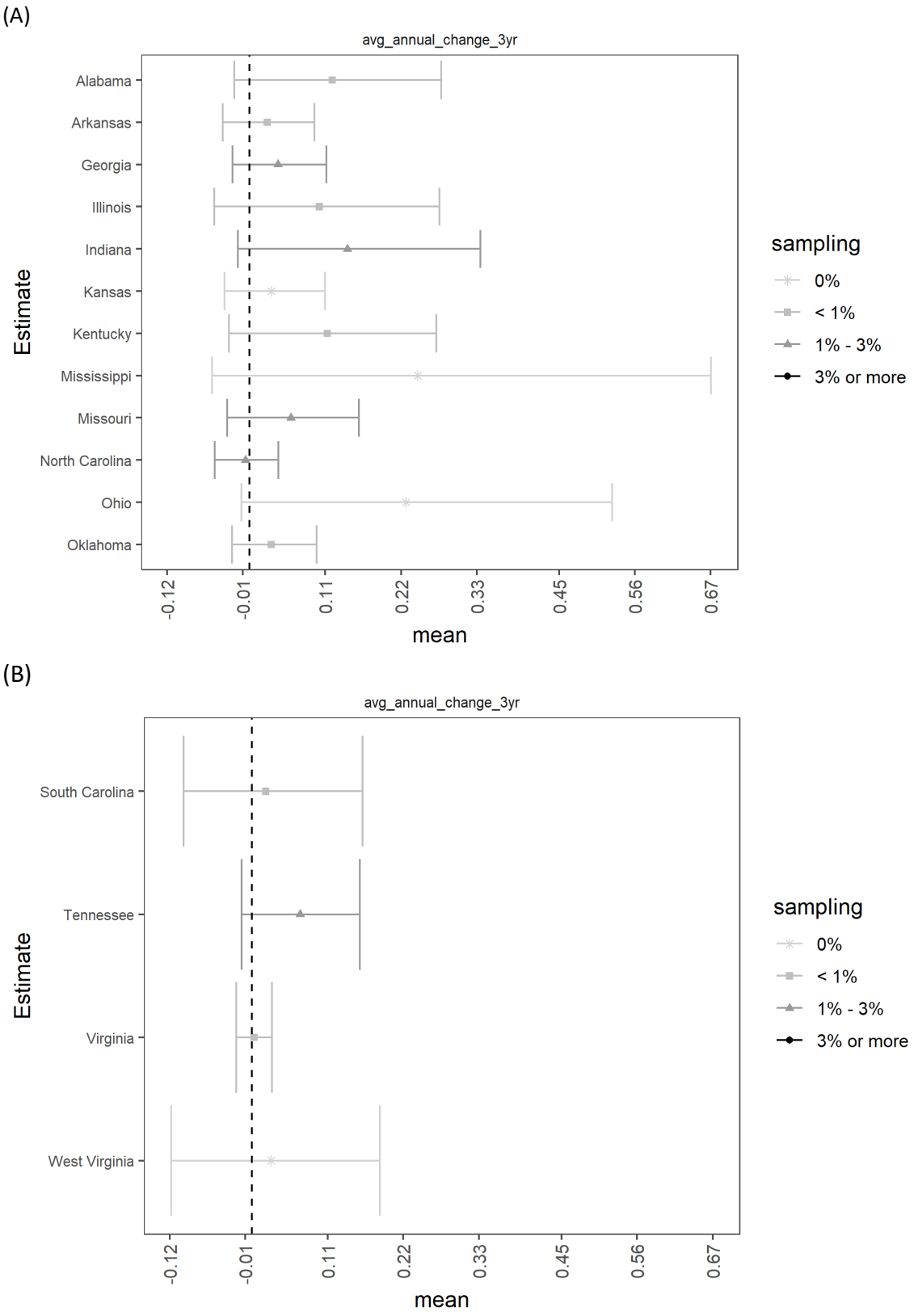

Figure B.14. Average annual rates of change in mean occupancy probabilities (avg_annual_change = lambda_avg - 1) for *Myotis grisescens* (MYGR) between years over the three-year (2016-2019) time

period aggregated across a state within the modeled species range. For example, avg_change_3yr = -0.05, the mean occupancy rate has declined on average by 5% each year over the three years since 2016. Means (points) and 95% credible intervals (bars) are depicted based on the average percent of grid cells sampled (legend) across all years in the timeframe of interest for each state. Note that when credible intervals do not overlap zero, we have at least 95% certainty that these trends in species occupancy are either negative or positive. When credible intervals overlap zero, we have less than 95% certainty that these trends are different than zero. U.S. states appear in alphabetic order (A-B).

(A)

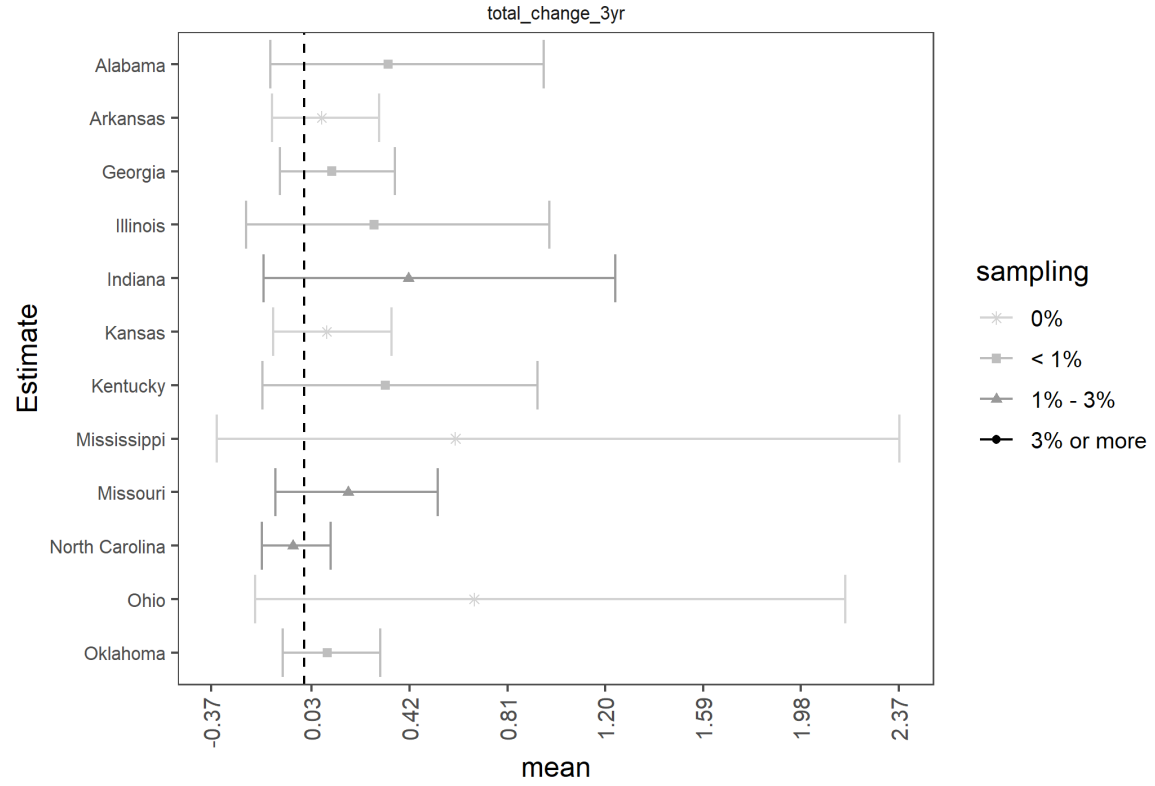
total_change_3yr
Alabama
Arkansas
Georgia
Illinois
Indiana
Kansas
Kentucky
Mississippi
Missouri
North Carolina
Ohio
Oklahoma
Estimate
-0.37
0.03
0.42
0.81
1.20
1.59
1.98
2.37
mean
sampling
0%
< 1%
1% - 3%
3% or more

(B)

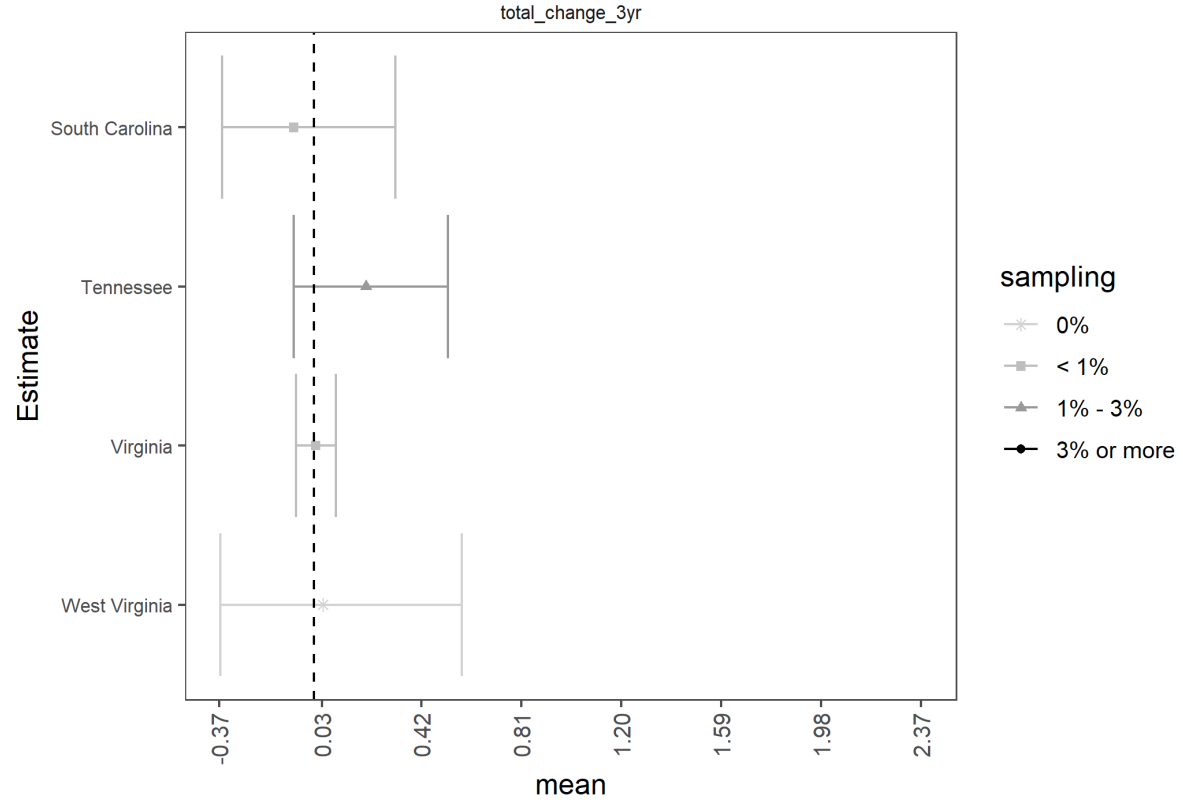
total_change_3yr
South Carolina
Tennessee
Virginia
West Virginia
Estimate
-0.37
0.03
0.42
0.81
1.20
1.59
1.98
2.37
mean
sampling
0%
< 1%
1% - 3%
3% or more

Figure B.15. The total change rate in mean occupancy (total_change = lambda_tot - 1) for *Myotis grisescens* (MYGR) given the mean occupancy estimate in last year of sampling (2019) and the mean occupancy estimates three years (2016) prior aggregated across a state within the modeled species range. For example, if total_change_3yr = -0.25, the mean occupancy rate has declined by 25% over the nine years since 2016, while a value of 0.25 would indicate an increase of 25%. Means (points) and 95% credible intervals (bars) are depicted based on the average percent of grid cells sampled (legend) in the first and last years of the timeframe of interest for each state. Note that when credible intervals do not overlap zero, we have at least 95% certainty that these trends in species occupancy are either negative or positive. When credible intervals overlap zero, we have less than 95% certainty that these trends are different than zero. U.S. states appear in alphabetic order (A-B).

B.6 *Myotis leibii*

(A)

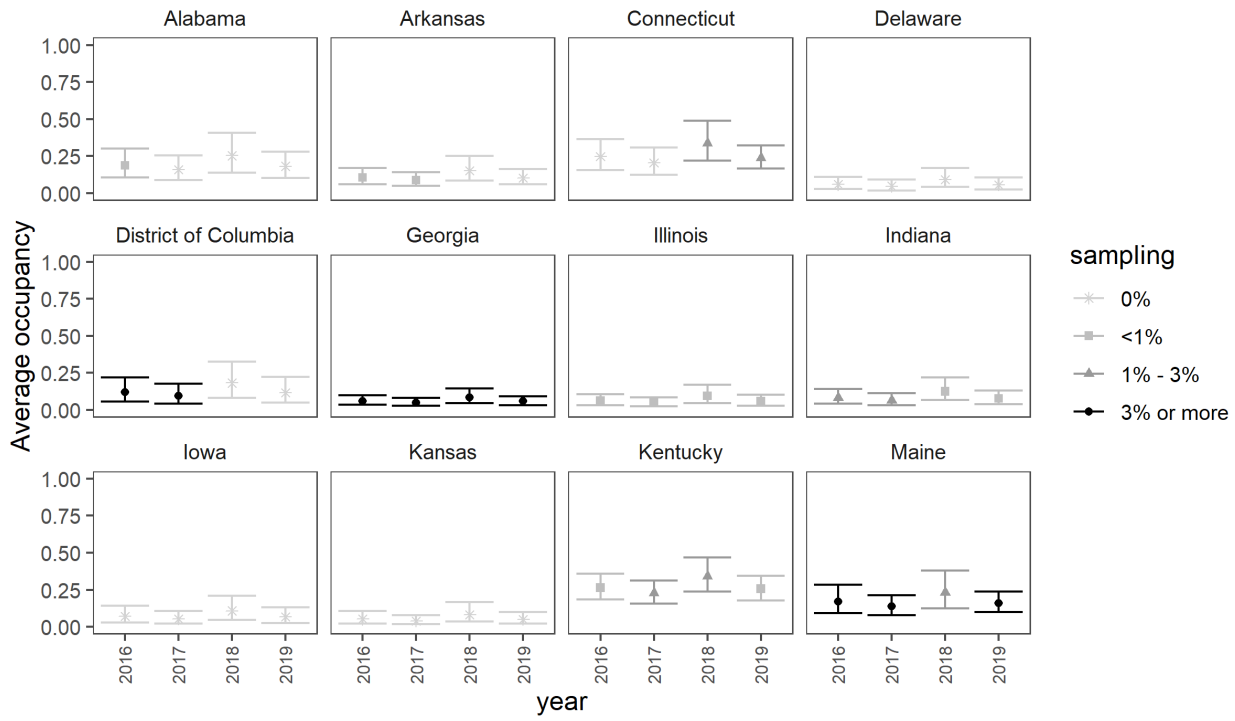

(B)

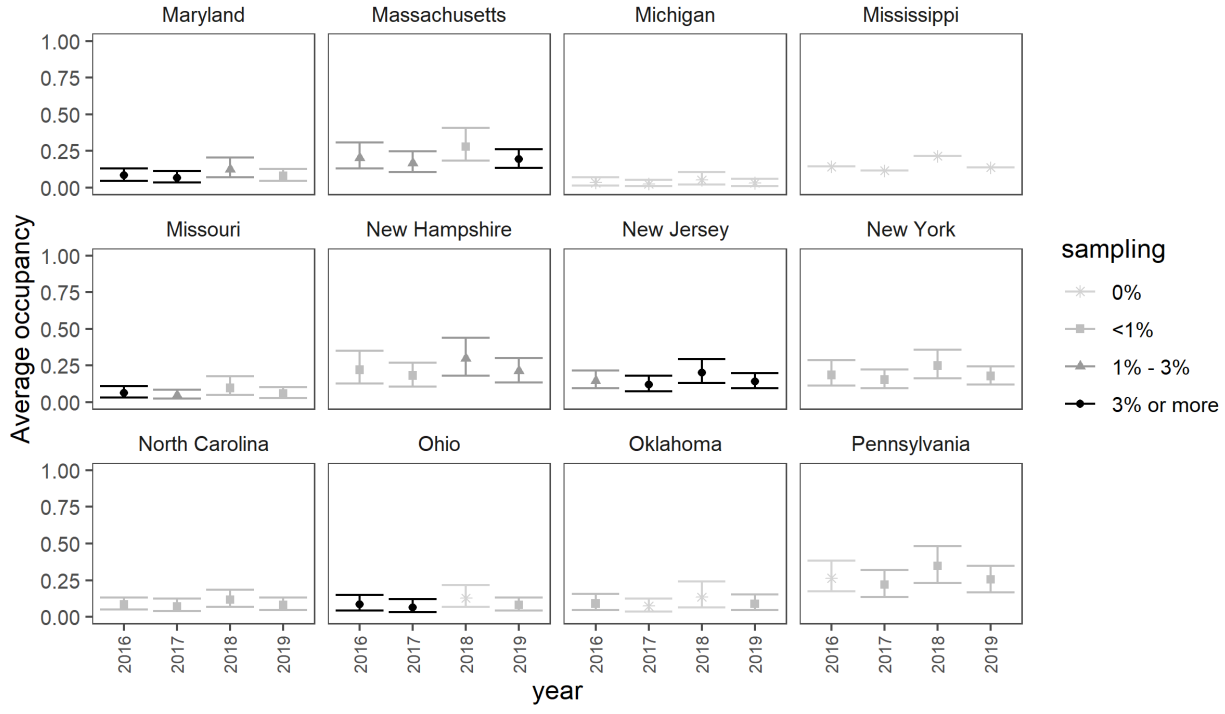

(C)

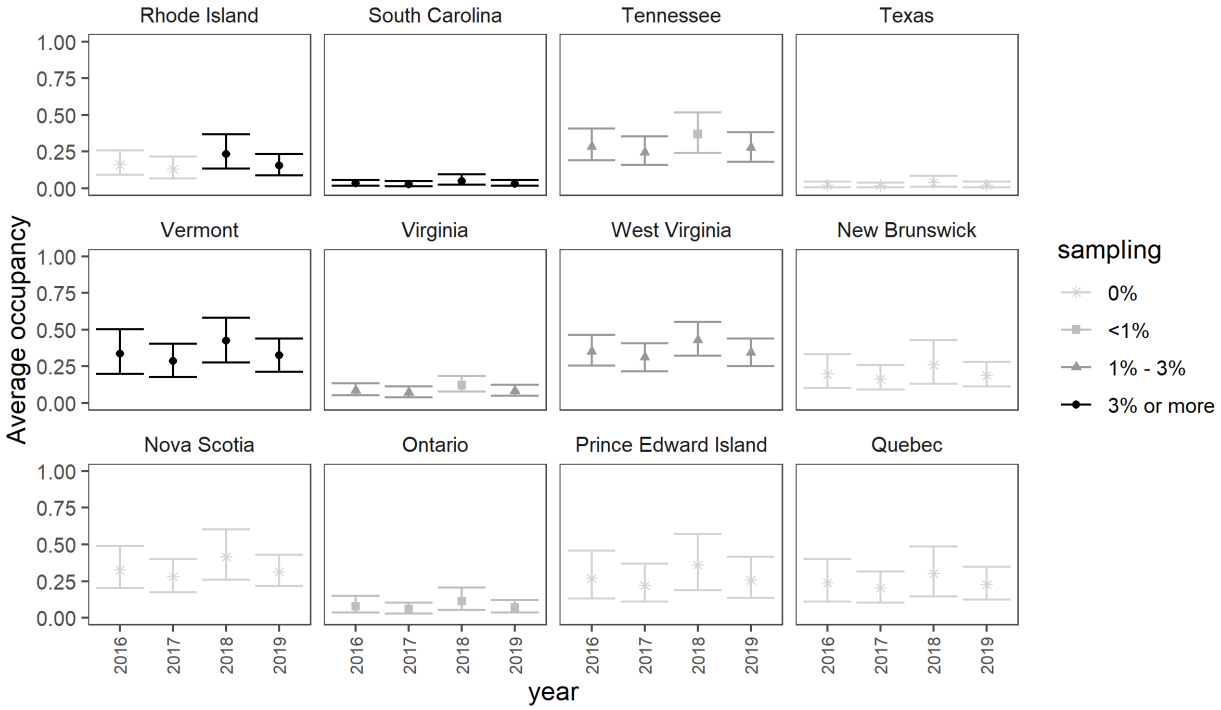

Figure B.16. Estimates of the average occupancy probability ($\hat{\psi}_t$) for *Myotis leibii* (MYLE) aggregated over all grid cells for each state in the modeled species range each year. Means (points) and 95% credible intervals (bars) are depicted according to the percent of grid cells sampled (legend in the entire state each year (A-C). U.S. states appear first in alphabetic order (A-C), followed by Canadian territories and provinces in alphabetic order (C).

(A)

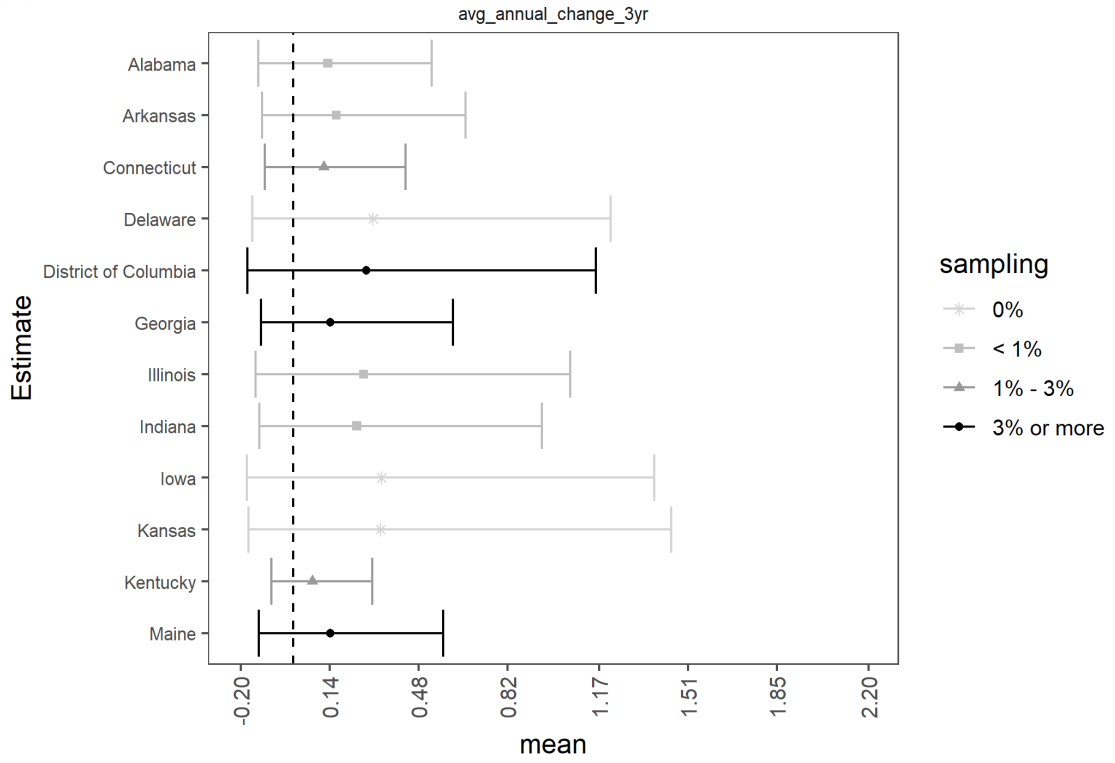
avg_annual_change_3yr
Alabama
Arkansas
Connecticut
Delaware
District of Columbia
Georgia
Illinois
Indiana
Iowa
Kansas
Kentucky
Maine
Estimate
-0.20
0.14
0.48
0.82
1.17
1.51
1.85
2.20
mean
sampling
0%
< 1%
1% - 3%
3% or more

(B)

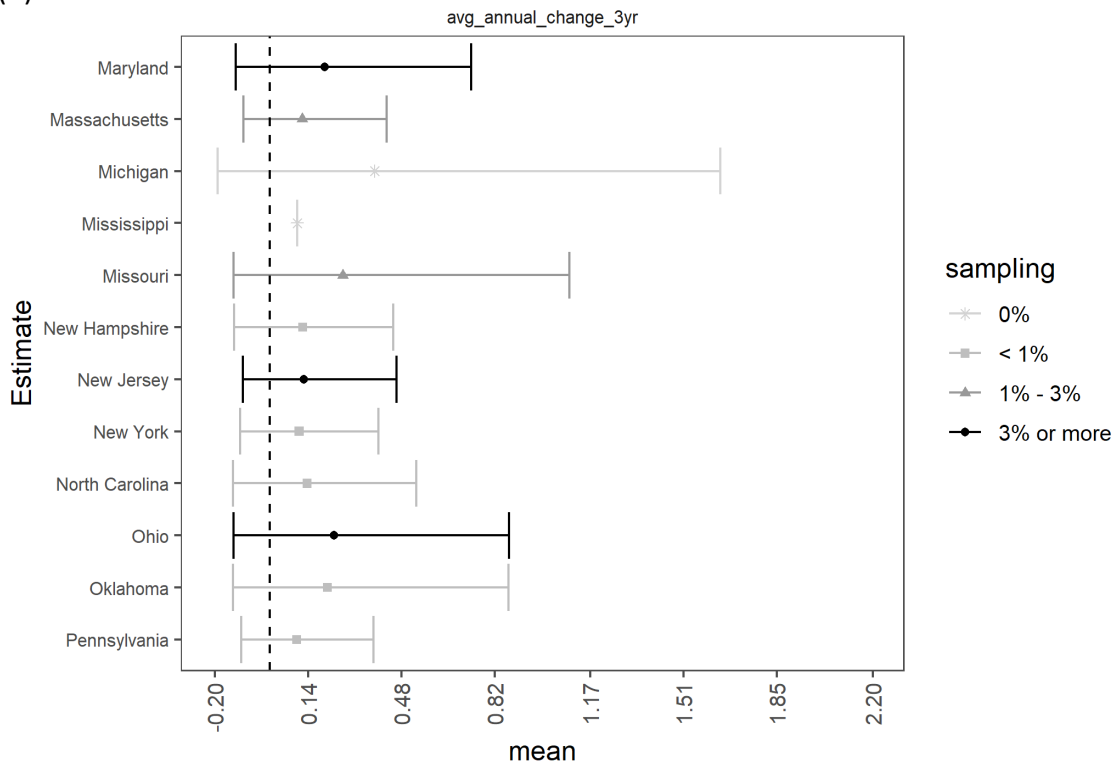
avg_annual_change_3yr
Maryland
Massachusetts
Michigan
Mississippi
Missouri
New Hampshire
New Jersey
New York
North Carolina
Ohio
Oklahoma
Pennsylvania
Estimate
-0.20
0.14
0.48
0.82
1.17
1.51
1.85
2.20
mean
sampling
0%
< 1%
1% - 3%
3% or more

(C)

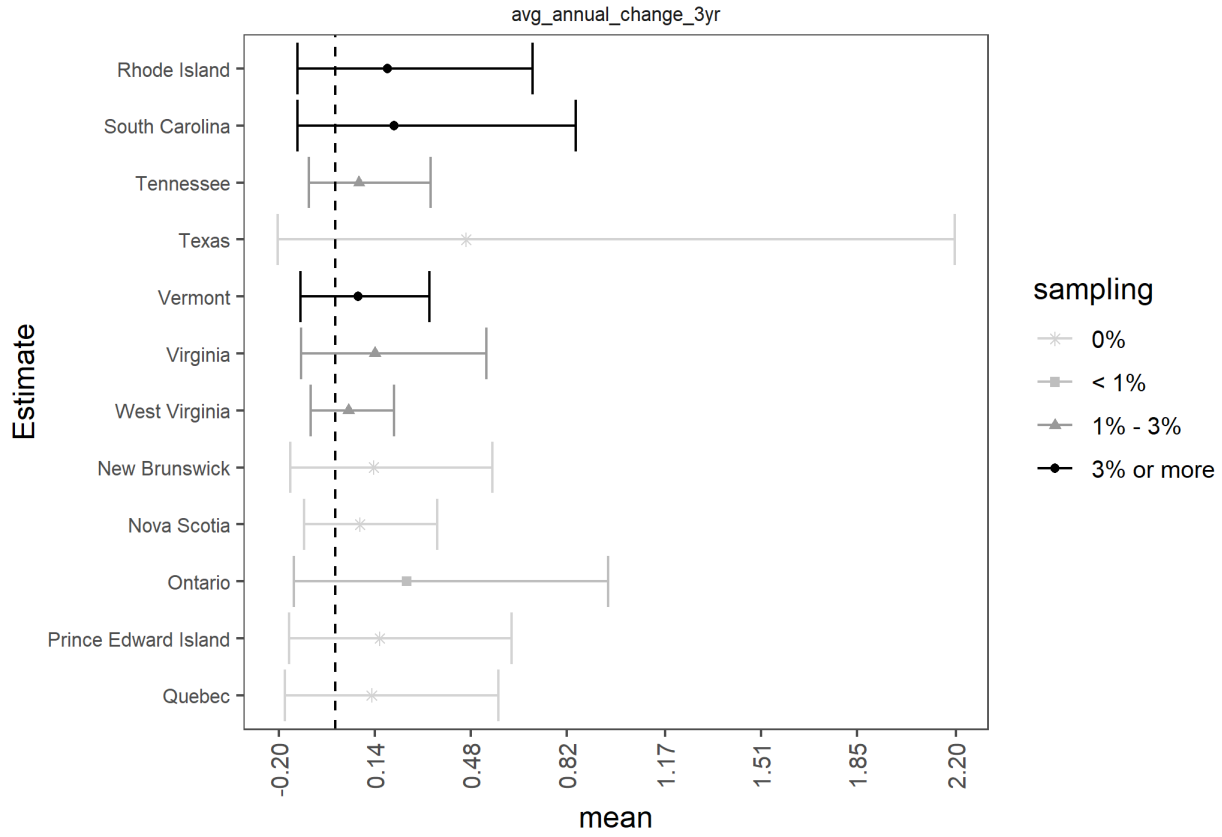

Figure B.17. Average annual rates of change in mean occupancy probabilities (avg_annual_change = lambda_avg - 1) for *Myotis leibii* (MYLE) between years over the three-year (2016-2019) time period aggregated across a state within the modeled species range. For example, avg_change_3yr = -0.05, the mean occupancy rate has declined on average by 5% each year over the three years since 2016. Means (points) and 95% credible intervals (bars) are depicted based on the average percent of grid cells sampled (legend) across all years in the timeframe of interest for each state. Note that when credible intervals do not overlap zero, we have at least 95% certainty that these trends in species occupancy are either negative or positive. When credible intervals overlap zero, we have less than 95% certainty that these trends are different than zero (A-C). U.S. states appear first in alphabetic order (A-C), followed by Canadian territories and provinces in alphabetic order (C).

(A)

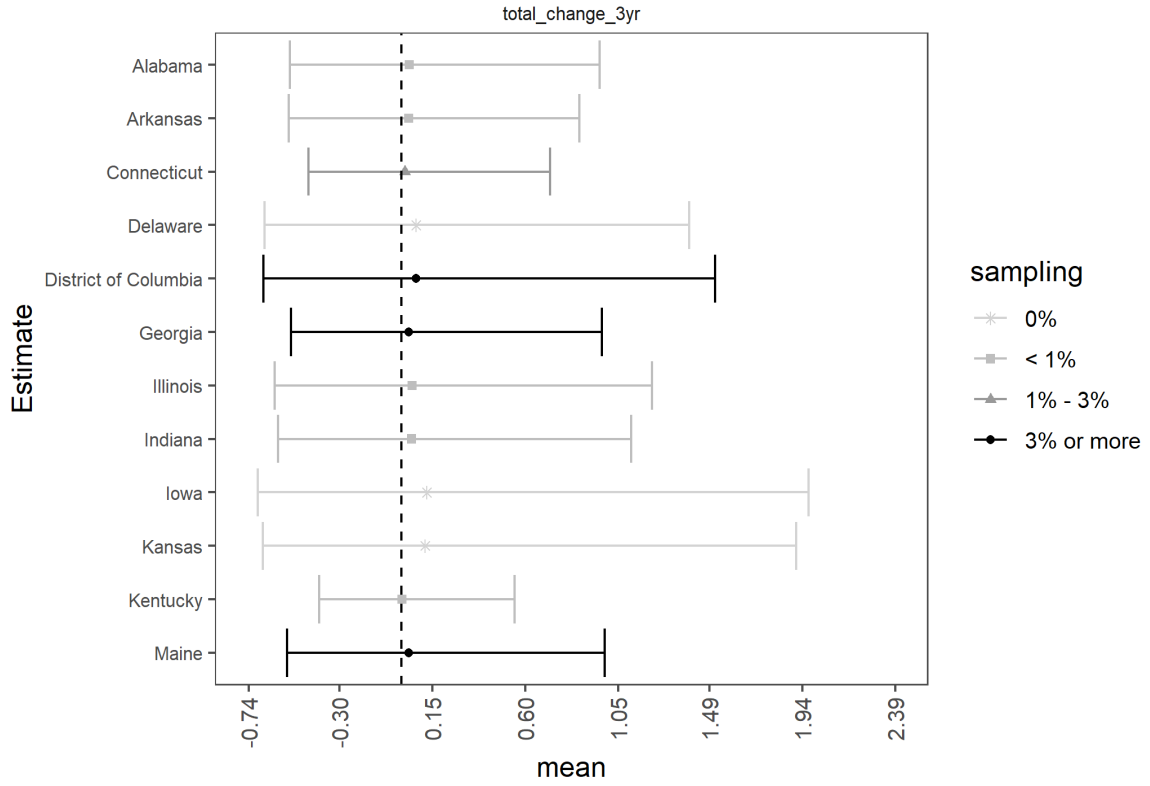
total_change_3yr
Alabama
Arkansas
Connecticut
Delaware
District of Columbia
Georgia
Illinois
Indiana
Iowa
Kansas
Kentucky
Maine
Estimate
-0.74
-0.30
0.15
0.60
1.05
1.49
1.94
2.39
mean
sampling
0%
< 1%
1% - 3%
3% or more

(B)

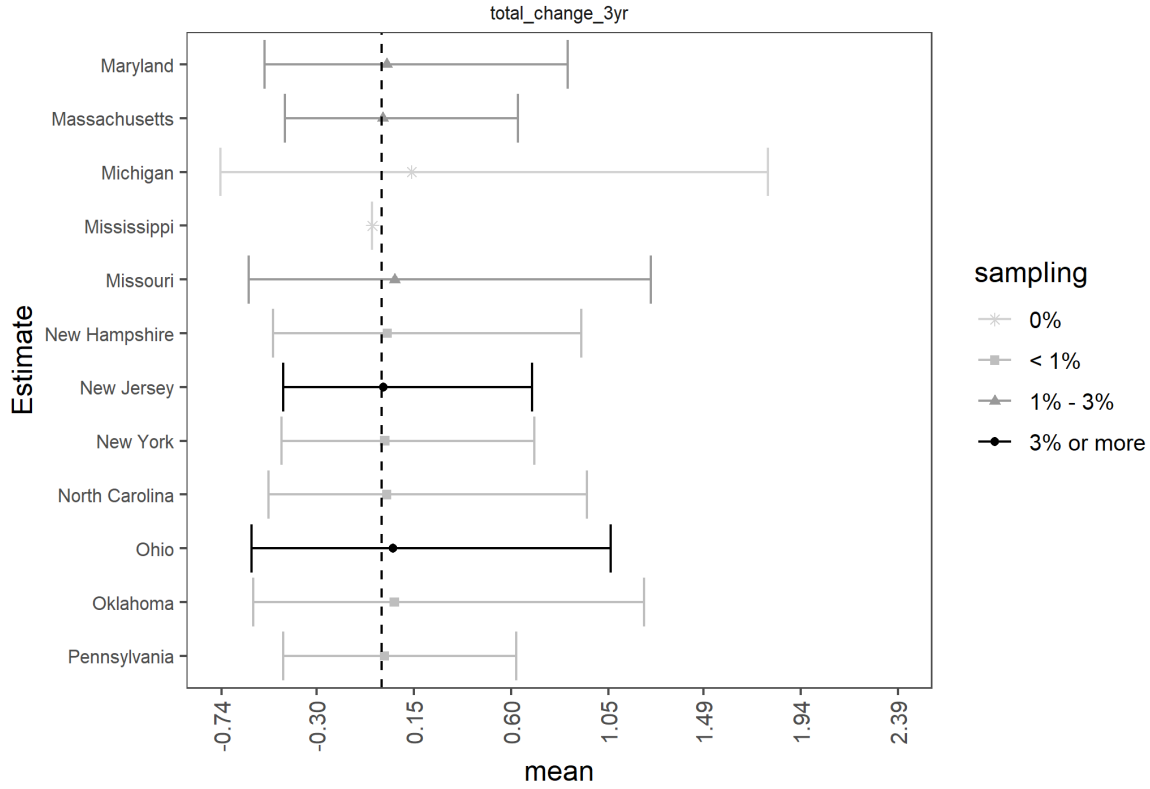
total_change_3yr
Maryland
Massachusetts
Michigan
Mississippi
Missouri
New Hampshire
New Jersey
New York
North Carolina
Ohio
Oklahoma
Pennsylvania
Estimate
-0.74
-0.30
0.15
0.60
1.05
1.49
1.94
2.39
mean
sampling
0%
< 1%
1% - 3%
3% or more

(C)

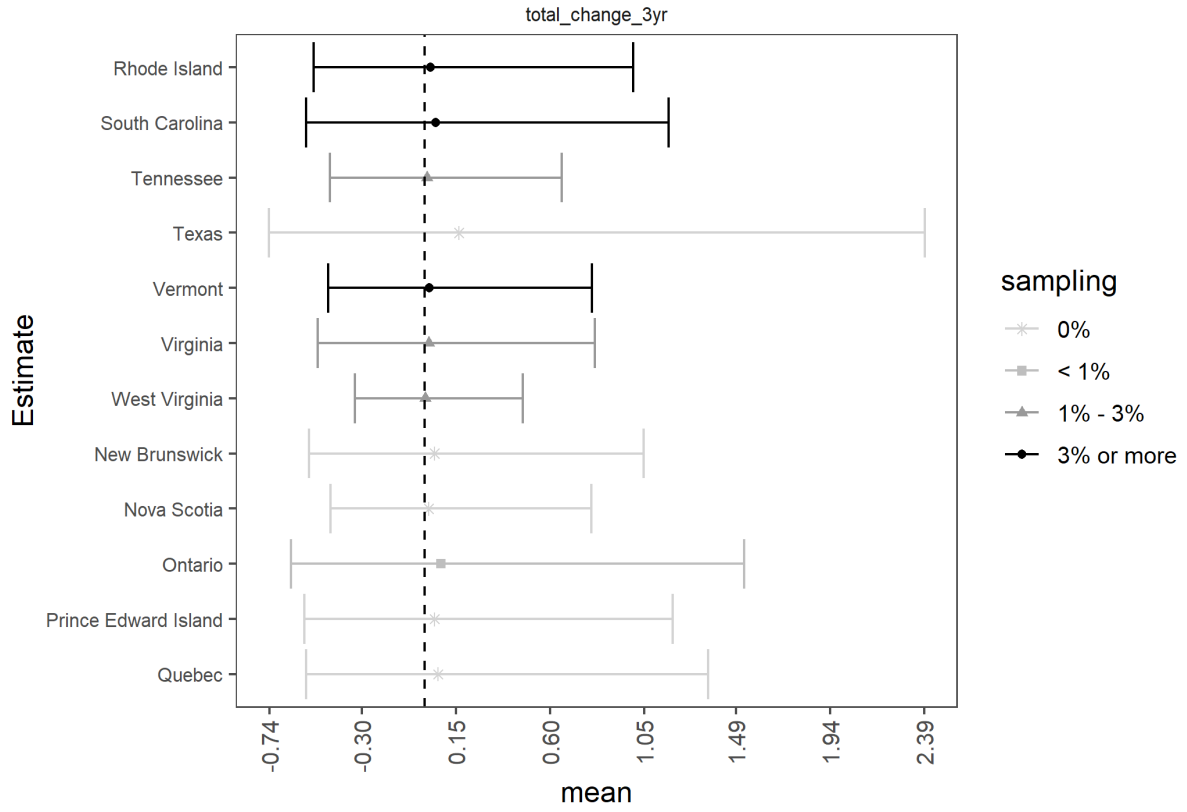

Figure B.18. The total change rate in mean occupancy (total_change = lambda_tot - 1) for *Myotis leibii* (MYLE) given the mean occupancy estimate in last year of sampling (2019) and the mean occupancy estimates three years (2016) prior aggregated across a state within the modeled species range. For example, if total_change_3yr = -0.25, the mean occupancy rate has declined by 25% over the nine years since 2016, while a value of 0.25 would indicate an increase of 25%. Means (points) and 95% credible intervals (bars) are depicted based on the average percent of grid cells sampled (legend) in the first and last years of the timeframe of interest for each state. Note that when credible intervals do not overlap zero, we have at least 95% certainty that these trends in species occupancy are either negative or positive. When credible intervals overlap zero, we have less than 95% certainty that these trends are different than zero. U.S. states appear first in alphabetic order (A-C), followed by Canadian territories and provinces in alphabetic order (C).

B.7 *Myotis thysanodes*

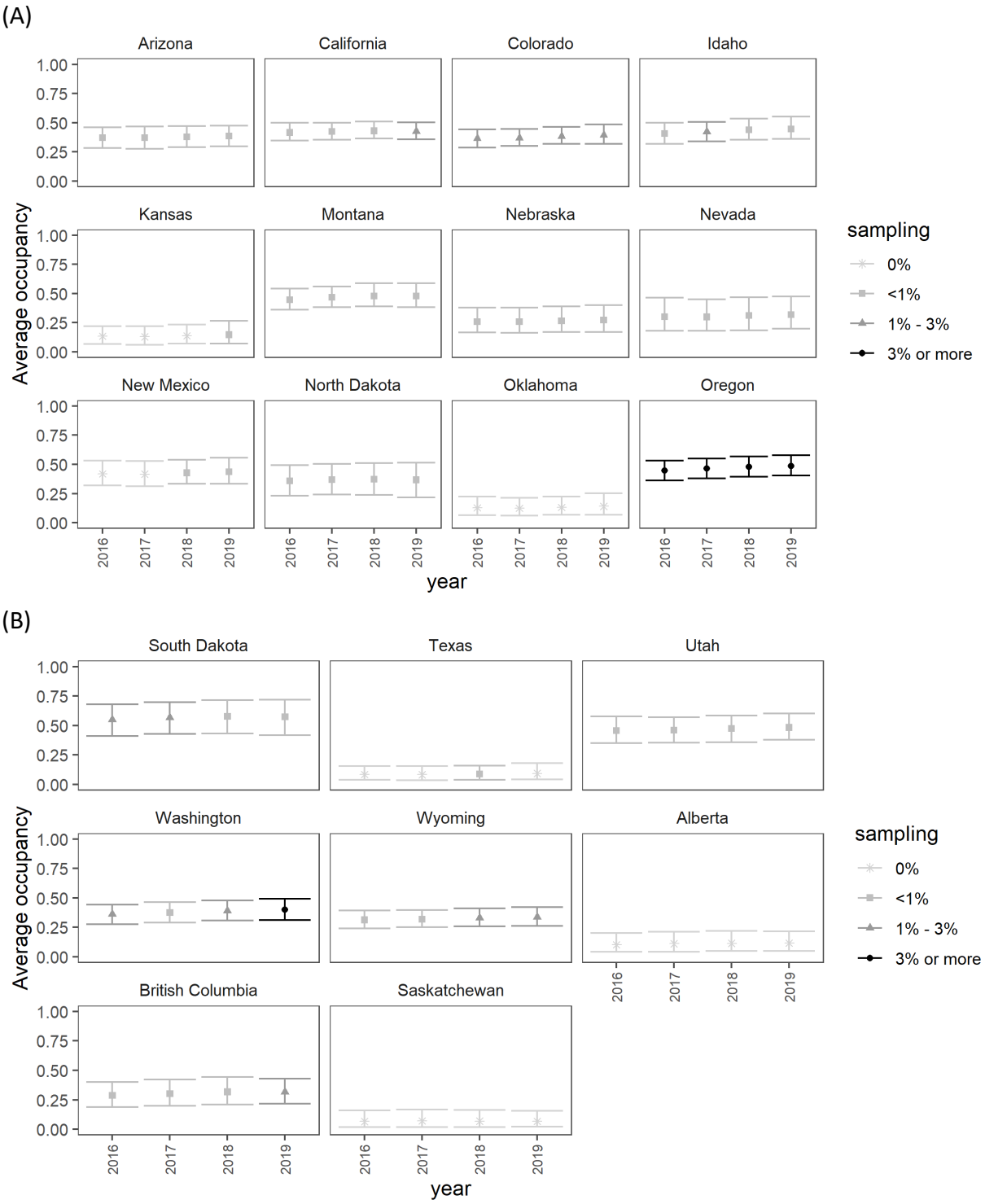

Figure B.19. Estimates of the average occupancy probability (psi_bar) for *Myotis thysanodes* (MYTH) aggregated over all grid cells for each state, territory or province in the modeled species range each year. Means (points) and 95% credible intervals (bars) are depicted according to the percent of grid cells sampled (legend) in the entire state, province or territory each year (A and B). U.S. states appear first in alphabetic order (A and B), followed by Canadian territories and provinces in alphabetic order (B).

(A)

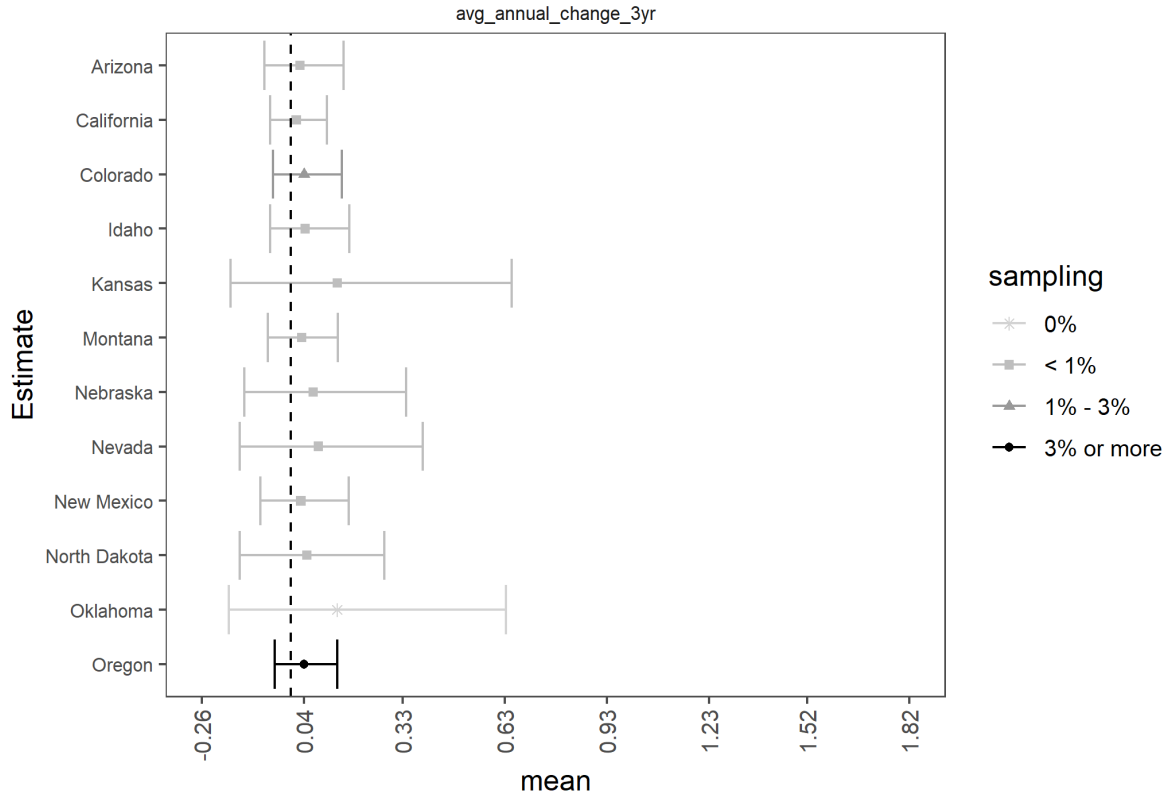
avg_annual_change_3yr
Arizona
California
Colorado
Idaho
Kansas
Montana
Nebraska
Nevada
New Mexico
North Dakota
Oklahoma
Oregon
Estimate
-0.26
0.04
0.33
0.63
0.93
1.23
1.52
1.82
mean
sampling
0%
< 1%
1% - 3%
3% or more

(B)

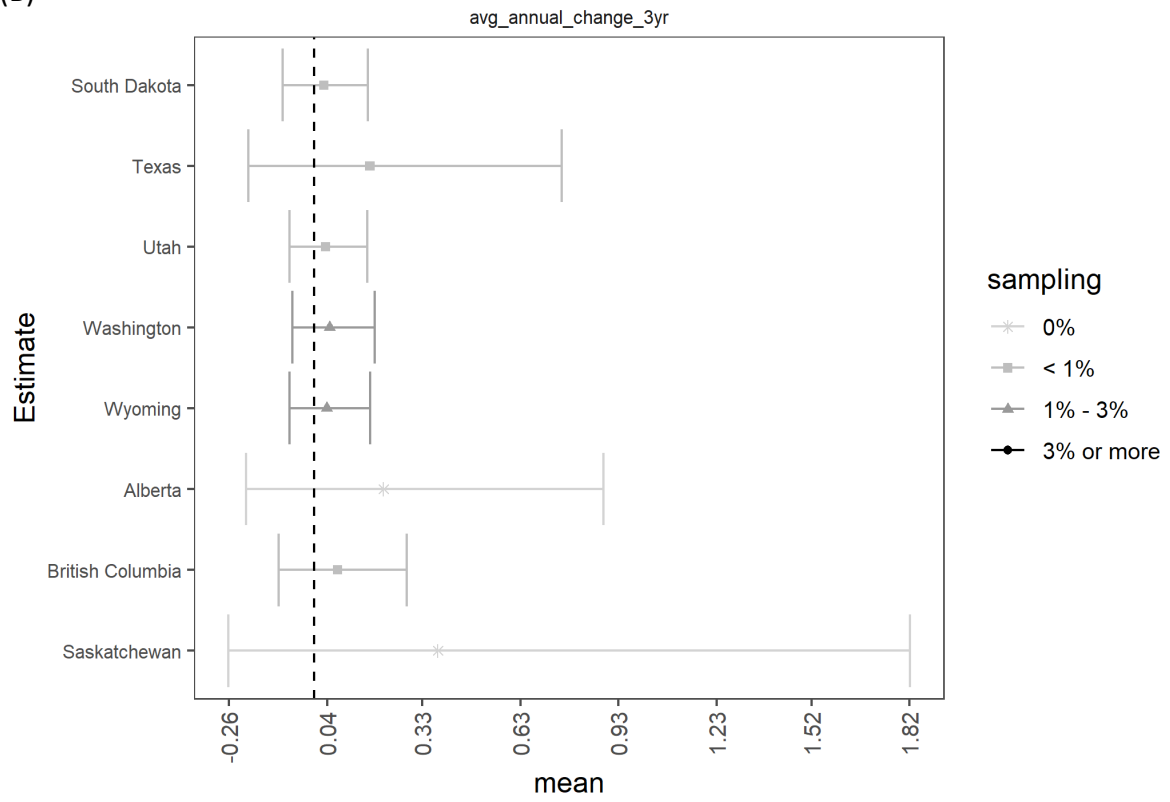
avg_annual_change_3yr
South Dakota
Texas
Utah
Washington
Wyoming
Alberta
British Columbia
Saskatchewan
Estimate
-0.26
0.04
0.33
0.63
0.93
1.23
1.52
1.82
mean
sampling
0%
< 1%
1% - 3%
3% or more

Figure B.20. Average annual rates of change in mean occupancy probabilities (avg_annual_change = lambda_avg - 1) for *Myotis thysanodes* (MYTH) between years over the three-year time (2016-2019) period aggregated across a state, province, or territory within the modeled species range. For example, if avg_change_3yr = -0.05, the mean occupancy rate has declined on average by 5% each year over the three years since 2016. Means (points) and 95% credible intervals (bars) are depicted based on the average percent of grid cells sampled (legend) across all years in the timeframe of interest for each state, province or territory (A and B). Note that when credible intervals do not overlap zero, we have at least 95% certainty that these trends in species occupancy are either negative or positive. When credible intervals overlap zero, we have less than 95% certainty that these trends are different than zero. U.S. states appear first in alphabetic order (A-B), followed by Canadian territories and provinces in alphabetic order (B).

(A)

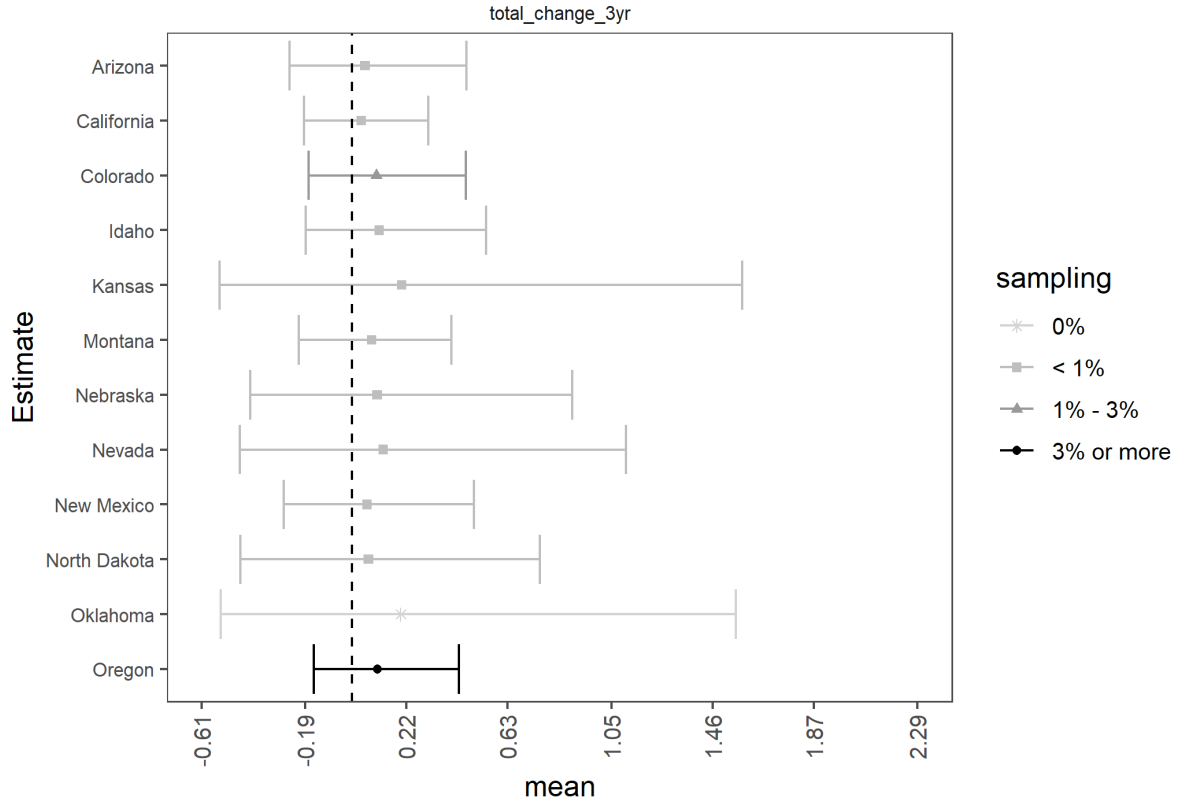
total_change_3yr
Arizona
California
Colorado
Idaho
Kansas
Montana
Nebraska
Nevada
New Mexico
North Dakota
Oklahoma
Oregon
Estimate
-0.61
-0.19
0.22
0.63
1.05
1.46
1.87
2.29
mean
sampling
0%
< 1%
1% - 3%
3% or more

(B)

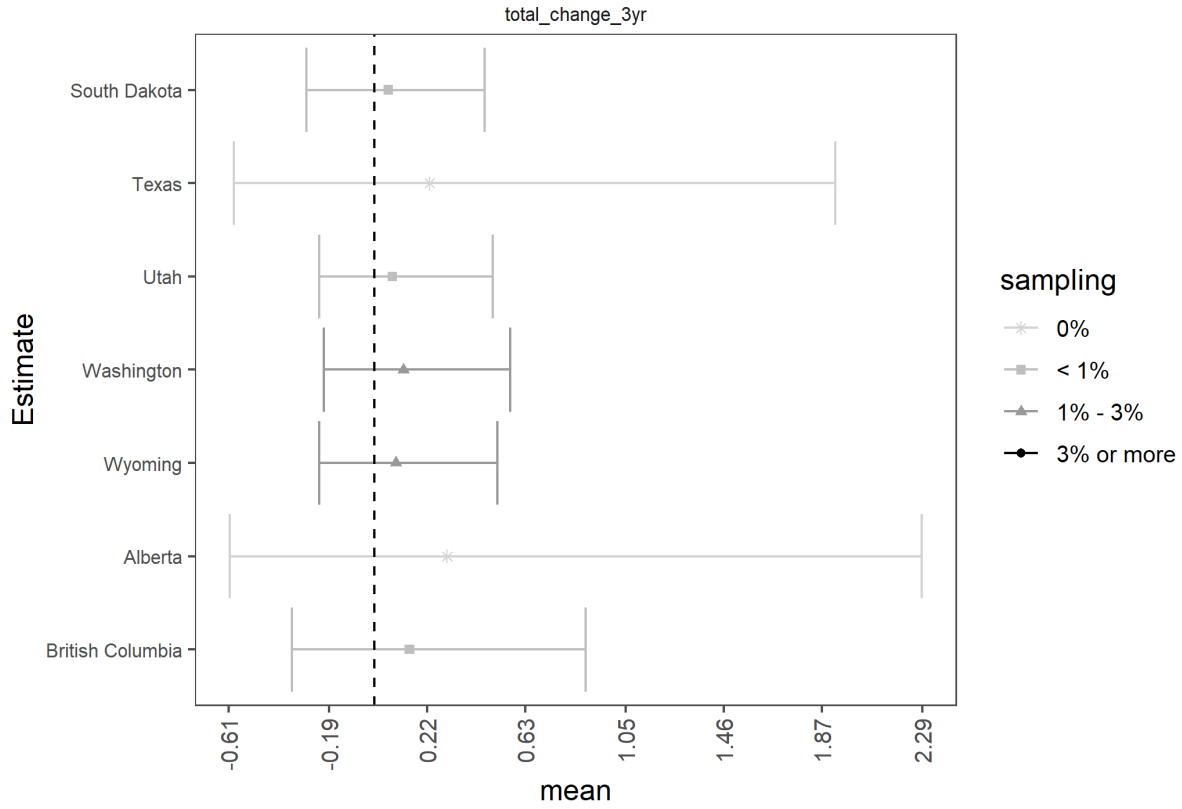
total_change_3yr
South Dakota
Texas
Utah
Washington
Wyoming
Alberta
British Columbia
Estimate
-0.61
-0.19
0.22
0.63
1.05
1.46
1.87
2.29
mean
sampling
0%
< 1%
1% - 3%
3% or more

Figure B.21. The total change rate in mean occupancy (total_change = lambda_tot - 1) for *Myotis thysanodes* (MYTH) given the mean occupancy estimate in last year of sampling (2019) and the mean occupancy estimates three years (2016) prior aggregated across a state, province, or territory within the modeled species range. For example, if total_change_3yr = -0.25, the mean occupancy rate has declined by 25% over the nine years since 2016, while a value of 0.25 would indicate an increase of 25%. Means (points) and 95% credible intervals (bars) are depicted based on the average percent of grid cells sampled (legend) in the first and last years of the timeframe of interest for each state, province or territory (A and B). Note that when credible intervals do not overlap zero, we have at least 95% certainty that these trends in species occupancy are either negative or positive. When credible intervals overlap zero, we have less than 95% certainty that these trends are different than zero. U.S. states appear first in alphabetic order (A-B), followed by Canadian territories and provinces in alphabetic order (B).

B.8 *Myotis volans*

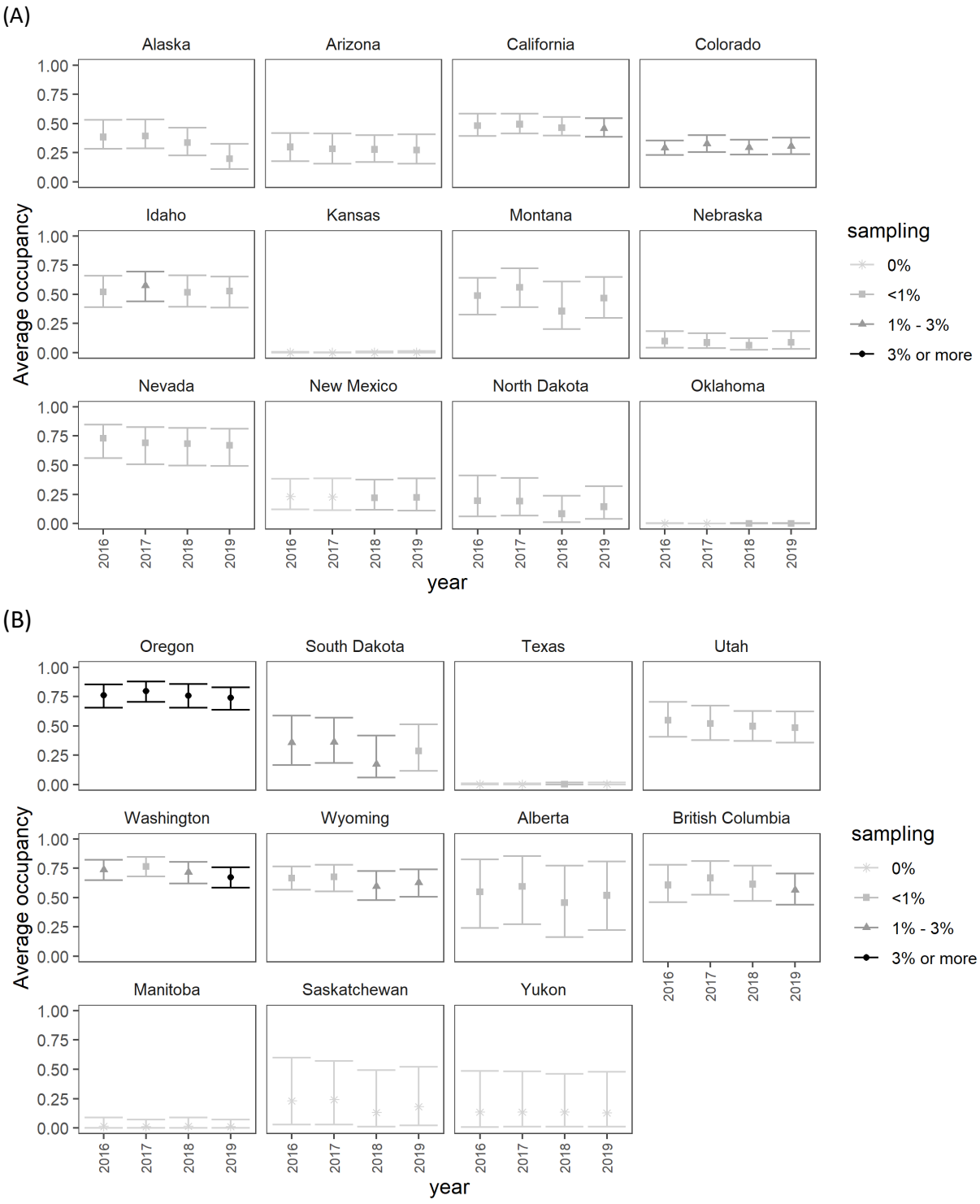

Figure B.22. Estimates of the average occupancy probability ($\widehat{\psi}_t$) for *Myotis volans* (MYVO) aggregated over all grid cells for each state, territory or province in the modeled species range each year. Means (points) and 95% credible intervals (bars) are depicted according to the percent of grid cells sampled (legend) in the entire state, province or territory each year (A and B). U.S. states appear first in alphabetic order (A and B), followed by Canadian territories and provinces in alphabetic order (B).

(A)

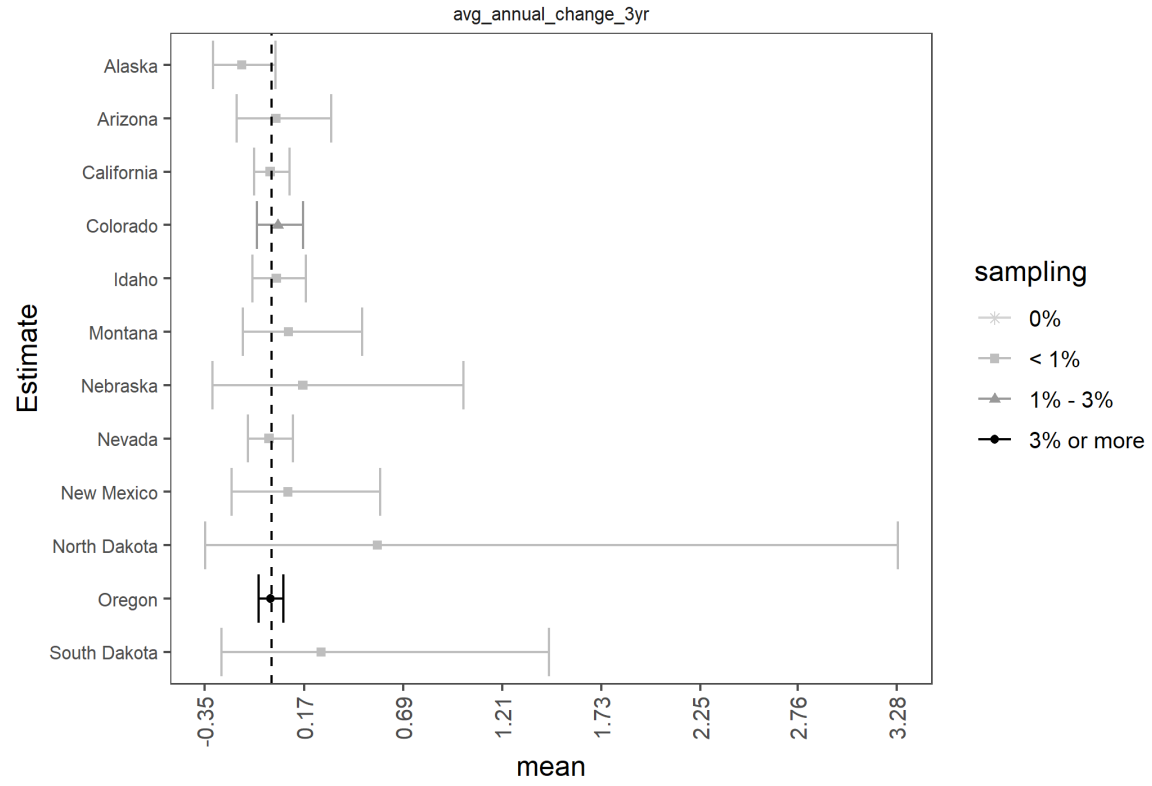
avg_annual_change_3yr
Alaska
Arizona
California
Colorado
Idaho
Montana
Nebraska
Nevada
New Mexico
North Dakota
Oregon
South Dakota
Estimate
-0.35
0.17
0.69
1.21
1.73
2.25
2.76
3.28
mean
sampling
0%
< 1%
1% - 3%
3% or more

(B)

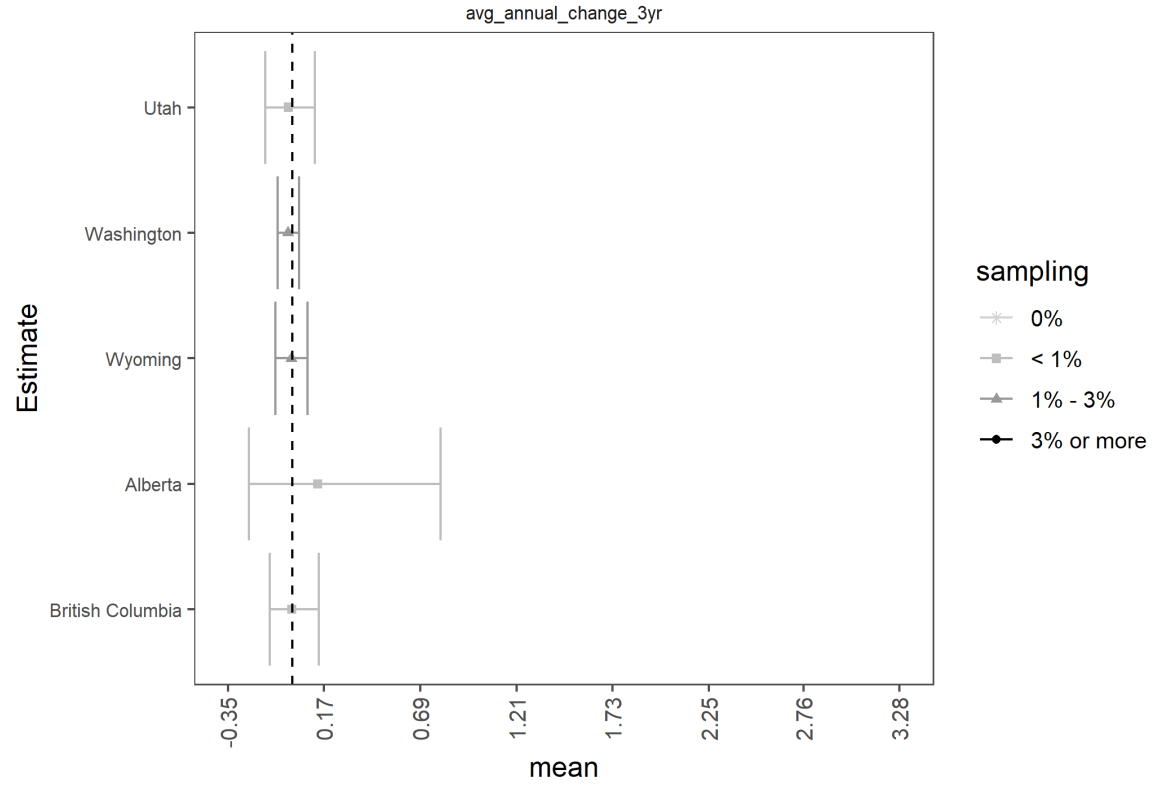
avg_annual_change_3yr
Utah
Washington
Wyoming
Alberta
British Columbia
Estimate
-0.35
0.17
0.69
1.21
1.73
2.25
2.76
3.28
mean
sampling
0%
< 1%
1% - 3%
3% or more

Figure B.23. Average annual rates of change in mean occupancy probabilities (avg_annual_change = lambda_avg - 1) for *Myotis volans* (MYVO) between years over the three-year (2016-2019) time period aggregated across a state, province, or territory within the modeled species range. For example, if avg_change_3yr = -0.05, the mean occupancy rate has declined on average by 5% each year over the three years since 2016. Means (points) and 95% credible intervals (bars) are depicted based on the average percent of grid cells sampled (legend) across all years in the timeframe of interest for each state, province or territory (A and B). Note that when credible intervals do not overlap zero, we have at least 95% certainty that these trends in species occupancy are either negative or positive. When credible intervals overlap zero, we have less than 95% certainty that these trends are different than zero. U.S. states appear first in alphabetic order (A-B), followed by Canadian territories and provinces in alphabetic order (B).

(A)

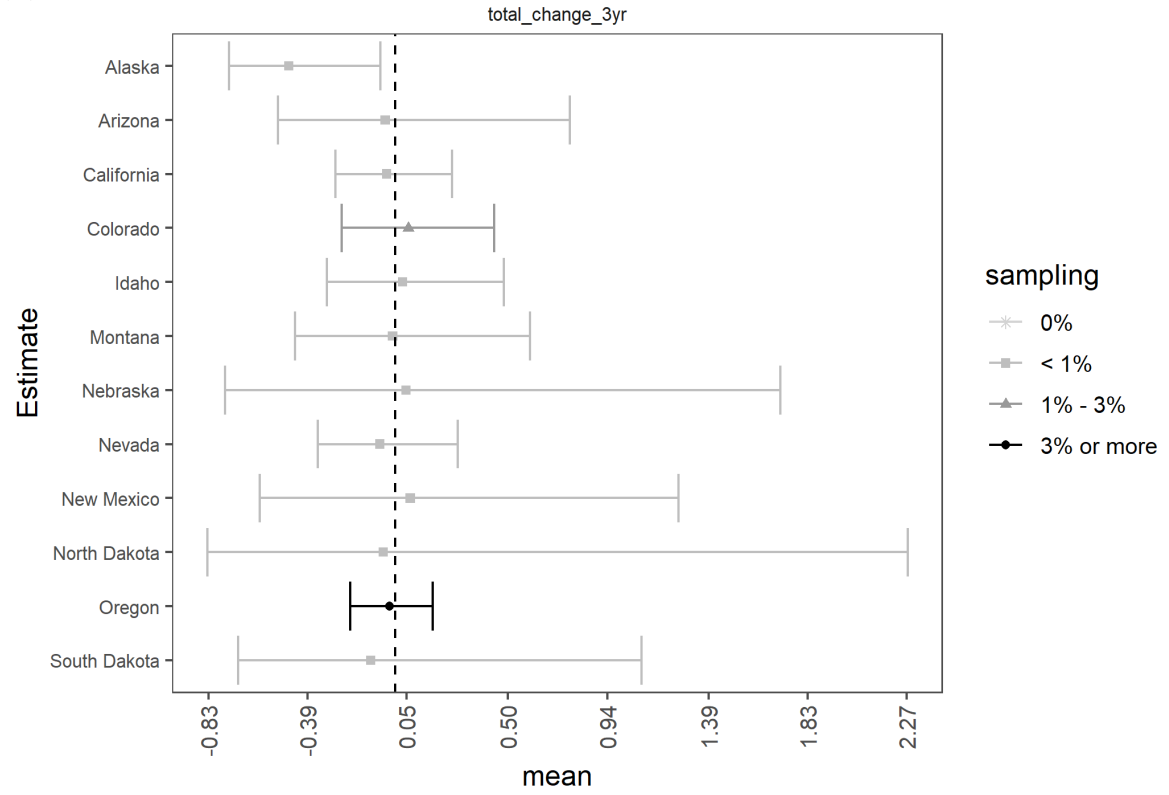
total_change_3yr
Alaska
Arizona
California
Colorado
Idaho
Montana
Nebraska
Nevada
New Mexico
North Dakota
Oregon
South Dakota
Estimate
-0.83
-0.39
0.05
0.50
0.94
1.39
1.83
2.27
mean
sampling
0%
< 1%
1% - 3%
3% or more

(B)

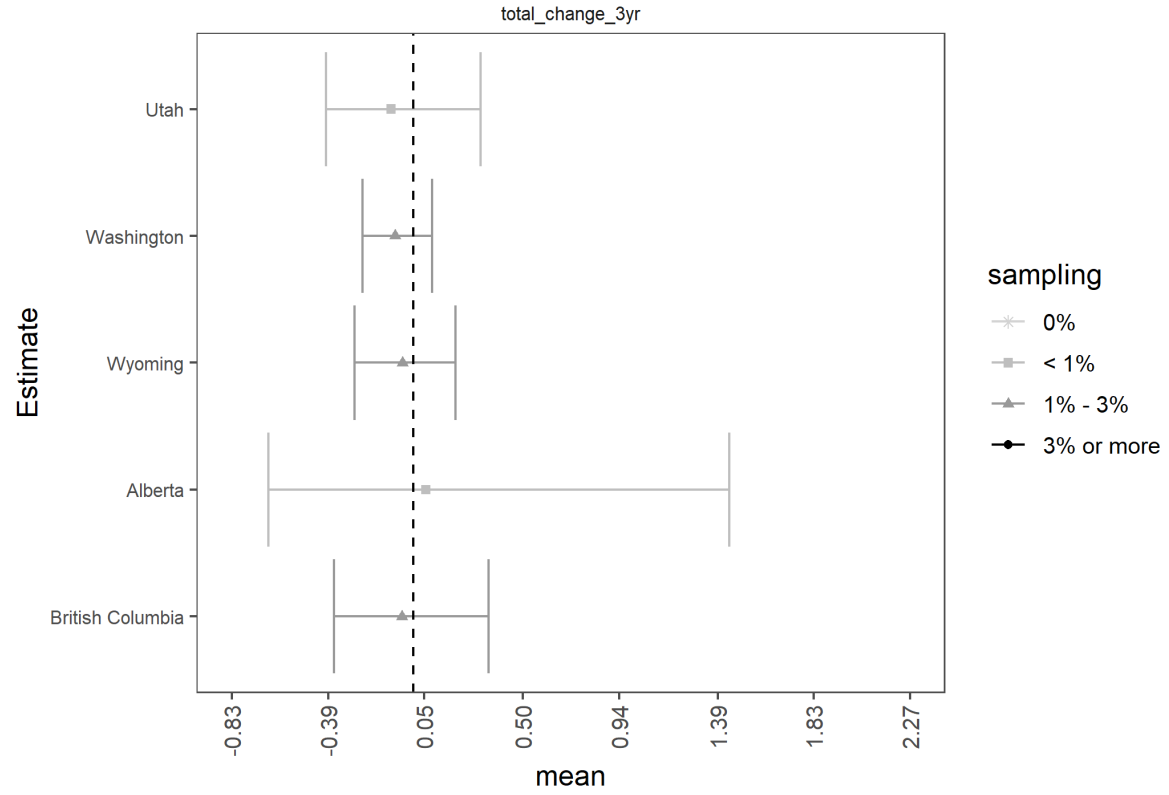
total_change_3yr
Utah
Washington
Wyoming
Alberta
British Columbia
Estimate
-0.83
-0.39
0.05
0.50
0.94
1.39
1.83
2.27
mean
sampling
0%
< 1%
1% - 3%
3% or more

Figure B.24. The total change rate in mean occupancy (total_change = lambda_tot - 1) for *Myotis volans* (MYVO) given the mean occupancy estimate in last year of sampling (2019) and the mean occupancy estimates three years (2016) prior aggregated across a state, province, or territory within the modeled species range. For example, if total_change_3yr = -0.25, the mean occupancy rate has declined by 25% over the nine years since 2016, while a value of 0.25 would indicate an increase of 25%. Means (points) and 95% credible intervals (bars) are depicted based on the average percent of grid cells sampled (legend) in the first and last years of the timeframe of interest for each state, province or territory (A and B). Note that when credible intervals do not overlap zero, we have at least 95% certainty that these trends in species occupancy are either negative or positive. When credible intervals overlap zero, we have less than 95% certainty that these trends are different than zero. U.S. states appear first in alphabetic order (A-B), followed by Canadian territories and provinces in alphabetic order (B).

B.9 *Myotis yumanensis*

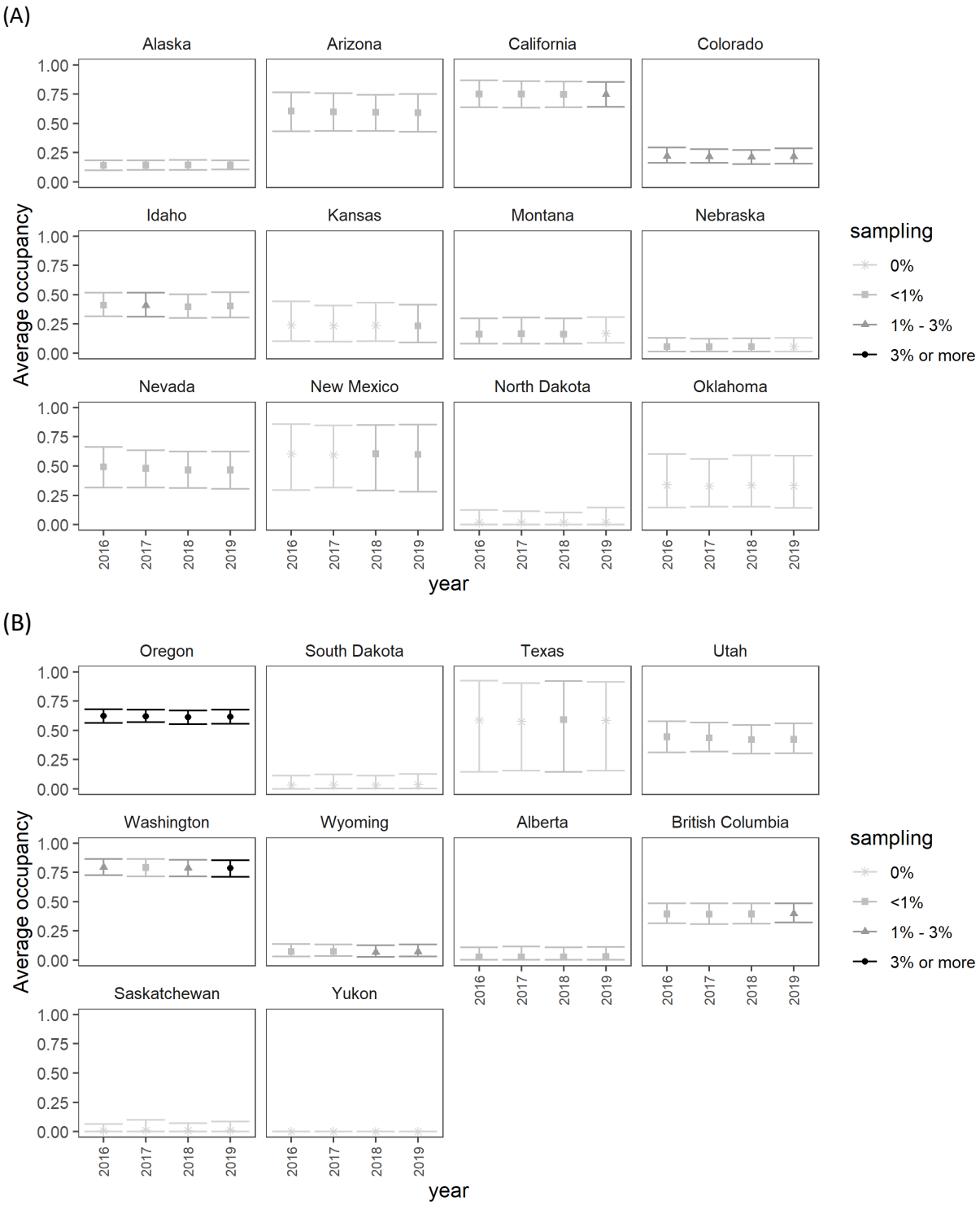

Figure B.25. Estimates of the average occupancy probability ($\widehat{\psi}_t$) for *Myotis yumanensis* (MYYU) aggregated over all grid cells for each state, territory or province in the modeled species range each year. Means (points) and 95% credible intervals (bars) are depicted according to the percent of grid cells sampled (legend) in the entire state, province or territory each year (A and B). U.S. states appear first in alphabetic order (A and B), followed by Canadian territories and provinces in alphabetic order (B).

(A)

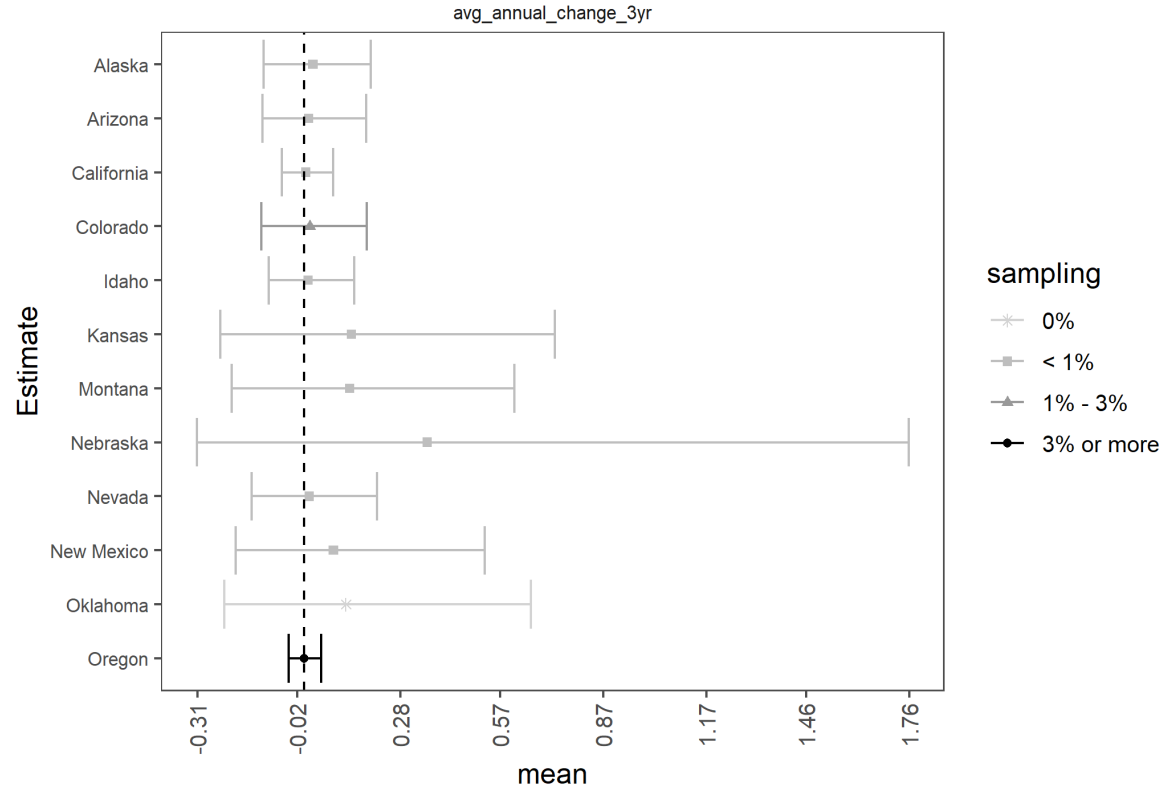
avg_annual_change_3yr
Alaska
Arizona
California
Colorado
Idaho
Kansas
Montana
Nebraska
Nevada
New Mexico
Oklahoma
Oregon
Estimate
-0.31
-0.02
0.28
0.57
0.87
1.17
1.46
1.76
mean
sampling
0%
< 1%
1% - 3%
3% or more

(B)

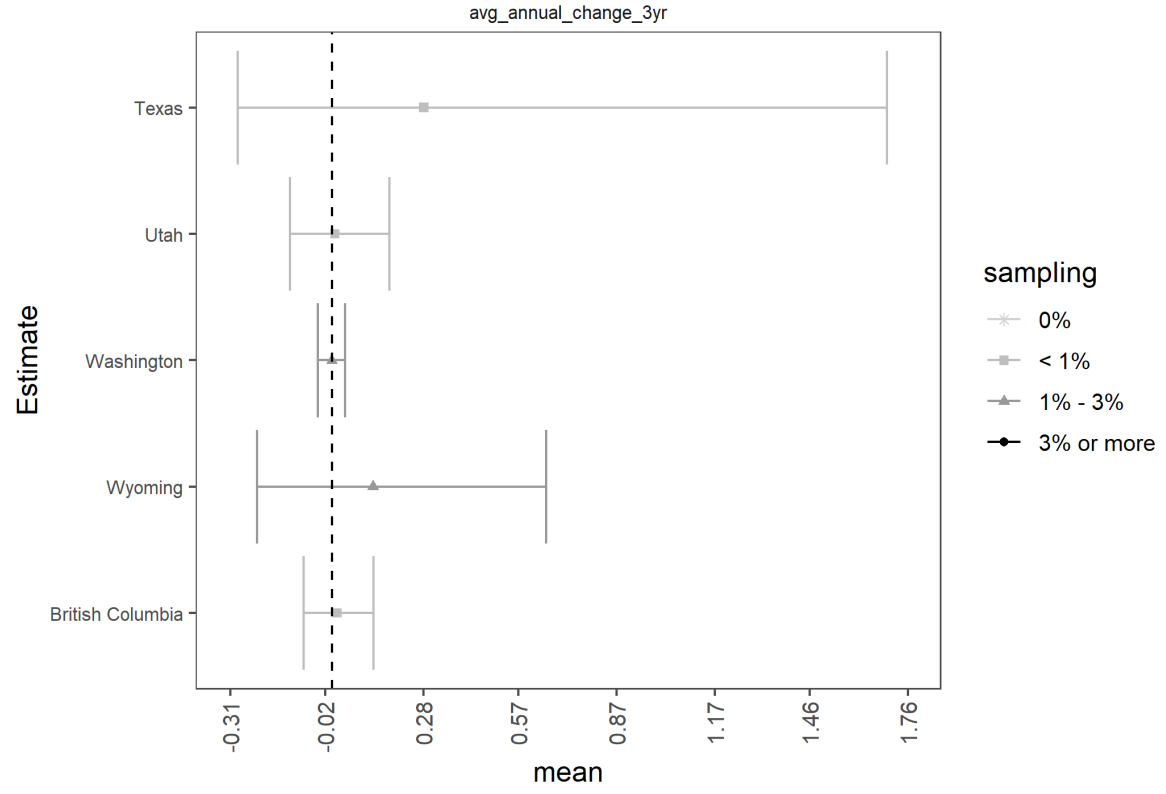
avg_annual_change_3yr
Texas
Utah
Washington
Wyoming
British Columbia
Estimate
-0.31
-0.02
0.28
0.57
0.87
1.17
1.46
1.76
mean
sampling
0%
< 1%
1% - 3%
3% or more

Figure B.26. Average annual rates of change in mean occupancy probabilities (avg_annual_change = lambda_avg - 1) for *Myotis yumanensis* (MYYU) between years over the three-year (2016-2019) time period aggregated across a state, province, or territory within the modeled species range. For example, if avg_change_3yr = -0.05, the mean occupancy rate has declined on average by 5% each year over the three years since 2016. Means (points) and 95% credible intervals (bars) are depicted based on the average percent of grid cells sampled (legend) across all years in the timeframe of interest for each state, province or territory (A and B). Note that when credible intervals do not overlap zero, we have at least 95% certainty that these trends in species occupancy are either negative or positive. When credible intervals overlap zero, we have less than 95% certainty that these trends are different than zero. U.S. states appear first in alphabetic order (A-B), followed by Canadian territories and provinces in alphabetic order (B).

(A)

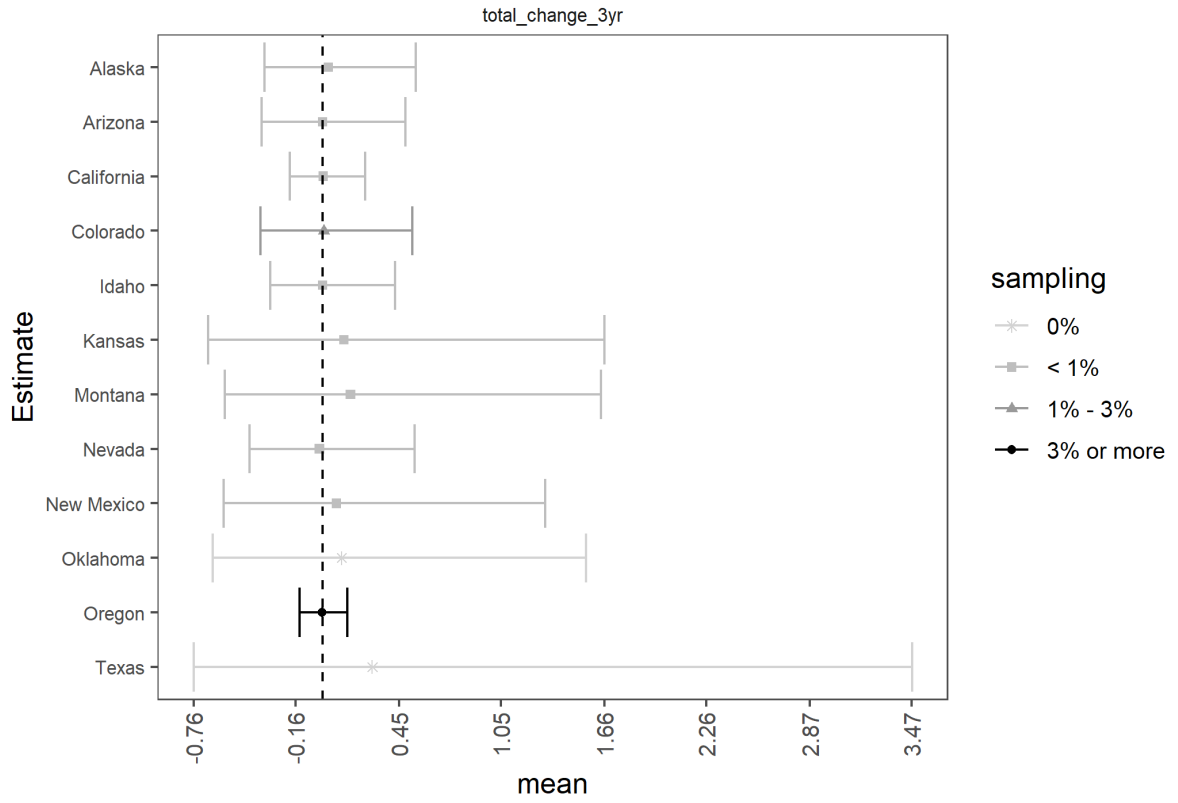
total_change_3yr
Alaska
Arizona
California
Colorado
Idaho
Kansas
Montana
Nevada
New Mexico
Oklahoma
Oregon
Texas
Estimate
-0.76
-0.16
0.45
1.05
1.66
2.26
2.87
3.47
mean
sampling
0%
< 1%
1% - 3%
3% or more

(B)

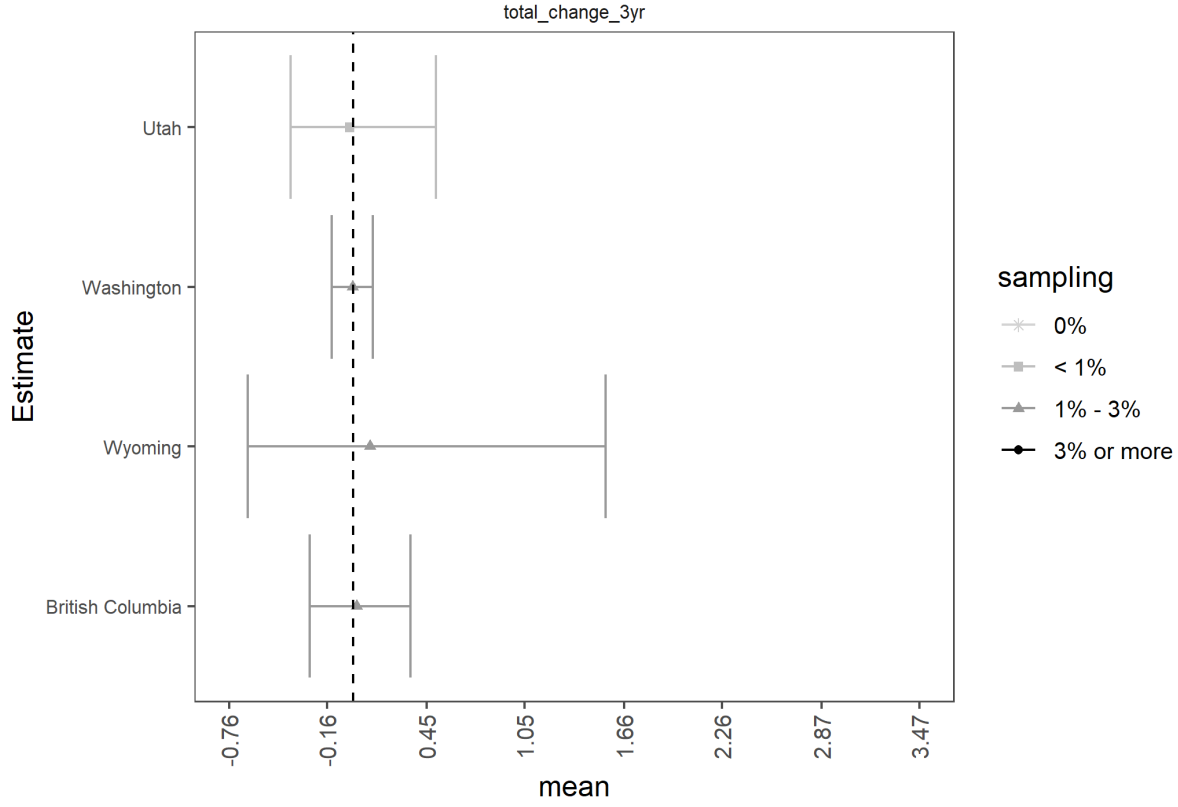
total_change_3yr
Utah
Washington
Wyoming
British Columbia
Estimate
-0.76
-0.16
0.45
1.05
1.66
2.26
2.87
3.47
mean
sampling
0%
< 1%
1% - 3%
3% or more

Figure B.27. The total change rate in mean occupancy (total_change = lambda_tot - 1) for *Myotis yumanensis* (MYYU) given the mean occupancy estimate in last year of sampling (2019) and the mean occupancy estimates three years (2016) prior aggregated across a state, province, or territory within the modeled species range. For example, if total_change_3yr = -0.25, the mean occupancy rate has declined by 25% over the nine years since 2016, while a value of 0.25 would indicate an increase of 25%. Means (points) and 95% credible intervals (bars) are depicted based on the average percent of grid cells sampled (legend) in the first and last years of the timeframe of interest for each state, province or territory (A and B). Note that when credible intervals do not overlap zero, we have at least 95% certainty that these trends in species occupancy are either negative or positive. When credible intervals overlap zero, we have less than 95% certainty that these trends are different than zero. U.S. states appear first in alphabetic order (A-B), followed by Canadian territories and provinces in alphabetic order (B).

B.10 *Eptesicus fuscus*

(A)

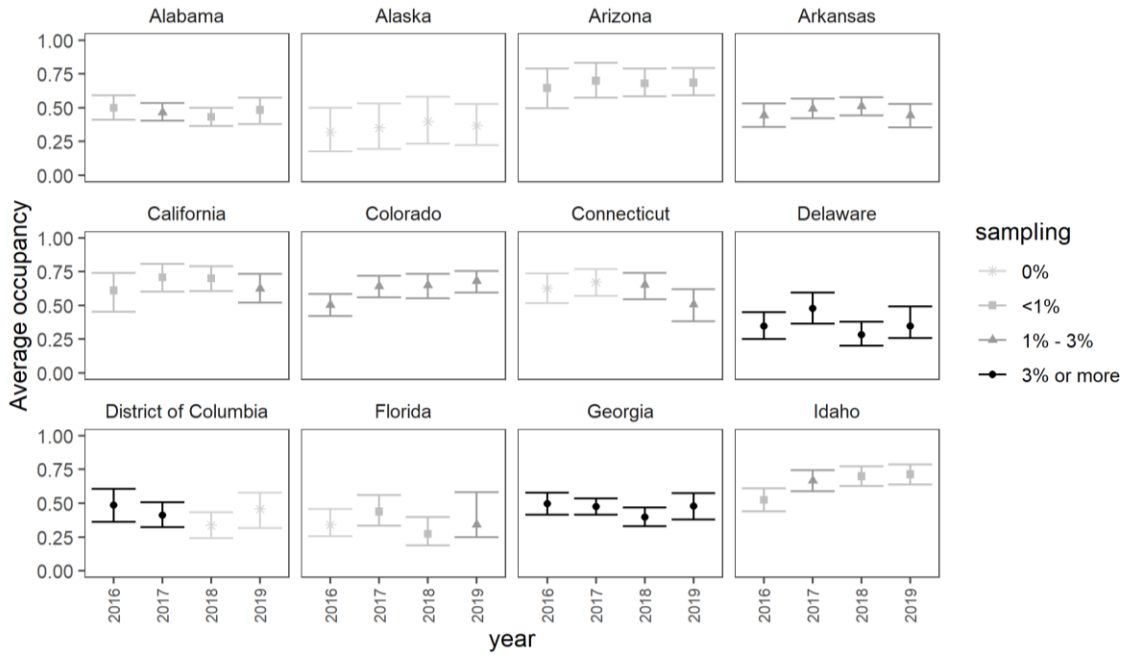

(B)

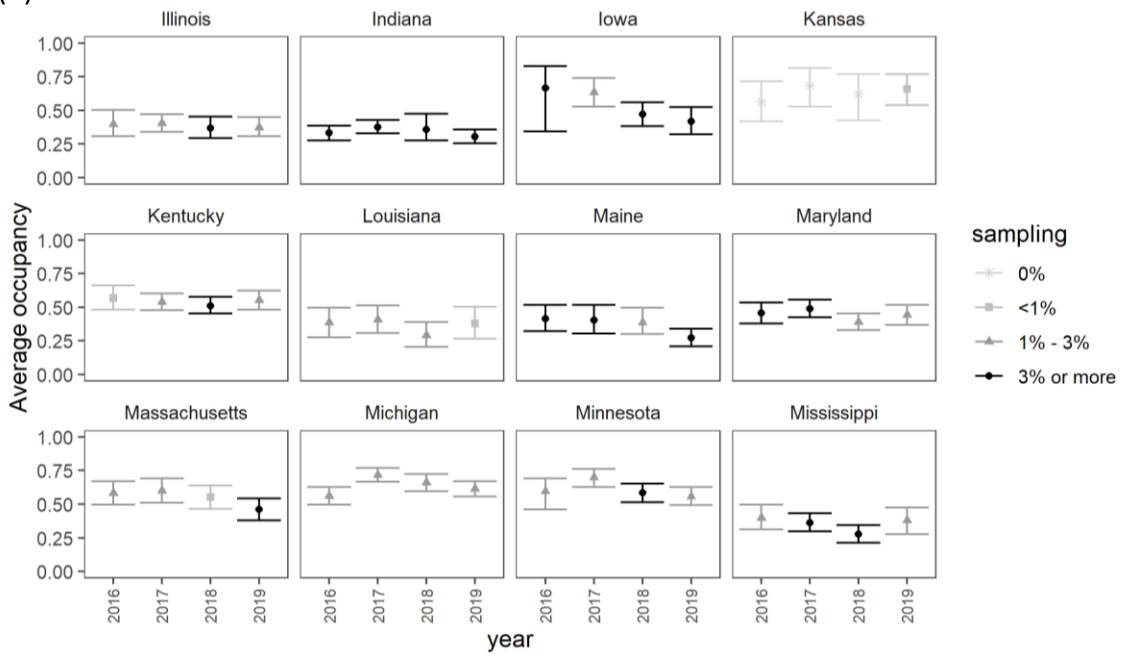

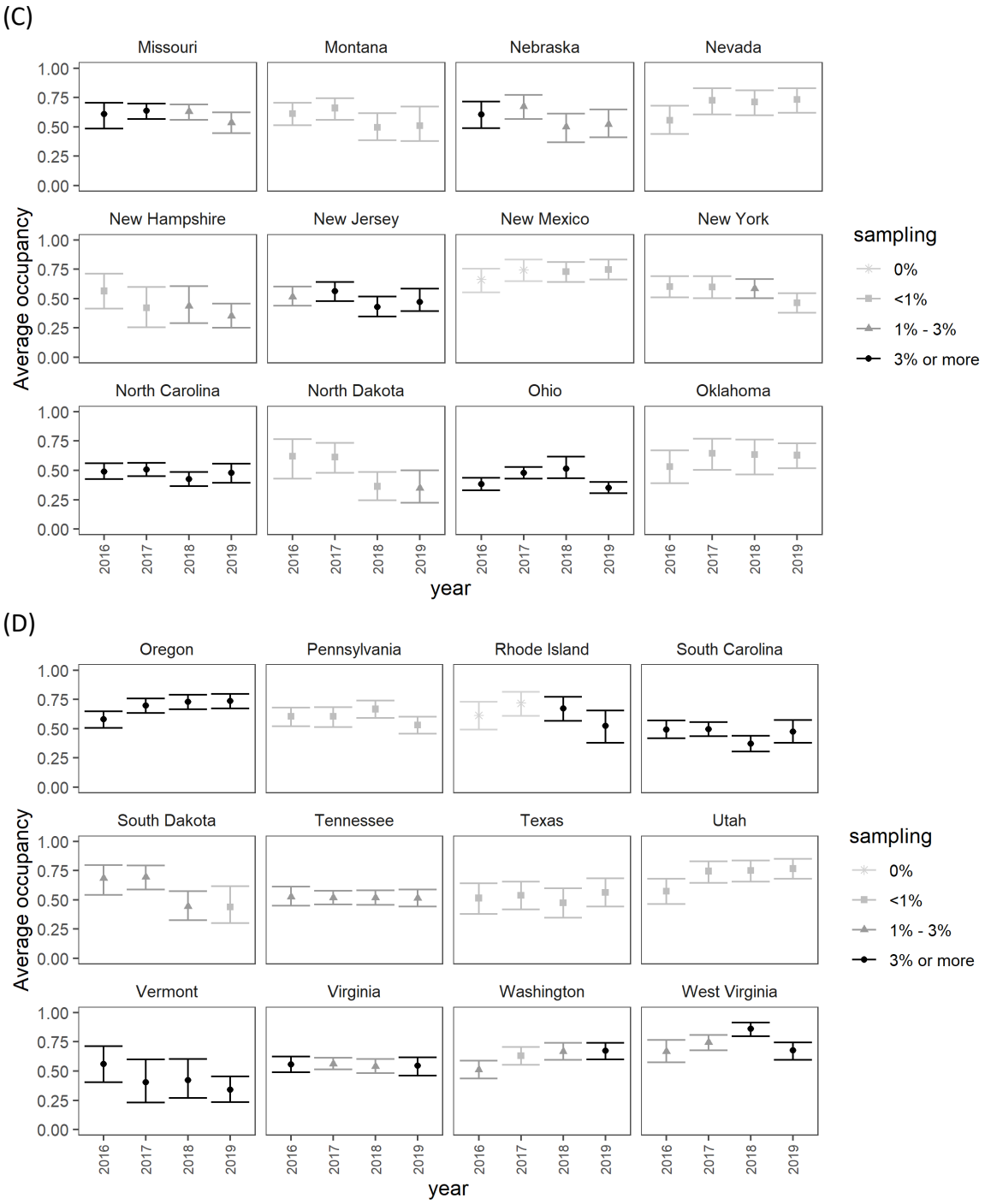

Figure B.28. Estimates of the average occupancy probability ($\widehat{\psi}_t$) for *Eptesicus fuscus* (EPFU) average occupancy probability aggregated over all grid cells for each state in the modeled species range each year. Means (points) and 95% credible intervals (bars) are depicted according to the percent of grid cells sampled (legend) in the entire state, province or territory each year (A-D). U.S. states appear in alphabetic order (A-D. Note the results for EPFU were inconclusive due issues reported in section 3.12.

(A)

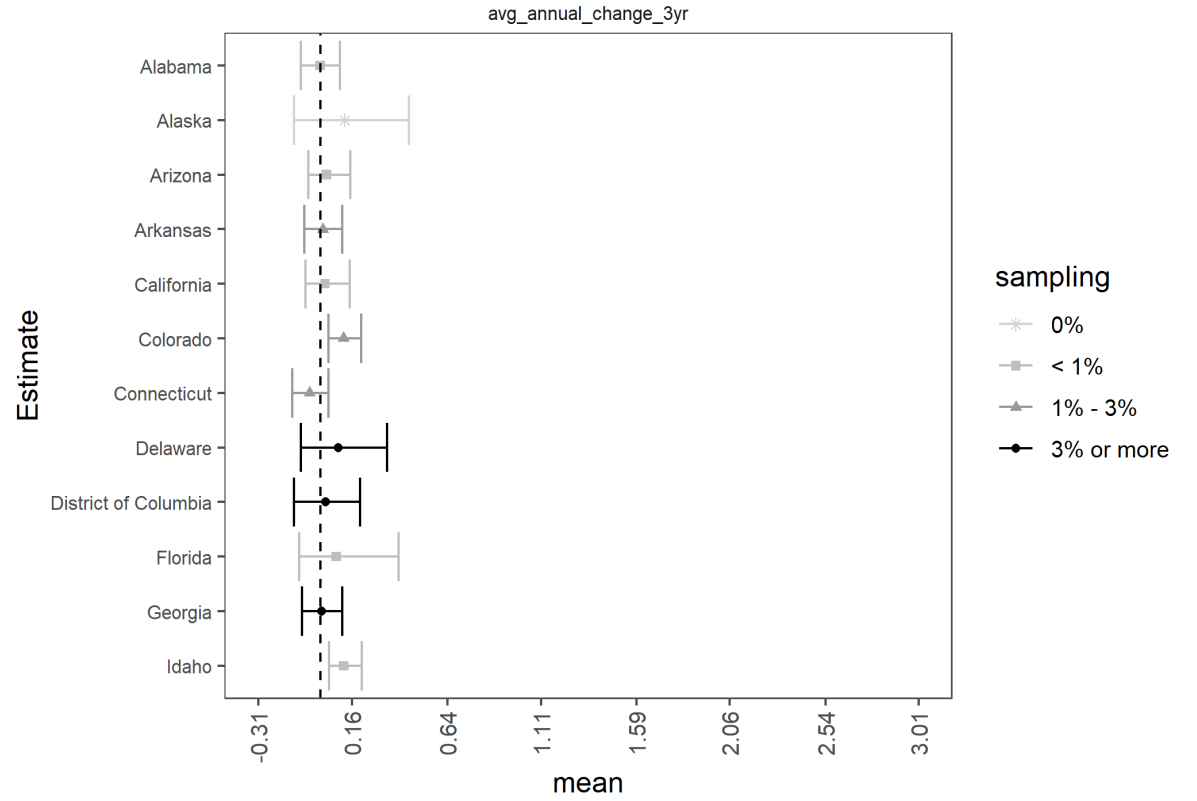
avg_annual_change_3yr
Alabama
Alaska
Arizona
Arkansas
California
Colorado
Connecticut
Delaware
District of Columbia
Florida
Georgia
Idaho
Estimate
-0.31
0.16
0.64
1.11
1.59
2.06
2.54
3.01
mean
sampling
0%
< 1%
1% - 3%
3% or more

(B)

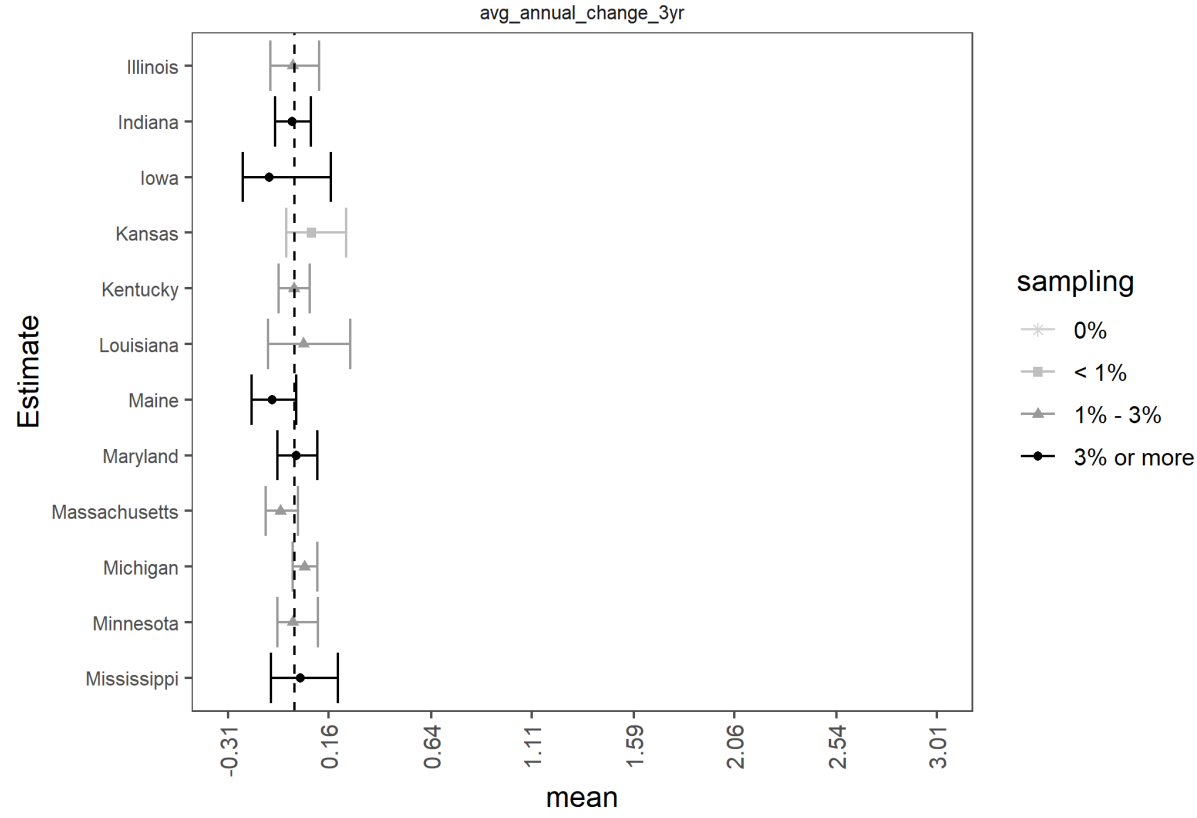
avg_annual_change_3yr
Illinois
Indiana
Iowa
Kansas
Kentucky
Louisiana
Maine
Maryland
Massachusetts
Michigan
Minnesota
Mississippi
Estimate
-0.31
0.16
0.64
1.11
1.59
2.06
2.54
3.01
mean
sampling
0%
< 1%
1% - 3%
3% or more

(C)

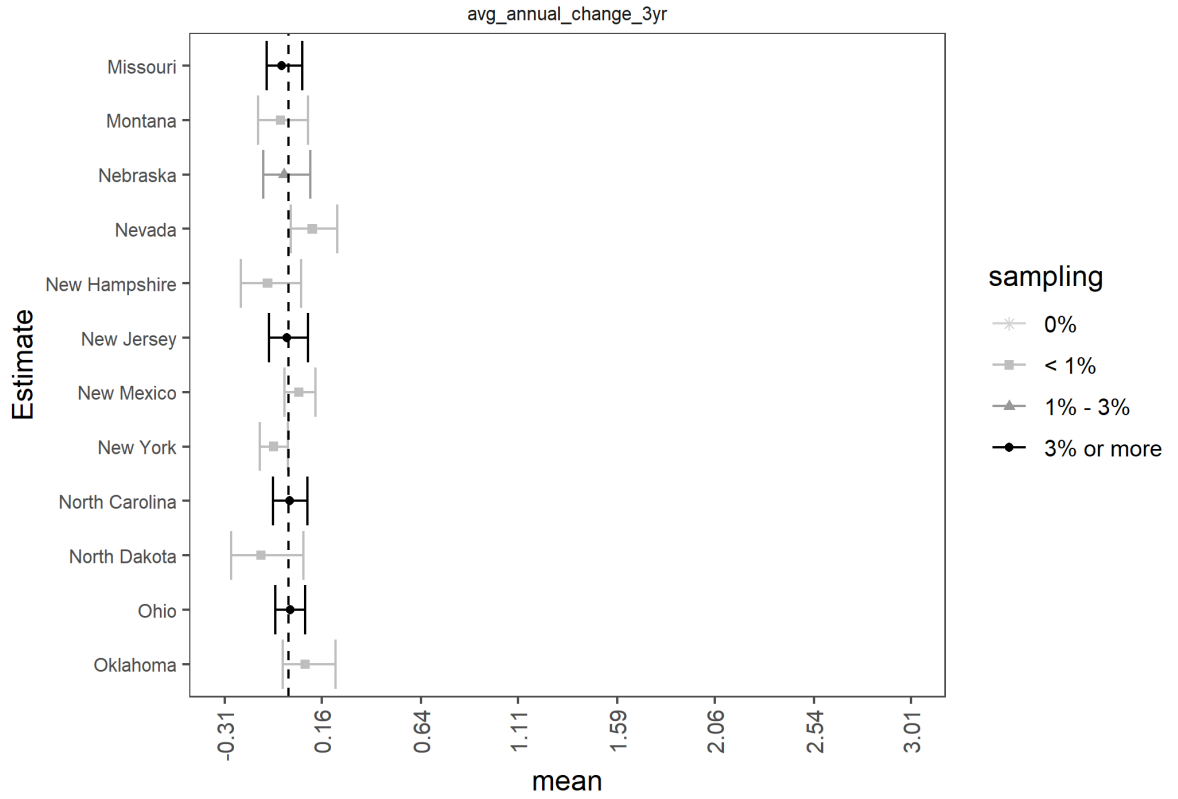
avg_annual_change_3yr
Missouri
Montana
Nebraska
Nevada
New Hampshire
New Jersey
New Mexico
New York
North Carolina
North Dakota
Ohio
Oklahoma
Estimate
-0.31
0.16
0.64
1.11
1.59
2.06
2.54
3.01
mean
sampling
0%
< 1%
1% - 3%
3% or more

(D)

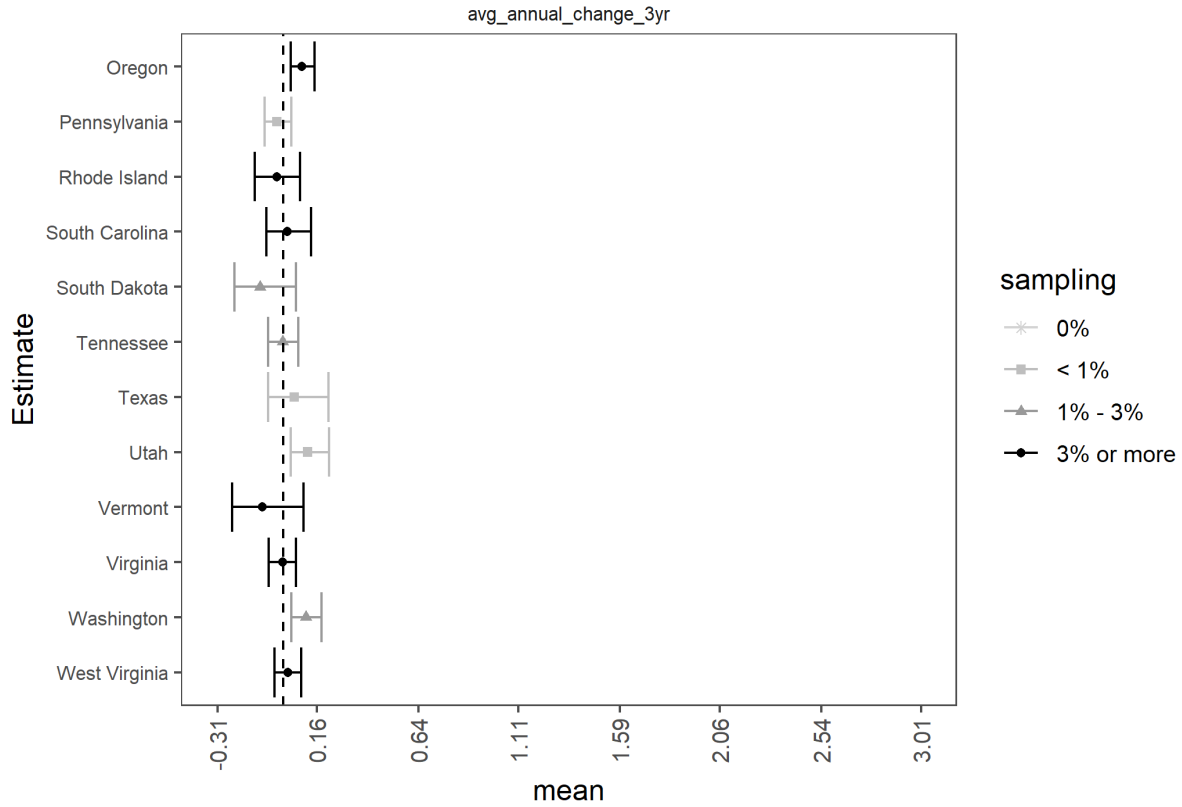
avg_annual_change_3yr
Oregon
Pennsylvania
Rhode Island
South Carolina
South Dakota
Tennessee
Texas
Utah
Vermont
Virginia
Washington
West Virginia
Estimate
-0.31
0.16
0.64
1.11
1.59
2.06
2.54
3.01
mean
sampling
0%
< 1%
1% - 3%
3% or more

Figure B.29. Average annual rates of change in mean occupancy probabilities (avg_annual_change = lambda_avg - 1) for *Eptesicus fuscus* (EPFU) between years over the three-year (2016-2019) time period aggregated across a state, province, or territory within the modeled species range. For example, if avg_change_3yr = -0.05, the mean occupancy rate has declined on average by 5% each year over the three years since 2016. Means (points) and 95% credible intervals (bars) are depicted based on the average percent of grid cells sampled (legend) across all years in the timeframe of interest for each state (A-D). Note that when credible intervals do not overlap zero, we have at least 95% certainty that these trends in species occupancy are either negative or positive. When credible intervals overlap zero, we have less than 95% certainty that these trends are different than zero. U.S. states appear in alphabetic order (A-D). Note the results for EPFU were inconclusive due issues reported in section 3.12.

(A)

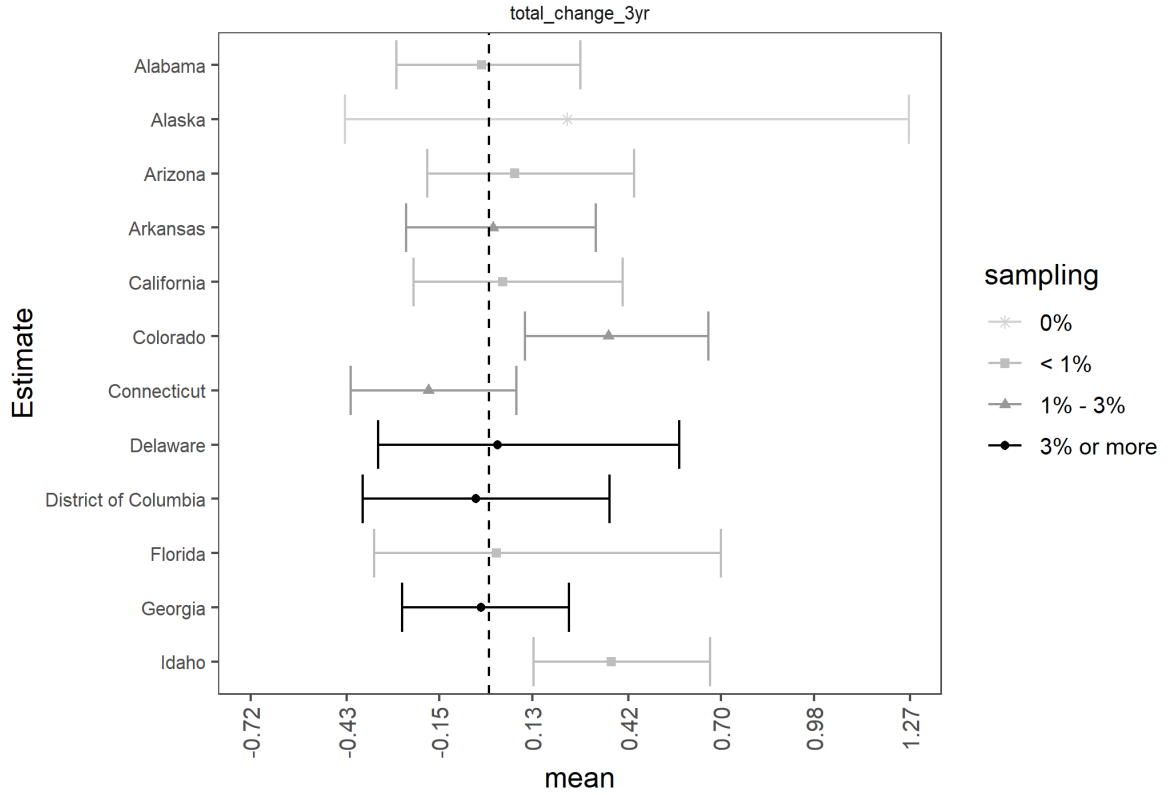
total_change_3yr
Alabama
Alaska
Arizona
Arkansas
California
Colorado
Connecticut
Delaware
District of Columbia
Florida
Georgia
Idaho
Estimate
-0.72
-0.43
-0.15
0.13
0.42
0.70
0.98
1.27
mean
sampling
0%
< 1%
1% - 3%
3% or more

(B)

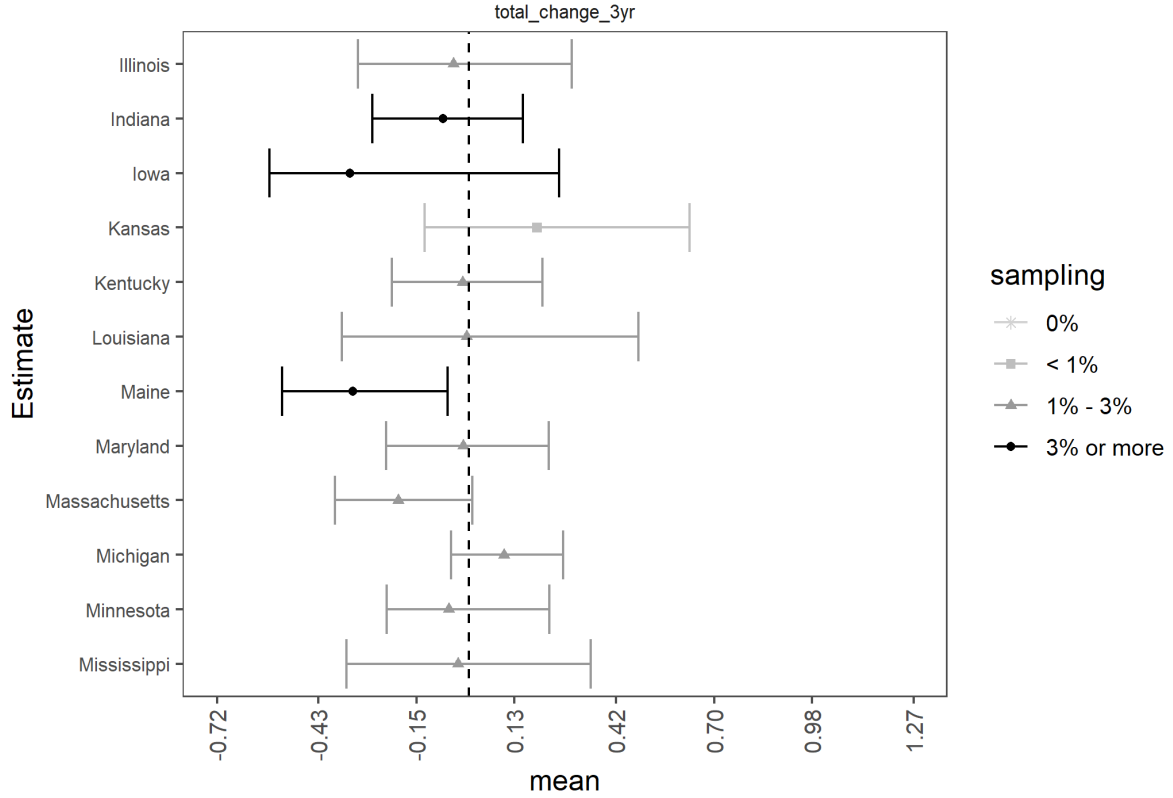
total_change_3yr
Illinois
Indiana
Iowa
Kansas
Kentucky
Louisiana
Maine
Maryland
Massachusetts
Michigan
Minnesota
Mississippi
Estimate
-0.72
-0.43
-0.15
0.13
0.42
0.70
0.98
1.27
mean
sampling
0%
< 1%
1% - 3%
3% or more

(C)

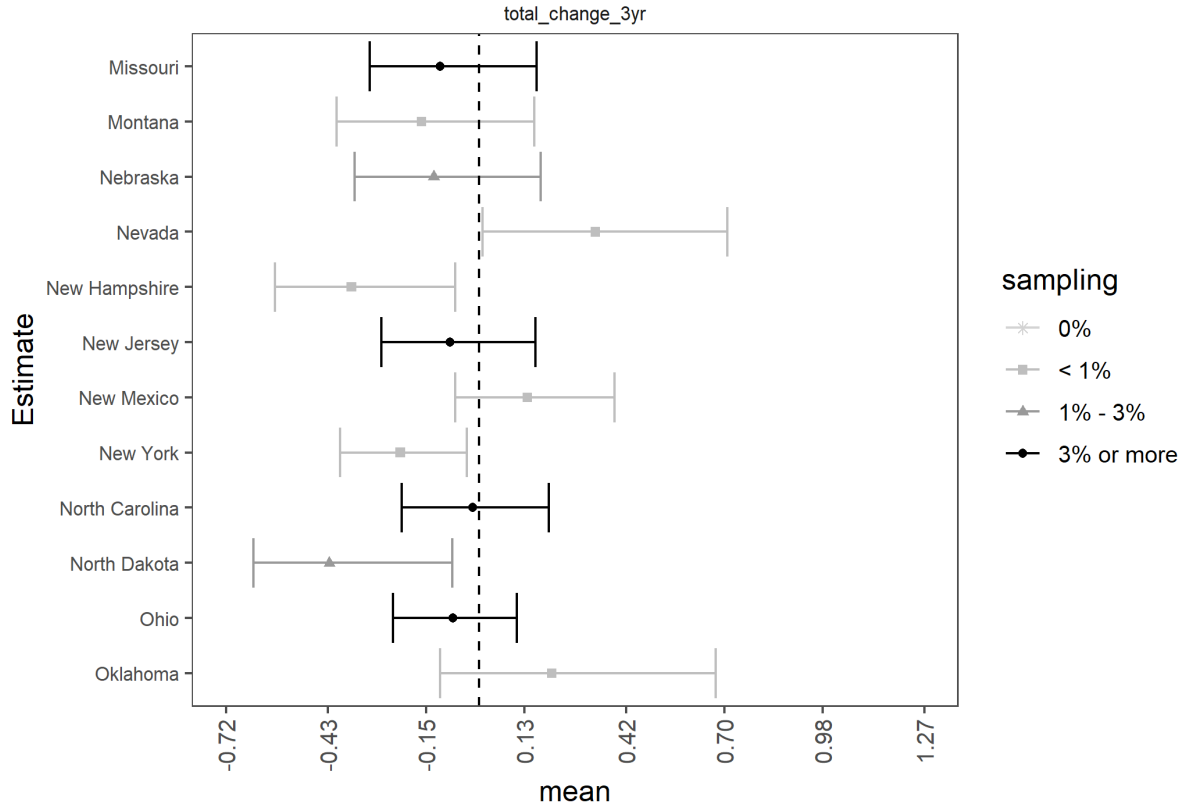
total_change_3yr
Missouri
Montana
Nebraska
Nevada
New Hampshire
New Jersey
New Mexico
New York
North Carolina
North Dakota
Ohio
Oklahoma
Estimate
-0.72
-0.43
-0.15
0.13
0.42
0.70
0.98
1.27
mean
sampling
0%
< 1%
1% - 3%
3% or more

(D)

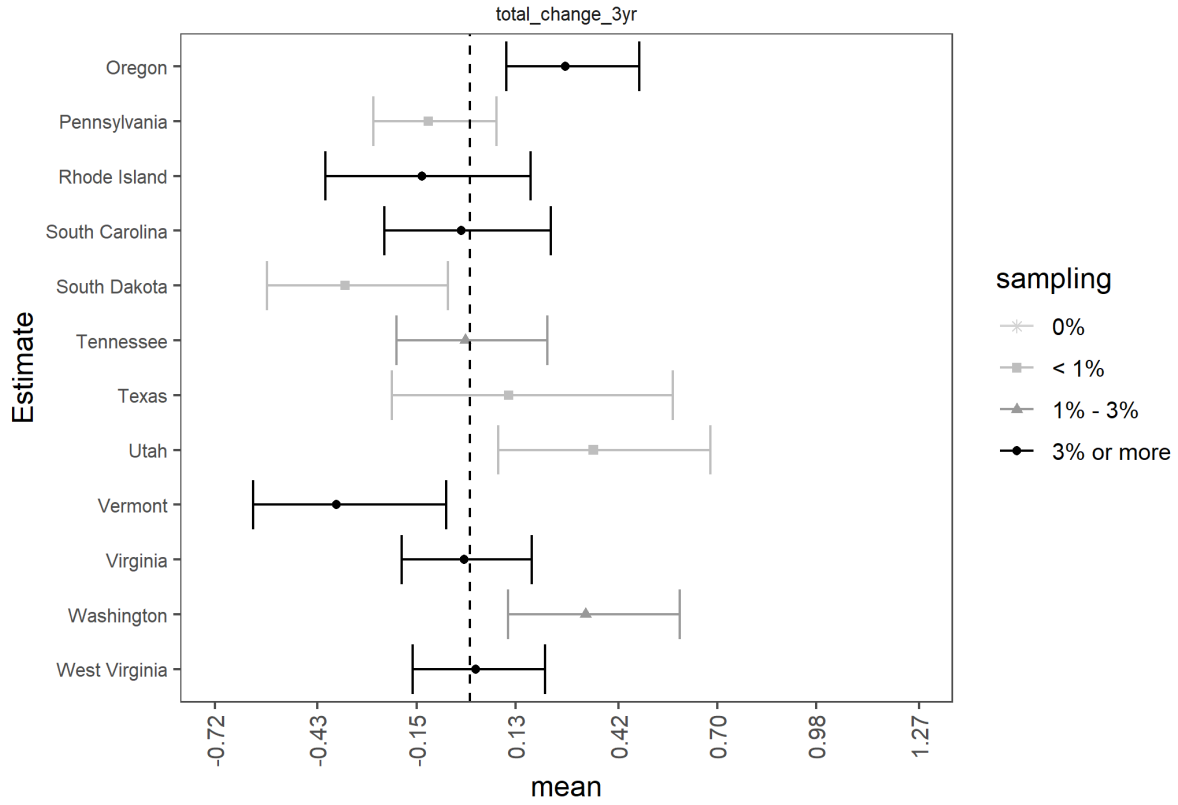
total_change_3yr
Oregon
Pennsylvania
Rhode Island
South Carolina
South Dakota
Tennessee
Texas
Utah
Vermont
Virginia
Washington
West Virginia
Estimate
-0.72
-0.43
-0.15
0.13
0.42
0.70
0.98
1.27
mean
sampling
0%
< 1%
1% - 3%
3% or more

Figure B.30. The total change rate in mean occupancy (total_change = lambda_tot - 1) for *Eptesicus fuscus* (EPFU) given the mean occupancy estimate in last year of sampling (2019) and the mean occupancy estimates three years (2016) prior aggregated across each state within the modeled species range. For example, if total_change_3yr = -0.25, the mean occupancy rate has declined by 25% over the nine years since 2016, while a value of 0.25 would indicate an increase of 25%. Means (points) and 95% credible intervals (bars) are depicted based on the average percent of grid cells sampled (legend) in the first and last years of the timeframe of interest for each state, province or territory (A-D). Note that when credible intervals do not overlap zero, we have at least 95% certainty that these trends in species occupancy are either negative or positive. When credible intervals overlap zero, we have less than 95% certainty that these trends are different than zero. U.S. states appear in alphabetic order (A-D). Note the results for EPFU were inconclusive due issues reported in section 3.12.

B.11 *Lasionycteris noctivagans*

(A)

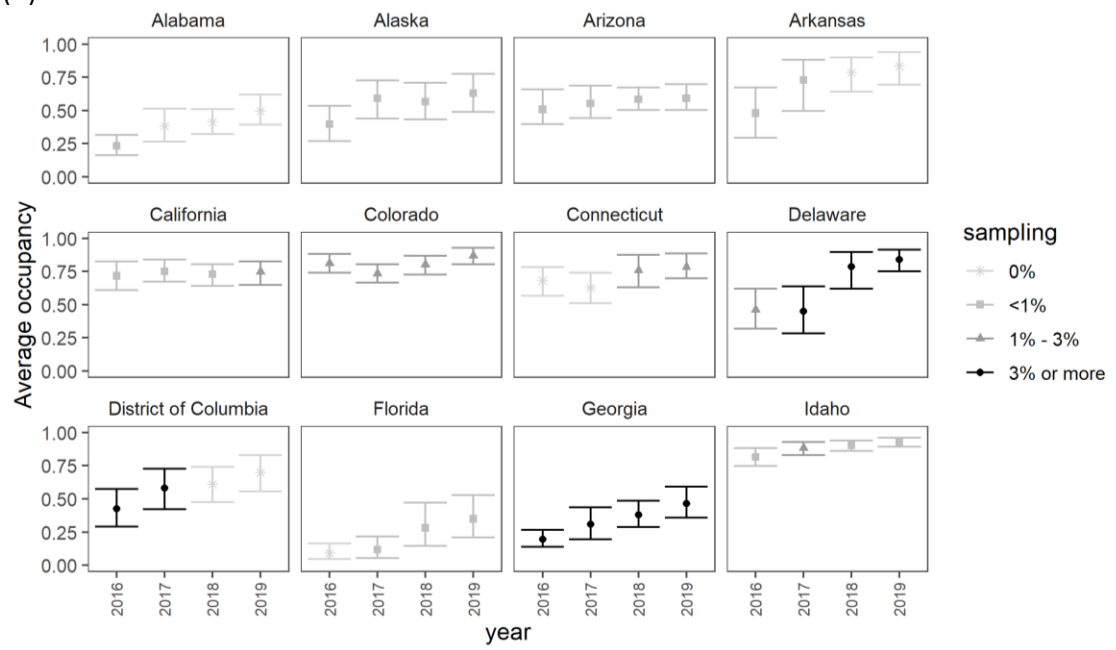

(B)

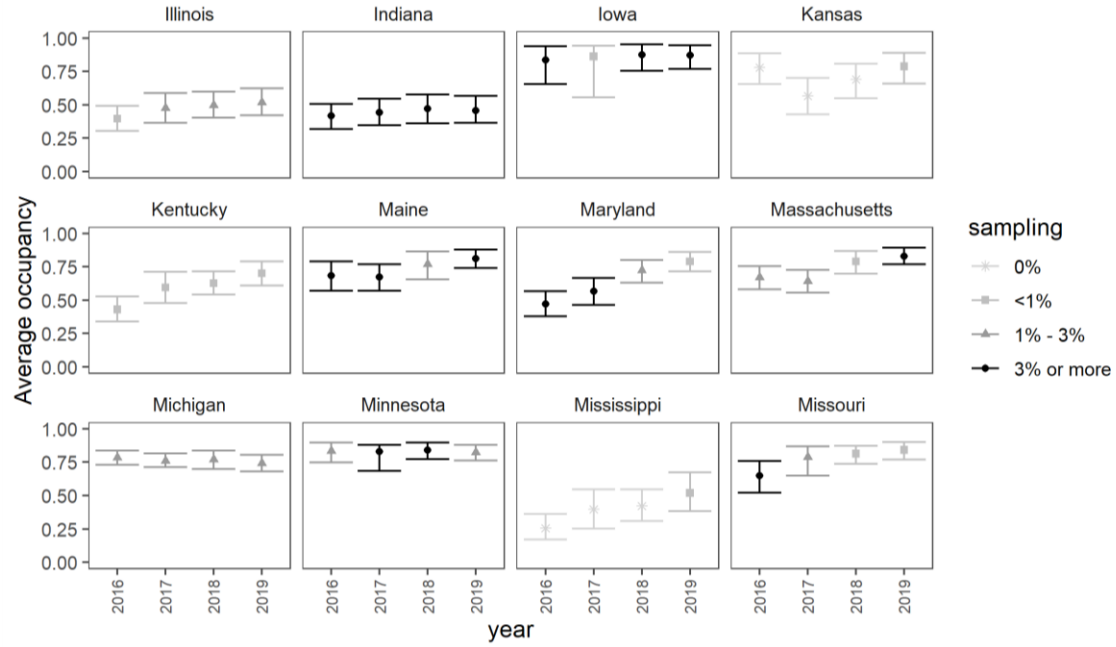

(C)

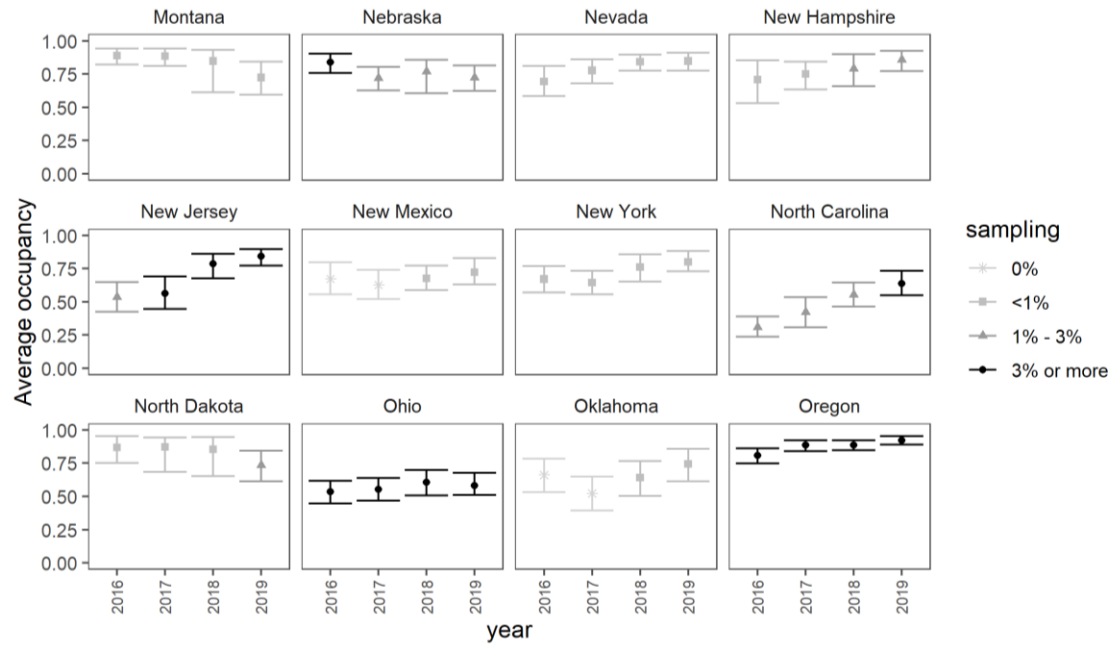

(D)

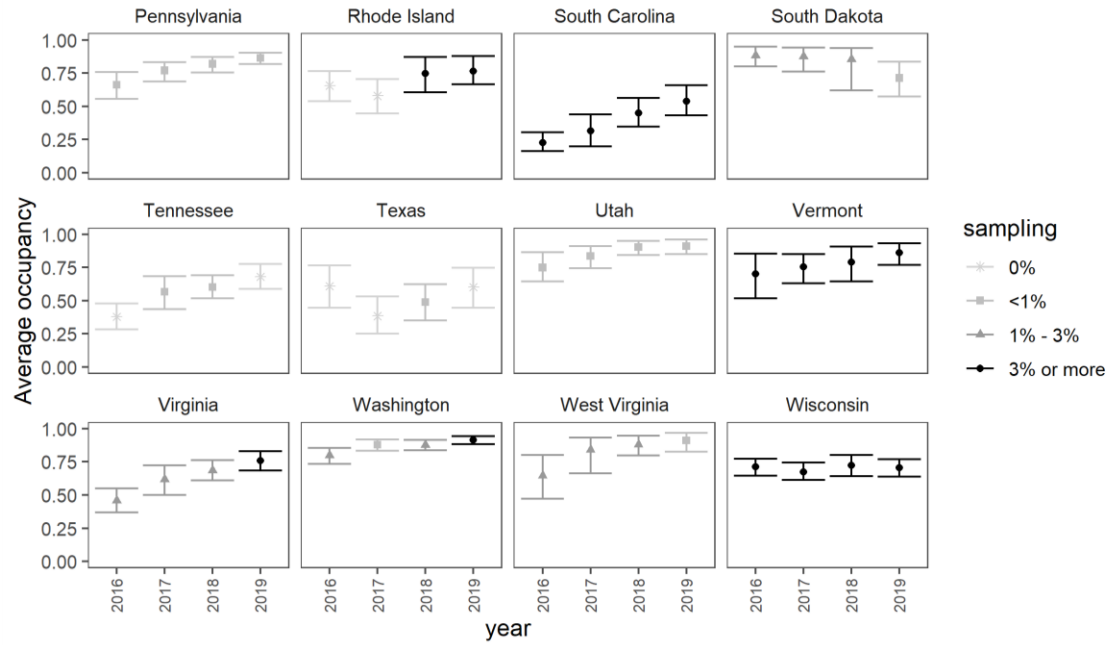

Figure B.31. Estimates of the average occupancy probability ($\widehat{\psi}_t$) for *Lasionycteris noctivagans* (LANO) aggregated over all grid cells for each state in the modeled species range each year. Means (points) and 95% credible intervals (bars) are depicted according to the percent of grid cells sampled (legend) in the entire state each year (A-D). U.S. states appear in alphabetic order (A-D). Note the results for LANO were inconclusive due issues reported in section 3.12.

(A)

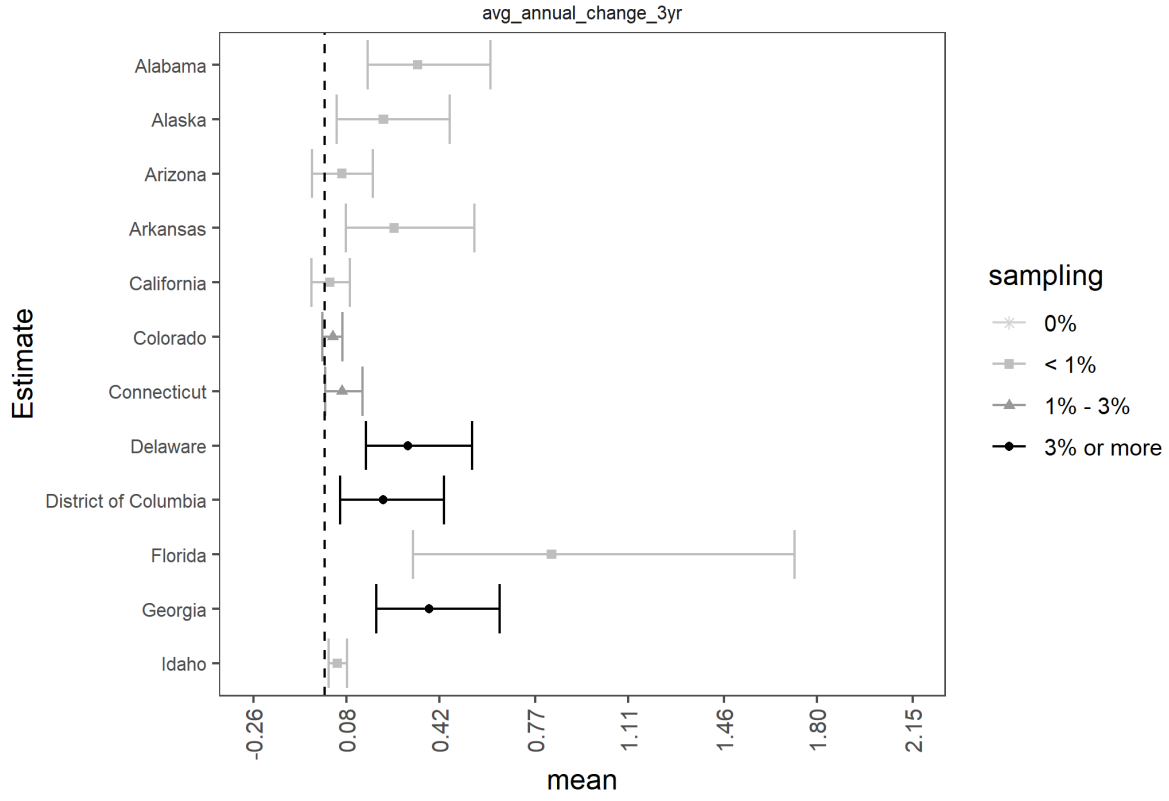
avg_annual_change_3yr
Alabama
Alaska
Arizona
Arkansas
California
Colorado
Connecticut
Delaware
District of Columbia
Florida
Georgia
Idaho
Estimate
-0.26
0.08
0.42
0.77
1.11
1.46
1.80
2.15
mean
sampling
0%
< 1%
1% - 3%
3% or more

(B)

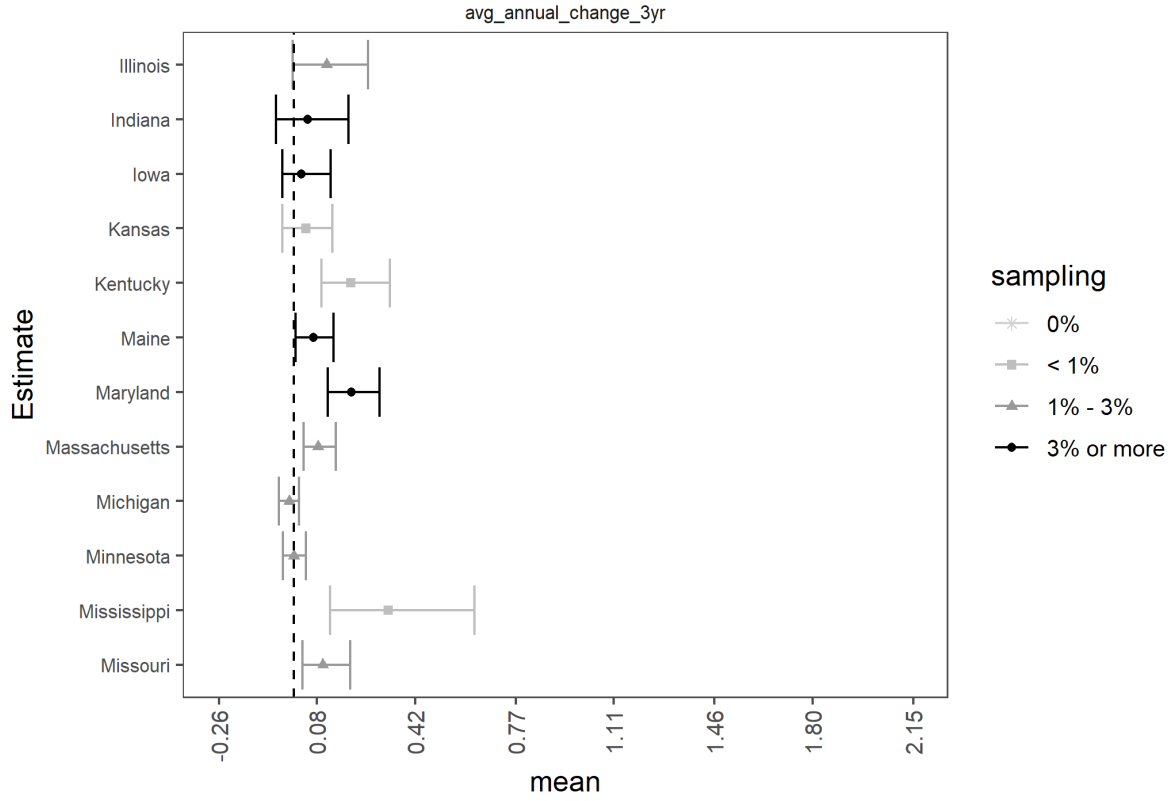
avg_annual_change_3yr
Illinois
Indiana
Iowa
Kansas
Kentucky
Maine
Maryland
Massachusetts
Michigan
Minnesota
Mississippi
Missouri
Estimate
-0.26
0.08
0.42
0.77
1.11
1.46
1.80
2.15
mean
sampling
0%
< 1%
1% - 3%
3% or more

(C)

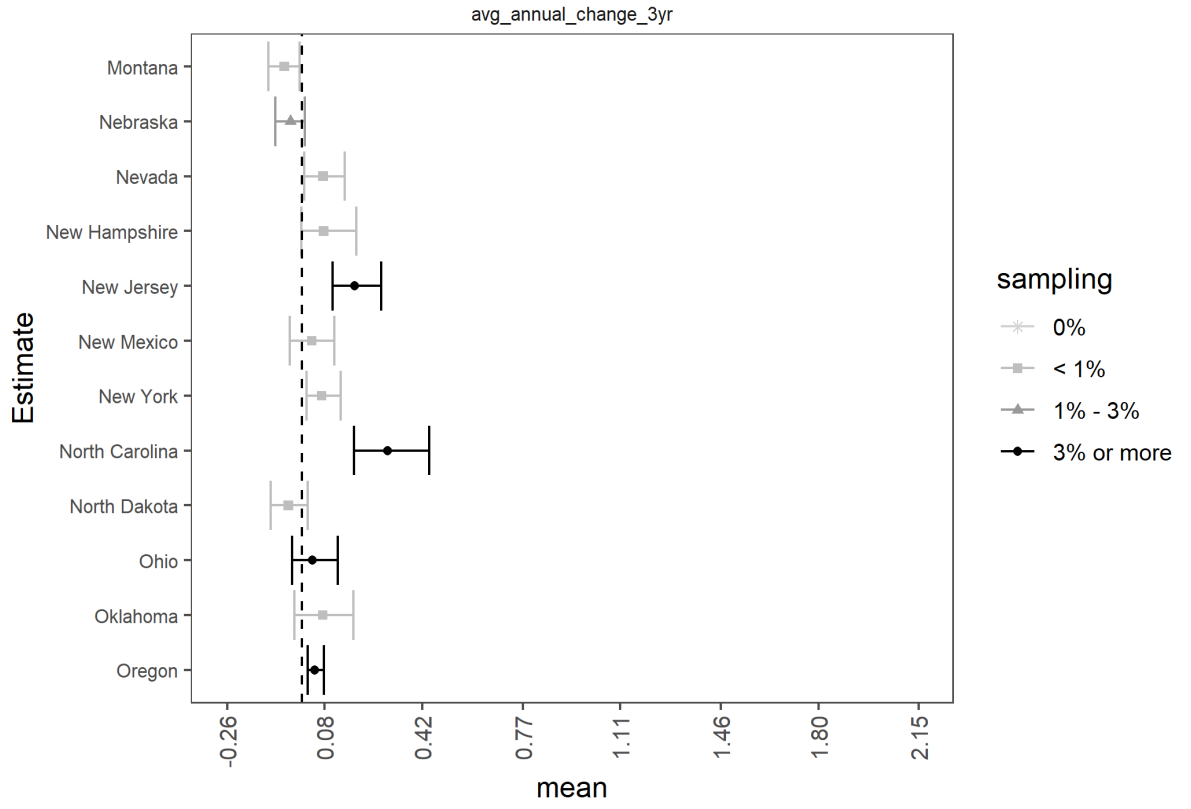
avg_annual_change_3yr
Montana
Nebraska
Nevada
New Hampshire
New Jersey
New Mexico
New York
North Carolina
North Dakota
Ohio
Oklahoma
Oregon
Estimate
-0.26
0.08
0.42
0.77
1.11
1.46
1.80
2.15
mean
sampling
0%
< 1%
1% - 3%
3% or more

(D)

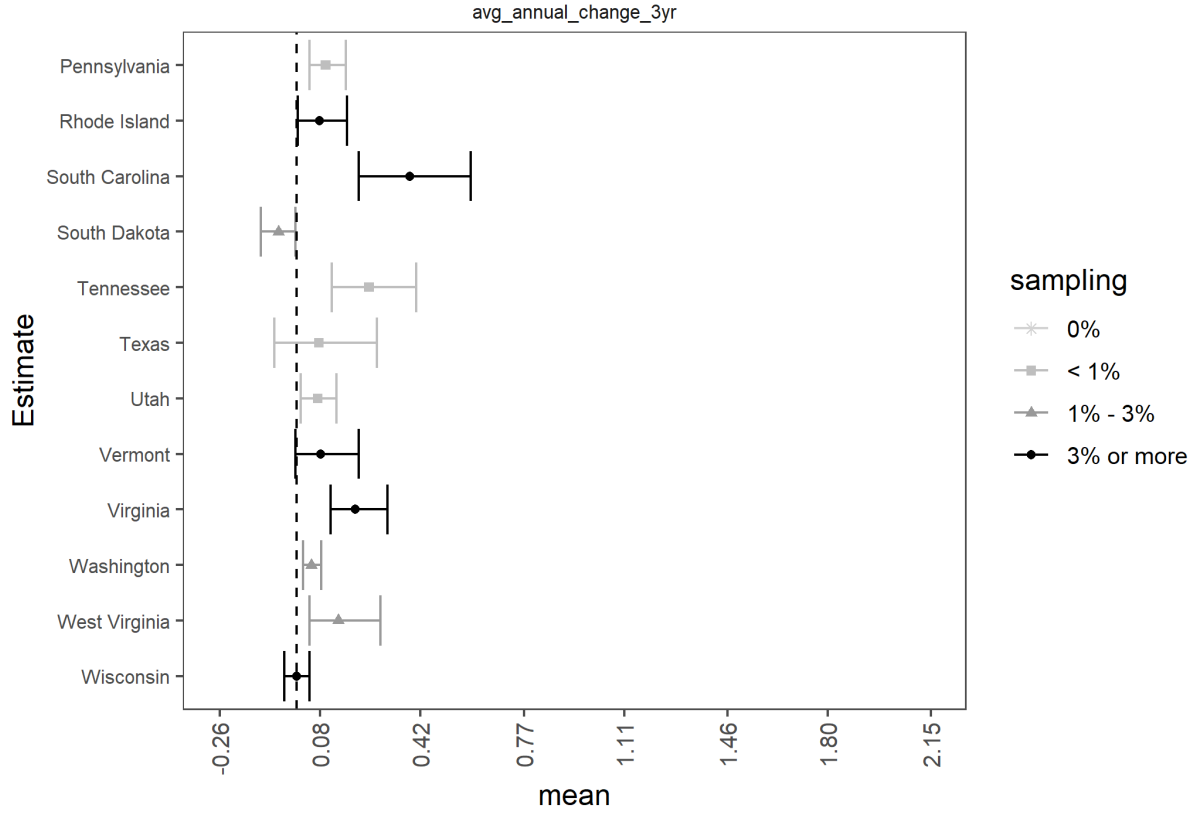
avg_annual_change_3yr
Pennsylvania
Rhode Island
South Carolina
South Dakota
Tennessee
Texas
Utah
Vermont
Virginia
Washington
West Virginia
Wisconsin
Estimate
-0.26
0.08
0.42
0.77
1.11
1.46
1.80
2.15
mean
sampling
0%
< 1%
1% - 3%
3% or more

Figure B.32. Average annual rates of change in mean occupancy probabilities (avg_annual_change = lambda_avg - 1) for *Lasionycteris noctivagans* (LANO) between years over the three-year (2016-2019) time period aggregated across a state within the modeled species range. For example, if avg_change_3yr = -0.05, the mean occupancy rate has declined on average by 5% each year over the three years since 2016. Means (points) and 95% credible intervals (bars) are depicted based on the average percent of grid cells sampled (legend) across all years in the timeframe of interest for each state (A-D). Note that when credible intervals do not overlap zero, we have at least 95% certainty that these trends in species occupancy are either negative or positive. When credible intervals overlap zero, we have less than 95% certainty that these trends are different than zero. U.S. states appear in alphabetic order (A-D). Note the results for LANO were inconclusive due issues reported in section 3.12.

(A)

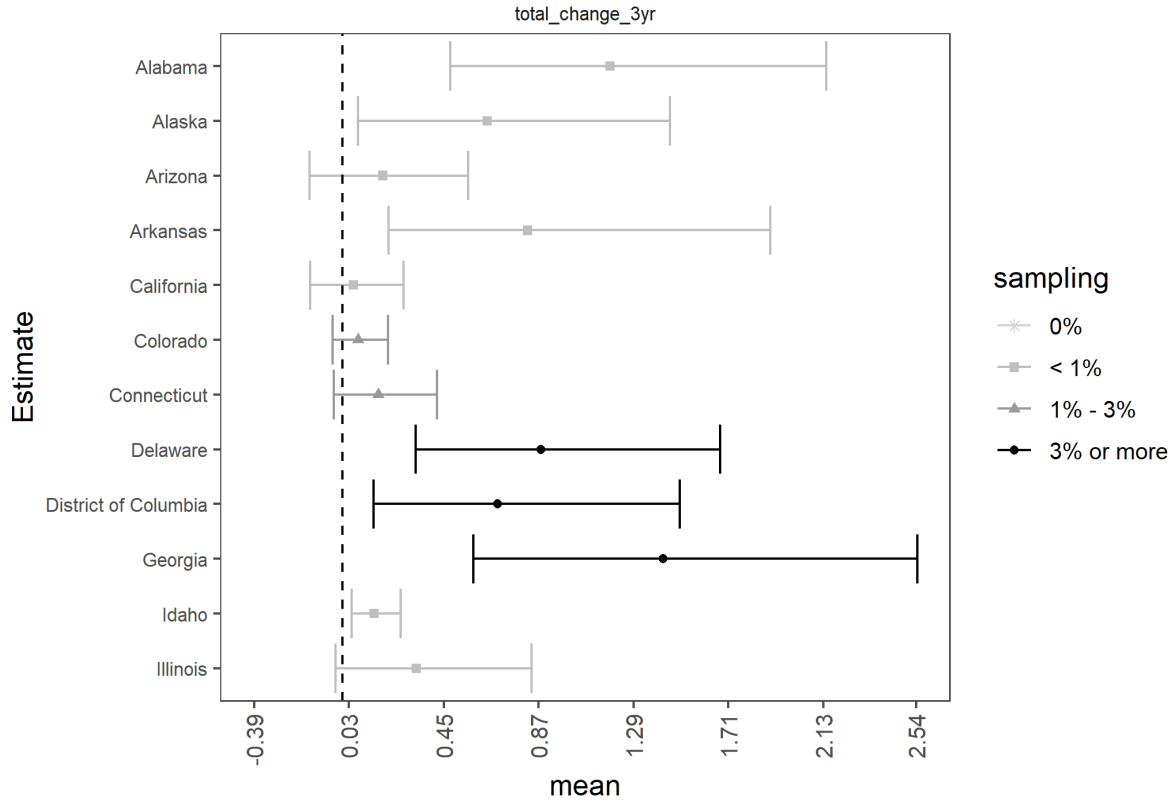
total_change_3yr
Alabama
Alaska
Arizona
Arkansas
California
Colorado
Connecticut
Delaware
District of Columbia
Georgia
Idaho
Illinois
Estimate
-0.39
0.03
0.45
0.87
1.29
1.71
2.13
2.54
mean
sampling
0%
< 1%
1% - 3%
3% or more

(B)

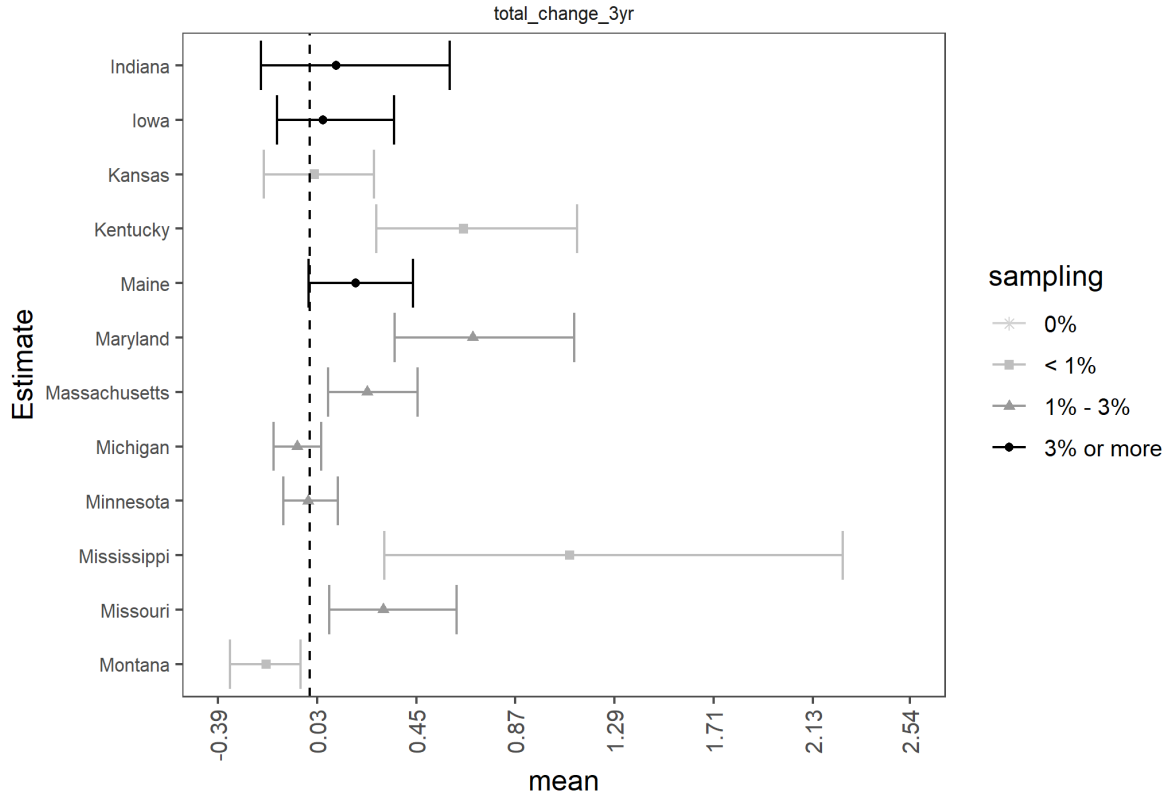
total_change_3yr
Indiana
Iowa
Kansas
Kentucky
Maine
Maryland
Massachusetts
Michigan
Minnesota
Mississippi
Missouri
Montana
Estimate
-0.39
0.03
0.45
0.87
1.29
1.71
2.13
2.54
mean
sampling
0%
< 1%
1% - 3%
3% or more

(C)

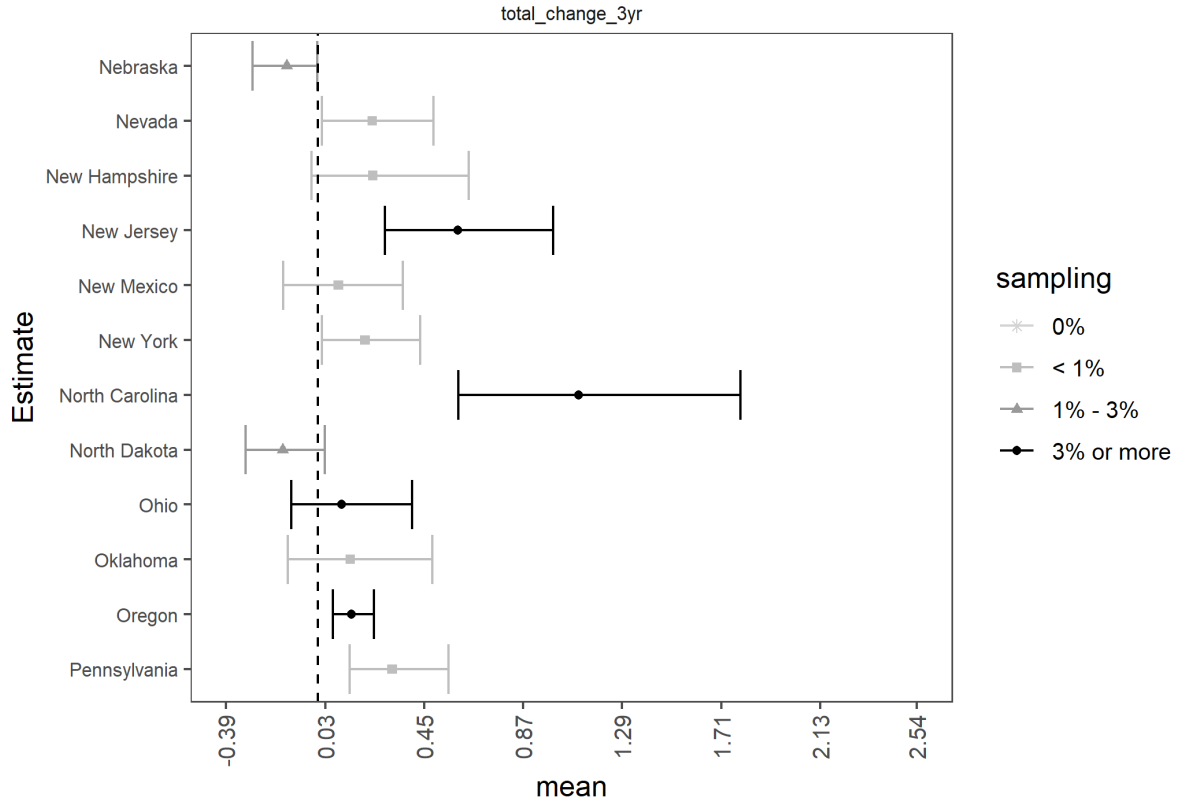
total_change_3yr
Nebraska
Nevada
New Hampshire
New Jersey
New Mexico
New York
North Carolina
North Dakota
Ohio
Oklahoma
Oregon
Pennsylvania
Estimate
-0.39
0.03
0.45
0.87
1.29
1.71
2.13
2.54
mean
sampling
0%
< 1%
1% - 3%
3% or more

(D)

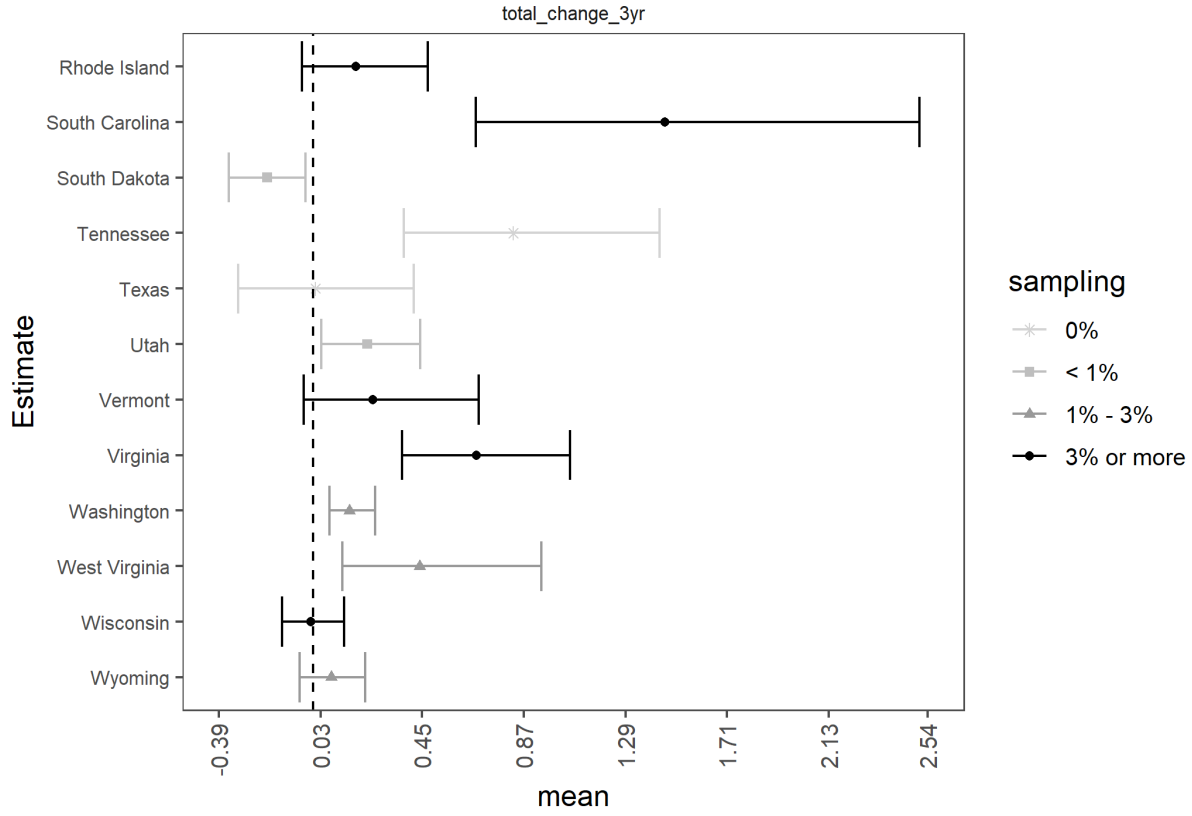
total_change_3yr
Rhode Island
South Carolina
South Dakota
Tennessee
Texas
Utah
Vermont
Virginia
Washington
West Virginia
Wisconsin
Wyoming
Estimate
-0.39
0.03
0.45
0.87
1.29
1.71
2.13
2.54
mean
sampling
0%
< 1%
1% - 3%
3% or more

Figure B.33. The total change rate in mean occupancy (total_change = lambda_tot - 1) for *Lasionycteris noctivagans* (LANO) given the mean occupancy estimate in last year of sampling (2019) and the mean occupancy estimates three years (2016) prior aggregated across a state within the modeled species range. For example, if total_change_3yr = -0.25, the mean occupancy rate has declined by 25% over the nine years since 2016, while a value of 0.25 would indicate an increase of 25%. Means (points) and 95% credible intervals (bars) are depicted based on the average percent of grid cells sampled (legend) in the first and last years of the timeframe of interest for each state (A-D). Note that when credible intervals do not overlap zero, we have at least 95% certainty that these trends in species occupancy are either negative or positive. When credible intervals overlap zero, we have less than 95% certainty that these trends are different than zero. U.S. states appear in alphabetic order (A-D). Note the results for LANO were inconclusive due issues reported in section 3.12.

B.12 *Lasiurus cinereus*

(A)

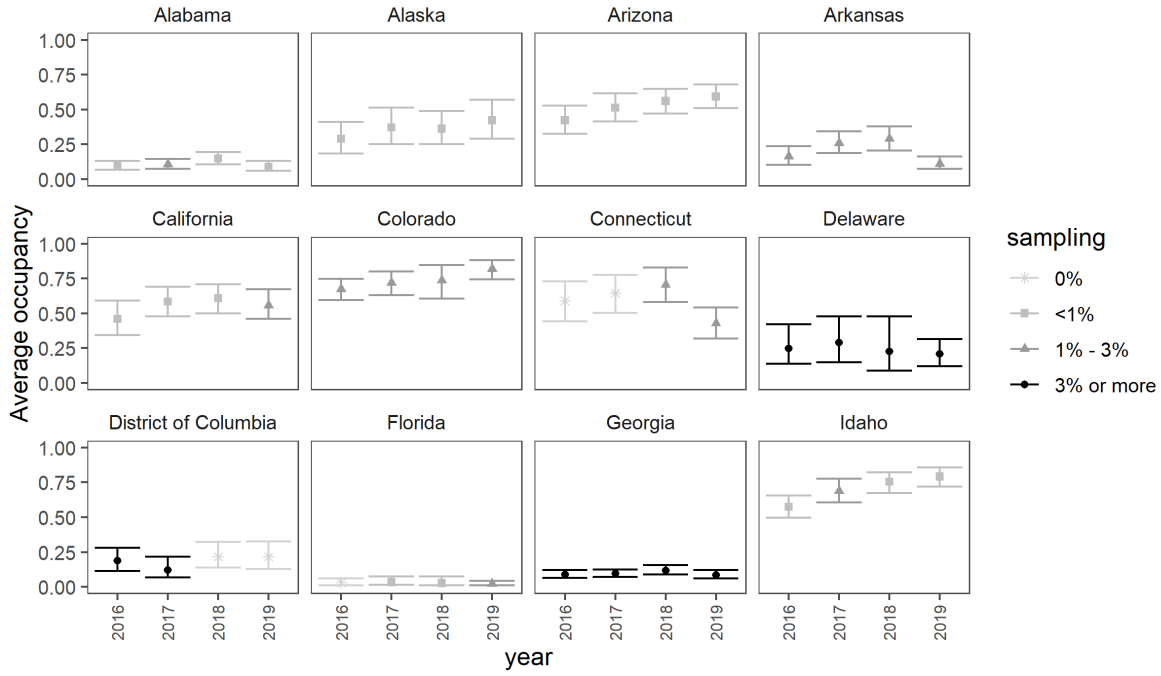

(B)

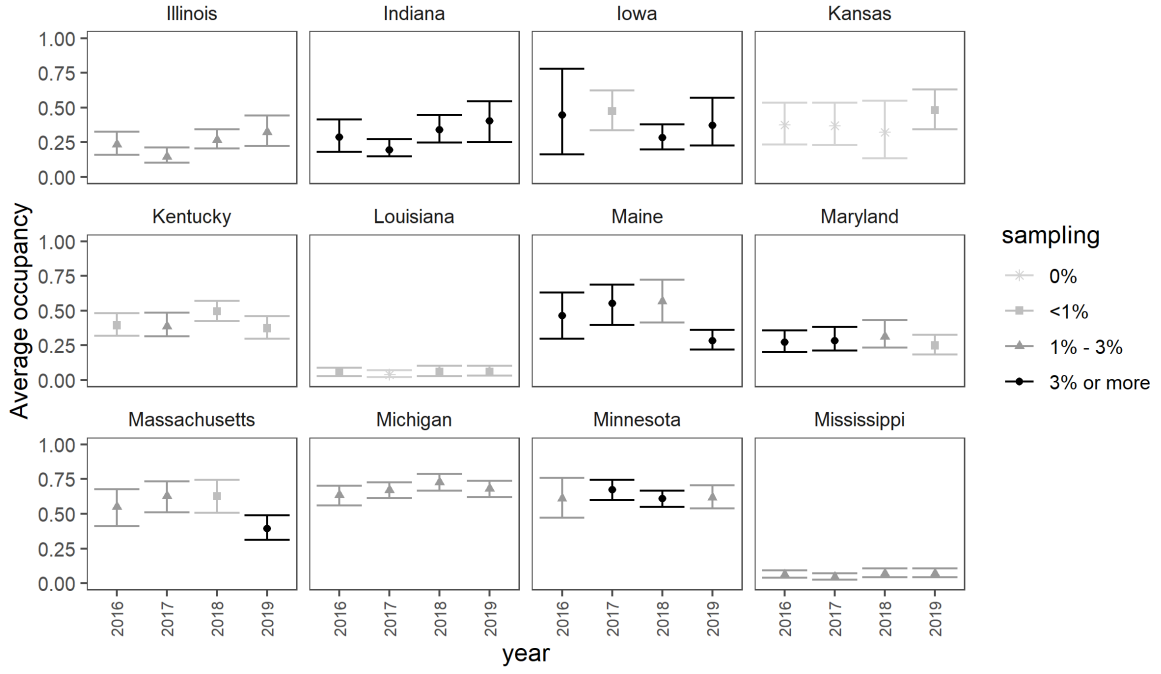

(C)

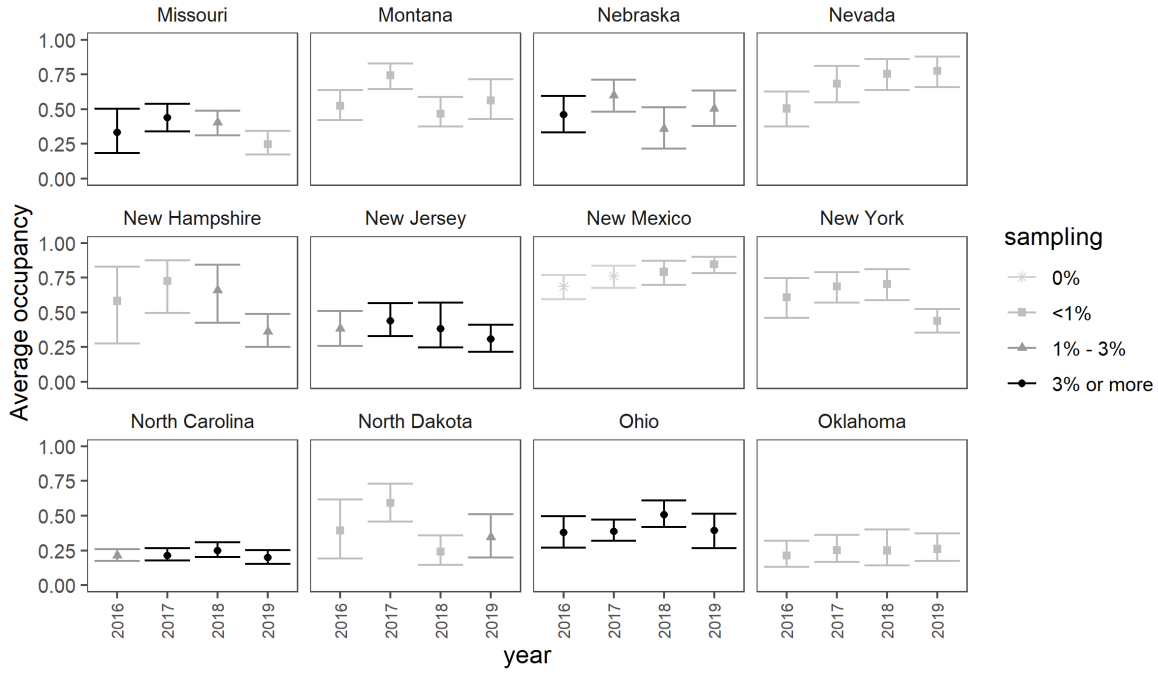

(D)

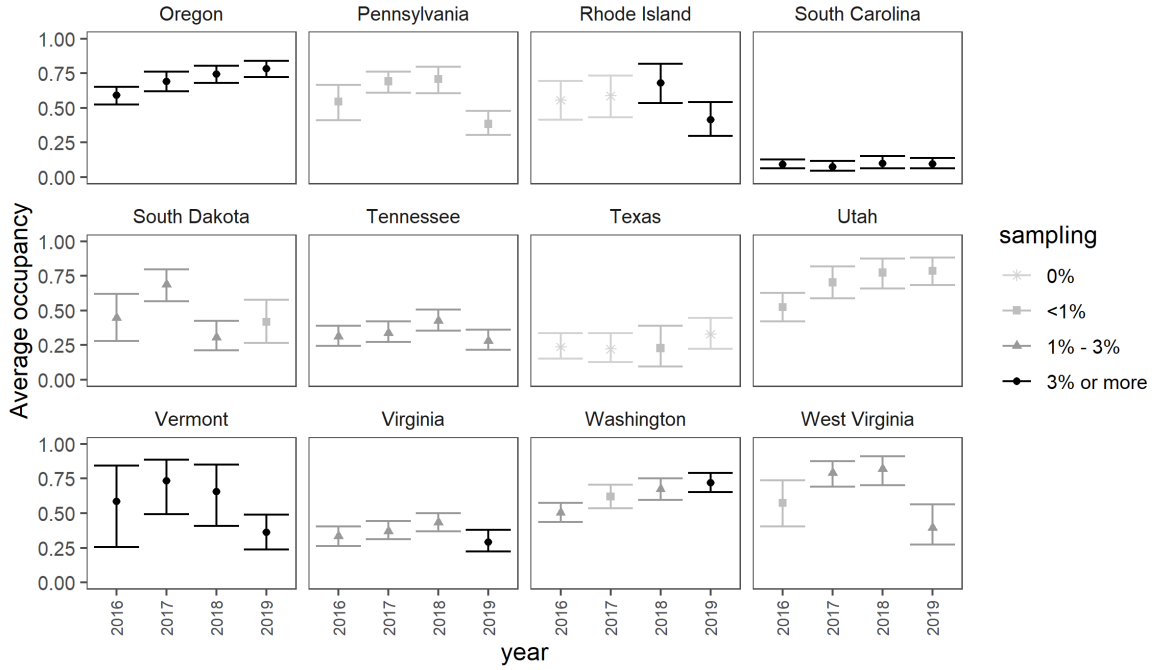

Figure B.34. Estimates of the average occupancy probability ($\widehat{\psi}_t$) for *Lasiurus cinereus* (LACI) aggregated over all grid cells for each state in the modeled species range each year. Means (points) and 95% credible intervals (bars) are depicted according to the percent of grid cells sampled (legend) in the entire state, province or territory each year (A-D). U.S. states appear in alphabetic order (A-D). Note the results for LACI were inconclusive due issues reported in section 3.12.

(A)

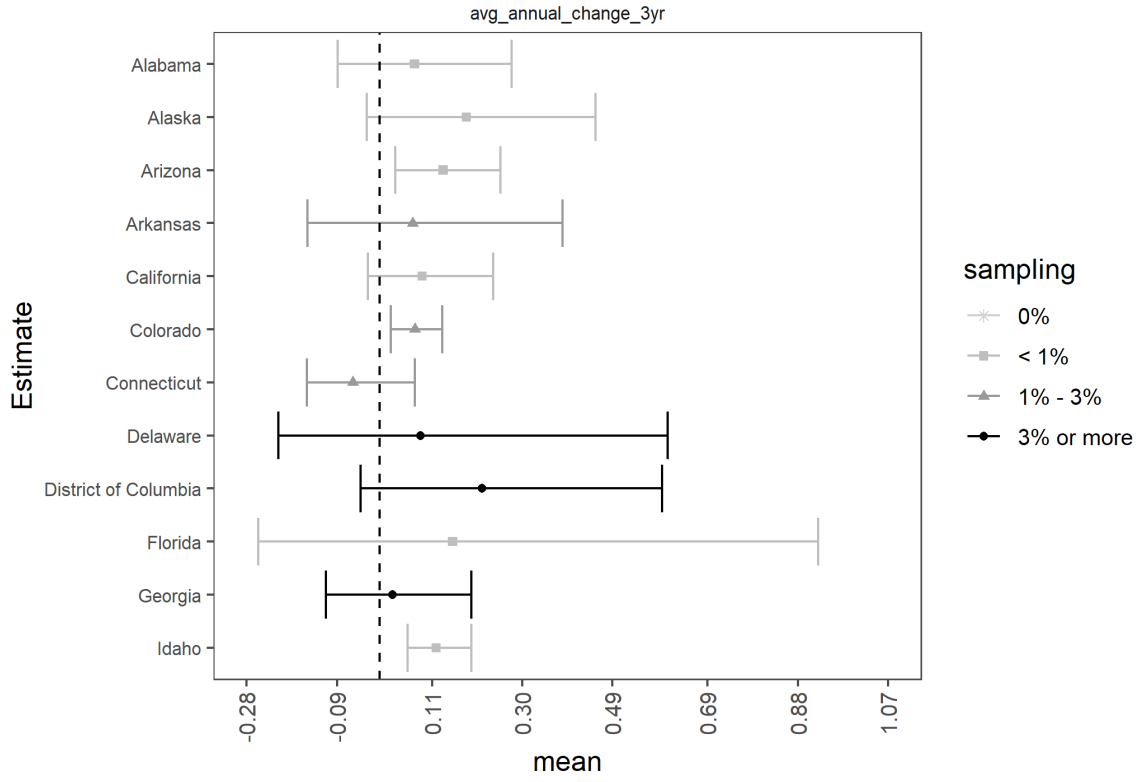
avg_annual_change_3yr
Alabama
Alaska
Arizona
Arkansas
California
Colorado
Connecticut
Delaware
District of Columbia
Florida
Georgia
Idaho
Estimate
-0.28
-0.09
0.11
0.30
0.49
0.69
0.88
1.07
mean
sampling
0%
< 1%
1% - 3%
3% or more

(B)

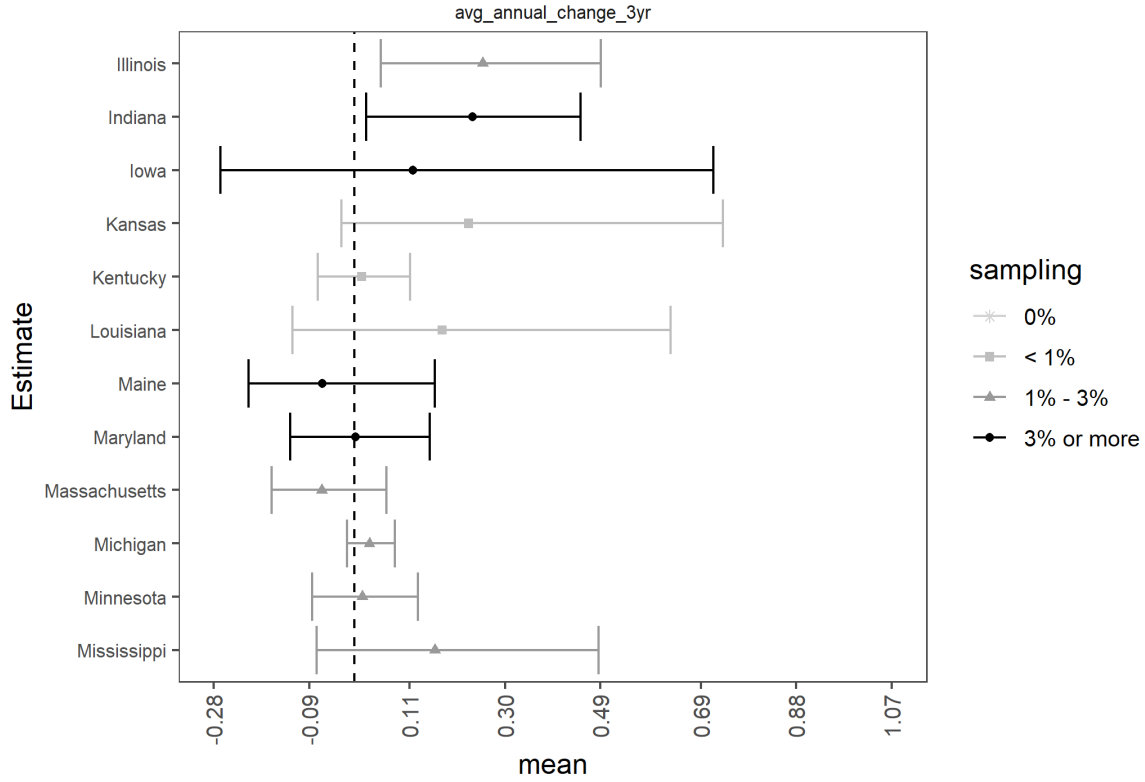
avg_annual_change_3yr
Illinois
Indiana
Iowa
Kansas
Kentucky
Louisiana
Maine
Maryland
Massachusetts
Michigan
Minnesota
Mississippi
Estimate
-0.28
-0.09
0.11
0.30
0.49
0.69
0.88
1.07
mean
sampling
0%
< 1%
1% - 3%
3% or more

(C)

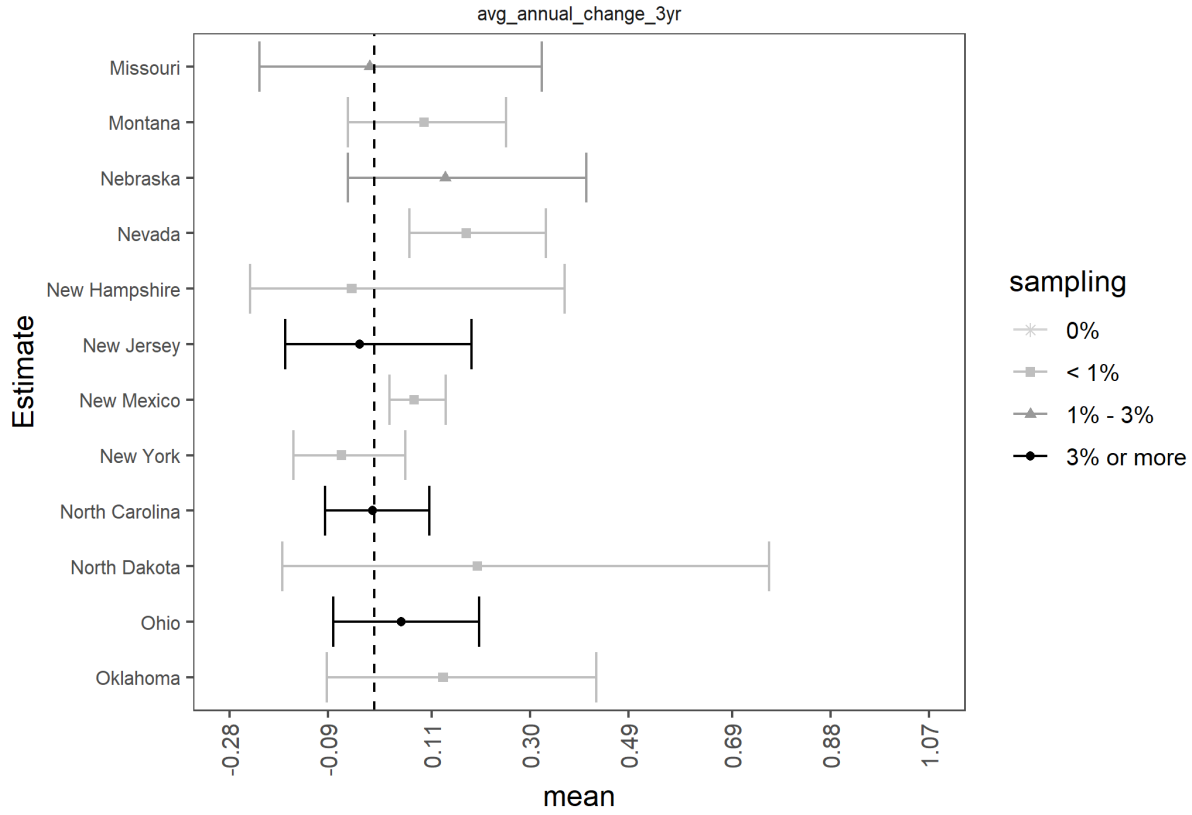
avg_annual_change_3yr
Missouri
Montana
Nebraska
Nevada
New Hampshire
New Jersey
New Mexico
New York
North Carolina
North Dakota
Ohio
Oklahoma
Estimate
-0.28
-0.09
0.11
0.30
0.49
0.69
0.88
1.07
mean
sampling
0%
< 1%
1% - 3%
3% or more

(D)

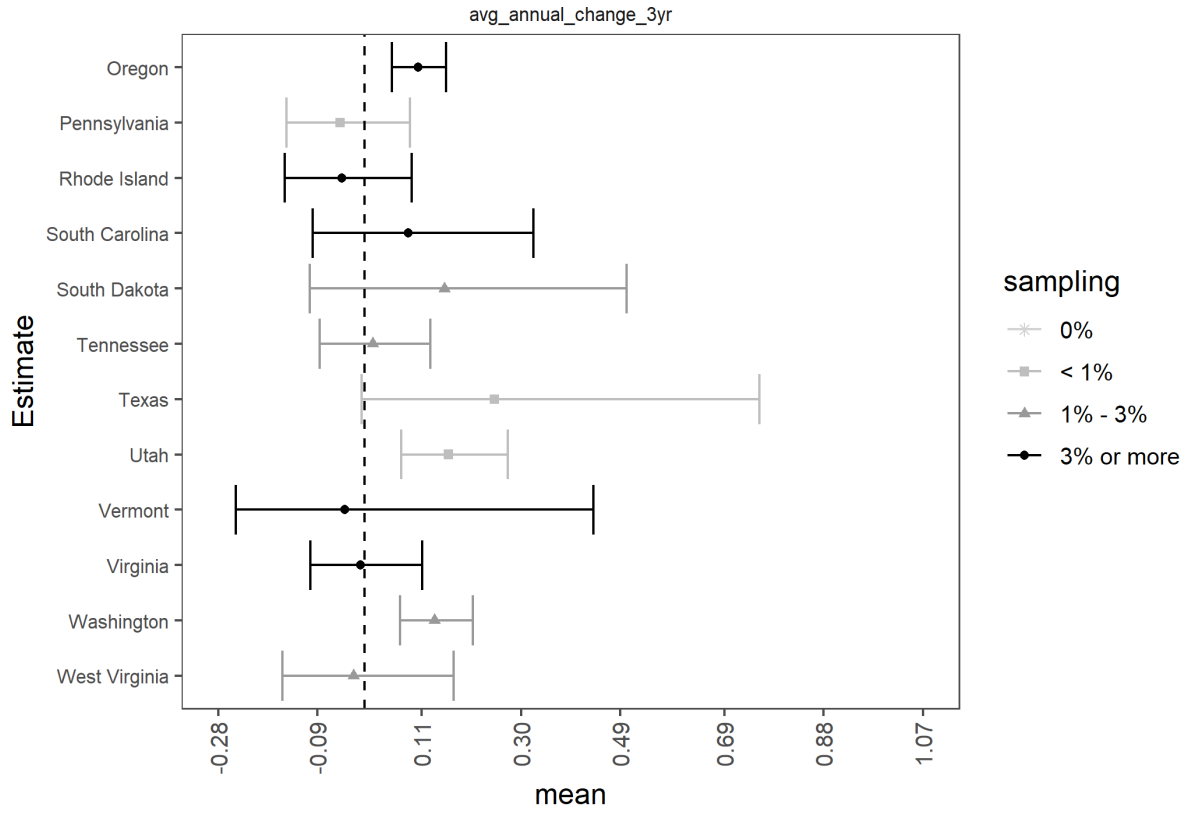
avg_annual_change_3yr
Oregon
Pennsylvania
Rhode Island
South Carolina
South Dakota
Tennessee
Texas
Utah
Vermont
Virginia
Washington
West Virginia
Estimate
-0.28
-0.09
0.11
0.30
0.49
0.69
0.88
1.07
mean
sampling
0%
< 1%
1% - 3%
3% or more

Figure B.35. Average annual rates of change in mean occupancy probabilities (avg_annual_change = lambda_avg - 1) for *Lasiurus cinereus* (LACI) between years over the three-year (2016-2019) time period aggregated across a state within the modeled species range. For example, avg_change_3yr = -0.05, the mean occupancy rate has declined on average by 5% each year over the three years since 2016. Means (points) and 95% credible intervals (bars) are depicted based on the average percent of grid cells sampled (legend) across all years in the timeframe of interest for each state (A-D). Note that when credible intervals do not overlap zero, we have at least 95% certainty that these trends in species occupancy are either negative or positive. When credible intervals overlap zero, we have less than 95% certainty that these trends are different than zero. U.S. states appear in alphabetic order (A-D). Note the results for LACI were inconclusive due issues reported in section 3.12.

(A)

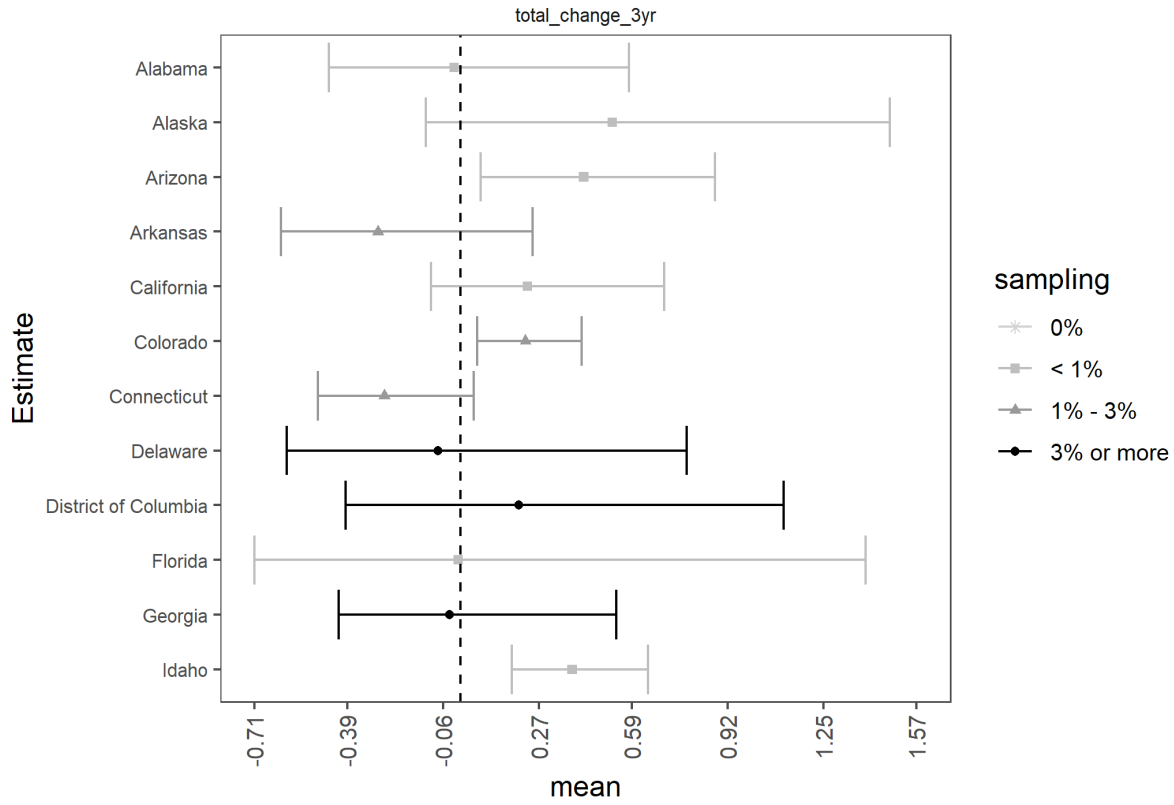
total_change_3yr
Alabama
Alaska
Arizona
Arkansas
California
Colorado
Connecticut
Delaware
District of Columbia
Florida
Georgia
Idaho
Estimate
-0.71
-0.39
-0.06
0.27
0.59
0.92
1.25
1.57
mean
sampling
0%
< 1%
1% - 3%
3% or more

(B)

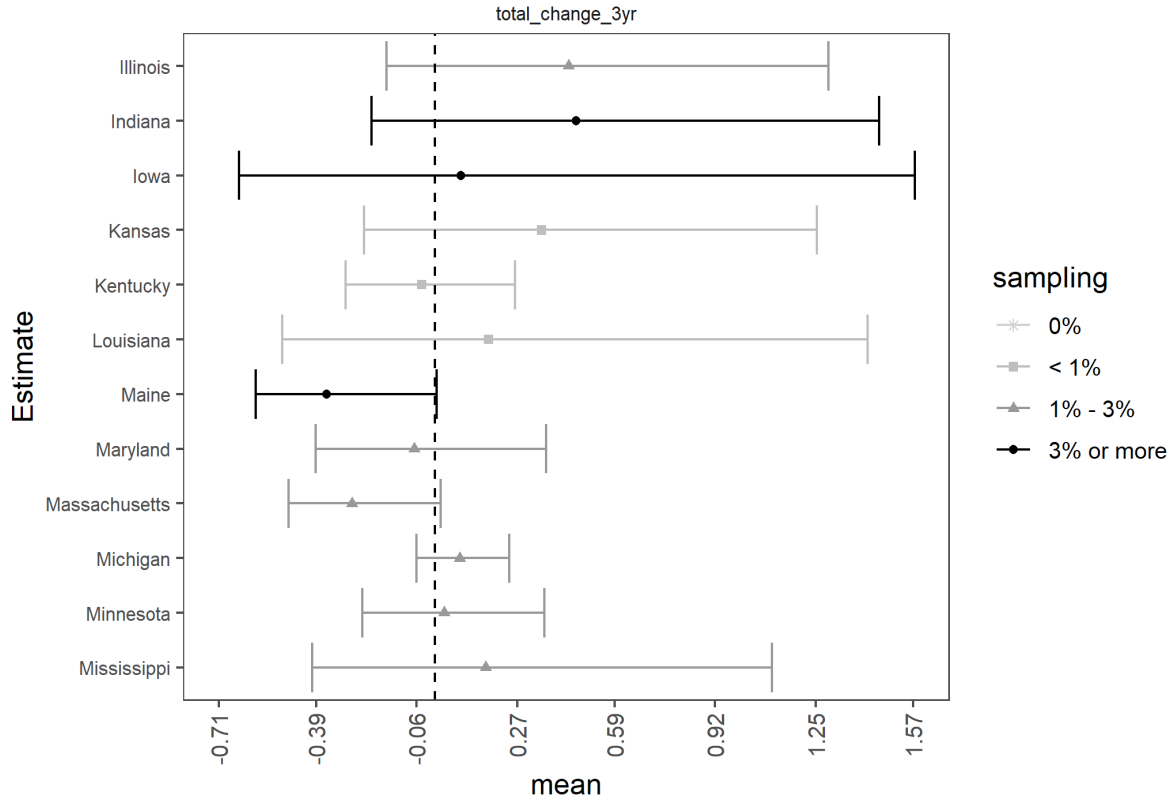
total_change_3yr
Illinois
Indiana
Iowa
Kansas
Kentucky
Louisiana
Maine
Maryland
Massachusetts
Michigan
Minnesota
Mississippi
Estimate
-0.71
-0.39
-0.06
0.27
0.59
0.92
1.25
1.57
mean
sampling
0%
< 1%
1% - 3%
3% or more

(C)

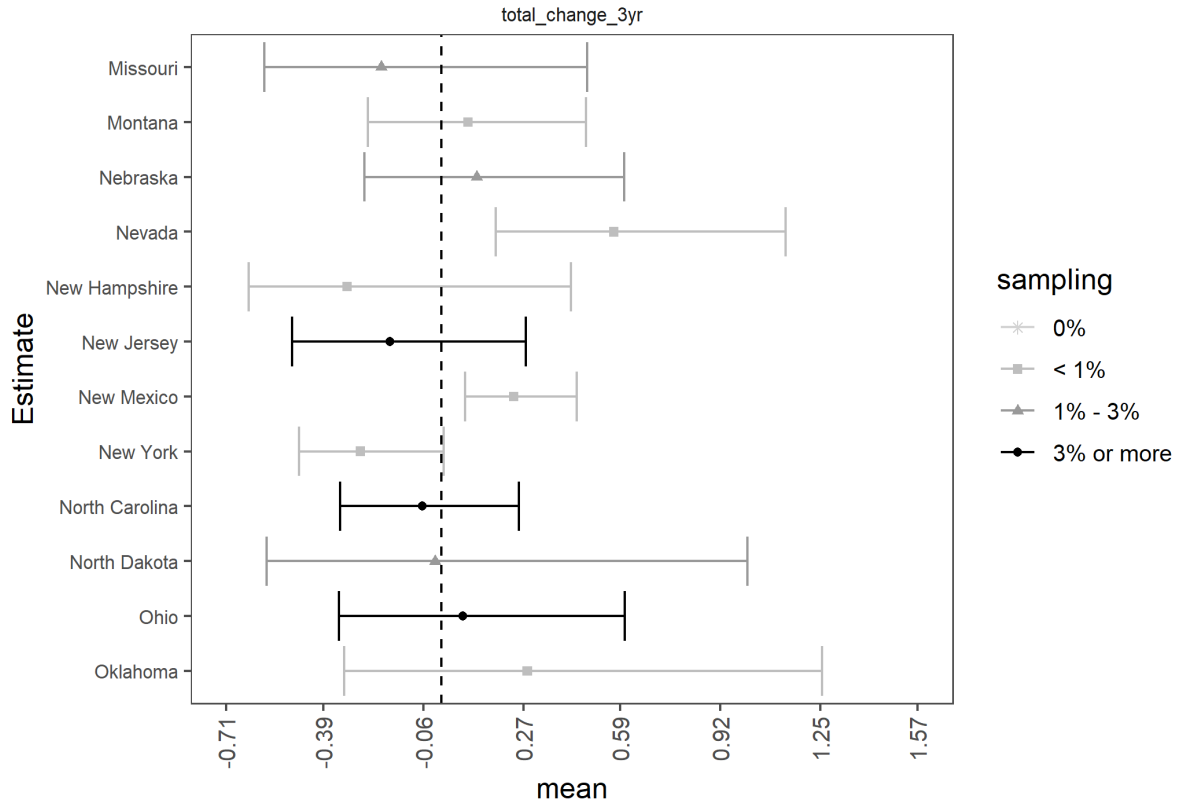
total_change_3yr
Missouri
Montana
Nebraska
Nevada
New Hampshire
New Jersey
New Mexico
New York
North Carolina
North Dakota
Ohio
Oklahoma
Estimate
-0.71
-0.39
-0.06
0.27
0.59
0.92
1.25
1.57
mean
sampling
0%
< 1%
1% - 3%
3% or more

(D)

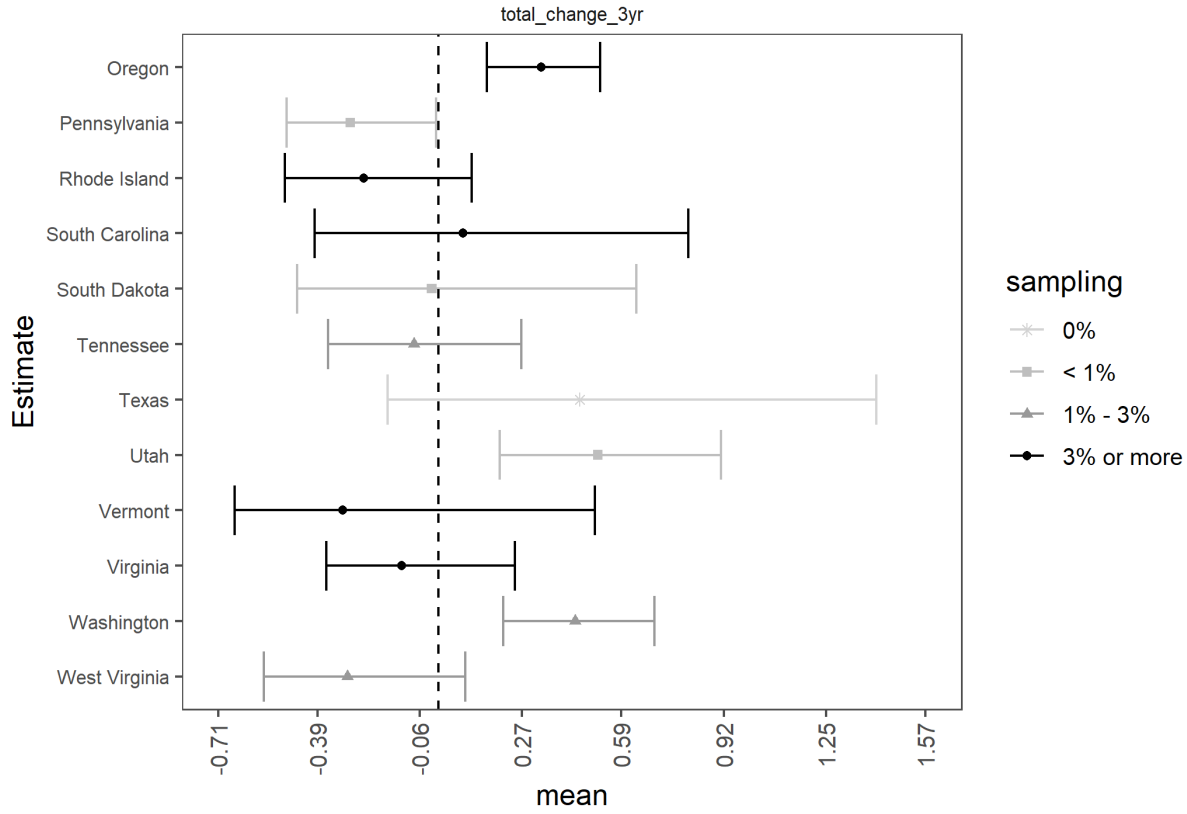
total_change_3yr
Oregon
Pennsylvania
Rhode Island
South Carolina
South Dakota
Tennessee
Texas
Utah
Vermont
Virginia
Washington
West Virginia
Estimate
-0.71
-0.39
-0.06
0.27
0.59
0.92
1.25
1.57
mean
sampling
0%
< 1%
1% - 3%
3% or more

Figure B.36. The total change rate in mean occupancy (total_change = lambda_tot - 1) for *Lasiurus cinereus* (LACI) given the mean occupancy estimate in last year of sampling (2019) and the mean occupancy estimates three years (2016) prior aggregated across a state within the modeled species range. For example, if total_change_3yr = -0.25, the mean occupancy rate has declined by 25% over the nine years since 2016, while a value of 0.25 would indicate an increase of 25%. Means (points) and 95% credible intervals (bars) are depicted based on the average percent of grid cells sampled (legend) in the first and last years of the timeframe of interest for each state (A-D). Note that when credible intervals do not overlap zero, we have at least 95% certainty that these trends in species occupancy are either negative or positive. When credible intervals overlap zero, we have less than 95% certainty that these trends are different than zero. U.S. states appear in alphabetic order (A-D). Note the results for LACI were inconclusive due issues reported in section 3.12.

Appendix C: Occupancy Modeling Covariate Effects

C.1 *Myotis lucifugus*

Model occupancy covariates

For *Myotis lucifugus* (MYLU), the occupancy probability in each grid cell and year was modeled using a logit link. The intercept (mean occupancy) was modeled using hierarchical ecoregion effects to account for spatial and temporal autocorrelation (See Appendix A, Section A.2.3 and Table A.1 for more details and equations). Note, the variances of the spatial effects were constrained to be relatively small so that they did not overpower the site-level covariate effects.
Grid cell level covariates:
Max elevation (quadratic effects allow for downward bending curves or upward bending curves)
Average temperature (climatological mean not yearly differences, quadratic effects)
Average physiographic diversity
Average precipitation (climatological mean not yearly differences)
Percent forest cover
Percent wetlands
Karst in the east (east of the 100 degree W longitude) as an indicator variable
Distance to the nearest mines in the east (east of the 100 degree W longitude)
Winter-to-summer connectivity (a value in each grid cell and year)

A winter-to-summer connectivity metric was used to link the modeled winter count at each hibernaculum each year (Cheng et al. 2021b) to each grid cell based on the species-specific average winter to summer migration distance. This parameter influences summertime occupancy in both space and time (for example, capturing the effects of spatial proximity to large hibernacula, and the effects of declining abundances over time due to WNS, Section 2.2.3, Figure 1). Note, this connectivity metric models the effects of known hibernacula counts on the summer distribution; however, there are large portions of MYLU's summer range for which colony counts at hibernacula are quite rare despite the known presence of MYLU. Thus, this metric is most relevant for portions of the range with known colony counts. To remove the effect of connectivity in these regions for which the covariate was unrepresentative (largely in the western United States and Canada), we set the effect of this covariate to zero for all Ecoregion level-3's where the mean connectivity value across all sampled points in the ecoregion was less was than -2.5, which on a logit scale corresponds to a value of 0.076.

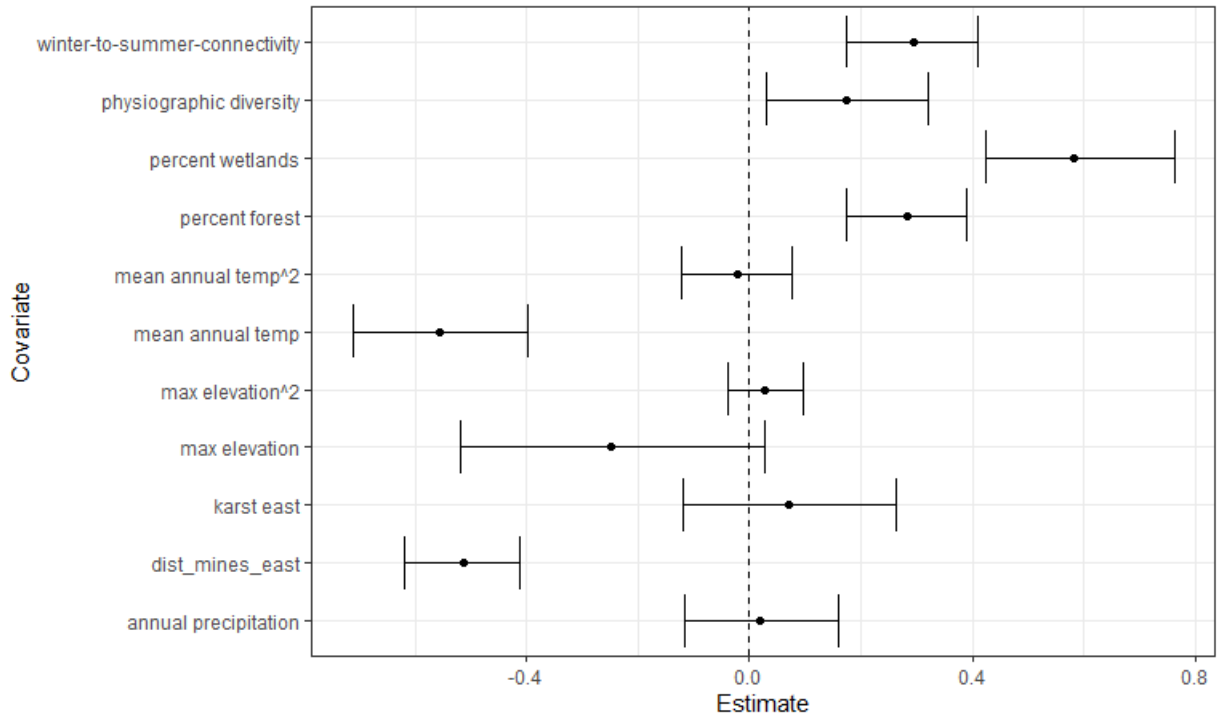

Figure C.1. Estimates of covariate effects on grid cell occupancy for *Myotis lucifugus* (MYLU), excluding intercept estimates which varied by ecoregions and year.

Model detection covariates

The intercept for p11 (detectability), p10 (false-positive rate), and b (confirmation rates) were modeled as random effects by Ecoregion level-3 and year. Additional observation level covariates were modeled on p11 including: day length, water vapor pressure, precipitation indicator, effort (length of the detection history aggregated across for each observation period), the day of year. Effort was also included as an additional covariate on the false positive rate p10. No additional covariates were fitted on the confirmation rate, *b*. Note that all three observation parameter types (p11, p10, and b) are rates corresponding with observation events aggregated over 7-day periods, and are not the same as nightly rates.

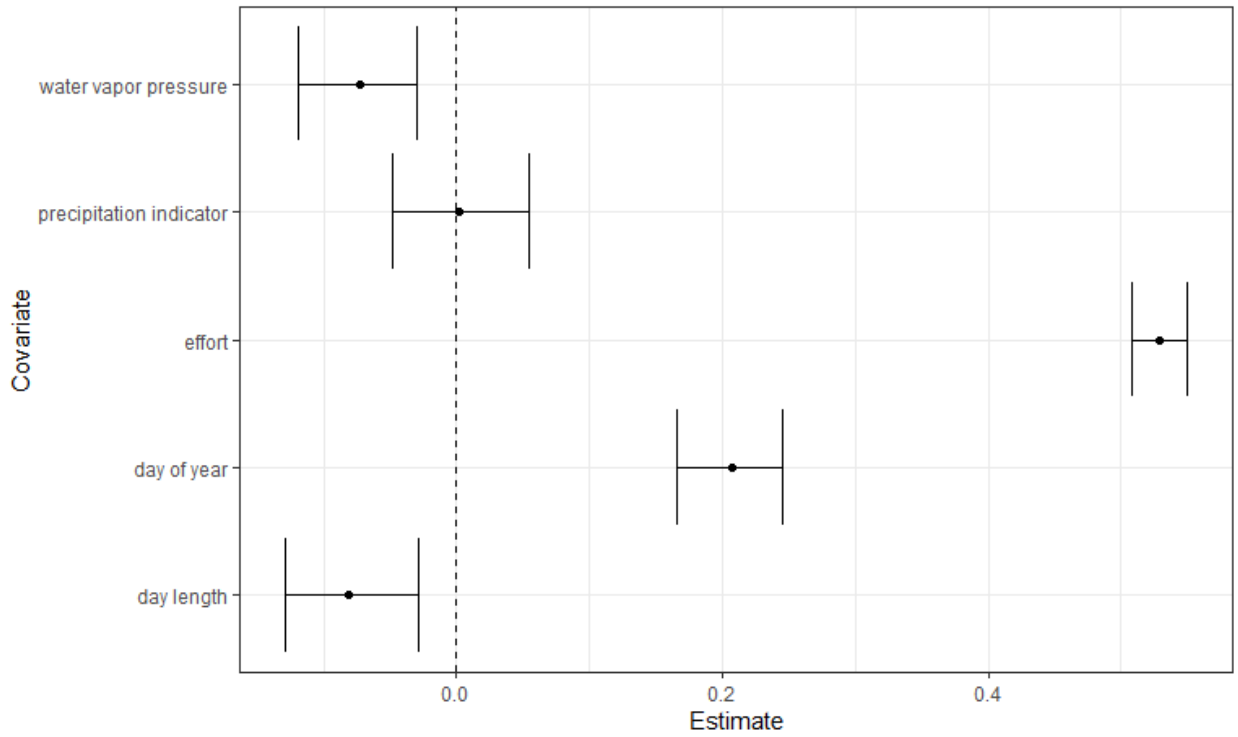

Figure C.2. Estimates of observation covariates on the detection rate for *Myotis lucifugus* (MYLU).

C.2 *Myotis septentrionalis*

Model occupancy covariates

For *Myotis septentrionalis* (MYSE), the occupancy probability in each grid cell and year was modeled using a logit link with the following assumptions: 1) the intercept (mean occupancy) with a random effect by year from a multivariate normal autoregressive (AR1) time process and 2) a time varying effect of karst (different each year) given a multivariate normal AR1 time process.

Other grid cell-level covariates:

- Max elevation (quadratic effects allow for downward bending curves or upward bending curves)
- Average temperature (climatological mean not yearly differences, quadratic effects)
- Average physiographic diversity
- Average precipitation (climatological mean not yearly differences)
- Percent forest cover
- Percent wetlands
- Distance to the nearest mines in the east (east of the 100 degree W longitude)
- Winter-to-summer connectivity (a value in each grid cell and year)

A winter-to-summer connectivity metric was used to link the modeled winter count at each hibernacula each year (Cheng et al. 2021b) to each grid cell based on the species-specific

average winter to summer migration distance. This parameter influences summertime occupancy in both space and time (for example, capturing the effects of spatial proximity to large hibernacula, and the effects of declining abundances over time due to WNS, Section 2.2.3, Figure 1). The addition of time varying karst effects and distance to mine effects were included based on conversations with species experts, and recent empirical study in the literature (Barr et al. 2021). Note that percent forest (of any kind) has a strong and positive correlation with physiographic diversity and winter-to-summer connectivity, thus forest effects are soaked up between strong positive effects of physiography diversity and winter to summer connectivity. Thus, caution should be used when interpreting individual covariate effects in isolation of correlated predictor effects.

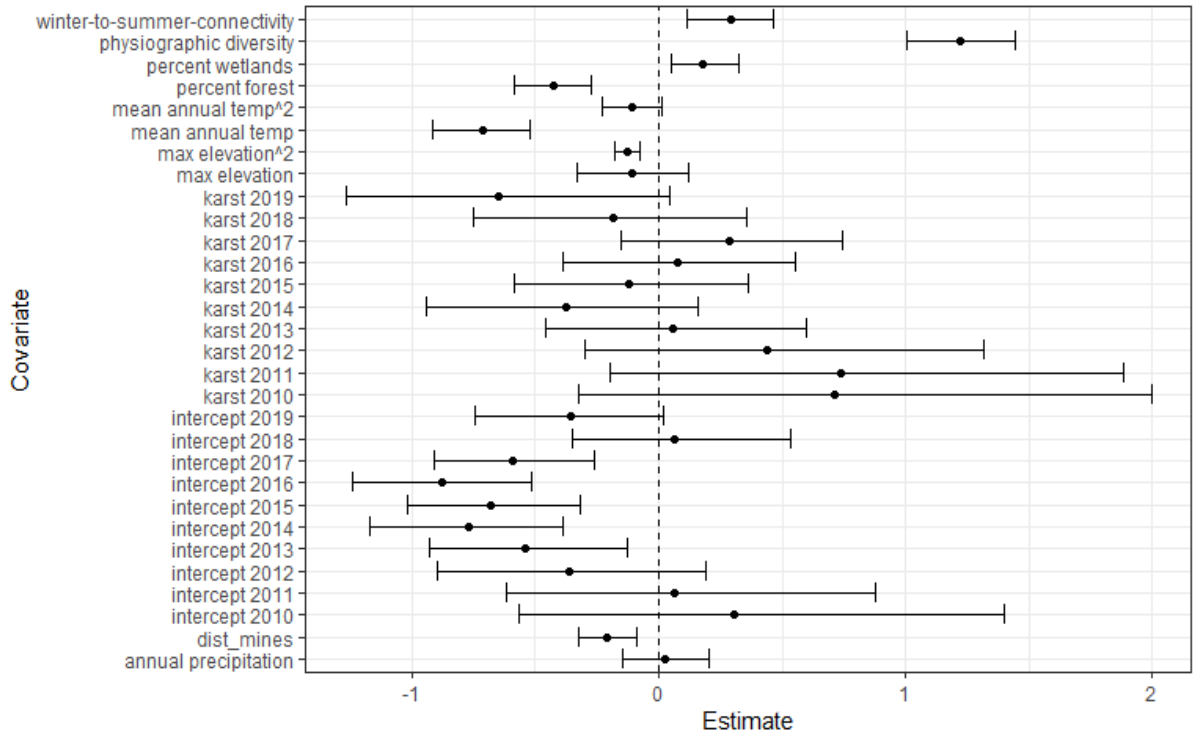

Figure C.3. Estimates of occupancy and detection covariates for *Myotis septentrionalis* (MYSE).

Model detection covariates

The intercept for p11 (detectability), p10 (false-positive rate), and b (confirmation rates) were modeled as random effects by Ecoregion level-3 and year. Additional observation level covariates were modeled on p11 including: day length, minimum temperature, water vapor pressure, precipitation indicator (0/1), effort (length of the detection history aggregated across for each observation period), the day of year. Effort was also included as an additional covariate on the false positive rate p10. No additional covariates were fitted on the confirmation rate, *b*. Note that all three observation parameter types (p11, p10, and b) are rates corresponding with observation events aggregated over 7-day periods, and are not the same as nightly rates.

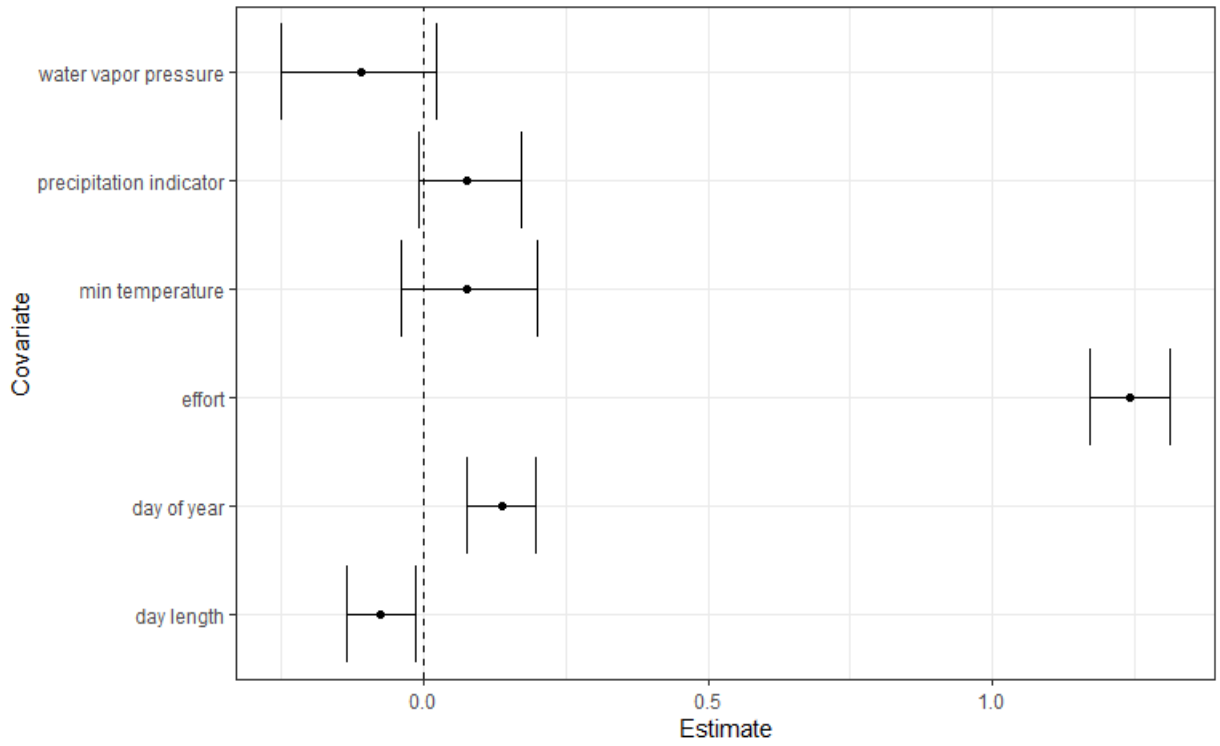

Figure C.4. Estimates of occupancy and detection covariates *Myotis septentrionalis* (MYSE).

C.3 *Perimyotis subflavus*

Model occupancy covariates

For *Perimyotis subflavus* (PESU), the occupancy probability in each grid cell and year was modeled using a logit link. The intercept (mean occupancy) was modeled using hierarchical ecoregion effects to account for spatial and temporal autocorrelation (See Appendix A, Section A.2.3 and Table A.1 for more details and equations). Note, the variances of the spatial effects were constrained to be relatively small (i.e., SD < 0.5 at each level in most cases) so that they did not overpower the site-level covariate effects.

Grid cell level covariates:

- Max elevation (quadratic effects allow for downward bending curves or upward bending curves)
- Average temperature (climatological mean not yearly differences, quadratic effects)
- Average physiographic diversity
- Average precipitation (climatological mean not yearly differences)
- Percent forest cover
- Percent wetlands
- Karst
- Distance to the nearest mines
- Winter-to-summer connectivity (a value in each grid cell and year)

A winter-to-summer connectivity metric was used to link the modeled winter count at each hibernacula each year (Cheng et al. 2021b) to each grid cell based on the species-specific average winter to summer migration distance. This parameter influences summertime occupancy in both space and time (for example, capturing the effects of spatial proximity to large hibernacula, and the effects of declining abundances over time due to WNS, Section 2.2.3, Figure 1).

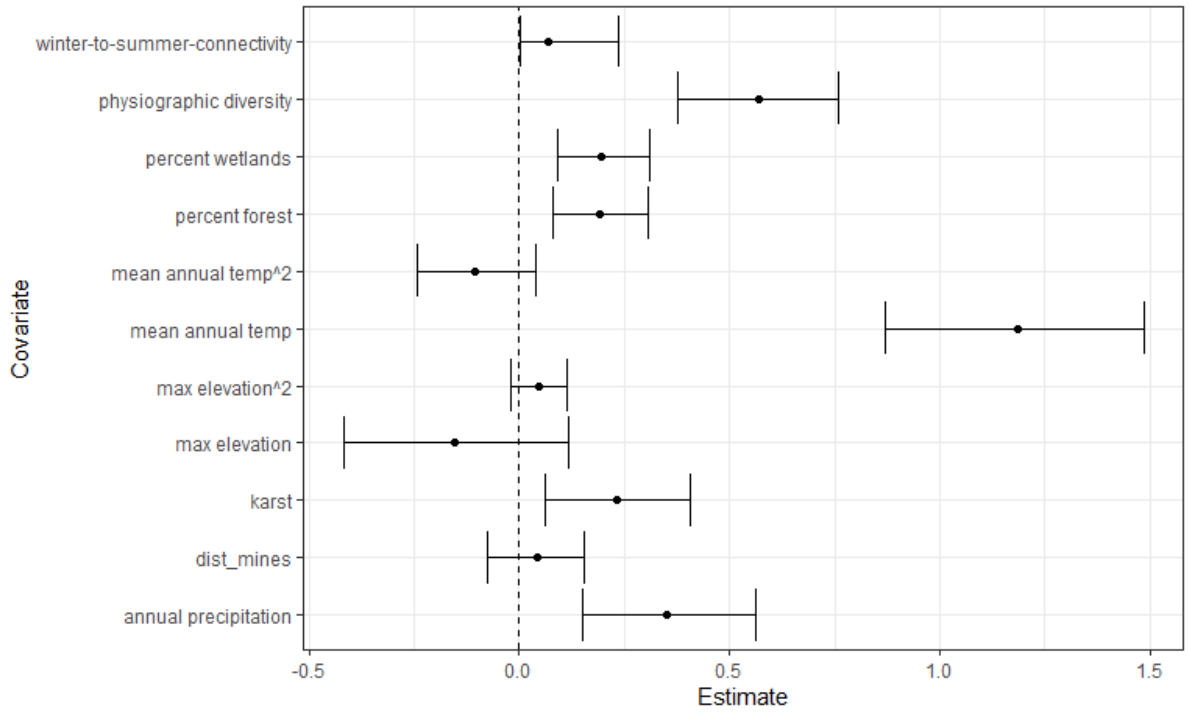

Figure C.5. Estimates of occupancy and detection covariates for *Perimyotis subflavus* (PESU).

Model detection covariates

The intercept for p11 (detectability), p10 (false-positive rate), and b (confirmation rates) were modeled as random effects by Ecoregion level-3 and year. Additional observation level covariates were modeled on p11 including: day length, water vapor pressure, precipitation indicator, effort (length of the detection history aggregated across for each observation period), the day of year. Effort was also included as an additional covariate on the false positive rate p10. No additional covariates were fitted on the confirmation rate, *b*. Note that all three observation parameter types (p11, p10, and b) are rates corresponding with observation events aggregated over 7-day periods, and are not the same as nightly rates.

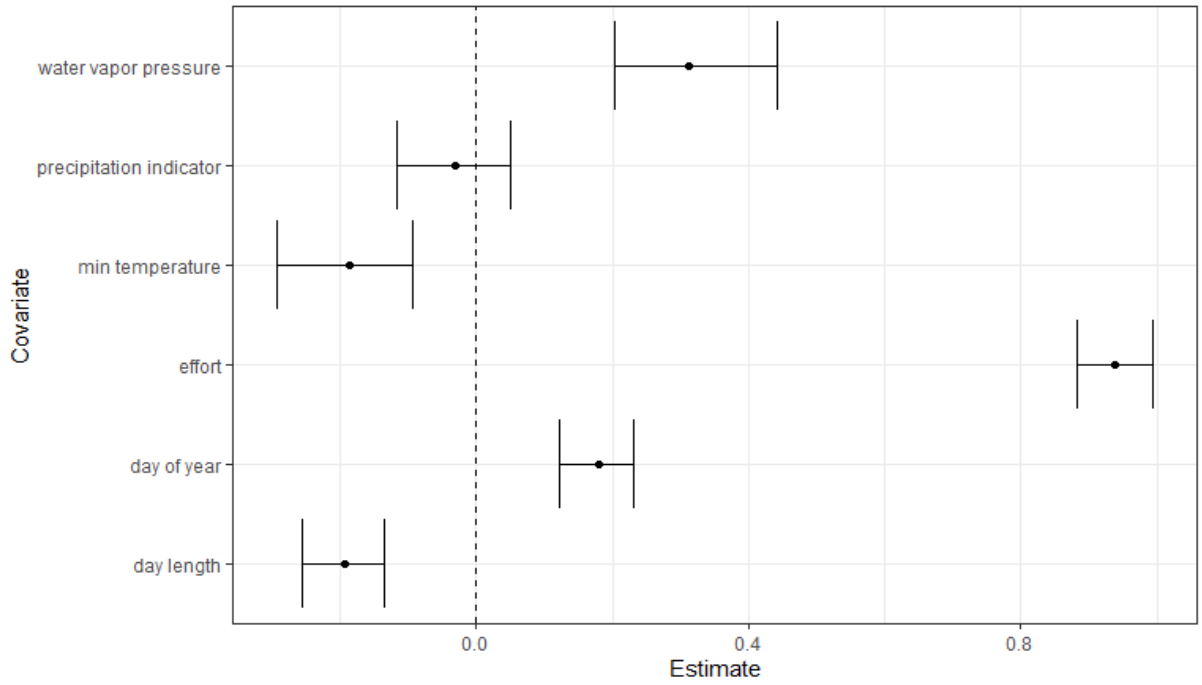

Figure C.6. Estimates of occupancy and detection covariates for *Perimyotis subflavus* (PESU).

C.4 *Myotis evotis*

Model occupancy covariates

For *Myotis evotis* (MYEV), the occupancy probability in each grid cell and year was modeled using a logit link. The intercept (mean occupancy) was modeled using hierarchical ecoregion effects to account for spatial and temporal autocorrelation (See Appendix A, Section A.2.3 and Table A.1 for more details and equations). Note, the variances of the spatial effects were constrained to be relatively small (i.e., SD < 0.5 at each level in most cases) so that they did not overpower the site-level covariate effects.

Other grid cell-level covariates:

- Max elevation (quadratic effects allow for downward bending curves or upward bending curves)
- Average temperature (climatological mean not yearly differences, quadratic effects)
- Average physiographic diversity
- Average precipitation (climatological mean not yearly differences)
- Percent forest cover
- Percent wetlands

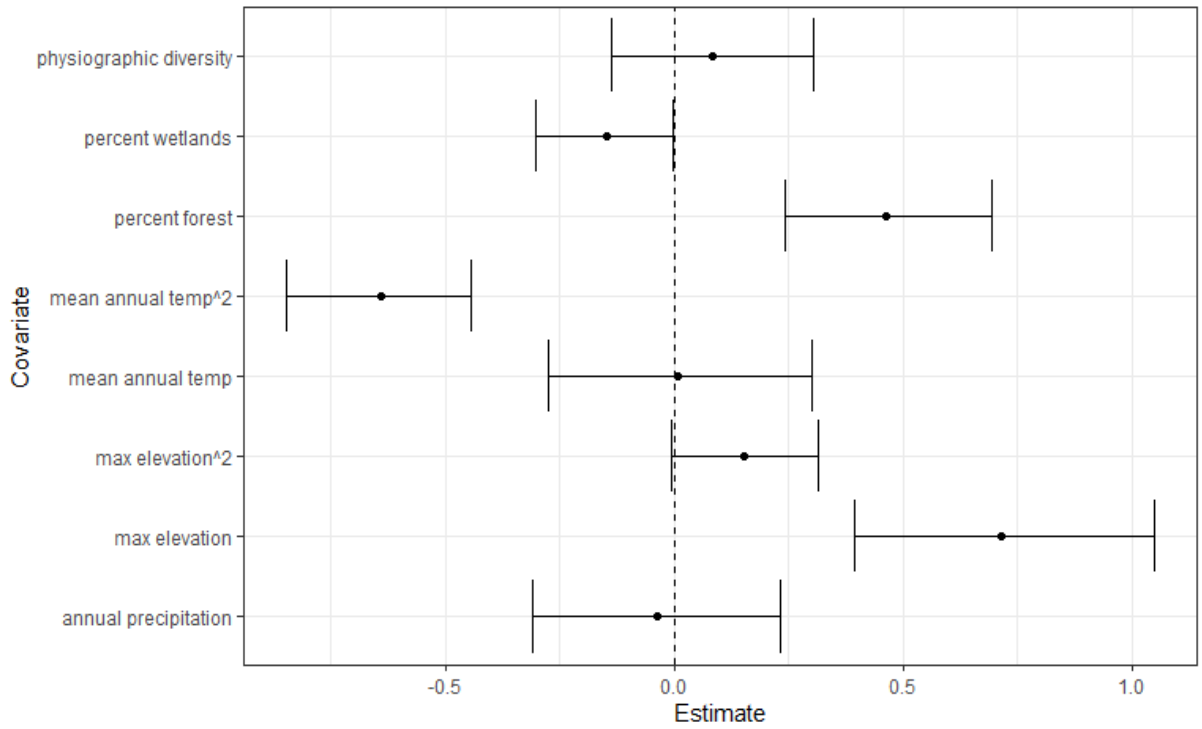

Figure C.7. Estimates of occupancy and detection covariates for *Myotis evotis* (MYEV).

Model detection covariates

The intercept for p11, p10, and b were modeled as random effects by Ecoregion level-3 and year. Additional observation level covariates were modeled on p11 including: day length, minimum temperature, water vapor pressure, precipitation indicator, effort (number of total rows of data aggregated across for each observation periods, e.g., detector nights for stationary), and the day of year. Effort was also included as an additional covariate on the false positive rate p10. No additional covariates were fitted on the confirmation rate, *b*.

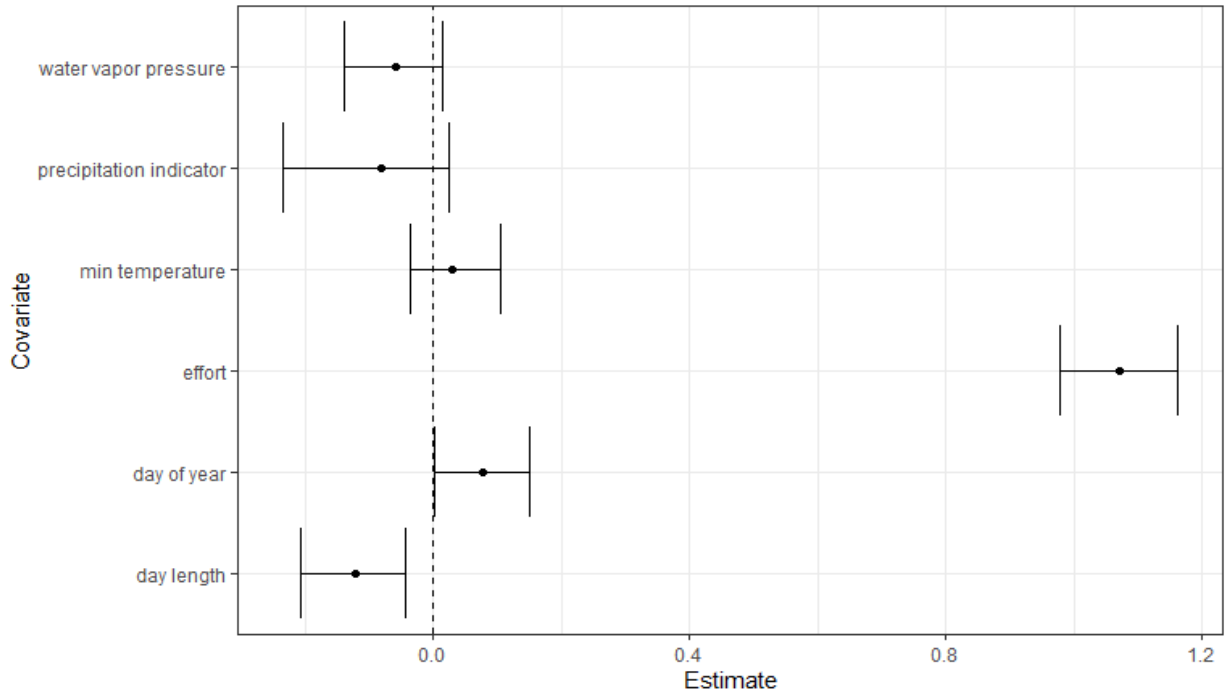

Figure C.8. Estimates of occupancy and detection covariates for *Myotis evotis* (MYEV).

C.5 *Myotis grisescens*

Model occupancy covariates

For *Myotis grisescens* (MYGR), the occupancy probability in each grid cell and year was modeled using a logit link with the following assumptions: 1) the intercept (mean occupancy) with a random effect by year from a multivariate normal AR1 time process, 2) a time varying effect of karst (different each year) given a multivariate normal AR1 time process, and 3) a time varying effect of river/shoreline presence in each grid cell given a multivariate normal AR1 time process.

Other grid cell-level covariates:

- Max elevation (quadratic effects allow for downward bending curves or upward bending curves)
- Average temperature (climatological mean not yearly differences, quadratic effects)
- Average physiographic diversity
- Average precipitation (climatological mean not yearly differences)
- Percent forest cover
- Percent wetlands

Note that physiographic diversity and percent forest have a very strong positive correlation, thus forest effects are soaked up between strong positive effects of physiography diversity and Ecoregion spatial effects. Despite a negative marginal effect of percent forest, occupancy values

given all other variables show strong positive relationships when regressing only percent forest against occupancy.

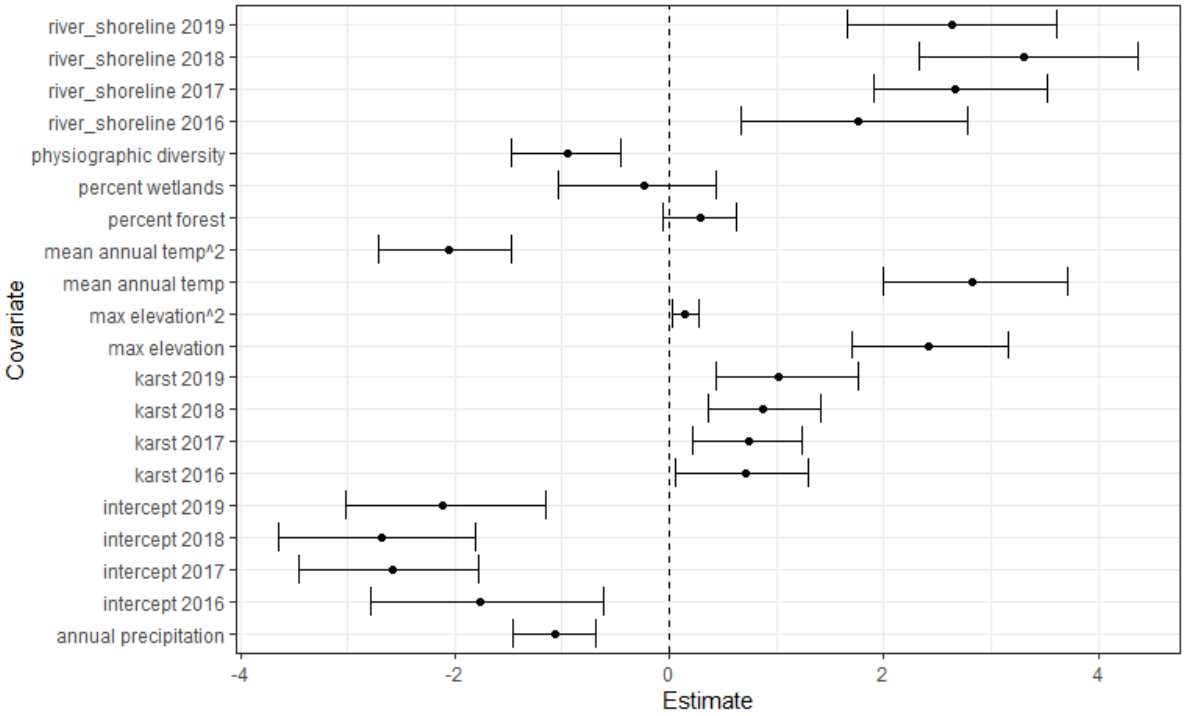

Figure C.9. Estimates of occupancy and detection covariates for *Myotis grisescens* (MYGR).

Model detection covariates

The intercept for p11, p10, and b were modeled as random effects by Ecoregion level-3 and year. Additional observation level covariates were modeled on p11 including: day length, minimum temperature, water vapor pressure, precipitation indicator, effort (number of total rows of data aggregated across for each observation periods, e.g., detector nights for stationary), and the day of year. Effort was also included as an additional covariate on the false positive rate p10. No additional covariates were fitted on the confirmation rate, *b*.

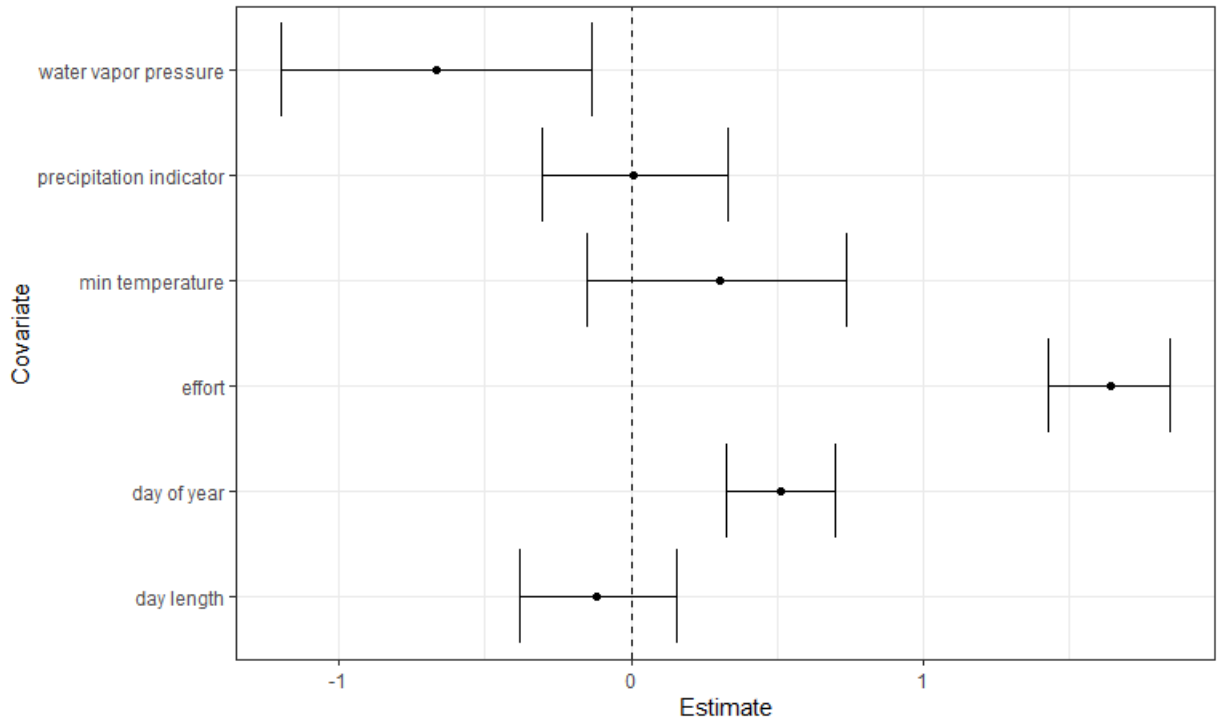

Figure C.10. Estimates of occupancy and detection covariates for *Myotis grisescens* (MYGR).

C.6 *Myotis leibii*

Model occupancy covariates

For *Myotis leibeii* (MYLE), the occupancy probability in each grid cell and year was modeled using a logit link. The intercept (mean occupancy) was modeled using hierarchical ecoregion effects to account for spatial and temporal autocorrelation (See Appendix A, Section A.2.3 and Table A.1 for more details and equations).

Other grid cell-level covariates:Max elevation (quadratic effects allow for downward bending curves or upward bending curves)

- Average temperature (climatological mean not yearly differences, quadratic effects)
- Average physiographic diversity
- Average precipitation (climatological mean not yearly differences)
- Percent forest cover
- Percent wetlands

Note that physiographic diversity and percent forest have a very strong positive correlation, thus forest effects are soaked up between strong positive effects of physiography diversity and Ecoregion spatial effects. Despite a negative marginal effect of percent forest, occupancy values given all other variables show strong positive relationships when regressing only percent forest against occupancy.

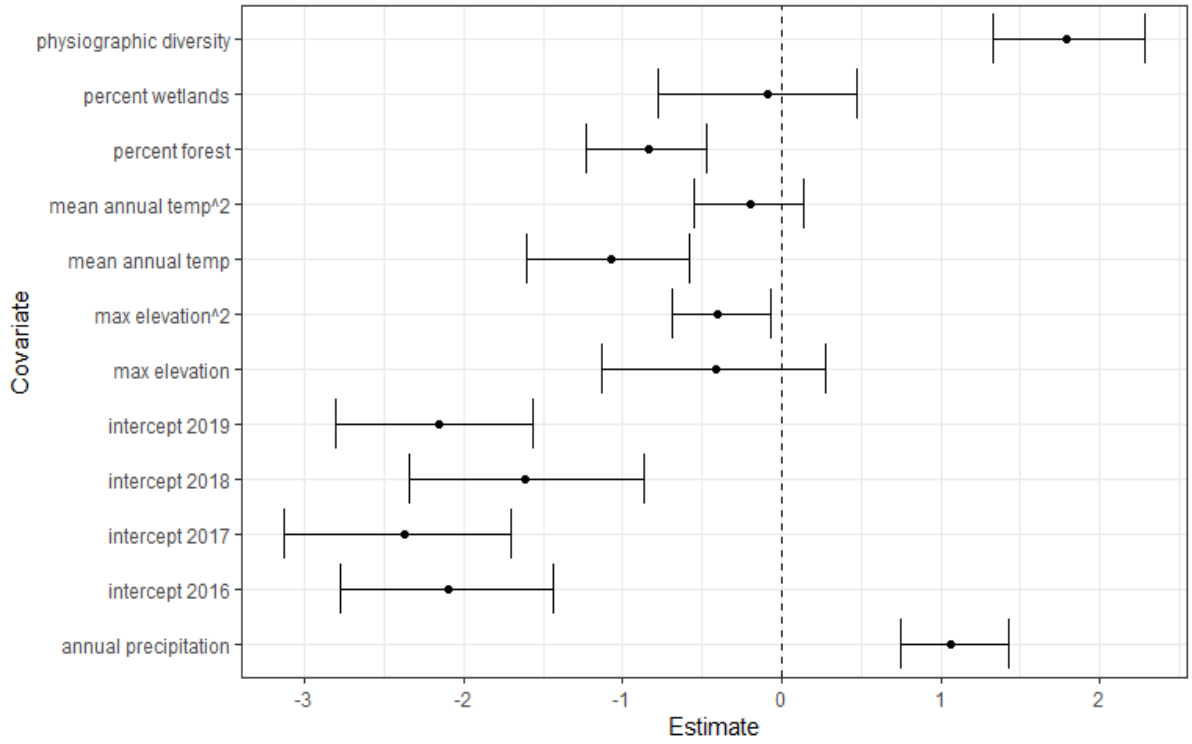

Figure C.11. Estimates of occupancy and detection covariates for *Myotis leibii* (MYLE).

Model detection covariates

The intercept for p11, p10, and b were modeled as random effects by Ecoregion level-3 and year. Additional observation level covariates were modeled on p11 including: day length, minimum temperature, water vapor pressure, precipitation indicator, effort (number of total rows of data aggregated across for each observation periods, e.g., detector nights for stationary), and the day of year. Effort was also included as an additional covariate on the false positive rate p10. No additional covariates were fitted on the confirmation rate, *b*.

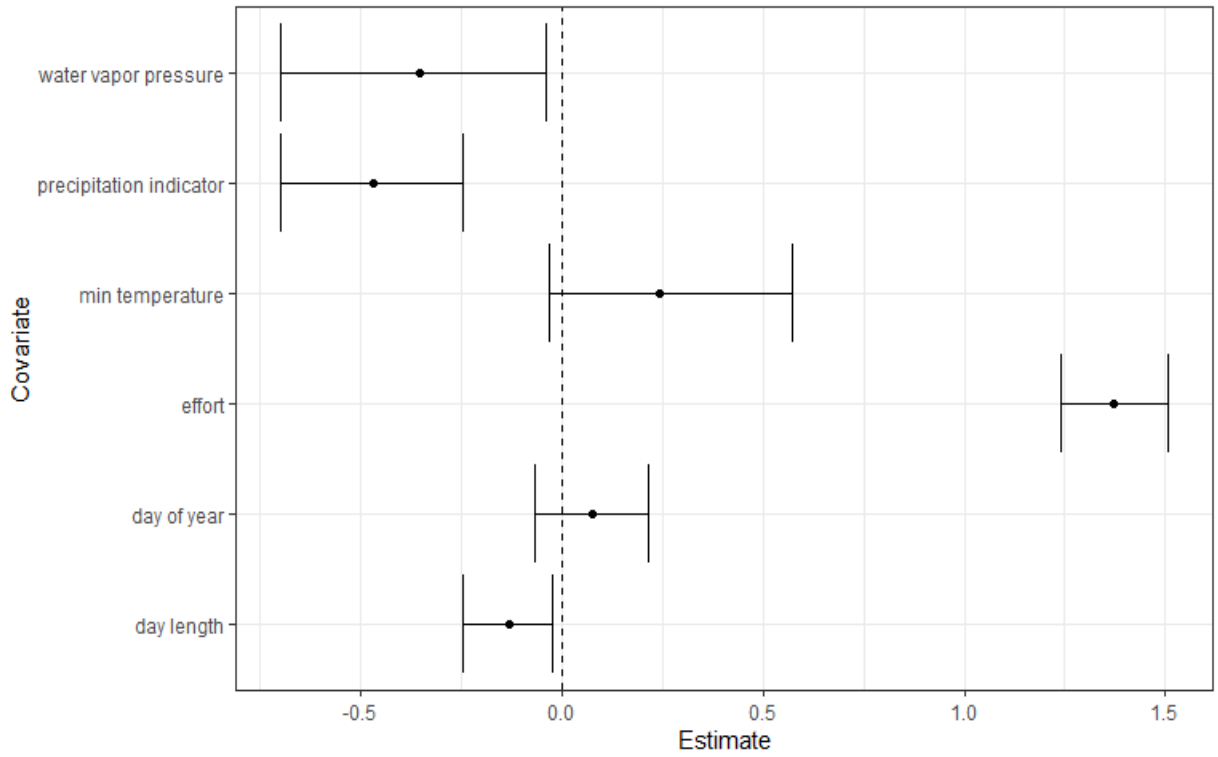

Figure C.12. Estimates of occupancy and detection covariates for *Myotis leibii* (MYLE).

C.7 *Myotis thysanodes*

Model occupancy covariates

For *Myotis thysanodes* (MYTH), the occupancy probability in each grid cell and year was modeled using a logit link. The intercept (mean occupancy) was modeled using hierarchical ecoregion effects to account for spatial and temporal autocorrelation (See Appendix A, Section A.2.3 and Table A.1 for more details and equations). Note, the variances of the spatial effects were constrained to be relatively small (i.e., SD < 0.5 at each level in most cases) so that they did not overpower the site-level covariate effects.

Other grid cell-level covariates:

- Max elevation (quadratic effects allow for downward bending curves or upward bending curves)
- Average temperature (climatological mean not yearly differences, quadratic effects)
- Average physiographic diversity
- Average precipitation (climatological mean not yearly differences)
- Percent forest cover
- Percent wetlands

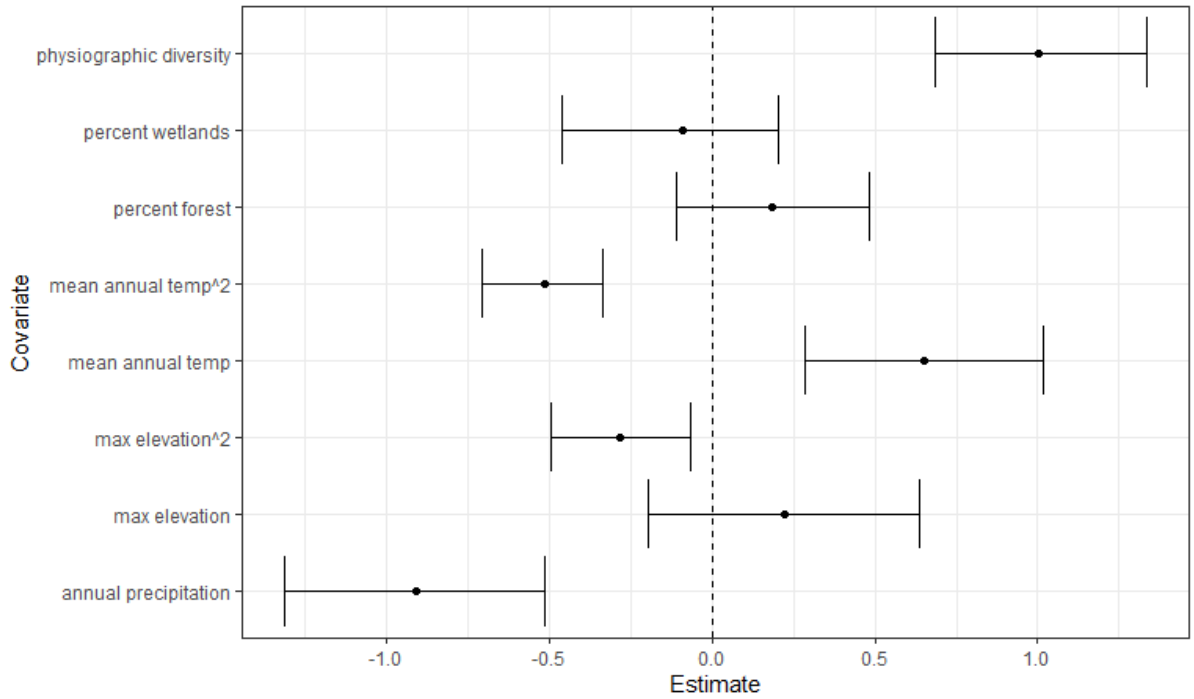

Figure C.13. Estimates of occupancy and detection covariates for *Myotis thysanodes* (MYTH).

Model detection covariates

The intercept for p11, p10, and b were modeled as random effects by Ecoregion level-3 and year. Additional observation level covariates were modeled on p11 including: day length, minimum temperature, water vapor pressure, precipitation indicator, effort (number of total rows of data aggregated across for each observation periods, e.g., detector nights for stationary), and the day of year. Effort was also included as an additional covariate on the false positive rate p10. No additional covariates were fitted on the confirmation rate, *b*.

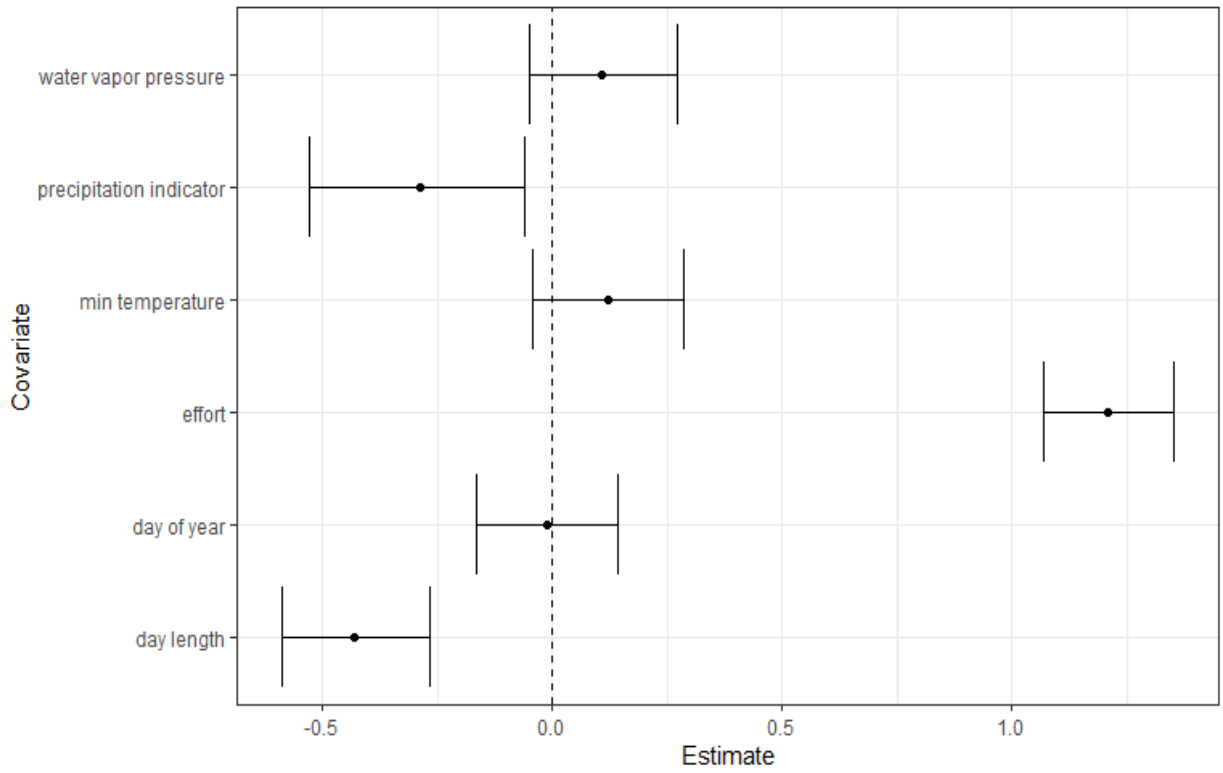

Figure C.14. Estimates of occupancy and detection covariates for *Myotis thysanodes* (MYTH).

C.8 *Myotis volans*

Model occupancy covariates

For *Myotis volans* (MYVO), the occupancy probability in each grid cell and year was modeled using a logit link. The intercept (mean occupancy) was modeled using hierarchical ecoregion effects to account for spatial and temporal autocorrelation (See Appendix A, Section A.2.3 and Table A.1 for more details and equations). Note, the variances of the spatial effects were constrained to be relatively small (i.e., SD < 0.5 at each level in most cases) so that they did not overpower the site-level covariate effects.

Other grid cell-level covariates:

- Max elevation (quadratic effects allow for downward bending curves or upward bending curves)
- Average temperature (climatological mean not yearly differences, quadratic effects)
- Average physiographic diversity
- Average precipitation (climatological mean not yearly differences)
- Percent forest cover
- Percent wetlands

A grid cell level, multivariate Gaussian spatial smooth was implemented as a tensor product interaction with 25 knots (five in each dimension) to capture large-scale spatial autocorrelation.

This effect was included after discussions with species experts, after finding it greatly improved predictions in Colorado based on expected elevational effects compared to models without the spatial smooth.

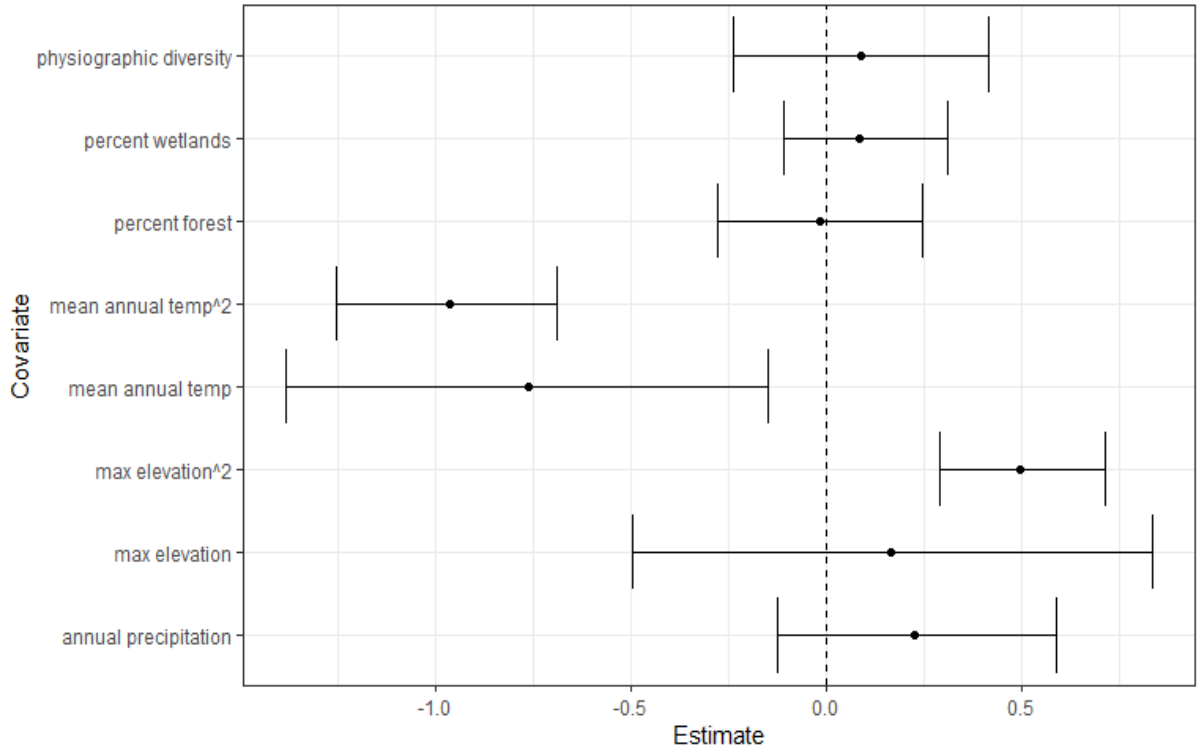

Figure C.15. Estimates of occupancy and detection covariates for *Myotis volans* (MYVO).

Model detection covariates

The intercept for p11, p10, and b were modeled as random effects by Ecoregion level-3 and year. Additional observation level covariates were modeled on p11 including: day length, minimum temperature, water vapor pressure, precipitation indicator, effort (number of total rows of data aggregated across for each observation periods, e.g., detector nights for stationary), and the day of year. Effort was also included as an additional covariate on the false positive rate p10. No additional covariates were fitted on the confirmation rate, *b*.

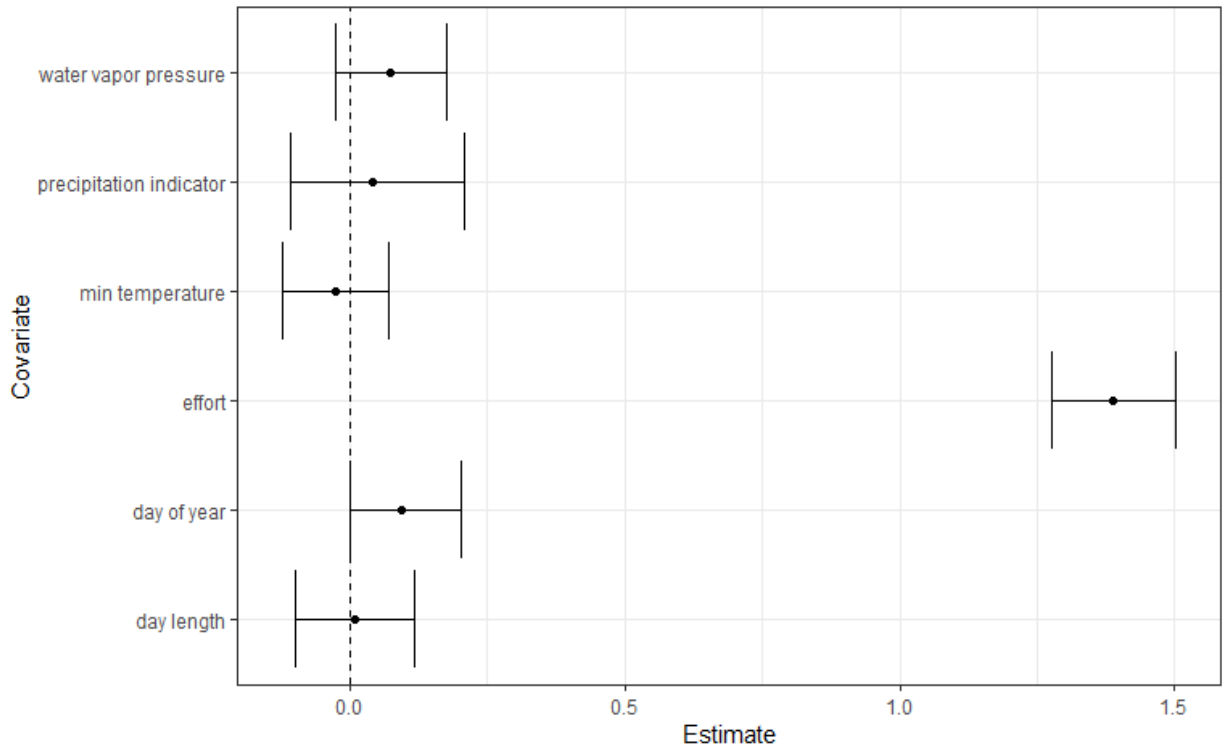

Figure C.16. Estimates of occupancy and detection covariates *Myotis volans* (MYVO).

C.9 *Myotis yumanensis*

Model occupancy covariates

For *Myotis yumanensis* (MYYU), the occupancy probability in each grid cell and year was modeled using a logit link. The intercept (mean occupancy) was modeled using hierarchical ecoregion effects to account for spatial and temporal autocorrelation (See Appendix A, Section A.2.3 and Table A.1 for more details and equations). Note, the variances of the spatial effects were constrained to be relatively small (i.e., SD < 0.5 at each level in most cases) so that they did not overpower the site-level covariate effects.

Other grid cell-level covariates:

- Max elevation (quadratic effects allow for downward bending curves or upward bending curves)
- Average temperature (climatological mean not yearly differences, quadratic effects)
- Average physiographic diversity
- Average precipitation (climatological mean not yearly differences)
- Percent forest cover
- Percent wetlands

A grid cell level, multivariate Gaussian spatial smooth was implemented as a tensor product interaction with 25 knots (5 in each dimension) to capture large-scale spatial autocorrelation.

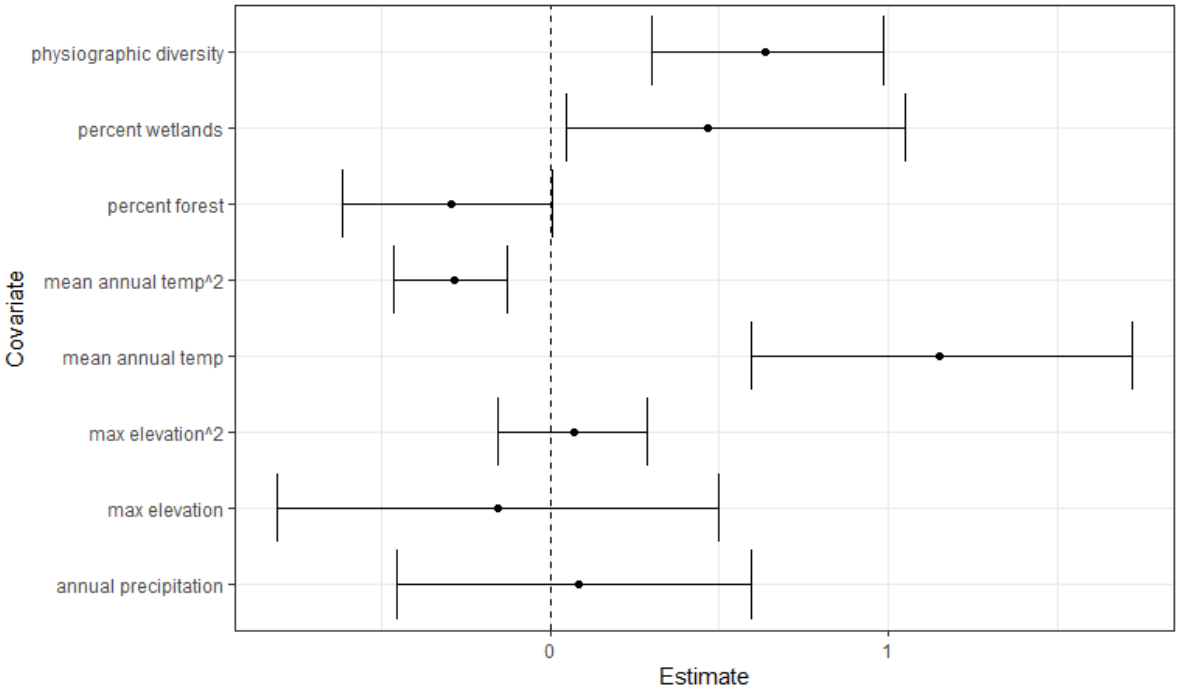

Figure C.17. Estimates of occupancy and detection covariates for *Myotis yumanensis* (MYYU).

Model detection covariates

The intercept for p11, p10, and b were modeled as random effects by Ecoregion level-3 and year. Additional observation level covariates were modeled on p11 including: day length, minimum temperature, water vapor pressure, precipitation indicator, effort (number of total rows of data aggregated across for each observation periods, e.g., detector nights for stationary), and the day of year. Effort was also included as an additional covariate on the false positive rate p10. No additional covariates were fitted on the confirmation rate, *b*.

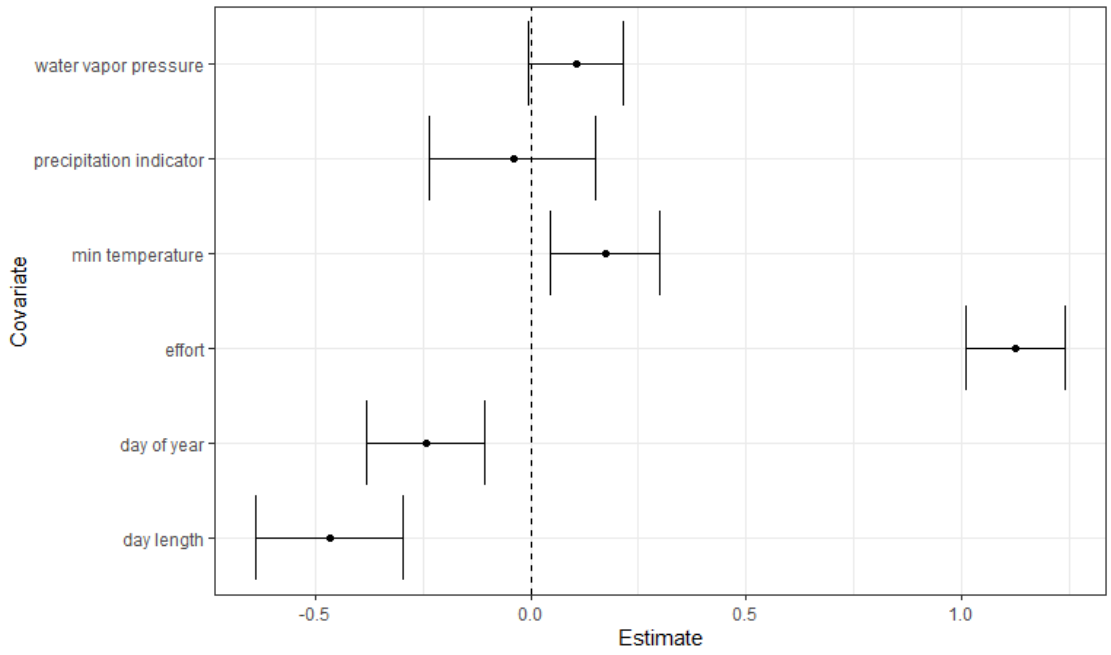

Figure C.18. Estimates of occupancy and detection covariates *Myotis yumanensis* (MYYU).

C.10 *Eptesicus fuscus*

Model occupancy covariates

For *Eptesicus fuscus* (EPFU), the occupancy probability in each grid cell and year was modeled using a logit link. The intercept (mean occupancy) was modeled using hierarchical ecoregion effects to account for spatial and temporal autocorrelation (See Appendix A, Section A.2.3 and Table A.1 for more details and equations). Note, the variances of the spatial effects were constrained to be relatively small (i.e., SD < 0.5 at each level in most cases) so that they did not overpower the site-level covariate effects.

Other grid cell-level covariates:

- Max elevation (quadratic effects allow for downward bending curves or upward bending curves)
- Average temperature (climatological mean not yearly differences, quadratic effects)
- Average physiographic diversity
- Average precipitation (climatological mean not yearly differences)
- Percent forest cover
- Percent wetlands

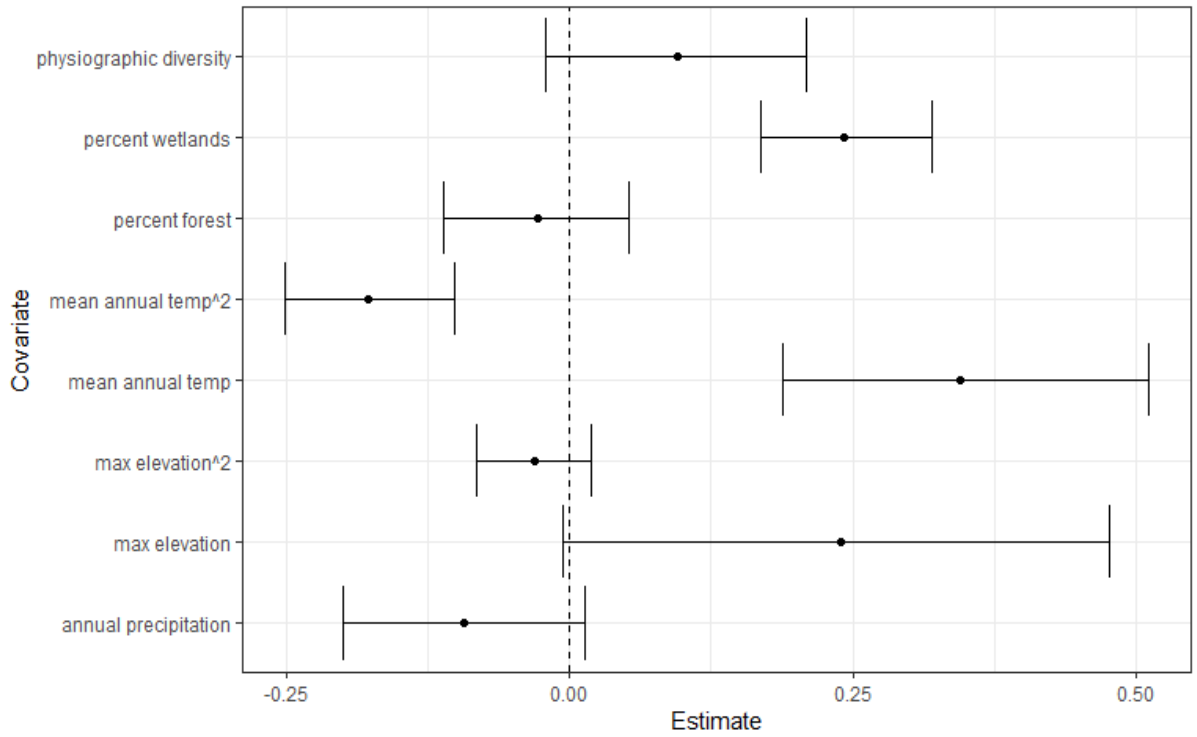

Figure C.19. Estimates of occupancy and detection covariates for *Eptesicus fuscus* (EPFU).

Model detection covariates

The intercept for p11, p10, and b were modeled as random effects by Ecoregion level-3 and year. Additional observation level covariates were modeled on p11 including: day length, minimum temperature, water vapor pressure, precipitation indicator, effort (number of total rows of data aggregated across for each observation periods, e.g., detector nights for stationary), and the day of year. Effort was also included as an additional covariate on the false positive rate p10. No additional covariates were fitted on the confirmation rate, *b*.

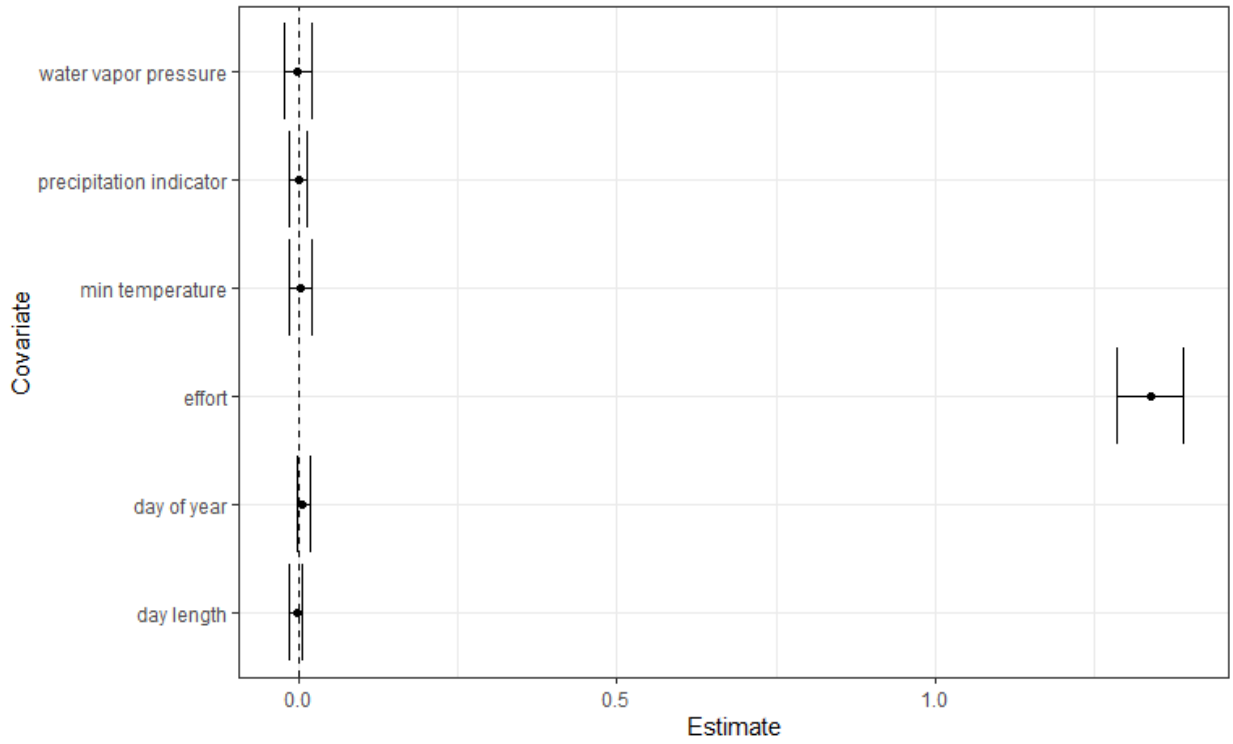

Figure C.20. Estimates of occupancy and detection covariates for *Eptesicus fuscus* (EPFU).

C.11 *Lasionycteris noctivagans*

Model occupancy covariates

For *Lasionycteris noctivagans* (LANO), the occupancy probability in each grid cell and year was modeled using a logit link. The intercept (mean occupancy) was modeled using hierarchical ecoregion effects to account for spatial and temporal autocorrelation (See Appendix A, Section A.2.3 and Table A.1 for more details and equations). Note, the variances of the spatial effects were constrained to be relatively small (i.e., SD < 0.5 at each level in most cases) so that they did not overpower the site-level covariate effects.

Other grid cell-level covariates:

- Max elevation (quadratic effects allow for downward bending curves or upward bending curves)
- Average temperature (climatological mean not yearly differences, quadratic effects)
- Average physiographic diversity
- Average precipitation (climatological mean not yearly differences)
- Percent forest cover
- Percent wetlands

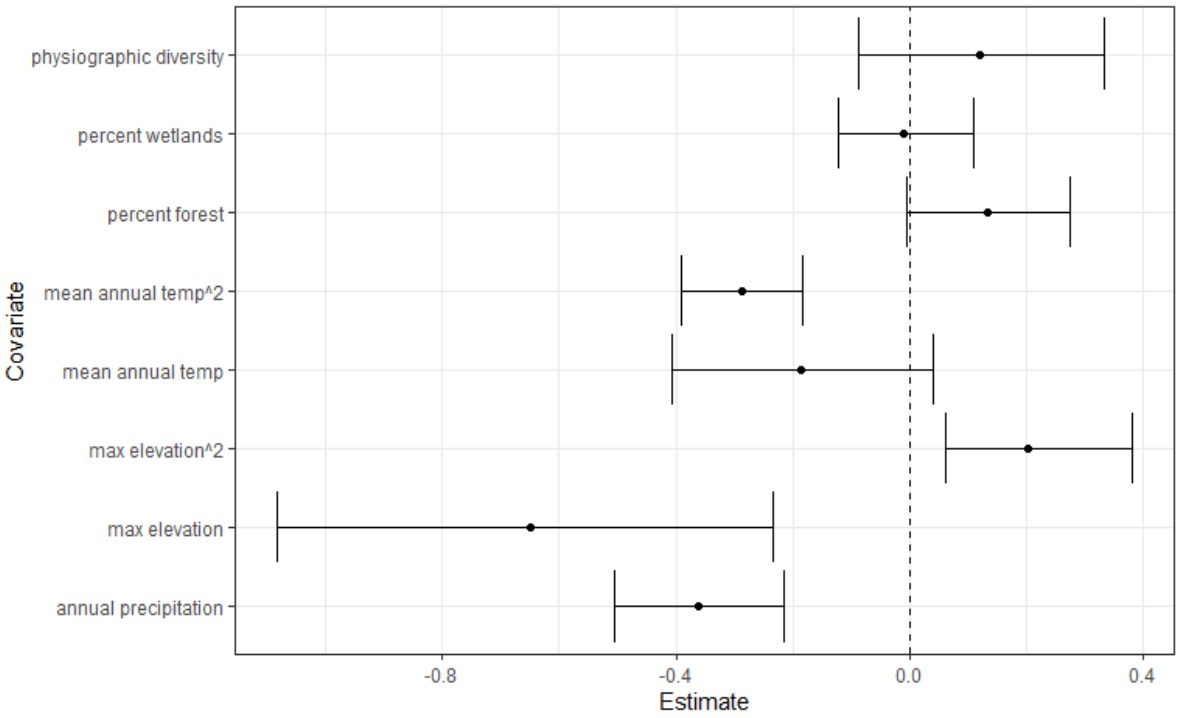

Figure C.21. Estimates of occupancy and detection covariates for *Lasionycteris noctivagans* (LANO).

Model detection covariates

The intercept for p11, p10, and b were modeled as random effects by Ecoregion level-3 and year. Additional observation level covariates were modeled on p11 including: day length, minimum temperature, water vapor pressure, precipitation indicator, effort (number of total rows of data aggregated across for each observation periods, e.g., detector nights for stationary), and the day of year. Effort was also included as an additional covariate on the false positive rate p10. No additional covariates were fitted on the confirmation rate, *b*.

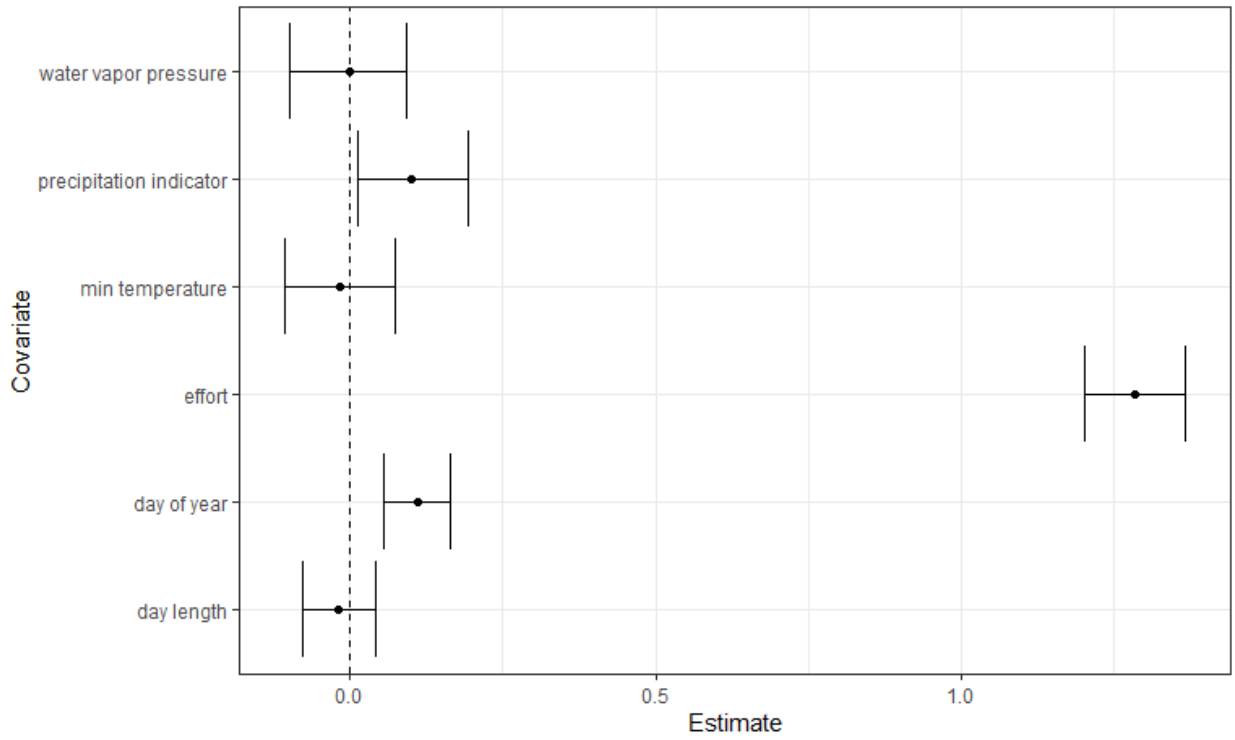

Figure C.22. Estimates of occupancy and detection covariates *Lasionycteris noctivagans* (LANO).

C.12 Lasiurus cinereus

Model occupancy covariates

For *Lasiurus cinereus* (LACI), the occupancy probability in each grid cell and year was modeled using a logit link. The intercept (mean occupancy) was modeled using hierarchical ecoregion effects to account for spatial and temporal autocorrelation (See Appendix A, Section A.2.3 and Table A.1 for more details and equations). Note, the variances of the spatial effects were constrained to be relatively small (i.e., SD < 0.5 at each level in most cases) so that they did not overpower the site-level covariate effects.

Other grid cell-level covariates:

- Max elevation (quadratic effects allow for downward bending curves or upward bending curves)
- Average temperature (climatological mean not yearly differences, quadratic effects)
- Average physiographic diversity
- Average precipitation (climatological mean not yearly differences)
- Percent forest cover
- Percent wetlands

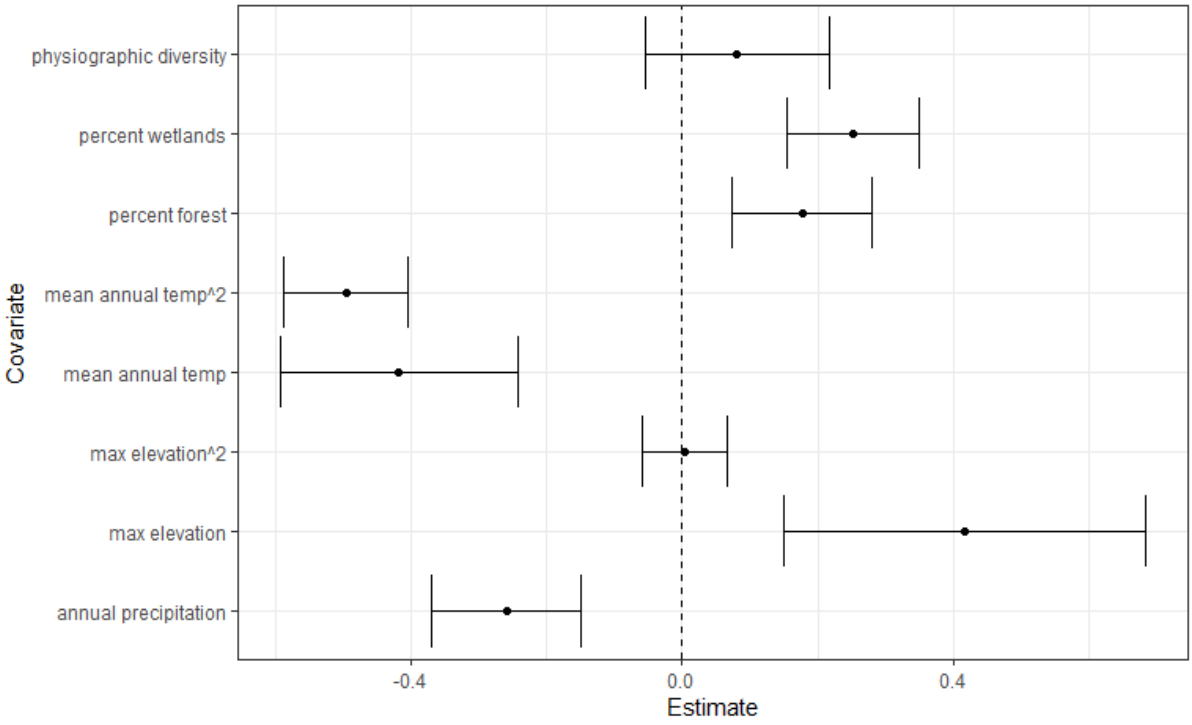

Figure C.23. Estimates of occupancy and detection covariates for *Lasiurus cinereus* (LACI).

Model detection covariates

The intercept for p11, p10, and b were modeled as random effects by Ecoregion level-3 and year. Additional observation level covariates were modeled on p11 including: day length, precipitation indicator, effort (number of total rows of data aggregated across for each observation periods, e.g., detector nights for stationary), and the day of year. Effort was also included as an additional covariate on the false positive rate p10. No additional covariates were fitted on the confirmation rate, *b*.

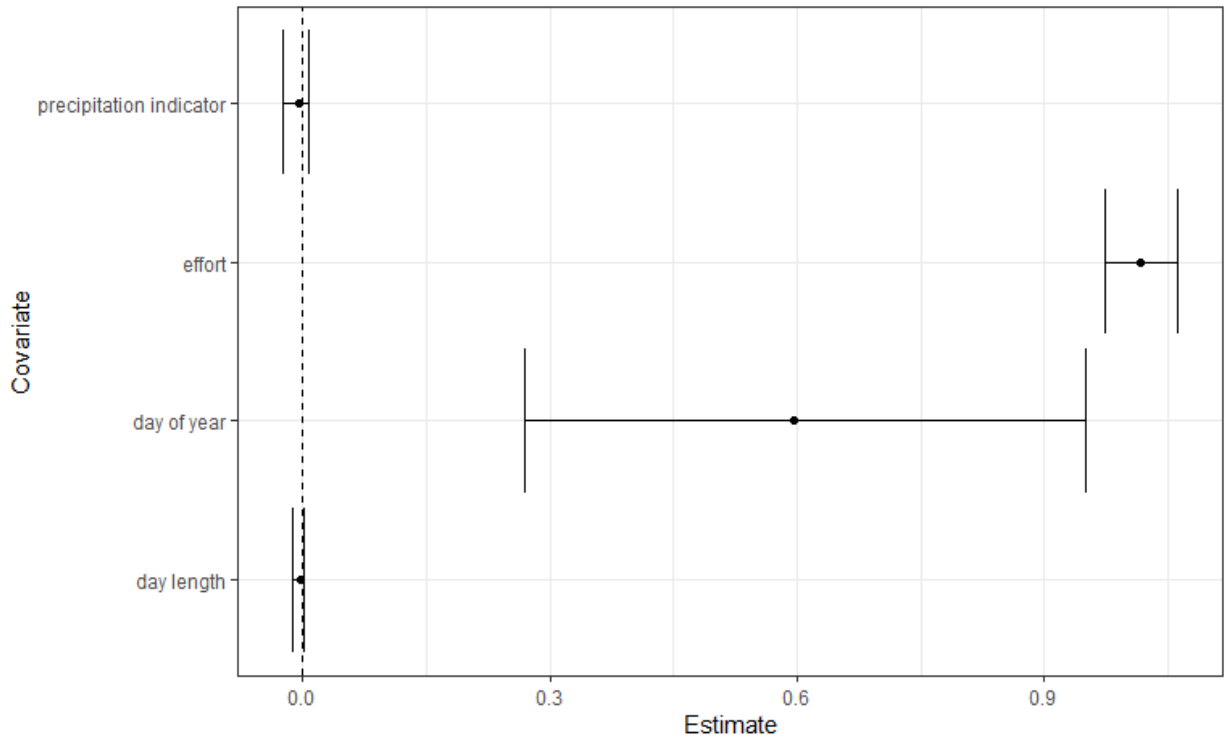

Figure C.24. Estimates of occupancy and detection covariates for *Lasiurus cinereus* (LACI).

Appendix D: Comparing predicted occupancy probabilities to monitoring data

In this section, we provide figures comparing the predicted occupancy probabilities of each grid cell to the highest level of species detection observed each year in monitored locations. This serves as an informal means of model assessment. It is informal because truth is only known for the grid cells and years with unambiguous detections (e.g., manually vetted acoustic records or capture data), while non-detections and ambiguous detections could result from either the presence or absence of a species. For example, it is possible to get 'no-detections' from true species absence, or from species presence but lack of detection. Ambiguous detections can occur from true species' detections and from false positives. Model sensitivity (i.e., the probability of correctly predicting species presence) can be evaluated based on the distribution of predicted occupancy probabilities corresponding with unambiguous detections, where we expect to see a high concentration of values near one with high sensitivity. However, model specificity (i.e., the probability of correctly predicting species absence) cannot be evaluated from the monitoring data alone.

In general, the distribution of predicted occupancy probability values that correspond with unambiguous detections should be higher than those corresponding with non-detections and ambiguous detections. Similarly, occupancy probabilities in grid cells with ambiguous detections should generally be higher than those with no detections, especially since we assume in the analyses that the true positive rate is higher than the false positive rate. In some cases, predicted occupancy probabilities of grid cells can be high in locations with no detections, especially if grid cell level occupancy covariates and observation level covariates suggest it is more likely the species was present but not detected. In general, we expect this more for species that are wide-spread (i.e., with high baseline occupancy probabilities) and/or have low-detectability. Similarly, some predicted occupancy probabilities corresponding with ambiguous detections can be quite low if occupancy covariates or observation covariates suggest the species is more likely absent and detected in error (false positives). Finally, if there is little difference in the occupancy probability distributions between no-detections and ambiguous detections, this suggests that the ambiguous detections provide relatively little information to the species occupancy process due to the model's poor ability to distinguish between false positives and true positives.

D.1 *Myotis lucifugus*

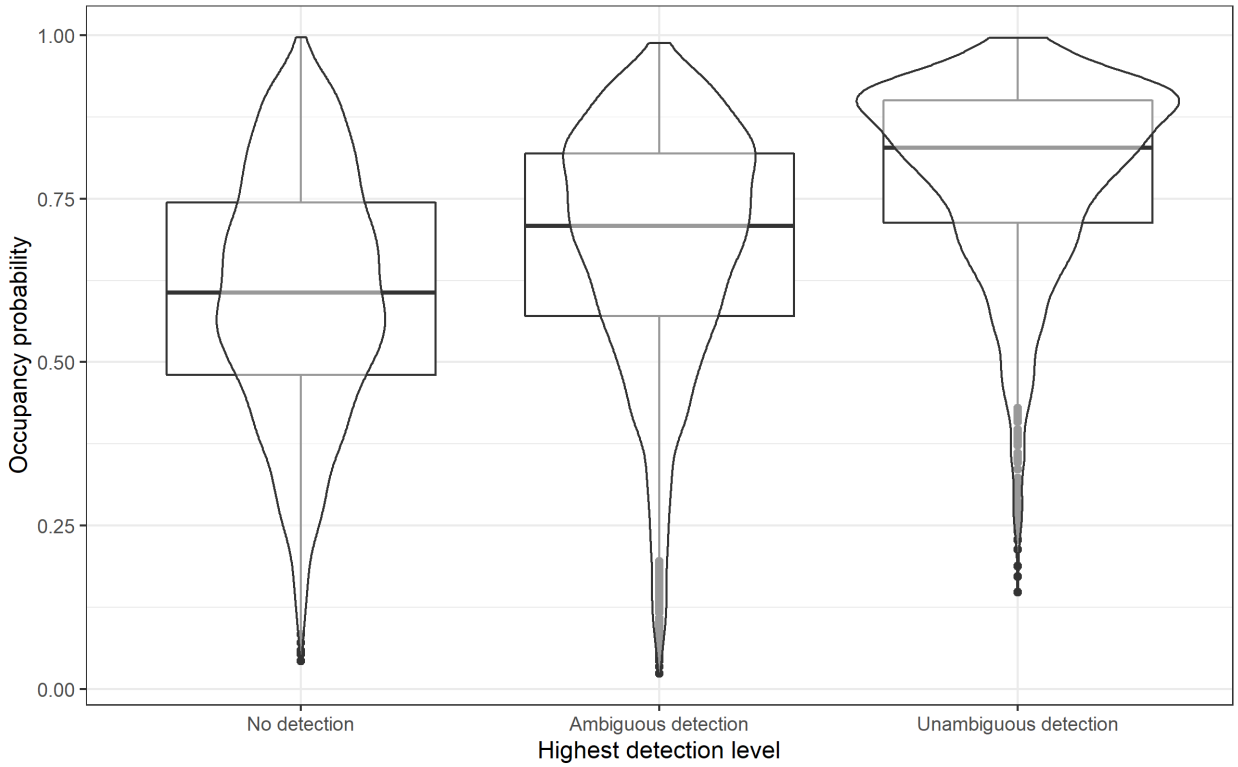

Figure D.1. Violin plots depict predicted occupancy probabilities for *Myotis lucifugus* (MYLU) compared to the highest level of species detection observed for each grid cell and year. The distributions of predicted occupancy probabilities (y-axis) are plotted against the highest level of detection observed in each grid cell and year (x-axis).

D.2 *Myotis septentrionalis*

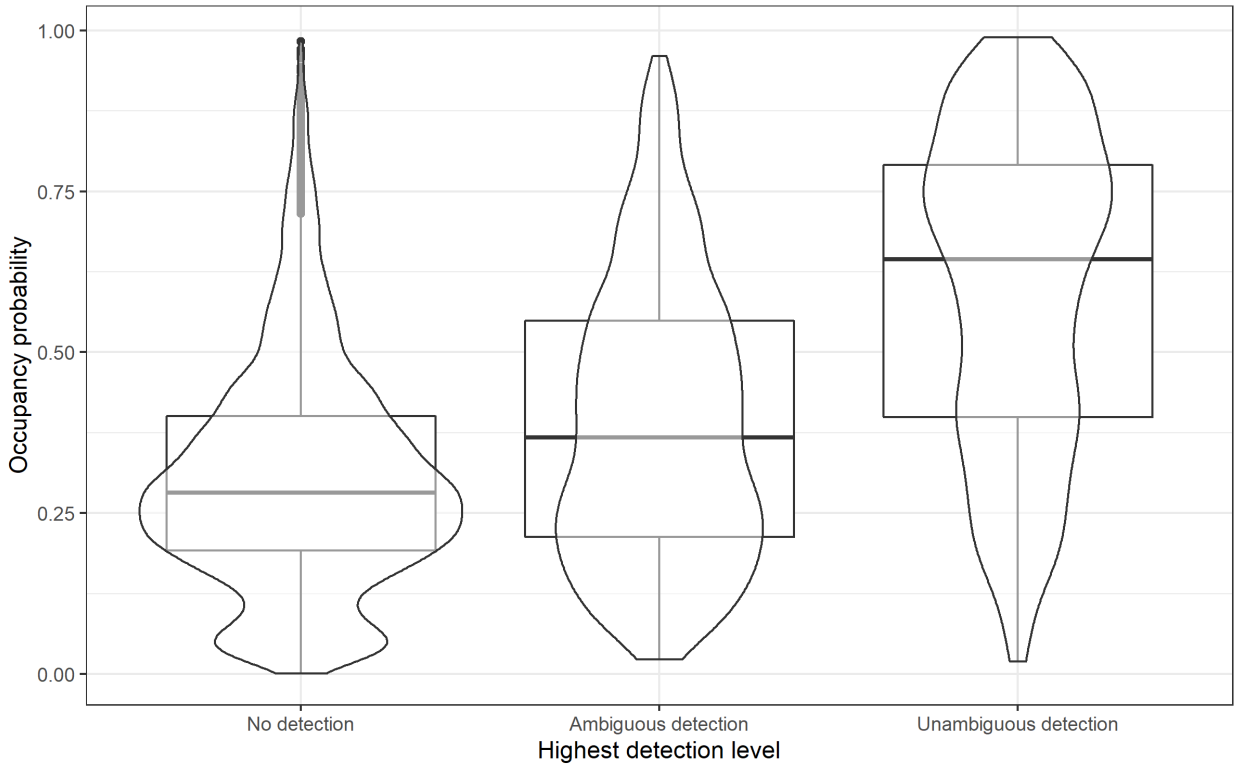

Figure D.2. Violin plots depict predicted occupancy probabilities for *Myotis septentrionalis* (MYSE) compared to the highest level of species detection observed for each grid cell and year. The distributions of predicted occupancy probabilities (y-axis) are plotted against the highest level of detection observed in each grid cell and year (x-axis).

D.3 *Perimyotis subflavus*

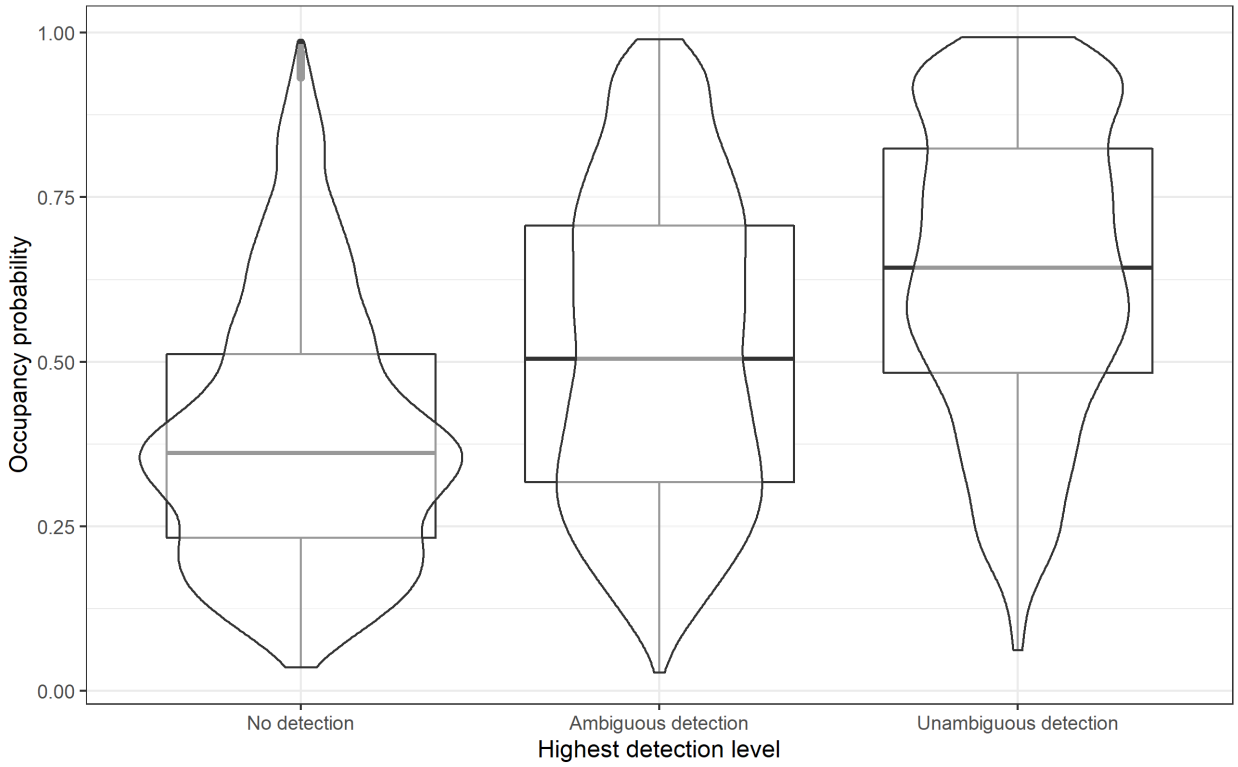

Figure D.3. Violin plots depict predicted occupancy probabilities for *Perimyotis subflavus* (PESU) compared to the highest level of species detection observed for each grid cell and year. The distributions of predicted occupancy probabilities (y-axis) are plotted against the highest level of detection observed in each grid cell and year (x-axis).

D.4 *Myotis evotis*

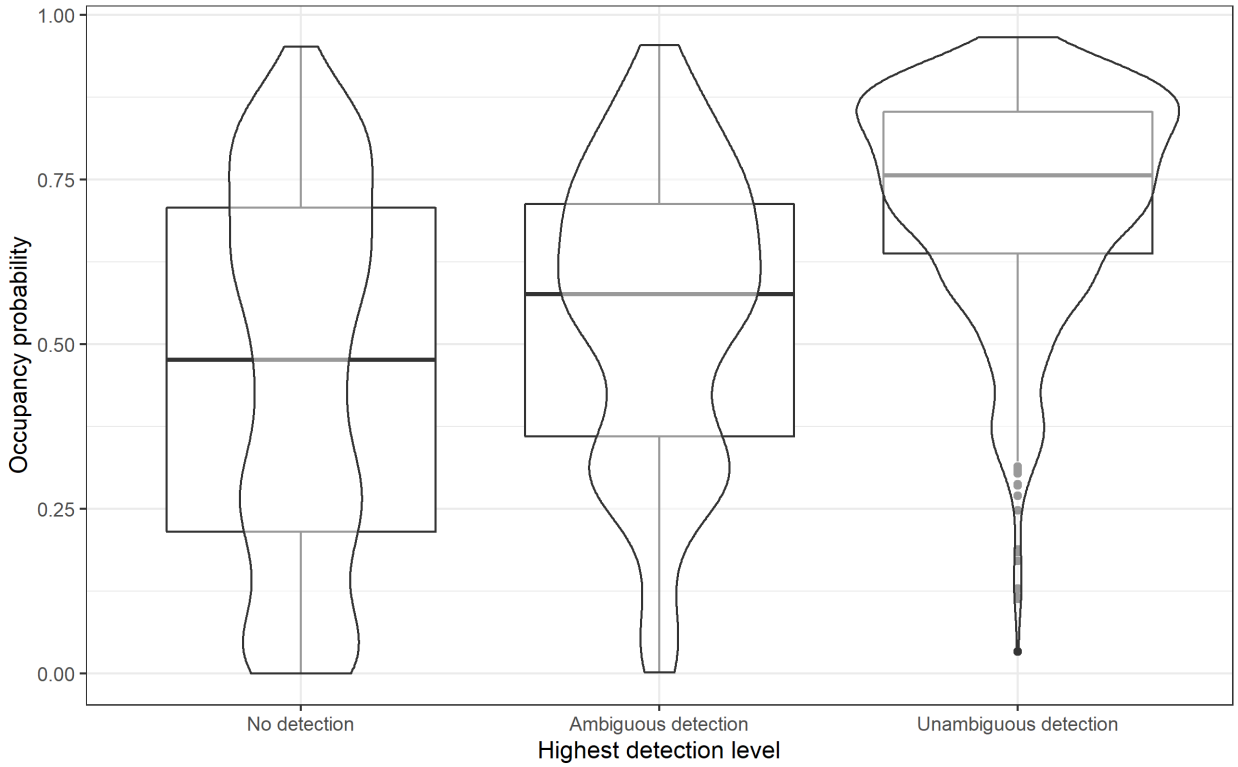

Figure D.4. Violin plots depict predicted occupancy probabilities for *Myotis evotis* (MYEV) compared to the highest level of species detection observed for each grid cell and year. The distributions of predicted occupancy probabilities (y-axis) are plotted against the highest level of detection observed in each grid cell and year (x-axis).

D.5 *Myotis grisescens*

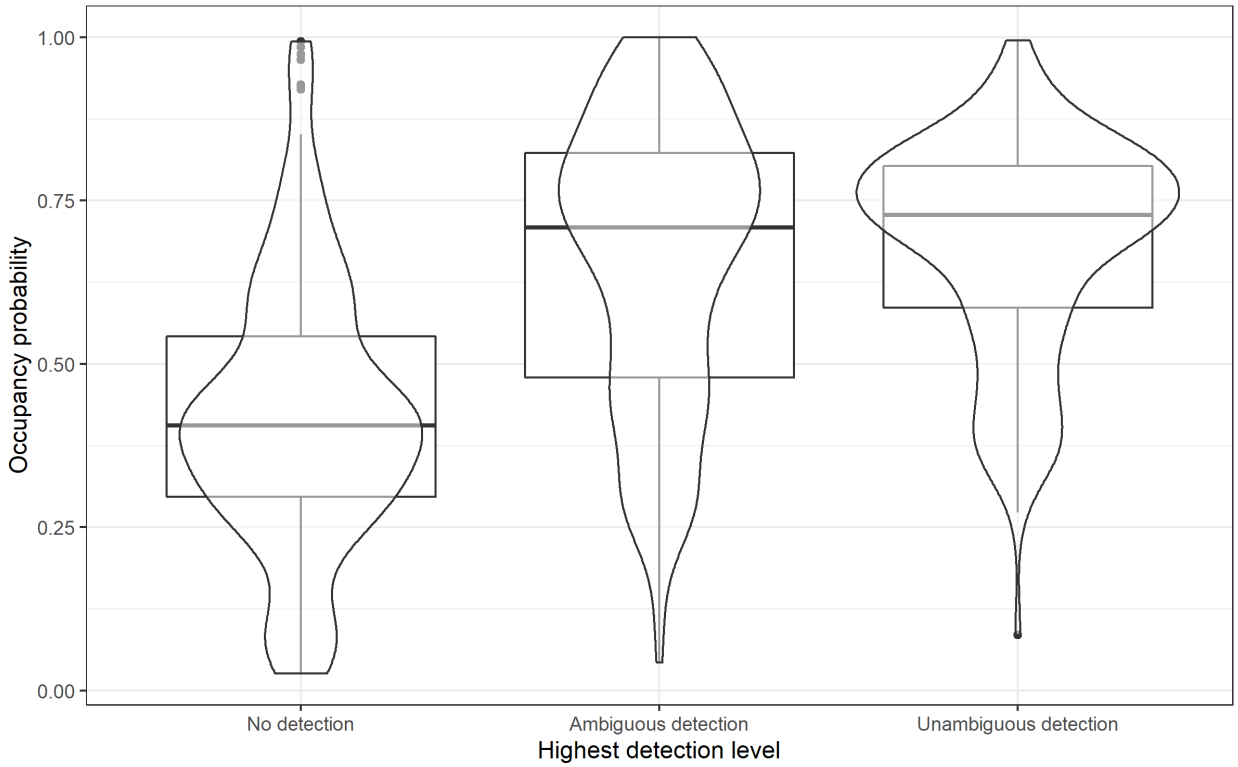

Figure D.5. Violin plots depict predicted occupancy probabilities for *Myotis grisescens* (MYGR) compared to the highest level of species detection observed for each grid cell and year. The distributions of predicted occupancy probabilities (y-axis) are plotted against the highest level of detection observed in each grid cell and year (x-axis).

D.6 *Myotis leibii*

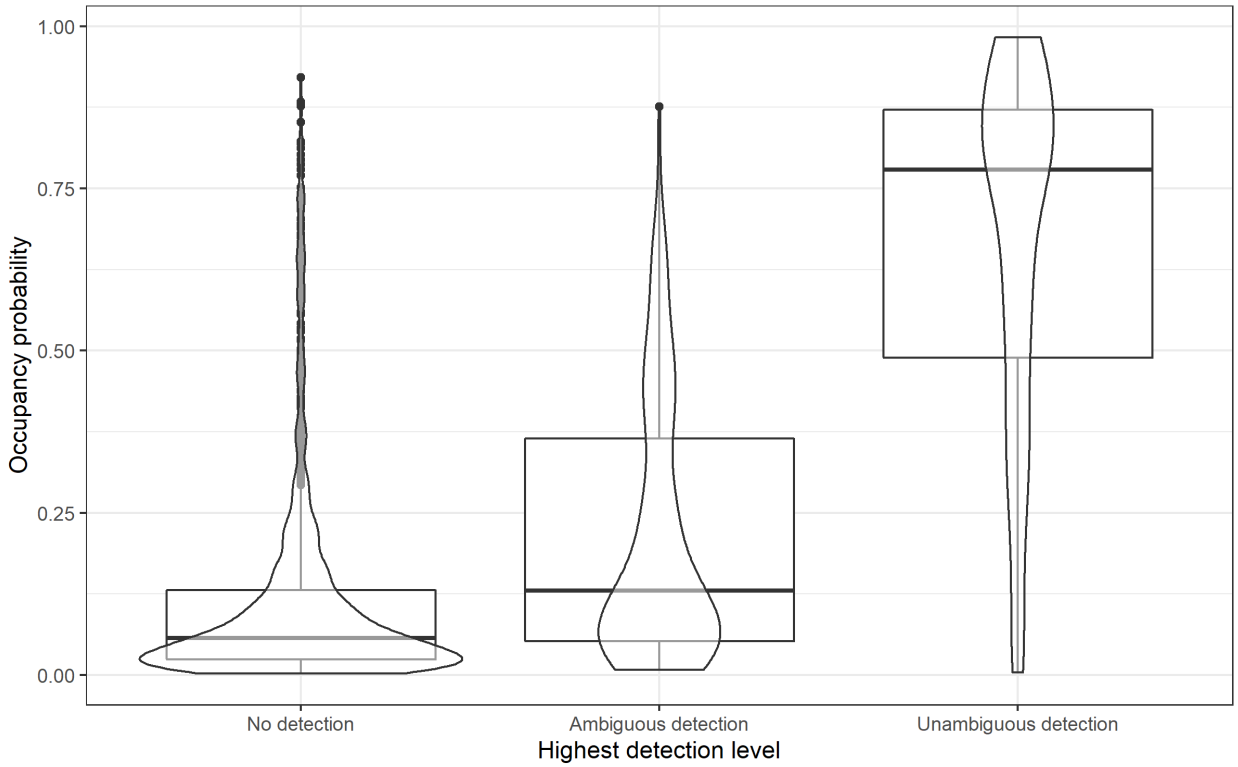

Figure D.6. Violin plots depict predicted occupancy probabilities for *Myotis leibii* (MYLE) compared to the highest level of species detection observed for each grid cell and year. The distributions of predicted occupancy probabilities (y-axis) are plotted against the highest level of detection observed in each grid cell and year (x-axis).

D.7 *Myotis thysanodes*

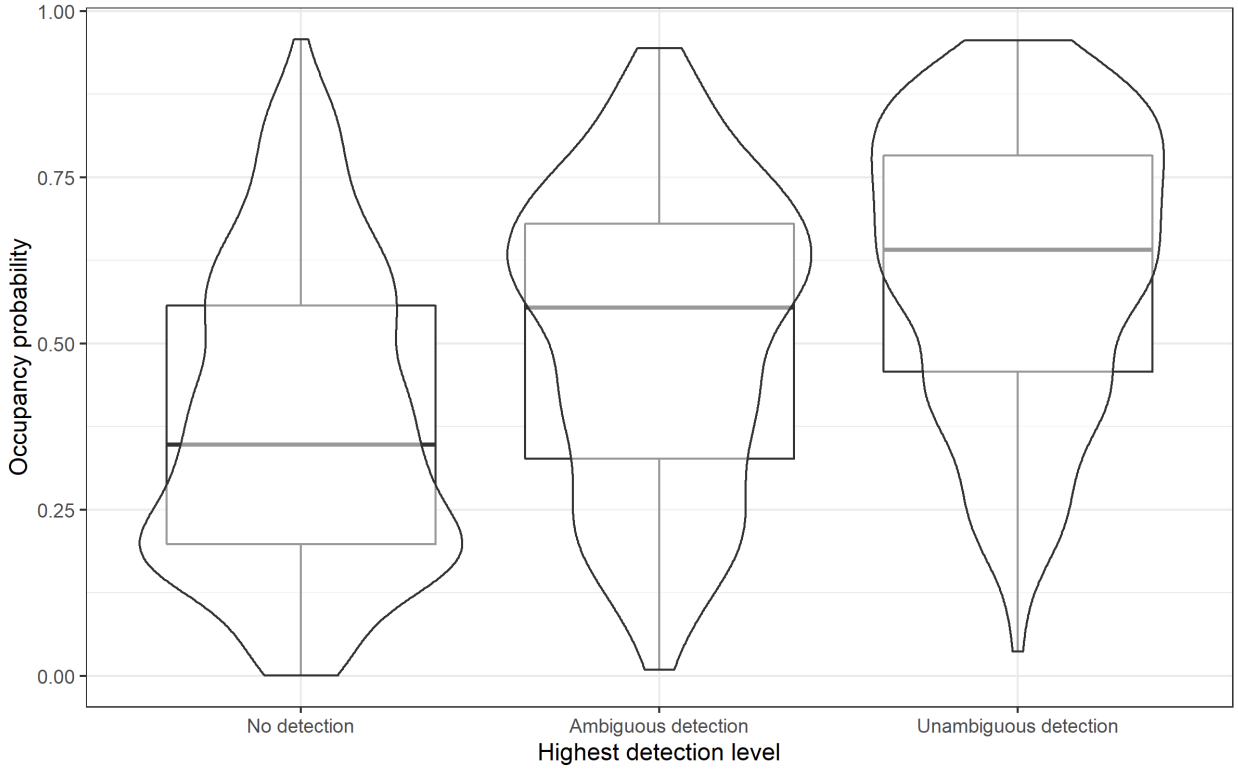

Figure D.7. Violin plots depict predicted occupancy probabilities for *Myotis thysanodes* (MYTH) compared to the highest level of species detection observed for each grid cell and year. The distributions of predicted occupancy probabilities (y-axis) are plotted against the highest level of detection observed in each grid cell and year (x-axis).

D.8 *Myotis volans*

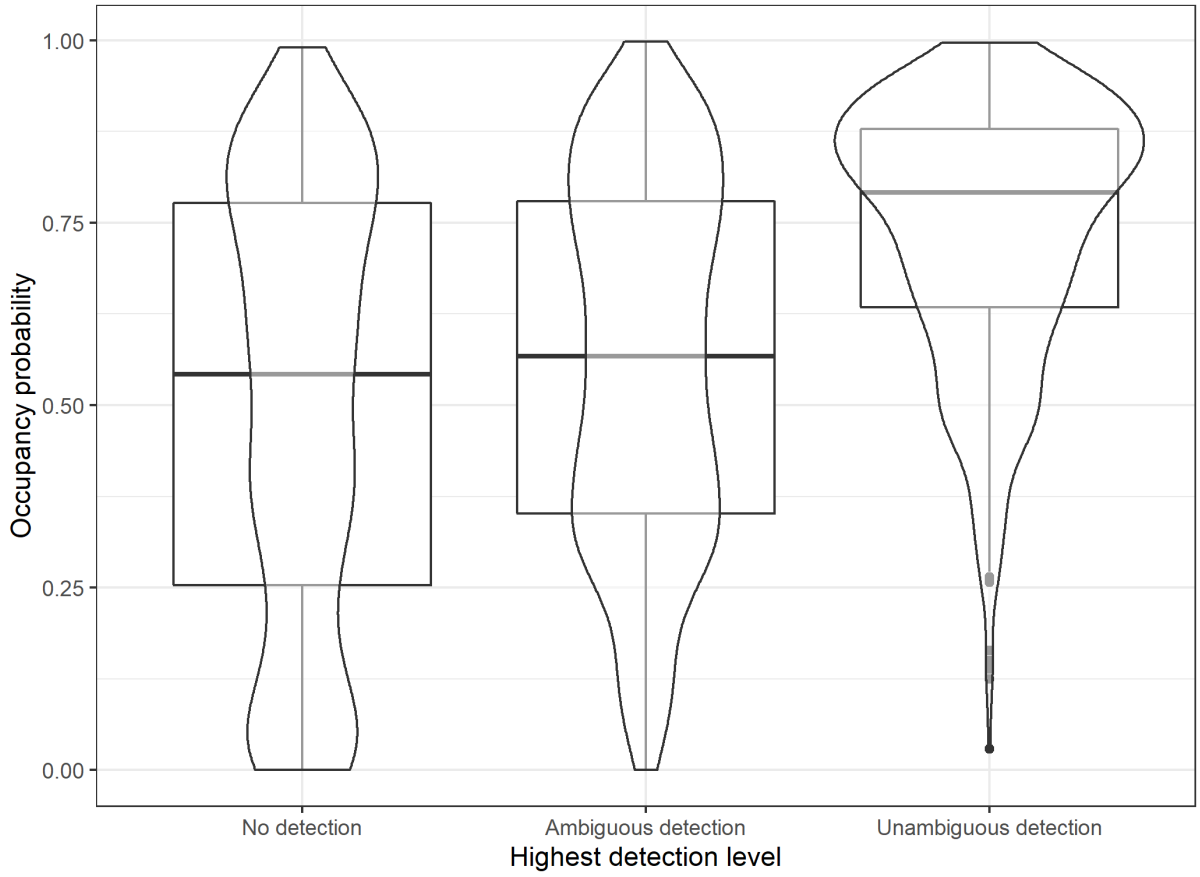

Figure D.8. Violin plots depict predicted occupancy probabilities for *Myotis volans* (MYVO) compared to the highest level of species detection observed for each grid cell and year. The distributions of predicted occupancy probabilities (y-axis) are plotted against the highest level of detection observed in each grid cell and year (x-axis).

D.9 *Myotis yumanensis*

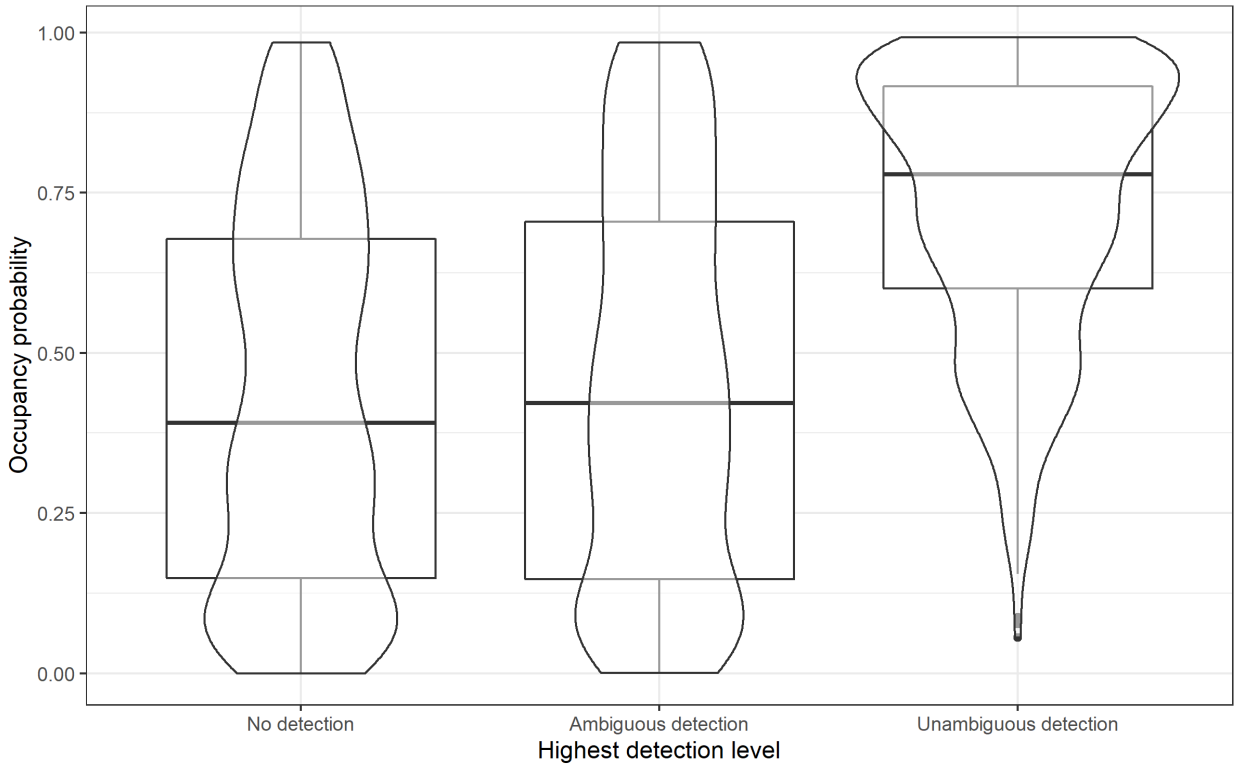

Figure D.9. Violin plots depict predicted occupancy probabilities for *Myotis yumanensis* (MYYU) compared to the highest level of species detection observed for each grid cell and year. The distributions of predicted occupancy probabilities (y-axis) are plotted against the highest level of detection observed in each grid cell and year (x-axis).

D.10 *Eptesicus fuscus*

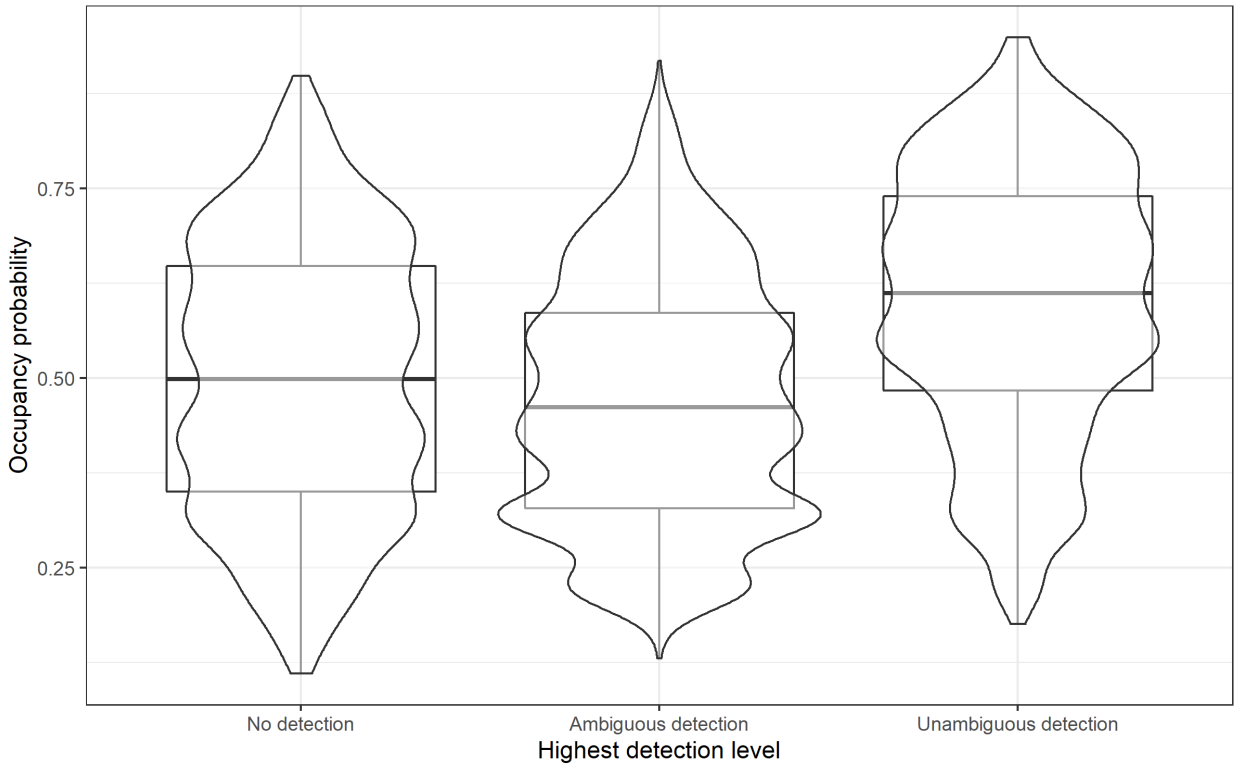

Figure D.10. Violin plots depict predicted occupancy probabilities for *Eptesicus fuscus* (EPFU) compared to the highest level of species detection observed for each grid cell and year. The distributions of predicted occupancy probabilities (y-axis) are plotted against the highest level of detection observed in each grid cell and year (x-axis).

D.11 *Lasionycteris noctivagans*

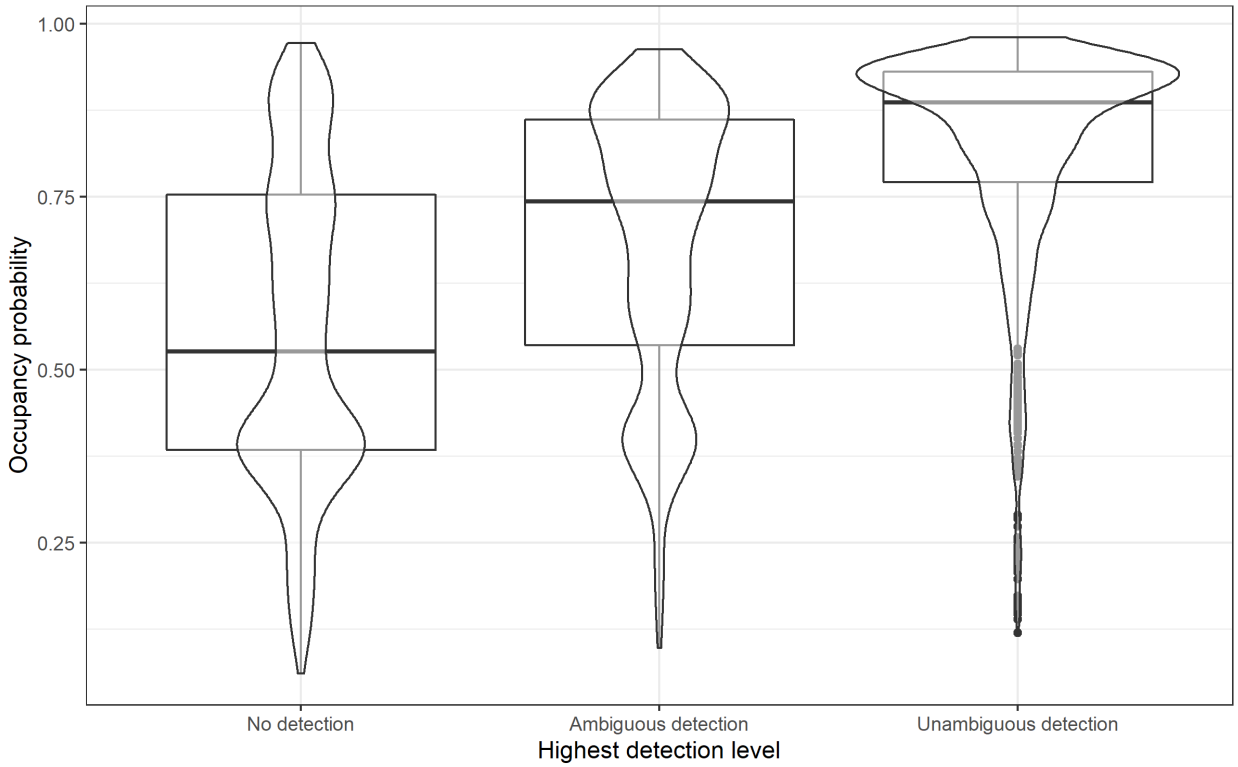

Figure D.11. Violin plots depict predicted occupancy probabilities for *Lasionycteris noctivagans* (LANO) compared to the highest level of species detection observed for each grid cell and year. The distributions of predicted occupancy probabilities (y-axis) are plotted against the highest level of detection observed in each grid cell and year (x-axis).

D.12 *Lasiurus cinereus*

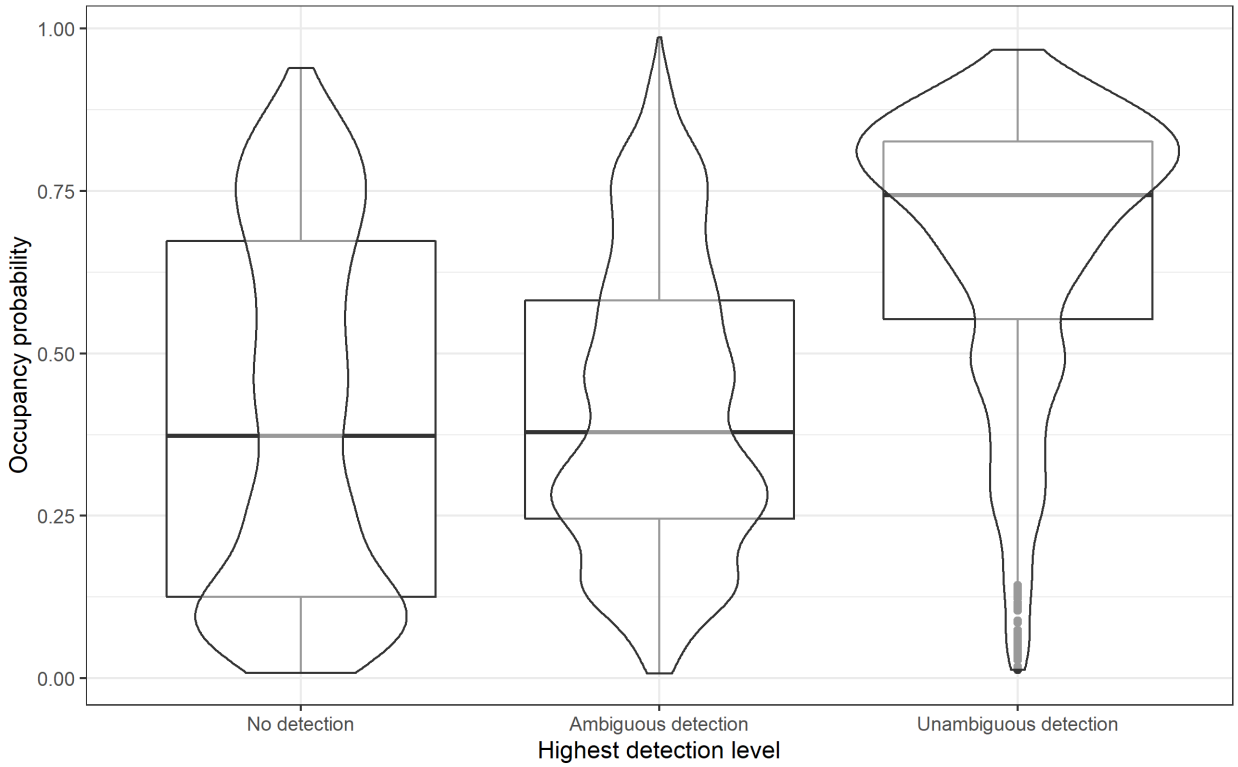

Figure D.12. Violin plots depict predicted occupancy probabilities for *Lasiurus cinereus* (LACI) compared to the highest level of species detection observed for each grid cell and year. The distributions of predicted occupancy probabilities (y-axis) are plotted against the highest level of detection observed in each grid cell and year (x-axis).